

http://researchcommons.waikato.ac.nz/

Research Commons at the University of Waikato

Copyright Statement:

The digital copy of this thesis is protected by the Copyright Act 1994 (New Zealand).

The thesis may be consulted by you, provided you comply with the provisions of the Act and the following conditions of use:

- Any use you make of these documents or images must be for research or private study purposes only, and you may not make them available to any other person.
- Authors control the copyright of their thesis. You will recognise the author's right to be identified as the author of the thesis, and due acknowledgement will be made to the author where appropriate.
- You will obtain the author's permission before publishing any material from the thesis.

Site Characterisation and Assessment of Sediments For Beach Renourishment

A thesis
submitted in partial fulfilment
of the requirements for the Degree
of
Master of Science in Earth Sciences
at the
University of Waikato
by

Peter Clifford Longdill

April 2004

coastal marine group
University of Waikato

The University of Waikato
Te Whare Wānanga o Waikato

ABSTRACT

Marsden Point, Northland, New Zealand, is a Holocene, prograded barrier spit at the tidal inlet to Whangarei Harbour. The development of the Northport timber export port at Marsden Point in late 2000 modified the tidal inlet dynamic equilibrium due to a large reclamation (32.6 ha) and dredged turning basin (31.8 ha to 13 m below Chart Datum). The effects of the Northport development on the inlet morphodynamics and the potential use of dredge sediments as beach nourishment fill are the foci of this study.

Regional sediment transport patterns adjacent to the Northport development were inferred and documented through the interpretation of sediment grain size distributions, geomorphic analysis of historical shoreline and bathymetry data, analysis of beach profiles, identification of seabed sediment transport pathways, and calculation of potential sediment transport vectors from hindcast wind-wave and current meter data.

Sediments found in the lower harbour are consistent with Schofield's (1975) Hauraki (B) facies. Shelly lag sediments, which armour and stabilise the bed, were observed in similar locations to those present in 1983. Sediment transport directions inferred from sediment textural analyses were generally in agreement with directions found from beach profile analysis, morphologic interpretation and calculation of potential sediment transport vectors.

Analysis of thirteen rectified and geo-referenced vertical aerial photographs of the Marsden Point region over the period 1984 to 2001, indicated a general reduction in dry beach widths within the harbour, and an increase in beach width at Marsden Point, where opposing sediment transport vectors meet and the ebb tidal delta of Mair Bank became *'welded'* to the shoreline. This area exhibits highly variable beach profiles and offshore bathymetry, indicative of the relatively large potential sediment vectors meeting at this location.

Comparison of digital bathymetric surveys, sediment transport pathways and bedform locations both pre and post-development, indicates changes have been limited to the local reclamation and dredge basin areas. Reduced post-development sediment transport potentials were found in the northern areas of the dredge basin. There is potential for scour and the development of a shell lag at the dredge basin's eastern edge. Small-scale (~1,000m^3yr^{-1}) accretion has been observed against both western and eastern edges of the Northport reclamation. Accretion is occurring due to dominant longshore sediment transport patterns (western edge) and the creation of a *'current transport shadow zone*' (eastern edge). Dredge basin sedimentation is expected to increase over the next 5-10 years to reach 15-20,000 m^3yr^{-1} as the beach profile against Northport's western edge '*fills*' with sediment.

Sediment grain size comparisons and sediment transport patterns have been used to develop an effective beach nourishment plan for Marsden Bay (West and Central) using sediments sourced from Northport's dredge basin.

The Northport development has caused only local modifications to sediment transport processes operating within the lower Whangarei Harbour. There have been no large-scale changes in sediment transport patterns or morphology observed post-development.

ACKNOWLEDGEMENTS

This thesis evaluates data and measurements resulting from the combined efforts of many people. First and foremost I would like to thank my supervisor Professor Terry Healy, who has supported my work through its entirety. Thank you for being so enthusiastic with my studies and guiding me through any problems encountered. Thanks also to John Palmer of Northport for providing key contacts, advice and help. This study has been made possible through the assistance of Northport and the Foundation of Research, Science and Technology, Contract No. NPRT0201.

To the University of Waikato team, Dirk Immenga and Ian Blair, your assistance in the field was invaluable, thanks for the good company and knowledgeable direction. Also to Arne Pallentin for making sense of the many projections, data formats and GIS issues. The team at Northport including Bruce, Joan, Trevor, and Craig from International Stevedoring, thanks for the prompt assistance and kind words when they were needed. I am still amazed by your willingness and eagerness to lend assistance. To Glenys Mulooly and Harvey Schroyen of the Whangarei District Council, Bruce Howse of the Northland Regional Council, Mike Swords of the New Zealand Refining Company, Kathy Walter of NIWA, Alastair Barnett, Sidney Wright, and Owen Maynard thank you for your assistance with providing accurate and relevant data.

Many thanks to my gran, Isabel for providing many dinners and a place to stay during my overnight trips to Hamilton.

Most importantly, Menderson, Bungle and my family, Doug, Judi, Simon and Anna; your support has been invaluable and greatly appreciated, without your influence I would surely be much worse off and I am sure that this work would not be what it is.

TABLE OF CONTENTS

ABSTRACT ii
ACKNOWLEDGEMENTS iii
TABLE OF CONTENTS iv
LIST OF FIGURES ix
LIST OF TABLES xii

1 INTRODUCTION 1
1.1 Background 1
1.2 Objectives of This Thesis 6
1.3 Thesis Structure 7
1.4 The Site 9
1.5 Summary 10

2 REVIEW OF HARBOUR STUDIES 11
2.1 Introduction 11
2.2 Geological Background 11
2.2.1 Sub-Surface Investigations - Marsden Point barrier system 12
2.2.2 Morphologic Features 13
2.3 The seabed and its Sediments 14
2.3.1 General 14
2.3.2 Sediment Inputs 14
2.3.3 Harbour Sediments 14
2.4 Bathymetry 16
2.4.1 General 16
2.4.2 Dredging and Reclamation 17
2.4.3 Bathymetric Change 17
2.5 Sediment Transport 18
2.5.1 Harbour Entrance and Channels 18
2.5.2 Modes of Sediment Transport 19
2.5.3 Volume of Sediment Movement 19
2.5.4 Sediment Pathways 20
2.5.5 The Marsden Bay – One Tree Point Region 22
2.5.6 The Bream Bay Beach Region 23
2.6 Hydraulics and Hydrodynamics 25
2.6.1 General Characteristics 25
2.6.2 Waves 25
2.6.3 Currents Near the Harbour Entrance 26
2.7 Wind Conditions 28
2.8 Shoreline Change 29
2.8.1 Bream Bay Beach 29
2.8.2 Shoreline Change Within the Harbour 30
2.9 Ecology 30
2.10 Developments in the Region and Associated Studies 32
2.10.1 Temporary Offloading Wharf 32
2.10.2 Beach Protection: Marsden Bay – One Tree Point 32
2.10.3 Port Facilities at Marsden Point 33
2.11 Modelling of the Lower Harbour 35
2.11.1 Background 35
2.11.2 DHI's Physical Model 35
2.11.3 Mathematical Models 36
2.11.4 Sediment Transport Modelling 38

3 GRAIN SIZE PATTERNS OF THE LOWER HARBOUR 43
3.1 Introduction 43
3.2 Background 43
3.3 Methods 44
3.4 Sediment Sampling Results 48
3.4.1 Shell Lag 48
3.4.2 Mean Grain Size 50
3.4.3 Spatial Variation of Class Size Abundance 52
3.4.4 Higher Moment Measures 56
3.4.4.1 Interpretation of Higher Moment Measures 56
3.4.4.2 Sediment Transport Inferred From Higher Moment Measures 57
3.5 Summary 62

4 MEDIUM–LONG TERM COASTAL CHANGE SURROUNDING MARSDEN POINT 63
4.1 Introduction 63
4.2 Previous Investigations and Data Available 63
4.3 Methods 64
4.3.1 Overview of Procedures 64
4.3.2 Registration and Rectification 65
4.3.3 Errors in the Rectified Geo-Referenced Images 67
4.3.4 Shore-line Delineation 69
4.3.5 Methods of shoreline Analysis 71
4.4 Beach trends from air photographs – Results / Discussion 72
4.4.1 Marsden Point 72
4.4.2 One Tree Point – Central 75
4.4.3 One Tree Point – South 78
4.4.4 Marsden Bay – West and Central 81
4.4.5 Marsden Bay – East and Blacksmiths Creek 83
4.4.6 Marsden Spit 87
4.5 Summary of Trends from Air photo Interpretation 88

5 BEACH PROFILES OF THE SHORELINE SURROUNDING MARSDEN POINT 91
5.1 Introduction 91
5.1.1 Structure of Chapter 91
5.2 Survey Methods and Errors 92
5.2.1 Profile Locations 92
5.4 Profile Trends 94
5.4.1 Terminology 94
5.4.2 Analytic Techniques and Methods 94
5.4.2.1 Envelope of Change 95
5.4.2.2 Standard Deviations 95
5.4.3 Features and Trends of the Raw Profiles 96
5.4.3.1 Marsden Point (NZRC jetties, profiles A-G) 96
5.4.3.2 Between the NZRC jetties and Northport (Profiles 1 and 2) 100
5.4.3.3 Port Site Profiles 102
5.4.3.4 Marsden Spit Profiles 106
5.4.3.5 Marsden Bay 108
5.4.3.6 One Tree Point Profiles 110
5.5 Closure Depth From the Raw Profiles 115
5.5.1 Definition 115
5.5.2 Depth of Closure From Profile Changes at Marsden Point 116
5.6 Volumetric Changes 119
5.6.1 Analytic Techniques and Methods 119
5.6.2 Results and discussion 121

5.7 Even-Odd Analysis at the Northport site 123
5.7.1 Longshore Sediment Transport and Even-Odd Analysis 123
5.7.2 Even-Odd Analysis at the Port Site 125
5.7.3 Results and discussion 126
5.8 Principle Components Analysis 129
5.8.1 Background 129
5.8.2 Statistical method 130
5.8.3 Application to the Marsden Point Profiles 133
5.8.4 Interpretation of Eigenfunctions 134
5.8.5 Eigenfunctions at Marsden Point 135
5.9 An Inter-tidal Sediment Budget 142
5.10 Summary and Conclusions 146

6 BATHYMETRY AND HYDROGRAPHY OF MARSDEN POINT 147
6.1 Introduction 147
6.2 Previous Investigations 147
6.3 Recent surveys 150
6.3.1 Surveying Scheme and Resolution 151
6.3.2 Datum position at Marsden Point 151
6.4 Digital Elevation Model (DEM) Generation 152
6.4.1 Error Checking 152
6.4.2 Gridding Operations 152
6.4.2.1 Spatial Extent of DEMs 153
6.4.3 Error Analysis of Gridded Bathymetry 153
6.5 DEM Calculations 155
6.5.1 Calculating Bed Level Changes 155
6.5.2 Removing Artefacts of the Gridding Process 155
6.5.3 Volume calculations 156
6.6 Bathymetry Changes Prior to Port Development 157
6.6.1 May 1995 to November 1995 (Figure 6.3) 158
6.6.2 November 1995 to May 1996 (Figure 6.4) 160
6.6.3 May 1996 to May 1998 (Figure 6.5) 162
6.6.4 May 1998 to December 2000 (Figure 6.6) 162
6.6.5 Pre-Construction trends 165
6.7 Bathymetric Changes During and Post Port Construction 166
6.7.1 December 2000 to May 2001 (Figure 6.7) 166
6.7.2 May 2001 to November 2001 (Figure 6.8) 168
6.7.3 November 2001 to November 2002 (Figure 6.9) 170
6.7.4 During and Post-Construction Trends 172
6.8 Comparison of Pre and Post Construction Trends 173
6.9 Predictions of sediment transport models 177
6.10 Sediment budget for Marsden Point 181
6.11 Summary 183

7 MORPHODYNAMICS OF THE LOWER HARBOUR 185
7.1 Introduction 185
7.2 Instrumentation 185
7.3 Methods 186
7.3.1 Side Scan Sonar Survey 186
7.3.2 Sonograph Interpretation Methods 187
7.3.4 Bedform Classification 189
7.4 Side Scan Sonar Survey Results 191
7.4.1 Sediment Facies Units 191
7.4.2 Bedform Orientation 195
7.5 Discussion 198
7.6 Conclusions 199

8 SEDIMENT TRANSPORT AT MARSDEN POINT 201
8.1 Introduction 201
8.2 Instrumentation 202
8.2.1 Autonomous ADP Surveys 202
8.2.2 Shipboard, Downward-Looking ADP Survey 204
8.2.3 Current Velocity Measurements Over the Inter-tidal Zone 207
8.3 Sediment Transport Over the Channels and Channel Margins 210
8.3.1 Introduction 210
8.3.2 Sediment Thresholds 210
8.3.3 Residual Velocity Definition 211
8.3.4 Residual Distance Definition and Calculation 213
8.3.5 Morphologic and Erosional / Depositional Implications 213
8.3.6 Spring-Neap tide differences 214
8.3.7 Tidal Cycle Residual Distances 216
8.3.7.1 Un-scaled Residuals 216
8.3.7.2 Residual Distances Scaled to a Constant Tidal Range 218
8.3.7.3 Residuals From Boat Mounted Survey 220
8.3.8 Comparison with Previous Sediment Transport Investigations 224
8.3.8.1 Tidal Cycle Residual Distances 224
8.3.8.2 Transport Pathways 226
8.4 Transport by Tidal Currents Over Inter-tidal Zones 227
8.4.1 Introduction 227
8.4.2 Limitations and Assumptions 228
8.4.3 Methods 229
8.4.3.1 Sediment Thresholds 229
8.4.3.2 Calculation of Tidal Cycle Sediment Transport 230
8.4.3.3 Distribution of Tidal Ranges 232
8.4.3.4 Annual Sediment Transport Rates 232
8.4.4 Results 233
8.4.5 Comparison to Previous Calculations 236
8.5 Longshore Transport by Waves at the Beach Face 236
8.5.1 Introduction 236
8.5.2 Methods 237
8.5.2.1 Longshore Wave Power and Transport 237
8.5.2.2 Limitations and assumptions 238
8.5.2.3 Wave Hindcasting 239
8.5.2.3.1 Fetch Lengths 239
8.5.2.3.2 Water Depths 240
8.5.2.3.3 Wave Heights 240
8.5.2.4 Time Averaging of Wave Energy 243
8.5.3 Results 243
8.6 Longshore Transport by Waves and Currents Over the Inter-tidal Zone 246
8.6.1 Introduction 246
8.6.2 Methods 246
8.6.2.1 Longshore Current Method 247
8.6.2.2 Methods of Calculation 248
8.6.2.3 Limitations and Assumptions 249
8.6.3 Results 250
8.7 Northport – One Tree Point Inter-tidal Area Sediment Transport 253
8.7.1 Inter-tidal Transport at Site I-1 (Marsden Point) 255
8.7.2 Inter-tidal Transport at Site I-2 (Bream Bay Beach) 256
8.7.3 Inter-tidal Transport at Site I-3 (Marsden Bay) 257
8.7.4 Inter-tidal Transport at Sites I-4, I-5 and I-6 (Paradise Point to One Tree Point 259
8.8 Summary of Sediment Transport, Debits and Credits at Marsden Point 259
8.9 Implications of Sediment Transport 262
8.10 Conclusions 263

9 POTENTIAL BEACH RENOURISHMENT, MARSDEN POINT–ONE TREE POINT **265**
9.1 Introduction 265
9.2 The Case for Renourishment 265
9.3 Potential Sites for Renourishment 266
9.4 Suitability of Available Sediments 268
9.4.1 Calculation of the Overfill Factor 270
9.5 Selection of Nourishment Site 271
9.6 A Plan for Nourishment 273
9.6.1 Volumes of Sediment 273
9.6.2 The Construction Profile 274
9.6.3 Methods of Placement 274
9.6.4 Life Expectancy 276
9.6.5 A Monitoring Program 276
9.6.6 Estimated Costs of Nourishment 279
9.7 Summary 279

10 SUMMARY AND CONCLUSIONS **281**
10.1 Introduction 281
10.2 General Summary 281
10.3 Grain Size Patterns 282
10.4 Medium – Long Term Coastal Change 282
10.5 Beach Profile Analysis 284
10.6 Bathymetry and Hydrography 285
10.7 Morphodynamics of the Lower Harbour 286
10.8 Sediment Transport at Marsden Point 287
10.9 Potential Beach Renourishment 288
10.10 Aims Achieved 289
10.11 Suggestions for Further Research 289

REFERENCES **291**

APPENDICIES (A,B,C,D,E,F,G) **303**

LIST OF FIGURES

Figure 1.1 – Whangarei Harbour, located on the northeast coast of New Zealand. 2
Figure 1.2 – Northport is sited on the barrier spit of Marsden Point. 4
Figure 1.3 – Major developments at the Northport site. 4
Figure 1.4 – Whangarei Harbour extent. 5
Figure 1.5 – Place names used throughout the study. 9
Figure 2.1 – Geology of the Whangarei Harbour and Marsden Point region. 11
Figure 2.2 – Sediment transport loops and pathways. 21
Figure 2.3 – Geomporphic evidence of easterly directed net sediment transport. 22
Figure 2.4 – Sediment Budget of Bream Bay Beach in 1982. 24
Figure 2.5 – Wind rose from Marsden Point. 28
Figure 3.1 – Flow chart illustrating the analysis procedure for sediment samples 46
Figure 3.2 – Shelly and active sediment transport zones from Black (1983). 48
Figure 3.3 – Location and mean grain size of samples collected for this study. 49
Figure 3.4 – Interpolated mean grain size of lower Whangarei H arbour. 51
Figure 3.5 – Abundance of coarse and very coarse sands. 54
Figure 3.6 – Abundance of medium sands. 54
Figure 3.7 – Abundance of fine sands. 55
Figure 3.8 – Abundance of very fine sands. 55
Figure 3.9 – Spatial trends of mean grain size and sorting. 57
Figure 3.10 – Spatial variation of standard deviation. 58
Figure 3.11 – Spatial variation of skewness. 60
Figure 4.1 – GCPs used for image rectification and referencing. 66
Figure 4.2 – Road centrelines and wharves at Marsden Point. 68
Figure 4.3 – Identifiable indicators of shoreline movement. 70
Figure 4.4 – Location of areas for analysis of trends from Air Photographs. 71
Figure 4.5 – Location of Healy's (1980) transects. 73
Figure 4.6 – Decrease in beach width at One Tree Point – Central 77
Figure 4.7 – Decrease in beach width at One Tree Point – South. 79
Figure 4.8 – One Tree Point- South, narrowing in a southeast (down harbour) direction, indicative of longshore sediment transport up harbour. 79
Figure 4.9 – Sediment accumulation on the northwestern side promontory. 80
Figure 4.10 – The Marsden Bay – West shoreline. 82
Figure 4.11 – Blacksmiths Creek channel, along the shoreline of Marsden Bay. 85
Figure 4.12 – Shoreline change at Marsden Bay East and Marsden Spit. 86
Figure 4.13 – Shoreline change rates. 88
Figure 5.1 – Location of beach profiles at Marsden Point - One Tree Point. 92
Figure 5.2 – Profile of a typical inter-tidal estuarine. 94
Figure 5.3 – Profile A raw data. 97
Figure 5.4 – Profile B raw data. 97
Figure 5.5 – Profile C raw data. 98
Figure 5.6 – Profile D raw data. 98
Figure 5.7 – Profile E raw data. 99
Figure 5.8 – Profile F raw data. 99
Figure 5.9 – Profile G raw data. 100
Figure 5.10 – Profile 1 raw data. 101

Figure 5.11 – Profile 2 raw data. 101
Figure 5.12 – Profile 215E raw data. 103
Figure 5.13 – Profile 55E raw data. 103
Figure 5.14 – Profile 15E raw data. 104
Figure 5.15 – Profile 15W raw data. 104
Figure 5.16 – Profile 55W raw data. 105
Figure 5.17 – Profile 215W raw data. 105
Figure 5.18 – Profile 3 raw data. 107
Figure 5.19 – Profile 4 raw data. 107
Figure 5.20 – Profile 5 raw data. 109
Figure 5.21 – Profile 6 raw data. 109
Figure 5.22 – Profile 7 raw data. 110
Figure 5.23 – Profile 7-1 raw data. 111
Figure 5.24 – Profile 8 raw data. 112
Figure 5.25 – Profile 9 raw data. 112
Figure 5.26 – Profile 10 raw data. 113
Figure 5.27 – Profile 11 raw data. 113
Figure 5.28 – Profile 12 raw data. 114
Figure 5.29 – Profile 13 raw data. 114
Figure 5.30 – Standard deviations of Profile lines A-G. 116
Figure 5.31 – Standard deviations of Profile lines 1-4 (incl. 215E-215W). 117
Figure 5.32 – Standard deviations of Profile lines 5-13. 118
Figure 5.33 – Areas for volumetric analysis of beach sediments. 121
Figure 5.34 – Changes in sand volume of, 1997 – 2003. 122
Figure 5.35 – Even-Odd analysis of the St. Lucie Inlet, Florida. 124
Figure 5.36 – Odd Component of shoreline change about causeway 1996-2000. 126
Figure 5.37 – Odd Component of volumetric sediment change 1996-2000. 127
Figure 5.38 – Odd Component of volumetric sediment change about Northport. 128
Figure 5.39 – Schematic decomposition of profiles. 130
Figure 5.40 – Eigenfunctions at profile B, Marsden Point. 137
Figure 5.41 – Eigenfunctions for Torrey Pines Beach, California. 138
Figure 5.42 – Eigenfunctions at profile 2, Marsden Point. 139
Figure 5.43 – Eigenfunctions at profile 4, Marsden Point. 141
Figure 5.44 – Sediment transport quantities, Marsden Point 1998-2003. 145
Figure 6.1 – Bathymetric changes at Marsden Point. 148
Figure 6.2 – Time line of bathymetric surveys and development works. 157
Figure 6.3 – Bed level changes, May 1995 to November 1995. 159
Figure 6.4 – Bed level changes, November 1995 to May 1996. 161
Figure 6.5 – Bed level changes, May 1996 to May 1998. 163
Figure 6.6 – Bed level changes, May 1998 to December 2000. 164
Figure 6.7 – Bed level changes, 2000 to May 2001. 167
Figure 6.8 – Bed level changes, May 2001 to November 2001. 169
Figure 6.9 – Bed level changes, November 2001 to November 2002. 171
Figure 6.10 – Observed and Predicted changes in bed level. 178
Figure 6.11 – Bathymetry based sediment budget for lower Whangarei Harbour. 182
Figure 7.1 – Side scan sonar system. 186
Figure 7.2 – Sediment classification scheme based on four end-member. 188
Figure 7.3 – Differences between shell lag and medium sand zones. 189
Figure 7.4 – Subaqueous bedforms. 191

Figure 7.5 – Sonograph of the lower Whangarei Harbour. 192
Figure 7.6 – Bottom sediments interpreted from sonograph. 193
Figure 7.7 – Bottom types from side scan sonar survey. 194
Figure 7.8 – Mean water depth and depth range of the dominant facies units. 194
Figure 7.9 – Bed from orientation and wavelength. 196
Figure 7.10 – Side-scan sonar summary of inner harbour, 1983. 197
Figure 8.1 – Location of instruments. 203
Figure 8.2 – Tidal elevation during autonomous ADCP survey. 205
Figure 8.3 – Tide height during boat mounted ADCP surveys. 206
Figure 8.4 – Frame, FSI current meter, Dobie wave gauge and OBS. 207
Figure 8.5 – Spring (blue) and neap (red) tidal cycle residual distances. 215
Figure 8.6 – Tidal cycle residual distances at 1 m above the bed. 216
Figure 8.7 – Tidal cycle residual distances at 1 m above the bed. 217
Figure 8.8 – Tidal cycle residual distances at 1 m above the bed. 219
Figure 8.9 – Tidal cycle residual distances at 1 m above the bed. 219
Figure 8.10 – Measured tidal cycle residual distances at 1 m above the bed. 221
Figure 8.11 – Measured tidal cycle residual distances at 1 m above the bed. 221
Figure 8.12 – Sediment transport directions inferred from residual distances. 223
Figure 8.13a, b and c – Tidal cycle residual distances at 1 m above the bed. 225
Figure 8.14 – Sediment transport pathways inferred from tidal cycle residuals. 227
Figure 8.15 – Annual tidal current (in isolation) induced sediment transport. 234
Figure 8.16– Longshore and cross-shore directions. 237
Figure 8.17 – Potential longshore sediment transport at sites I-1,I-3,I-4 and I-5. 244
Figure 8.18 – Annual longshore transport vectors due to wave action. 245
Figure 8.19 – Longshore velocity, on/offshore velocity, significant wave height, mean spectral period of waves and calculated longshore sediment transport. 251
Figure 8.20 – Net (and Gross) sediment transport over individual tidal. 252
Figure 8.21 – Sediment transport over inter-tidal areas surrounding Northport. 254
Figure 8.22– Observed and potential sediment transport. 260
Figure 8.23 – Schematic diagram of potential sediment transport. 261
Figure 9.1 – Area boundaries used for analysis of aerial photographs. 267
Figure 9.2 – Particle size distributions for native beach and dredge sediments. 269
Figure 9.3 – Isoline diagram for the evaluation of overfill ratio (RA). 271
Figure 9.4 – Sediment transport vectors and James' (1975) overfill ratios. 272
Figure 9.5 – Planform of proposed beach nourishment at Marsden Bay. 275
Figure 9.6 – Beach profile, design and construction profiles at Marsden Bay. 276

LIST OF TABLES

Table 3.1 – Wentworth grain size classification scheme. 45
Table 4.1 – Aerial Photographs available for analysis. 64
Table 4.2 – Air photograph analysis of change in dune line. 74
Table 4.3 – Beach width at One Tree Point–Central. 76
Table 4.4 – Width of dry beach. 76
Table 4.5 – Beach width at One Tree Point – South. 78
Table 4.6 – Shoreline rates of change from Gibb (1998). 81
Table 4.7 – Shoreline change rates along Marsden Bay West and Central. 81
Table 4.8 – Dune-line movement at Marsden Bay East and Blacksmiths Creek. 83
Table 4.9 – Movement of Marsden Spit 1906 – 1997. 87
Table 5.1 – Errors in volumetric change estimates. 120
Table 5.2 – Empirical eigenfunction analysis. 136
Table 6.1 – Recent bathymetric surveys at Marsden Point. 150
Table 6.2 – Datum Benchmarks at Marsden Point. 151
Table 6.3 – Characteristic volumes of sediment movement in the Lower harbour. 176
Table 7.1 – Basic map units used in the interpretation of the sonograph. 188
Table 8.1 – ADCP set-up information. 202
Table 8.2 – Set-up parameters for Boat-mounted ADP survey. 206
Table 8.3 – Set-up information for FSI current/wave meter. 208
Table 8.4 – Deployment locations, inter-tidal series of measurements. 208
Table 8.5 – Threshold velocity at inter-tidal sites (I-1 to I-6). 230
Table 8.6 – Annual tidal current (in isolation) induced sediment transport rates. 233
Table 8.7 – Fetch lengths and beach angles for the wave hindcasting sites. 240
Table 8.8 – Elevations of intertidal terrace from beach profiles. 240
Table 8.9 – Example spreadsheet of longshore sediment transport from wind hindcasting using CERC (1984) formulae. 242
Table 8.10 – Weighted net yearly transport rates at the foreshore due to wind generated waves. 244
Table 8.11 – Net and Gross potential sediment transport rates at Sites I-1 to I-4. 251
Table 8.12 – Previous estimations of longshore sediment transport at northern Bream Bay Beach (Site I-2). 256
Table 9.1 – Dry-beach width and beach narrowing. 267
Table 9.2 – Sediment sizes and sorting at nourishment sites and dredge basin. 268

1 INTRODUCTION

1.1 Background

During the 1960's and 1970's there was a boom in the planting of exotic pines in Northland. The growth was stimulated by the equitable climate, large areas of under-utilised scrubland and hilly country, the opportunity to use Maori leasehold land, and assessments that there would be a ready export market for timber and timber products in the years to come. Large-scale forest plantations were initiated by the state in the 1960's, followed by private companies in the 1970's.

In September 1978, with timber exports through Port Whangarei (Figure 1.1) totalling 240,000 tonnes, the Northland Regional Development Council (NRDC) forecast that timber exports would rise to 500,000 tonnes by 1990 and 2 million tonnes by 2005 (NFPWC, 1980). Ten years later, in 1998, Port Whangarei handled 600,000 tonnes of logs and forest products. Export predictions were revised in 2000 (NPC, 2000) to 2.4 million tonnes by 2004.

Following a number of studies the 1980 Northland Forestry Port Working Committee Report concluded:

> *"That Marsden Point be developed as a deep water port for the export of Northland forest products".*

The Northland Port Corporation and the Port of Tauranga formed the joint venture company *'Northport Ltd'* in 2000 following the issuing of resource consents for a 2-berth port. Construction of the ~$65 million Northport development began in October 2000, with the first log carrier berthing in June 2002. Currently (2003) the port is solely exporting logs and timber products, although it has been designed to accommodate more general cargo facilities also. The export of other types of cargo is likely to become a reality as Port Whangarei becomes increasingly uneconomic due to its reduced capacity for large carriers.

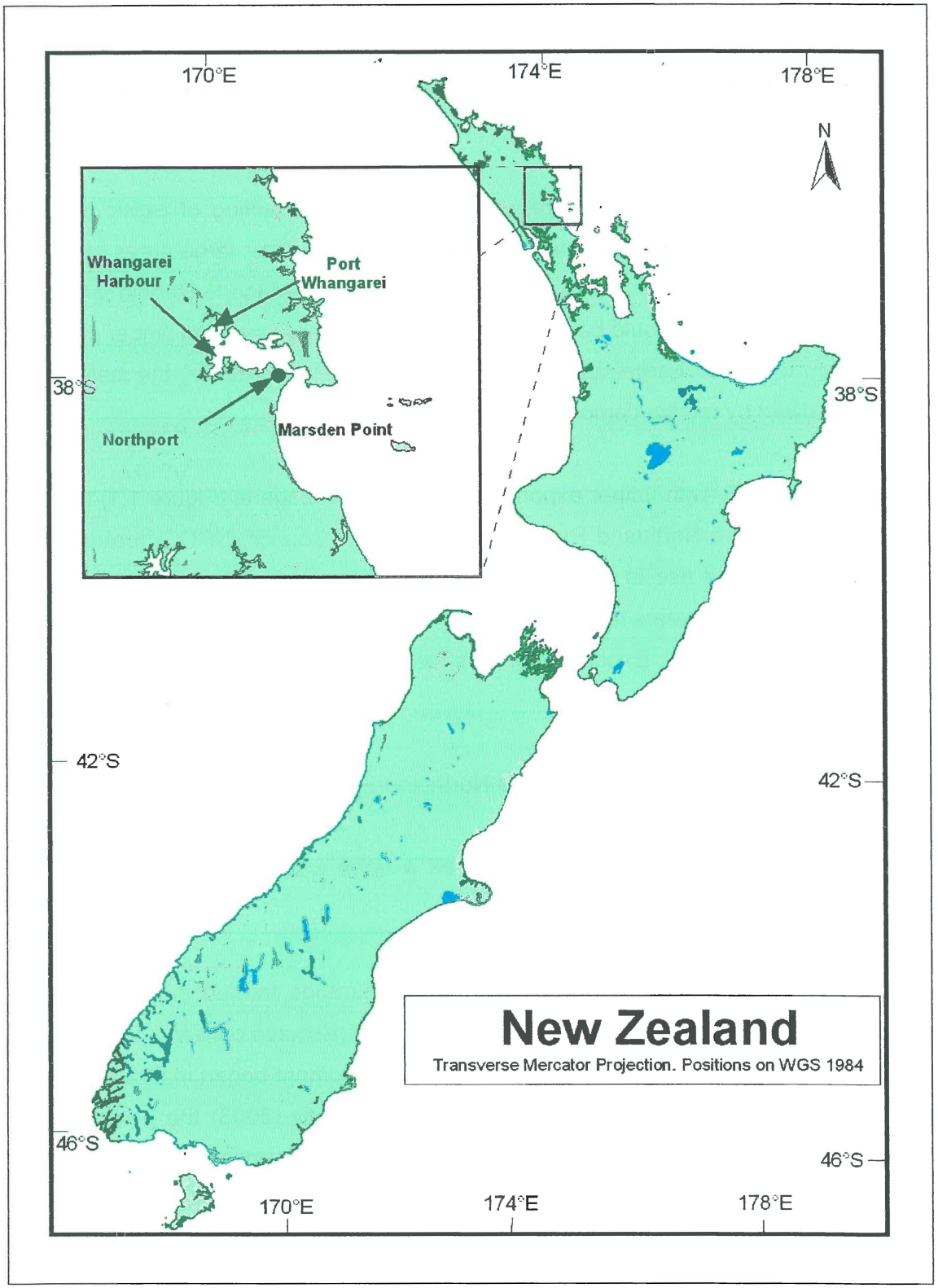


Figure 1.1- *Whangarei Harbour, located on the northeast coast of New Zealand's North Island.*

Northport is sited on the barrier spit of Marsden Point, adjacent to the flood tidal delta of Snake Banke (Figures 1.3 and 1.4). Construction involved a 32.6 ha reclamation of intertidal flats at Marsden Point providing 390 m of deep water berthage (Figure 1.3). A 31.8 ha turning basin was dredged to a depth of 13 m (below Chart Datum [C.D]). The 2.4 million m^3 of capital dredging tailings, comprising unconsolidated marine sands and shelly gravel, were used as fill for the reclamation (Figures 1.2 and 1.3). Additional development at the site has included a sophisticated stormwater collection system with an associated 15 ha storage pond, along with roading improvements, water taxi wharves and restorative areas of native trees and other developments (Figure 1.3).

Initial expectations of the maintenance dredging requirements in the turning basin based on sediment transport model investigations, are 50,000 m^3y^{-1} (Montgomery Watson, 1997; Northland Port Corporation, 2000).



Figure 1.2 – *Northport (mid-construction) is sited on the barrier spit of Marsden Point adjacent to the flood tidal delta. Dredge tailings were used as fill for the reclamation. NZRC facility and wharves are located on the tip of Marsden Point. In the background is Home Point, Busby Head and Bream Head.*

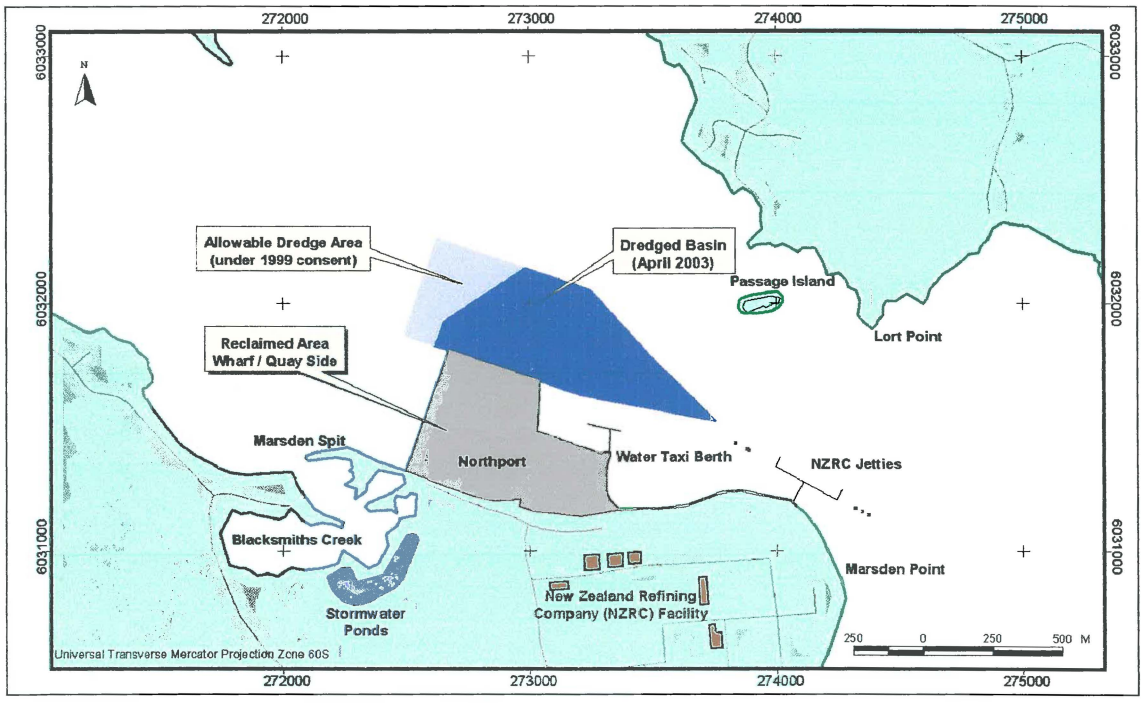


Figure 1.3 - *Major developments at the Northport site, Marsden Point, Northland, New Zealand. Developments have included large-scale reclamation, dredging, roading and stormwater runoff settling ponds.*

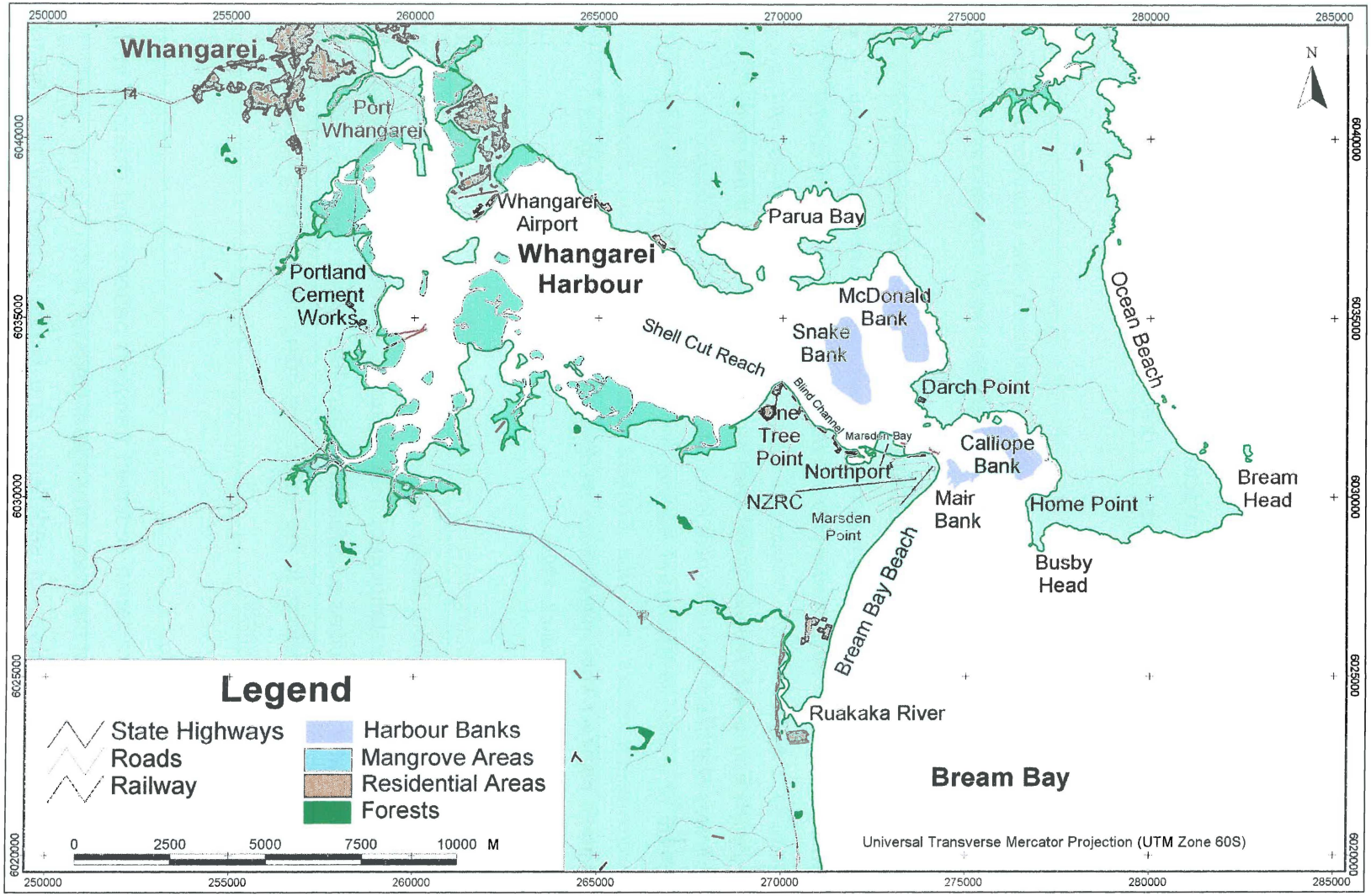


Figure 1.4 - *Whangarei Harbour extent, including common place names in the region.*

1.2 Objectives of This Thesis

"*Many coastal failures can be traced back to inadequate site characterisation analyses. Site characterisation involves identifying distinguishing qualities and features of a region that have a direct and indirect impact on the conception, design, economics, aesthetics, construction, and maintenance of a coastal project.*" (CERC, 2002).

This thesis aims to undertake a site characterisation of the lower Whangarei Harbour with respect to the Northport reclamation, dredge basin and a potential beach nourishment project.

In issuing the resource consents for the port construction, the Northland Regional Council specified in '*Decision #12: Land Use Consent No.2*', special condition no.9 that:

> *"The Consent Holder shall commission a study to investigate the feasibility of using the maintenance dredging material for beach renourishment purposes in Whangarei Harbour within twelve (12) months of the commencement of capital dredging. A person with recognised expertise in coastal processes and experience in beach renourishment shall supervise this study. If the study indicates that beach renourishment is an appropriate method of mitigating the effects of erosion in Whangarei Harbour and / or would result in beneficial environmental effects, then the Consent Holder shall make any suitable material obtained from maintenance dredging available for these purposes." (Northland Regional Council, 1999)*

Accurate appraisal of the *'distinguishing qualities and features'* of the lower harbour, with respect to the reclamation, dredge basin, and potential beach nourishment, will allow a more complete understanding of their impacts and effects on the environment. It is envisaged that the *'qualities and features'* identified within this thesis will allow a scientifically defendable position to be taken regarding the impacts (perceived or otherwise) of the coastal projects.

Specifically this study aims to:

1) Identify and characterise sediment transport patterns and changes in the geomorphology of the lower Whangarei Harbour; and
2) assess the suitability of sediments, and create a plan for the effective artificial nourishment of adjacent beach areas with sediment dredged from Northport's turning basin.

In order to achieve these aims, the following objectives are identified:

i. Identify sediment grain size distributions over the beach faces of the lower Whangarei Harbour, to be compared to dredge basin sediments for their compatibility for potential nourishment;
ii. identify medium – long term changes in the morphology of features in the lower Whangarei Harbour, including its spits, beaches, channels, and ebb and flood tidal deltas in order to isolate recent trends (post Northport development) from any pre-existing trends;
iii. determine changes in beach sediment volume over time for the One Tree Point – Marsden Point region;
iv. identify sediment transport directions, magnitudes and pathways within the lower Whangarei Harbour, including channels, channel margins, inter-tidal terraces and beach faces;
v. identify variations with, or similarities to, previous investigations of sediment transport and morphology change in the lower Whangarei Harbour; and
vi. determine the most suitable site and create a plan for beach nourishment within the lower harbour using dredge basin sediments.

1.3 Thesis Structure

Chapter 2 presents a review of past studies conducted within and surrounding the Whangarei Harbour and Marsden Point. The chapter aims to detail and describe previous work undertaken in the area, and the knowledge obtained from it. The chapter provides a base-level in terms of the current knowledge, it details previously identified trends in order to allow comparisons with those evaluated within this study,

Chapter 3 presents sediment textural properties surrounding Northport and the One Tree Point – Marsden Point coastline. Sediment textural patterns are detailed and comparisons drawn with previous investigations. Sediment transport directions are inferred from textural patterns obtained.

Chapter 4 details the medium – long term morphologic changes of the beaches from One Tree Point to Marsden Point. Shoreline advance and retreat rates are determined from aerial photograph interpretation. Limited inference of sediment transport directions is made based on the morphology of coastal features.

Chapter 5 examines beach profiles of the One Tree Point – Marsden Point region to determine closure depths, variations in beach sediment volume, infer longshore sediment transport rates and directions, and characteristic onshore-offshore sediment movement across the profile.

Chapter 6 investigates bathymetric changes of the lower Whangarei Harbour prior-to and post port development. Variations observed are compared with previous findings, and the influence of the port reclamation and dredging is assessed with respect to characteristic bathymetric changes surrounding Marsden Point. Limited inference of sediment transport directions and volumes is made.

Chapter 7 provides a summary of the morphodynamics of the lower Whangarei Harbour seabed. Sediment character, bedforms and transport pathways are described from the interpretation of a Side Scan Sonar (SSS) sonograph. A sediment facies map and sediment transport directions inferred from bedforms are compared with those of previous researchers.

Chapter 8 determines sediment transport vectors arising from tidally generated flows, wave generated flows and the combined action of tides and waves at the channels, channel margins, inter-tidal terraces, and beach faces of the lower Whangarei Harbour. Potential sediment transport vectors calculated are compared with previous researches conclusions and also the findings of other chapters within this thesis. A summary of potential sediment transport and sediment debits and credits is created for the lower Whangarei Harbour.

Chapter 9 integrates information obtained from previous chapters to identify the most appropriate site for artificial beach nourishment using sediments from Northport's dredge basin. A nourishment and monitoring plan is developed and costs are evaluated.

Chapter 10 provides a summary and conclusion to the study. The chapter draws on the preceding chapters to evaluate the morphologic state of the lower Whangarei Harbour and morphologic impacts of the Northport development. Recommendations for future research are made.

1.4 The Site

Whangarei Harbour is a 98 km^2 drowned river valley, located on the northeast coast of New Zealand's North Island (Figure 1.1). Bounded by Tertiary volcanics on the northern side and a Holocene, prograded, sandy barrier spit on the southern side forming Marsden Point (Healy, 1980; Millar, 1980; Black, 1983), the harbour entrance is located at the northern end of Bream Bay. The entrance is 730 m wide at its narrowest point and reaches a depth of 31m below chart datum. The harbour extends roughly 18 km from Marsden Point to the city of Whangarei.

Bream Bay and Marsden Point tides are meso-tidal, ranging from 2.2 m to 1.6 m for spring and neap tides respectively. The average tidal range is 1.9 m (Black and Healy, 1982; Black, 1983a; Barnett, 2002). Major hydrographic features include the four tidal inlet deltas, colloquially known as "*banks*". Snake and McDonald Banks (Figure 1.5) are morphodynamically flood-tidal deltas. Calliope and Mair Banks are ebb-tidal deltas formed outside the inlet gorge on either side of the main channel.

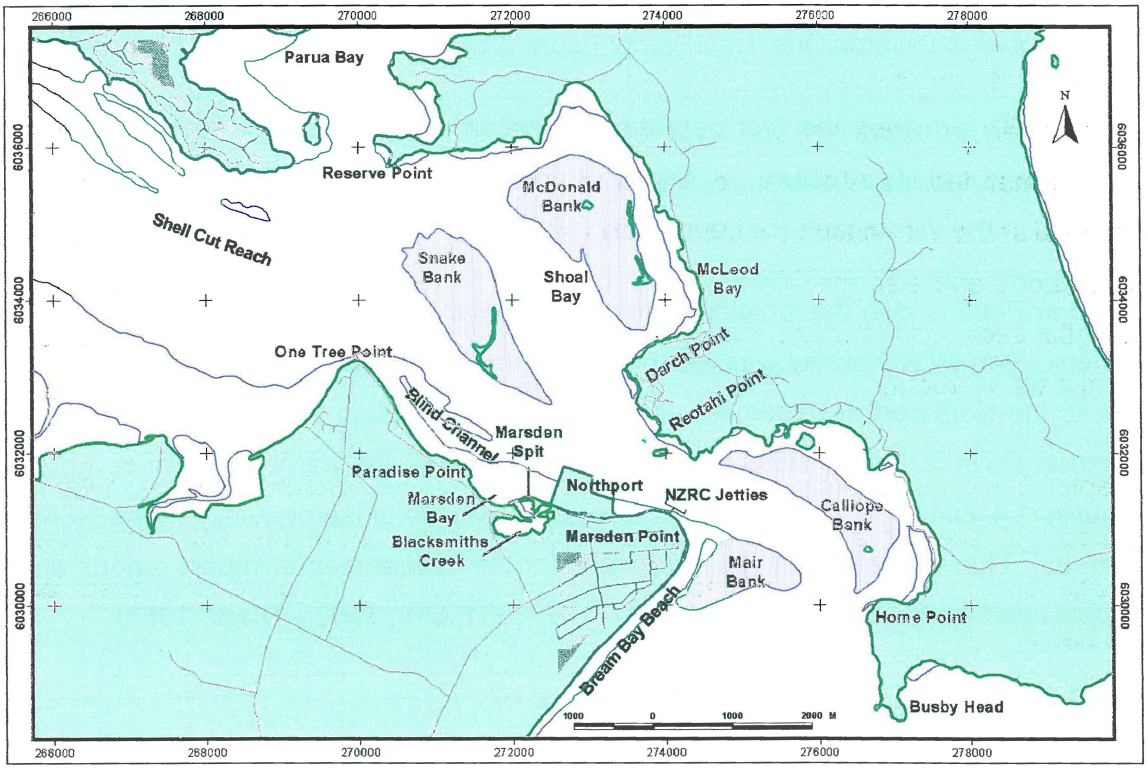


Figure 1.5 - Place names used throughout the study in the immediate environs of Marsden Point and Northport.

The Whangarei harbour is topographically a drowned river valley type estuary, with polygenetic origins. "*The course of the original river valley appears to have been controlled by the harbour fault and the entrance has been restricted by Holocene sand-spit and dune ridge formations*" (Millar, 1980).

Hume and Herdendorf (1988), focussing on the development of the Marsden Point barrier system, classified the harbour as a Pleistocene barrier enclosed estuary. The harbour owes its formation partly to tectonic activity, partly to its location on a drowned river valley and partly to the enclosing Marsden Point barrier spit system.

The orientation of the Marsden Point spit (extending in a roughly northerly direction) is consistent with similar spit developments at Mangawhai and Omaha to the south and Ocean Beach and Ngunguru to the north. The harbour is aligned along a fault that passes through the harbour entrance. The north-northwest trending fault is parallel with another that follows the Ruakaka River valley (Thompson, 1961; Markham, 1981).

Inside the harbour, the main shipping channel toward Whangarei runs not between the two flood-tidal deltas, but to the south of both along the channel named '*Shell Cut Reach*' (Figures 1.4 and 1.5). This channel has been dredged and cuts through a shallow region known as Shell Bank. Shell Bank separates the natural channel of the middle harbour from the lower harbour (Millar, 1980). A '*Blind Channel*', which separates from the main channel immediately to the west of the port site extends close to the shoreline towards One Tree Point (Figure 1.5) and is used for local boat access.

Millar (1980) provided the first detailed description of the harbours sediments, tidal currents and salinity structure. A history of dredging activities at Port Whangarei can be found in the Whangarei Harbour Study (1988).

Marsden Point is also the location of the New Zealand Refining Company (NZRC) oil refinery. The NZRC facility was established in the 1960's and is located immediately next to the Northport development. The NZRC wharf, built in 1963, extends out from Marsden Point and is located in the narrowest part of the harbour entrance gorge (Figures 1.4 and 1.5). The Northport development is in close proximity to the NZRC wharves. This is one specific point of focus for the environmental impact reports and models used for the design of Northport (NHB, 1981; DHI, 1982a; Black, 1983).

1.5 Summary

A forecast increase in timber export volumes led to the development of a timber export port at Marsden Point, Northland, New Zealand. The export port has been built on reclaimed inter-tidal terraces and incorporates a 32 ha dredge basin. The port represents significant development in the coastal zone. This thesis identifies distinguishing features and qualities of the Marsden Point physical environment that have the capability to impact on the port and on the potential use of dredge basin sediments as artificial beach fill.

2 REVIEW OF HARBOUR STUDIES

2.1 Introduction

A summary of past studies conducted in and around the Whangarei Harbour and Marsden Point is relevant in that it provides a level of knowledge on which to base comparisons with the present study. The aim of the chapter is not to provide detailed specifics of each and every study conducted in the region, but rather to summarise, draw comparisons and identify the main differences between them.

2.2 Geological Background

The general geology of the region has been identified and described by Ferrar (1925, 1934), updated by Thompson (1961) and Markham (1981), and is well summarised in Millar (1980). Figure 2.1 provides a summary of the geology of the Whangarei Harbour and Marsden Point.

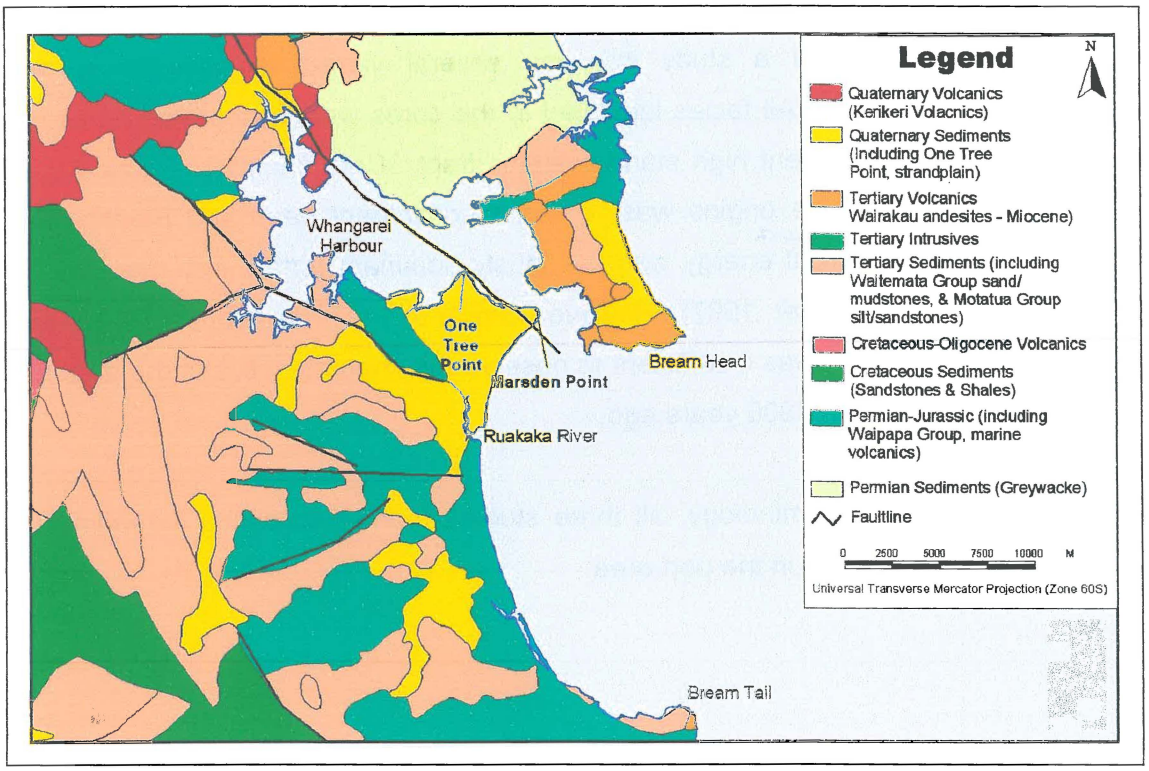


Figure 2.1 - *Geology of the Whangarei Harbour and Marsden Point region, based on Thompson (1961), Millar (1980), Markham (1981) and Nichol (1997).*

2.2.1 Sub-Surface Investigations - Marsden Point barrier system

Blacksmiths Creek and One Tree Point have been the sites of recent sub surface studies of geologic character. Healy (1980) reported on borehole investigations in the area from 1960, 1965 and 1969 by the Delft Soil Mechanics Laboratory, Brickell-Moss & Partners and Tonkin & Taylor respectively. Dredging in the port area (to 13 m CD) was expected to encounter non-cohesive fine to medium sized sands (Healy, 1980). It appears that this fine-to-medium sand layer extends to greater depths below the surface at the port site than at Marsden Bay.

Beca Carter Hollings and Ferner Ltd (BCHF, 1992), using nine boreholes of up to 36 m below Chart Datum (CD), conducted a more rigorous investigation of subsurface geology. The Beca Carter (BCHF, 1992) study provided information on subsurface conditions for the construction of port foundations. Boreholes adjacent to Marsden Bay (of interest to this study for it's proximity to the port and nearby beaches, Figure 1.5) revealed a surface layer with a thickness ranging from 4.8 m to 12.5 m, with a mean width of 9.0 m, concurring with Healy's (1980) earlier investigations at the port area. The layer was described as '*Light greyish, green-grey, fine and medium sand with trace silt and shelly layers*' (BCHF, 1992).

Glover (1997) conducted a study involving several vibra-core samples in the Blacksmiths Creek area. All facies identified in the cores were interpreted as being deposited during the present high stand systems tract. Core samples revealed that sand derived from marine origins was "*a major constituent deep into Blacksmiths Creek*", indicating that tidal energy was previously dominant further into the estuary than the present day (Glover, 1997). However, Glover's (1997) distribution of a limited number (5) of vibracores was insufficient to observe the characteristics of the area for time periods greater than 7000 years ago.

Despite differences in terminology, all three studies found fine sands extending to depths of ~20 m below CD in the port area.

2.2.2 Morphologic Features

Tertiary volcanics provide the base for the northern side of the harbour, whilst the coastal barrier on the southern side is made up of Quaternary sediments (Figure 2.1). The primary source of sediment for barrier construction has been near-shore and inner shelf deposits on the floor of Bream Bay (Schofield, 1970; Nichol, 2002).

Dune ridges and intervening swales, oriented in a general north-south direction and elevated roughly 10m above sea level, form the Pleistocene strand-plain around One Tree Point (WHSWC, 1988; Nichol, 1997). These dune sediments overlay sandy beach and near-shore deposits. Cliff outcrops at One Tree Point show cross-sections through many of these ridges, revealing their sedimentary structure and stratigraphy. This morphology of dune sediments overlying beach sands is characteristic evidence for a history of shoreline advance, caused by either a large sediment input or a fall in relative sea level. These relic coastal deposits were investigated using ground-penetrating radar (GPR) (Nichol, 1997; Nichol, 2002).

Focussing on the subsurface geology of One Tree Point and Blacksmiths Creek, Nichol (1997) concluded that the underlying geology in this area (to 12 m depth) is made up of seaward dipping beach sands underlying massive quartzose sands, interpreted as foredune deposits (Nichol, 1997). The One Tree Point strandplain was deposited during the last interglacial period and formed during an initial stage of relative sea level stability, then a subsequent fall in relative sea level (Nichol, 1997). The age of the strandplain was verified by thermoluminescence (TL) dating of samples from a One Tree Point cliff section. TL ages ranged from 85 $\pm$ 8 to 115 $\pm$ 19 ka Before Present (BP), thus indicating deposition during the last interglacial period (δO^{18} isotope sub-stage 5e to 5a) (Nichol, 2002), assuming no tectonic activity in the region. This assumption may not be entirely valid however, as evidence of nearby Holocene uplift at Pakiri for example does exist (pers. comm. T.R. Healy, 2003).

Using the orientation of the dune ridges, along with the assumption that the modern wave regime operating in Bream Bay also prevailed in the last interglacial, Nichol (2002) inferred that the swash aligned form among all ridges in the One Tree Point system was strong evidence for a dominantly shore normal sediment transport regime.

2.3 The seabed and its Sediments

2.3.1 General

Schofield (1970) provides a classical summary of the origins, textural and mineralogical properties of the coastal sands for the Northland area. The beach and dune sands of Bream Bay are identified as belonging to the Hauraki (B) facies, a derivative of the Hauraki (A) facies that covers much of the Hauraki Gulf (Schofield, 1970). Hauraki (A) sediments originate from the Waikato River when it flowed into the Hauraki Gulf and are derived from the central North Island volcanic plateau. Deposition occurred in an embayment near Great Barrier Island during glacial times when sea level was 120 m lower than present. Following deposition, these sediments were swept onshore with the postglacial rising sea level to create the Holocene dune deposits.

2.3.2 Sediment Inputs

Significant sediment discharge into the harbour's catchments and tributaries has occurred since the initiation of pastoral, forestry, urban and industrial development in the late 1800's and early 1900's (WHSWC, 1980), although the actual amounts are unknown. Both Millar (1980) and the Whangarei Harbour Study (WHSWC, 1988) provide summaries of historical sediment inputs to the harbour. Direct inputs have occurred in the upper harbour, as a result of dredge spoil dumping and cement washings. The largest direct input has been reject washings from Wilsons (NZ) Portland Cement Company, peaking at 250,000 tonnes in 1967 and averaging 106,000 tonnes from 1967 to 1981 (WHSWC, 1988). This was up to 20 times the natural sediment input in this part of the upper harbour (Millar, 1980).

2.3.3 Harbour Sediments

Both physical and textural sediment characteristics, based upon remote grab sampling and sieving, were determined by Millar (1980) at 75 sites within the harbour. Plots and maps of grain size distributions, sorting and skewness were presented. The channels of the lower harbour were typically armoured by gravel, remaining areas were found to be made up of *'pure sands'* and the upper harbour consisted of more silty and muddy sediments. Subsequently Black et al. (1981), investigating the sediment textural patterns in the lower harbour near Marsden Point, went farther to describe bedforms on the harbour bottom also.

From analysis of the distribution of sediments and from examination of Feldspar/Quartz ratios determined by X-ray diffraction, Millar (1980) interpreted the origins of sediments within the harbour. The sand sediments inside the lower harbour were essentially identical to those found on Bream Bay Beach. Mineralogical and textural parameters of the sands of the lower harbour indicated they were derived from Bream Bay (outside the Harbour) (Millar, 1980). Healy (1980) made use of the sedimentary data collected by Millar (1980), noting that due to the marine origin of the sands at the port site there must be a considerable net in-flow of sediment into the harbour in the long term.

The sediment grain size distribution led to conclusions that '*saltation is the most dominant method of transport in the lower harbour, while the movement of particles in suspension becomes a feature farther up harbour*' (Millar, 1980).

Lower harbour sediments have been classified into one of two facies by Millar (1980):

Facies one - mainly fine sands with a low skeletal carbonate content .

Facies two - coarser sands, minor fine gravels and a high skeletal carbonate content, possibly a "*lag*" deposit (subsequently confirmed by Black (1983)).

Facies two is found in the lower harbour channels whilst facies one is found in other areas of the lower harbour (Millar, 1980). Both are derived from Schofield's (1970) Hauraki (B) sediments, local biogenic shell and terrigenous gravels.

Black et al. (1981) went farther, separating the lower harbour sediments into five facies types based on both underwater photography and diver observations:

1) Predominant coarse shelly gravel lag cover.
   Found mainly in the channels.
2) 50% Cover of gravel and sand.
   Principally found as channel side and bank facies.
3) Dune bedforms.
   Located in the channel off One Tree Point and on the western side of the entrance opposite Busby Head.
4) Sandy rippled bottom.
   Found on the southern side of Mair Bank in 3.5-5 m depth, in the channel between Mair Bank and Marsden Point and in the zone between Snake Bank and McDonald Banks.
5) Flat, featureless fine sand bed.
   Found in the '*quieter bottom water conditions*'.

Black et al. (1981)

The Danish Hydraulic Institute (DHI) (1982a) did not distinguish between sand dunes and ripples, categorising the following as areas of '*ripples*':

i. North and east of One Tree Point
ii. Between One Tree Point and Marsden Point
iii. North of the Northland Harbour Board (NHB) wharf
iv. West of Darch Point. DHI (1982a)

Black et al. (1981) inferred sediment transport patterns from their observations. The most active transport zones were deemed to be the areas of dune bed-forms, followed by the rippled areas.

In his sedimentary analyses Black (1983) retained the skeletal carbonate components, contrasting to Millar's (1980) approach where they were dissolved. Black's (1983) approach was based on the effect of the shells on sediment transport in the channels, thus they were retained.

Shelly lag sediments occurring in the channels of the lower harbour are identified by Millar (1980), Black et al. (1981) and Black (1983). The effect of this lag acting as an armour layer, protecting the underlying sands from movement, is recognised also by the DHI (1982a), Black (1983) and Venus (1984).

Loosely packed sediments on the harbour beach between the NZRC wharf and the then NHB wharf (Northport site) indicate considerable sediment mobility in this area (Black, 1983).

2.4 Bathymetry

2.4.1 General

Rogers (1959) undertook one of the first studies of the harbour's physical characteristics in 1959 for the Whangarei Harbour Board. This study, based on a physical scale model of the harbour, was initiated to investigate plans for reducing and eliminating shoaling in the channel that was to be dredged through Shell Bank, west of One Tree Point. Whilst the model dealt with both tides and waves, it provided only general observations with few specific details and little data. Observations for model construction revealed that up to 1.2 m of sand had built up in the channels near Shell Bank between 1939 and 1955 (Rogers, 1959 in Millar, 1980). Both Millar (1980) and Black (1983) note that between the dredging of this area in the 1960's and their studies in the 1980's, the bathymetry remained stable, with no maintenance dredging required.

2.4.2 Dredging and Reclamation

A summary of dredging activities in the upper and middle harbour can be found in the Whangarei Harbour Study (WHSWC, 1988). Dredge tailing dumping grounds have included dredge ponds at Port Whangarei, areas in Bream Bay and occasionally unbunded sand banks adjacent the main channel within the harbour (WHSWC, 1988).

The tidal prism of the Whangarei Harbour was reduced by ~5% between 1939 and 1961 due to reclamations (Millar, 1980). Millar (1980) estimated that this value could have been doubled by 1980 as a result of an input of sediment from the Portland Cement Company washings between 1961 and 1980.

2.4.3 Bathymetric Change

Comparison of hydrographic surveys from 1849, 1939 and 1961 showed almost no changes in harbour features over these periods (Millar, 1980). Between Marsden Point and One Tree Point in the lower harbour, net erosion was experienced from 1961 to 1981 (Black, 1983). Healy (1980) had previously drawn the same conclusion for the period between 1974 and 1978. This indicates there is some evidence for a change in harbour processes around 1961.

Erosion of some 100,000 m^3 of material from the inlet entrance between 1974 and 1978 was documented by Healy (1980) using soundings provided by the NZRC. Erosion was located in areas adjacent the NZRC wharf and resulted in a lowering of the channel floor by 4 meters. This was consistent with a large-scale sediment flux through the entrance to the harbour (Healy, 1980). The bathymetry inside Marsden Point however, was found to be relatively stable (Healy, 1980; DHI, 1982a; Black, 1983).

Entrance cross-sections from 1959, 1974, 1978 and soundings from 1981 showed great stability of the entrance throat (Black and Healy, 1982; Black, 1983; Black et al., 1989). The only changes greater than the accuracy of the methods used were at Shell Cut Reach where the NHB had conducted dredging operations (WHSWC, 1988). The DHI (1982a) also report on the stability of the harbour over the period of 1959 to 1981, with the exception of the southern side of Mair Bank. The lower harbour, below One Tree Point is referred to as being *'close to equilibrium'* (DHI, 1982a). This conclusion contrasts slightly with both Healy's (1980) and Black's (1983) observations of net erosion in the lower harbour over this time period, despite the stability at the entrance throat.

Sediment accumulated on the southern and western sides of the ebb tidal delta of Mair Bank (Figure 1.5) between 1950 and 1981 (DHI, 1982a; Black and Healy, 1982; Black, 1983; Venus, 1984). Black and Healy (1982) suggests that the likely source of this sediment was the eroding Bream Bay Beach and lower harbour, agreeing with Healy's (1980) observations of erosion during this period from near the NZRC wharf. Marine charts from 1964 and 1974 analysed for differences in shoreline position were not conclusive due to the inherent errors of the charts and methods (Healy, 1980). Details of these changes are expanded upon in chapter 6.

More recently Barnett et al. (1993) compared bathymetries from digitised 1981 Royal New Zealand Navy (RNZN) hydrographic charts along with data surveyed in 1992 (based on his model grids 50 m spacing). No capital dredging occurred in the harbour over this period (Barnett et al. 1993). Significant changes found included a migration of the main channel, specifically in ~ 5 m depths, just down harbour from the flood tidal delta of Snake Bank and also at the entrance to the Blind Channel. The remainder of the lower harbour was relatively stable (Barnett et al., 1993).

2.5 Sediment Transport

2.5.1 Harbour Entrance and Channels

Rogers' (1959) physical model study was the first that observed sediment transport and changes in harbour morphology. Whilst some conclusions were based on field observations, the majority were from his physical scale model. Conclusions of note included:

i. On the flood tide material was transported into the harbour mainly in suspension;
ii. ebb flows generated a dominance of bed load movement; and
iii. material entering the harbour on the flood tide was transported along Bream Bay beach by a northward moving littoral drift.

(Rogers, 1959 in Millar, 1980)

During echo soundings for Rogers' (1959) model, it was reported that divers observed dunes on the sea bed with heights up to 1.2 m (Millar, 1980) in the region around Shell Cut Reach, although the specific location and orientation were not specified as the model was demolished after these tests.

Millar (1980) supported Rogers' (1959) conclusions regarding the transport of material into the harbour in suspension:

> *'Net movement of sand into the harbour most likely occurs during easterly storms when waves outside the entrance can suspend large amounts of sand. Once deposited within the harbour, tidal currents alone are unlikely to be able to return this sediment' (Millar, 1980).*

2.5.2 Modes of Sediment Transport

Dominant modes of sediment transport are suspension in the upper harbour and bedload in the lower harbour (Millar, 1980; DHI, 1982a, Black 1983). These conclusions were based upon observations of an up harbour decrease in mean sediment size, sorting and the variation of sediment sources.

Black et al. (1982) note that net bedload sediment transport is related to ebb and flood tidal dominance. Net bedload transport is directed out of the harbour in the channels (Black and Healy, 1982).

2.5.3 Volume of Sediment Movement

Suspended sediment concentrations were measured and found to be very low (<10 mgL^{-1}) (DHI, 1982a). Black (1983), using sediment traps and diver observations to measure the bed load transport in the lower harbour also found the quantities of sediment moving to be "*quite small*", which is consistent with the bathymetric stability mentioned above. Higher mean suspended sediment values of 29 mgL^{-1} on ebb flows and 32 mgL^{-1} on flood flows, recorded over eight stations have been reported by Poynter (1993).

The DHI (1982a) found no significant correlation between suspended sediment concentration and flow velocity or distance from the bed. Black and Healy (1982) reported that the suspended sediment transport rate varied with the $7\text{-}8^{th}$ power of the flow speed at 1 m above the bed (correlation 0.94). Several authors have noted that in the lower harbour there is no consistent relationship between suspended sediment concentrations and rainfall in the catchment (Millar, 1980; Poynter, 1993).

The observed sediment transport through the lower harbour is much less than is expected from the water velocites alone (Black, 1983). This is due to the armouring effect of the shell lag on the channel floors and is another contributor to Healy's (1980) observations of the morphologic stability of the region.

Encrusting sponges and erect algae were observed on some of the shell lag material in the channels by Black et al. (1981). The existence of these organisms on the shell lag is interpreted as an indicator that sediment transport magnitudes in these areas are very low, as the sponges and algae cannot withstand high sediment transport loads (Black, 1983). The absence of these algae on the shell lag at the harbour entrance indicates possible movement of sediment over the lag, or movement of the lag itself (Black et al., 1989).

Observations by divers indicated that the threshold of movement for the shell lag is greater than a velocity of 0.9 ms^{-1} at 1 m above the bed. During spring tide observations by Black et al. (1983), currents exceeded this 'shell' threshold.

2.5.4 Sediment Pathways

Regions of active sediment movement have been identified:

1) from Snake Bank towards the NZRC jetty;
2) on the south side of the shipping channel between One Tree Point and Marsden Bay;
3) on the north side of Snake Bank;
4) off Reotahi Bay;
5) off Marsden Point;
6) north of Mair Bank;
7) near Busby Head; and
8) between Marsden Point and Mair Bank.

sources 1.Black et al. (1981), 2-7 Black and Healy (1983), 8 (Black (1983)

Black and Healy (1982) proposed a model of sediment dynamics in the region, in which sediment entering the harbour is deposited on the northeast side of a sub-tidal extension of the flood tidal delta of Snake Bank. On the southwest side of the extension there is a net down harbour movement of sediment. This pattern was expanded by Black (1983) and Black et al. (1989), with the addition of sediment loops based on tidal cycle residuals (Figure 2.2).

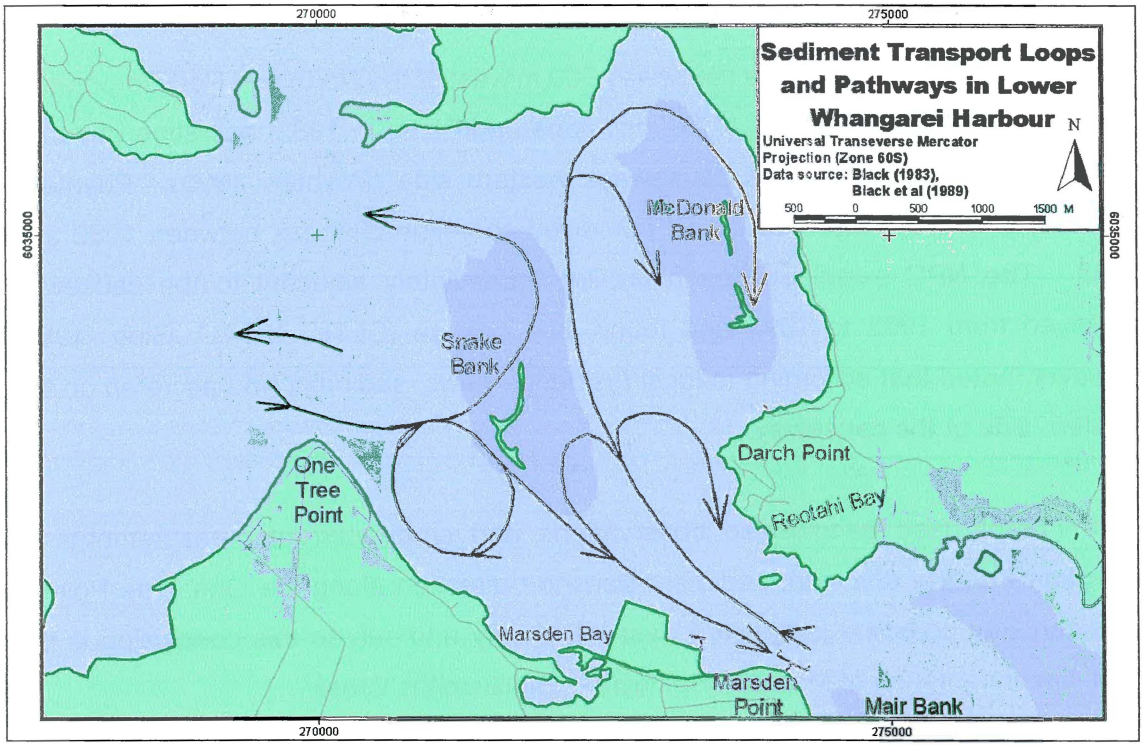


Figure 2.2 - *Schematic diagram showing sediment transport loops and pathways revealed by residual velocities from Black's (1983) 2-dimensional model along with field observations and measurements. (after Black (1983) and Black et al. (1989).*

The harbour's flood and ebb tidal deltas (Snake, McDonald, Mair and Calliope Banks) act as storage reservoirs, containing much of the unconsolidated sand in the harbour (Venus, 1984). Due to low water velocities on their crests the deltas are mostly stable (Black, 1983), (see Mair Bank below). They are however, flanked by narrow distended regions of sediment transport activity along the channel margins, where most bedload sediment transport is occurring (DHI, 1982; Black, 1983; Black and Healy, 1983; Venus, 1984).

Mair Bank has been identified as something of a special case, due to both its proximity to Bream Bay Beach and Marsden Point, and associated littoral currents. Black (1983) observed '*significant quantities*' of sand moving between Mair Bank and Marsden Point. Both the littoral drift and the tidal sediment transport are directed into the harbour at this location (Tonkin and Taylor, 1979a; Black and Healy, 1982; Black, 1983). Changes to the sediment transport loop centred on Mair Bank could have implications to the Marsden Point and the Bream Bay Beach shorelines.

Sediment transport over a mega-rippled bed at Whangarei Harbour was investigated by Black and Healy (1982). Observations of both mega-ripple advance and individual grain transport were taken. The sediment bed-load transport rate was estimated (and verified) by breaking the bed friction into two components, one due to form drag and the other due to skin friction. The concept is taken further in Black et al. (1989).

2.5.5 The Marsden Bay – One Tree Point Region

Following the construction of a causeway 300 m west of the Northland Port Corporation (NPC) wharf (now the middle of the developed port site) in 1983, accretion of sandy sediments was noted on the causeways western side (Poynter, 1993). Poynter's (1993) observations were based on perceived shoreline changes between 1983 and 1993. The NPC examined beach profiles immediately adjacent to the causeway surveyed from 1992 to 1994 and found little change (CFTE, 1994). Gibb (1998) however, noted that according to local resident's views, sediment had accreted on the western side of the causeway.

Gibb (1998) used geomorphic observations and crude current measurements to conclude that the dominant sediment transport direction along the One Tree Point – Marsden Bay coastline is directed east. The only anomaly to this conclusion is the east-west orientation of Marsden Spit across Blacksmiths Creek.

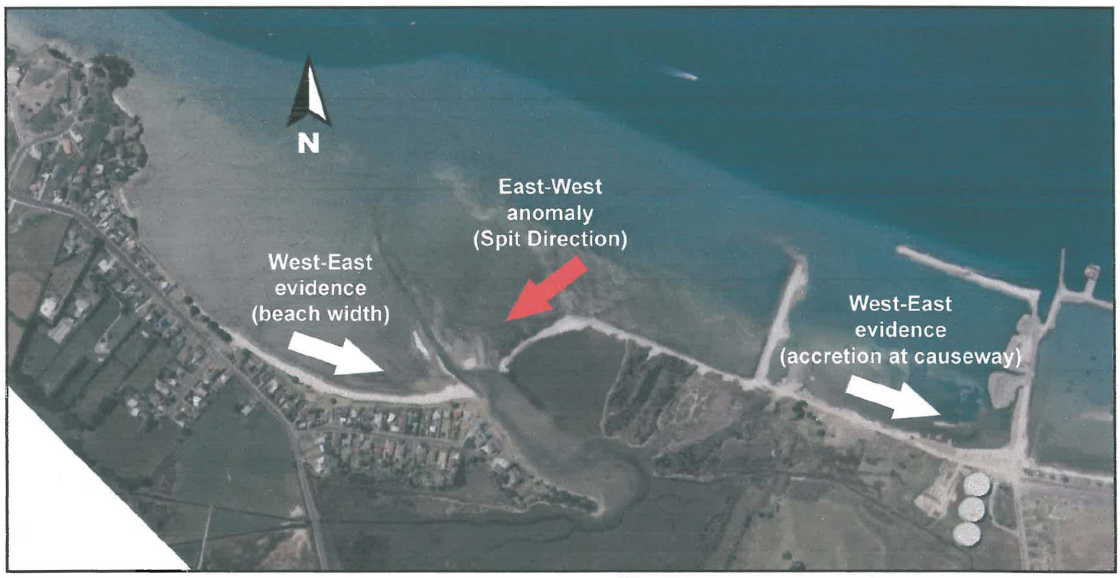


Figure 2.3 - *Vertical air photograph (5/1/2001) showing geomporphic evidence of easterly directed net sediment transport. The contradicting direction of Marsden Spit has been used as evidence that the spit is not formed by longshore drift (Gibb, 1998).*

Marsden Spit is likely the result of onshore migration of sand bars and not a free-form spit formed by longshore drift (Gibb, 1998). Current velocities were deemed incapable of entraining sediment without the assistance of wave action (Gibb, 1998), highlighting the importance of wave-generated currents in the transport of sediment over the inter-tidal zone.

2.5.6 The Bream Bay Beach Region

A severe erosive episode, occurring during the July 1978 storm, at Bream Bay Beach endangered the New Zealand Electricity Corporation (NZEC) facility and prompted various reports focussing on sediment e.g. Tonkin and Taylor (1979a,b,c, 1980, 1981). Various techniques were employed to estimate the sediment transport, including wave hindcasting, grain size analysis and daily observations.

Wave hindcasting using wind data from the Mokohinau Islands resulted in a littoral drift calculation that was predominantly northward with short periods of southward reversals. The net movement northward was deemed to be 140,000 m^3yr^{-1} (Tonkin and Taylor, 1979a). The limitations of this technique were outlined however and a warning that the estimates could '*be off by as much as a factor of three (3)*'.

Gibb (1979) (in Tonkin and Taylor, 1981) estimates a northward drift of less than 100,000 m^3yr^{-1}. Estimations made using the Coastal Engineering Research Center (CERC) - Longuet-Higgins (energy flux) method along with the 'Bijker' method gave transport rates between 45,000 m^3yr^{-1} to the south and 19,000 m^3yr^{-1} to the north between 1978 and 1980 (Tonkin and Taylor, 1981). The direction of littoral drift was calculated to be predominantly northerly in the north and southerly elsewhere (Tonkin and Taylor, 1979c) roughly agreeing with directions obtained from the hindcasting (Tonkin and Taylor, 1979a).

Black (1983) criticises the Tonkin and Taylor (1981) report for its assumptions when developing wave refraction patterns used in the determination of longshore transport rates. Tonkin and Taylor (1981) assume that a southeasterly swell will not impact the area due to protection by Great Barrier Island. Black (1983) however, showed that east to southeast waves can indeed impact on Mair Bank and it's environs.

The DHI (1982a) compiled a sediment budget for the region (Figure 2.4) basing values on beach profiles and air photos. Overall movement was calculated to be in the order of 150,000 m^3yr^{-1}, with 30,000 m^3yr^{-1} being removed from Bream Bay Beach resulting in the observed erosion at the NZEC site (DHI, 1982a).

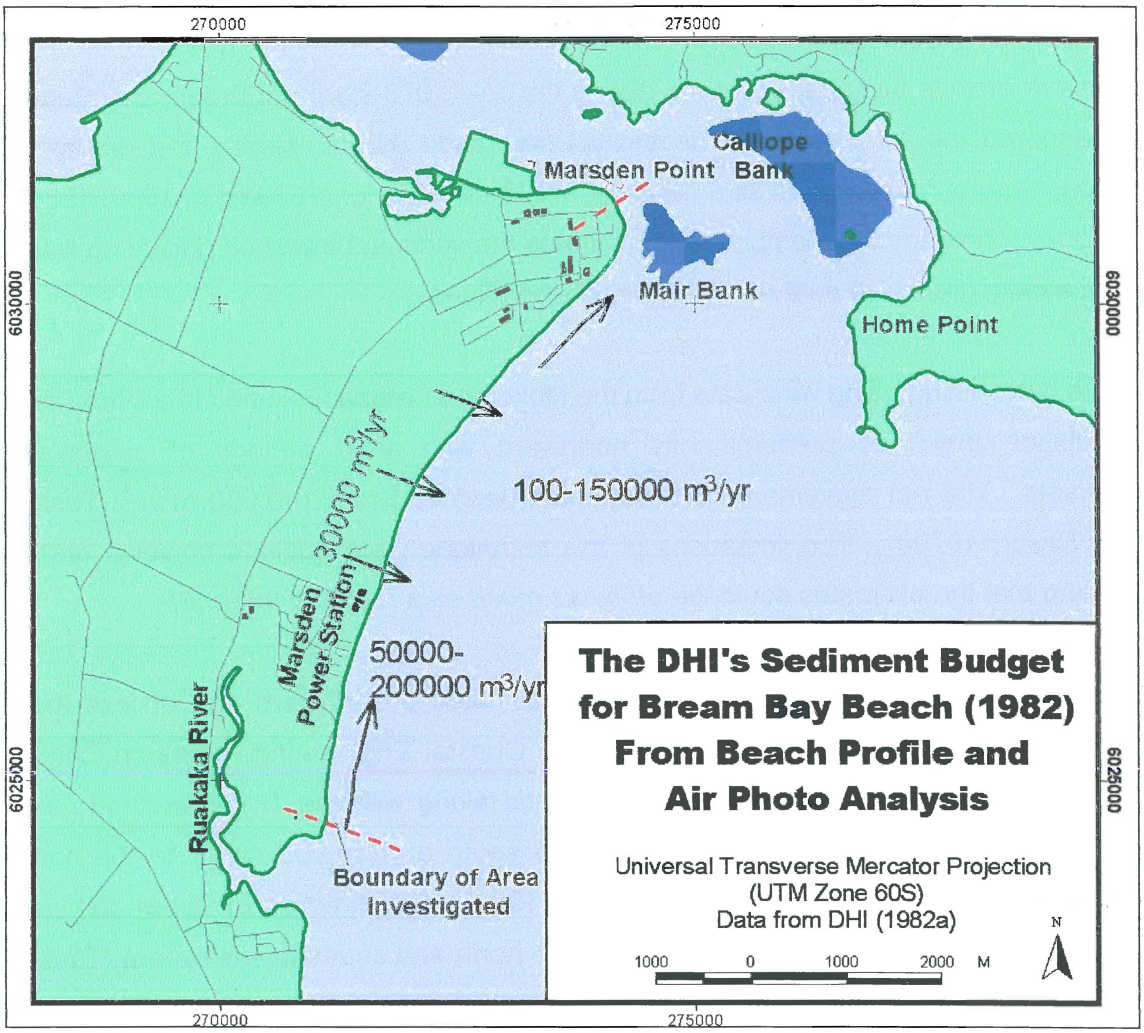


Figure 2.4 - *Sediment Budget of Bream Bay Beach in 1982, from data interpreted by the DHI (1982), including Beach Profiles and Air Photographs.*

While the estimates of the sediment transport along Bream Bay beach vary between 19,000 m^3yr^{-1} and 150,000 m^3yr^{-1}, the dominant littoral drift and net transport is recognised as being consistently northerly in direction.

2.6 Hydraulics and Hydrodynamics

2.6.1 General Characteristics

In terms of salinity structure, the lower harbour is well mixed and lacks major salinity or density stratification (Millar, 1980; Venus, 1984). Summer maximum temperatures are 24-25° C, whilst winter minimums are 13-14.5° C (Millar, 1980).

The tide at Whangarei Harbour is dominated by the principal lunar semi-diurnal (M2) tide with additional significant influence from the N2, S2 and K1 constituents (Barnett, 1995b; Barnett, 2002; Longdill et al. 2003b). The mean sea level at Marsden Point has demonstrated an increasing trend during the late 1990's of 6 mmy^{-1} (Barnett, 2002).

Flushing times of the harbour have been estimated to lie between 2.2 tidal cycles (using the tidal prism method) to 120 days (using fraction of freshwater method [summer]) (Millar, 1980). Venus (1984) reports a flushing time for the lower harbour segment only of 1.1 tidal cycles.

2.6.2 Waves

A wave buoy deployed off Mangawhai showed a variable wave climate for the region, with mean wave heights for the winters of 1995 and 1996 varying by 0.24 m (Barnett, 2002). Storm waves in Bream Bay have exceeded 5 m (Barnett, 2002), however the effects of these waves on northern Bream Bay, Marsden Point and within Whangarei Harbour is reduced due to the sheltering effect provided by the Whangarei Heads (Tonkin and Taylor, 1981; DHI, 1982; Black, 1983).

Using a capacitance type wave gauge, Black (1983) measured the wave climate at the port site, where over a six-week period the maximum significant wave height recorded was 0.36 m.

The only other wave data available for the lower Whangarei harbour consists of a wind-wave climate assessed by 'hindcasting' from wind data, and a swell wave climate assessed from offshore ship wave observations (BCHF, 1999). The Beca Carter (BCHF, 1999) report mentioned *"No site-specific wave data was available for this study"*, failing to recognise Black's (1983) data. The hindcasting method was therefore used along with ships observations. Beca Carter (BCHF, 1999) calculated wind waves with significant wave heights of around 1 m and periods of 3 s, occurring with a 10-year return period. Swell waves impacting on the Northport site with a 10-year return period had a significant wave height of 0.5 m and periods of 8-12 s (BCHF, 1999).

2.6.3 Currents Near the Harbour Entrance

Channel drogue tracking (Bioresearches, 1976; Black et al. 1982; Black, 1983; Barnett, 1995a; Longdill et al., 2003) has provided a significant quantity of information on water currents surrounding Marsden Point. Findings have included:

i. Convergence of different channel systems at Marsden Point leads to a considerable variation in the potential path taken by a drogue.
ii. Ebb currents dominate the main channel outside the entrance.
iii. Flood currents dominate the smaller distributaries outside the entrance (behind Calliope and Mair Banks).
iv. Ebb currents dominate the main channel inside the entrance.
v. Water moves at an angle to the sub-tidal extension of Snake Bank.
vi. Eddies occur behind Darch and Home Points on ebb flows.

Black's (1983) drogue tracking results from the Mair Bank - Home Point region of the harbour show faster ebb currents compared with flood flows, contrasting with Bioresearches (1976) who found stronger flood flows in these areas. The DHI (1982a) also reported on the drogue tracking conducted by Black et al. (1982). Variation in drogue tracking results between researchers highlights the inherent variability in this method of current measurement. Both wind effects and drogue design can influence movement. The method is nonetheless valuable in that it provides a *'real world'* indicator of water movement in a *'Lagrangian'* sense rather than fixed position *'Eulerian'* electronic measurement, in that the drogue follows the movement of the water through space.

Water current velocities have also been measured using Aanderra, Braystoke and in more recent years Acoustic Doppler Current Profiler (ADCP) current meters (DHI, 1982a; Black, 1983; Barnett, 1995a; Longdill et al., 2003). Ebb tide velocity curves are typically steeper and of shorter duration than flood curves, concurring with Miller's (1980) analysis of the Marsden Point tidal curve which found half-tidal periods of 6 hours 5 minutes for the ebb and 6 hours 20 minutes for the flood. Peak velocities occur nearer the time of high tide on both ebb and flood flows (Black, 1983).

Ebb flows continue past the time of low water and into the flooding stage (Black, 1983). Flooding oceanic water moves up harbour around the edge of the ebb jet via the marginal channel (between Mair Bank and Marsden Point / Ocean Beach), then along the southern shoreline of the harbour (Black, 1983).

The DHI (1982a) noted the regularity of the channel's currents, in both speed and direction;

> "*It appears that neither wind, waves nor storms have any significant effects on the currents in the main channels. Neither can the effect of any local freshwater runoff be observed*" (DHI, 1982a).

Snake Bank, morphologically a flood tidal delta has been shown to have zones of ebb dominant currents (Black et al., 1989). Snake Bank is now identified as a *'flood tidal delta relative to the entrance throat'*, while the up harbour end is termed *'partly an ebb shield and partly an ebb tidal delta relative to the constricted cross section of the harbour adjacent One Tree Point'* (Black et al., 1989). A shell ridge separates the two different hydrodynamic environments. The 'S' shape (giving Snake Bank its name) of the shell ridge is created by the opposing tidal residuals (Black et al., 1989).

Currents over the inter-tidal zone in the One Tree Point / Marsden Bay area have been crudely measured by Gibb (1998) using water filled plastic bottles. Gibb (1998) found an easterly moving current on both ebb and flood tides. Velocities were faster during ebb tides (0.05 - 0.33ms^{-1}) than for flood tides (0 - 0.03ms^{-1}) (Gibb, 1998). Although qualified by the statement *"as there was negligible wind and wave action during measurements the longshore current velocities are mostly tide generated"* the only data provided on wind and waves during the measurements are *"variable"* and *"calm"* respectively. The expected significant influence of winds on floating plastic bottles (due to above surface windage) and the lack of supporting wind data should be kept in mind if considering this data.

2.7 Wind Conditions

Wind conditions at Marsden Point, between January 1, 1983 and December 31st, 1987, have been summarised by the National Institute of Water and Atmospheric Research (NIWA), (NIWA, 1988). Wind recordings were made during *'all hours'* by a Munro anemometer situated atop a standard 10 m mast at a site with grid reference NZMS 260, 1:50,000 Q07 453949. The site is coastal and well exposed. Wind data recorded is shown in Figure 2.5 and contained in Appendix F.

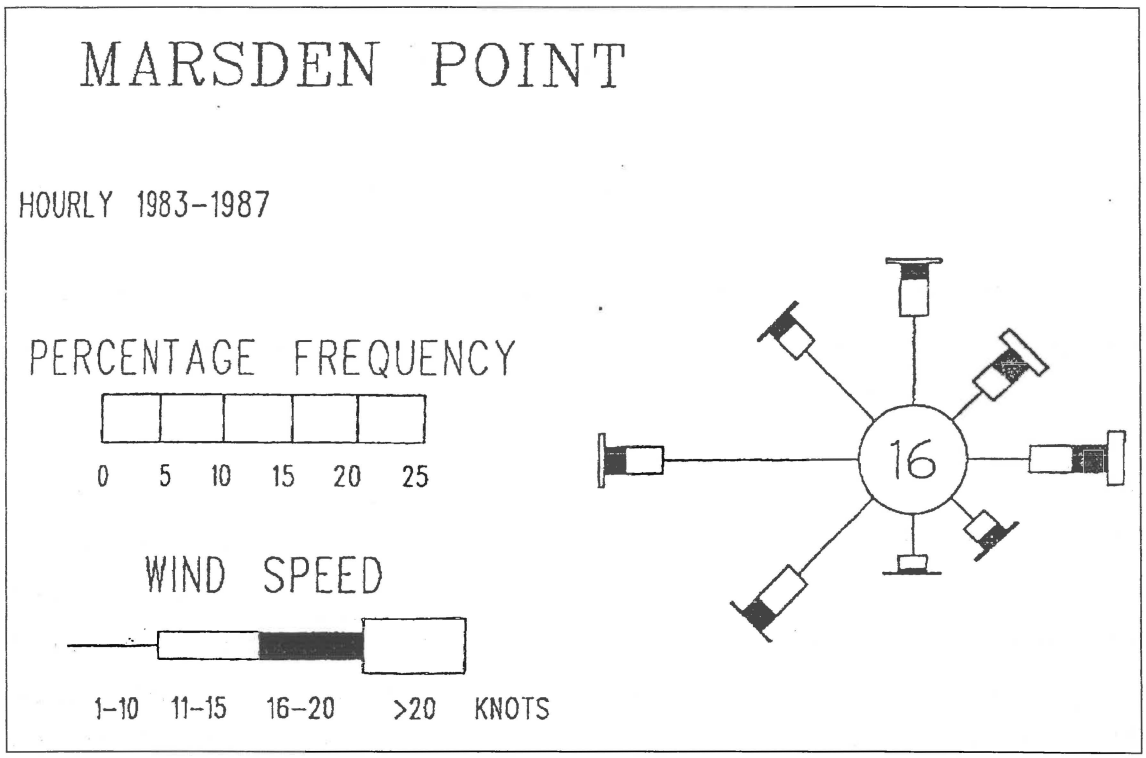


Figure 2.5 – *Wind rose from Marsden Point. Data recorded over all hours between January 1st, 1983 and December 31st, 1987. NIWA (1988).*

Analysis of the wind summary (Figure 2.5) shows that winds were most frequent from the west (prevailing 20% of the time), with southwesterlies second most frequent (prevailing 13% of the time). Calm to slight variable conditions occurred 16 percent of the time. Light winds (mean speeds in the range 1 to 10 knots [0.5 to 5 ms^{-1}]) prevailed 51% of the time. Strong winds (mean speeds at least 21 knots (10.9 ms^{-1}) occurred 3% of the time, being most frequent from the east.

2.8 Shoreline Change

2.8.1 Bream Bay Beach

Observations and measurements of landscape change have taken place in the area surrounding Marsden Point to quantify observed erosion patterns. New Zealand Electricity instigated measurements following a severe erosive episode adjacent to their plant at Bream Bay Beach in a storm of 17-19 July 1978. Similar storms in May and June of 1978 acted to initially deplete the *'reserve'* of sediment in the dunes, whilst the July storm following in quick succession acted on an already depleted beach, hence having a severe erosive effect. A summary of the storm of July 1978 is included in a New Zealand Meteorological Service report in Tonkin and Taylor (1979b).

Tonkin and Taylor provided a series of reports to the NZEC on coastal erosion, wave studies and foreshore protection at Bream Bay beach, Ruakaka (Tonkin and Taylor, 1979a, 1979b, 1979c, 1980, 1981). It is recognised in the reports that the NZEC power stations were located too close to the foredune to allow an adequate buffer for possible depletion of the foredune by storm episodes (Tonkin and Taylor, 1979a).

Between 1914 and 1962, Bream Bay Beach adjacent to the Marsden Power stations prograded (Tonkin and Taylor, 1979a; DHI, 1982a). This trend changed to retreat from 1962 to 1979, with rates of 0.7 - 1.4 myr^{-1} (DHI, 1982a). Corresponding accretion took place in the deeper areas of Mair Bank over the same time period as this erosion (Tonkin and Taylor, 1979a, 1979c; Black and Healy, 1982; DHI, 1982a; Black, 1983), only Tonkin and Taylor (1979c) and Black (1983) identified a likely link. During the same period there was significant clearing of hinterland forests, another potential sediment source for the Mair Bank accretion.

Accretion in this region typically occurs over periods of ~100 days, while erosive episodes occur over much shorter spans of time and are often due to single storm events (Black, 1983).

Sand extractions from the beach environment are detailed in Tonkin and Taylor (1979a), though many of these are minor amounts (the largest being 35,000 m^3yr^{-1} in 1974 / 1975). Extractions occurred in the Uretiti Beach area (Tonkin and Taylor, 1979a), well south of the Ruakaka River mouth this study's area of interest. The Whangarei Harbour Study (WHSWC, 1988) notes that through the mid 1970's sand was removed from Bream Bay. This ceased in 1979 to reduce the possibility of aggravating erosion at Marsden Point and of the beach in front of the NZEC power stations.

2.8.2 Shoreline Change Within the Harbour

Inside the harbour, retreat of the dune line near the eastern edge of the Northport site, accretion in the vicinity of the NZRC wharf and erosion of the ocean beach adjacent Mair Bank have been observed between 1942 and 1979 from air photo interpretation (Healy, 1980).

The beach between the NZRC wharf and Blacksmith's Creek (Northport currently occupies some of this region) showed great stability over a two-year period of measurements by Black (1983). However, after the development of a '*causeway*' here in 1983, accretion was noted on its western side (Poynter, 1993; Gibb, 1998), providing evidence of a flux of sediment in an easterly direction.

Shoreline retreat rates for the One Tree Point – Marsden Bay area were of the order of 8-130 mmy^{-1} over the period 1942 –1997 (Gibb, 1998). These values should however be used with caution, as an 8 mmy^{-1} rate of retreat over the 55 year period equates to a movement of 44 cm. Gibb (1998) reports the 1942 measurements have an accuracy of no greater than ± 2.0 m, making any reported value less than 37 mmy^{-1} within the reported error limits and incorrect. The long-term retreat of Marsden Spit, which impounds Blacksmiths Creek, is associated with this shoreline erosion. Spit retreat has accelerated over the period 1906-1998 to reach 1.58 myr^{-1} in 1998 (Gibb, 1998).

2.9 Ecology

The ecology of the harbour is summarised in a report by the Ministry of Agriculture and Fisheries (MAF, 1979). Other useful summaries include the Whangarei Harbour Study (WHSWC, 1988) and ecological surveys for the Environmental Impact Report (EIR) for port development (Bioresearches, 1980; Poynter, 1993). Details of biota found within the harbour sediments, their extent and references to other reports are made on the ecological aspects of the Whangarei Harbour.

Prolific shellfish populations in the harbour include cockles (*Chione stutchburyi*), dog cockles (*Dosinia subrosea* and *Glycimeris laticostata*), scallops (*Pectin nouvouzelandae*), pipis (*Paphies asutrale*), tuatua (*Paphies subtriangulatum*) and horse mussels (*Atrina zelandica*) (WHSWC, 1988). Shell detritus from these resident shellfish is important for the physical stability of the harbour entrance and channels through the armouring effect of the shells on the bed.

Encrustation of the lag in places by pink coralline algal growths (Black et al. 1989) provides evidence of stability, as the fragile algae will not grow in a '*sand-blasted*' environment. Absence of the algae in the harbour entrance is as much of an indicator as its presence, reflecting a likely flux of sediment or mobility of the shell detritus through the entrance (Black et al. 1989).

In 1966, eelgrass (*Zostera*) was found on many banks within the harbour and on both ebb tidal deltas (Mair and Calliope Banks) (WHSWC, 1988). Much of the eelgrass had disappeared by 1971 and in 1976 all major beds had vanished (WHSWC, 1988). The disappearance was attributed to eelgrass' sensitivity to suspended sediment and its effects in reducing the photosynthetic ability of the plant.

Major sediment sources over this period included the washings from Wilsons (NZ) Portland Cement Company and capital dredging in the main shipping channel at Port Whangarei (Millar, 1980; WHSWC, 1988). Whilst this was the likely cause of the depletion of the eelgrass beds, it is also possible that fungal infections with no relation to the cement company or dredging operations were responsible for their disappearance (WHSWC, 1988).

The Marsden Point region has been the focus of a series of Bioresearches (1978, 1979) reports compiled for the NZRC. These reports detail the findings of a monitoring programme aimed at determining long-term changes as a result of refinery operation or possible damage in the event of an oil spill (Bioresearches, 1978). Consultants to Northport have also conducted ecological monitoring (Poynter, 1993), for both the initial resource consents and also to monitor ongoing ecological effects of the development.

A cockle bed on the flood tidal delta of Snake Bank has been so plentiful it has been commercially harvested. Biomass figures are presented in the Whangarei Harbour Study (WHSWC, 1988). Potential effects of this harvesting on the shelly lag lined channels at the harbour entrance have not been investigated.

A trend of sand deposition between 1980 and 1992 at the '*proposed*' port site made the environment there less favourable to edible shellfish and other marine invertebrates (Poynter, 1993).

A bird roosting '*sanctuary*' exists in the inter-tidal zone at the entrance to Blacksmiths Creek.

2.10 Developments in the Region and Associated Studies

2.10.1 Temporary Offloading Wharf

An investigation into the environmental impacts of a '*Temporary Offloading Ramp*' located at the site where Northport is now located is included in the Bioresearches (1981) report. The proposal included dredging up to 115,000 m^3 from the area. Various options of disposal for the dredge spoil were considered, including artificial beach renourishment. Placement in the near-shore zone and direct placement at the toe of the dune were considered.

The preferred site for the '*near-shore zone*' option was along Bream Bay Beach, adjacent to the New Zealand Electricity power stations. Dredged tailings were to be deposited alongside the ebb tidal delta (Mair Bank), 300 - 1200 m offshore, at a depth of 5-8 m (Bioreasearches, 1981). This site had experienced significant erosion previously (Section 2.7.1). Whilst it was noted that the dredged sand was of a similar grain size to the potential nourishment site, detailed investigations required to confidently recommend this nourishment were not undertaken. The rejection of the beach renourishment options was based on the requirement that the contractors back fill the dredged zone once the offloading ramp had served its purpose and was no longer required (Bioresearches, 1981). A source of sand for the back fill would need to be found should the nourishment option have been recommended.

2.10.2 Beach Protection: Marsden Bay – One Tree Point

The area between One Tree Point and Blacksmiths Creek has a coastline approximately 5125 m long, of which by 1998, 55% had been modified by both legal and illegal property protection works (Gibb, 1998). Protection works range from vertical timber, concrete seawalls, rock revetments and makeshift seawalls of demolition piping and old car tires.

Since the construction of a vertical timber seawall at Marsden Bay in 1990, there has been erosion and a truncation of the beach profile. For the 56 years prior to this no erosion had been noticeable (Gibb, 1998). The Whangarei District Council (WDC) approved further property protection works in 1998 to mitigate erosion and destruction occurring to the existing protection structures.

A variety of works were undertaken in 1999 at Marsden Bay:

i. rock revetments were constructed at the foot of cliffs at Marsden Bay;
ii. two short retaining groynes were built;
iii. a stormwater pipe adjacent to Bermuda Place, acting as a groyne, was extended;
iv. eastern Marsden Bay was nourished with sand dredged from Shell Cut Reach (8,000 m^3); and
v. a new channel was excavated for Blacksmiths Creek providing sediment for:
    a. an artificial bird roosting island (150 m^3);
    b. a 95 m long rock training wall (100 m^3), constructed to 'train' Blacksmiths Creek and to retain the Marsden Bay Beach; and
    c. the nourishment of Marsden Spit (750 m^3).

(Gibb, 1998; Stevens, 1999)

2.10.3 *Port Facilities at Marsden Point*

The Northland Forestry Port Study (NFPWC, 1980), which summarised the need for a port, recommended:

> *'that Marsden Point be developed as a deep water port for the export of Northland forest products'. (NFPWC, 1980)*

Following that recommendation, an Environmental Impact Report (EIR) (NHB, 1981) and various contributions e.g. (Bioresearches, 1980; Healy, 1980) were undertaken. Most relevant to this study was that conducted by Healy (1980) who gave a brief appraisal of the tidal inlet hydraulics and stability, along with predictions on the effects of a proposed reclamation at the port site.

Sedimentation was predicted against both the eastern and western edges of the reclamation. With reference to the eastern edge of the port site, it was suggested that *'a new beach can be expected to form here'* (Healy, 1980), noting also the movement of sediment from Bream Bay Beach around Marsden Point to this location.

Calculation of tidal prisms and bottom shear stresses led Healy (1980) to conclude that:

> *'while the Whangarei Harbour entrance is in a state of sedimentary and hydraulic equilibrium, continued slow sedimentation is likely within the harbour' (Healy, 1980).*

An increase in the cross-sectional area of the entrance due to the dredging operations of the new port would lead to the possibility of sedimentation, thus requiring maintenance dredging (Healy, 1980).

The EIR (NHB, 1981), its subsequent audit (CFTE, 1981) and comments on the audit (NFPWC, 1982) outlined the need for a port and various cost benefit analyses that determined Marsden Point the most suitable location. No '*new*' data of interest to this study is presented.

The audit of the EIR questioned the data used in relation to the potential export volumes of forest products in the EIR and proposed that the existing ports of Opua and Whangarei would have the capacity to handle most of the early tonnages of forest product exports (CFTE, 1981). The audit dealt mainly with the projections of forest product exports in Northland, rather than environmental issues. However, it was recommended:

> *'that the Northland Harbour Board continue planning for hydraulic modelling with the intention of designing the study'* (CFTE, 1981).

Later modelling by the DHI (1982a, 1982b) showed that the port layout as sketched in the EIR was '*unacceptable*' due to excessive variations of currents both along and across the turning basin and alternate designs were recommended (DHI, 1982). Port, reclamation, seawall and wharf design specifications have since been published (Palmer et al., 2003). The consent process is summarised by Palmer (2003).

2.11 Modelling of the Lower Harbour

2.11.1 Background

The first '*model*' of the area was a physical scale model created by Rogers (1959) to examine shoaling on the shell bank and the potential effects of dredging this area to create '*shell cut reach*'.

The DHI (1982a, 1982b) developed both a two-dimensional mathematical (S21) and a physical model of the region. Concurrently, Black (1983) created both one and two-dimensional hydrodynamic models of the lower Whangarei Harbour. The DHI (1982a) model was updated in 1992 (Barnett et al., 1993) with the newer MIKE 21 software package (as opposed to System 21 in 1982). Hydrodynamic aspects of the two models are essentially identical (Barnett et al., 1993), with the advantage of MIKE 21 possessing an associated sediment transport module. Further study was undertaken with the same model (Barnett et al., 1993) in 1997 (Barnett, 1997) with the only variation being a modified dredge basin (more likely to be constructed), as such the predictions of this, more recent model are much more applicable than those of the earlier configurations.

2.11.2 DHI's Physical Model

The physical model developed by the DHI (1982a) was created with an inbuilt vertical distortion. The horizontal scale was 1:250 while the vertical scale was 1:81. This provided better vertical resolution at higher flow velocities and a more detailed flow pattern could be examined (DHI, 1982a). In order to maintain similtude, the Froude number (F) of the model and the actual harbour was made to be equal.

$$F = \frac{V}{\sqrt{(gD)}} \qquad (2.1)$$

Where:

V = characteristic horizontal velocity;

g = acceleration due to gravity; and

D = characteristic vertical length (depth).

The model was based on steady-state flows rather than the dynamic tidal flows found in nature. Comparisons of float tracking from the physical model with '*real world*' current measurements and drogue tracking were used along with mathematical model (S21) output, to calibrate the physical model (DHI, 1982).

2.11.3 Mathematical Models

Black's (1983) one-dimensional model will not be reviewed in detail as a two-dimensional model developed within the same thesis superseded it. Readers are referred to Black (1983) for further details.

The DHI's (1982a) two-dimensional model (S21) solved the hydrodynamic and continuity equations using an implicit finite difference scheme, whilst Black's (1983) two-dimensional model (2DD) used a semi explicit finite difference scheme. Black's (1983) choice of solution scheme was governed by computing limitations at the time.

Explicit schemes, while requiring less computation per time step are often limited by a stability criterion, which then requires a reassessment of the minimum time step. Black's (1983) 2DD initially used a grid size of 500 m, later refined to 250 m. The grid was oriented north south and east west (true) and time steps of 12 and 6 s respectively were used for the two grid sizes.

The DHI (1982a) initially used a finer grid resolution of 150 m (S21) then remodelled using a 50 m grid (SD1) and a smaller area, focussing on only the area immediately surrounding the proposed port location. The grid in both DHI models was rotated + 20° relative to true north (DHI, 1982a). The coarse grid model was used to calculate the boundary conditions for the fine grid model and time steps of 30 and 20 seconds where used respectively for the coarse and fine grid models. Barnett et al. (1993) and Barnett (1997) used the same 50 m grid as the DHI (1982a).

Both the DHI (1982a) and Black (1983) obtained bathymetry information by digitising Navy charts N.Z. 5213 (1974) and from soundings taken by the Royal New Zealand Navy in 1981.

The DHI / Barnett Consultants (Barnett et al.,1993) model used survey data recorded at a 1:1000 scale undertaken by the Northland Port Corporation.

Black (1983) used a constant roughness length of Z_o = 0.0007 m, obtained from the median value of Z_o calculated from several vertical velocity profiles in the Whangarei Harbour. This value was used to represent the entire modelled region. An eddy diffusion coefficient of 5 m^2s^{-1} was chosen as it provided the most realistic results. The DHI (1982a) used a manning number of 32 in the general harbour and 20 in mangrove areas, as this provided the most realistic results of water elevations at Port Whangarei.

Calibration and verification of Black's (1983) 2DD was undertaken using velocities measured at 20 independent sites. The model was found to be predicting the velocities well in all regions except for the channel near One Tree Point, this was attributed to the schematisation of the flood tidal delta of Snake Bank using the 250m grid resolution (Black, 1983). Maximum deviation of modelled and observed currents was 15%.

The DHI's (1982a) S21 (150 m grid) model was calibrated against four Aanderra current meters and a series of Braystoke current meter vertical velocity profile readings. The Aanderra current meters were deployed at mid depths to attempt to record velocities representative of the depth average (DHI, 1982). Braystoke measurements were obtained under different tidal ranges to that used in the model, and so were scaled to the modelled range using the Aanderra measurements from other sites (DHI, 1982a), a linear relationship between the Braystoke sites and Aanderra sites was assumed.

While linearity can be established between velocity and tidal range, it is essentially site specific (Black, 1983). The DHI (1982a) used a linear relationship over both varying tidal range and between the Aanderra and Braystoke sites. Black (1983) notes that this explains some of the scatter in the DHI (1982a) calibration plots. It may also have led to the situation where the model was correct and the field calibration / validation '*measured velocity*' may be subject to a poor scale factor (Black, 1983).

The DHI's (1982a) 50 m grid model (SD1) used output from S21 (150 m grid) as boundary conditions on both the up harbour and '*ocean*' boundaries. The fine grid model was calibrated using water level elevations and general observations of the drying of Snake Bank (DHI, 1982).

2.11.3.1 Findings and Predictions

To represent the proposed port development, Black (1983) used case A7 (DHI, 1982a, 1982b), essentially identical to case A3 (DHI, 1982a, 1982b) and examined extensively in DHI (1982a). Both cases have a 450 m wide, 13 m deep dredge basin and a 540 m long quay. The major difference between cases 'A7' and 'A3' is that in 'A3' the proposed port reclamation extended 20 m farther into the harbour than for 'A7'. It is notable that this difference is smaller than the model grid size used by Black (1983) and the DHI (1982a), thus noticeable effects on model output will be negligible as the models cannot actually distinguish the difference. The DHI (1982a) investigated case A7 in their physical model only, not their mathematical model.

Black's (1983) model suggested that Whangarei Harbour was typified by several closed or partially closed sediment transport loops, as indicated by residual velocities (Figure 2.2).

2.11.4 Sediment Transport Modelling

All three significant hydrodynamic models of the area (DHI, 1982; Black, 1983; Barnett, et al., 1993) have been expanded to incorporate sediment transport, with various methods and techniques being used. Black's (1983) model was one of the first globally to link the physics of sediment transport to the dynamics of the modelled fluid movements in order to calculate sediment transport potentials at each node in the grid.

2.11.4.1 Methods of Calculation

The DHI (1982a) model results were used to calculate sediment transport. The calculations were however, not automated within the model. Sediment transport was not based on the actual velocity field output by the model, but rather on a sinusoidal velocity curve that was fitted to selected model outputs at selected locations (DHI, 1982a). This contrasts with Black's (1983) approach where the actual modelled velocities were used to estimate transport at each node and at each time step of the model. The DHI (1982a) used output from their fine-grid two-dimensional, hydrodynamic model (SD1) to investigate sedimentation in three key areas, the dredge basin, the area surrounding the NZRC wharfs, and the main channels. Formulae used were based on the sediment transport by tidal currents model proposed by Engelund and Fredsoe (1976), which separates the sediment load into bedload and suspended sediment components. Details of the predictions and sediments follow in Sections 2.11.4.2 and 2.4.11.3.

Black (1983) used water velocities and amplitudes from 2DD, his two-dimensional hydrodynamic model, along with the principle of conservation of mass to calculate sediment volume changes between model grid cells. The model estimated sedimentation rates, maintenance dredging requirements and the sedimentary impact of the construction of a port. Black (1983) investigated the sensitivities of many sediment transport formulae before settling on the Yallin (1963) equation for bedload and an empirically determined equation developed at Whangarei from his own experiments for the suspended load.

To obtain annual fluxes, Black's (1983) model was run for one complete tidal cycle at both neap and spring tidal ranges with bed level changes being predicted. Output from each run was scaled to the mean tidal range and averaged. Predictions were extrapolated to annual sediment fluxes by weighting the sediment fluxes predicted at a known tidal range to a normal distribution of observed tidal ranges over a typical year at Marsden Point. The DHI (1982a) simulated velocities at a single tidal range (2.70 m). Output water velocities were scaled with values of 1.0, 0.84 and 0.66 to simulate tidal ranges of 2.70 m, 2.17 m and 1.54 m, assumed to be representative for 9%, 49% and 42% of the time respectively. Sediment fluxes for each of the tidal ranges were calculated and weighted to determine a yearly average.

The DHI (1982a) transport modelling technique was improved upon in 1993 when the sediment transport was calculated at each node of the model, based on the actual modelled flow velocities (Barnett et al., 1993). The newer models (Barnett et al., 1993) yearly calculation of sediment flux was also improved, with sediment transport being simulated at the three tidal ranges, rather than scaled from a single model run. Fluxes obtained were weighted accordingly, providing more accurate results as the effects of differing tidal ranges were actually modelled rather than assumed from a single model run. The report of Montgomery Watson (Barnett, 1997) was based on entirely the same model set up as that of Barnett et al., (1993), however the bathymetry of the dredge basin had been modified to a more *'likely'* scenario.

Interestingly in Blacks (1983) sediment transport model, sediment movement by waves was incorporated at the boundary only and not within the model grid itself. This should be kept in mind when considering model output near inter-tidal areas, as Black (1983) himself notes that surface waves were the dominant influence on the sediment transport in the inter-tidal zone (Black, 1983). Both DHI models (DHI, 1982a; Barnett et al., 1993) also neglected sediment transport by waves.

All three models were generally focused on sediment transport in the channels, where wave effects are minimal, as opposed to the inter-tidal zone. This arises from the need for the models to accurately estimate maintenance dredging requirements in the ship turning basin. It does however mean the modelling of potential morphologic change in the shallow inter-tidal areas is somewhat doubtful.

2.11.4.2 *Bed Sediments used for Calculations*

The nature of the bed sediments and the effects of the shell lag in the channels were taken into account by Black (1983) through the addition of two parameters to characterise the seabed. Values of erodibility and availability (between 0-100) were assigned to each node in the model grid to represent the percentage of the area surrounding the node covered in sandy sediment and the cohesiveness of those sediments (Black, 1983). Values were obtained from sea floor observations from underwater photography, sediment sampling, diver observations and side scan sonar imaging of the sea floor (Millar, 1980; Black et al., 1981; Black, 1983; Black and Healy, 1983).

The DHI (1982a) in their calculations used sediment grain sizes obtained from Millar (1980), who dissolved all calcium carbonate (shell) fragments from samples before analysis. This resulted in the DHI models (DHI, 1982a; Barnett et al., 1993) failing to accurately account for the effects of the shelly lag when calculating sediment fluxes. This was recognised and a *'scaling factor'* employed to correct the results. The scaling factor was calculated as one (1) minus the percentage of the bed area covered by shells (DHI, 1982a). The factor is similar to Black's (1983) erodibility value, but is somewhat less accurate as it is used to represent a much larger area of the bed.

Failing to take into account areas of bed stabilised by shell layers will affect comparisons of model output with the *'real'* situation post development. The DHI (1982a) models main concern was however, the differences between various modelled scenarios and the *'no development'* situation; as errors would be the same for each case this deficiency was acceptable. Care should be taken however when comparing these predicted changes to actual observed changes.

In using Millar's (1980) sediment data, the DHI (1982a) may have caused their model to indicate:

> *"suspended load transport is dominant for flow velocities above 1 ms^{-1}"*
>
> (DHI, 1982a).

The same authors observed

> *"suspended fine material in this part of Whangarei Harbour is very low (< 10 mgL^{-1})"* and
>
> *"There appeared to be no reliable correlation between the flow velocity and the concentrations"* (DHI, 1982a).

This discrepancy is not explained in their text.

Black (1983) used a roughness length of Z_o=0.0010m to model the harbour as it provided the best calibration results. The value compares favourably with the average roughness length of Z_o=0.0007m, obtained from velocity profile measurements throughout the lower harbour (Black and Healy, 1982). The modelled value may however result in sediment fluxes being slightly over-estimated in sandy regions during high current flows.

2.11.4.3 Sedimentation Predictions

Sedimentation will occur in the dredge basin due to:

1) Net sediment transport directed toward the dredge basin; and
2) Downslope movement of material agitated along the batter slopes of the dredge basin.

(DHI, 1982a; Black, 1983)

In all three models the underlying hydrodynamic models were calibrated, while the sediment transport '*extensions*' were not. It is recognised that the calibration of sediment transport models is a task often requiring quantities of time and money not available to those modelling the area (Davies, 2002; Haas, 2003). Black (1983) attempted to minimise non-calibration effects through the use of erodiblity and availability values. The DHI (1982a) model however, has the potential to predict erosion in areas covered by rock or shell.

Predicted changes by all the models represent, in reality, initial potential changes. In all three cases, longer-term morphologic simulations involving a continuous update of the bathymetry has not been undertaken.

The rate of accretion and erosion during the ebb and flood phases of a singe tidal cycle were found to be an order of magnitude larger than the predicted long-term impacts (Barnett, 1997). This indicates long-term stability, despite a short-term potential for sediment transport. Inter-tidal areas of Snake Bank and to the west of Northport are not affected by any predicted erosion or accretion (Barnett, 1997).

Black (1983) used *'port layout case A7'* (DHI, 1982a) which was superseded by a new dredge basin layout in 1997 (Barnett, 1997). The new layout was used in the predictions of Barnett (1997). The results of Black (1983) and Barnett (1997) will be detailed as they used differing models to obtain solutions. Only Barnett's (1997) predictions are investigated for the DHI family of models as it is the most recent and uses the most up to date bathymetry layout. However, the slightly differing dredge basin layouts should be kept in mind when comparing predictions between Black (1983) and the DHI family (DHI, 1982a & b; Barnett et al., 1993; Barnett, 1997).

Black's (1983) model predicted accretion on the northern side of the dredge basin with the material being sourced from the ebb-tidal spit of the flood-tidal delta of Snake Bank, extending towards the dredge basin. Much of the dredge basin is predicted to erode or stabilise if shelly or cohesive sediments are exposed, with the exception of slight accretion on the western margin. Approximately 20,000 m^3y^{-1} of sediment was expected to accumulate in the dredged basin due to transport by tidal currents and gravitational down-slope movement (P=0.45, mean grain size = 0.3 mm) (Black, 1983). Only minor effects were predicted surrounding the NZRC jetties and on the shipping channel.

Barnett (1997) predicted accretion on the batter slope to the west of the dredged basin and erosion in the basin's centre until a shell lag develops or stable strata is exposed, agreeing with Black (1983) on both predictions. Quantities of erosion and accretion in the immediate vicinity of the dredge basin are expected to balance and allowing for down-slope movement 50,000 m^3y^{-1} of sediment (60% relative density) is predicted to accumulate in the dredge basin (Barnett, 1997).

3 GRAIN SIZE PATTERNS OF THE LOWER HARBOUR

3.1 Introduction

Grain size distribution statistics, such as moment measures are essential information in beach nourishment projects (NRC, 1995) and assist in the determination of different transport-depositional environments. In this regard it is necessary to know the textural characteristics of the '*in-situ*' and deposited sediments.

A surficial sediment-sampling program was implemented in order to obtain information regarding sediments and transport patterns surrounding Marsden Point and Northport. The samples also provide essential baseline data needed to ground-truth the side-scan sonar survey record (Chapter 7).

3.2 Background

There are limited sediment sources for the lower Whangarei Harbour. Streams discharging sediments drain relatively small catchments, covering a combined area of 300 km^2, and do not influence the lower harbour significantly (Millar, 1980). Inputs from headland and cliff erosion are relatively low, due to the resistant volcanic (andesite) lithology of Bream Head and Bream Tail (Nichol, 2002).

The beach and dune sands of Bream Bay Beach have previously been identified as belonging to Schofield's (1975) Hauraki (B) facies (Miller, 1980), a derivative of the Haruraki (A) facies covering much of the Hauraki Gulf and originating from the ancestral Waikato River when it flowed through the Hauraki lowlands and into the Hauraki Gulf (Schofield, 1975). Both Millar (1980) and Healy (1980) have concluded that the sandy sediments of the lower harbour (One Tree Point to Marsden Point) are derived from the Hauraki (B) sediments of Bream Bay.

Much of this deposited sediment (Hauraki (B)) was '*swept*' onshore with the post-glacial rising sea level (Holocene transgression) between 10,000 and 6,500 years Before Present (BP) (Schofield, 1975). Presently, there is very little cross shelf (diabathic) movement of sand toward the beaches such as Bream Bay Beach from the inner shelf nearby (Hume et al., 2000).

On a regional scale, previous studies (Pakiri) have identified that there are only narrow and discontinuous pathways of sand transport around the headlands (e.g. Bream Head and Bream Tail, to the south of Bream Bay), indicating that the total amount of sand leakage / input around headlands is small (Hume et al., 2000).

3.3 Methods

Fifty sediment samples were collected from the lower Whangarei harbour on July 5th and 6th and October 16th, 2003. Positional information was obtained by differential GPS to within ± 1.0 m. Samples were taken either by hand (from beach sites), by SCUBA diver or with a Smith-McIntyre type sediment grab sampler. Sampling locations were based on areas identified in the initial Side Scan Sonar survey (February 2003) and also at key locations in the lower Harbour such as the beach profile survey locations and the dredge basin (Appendix A).

Several locations proved difficult to sample using the grab sampler, such as those of depth greater than 30 m, or those having a hard compact '*armoured*' or '*lagged*' bed from which no sediment could be obtained with the sampler. Locations such as these have been disregarded, as no data were immediately available for them.

Grain size distributions were determined using the Rapid Sediment Analyser (RSA) at the University of Waikato. Statistics were calculated by moment measures (Appendix A). Particle size was expressed in phi (Φ) units based on Wentworth classification system (Table 3.1). Phi units are related to the grain size in millimetres by the relation $D_\Phi = -\log_2 D_{mm}$ where D_Φ and D_{mm} is the diameter in phi and millimetres respectively.

Grain Size Scales for Sediments					
Sieve Mesh #	Millimetres	Microns	Phi (Φ)	BS Sieve	Wentworth Size Class
5	4	4000	-2.0		
6	3.36		-1.75		
7	2.83		-1.5		Granule
8	2.38		-1.25		
10	2.00	2000	-1.0	2000	
12	1.68		-0.75	1700	
14	1.41		-0.5	1400	Very coarse sand
16	1.19		-0.25	1180	
18	1.0	1000	0.0	1000	
20	0.84	840	0.25	850	
25	0.71	710	0.5	710	Coarse sand
30	0.59	590	0.75	600	
35	0.50	500	1.0	500	
40	0.42	420	1.25	425	
45	0.35	350	1.5	355	Medium sand
50	0.30	300	1.75	300	
60	0.25	250	2.0	250	
70	0.210	210	2.25	212	
80	0.177	177	2.5	180	Fine sand
100	0.149	149	2.75	150	
120	0.125	125	3.0	125	
140	0.105	105	3.25	106	
170	0.088	88	3.5	90	Very fine sand
200	0.074	74	3.75	75	
230	0.063	62.5	4.0	63	
270	0.053	53	4.25	53	
325	0.044	44	4.5	45	Coarse silt
	0.037	37	4.75	38	
	0.031	31	5.0		
	0.0156	15.6	6		Medium silt
	0.0078	7.8	7		Fine silt
	0.0039	3.9	8		Very fine silt
	0.0020	2	9		
	0.00098	0.98	10		
	0.00049	0.49	11		Clay
	0.00024	0.24	12		
	0.00012	0.12	13		
	0.00006	0.06	14		

Table 3.1 – *Wentworth grain size classification scheme. (after Folk, 1966)*

Sediment samples containing **large** shell content were wet sieved through a -2.00 Φ (4.00 mm) sieve (Figure 3.1). Only shell content larger than –2.00 Φ (4.00 mm) was removed, smaller broken shells were allowed to remain in the sample. The large shell content was removed to assess the location of *armoured* or *lagged* beds, smaller shell content will have little armouring effect. The RSA system is designed to cope with large shells (e.g. cockles, *Chione stuchburyi* ~ 3 cm), thus any large shell component present remained separated (Figure 3.1). Following the drying of both fractions the percentage of large shell material was determined.

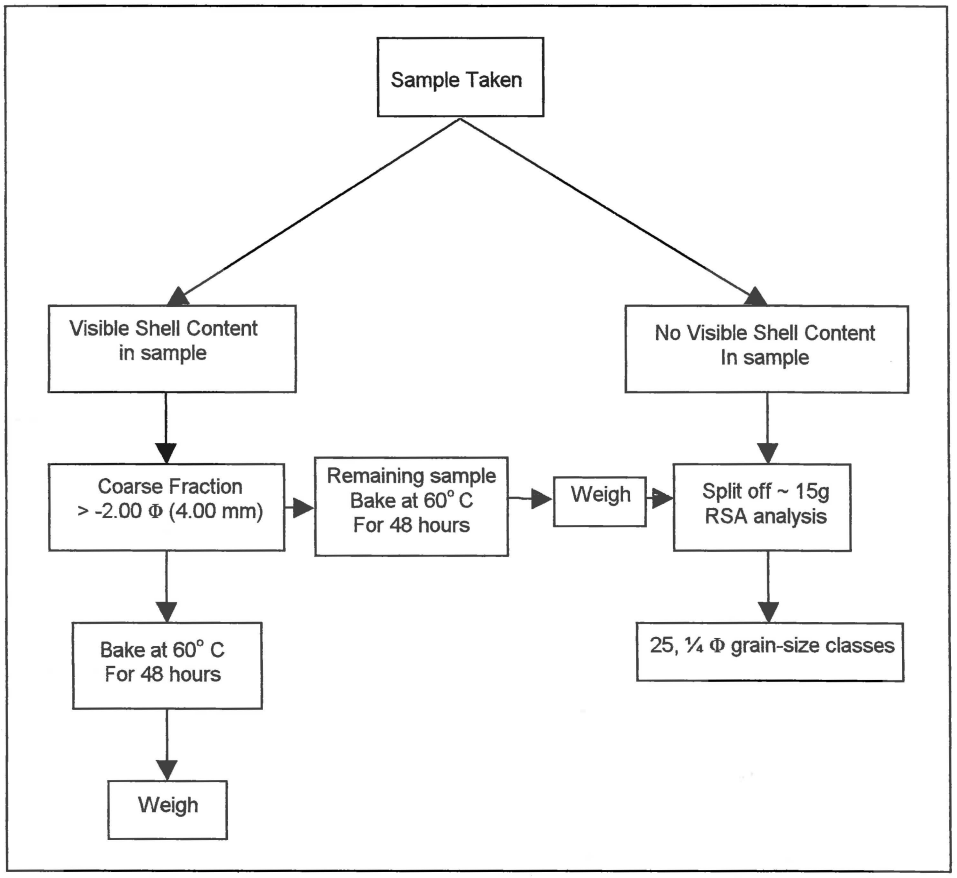


Figure 3.1 - *Flow chart illustrating the analysis procedure for sediment samples*

The finer, sandy material was subjected to analysis in the RSA at the University of Waikato. This technique determines the sediment grain size using an empirical equation derived by relating the fall velocity of the spherical quartz grains (density =2650 kgm^3) through a fluid medium to the grain diameter.

Grain size is calculated from the settling velocity using the Gibbs et al. (1971) equation:

$$r = \frac{0.055804V^2\rho + \sqrt{0.003114V^2\rho + [g(\rho_s - \rho)](4.5\eta V + 0.008705V^2\rho)}}{[g(\rho_s - \rho)]}$$

(3.1) - *Grain size calculation from settling velocity (Gibbs et al., 1971).*

Where: V is the velocity (cms^{-1}),
g is the gravitational acceleration (cms^{-1}),
η is the dynamic viscosity (poise),
ρ is the density of the fluid (gcm^{-3}),
ρ_s is the density of a sphere (gcm^{-3}) and
r is the sphere radius (cm).

The fall distance through the RSA tube filled with fresh water at 20°C was 1.88 m. Data from the collection pan hanging below an electronic balance was recorded for 600 seconds triggered by the release of the sample.

de Lange et al. (1997) compared sieve and RSA textural determinations and found that agreement was generally poor. They recommended the analysis of sub-samples between 20-30 g in the RSA, as these gave the least variability. Larger quantities have been identified as causing inter-particle vortex interference, leading to decreased fall velocities for high concentrations as the drag coefficient increases (Allen, 1985; Ross and Mehta, 1989). The National Research Council (NRC) (1994) record that:
"*Fall velocity determines the important hydraulic characteristics of the sediment, the near-shore beach slope and equilibrium beach-slope*" (NRC, 1994). This, along with the speedy nature of the analysis led to the use of the RSA.

The cumulative weight was recorded at 0.25 Φ intervals. A computer connected to the RSA calculated statistics using moment measures. Moment measure equations (Krumbein and Pettijohn, 1938) and grain size distribution data are compiled within Appendix A.

3.4 Sediment Sampling Results

3.4.1 Shell Lag

Shell lag deposits have previously been identified in the lower Whangarei Harbour (Millar, 1980; Black, 1983) (Figure 3.2). Found on the channel floors, the lag is the cause of reduced sediment transport potentials and the overall stability of the harbour (Black, 1983).

Figure 3.3 indicates the areas where shell was present in the samples of 2003. The channel floor is characterised by high shell content. Shell lag deposits were found:

i. in the harbour channel off Marsden Point (sites 45, 48 and 51 Figure 3.3 c.f. Figure 3.2) and
ii. in front of the Northport site, adjacent to the dredged turning basin (sites 23, 25, 27 and 46, Figures 3.3 and 3.2).

Both locations are in agreement with Black's (1983) summary (Figure 3.2).

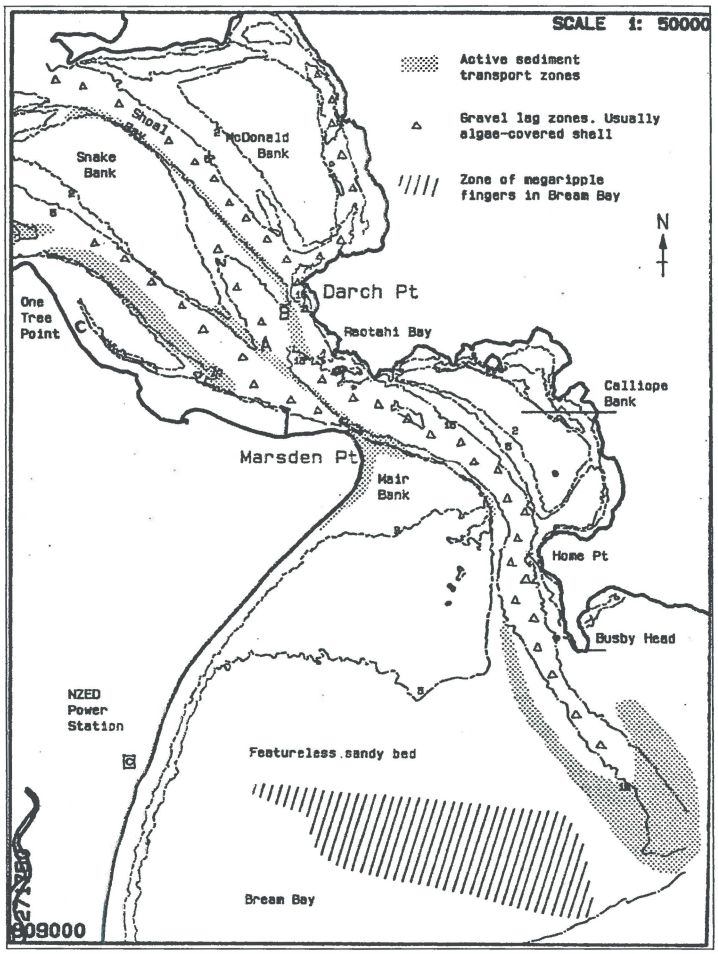


Figure 3.2– *Shelly and active sediment transport zones from Black (1983).*

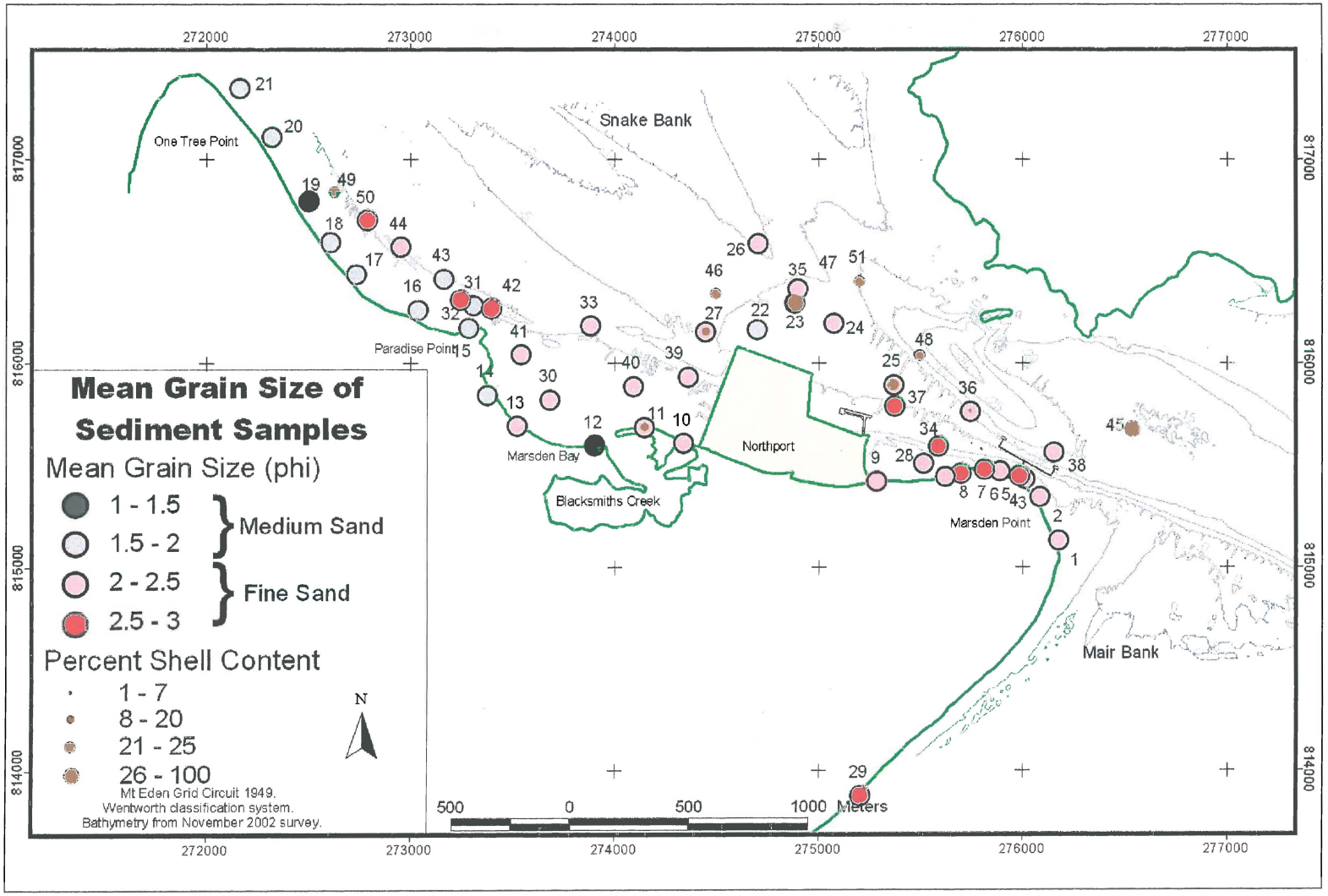


Figure 3.3 - *Location and mean grain size of samples collected for this study. See Appendix A for specific details and locations.*

Shell content was also found at sites 11 and 49. At Site 11, close to the shoreline, the shell content was relatively *'fresh'* and un-reworked, thus it is likely sourced nearby. Site 49 is the location of a *chenier shell ridge,* not identified by either Millar (1980) or Black (1983). The non-identification of this feature by previous authors cannot be used as evidence for its recent formation due to the sampling strategies employed in these previous studies.

There is an absence of shelly material on the sub-tidal extension of Snake Bank (identified by the -5.0 m contour) at sites 24, 26 and 35 (Figure 3.3), agreeing with Black's (1983) findings (Figure 3.2) where the extension was deemed an active sediment transport zone.

The broad scale areal distribution of shell lag sediments in the lower Whangarei Harbour has not changed greatly between 1983 and 2003. Very similar patterns of shell content are observed adjacent to the port site.

3.4.2 Mean Grain Size

Mean grain size is a function of both the size of the available materials and the amount of energy apparent on the sediment (stresses from current velocities and turbulence).

Mean grain size (non-shell component) is thematically mapped in Figure 3.3. The size range found (1 – 3 Φ or 0.125 – 0.50 mm) is consistent with that observed by Schofield (1975) in the surrounding areas (0.13 – 0.45 mm). The mean grain size observed on the beach face near the NZRC jetties (Sites 1 to 8, Figure 3.3) is between 2 and 3 Φ (0.125 – 0.25 mm), agreeing with Schofield's (1975) results of grain sizes between 0.16 and 0.19 mm (2.64 to 2.40 Φ) on the *'beach near Marsden Point'*.

To assist further presentation, Inverse Distance Weighting (IDW) interpolation was carried out on a 50 m grid in ArcView 3.2a® to create a surface of mean grain size. It should be noted that the surface represented (Figure 3.4) can only be reliably interpreted over the area covered by the original data points (Figure 3.3) and that the accuracy of the surface is proportional to the density of data points. The surface represented (Figure 3.4) has been masked to show only the area covered by the original data points.

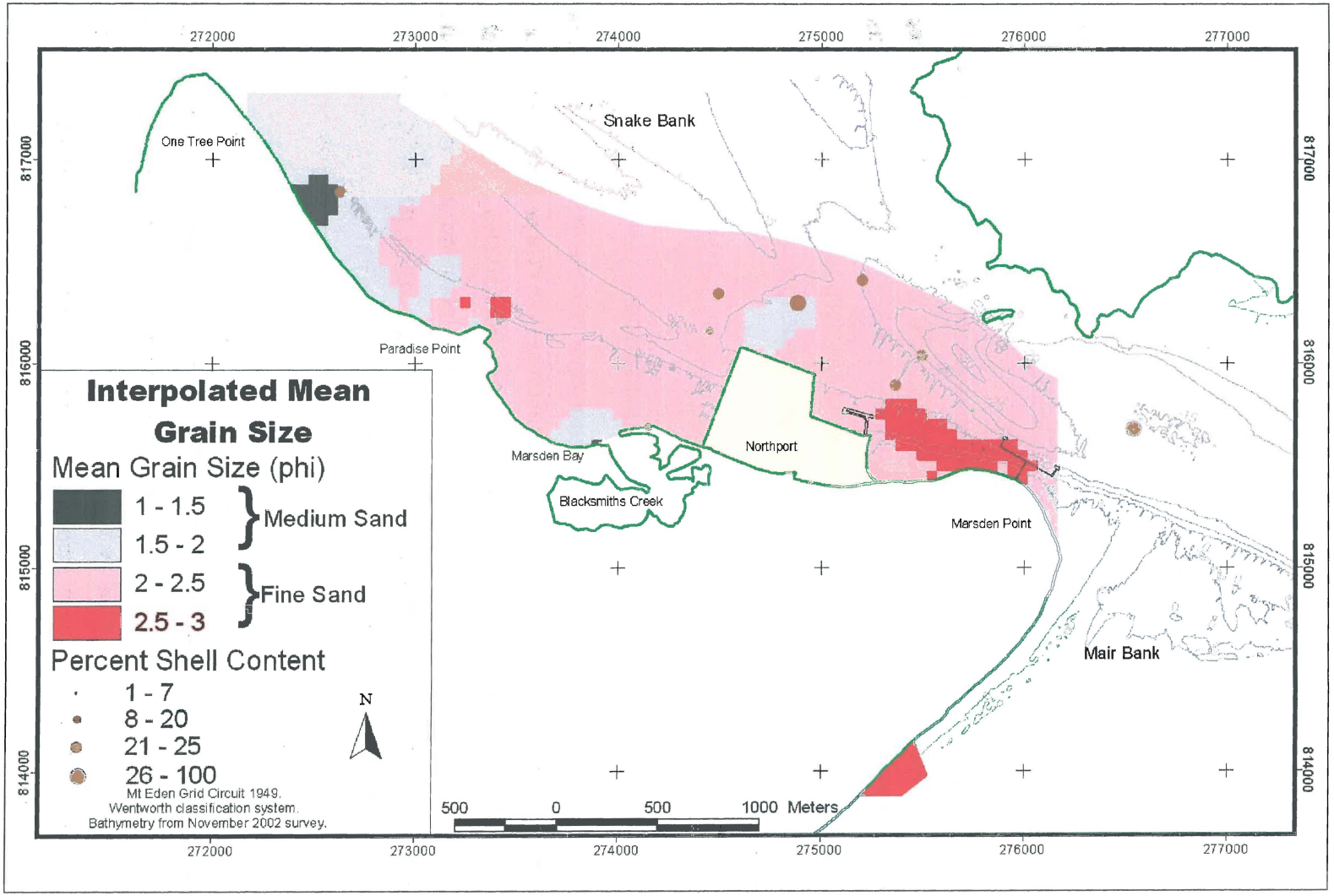


Figure 3.4 - *50 m grid of interpolated mean grain size of lower Whangarei Harbour, from samples taken in 2003.*

Fine sands extend over much of the region covered by the samples, medium sands occur in and alongside the dredge basin adjacent Northport and also on the beaches and inter-tidal areas of Marsden Bay and One Tree Point.

The region of medium sands adjacent to Northport corresponds with an area identified by Millar (1980) as having a mean grain size between 1.0 – 2.0 Φ (0.25 – 0.50 mm) (medium sands in the Wentworth classification). Remaining areas, shown in Figure 3.4, were identified by Millar (1980) as having a mean grain size of between 2.0 – 2.5 Φ (0.177 – 0.25 mm) (fine sand). Millar's (1980) sampling locations however, did not incorporate the inter-tidal and beach areas at Marsden Bay and One Tree Point where the larger medium grain sizes have been observed (Figures 3.3 and 3.4).

Sediments surrounding Northport are typically fine sands. Within and immediately adjacent to the dredge basin, grain sizes are slightly larger, a pattern observed both in 1980 (Millar, 1980) and in 2003. Near the shoreline, between Marsden Bay and One Tree Point, medium sands are dominant. This trend has not previously been identified, possibly due to sediment sampling strategies largely ignoring the inter-tidal and beach face areas.

3.4.3 Spatial Variation of Class Size Abundance

The 25 one-quarter phi grain size classes determined by the RSA analysis were summarised according to the Wentworth classification system (Table 3.1), results were expressed as the abundance (percent-weight) of sand sized particles, from coarse/very coarse to very fine sand (Figures 3.5 to 3.8). Values obtained at each sampling location were interpolated onto a grid (50 m resolution, using IDW). Class size abundance plots (Figures 3.5 to 3.8) reveal grain size patterns in much greater detail than the over-simplified mean grain size plots (Figures 3.3 and 3.4). Specific differences in grain sizes are tabulated in Appendix A.

Very coarse/coarse sands dominate more in the dredge basin adjacent to Northport and locally off Paradise Point than in other areas of the lower harbour (Figure 3.5). Black (1983) observed an abundance of coarse sands in an area stretching between these two sites. The proportion of coarse sediment noted by Black (1983) in these areas (> 69%) is greater than that measured in 2003. Black (1983) however, included all shell content in his analysis, contrasting slightly with the present method. These areas also contain a relatively large percentage of very fine sized sediments (Figure 3.8).

Medium sands are abundant (> 60%) adjacent to the shoreline from One Tree Point to Marsden Bay. This size class also appears to be the dominant sediment exiting Blacksmiths Creek (Figure 3.6). Fine sands dominate on the southern side of the Harbour eastwards of Blacksmiths Creek, with the exception of the Northport dredge basin.

To the east of Northport, extending from the beach to deeper water, sediments are generally homogenous in terms of grain class size abundance. To the west of Northport (Marsden Bay and One Tree Point coastline) the sediments show a general trend of decreasing proportions of coarser material and an increase in fines, extending from the beach to deeper water.

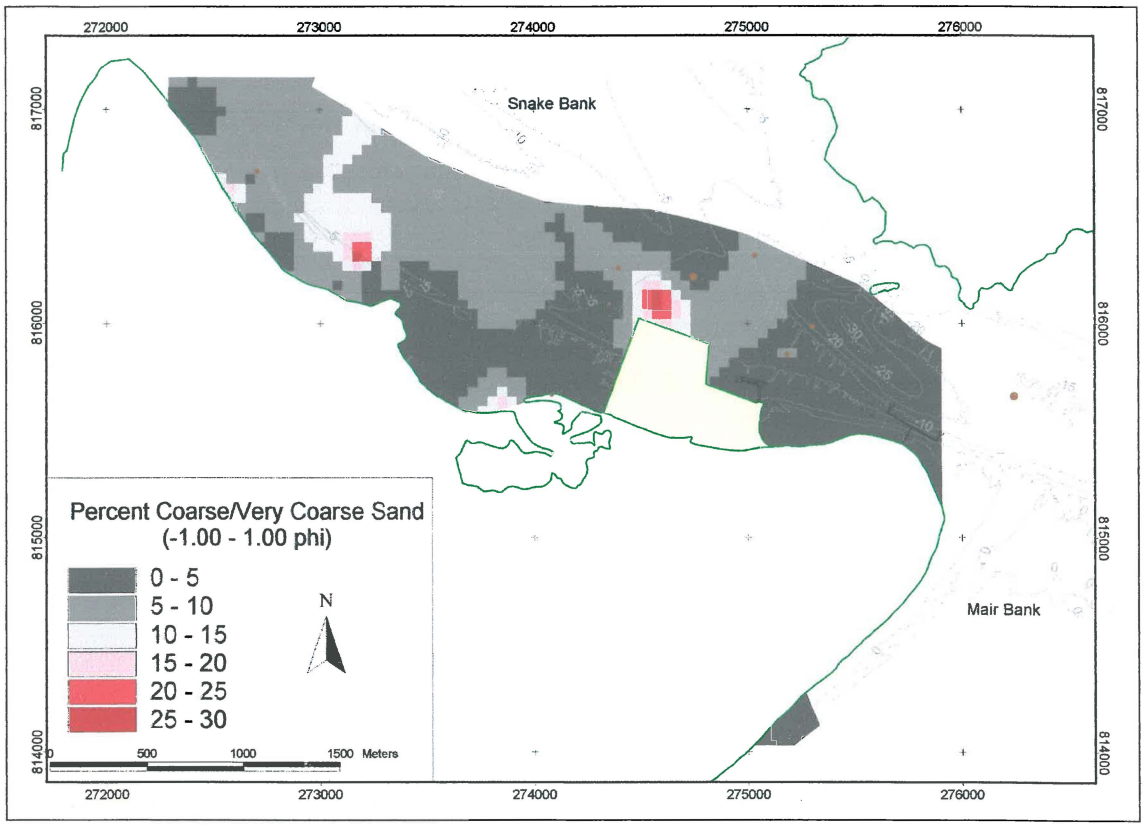


Figure 3.5 - *Abundance of coarse and very coarse sands, expressed as percent weight (50 m grid interpolation).*

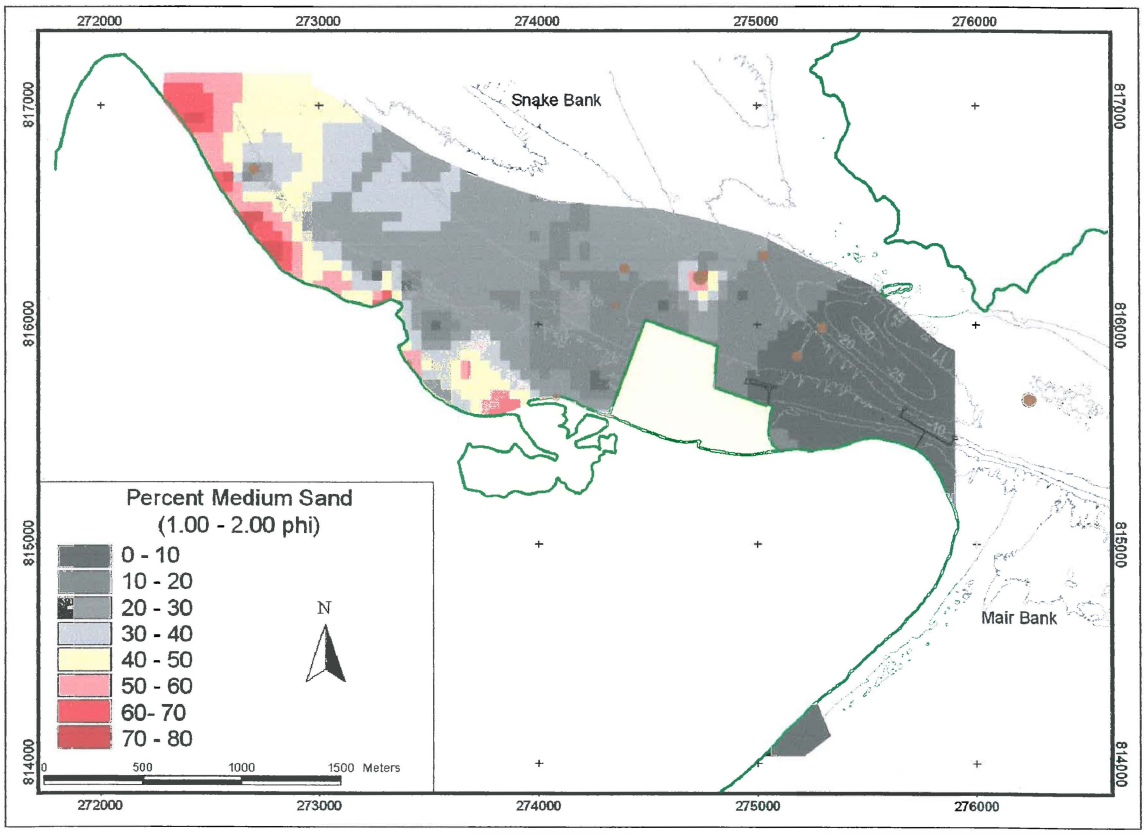


Figure 3.6 - *Abundance of medium sands, expressed as percent weight (50 m grid interpolation).*

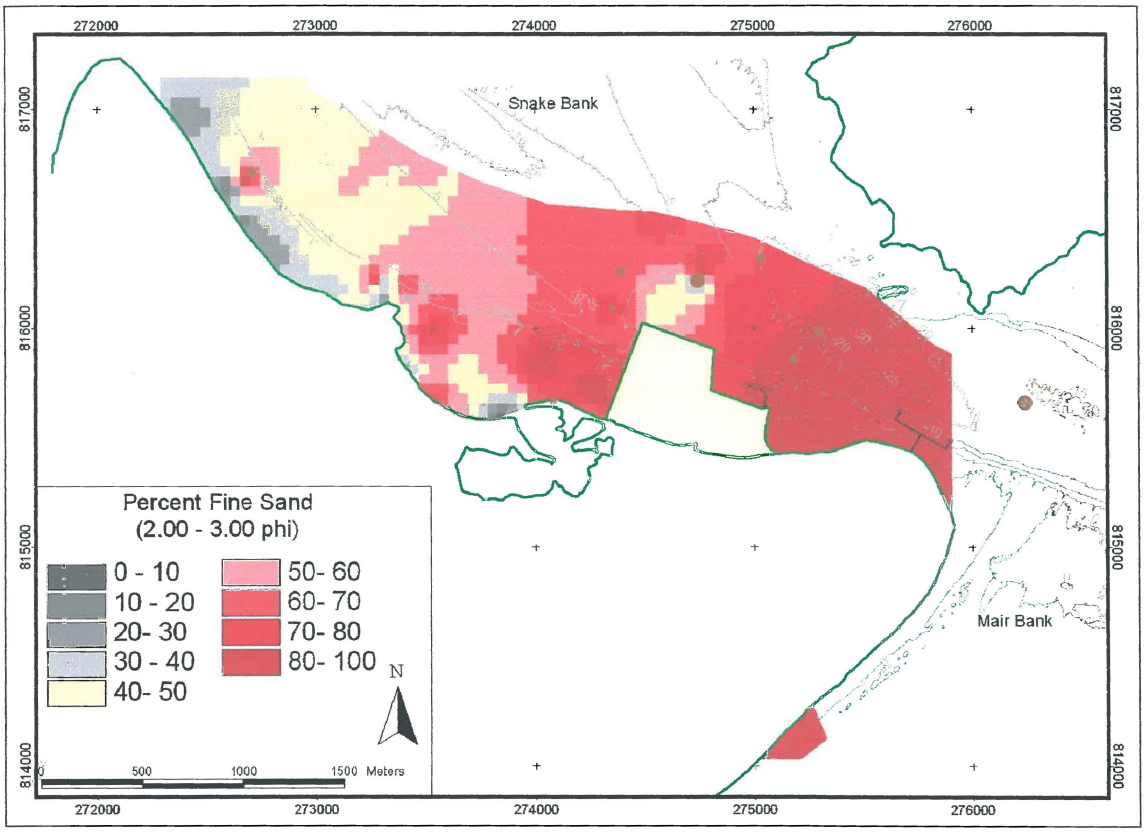


Figure 3.7 - *Abundance of fine sands, expressed as percent weight (50 m grid interpolation).*

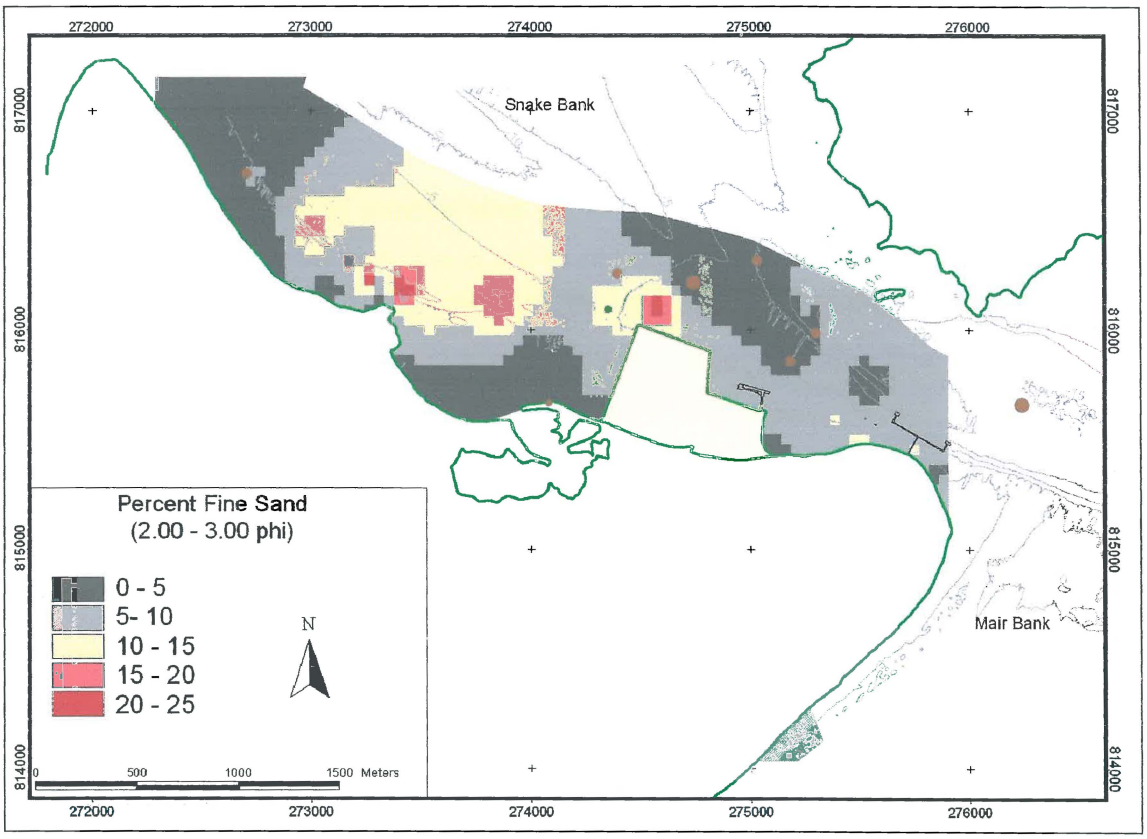


Figure 3.8 - *Abundance of very fine sands, expressed as percent weight (50 m grid interpolation).*

3.4.4 Higher Moment Measures

Higher moment measures: sorting, skewness and kurtosis, the 2nd, 3rd and 4th moment measures respectively, describe progressively more about the behaviour of the tails of the sediment grain size distribution. Descriptive terms are taken from Larsen et al. (1997) and are listed in Appendix A.

Sorting is the standard deviation of the grain size distribution and describes the spread of grains about the mean. Sorting is dependent on four major factors:

i. the size range of the material supplied;
ii. the type of deposition;
iii. the current characteristics (*e.g.* degree of turbulence); and
iv. the rate of sediment supply c.f. the efficiency of the sorting process.

In general, sorting improves along the sediment transport path (Tucker, 1991)

Skewness is a measure of the symmetry of the distribution about the mean. If there is a fine '*tail*', i.e. excess fine sediments, then the sample is fine (positively) skewed (> 0.1). If there is a coarse '*tail*', i.e. excess coarse sediments, then the sample is coarse (negatively) skewed (< -0.1). In general, sediment becomes more coarsely skewed (and finer grained) along its transport path, whereas the lag becomes more finely skewed and relatively coarser (McLaren and Bowles, 1985).

The coefficient of kurtosis is a measure of the peakedness of the distribution; that is, the proportion of the sediment in the middle of the distribution relative to the amount in both tails. Interpretation of the kurtosis value is difficult, as no consistent expression relating kurtosis and energy level exists (Tanner, 1995).

3.4.4.1 Interpretation of Higher Moment Measures

Textural parameters have frequently been used as indicators of sediment transport direction (Sunamura and Horikawa, 1972; McLaren, 1981; McLaren and Bowles, 1985). The model of Sunamura and Horikawa (1972) has previously been applied in New Zealand with success (Bridgewater, 1986; de Lange and Healy, 1990). The model compares spatial trends of median size (settling velocity) and sorting. Of the possible combinations of trends which may be obtained, four are considered to define transport directions (Figure 3.9)

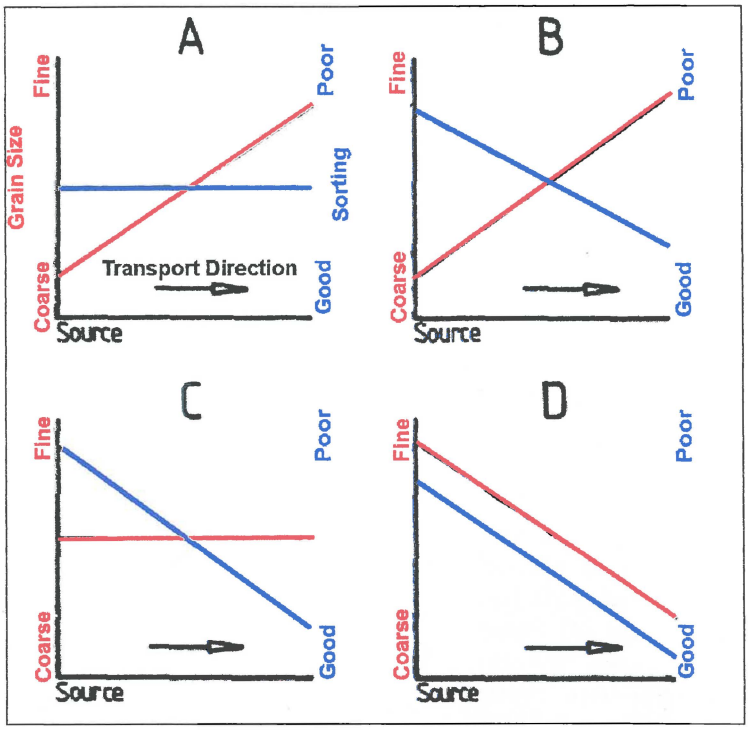


Figure 3.9 – *Spatial trends of mean grain size and sorting which are considered significant in terms of defining sediment transport direction (After Sunamura and Horikawa, 1972 and de Lange and Healy, 1990).* ***A*** *indicates a progressive fining of the sediment with no change in sorting;* ***B*** *indicates a fining of the sediment with improved sorting;* ***C*** *indicates no change in mean grain size with an improvement in sorting; and* ***D*** *indicates a coarsening of the sediment with an improvement in sorting.*

McLaren and Bowles (1985), relating skewness to transport direction sediment, note that sediment becomes more coarsely skewed (and finer grained) along its transport path, whereas the lag becomes more finely skewed and relatively coarser.

These models are used to assess potential sediment transport directions from textural patterns of sediments in the lower Whangarei Harbour.

3.4.4.2 Sediment Transport Inferred From Higher Moment Measures

The spatial distribution of the sorting parameter is shown in Figure 3.10, and skewness in Figure 3.11. The spatial variation in sorting and skewness is used, along with the mean grain size (Figure 3.4), to infer sediment transport directions based on the models of Sunamura and Horikawa (1972) (Figure 3.9) and McLauren and Bowles (1985) respectively.

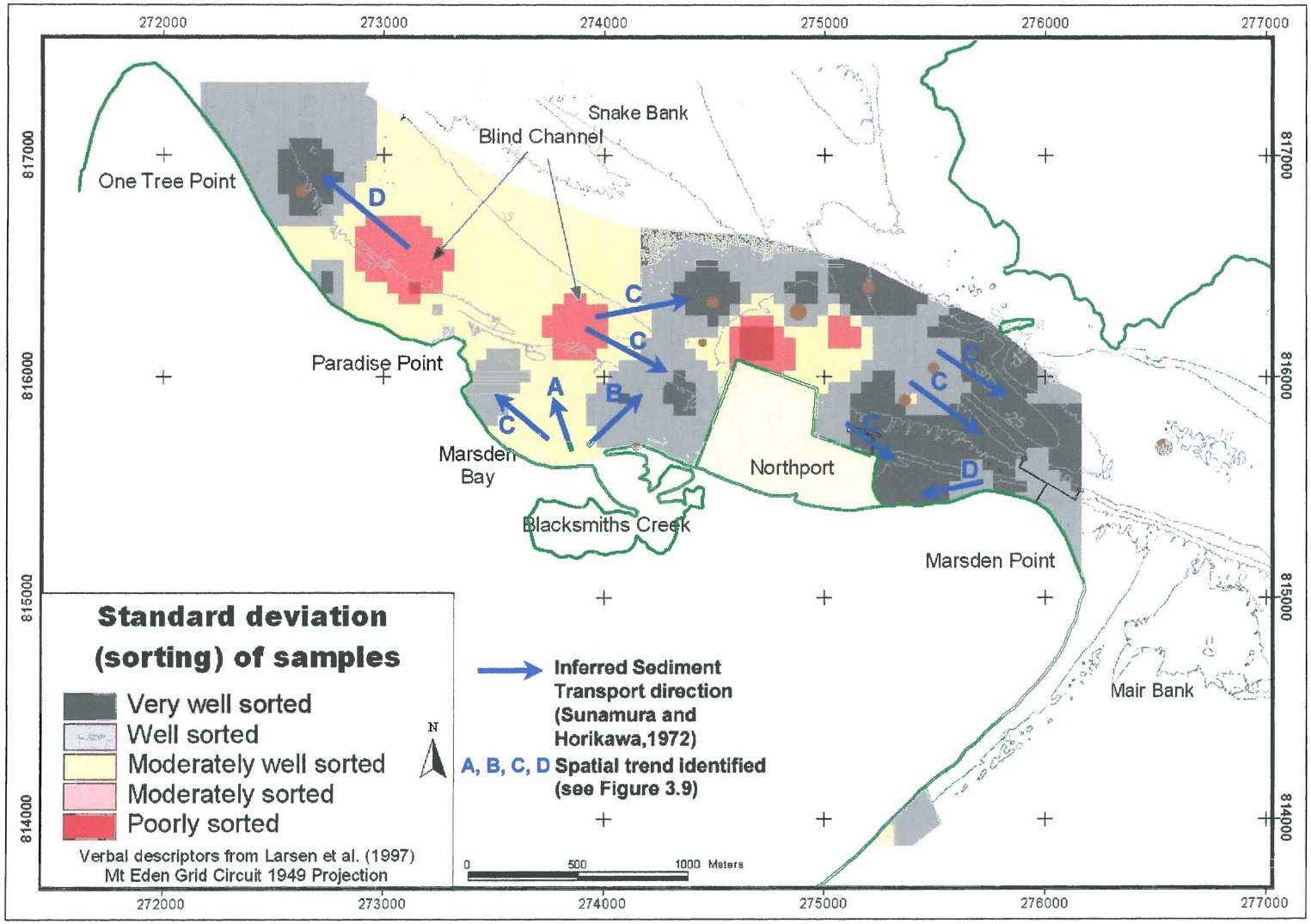


Figure 3.10 - *Spatial variation of standard deviation (measure of sorting) of the grain size distribution. Sediment transport directions inferred using theory of Sunamura and Horikawa (1972) (Figure 3.9) in conjuction with mean grain size (Figure 3.4). Dredge basin not considered due to 'mixing' of sediments.*

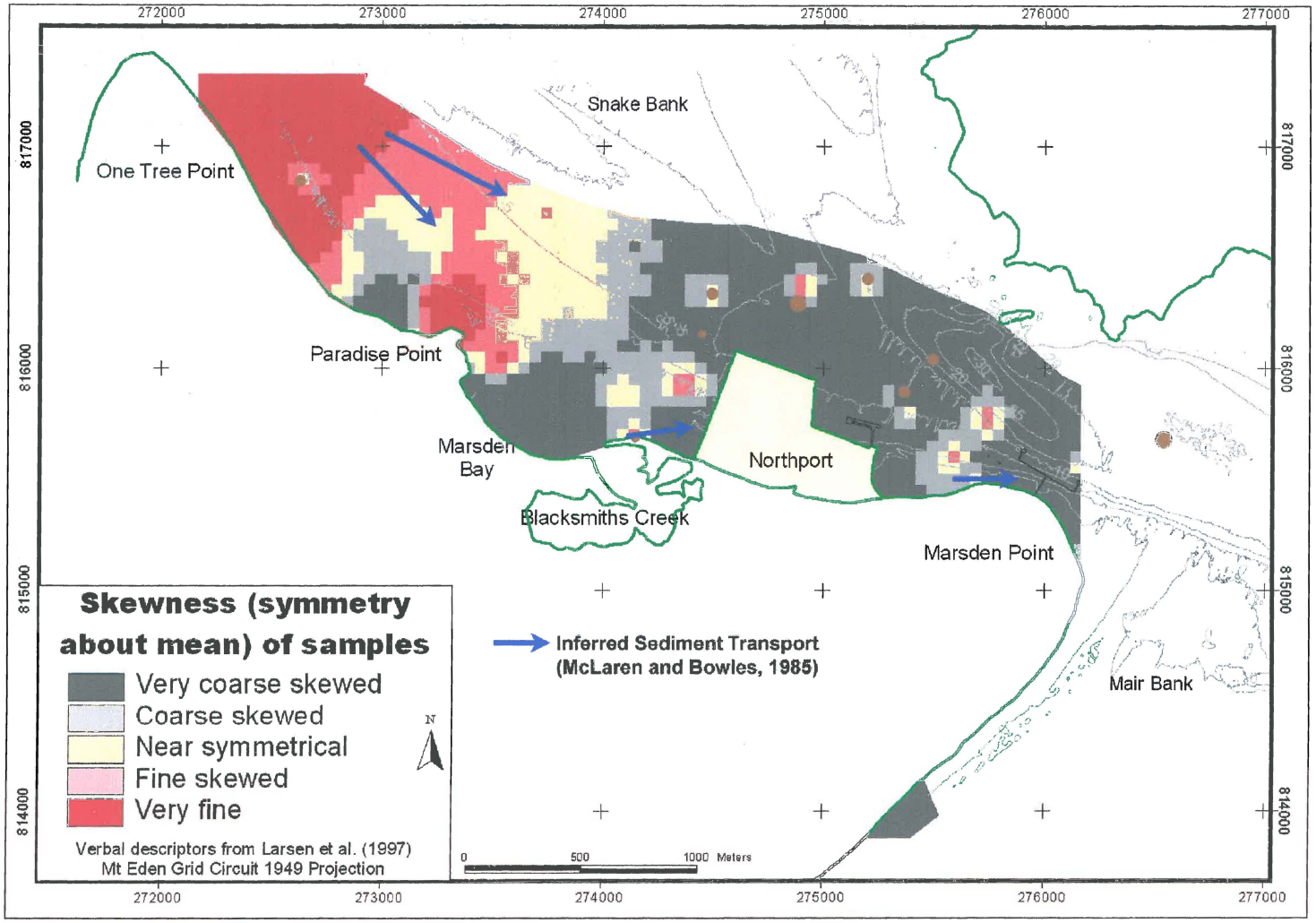


Figure 3.11 - *Spatial variation of skewness (symmetry about the mean) of the grain size distributions. Sediment transport directions inferred using theory of McLaren and Bowles (1985) (Section 3.3.3.1) in conjunction with mean grain size variations (Figure 3.4). Dredge basin not considered due to 'mixing of sediments.*

Sediments in the dredge basin are moderately-to-poorly sorted (Figure 3.10) and are made up of a much greater proportion of very fine (Figure 3.8) and very coarse (Figure 3.5) sediments than surrounding locations. Possible explanations for the poor sorting in the dredge basin include:

i. mixing of sediments (and therefore grain sizes) as a result of sediment stirring and turbulence created by the operation of a cutter suction dredge. Sampling was undertaken two months after the completion of the dredging; and
ii. the dredging may have exposed coarse sediments. Accretion in the dredge basin (post dredging) is likely to be initially dominated by fine sediments preferentially transported. This would lead to a mixture of coarse and fine sediments, with a relative lack of *medium* sized sediments.

Dredge basin sediments have been excluded from any inference of sediment transport direction based on their textural properties due to the influences of factors other than sediment transport on the grain size distributions.

Both models indicate that sediments are accumulating against the western edge of the reclamation (Figures 3.10 and 3.11), both mathematical models of the area (Black, 1983; Barnett, 1997) predicted sedimentation in this region near the dredge basin.

The two sediment textural models present conflicting directions of sediment transport near the shore between Northport and the NZRC jetties, the methods of Sunamura and Horikawa (1972) indicate transport toward Northport, while those of McLaren and Bowles (1985) indicates transport toward the NZRC jetties.

On the beach face and inter-tidal terrace of Marsden Bay and One Tree Point–Paradise Point, the model of Sunamura and Horikawa (1972) indicates longshore movement of sediment in a northwesterly direction, towards Paradise Point and One Tree Point respectively.

A general down harbour movement of sediment is identified in the deeper areas of the harbour near Northport (Figure 3.10) and also closer to One Tree Point (Figure 3.11).

3.5 Summary

- A surficial sediment textural survey undertaken in the lower Whangarei Harbour and its beaches has provided essential baseline data on sediment textural properties in the region.

- Sediments of the lower Whangarei Harbour are consistent with properties observed by Schofield (1975) in his Hauraki (B) facies.

- Shell lag sediments exist in very similar locations to those in identified in a previous survey conducted in 1983 by Black (1983).

- Mean grain sizes for the region are broadly fine sands, with coarser sediments in the dredge basin. This pattern is consistent with previous investigations (Millar, 1980). Coarser sediments are also found along the beach face from Marsden Bay to One Tree Point.

- Dredge basin sediments are made up of a much more even distribution of grain sizes than elsewhere in the lower harbour. It is concluded that agitation of sediments, due to dredging activities, has mixed sediments in the dredge basin resulting in the more even distribution of grain sizes.

- Sediments are being transported in an easterly direction and are accumulating against the western edge of the Northport reclamation.

- Sediment is being transported in a northwesterly-direction along the beach face of Marsden Bay and One Tree Point – Paradise Point.

- There is ambiguity as to the direction of sediment transport along the beach face and inter-tidal terrace between Northport and the NZRC jetties.

- There is a general down harbour movement of sediment in the channels and deeper areas of the harbour.

4 MEDIUM – LONG TERM COASTAL CHANGE SURROUNDING MARSDEN POINT

4.1 Introduction

'A review of historic maps and photographs is mandatory to fully understand the nature and processes at work, evolutionary trends, and natural ranges of variability' (USACE, 2002).

The principal tool in recognising the changes involved in shaping the coast is observation of the changing features and comparisons with historical records (Gorman et al., 1998; White, 1998). Aerial photographs provide a wealth of useful information for the interpretation of geologic coastal processes and coastal evolution. A Geographic Information System (GIS) is used to facilitate the consolidation of thirteen aerial photographs of the Marsden Point – One Tree Point shoreline recorded in 1984 and 2000/2001. Measurements are then made of changes in linear distance and areal extent of beaches and near-shore features. These changes are used to infer sediment transport directions and underlying patterns of shoreline advance and retreat.

4.2 Previous Investigations and Data Available

Aerial photographs of the lower Whangarei Harbour from 1942, 1950, 1966, 1971 and 1979 have previously been investigated for changes in the dune line and channel margins (Healy, 1980). Cliff cutback rates at 190 sites from One Tree Point to Marsden Point have been investigated using aerial photographs from 1942 to 1997 and more recently with GPS measurements (Gibb, 1998).

Rather than repeat the work of Healy (1980) and Gibb (1998), more recent photographs (detailed in Table 4.1) are analysed. Healy's (1980) historical trends are compared with changes occurring in the 20 years since his work and Gibb's (1998) long-term cliff retreat rates are compared with more recent beach and cliff movement trends using independent data sources.

Northport Ltd made several aerial photographs available for this study. Photographs used are documented in Table 4.1 and illustrated in Appendix B.

Date	Colour	General Location	Altitude
20/2/84	Black and White	Marsden Bay	
20/2/84	Black and White	Northport	
20/2/84	Black and White	Bream Bay Beach	
19/12/84	Black and White	One Tree Point	
19/12/84	Black and White	Marsden Bay	
19/12/84	Black and White	Northport	
9/12/00	Colour	One Tree Point	3250ft
9/12/00	Colour	Blacksmiths Creek	3250ft
9/12/00	Colour	Mair Bank	3250ft
5/1/01	Colour	One Tree Point	7500ft
5/1/01	Colour	Northport	7500ft
5/1/01	Colour	Mair Bank	7500ft
5/1/01	Colour	Marsden Bay	7500ft

Table 4.1 - *Aerial Photographs available for analysis*

4.3 Methods

4.3.1 Overview of Procedures

Aerial imagery has been used for detailed investigation of coastal processes and landforms since 1934 (O'Regan and Chalmers, 1993). O'Regan and Chalmers (1993) provide a history of the use of aerial photographs in assessing coastal shoreline changes. The reader is also referred to Dolan et al. (1980), Crowell et al., (1991 and 1993), Dolan et al., (1991), Fenster and Dolan (1993) and Gorman et al. (1998) for a summary of various techniques to estimate shoreline change from historical data.

Seasonal beach width variations and other short-term changes should be filtered out of the record. Ideally the best approach is to use only aerial photographs from the same season, preferably summertime, when the beach is exposed at its maximum width (Gorman et al., 1998). The current photographs are all taken during the summer season (Table 4.1). The range of photographs used for analysis (approx 20 years) is in the range of medium term, slightly less than that recommended by Dolan et al. (1991) and Crowell et al. (1993) to determine long term trends. Long-term trends however will be able to be established by considering the findings of Healy (1980) and Gibb (1998).

Photographs (Table 4.1) were scanned at a resolution of 600dpi, with a flat bed Microtek® scanner. Images were saved an uncompressed TIFF image files and imported to ArcGis® 8.

The photographs underwent the following phases:

i. Rectification and registration;
ii. Photo-Interpretation and shore line delineation;
iii. Classification of changes and
iv. Change analysis and presentation.

4.3.2 Registration and Rectification

In order to compare objects in one image to the same objects in another image (taken at a different time), it is necessary to locate them in space such that they accurately overly mapped features. Photographs must be registered to a common datum and coordinate system.

Land Information New Zealand's (LINZ's) digital data set of topographic features for the Northland region was used as the base on which to register the images. The data set contains information on the location of roads, fences, coastlines, mangrove areas, pipelines, wharves, prominent buildings etc and was thus well suited to the task. The LINZ data set is referenced to the Universal Transverse Mercator Projection system in Zone 60 South. By using this data set as the reference, the images were registered to the same projection.

ArcGis 8® and specifically its geo-referencing extension was used for the registration and rectification process. With both the LINZ data set and an image displayed, Ground Control Points (GCP), which were easily identifiable in both the photograph and the LINZ data, were identified and linked. It is critical in this process to have a significant number of evenly distributed points. Locations chosen were point definable features (to minimize errors in both the x and y directions) (Crowell et al., 1991), flat lying, all near the same elevation and as close to the shore as possible.

An example of the GCPs used is shown in Figure 4.1.

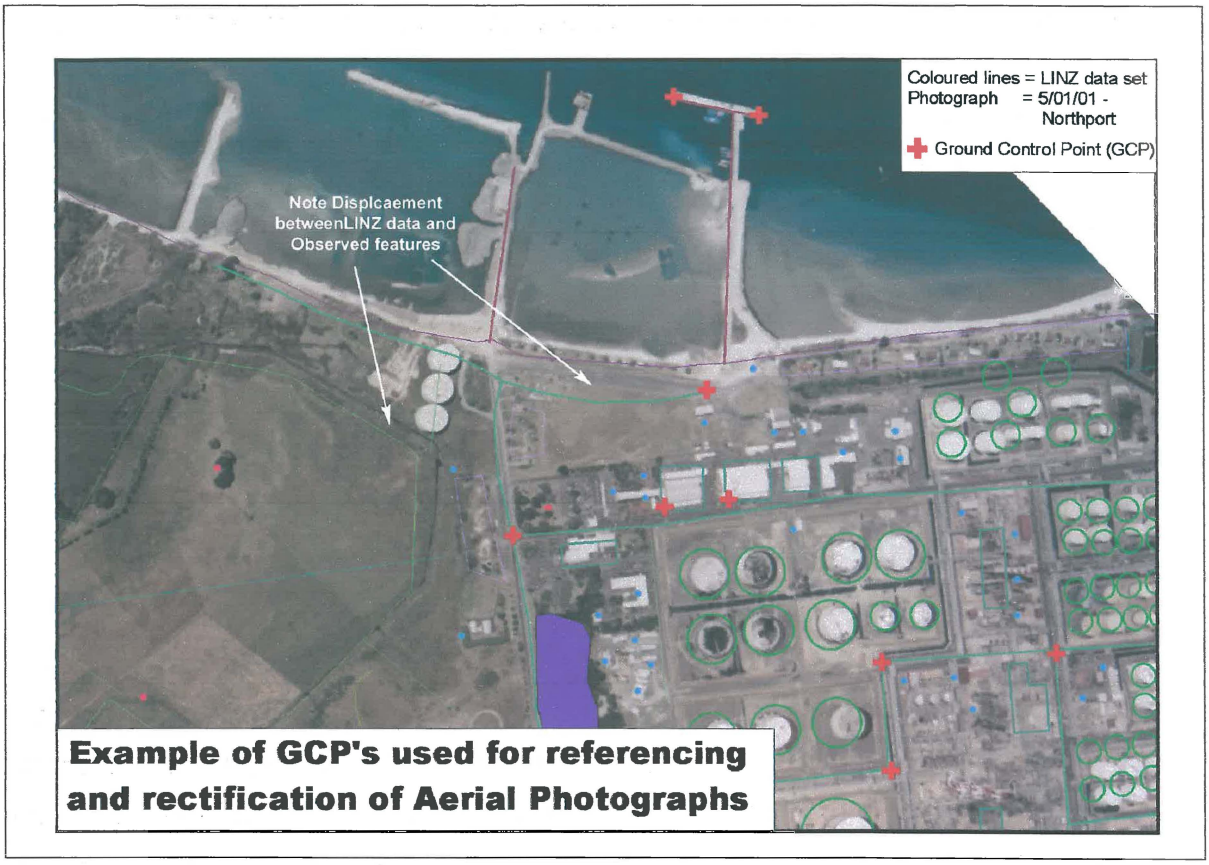


Figure 4.1 - *The GCPs used were picked to cover as much of the image as possible and to represent flat lying and point-definable features.*

Between 12 and 39 GCPs were identified for each photograph. Locations of GCPs used for each photograph are detailed in Appendix B.

The image was then subjected to the rectification process within ArcGIS 8®. Rectification *'warps'* an image, utilising a polynomial transformation whereby the original image is '*shifted, rotated, scaled and squeezed – to provide the best fit with the given control points'* (Novak, 1992). ArcGIS® provides the option of using either a conventional or a higher order polynomial transform, if enough GCPs are specified.

Conventional transformations (first order) warp the image uniformly across the entire image, whilst higher order polynomial transformations apply increasingly more and varied amounts of '*warping*' throughout the image. While the use of a higher order polynomial can offer superior accuracy, it was found to be highly dependent on the location of the GCPs used.

Photographs were transformed using the most appropriate affine transform, determined visually by the researcher. Often it was found that due to the restriction of GCPs to the land area of the image, a higher order transform, could badly manipulate other areas of the image. The use of higher order transforms was therefore restricted to images where many GCPs could be distributed throughout the entire image (Appendix B).

Once GCPs had been identified and the method of transform decided, the image was subjected to a pixel-level re-sampling to create the geo-referenced and rectified image file. Appendix B contains the rectified and geo-referenced images, along with appropriate co-ordinates.

4.3.3 Errors in the Rectified Geo-Referenced Images

Rectification based on polynomials is inferior to methods using projective transformation and differential rectification, as polynomial rectification does not adequately correct for relief displacements (Novak, 1992; O'Regan and Chalmers, 1993). O'Regan and Chalmers (1993) note however that relief displacement errors are small when maximum elevation differences are less than 9 m in magnitude. The One Tree Point sea cliffs (the highest relief in the area) are of the order of 6 m in elevation, within this range.

The diagnostic parameter in the rectification process is the Root Mean Square (RMS) error. RMS values for the rectified photos ranged from 5 to 12 m (Appendix B). When compared with values obtained by O'Regan and Chalmers (1993) at Te Puru, these errors seem high. The most obvious explanation is the quality of data used as the base for the rectification.

O'Regan and Chalmers (1993) had the advantage of cadastral data, which detailed each parcel of titled land at a much higher level of accuracy than the LINZ data set which had been digitised from 1:50,000 topographic map sheets. Any errors in the location of the features on the topographic map sheets, along with any errors from the digitising process undertaken by LINZ, are carried forward and into the current rectification process.

Observation of roads, fence lines and buildings in the LINZ data set in Figure 4.1 indicate that there are indeed significant errors in this set of data. This reduces the analytic capability of the rectified photographs.

To obtain a secondary estimate of these errors, fixed, non-moving features such as road centrelines and wharves were digitised from each of the rectified photographs (Figure 4.2). Maximum displacements are of the order of 7 m.

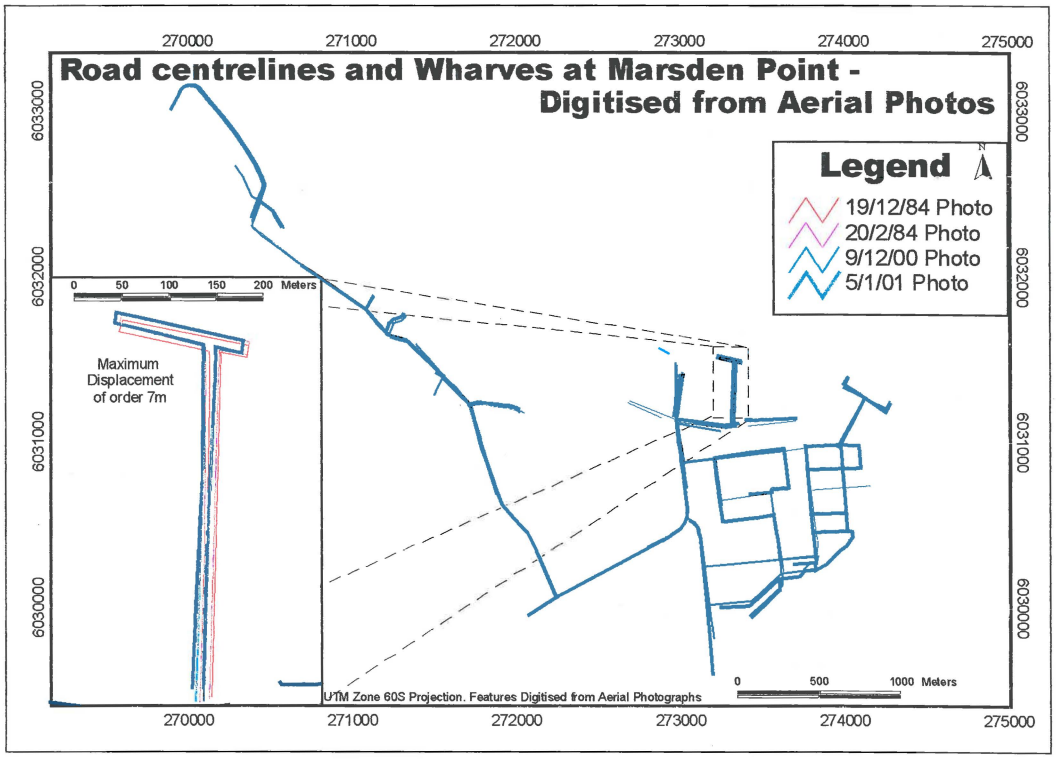


Figure 4.2 - *Road centrelines and wharves at Marsden Point, as digitised from Aerial Photographs, as described in Table 4.1.*

With displacements of up to 7 m between geo-referenced images, comparisons between features digitised from the various photographs are severely limited. A comparison similar to the technique used by O'Regan and Chalmers (1993), where the absolute shoreline position and change was measured and illustrated photographs, is not appropriate given these errors.

Whilst the absolute position of features in the rectified images contains these errors, each image pixel still represents a specific area on the ground. The physical distance represented by each pixel is not subject to this *'absolute position'* error. Using this information and a different approach, based generally on techniques documented by Gorman et al. (1998) valid comparisons between the 1984 and 2000/2001 photographs can still be made.

4.3.4 Shore-line Delineation

The shoreline is defined as the interface between land and water (Dolan et al., 1980). A primary consideration with aerial surveys is the interpretation of the high-water shoreline position (Gorman et al., 1998). Challenges arise as the shoreline position varies through time. The definition of Dolan et al. (1980) is somewhat inadequate in this situation as it fails to account for the dynamic nature of coastal water levels (waves, tides, storm surge, run-up, etc.). It must be recognised that the instantaneous shoreline position may not represent normal or average conditions. Over short time scales, tidal stage, local weather and wave conditions, and beach slope can influence the shoreline position.

Due to the dynamic nature of the shoreline, most coastal researchers use shoreline indicators (Boak and Turner, 2003). A shoreline indicator is a proxy based on a visually discernable feature used to represent actual shoreline position. Examples of indicators that can be used include:

i. instantaneous water line;
ii. groundwater exit point;
iii. current run-up maximum;
iv. previous high tide line;
v. older high tide line and the
vi. storm - debris line.

(Boak and Turner, 2003)

In many situations the High Water Line (HWL) has been found to be the best indicator of the land-water interface at the coastline (Crowell et al., 1991). The HWL is easily recognisable in the field and can often be approximated from aerial photographs by a change in colour or shade of the beach sand or a line of seaweed and debris (Gorman et al., 1998). O'Regan and Chalmers (1993) used both the high water line and the seaward toe of the frontal dune as reliable indicators of the land-water contact.

The nature of the coastline in the One Tree Point, Marsden Bay region determines which indicator will be of most use for the rectified photographs. The One Tree Point area is characterised by a beach at the bottom of 5-6 m cliffs, making the use of a frontal fore dune impossible. The Marsden Bay area however, while not having large fore dune deposits is characterised by a small well vegetated bank approximately 0.5 – 1.0 m high.

Observation of the aerial photographs available for analysis reveals that the following can be reliably identified (Figure 4.3):

i. High Water Line (change in shade of beach sand);
ii. small vegetated bank (where it exists);
iii. cliff edge (One Tree Point); and the
iv. instantaneous water line.

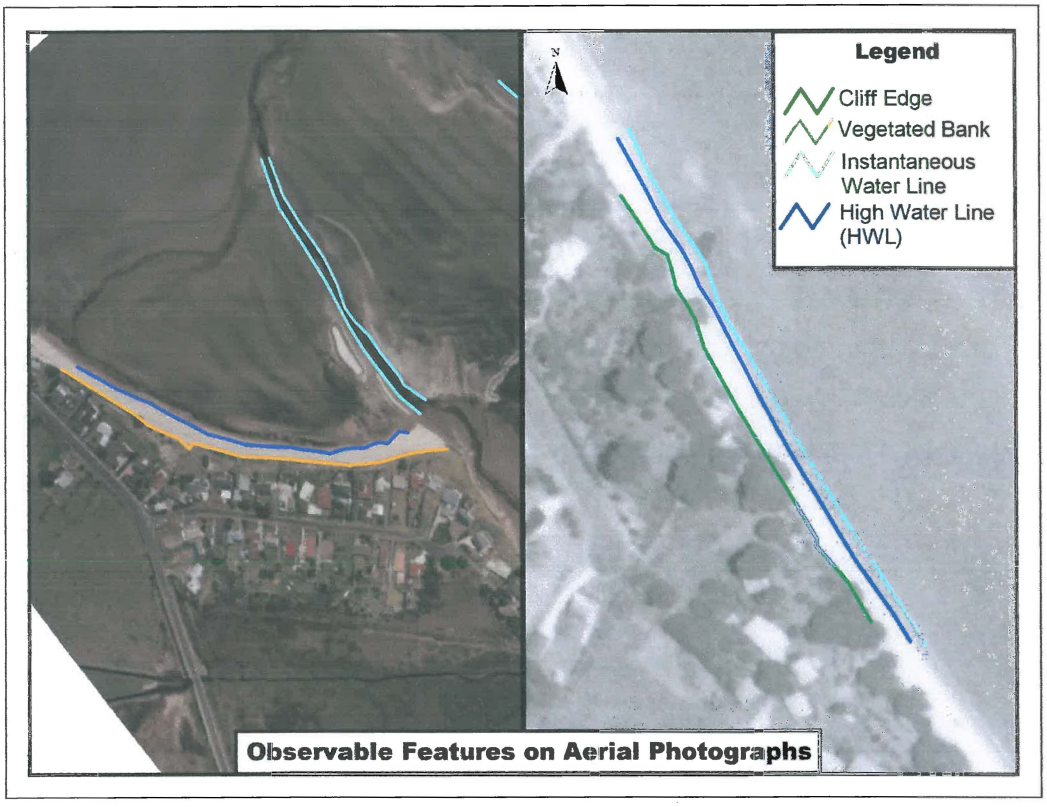


Figure 4.3 - *Aerial Photographs, showing identifiable indicators of shoreline movement.*

The use of the HWL and (where available) the seaward toe of the fore dune reduces the influences of short-term changes in sea level. Conclusions can be drawn from photographs taken at an unknown tidal stage, as is the case with the current set of photographs.

Recent literature (Turner et al., 2000; Boak and Turner, 2003) has described pixel level techniques applicable to digital images to delineate the boundary between the wet and dry beach areas. The Pixel Intensity Clustering (PIC) method uses differences in the Hue (H), Saturation (S) and Value (V) to separate clusters in HSV space and hence define areas of 'wet' and 'dry' beach. As light penetrates a water surface wavelengths from the red end (~700 nm) of the spectrum are attenuated more rapidly than those from the blue end (~400 nm). The 'water' pixels are then coloured with a greater mixture of blue and green components (as the red has been absorbed), areas of dry sands will contain all three components (Boak and Turner, 2003).

An alternate Colour Band Divergence (CBD) technique works in the Red, Green, Blue (RGB) colour space to detect a shoreline where the red, green and blue pixels diverge between the 'wet' and 'dry' sand (Boak and Turner, 2003).

These methods are applicable to the more recent colour photographs, but not so to the older greyscale images as the pixels contain no 'colour' information, only a shade of black.

4.3.5 Methods of shoreline Analysis

Using methods described by Gorman et al. (1998) as a guideline, the coastline is divided up into segments based on the general orientation of the shoreline. Attention is also paid to natural features such as headlands, which form natural breaks between segments. Data pairs are generated from shoreline locations relative to some arbitrary axis system that can be easily established in each photograph. Baselines for the axis system are chosen so that segments are parallel to the shoreline and a standard Cartesian co-ordinate system is assigned to each segment.

The area surrounding Marsden Point is separated and dealt with individually due to its rapidly curving morphology. The One Tree Point – Marsden Bay coastal sector is divided into eight segments for analysis (Figure 4.4).

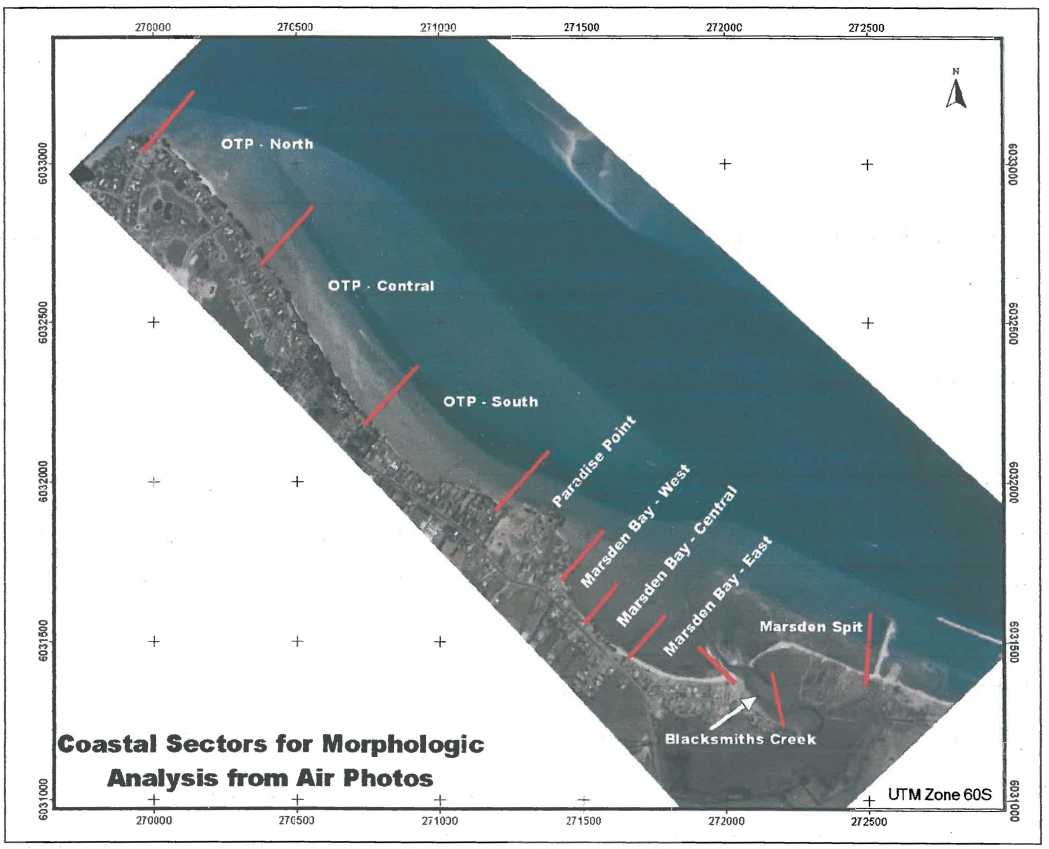


Figure 4.4 - *Location of areas for analysis of trends from Air Photographs and for comparison with Gibbs (1998) observations. OTP = One Tree Point.*

Areas are the same as that used by Gibb (1998). One Tree Point – north has not been used however, as there is no record of the sector in the 1984 photographs (Table 4.1 and Appendix B). Segments considered are:

i. One Tree Point – Central;
ii. One Tree Point – South;
iii. Paradise Point (not examined as characterised by cliffs and largely absent of beach);
iv. Marsden Bay – West;
v. Marsden Bay – Central;
vi. Marsden Bay – East;
vii. Blacksmiths Creek; and
viii. Marsden Spit.

Precise locations of the boundaries of these regions are provided in Appendix B.

Gibb (1998) determined cliff retreat rates at One Tree Point and foredune retreat in Marsden Bay from both air photographs and surveyed data. Vertical air photographs from 1942 and 1985 were used to fix the position of the dune line (Marsden Bay) and cliff top (One Tree Point) to an accuracy of ± 2 m (1942) and ± 0.75 m (1985). Professional surveyors surveyed the cliff position in 1997 to an accuracy of ± 0.10 m. Gibb (1998) calculated retreat rates at 190 equally spaced (20 m) transects between One Tree Point and Marsden Spit. Using only digitised cliff line position data near One Tree Point prevented Gibb (1998) from identifying any trends relating to the beach below.

4.4 Beach trends from air photographs – Results / Discussion

4.4.1 Marsden Point

Marsden Point dune line and channel movement between 1942, 1950, 1966, 1971 and 1979 has been analysed by Healy (1980). Nine transects perpendicular to the shoreline were created, with end point retreat rates being calculated. Similar techniques have been employed by Dolan et al. (1991), Fenster and Dolan (1993) and Gorman et al. (1998).

It is unfortunate that the exact locations of the transects are not provided. Where possible however (3 from 9 transects), the written explanation of transect location allowed reliable identification of the site and of transect angle allowing the re-measurement of rates in these areas. Figure 4.5 shows the location of transects used (positions provided in Appendix B).

Additional transects (A, B, C) provide further comparison, if only between 1984 and 2000 (2001). Lack of coverage of areas surrounding the NZRC jetty in the 1984 photographs (Appendix B) prevented any comparisons at this location.

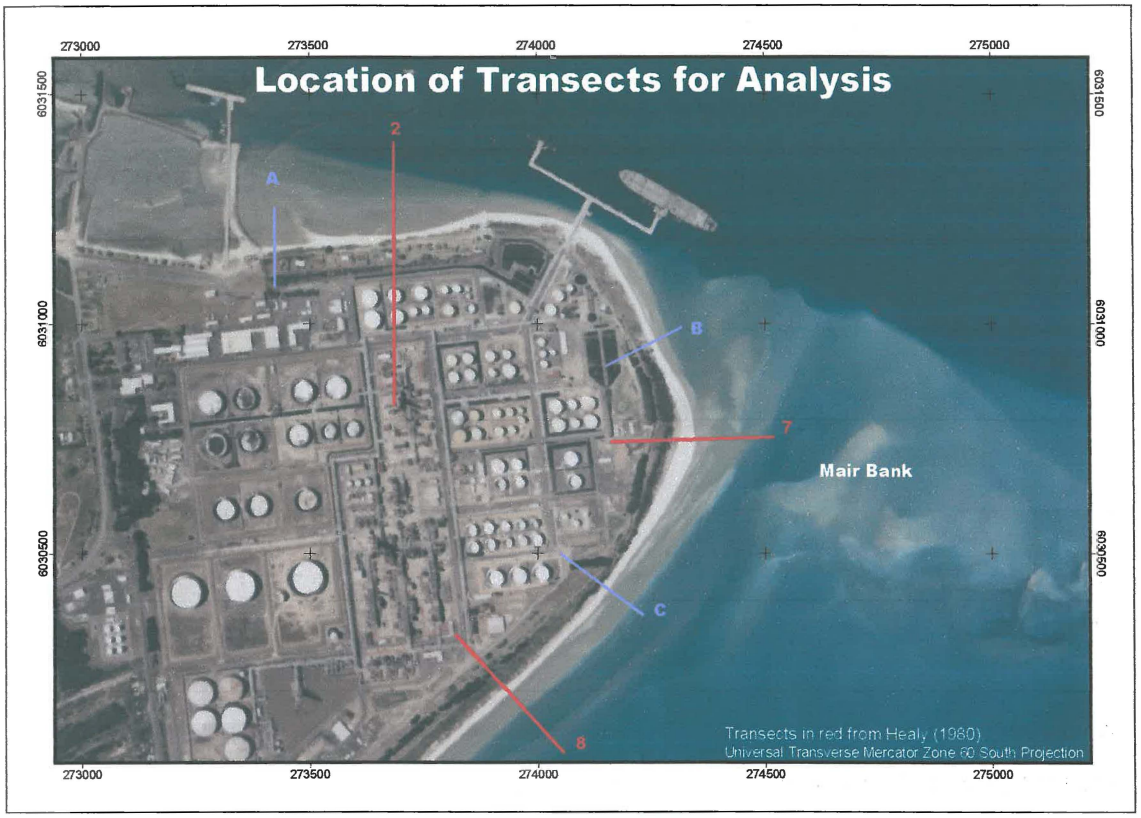


Figure 4.5 - *Location of Healy's (1980) transects that have been updated with analysis of photographs from 1984, 2000 and 2001 (in red). Additional comparisons have been made on three further transects (blue).*

Healy (1980) used the seaward toe of the foredune as an indicator to determine shoreline movement rates. To maintain consistency, the seaward edge of the foredune has been used for the current comparison. This line can be identified by the tonal contrast between the vegetation on the dune or small Bank and the sand of the beach (O'Regan and Chalmers, 1993) (Figure 4.3).

While some areas of Marsden Point have a well-formed dune (e.g. Bream Bay Beach), beaches inside the harbour lack a dune (in the sense of an aeolian feature composed of sand), e.g. Marsden Bay and the beach between the NZRC jetties and Northport. In these areas the smaller vegetated bank (0.5 – 1.0 m high) is used as the indicator.

Table 4.2 displays shoreline movement rates from Healy (1980), updated values and additional transects. Changes have been measured on both photographs of 9/12/2000 and of 5/1/2001. Minimal changes are expected in this 27-day period, providing an independent check on the accuracy of the measurements.

Transect	Location (UTM 60S)	Period	Net Change (m) - = retreat + = advance	Max Fluc. (m)	Rate (From Healy, 1980) myr^{-1}	Change 1984-2000 (2001)	Rate (1984-2000) myr^{-1}
A	273425mE, 6031161mN					**0.0**	**0.0**
2	*Due north in front of flare chimney* 273686mE, 6031186mN	*1942-1979*	*-7*	*15*	**- 0.19**	**-12.6 (-12.6)**	**- 0.79**
B	274258mE, 6030956mN					**+5.3 (+5.1)**	**+0.33**
7	*Eastern extremity of Marsden Point* 274312mE, 6030744mN	*1966-1979*	*+3*	*8*	**+ 0.23**	**+27.8 (+36.0)**	**+ 1.74**
C	274153mE, 6030425mN					**-12.0**	**-0.75**
8	*Off south-eastern corner of refinery storage tanks, near drain outlet* 273931mE, 6030200mN	*1966-1979*	*+8*	*8*	**+ 0.62**	**-2 (-1)**	**- 0.13 (limits of accuracy)**

Table 4.2 - *Air photograph analysis of change in dune line (Healy, 1980) and vegetation line (1984 – 2000 (2001)). Italicised data from Healy (1980) errors estimated at ± 2m. Data in bold from 1984, 2000 and 2001 photographs, measurement error ± 0.69m (pixel width).*

Transects 2, B and 8 exhibit good consistency between the values obtained from the 2000 and 2001 photographs.

Transect A, close to the old NHB wharf and the eastern edge of the Northport reclamation (Figure 4.5) showed no change over the 1984 – 2000 period (Table 4.2) (error estimate ± 1.5 m). Two hundred and fifty meters eastwards, the long-term trend of shoreline retreat at Transect 2 seems to be continuing. The rate appears to have increased from 1984 to 2000, however the change is within the fluctuations observed by Healy (1980) from 1942 to 1979 (Table 4.2). The data do not provide evidence for a change in trend, but rather a continuation of the long-term pattern of retreat.

Both transects B and 7, located adjacent the ebb tidal delta of Mair Bank (Figure 4.5) at the eastern extremity of Marsden Point show progradation of the vegetated dune line. The Transect 7 data show a discrepancy of 8.2 m in the values obtained by using photos taken only 27 days apart. Nonetheless, it is apparent this section of coast has experienced large-scale shoreline advance between 1984 and 2000. The change at transect 7 is larger than the fluctuations observed by Healy (1980) using a longer time period (Table 4.2).

These transects are located adjacent the ebb tidal delta of Mair Bank (Figure 4.5), which has shown to be variable in form and sediment volume (DHI, 1982a; Black and Healy, 1982; Black, 1983; Venus, 1984; and also in Chapter 6 of this thesis). Sediment accumulated on the southern and western edges of Mair Bank between 1959 and 1981 (DHI, 1982a; Black, 1983). The source of the sediment was deemed to be the eroding Bream Bay Beach and lower harbour in the region of the NZRC jetty (Black and Healy, 1982). The accumulation of sediment in the near-shore, adjacent transects B and 7 (Figure 4.5), could have provided the sediment necessary for the observed progradation of the shoreline.

Transect C, farther along Bream Bay Beach, experienced retreat of the dune line between 1984 and 2000, while transect 8 exhibited little change between 1984 and 2000. The change at transect 8 was within the accuracy of the method. It can only be concluded that the coastline here showed relative stability through the period 1984 to 2000.

4.4.2 One Tree Point – Central

The cliffs over this section of coast have been the most stable in the region with only 15% of measurements in this area exhibiting retreat between 1942 and 1997, at an average rate of 8 mmy^{-1} (Gibb, 1998). This measurement is in fact within the bounds of Gibb's (1998) errors, even though he does not acknowledge it (Section 2.8.2) and should be correctly interpreted as no measurable movement of the cliff face.

While the absolute positioning errors in the geo-referenced photographs are of the order of ±10 m, conclusions regarding the retreat rates of the cliff and the width of the beach below can be calculated with greater accuracy.

Measurement of the beach width is not dependent on the absolute position and hence is not subject to its errors. Any retreat of the cliff between 1984 and 2000 / 2001 will act to widen the beach.

The beach width was measured at 12 locations along the One Tree Point – Central shoreline, on the 1984, 2000 and 2001 photographs (Table 4.3). To provide a measure of accuracy, road widths were also measured on the three photographs.

Location (UTM60S)		Dry Beach Width (m)				
Easting	Northing	19/12/1984	9/12/2000	5/01/2001	Average Change	Rate (my^{-1})
270395.6	6032722.3	14.0	8.5	8.2	**-5.7**	**-0.36**
270415.9	6032688.4	12.5	9.5	8.7	**-3.4**	**-0.21**
270441.9	6032647.8	16.8	10.4	10.5	**-6.4**	**-0.40**
270472.4	6032600.3	12.0	8.0	8.1	**-4.0**	**-0.25**
270506.3	6032548.4	15.5	12.5	11.0	**-3.8**	**-0.24**
270536.8	6032498.7	17.3	8.2	6.1	**-10.2**	**-0.64**
270562.7	6032456.9	15.0	12.6	12.6	**-2.4**	**-0.15**
270594.4	6032401.5	10.6	5.9	5.6	**-4.9**	**-0.31**
270626.0	6032355.2	10.0	6.0	6.9	**-3.6**	**-0.23**
270657.6	6032303.3	10.5	9.7	9.2	**-1.1**	**-0.07**
270682.5	6032262.6	9.0	7.8	7.6	**-1.3**	**-0.08**
270715.2	6032223.1	8.3	5.3	5.0	**-3.2**	**-0.20**
		Average change (OTP- central)			**-4.1**	**-0.26**

Road width (m)			
19/12/1984	9/12/2000	5/01/2001	Average Change (apparent)
4.7	4.6	5.7	**0.5**
5.4	5.1	5.4	**-0.2**
4.9	5.0	5.4	**0.3**
5.9	6.2	6.4	**0.4**
6.2	6.2	6.4	**0.1**

Table 4.3 - *Beach width measured from vertical aerial photographs for One Tree Point–Central. Digitising and measuring error estimate from apparent change in road width (± 0.03 my^{-1}).*

Measurement of road widths indicates that the dry beach distances are accurate to within ± 0.5 m (Table 4.3), corresponding to two pixels (0.23m) in the images. Data pairs from transects indicate an average narrowing of 4.1 meters of the dry beach between 1984 and 2000 (2001).

Additionally the beach area was digitised in ArcView ® GIS, using the cliff edge and the wet-dry sand boundary. Measurement of the area of beach was calculated within the GIS for each photograph, along with the average beach width change (Table 4.4).

Date of Photograph	Area of Dry Beach (ha)	Average width change (m)
19/12/1984	0.78	N/A
9/12/2000	0.64	-2.1
5/1/2001	0.61	-2.5

Table 4.4 - *Width of dry beach, measured in Arc View GIS®, using digitised position of cliff and wet-dry sand boundary.*

Figure 4.6 shows the photographs used for the analysis and provides a graphic picture of the narrowing of the beach.

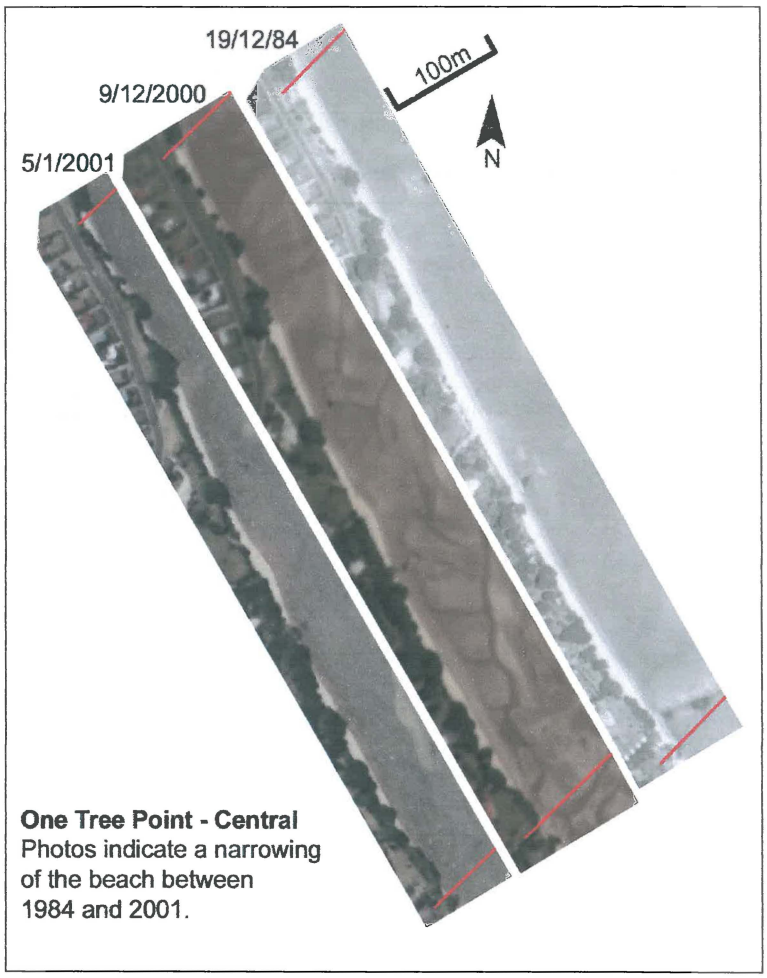


Figure 4.6 - *Air photographs showing the decrease in beach width at One Tree Point – Central from 1984 to 2001. All photographs have been maintained at a consistent scale, to indicate the change.*

The photograph of 9/12/2000 has been taken near the time of low tide, while the photograph of 5/1/2001 has been taken nearer high tide (Figure 4.6). Both photographs show the narrowing of the beach clearly, indicating the reliability of using HWL as an indicator of shoreline movement.

The lack of beach profile data for this region between 1984 and 1998 prevents an accurate estimate of the volume of sediment movement. While the area of beach loss can be calculated (Table 4.4), estimations of the vertical change in profile would be pure speculation. Morphologic evidence indicates that there has been a net loss of sediment for this region between 1984 and 2001.

While Gibb's (1998) data (digitised cliff lines rather than actual photographs) do not allow the identification of this trend, the importance of the beach in terms its protective effect on the cliffs was noted.

The location of the blind channel along this section of coast (Figure 4.4) was also digitised from the photographs. The channel displayed stability and no changes greater than the accuracy of the photographs was measured.

4.4.3 One Tree Point – South

The One Tree Point – south shoreline is characterised by a generally narrower beach and less stable cliffs, than the shoreline immediately to the north. Recent rates of cliff retreat have ranged between 10 and 100 $mmyr^{-1}$, with an average of 30 $mmyr^{-1}$ (Gibb, 1998). However, as noted previously (Section 2.7.2) while Gibb (1998) claims *'slower'* retreat rates, the methods used could only reveal patterns greater than 37 mmy^{-1}.

Measurement of beach widths from the 1984, 2000 and 2001 photographs indicate stability, with only one transect showing a slight reduction in beach width over the time period (Table 4.5). Figure 4.7 shows a graphic display of the changes.

Location (UTM60S)		Dry Beach Width (m)				
Easting	**Northing**	**19/12/1984**	**9/12/2000**	**5/01/2001**	**Average Change**	**Rate (my^{-1})**
270773.3	6032138	14.1	14.1	13.6	-0.3	0 (within errors)
270804	6032109	12.4	11.6	11.0	-1.1	0 (within errors)
270835.9	6032077	12.4	8.0	7.9	-4.5	-0.28
270871.8	6032042	10.7	9.7	9.3	-1.2	0 (within errors)
270901.7	6032013	6.2	7.0	7.2	+ 0.9	0 (within errors)
Average change (OTP- south)					**-1.2**	**0 (within errors)**

Table 4.5 - *Beach width measured from Air Photographs for One Tree Point – South.*

Both the photographs (Figure 4.7) and a plot of beach width for the area (Figure 4.8) indicate a narrowing trend in the southeast direction.

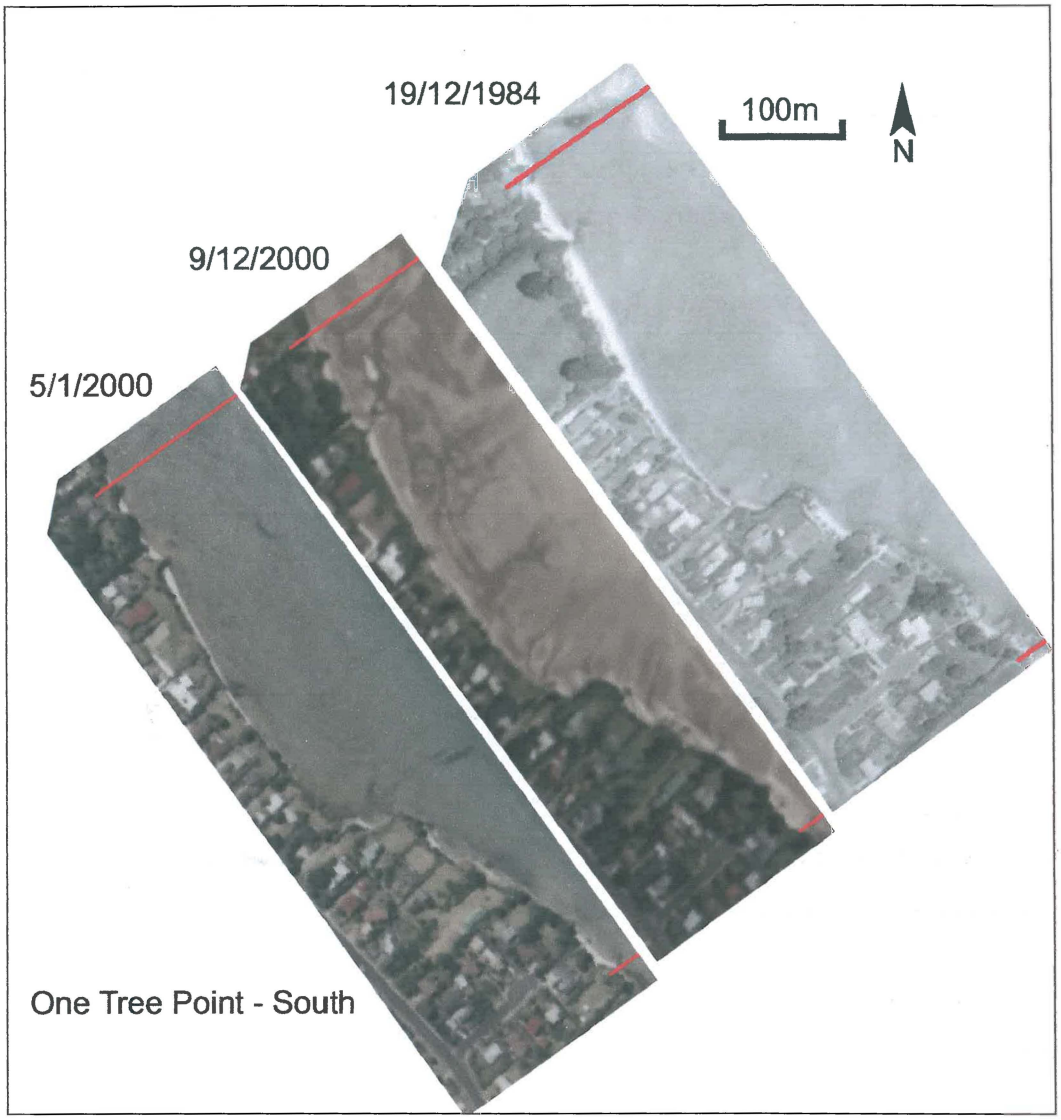


Figure 4.7 - *Air Photographs showing the decrease in beach width at One Tree Point – south from 1984 to 2001. All photographs have been maintained at a consistent scale, to indicate the change.*

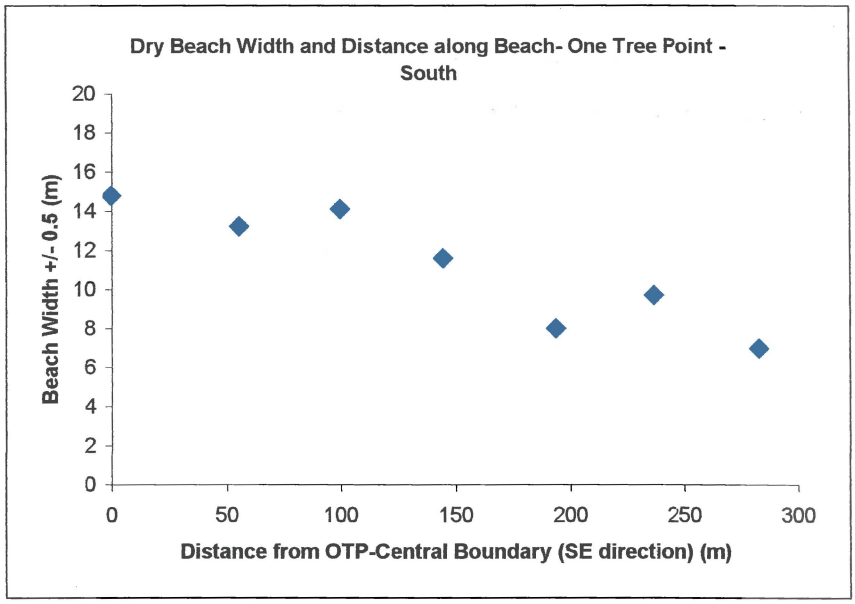


Figure 4.8 - *Beach width at One Tree Point- south indicates a trend toward narrowing in a southeast (down harbour) direction, indicative of longshore sediment transport to the northwest (up harbour).*

The narrowing trend can be used as evidence of a net drift direction toward the northwest. Observation on a smaller scale however, reveals beach advance on the northwest side of sandstone promontories (Figure 4.9), indicating a drift to the southeast. Gibb (1998) describes the drift direction along the coast here as directed southeast, while noting the narrowing beach he fails to explain the reasons for the morphology.

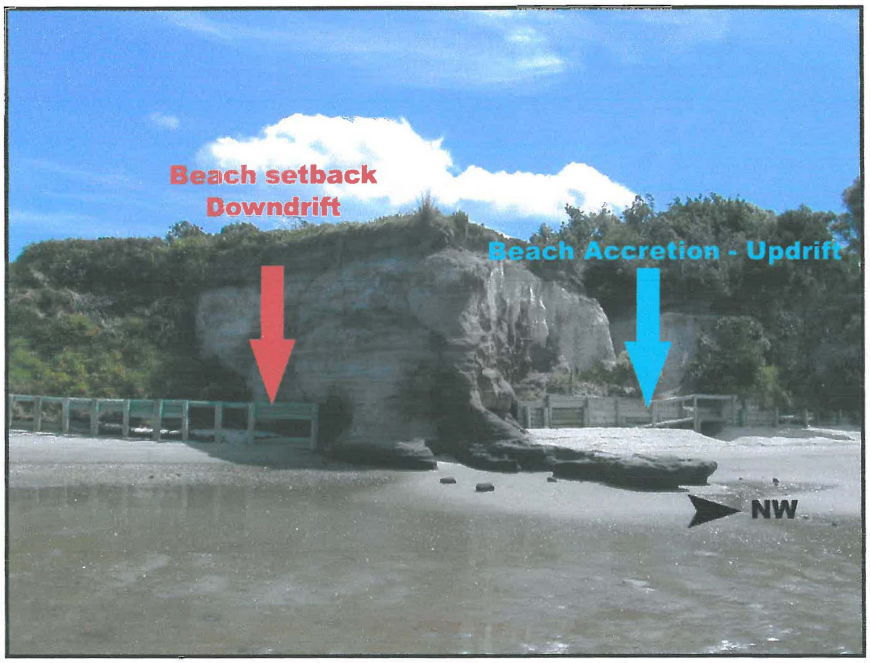


Figure 4.9 - *Photograph showing sediment accumulation on the northwestern side of a rock promontory.*

Field observations revealed that timber and concrete sea walls have been constructed along the southeastern section of the One Tree Point shoreline, where the beach is narrowest. A potential reason for the narrowing of the beach in a southeast direction is due to the action of these sea walls. The effects of seawalls on beaches are well documented and can include enhanced erosion and scour rates (Kraus, 1988; Kraus and McDougal, 1996).

It is possible that the narrow or absent beach on this south eastern section, has allowed the sea to break against the sea cliffs and sea walls, promoting the erosion of the beach through scour and the reflectance of wave energy.

4.4.4 Marsden Bay – West and Central

Shoreline movement rates along Marsden Bay have previously been evaluated using aerial photographs and the seaward toe of the fore dune as an indicator (Gibb, 1998). Findings from this analysis are summarised in Table 4.6

Marsden Bay West		
Date	**Duneline Movement (my^{-1})**	**Notes**
1928 – 1942	-0.71 - -0.92	Beach evident
1942 – 1955	-0.23	Beach evident
1955 – 1998	No Movement due to seawall	Seawall built 1955, Beach absent
Marsden Bay Central		
1928 – 1942	+0.36 - +0.71	
1942 – 1985	-0.07 - +0.16	
1990 – 1998	-0.125 - -0.4375	Seawall built in 1990 and backfilled

Table 4.6 - *Shoreline rates of change from Gibb (1998).*

Analysis of the 1984, 2000 and 2001 aerial photographs (Figure 4.10 and Table 4.7) provides no further information at Marsden Bay West, there is no 'dry' beach present adjacent to the seawall. A small pocket beach (Table 4.7, Location 1) exists at the northern end of Marsden Bay. This sediment is somewhat protected from sand removal by longshore drift by the groyne effects of Paradise Point to the north and a boat ramp to the south. This sandy area has not changed significantly between 1984 and 2000 (Table 4.7).

Marsden Bay West							
Location (UTM60S)		**Dry Beach Width (m)**					
Easting	**Northing**	**20/2/1984**	**19/12/1984**	**9/12/2000**	**5/01/2001**	**Avg. Change**	**Rate of change (my-1)**
271429	6031612	8.1	7.7	7.9	7.8	-0.05	0 (within errors)
271453	6031562	0	0	0	0	0	0
271477	6031529	0	0	0	0	0	0
271514	6031489	0	0	0	0	0	0
Marsden Bay Central							
Location (UTM60S)		**Dry Beach Width (m)**					
Easting	**Northing**	**20/2/1984**	**19/12/1984**	**9/12/2000**	**5/01/2001**	**Avg Change**	**Rate of change (my-1)**
271525	6031474	0	0	0	0	0	0
271544	6031445	10.2	11.4	7.4	7.5	-3.35	-0.21
271565	6031423	11.2	11.9	4.5	4.1	-7.25	-0.45
271589	6031405	14.5	13.3	6.0	5.4	-8.2	-0.51
271611	6031389	13.5	13.4	7.9	8.3	-5.35	-0.33
271632	6031374	14.6	15.1	17.4	17.8	+2.75	+0.17
271657	6031359	11.2	10.8	9.7	10.2	-1.05	0 (within errors)

Table 4.7 - *Shoreline change rates along Marsden Bay West and Central, 1984-2000(1).*

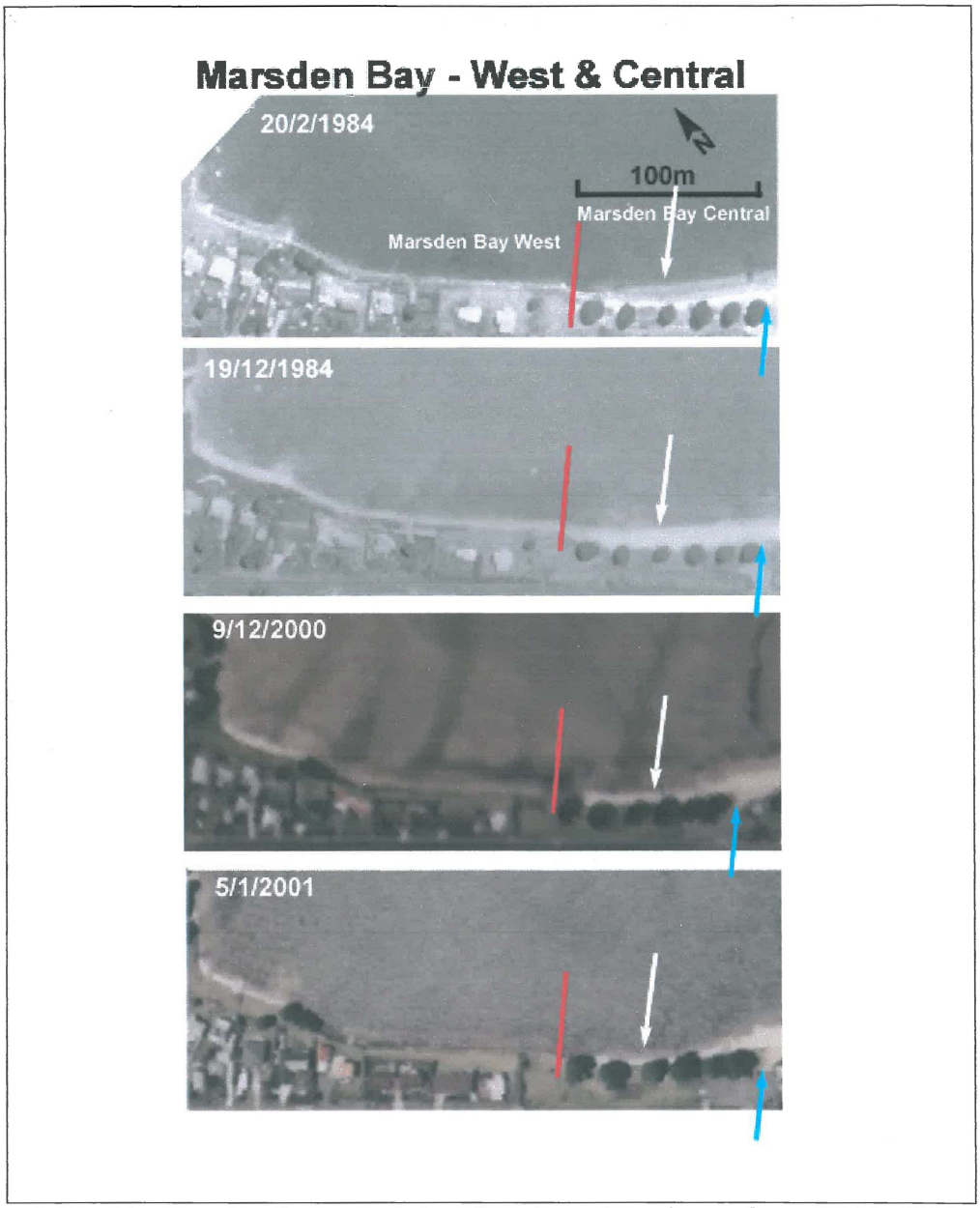


Figure 4.10 - *The Marsden Bay – west shoreline shows little change from 1984 to 2001, due to the absent beach and sea wall present. Farther along however the white arrows indicate beach narrowing adjacent the pohutukawa trees at Marsden Bay Reserve. Blue Arrows show location of minor shoreline advance near boat ramp.*

The sea wall at Marsden Bay-West has halted the previous erosive trend (Tables 4.6 and 4.7). This has been at the expense of the adjacent beach. At high tide, waves break against the sea wall. Wave reflection from the seawall has prevented the natural recovery of the beach through accretion (Gibb, 1998).

Marsden Bay – Central is adjacent to 7 pohutukawa trees planted in 1954 (Figure 4.10) (Gibb, 1998). The shoreline is cut by a concrete boat ramp and storm water drains which act as groynes, trapping sediment. The beach adjacent to the pohutukawa trees is protected by a continuous vertical timber seawall constructed in 1990 below the line of Mean High Water Springs (MHWS) and backfilled (Gibb, 1998).

The measured values of changes in beach width at Marsden Bay - Central, compare well with Gibbs (1998) values of dune line movement over the same period (Tables 4.6 and 4.7). Slight widening of the beach is noticeable in the area surrounding the boat ramp, which bisects the beach at the southeastern end of the area.

Figure 4.10 shows the narrowing of the beach in front of the pohutukawa trees (white arrows) and minor widening near the boat ramp (blue arrows).

Storms have caused significant periodic erosive events along the Marsden Bay central coastline. In 1997 tropical cyclone Drena damaged the sea wall and eroded the backfill behind the wall by between 1 and 3.5 m (Gibb, 1998).

4.4.5 Marsden Bay – East and Blacksmiths Creek

The 420 m shoreline along eastern Marsden Bay is adjacent to 20 residential properties. Houses were built in the early 1960's and protected by various seawalls constructed between 1960 and 1997 (Gibb, 1998). Values of dune line movement determined by Gibb (1998) are presented in Table 4.8. It is notable that there is some variation between the western and eastern areas of Marsden Bay – East.

	Marsden Bay East	
Date	**Duneline Movement (my^{-1}) (Western End)**	**Duneline Movement (my^{-1}) (Eastern End)**
1928 – 1942	+0.71 - +0.193	-0.36
1942 – 1985	+0.01 - +0.07	-0.05 - -0.13
	Blacksmiths Creek Channel Position	
1942 – 1958	Stable position, discharging straight into Marsden Bay	
1958 – 1967	Channel migrates 50m west along shore before swinging into bay.	
1967 – 1984	Channel migrates a further 30m west along the shore (now 80m)	
1984 – 1992	Channel migrates a further 120m west (now 200m)	
1992 – 1998	Channel migrates a further 80m west (now 280m along shore)	

Table 4.8 - *Dune-line movement at Marsden Bay East and Blacksmiths Creek (Gibb, 1998).*

The trends of progradation (western end) and retreat (eastern end) in Gibbs (1998) data can be explained by the meandering of the Blacksmiths creek channel (Figure 4.11). The shoreline along Blacksmiths creek was '*hardened*' with a vertical timber sea wall in 1960, despite the shoreline being relatively stable (Gibb, 1998). This may have acted to destabilised the creek and instigated its migration to the west, along the shoreline. The channelling of the flow, created by the hardened shoreline, prevented the creek from establishing its natural meander pattern across the inter-tidal flats.

The erosion Gibb (1998) noted along the eastern end of Marsden Bay (Table 4.8) can be explained by this migration of Blacksmiths Creek channel.

Significant works were undertaken in the area in 1999 (Stevens, 1998 and 1999) consisting of:

i. excavation of a new channel for Blacksmiths Creek through a recent breach in Marsden Spit;
ii. building a 95 m rock training wall alongside the new channel;
iii. building an artificial bird roosting island;
iv. placement of sand on Marsden Spit;
v. beach nourishment at Marsden Bay – East; and
vi. extension of storm-water pipes at Marsden Bay – East.

The new channel, training wall, roosting island, change in Marsden Spit and beach nourishment at Marsden Bay can be seen in Figure 4.11. The training wall and extension of the storm-water pipes were designed to act as groynes and trap the nourished sediment in Marsden Bay.

While initial proposals for the nourishment at Marsden Bay – East were for between 50,000 m^3 and 20,000 m^3 of sand (Stevens, 1998) the actual volume placed was 8,000 m^3 (Stevens, 1999; pers. comm. G. Mullooly) of material dredged from Shell Cut Reach, just up harbour of One Tree Point.

The nourishment was consented for the entire length of Marsden Bay, however due to the limited amount of sand available only the section from Marsden Spit to the Boat Ramp (Figures 4.10 and 4.11) (Marsden Bay Central and East) (Stevens, 1999).

Material from the excavation of Blacksmiths Creek (~1,000 m^3) was placed on Marsden Spit (750 m^3), used for the artificial bird roosting island (150 m^3) and for the training wall (100 m^3) (Stevens, 1999).

To graphically show the changes that occurred polygons, of change were created. The distribution of many houses close to the shoreline at Marsden Bay East allowed cropped aerial photographs to be more accurately geo-referenced, using house corners as control points. The RMS error of the cropped photographs is $\pm$ 1.5 m, allowing the HWL to be digitised and polygons of change created, using similar techniques to those applied by O'Regan and Chalmers (1993).

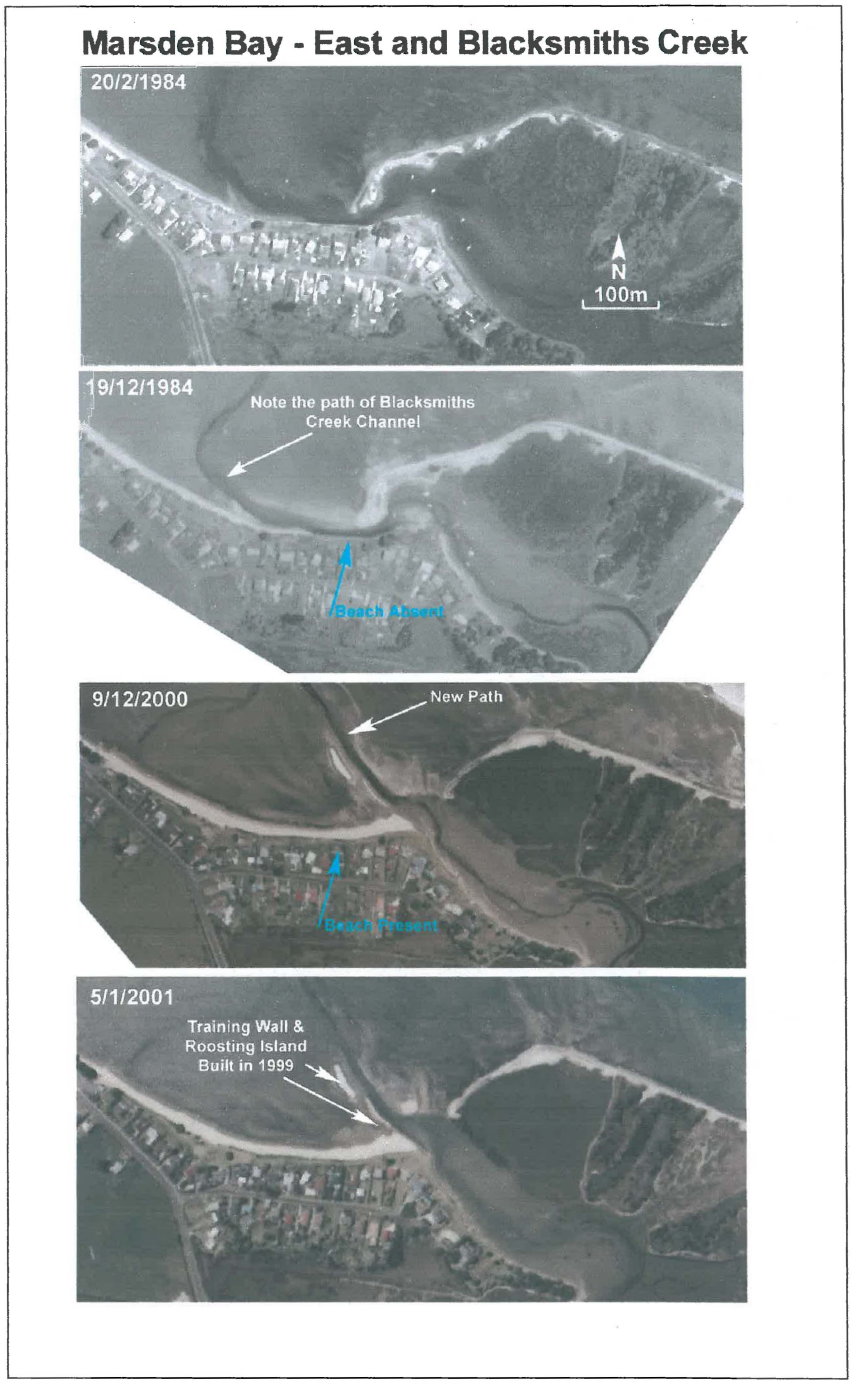


Figure 4.11 - *In 1984 the path of Blacksmiths Creek channel ran along the shoreline of Marsden Bay, preventing any beach from forming. The channel position was 'fixed' in 1999 with a rock-training wall and roosting island.*

This method is more effective than the *'transect'* method, used for the One Tree Point and Marsden Bay West/Central shoreline, in areas that show pronounced shoreline re-orientation (O'Regan and Chalmers, 1993) as it is not limited by needing to place transects perpendicular to a considerably changing shoreline. The method relies on the accuracy of the geo-referencing, preventing its use at other locations in Marsden Bay – One Tree Point.

Shorelines (HWLs) from 1984, 2000 and 2001 were digitised, then merged to form polygons of change in Arc View®. Polygons were assigned values based on whether they experiencing removal of material (erosion) or the deposition of material (accretion). Results are shown in Figure 4.12.



Figure 4.12 - *Shoreline change at Marsden Bay East and Marsden Spit, 1984 – 2000 largely due to works undertaken in 1999. Map produced by scanning digital images, then registering to a network of Ground Control Points (house corners). Subsequent rectification of the images has allowed changes in the shoreline position to be mapped. Root Mean Square (RMS) error of positional information ± 1.5 m.*

4.4.6 Marsden Spit

Marsden Spit partially impounds Blacksmiths Creek estuary. Previous data suggests an erosive trend (Gibb, 1998) (Table 4.9).

Marsden Spit		
Date	**Spit movement (at tip)(my^{-1})**	**Open Shore movement (my^{-1})**
1906 - 1942	- 0.83	-0.33
1942 – 1985	+0.42	-0.52 - -1.12
1985 – 1997	-5.2	-0.96 - -1.58

Table 4.9 – *Movement of Marsden Spit 1906 – 1997. Data drawn from Gibb (1998).*

The retreat of the spit is confirmed by field evidence consisting of mangrove stumps on the inter-tidal terrace, seaward of Marsden Spit. These mangroves would have grown inside Blacksmiths Creek estuary. It is apparent from Gibb's (1998) data (Table 4.9) the trend is for accelerating retreat of the spit and the adjacent shoreline.

The tip of the spit (Figures 4.11 and 4.12) has moved 120 m over a 16-year period (7.5 my^{-1}) (1984-2000), despite 750 m^3 of sediment being placed there in 1999 (Stevens, 1999).

Tropical Cyclones Fergus (29-30 December 1996), Drena (10-11 January 1997) and Gavin (10-13 March 1998) breached the spit by storm overwash (Gibb, 1998). Part of the flow from Blacksmiths Creek was naturally diverted through the breach. The breach was the foundation of the channel path excavated in 1999 and can be seen in the 2000 and 2001 images (Figure 4.11). The training wall built in 1999 and associated excavation works, diverted the entire flow through the breach. The sediment of the old tip of Marsden Spit was moved to the Marsden Bay – East shoreline to compliment the beach nourishment from dredge tailings from Shell Cut Reach occurring there.

4.5 Summary of Trends from Air photo Interpretation

- The coastline of One Tree Point – Marsden Bay – Marsden Point has experienced both retreat and advance between 1984 and 2000 (Figure 4.13). Rates of shoreline movement have been calculated from vertical air photographs of the region.

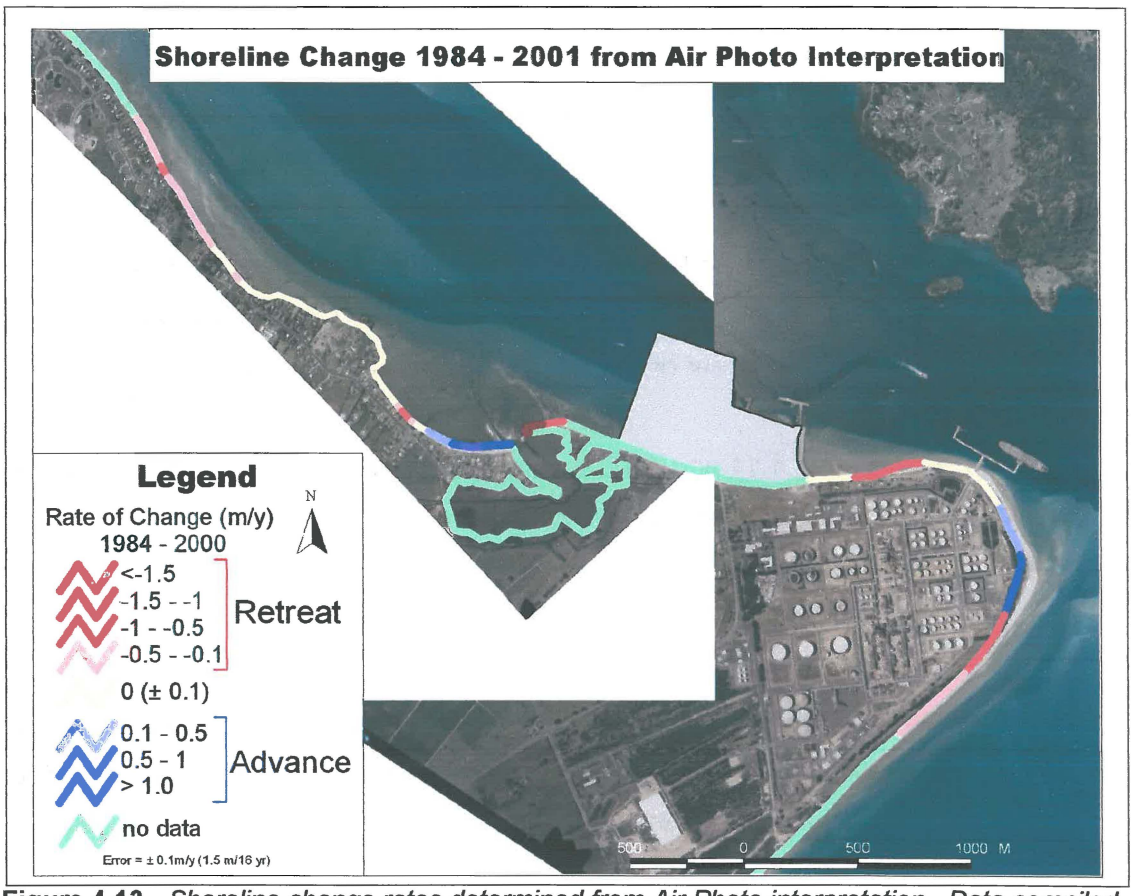


Figure 4.13 - *Shoreline change rates determined from Air Photo interpretation. Data compiled from morphologic analysis of rectified air photos from 1984, 2000 and 2001. Errors ± 0.1 m*

- The central section of the One Tree Point shoreline has experienced a narrowing of the dry beach at an average rate of 0.26 my^{-1}, cliff retreat rates here over the same period have been documented as 0.008 my^{-1}(Gibb, 1998). Care should be taken using these cliff retreat values however, as many of the rates presented in this report (Gibb, 1998) are within the errors of the methods used and should not be used as an indication of cliff retreat rates.

- The Paradise Point shoreline, separating One Tree Point and Marsden Bay, showed no changes greater than ± 0.1 my^{-1} between 1984 and 2001, cliff retreat rates here average 0.03 my^{-1} (Gibb, 1998).

- Patterns of beach narrowing indicate a longshore drift toward the northwest (One Tree Point) along the One Tree Point – Paradise Point beach face.

- A seawall along the western Marsden Bay shoreline has 'hardened' the shoreline. There is now no beach present.

- The central section of Marsden Bay has experienced a reduction in beach width, averaging 0.4 my^{-1} between 1984 and 2001. This value compares well with those obtained using independent data (retreat rates between 0.13 to 0.44 my^{-1} (Gibb, 1998).

- Eastern Marsden Bay was nourished in 1999 with 8,000 m^3 of material dredged from Shell Cut Reach. As a result of the nourishment the dry beach width has increased, the change in width increases towards Blacksmiths Creek.

- The breaching of Marsden Spit in 1996, 1997 and 1998 by tropical storms accelerated an already present trend of spit retreat. Average rates of retreat are within the range of 5 – 7.5 my^{-1} (1984 – 2001) despite small nourishment efforts (750 m^3) in 1999.

- Construction of a training wall in 1999 and associated works diverted the flow of Blacksmiths Creek away from the beach, increasing the likelihood of nourished sediment remaining on the beach.

- The Marsden Point shoreline adjacent to the ebb-tidal delta of Mair Bank, experienced progradation between 1984 and 2000. Areas farther south along Bream Bay Beach experienced minor retreat, as have inner harbour locations between the NZRC jetty and the Northport site.

5 BEACH PROFILES OF THE SHORELINE SURROUNDING MARSDEN POINT

5.1 Introduction

The elevations and contours of a shoreline are a response to the forcing of waves, winds and currents, and are dependant on the supply or loss of sediment to the beach. "*Periodic topographic and near-shore profile surveys constitute one of the most direct and accurate means of assessing geologic and geomorphic changes on the shore face to water depths of 10 or 15 m*" (Gorman et al., 1998).

Beach profiles vary with time, both seasonally as the wave climate changes and over longer time periods, responding to changes in sediment supply (erosion or accretion). Profiles surveyed at the same location over time reveal beach changes and allow calculation of shoreline change rates and volumetric sediment changes. Advanced analytical techniques allow information regarding both alongshore and onshore-offshore sediment transports to be gleaned from the time series of profiles.

5.1.1 Structure of Chapter

This chapter is divided into sections in order to initially describe the survey methods and profile locations before describing the changes in raw beach profiles. Several analytical techniques are applied to the data:

Standard Deviations and Profile Elevation	to determine closure depths (vertical limits of sediment movement)
Volumetric Analysis	to determine changes in sediment volume at specific locations along the beach
Even-Odd Analysis at the Port Site	to determine the impact of large structures on alongshore sediment transport (e.g. the causeway and rock-wall)
Principle Components Analysis	to determine characteristic locations of change along the profile and onshore-offshore sediment transport patterns and pivot points.

5.2 Survey Methods and Errors

Registered surveyors *'Simpson Shaw and Co'* conducted all surveys of the beach profiles analysed within this chapter. Conventional land surveying techniques were used, involving a transit, surveyor's rod and a tape to measure the profile. Profiles were measured at low tide to maximise the distance along the profile measured. The method allowed elevations to be measured to within 0.003 m and distances to within 0.03 m. Measurements were made at pronounced changes in beach slope. Operation error may take the form of measurement inaccuracies through poor instrument set up and collection techniques. Using the same surveyor for all surveys minimised these errors as much as possible.

All measurements were resolved to a common datum (Marsden Point), based on the known height of the benchmarks used for each profile line.

5.2.1 Profile Locations

Twenty-eight (28) profiles were repetitively surveyed almost annually between November 1996 and August 2003. The location of the profiles ranges from Bream Bay Beach (adjacent to the ebb tidal delta of Mair Bank) to One Tree Point (Figure 5.1). Specifics regarding the benchmark location, profile direction and date of survey are contained in Appendix C.

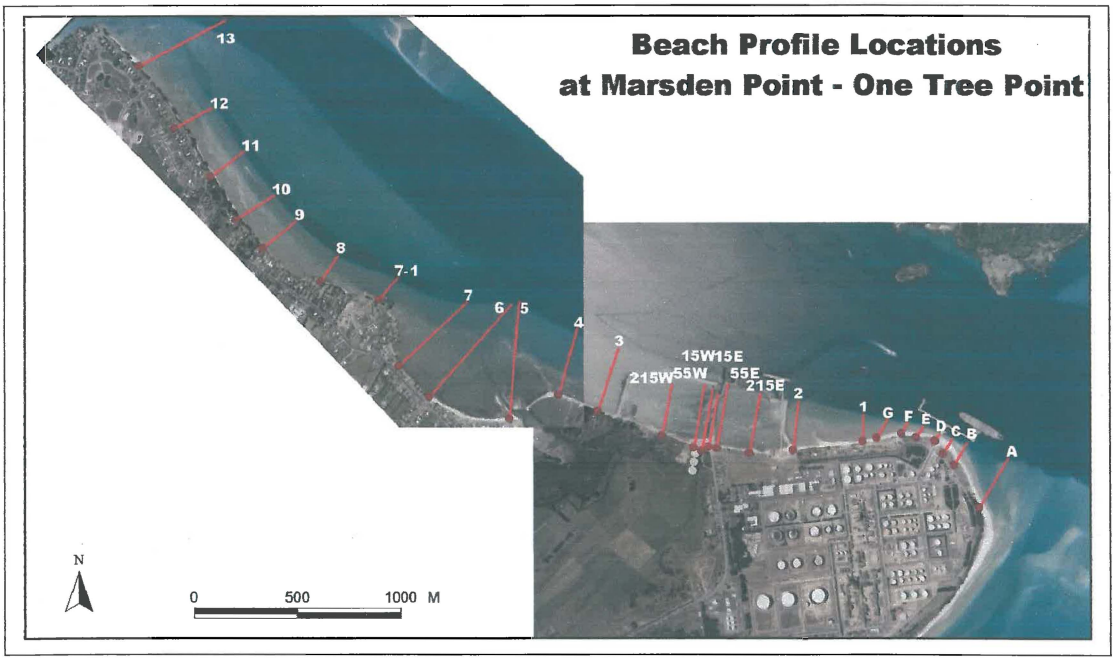


Figure 5.1 - *Location of beach profiles at Marsden Point - One Tree Point.*

Surveys were conducted in November 1996, May 1997, June 1998, July 1999, October 2000, June 2001, November 2002 and August 2003.

It is clear that the profiles can be grouped into smaller sub-sets representing characteristic sections along the coast:

Surrounding the NZRC Wharf

Profiles A-G are located on Marsden Point, adjacent to the NZRC wharf (Figure 5.1). Profile lines run parallel to the wharf structure. The area is characterised by a relatively large foredune adjacent to profile A, with the dune height decreasing around the point toward profile G. This area is subject to the greatest wave energy of the profile areas, due to its location and orientation with respect to Busby Head and Bream Bay Beach (Black, 1983).

Between the NZRC wharf and Northport

Profiles 1 and 2 cross the inter-tidal terrace between the NZRC jetties and the Northport reclamation (Figure 5.1). Profiles within the harbour itself lack a large dune (in the sense of an aeolian feature of sand), however they do generally have a small (0.5-1 m) vegetated bank (Chapter 4). Many of the harbour profiles consist wide inter-tidal terraces, which are exposed at low tide.

The Port Site

Profiles 215 East to 215 West cover the area over which the Northport reclamation occurred (Figure 5.1). The profiles are named corresponding to the distance (m) and direction of the profile from a causeway built in 1983. The causeway extended to the channel edge and impacted alongshore sediment transport. The causeway was located in the middle of what is now the Northport reclamation site.

Marsden Spit

Profiles 3 and 4 are located to the west of the Northport development (Figure 5.1) covering Marsden Spit, a variable feature enclosing Blacksmiths Creek estuary.

Marsden Bay Profiles

Profiles 5, 6 and 7 extend over the Marsden Bay region (Figure 5.1). The area has extensive inter-tidal terraces, which are cut by a channel draining Blacksmiths Creek. Extensive property protection works have modified the western end of Marsden Bay (Sections 4.4.4 and 4.4.5).

One Tree Point Profiles

Profiles 7-1 to 13 extend from Paradise Point to One Tree Point. The area contains sea cliffs ranging in height from 2 to 7 m that are retreating slowly (~0.8 – 30 mmy^{-1}) (Gibb, 1998), although some of this data has been questioned. The dry beach is generally narrow (Chapter 4, Sections 4.4.2 and 4.4.3) and inter-tidal terraces extend out to the Blind Channel.

5.4 Profile Trends

5.4.1 Terminology

Features sufficiently common in their occurrence to be recognised on most beaches have been given names that are in general usage. Figure 5.2 shows the morphological definitions of some important beach features.

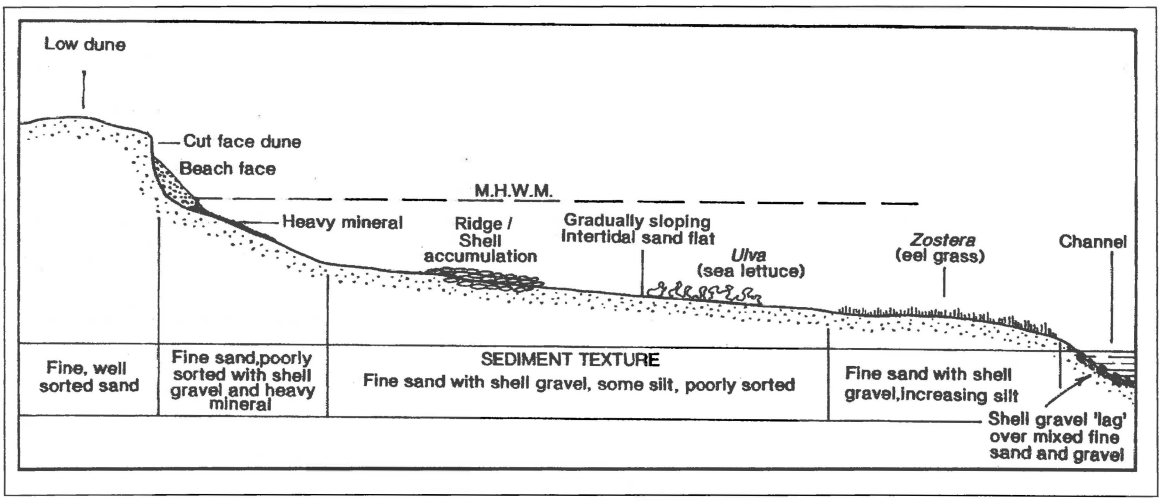


Figure 5.2 - *Profile of a typical inter-tidal estuarine shore showing characteristic features (after Healy et al., 1996).*

5.4.2 Analytic Techniques and Methods

Profile data were read into MATLAB® for plotting and analysis. Raw Profiles were plotted for each survey at each location (Figures 5.3 to 5.29). In addition to the raw profiles, two descriptors of the data were plotted - the envelope of change and standard deviation along the extent of the profile.

The data, consisting of data points with irregular offshore spacing, required some modification to obtain standard deviations and envelope of changes along the profiles. Data were required at regular intervals in the offshore direction to calculate the two properties at each interval.

A MATLAB® program (*'profile_sd_eoc.m'*, Appendix C) was written by this author to interpolate the profiles at 0.5 m intervals offshore, based on the original data. The programme uses one-dimensional linear interpolation (table look-up) between the data points. It returns values at intermediate points of a one-dimensional function *f(x)* that underlies the original data. The function uses a linear relationship between the data points and does not extrapolate for values outside the range of the raw data. The potential decrease in the resolution of the interpolated data from the original data is dependent on the interval chosen for the regular grid. Smaller intervals result in more accurate representation, but lead also to increased variable size and processing requirements. A 0.5 m grid (e.g. 300 data points along a 150 m profile) was selected as it accurately represented the original profiles.

5.4.2.1 Envelope of Change

With the profile data on a regular grid in the y direction, calculation of envelope heights and standard deviations can be made. Envelope of change values are calculated by subtracting the minimum profile elevation from the maximum at each position on the grid created in the offshore direction (lines 38–42 of *profile_sd_eoc.m* in Appendix C).

Envelope of change data can be used as an indicator of closure depth. Hallermeier (1981) defined the depth of closure to be where the envelope of change thinned to less than 0.3 m. Kraus and Harikai (1983) defined the depth of closure as the minimum depth where the standard deviation decreased markedly to a near constant value. Evaluated depths of closure from envelopes of change do not necessarily indicate reduced sediment transport below the specified depth. The depth of closure evaluated using this method indicates that there is no morphologic change (greater than the limits defined) below the specified depth. Sediment may still be transported below the depth although there is no net accumulation or removal.

5.4.2.2 Standard Deviations

Standard deviations were calculated from the interpolated profile data (lines 45-46 and 104-123 of *profile_sd_eoc.m* in Appendix C).

The program calculates standard deviations of the gridded data taking into consideration only the profiles that contain measured data at each point. i.e. if four profiles were recorded at y=50 m, all four elevations are taken into consideration (n=4), while if at y=150 m only three profiles have been measured, the standard deviation is calculated using only these profiles (n=3).

5.4.3 Features and Trends of the Raw Profiles

5.4.3.1 Marsden Point (NZRC jetties, profiles A-G)

As there have been only two surveys undertaken at profile D (Figure 5.6), no further analysis has been undertaken at this location. It is apparent that the profile taken during May 1997 at profile B is erroneous, thus this data will not be used for any further analysis.

Profile A (Figure 5.3) shows erosion of the dune and beach face between 1998 and 2001, an increase in elevation (~0.5 m) in the region of Mair Bank between 2002 and 2003. Closure depth would be evaluated at +0.4 m C.D. if not for the 2003 data. Taking this data into account however, the depth of closure is deeper than +0.3 m C.D. Profile A appears to rotate about a point located 80 m from the benchmark and at +0.4 m C.D.

Similar erosion of the beach face occurred over the same interval (1998-2001) at profile C (Figure 5.5), while profile B, between the two, accreted early in the period and experienced erosion from 2000-2001 (Figure 5.4).

The profiles indicate a narrowing of the beach width and a reduction in dune height along the shoreline from profile A to profile G. The dune and beach face also become more stable in this direction (see standard deviations of changes in Figures 5.3 to 5.9).

An interesting feature develops at profile G (Figure 5.9) between the October 2000 and June 2001 surveys. A '*wedge*' of sediment moves onshore at depths of +0.8 to +1.8 m C.D. The movement has widened and flattened the inter-tidal terrace while simultaneously steepening the slope towards the channel. The onshore movement of sediment in this manner is described in the Shore Protection Manual (CERC, 1984) as being "*characteristic of post-storm beach accretion under a wide range of wave, tide and sediment conditions*".

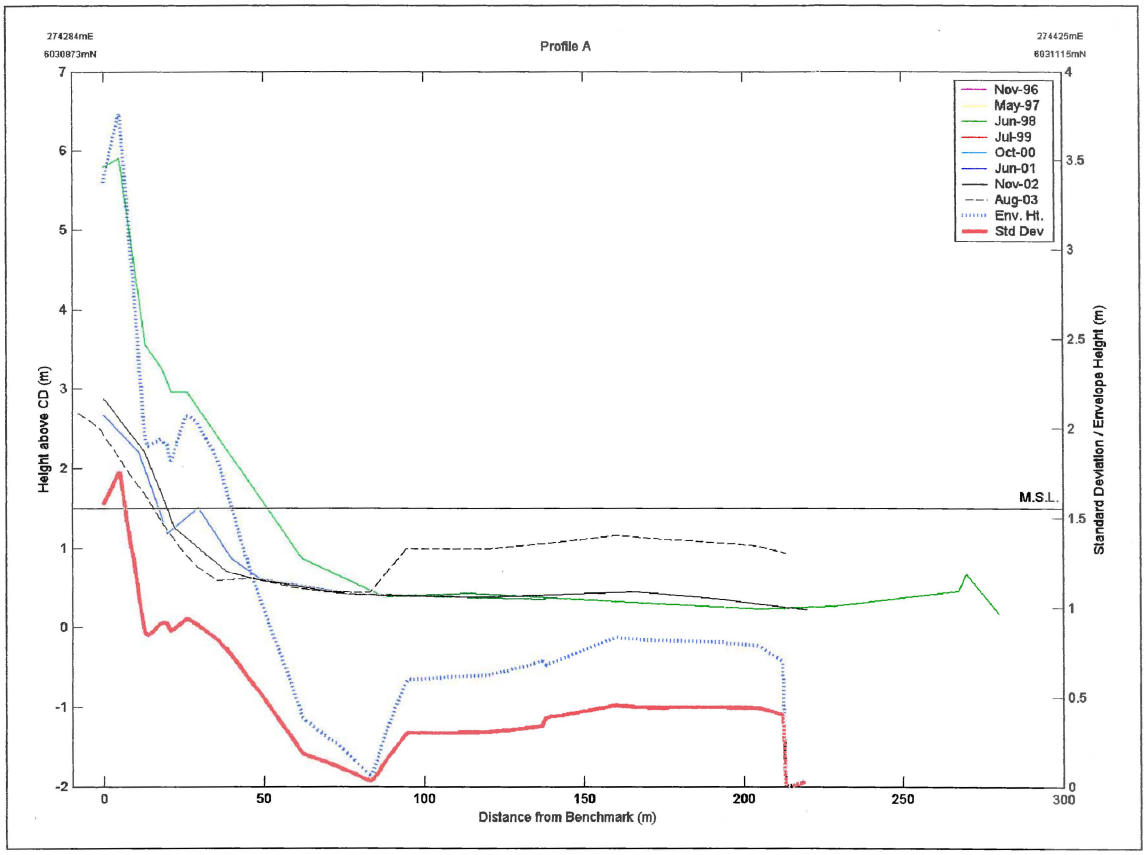


Figure 5.3 - *Profile A raw data, envelope of change and standard deviation from mean.*

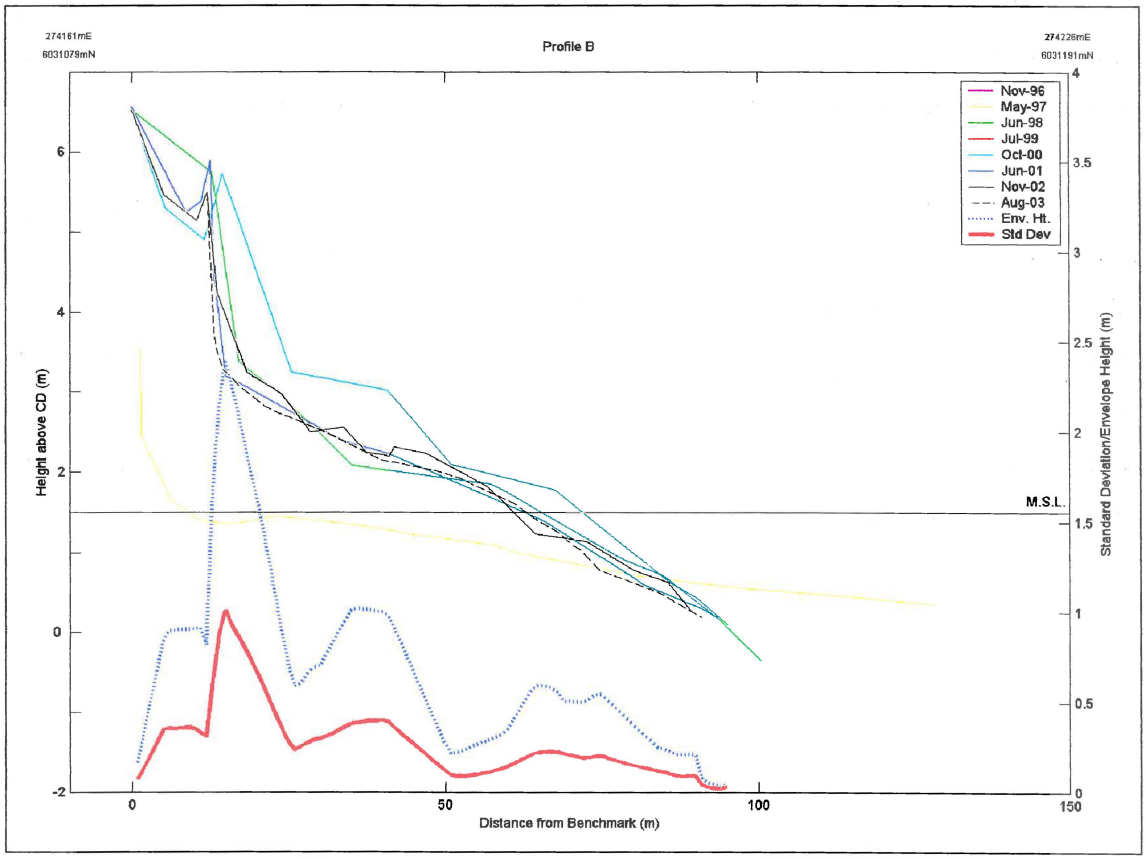


Figure 5.4 - *Profile B raw data, envelope of change and standard deviation from mean.*

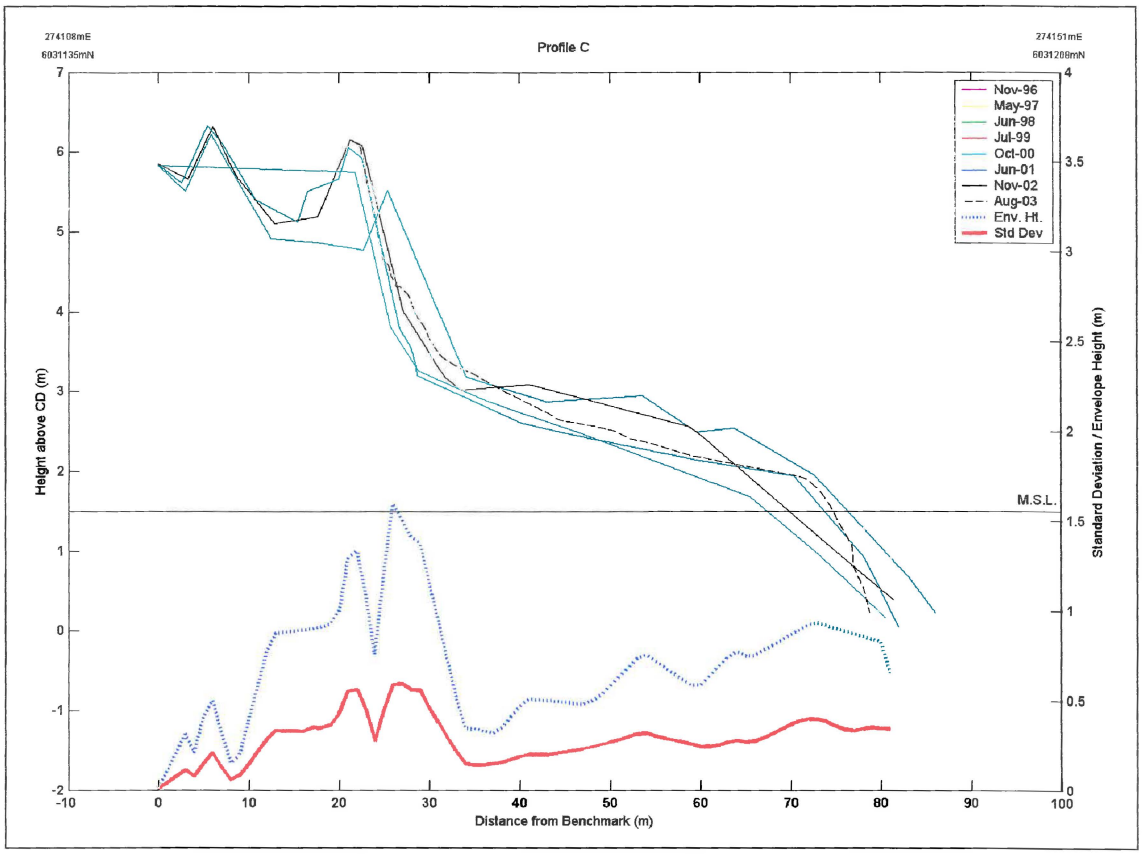


Figure 5.5 - *Profile C raw data, envelope of change and standard deviation from mean.*

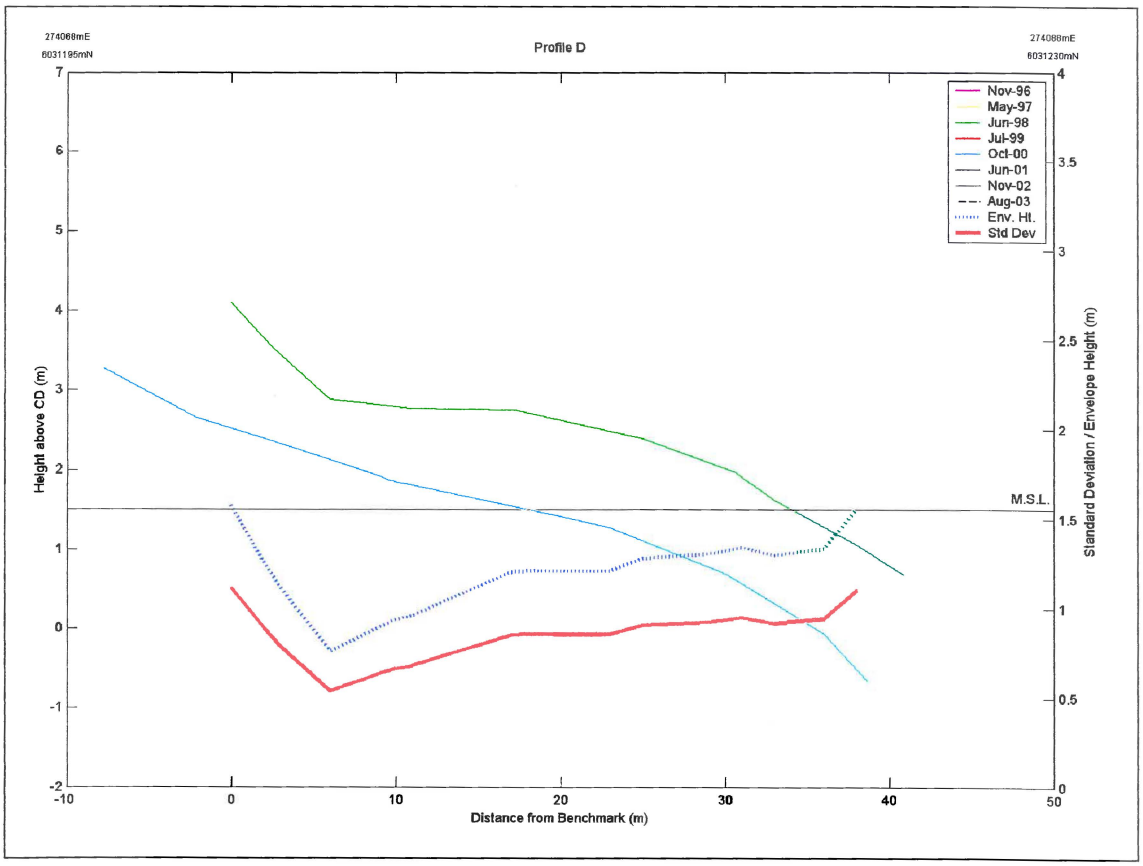


Figure 5.6 - *Profile D raw data, envelope of change and standard deviation from mean.*

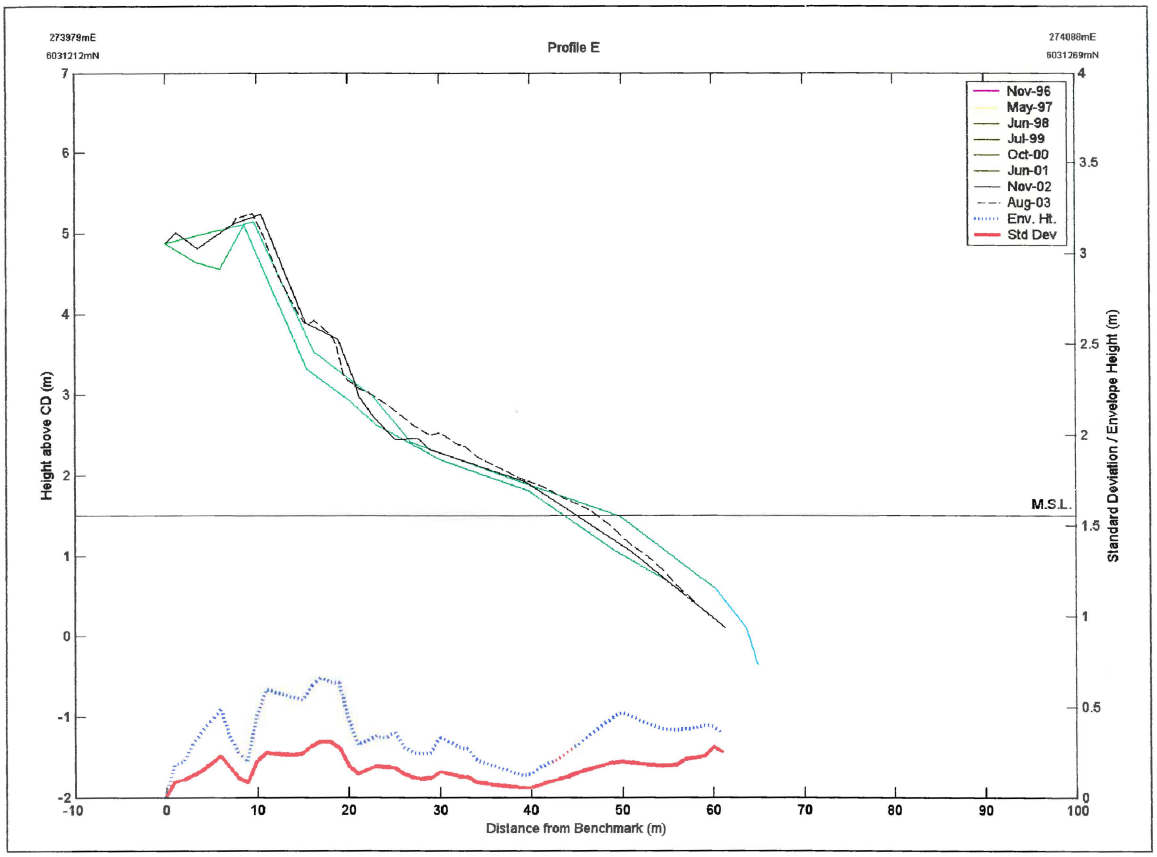


Figure 5.7 - *Profile E raw data, envelope of change and standard deviation from mean.*

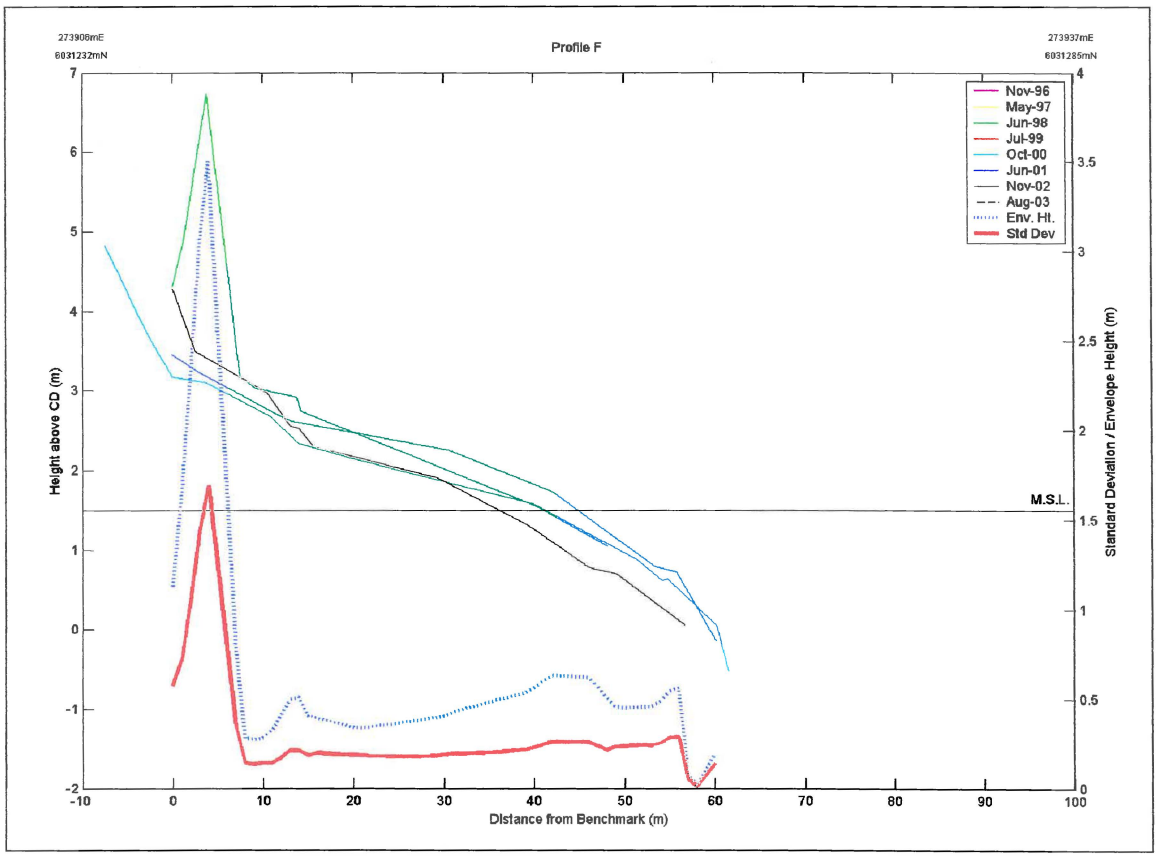


Figure 5.8 - *Profile F raw data, envelope of change and standard deviation from mean.*

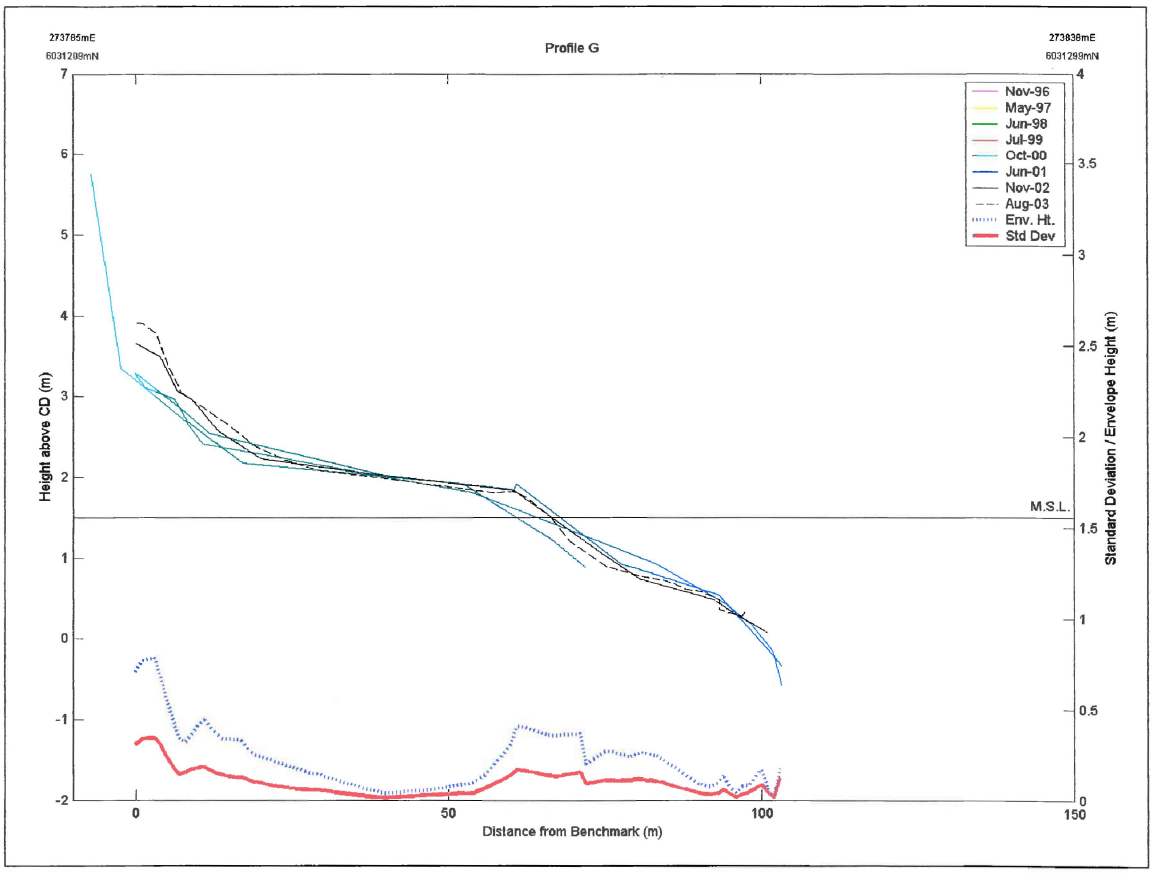


Figure 5.9 - *Profile G raw data, envelope of change and standard deviation from mean.*

5.4.3.2 Between the NZRC jetties and Northport (Profiles 1 and 2)

Profiles 1 and 2 show a beach face extending into a long terrace or inter-tidal flats (Figures 5.10 and 5.11). Profile 1, between October 2000 and June 2001, displays a similar pattern to that observed at profile G, a widening of the inter-tidal flats and steepening of the channel slope (Figure 5.10). The sediment deposited was subsequently eroded in the following 10-month period.

At both locations, the beach face (~ +2 to +3 m C.D) experienced the accretion of sediment from 2001 to 2002. Erosion occurred at the seaward edge of the inter-tidal terrace (~ 0.0 m C.D) over the same time period.

Profile 2 shows the development of a 0.5 m high bar or shell ridge at the edge of the inter-tidal zone between 2000 and 2002 (Figure 5.11). The sediment source for this bar has been from +1.5 to +0.9 m C.D.

The depth of closure estimated from the profile standard deviations and envelopes of change is +0.8 m C.D at both profiles.

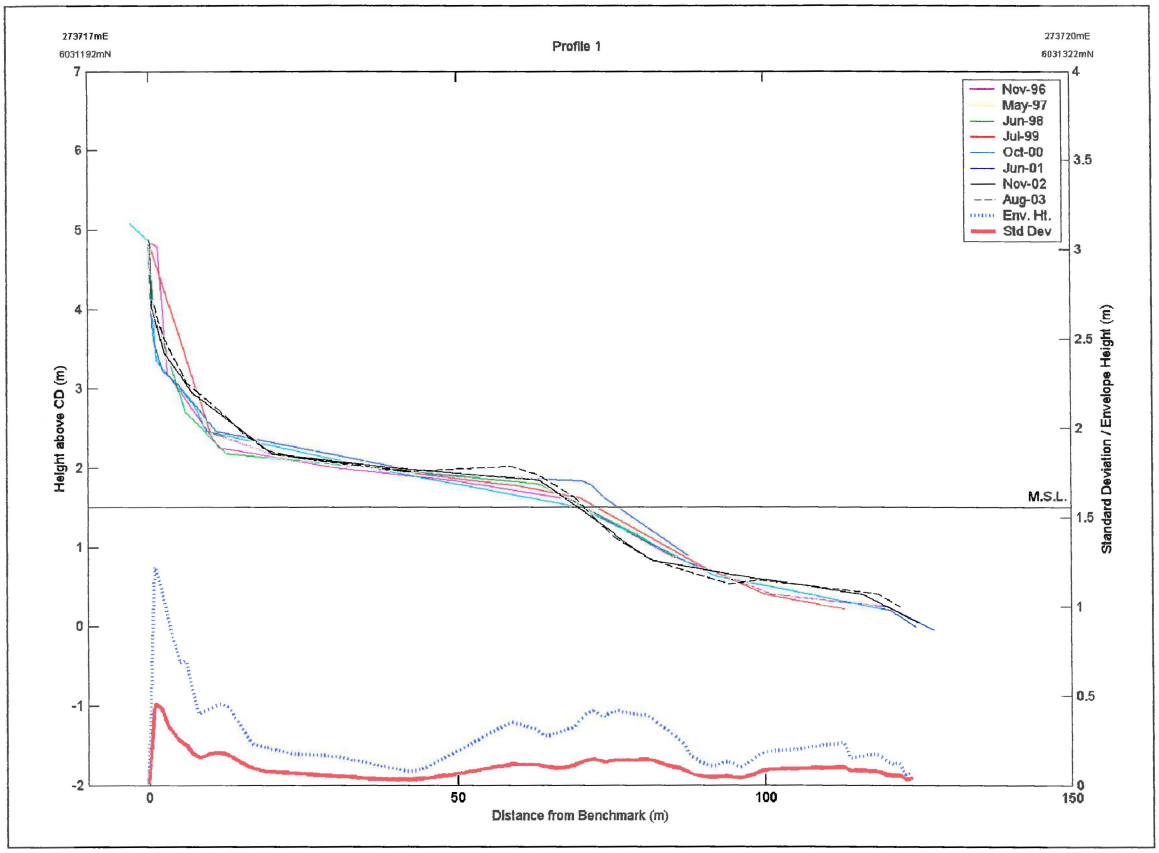


Figure 5.10 - *Profile 1 raw data, envelope of change and standard deviation from mean.*

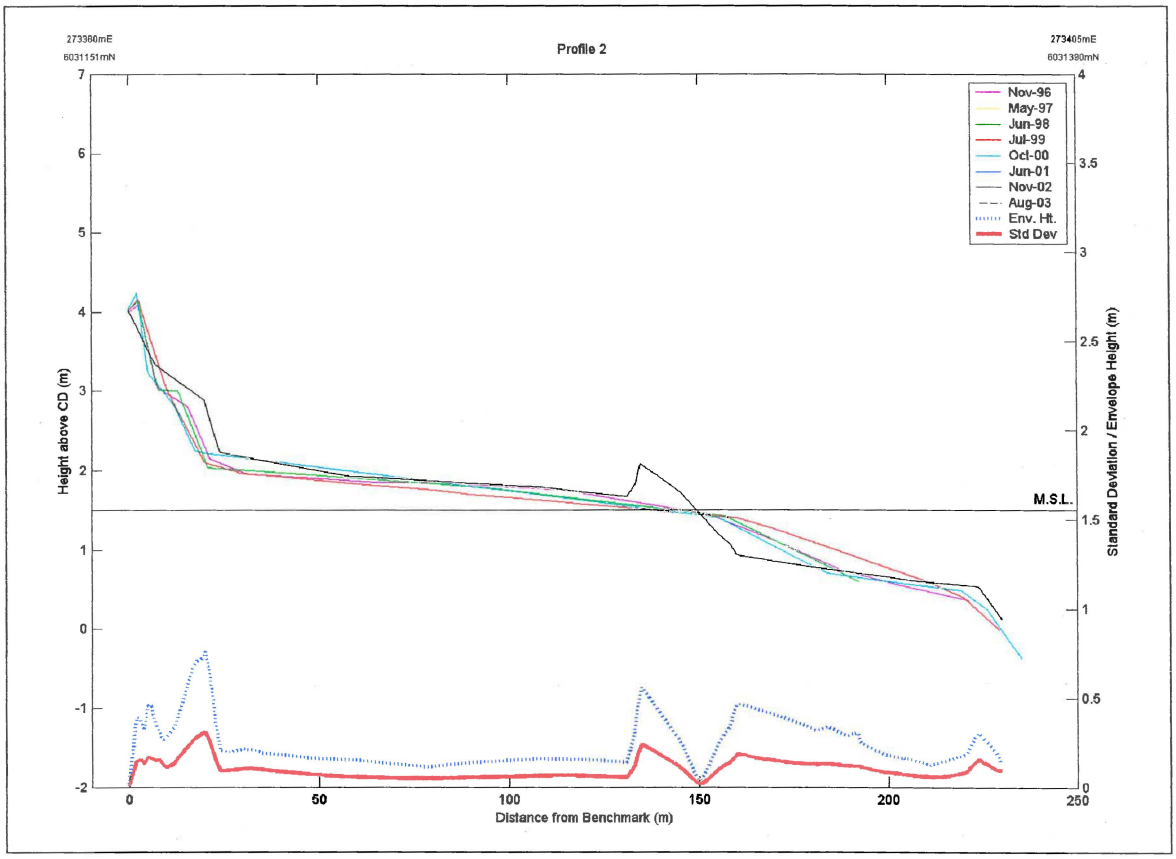


Figure 5.11 - *Profile 2 raw data, envelope of change and standard deviation from mean.*

5.4.3.3 Port Site Profiles

These profiles were separated by a causeway built in 1983, which has acted as a barrier to longshore sediment transport.

Profile 215E (215 m east of the causeway, Figure 5.1) experienced an increase in elevation of the inter-tidal flats (~ 0.25 m) from 1998 to 1999, the growth of a small bar is apparent at +1.5 m CD over the same period (Figure 5.12). While accumulating sediment, the bar moves closer to the beach face by 15 metres, characteristic of the initiation of beach accretion (CERC, 1984). Note that the growth of this bar occurs prior to a similar feature observed at profile 2. Profile 215E indicates a depth of closure of +0.8 m CD.

Profile 55E appears to be relatively stable if the data of June 1998 is not considered (Figure 5.13). The scale of the changes indicated by this profile and the consistent pattern of profiles preceding and postdating the June 1998 survey indicate that this data is likely somewhat erroneous.

Close to the causeway on the eastern side, profile 15E shows a relatively stable profile with a small envelope of change and standard deviation (Figure 5.14). Interesting to note is the large (2 m) high feature at the seaward edge of the profile. This ridge feature is relatively stable. The closure depth indicated by the standard deviation and envelope of change is +1.5 m CD, although it is likely that the relatively '*elevated*' depth of closure is due to sheltering effects from the nearby causeway.

Profiles to the west of the causeway exhibit more variable behaviour (Figures 5.12-5.17). Profile 15W shows large variability across the extent of the profile (Figure 5.15). The ridge (250 m from the perpendicular base line, Figure 5.15) is smaller (~1 m) and much less stable than that observed on the eastern side of the causeway (Figure 5.14). The depth of closure is deeper than +0.5 m C.D.

Profile 55W also shows variability with the only consistent trend being retreat of the dune line and shore face from 1997 to 2000 at an average rate of 5 my^{-1}, there is no ridge present and the depth of closure is +0.8 m C.D (Figure 5.16).

Profile 215W exhibits a stable dune slope and beach face (Figure 5.17). There is evidence of a small bar (0.5 m), closer to the shore face than in other profiles (Profiles 15W, 15E, 215E, Figures 5.15, 5.14 and 5.12 respectively). The ridge was moving onshore throughout the survey period (May 1997 – October 2000) and simultaneously material was being eroded from the channel margin. The depth of closure is deeper than +0.4 m C.D.

It is apparent that the beach morphology on the western side of the causeway was more variable than that on the eastern side. The depth of closure was also in general deeper on the western side compared with the eastern side, indicating a greater potential for sediment transport on the western side of the causeway.

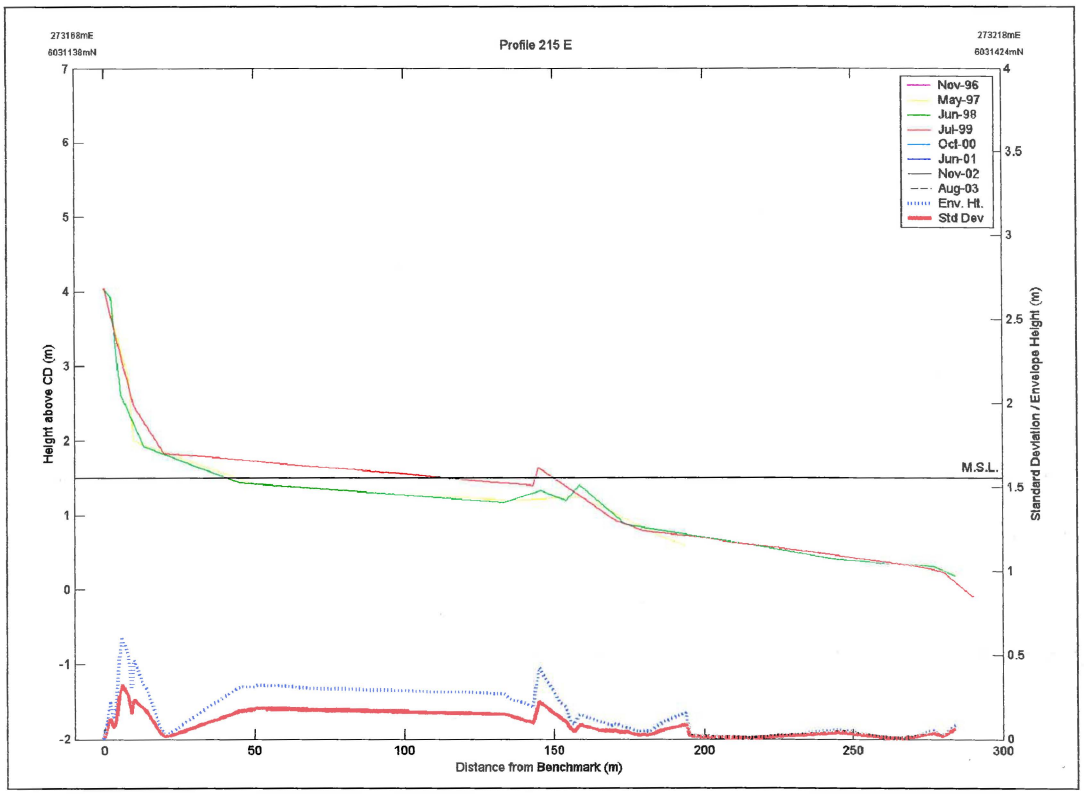


Figure 5.12 - *Profile 215E raw data, envelope of change and standard deviation from mean.*

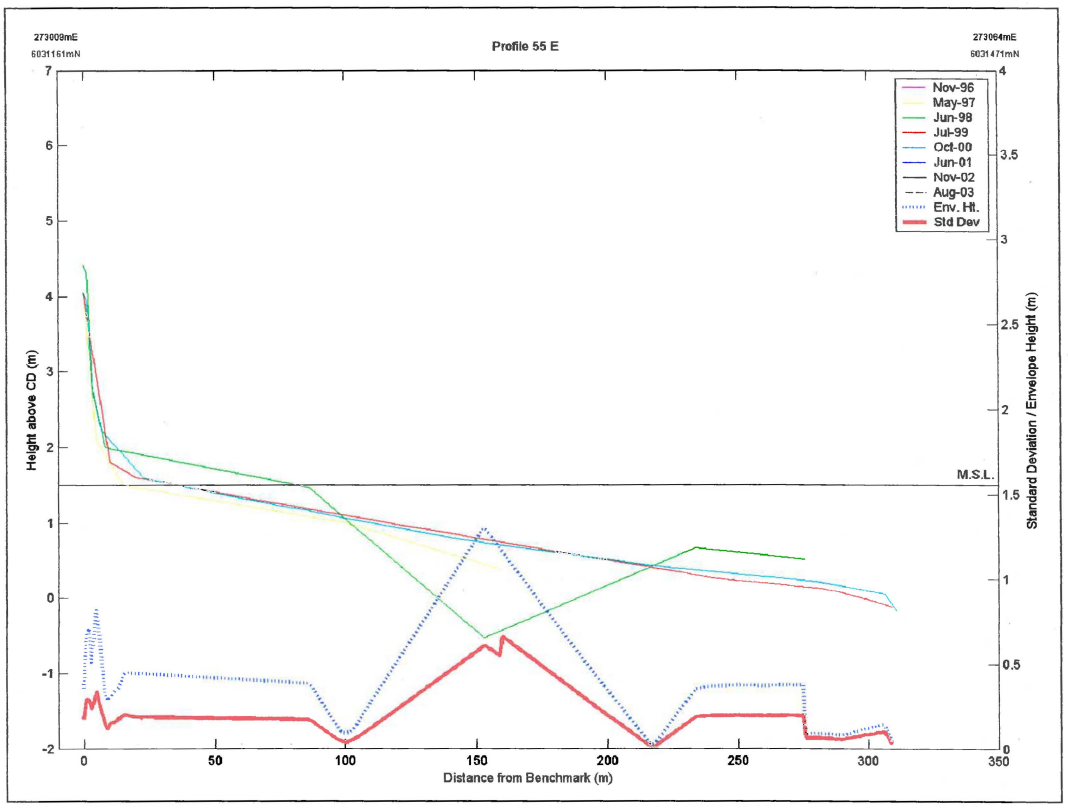


Figure 5.13- *Profile 55E raw data, envelope of change and standard deviation from mean.*

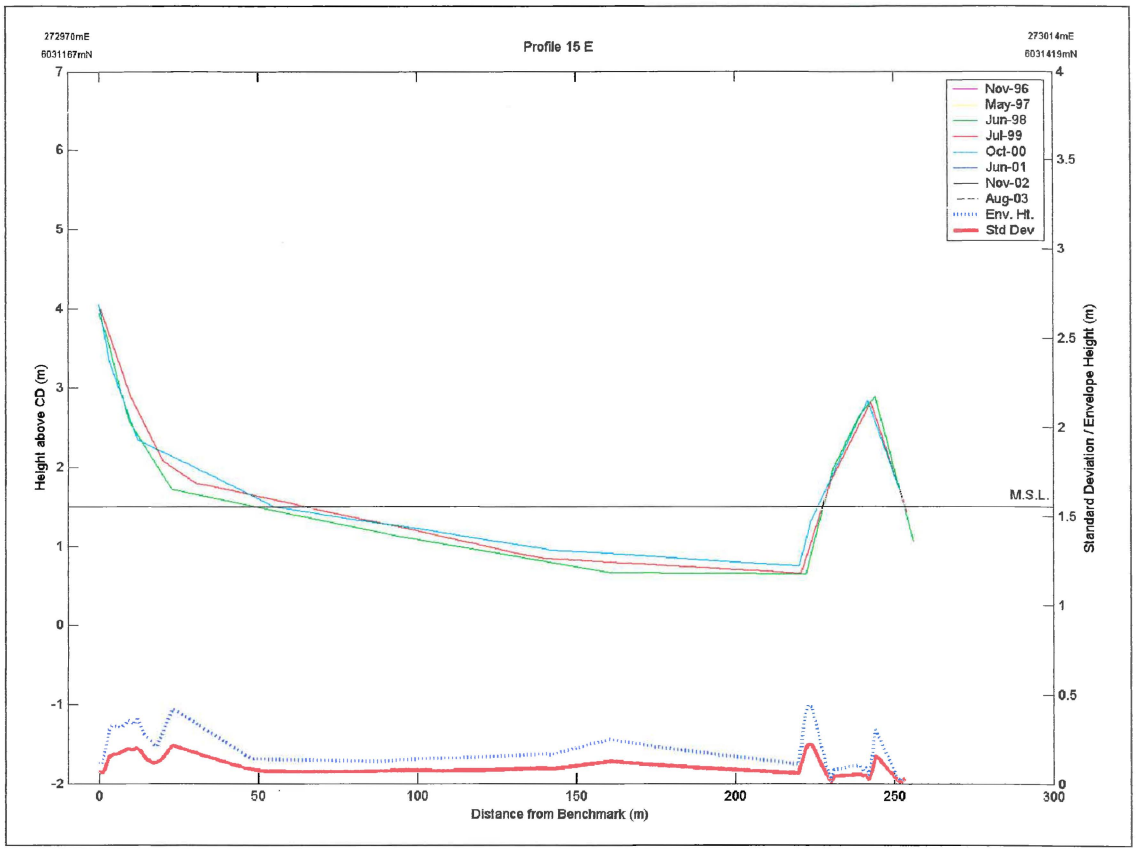


Figure 5.14 - *Profile 15E raw data, envelope of change and standard deviation from mean.*

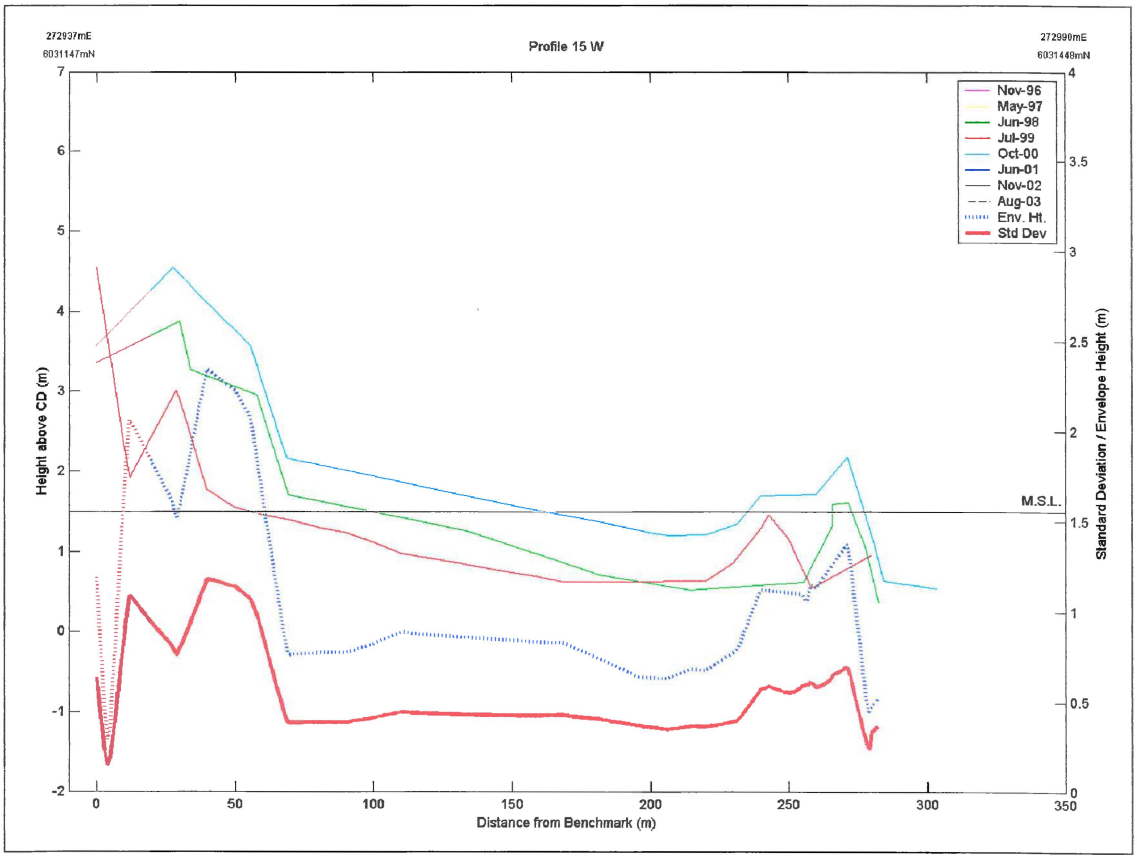


Figure 5.15 - *Profile 15W raw data, envelope of change and standard deviation from mean.*

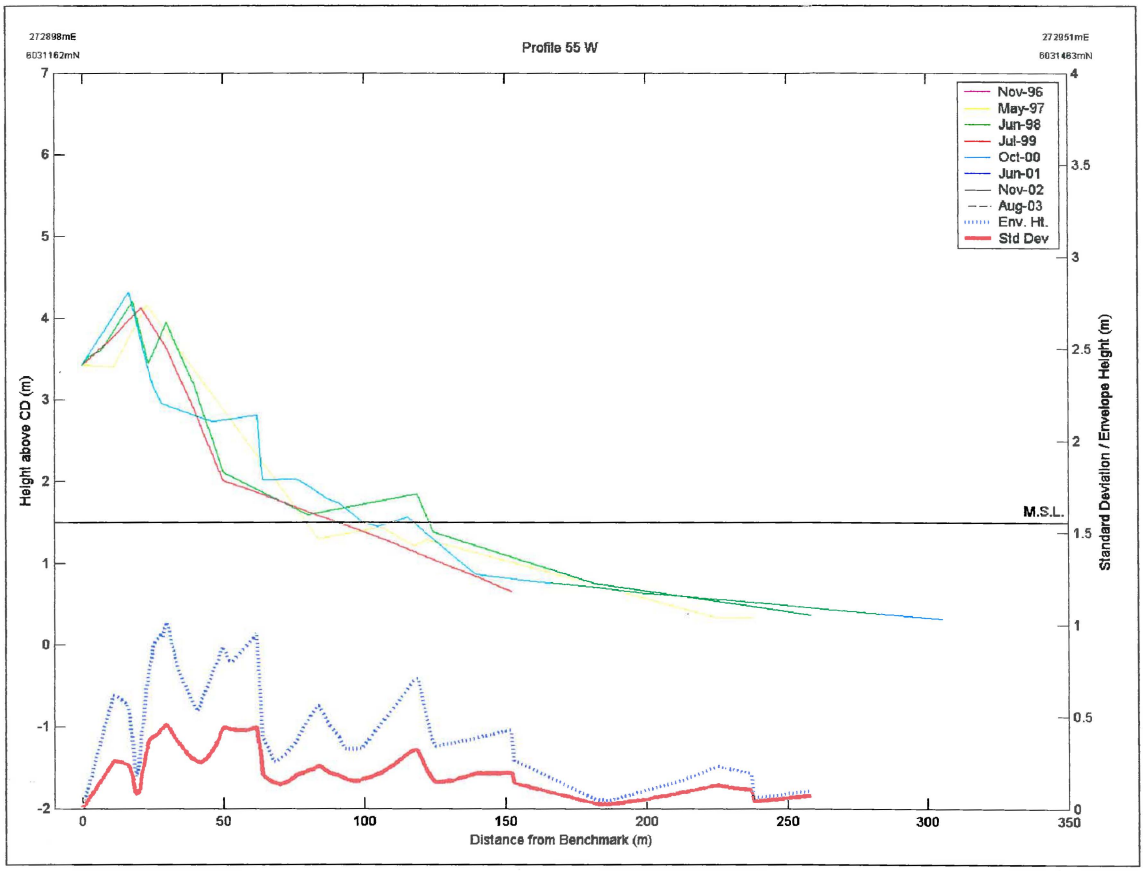


Figure 5.16- *Profile 55W raw data, envelope of change and standard deviation from mean.*

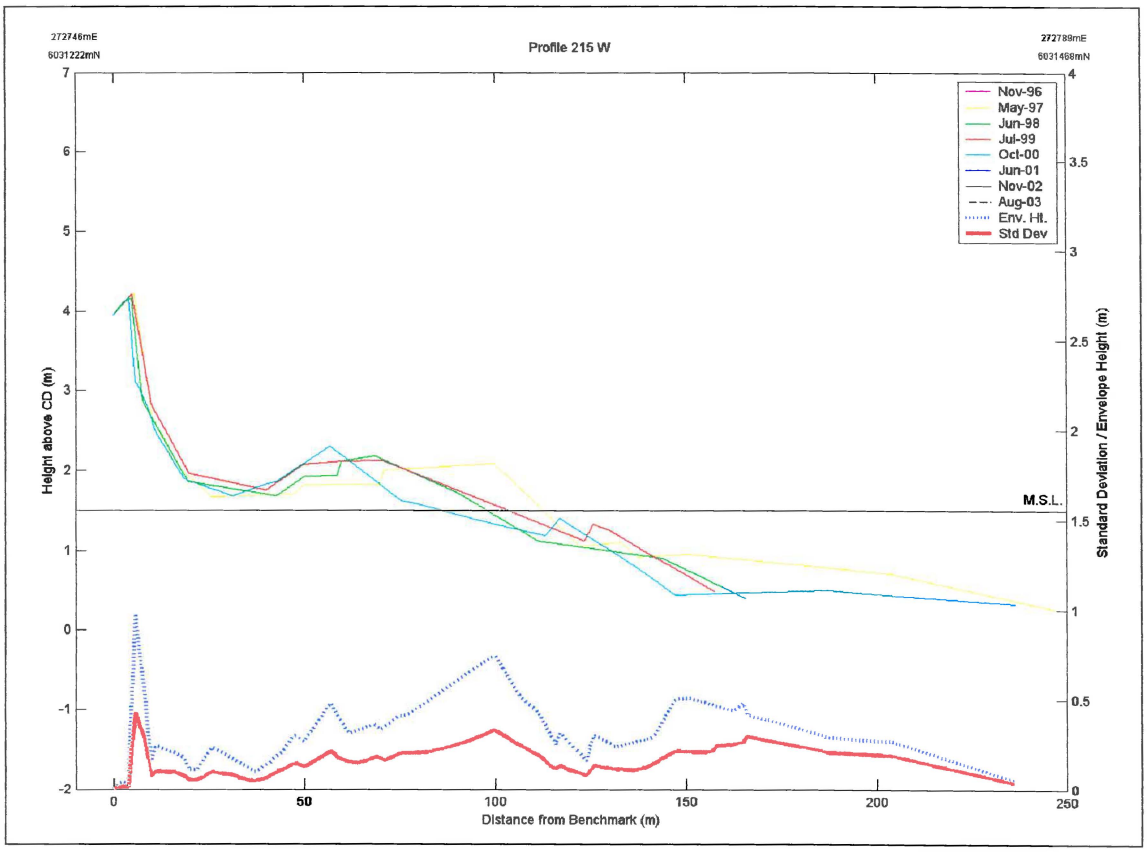


Figure 5.17 - *Profile 215W raw data, envelope of change and standard deviation from mean.*

5.4.3.4 Marsden Spit Profiles

Previous evidence from air photographs (Section 4.4.6) has indicated a long-term erosive trend at Marsden Spit. Significant storms occurred in December 1996, January 1997, March 1998 and April 2001. The spits morphology was altered in 1999 following the building of a rock-training wall for Blacksmiths Creek (Figure 4.12).

Profile 3 shows accretion over the entire profile between June 1998 and July 1999 (Figure 5.18). While the data looks to have potential for a datum error in that it is consistently 0.4 m '*higher*' than the majority of the other profiles, the fact that both the 1999 and 2000 profiles exhibit this shape (Figure 5.18) reduces the likelihood of the presence of datum errors in the data, as the error would need to have occurred twice (during each profile).

The May 1997 and June 1998 profiles (both similar) are likely '*eroded*' profiles caused by the storms that occurred prior to each survey. Elevated 1999 and 2000 profiles show a healthier, sediment rich beach, which had recovered from the previous storm episodes. A tropical cyclone in April 2001 eroded the profile back to the levels of 1997/1998, where the beach has remained through to the most recent profile (August 2003). There is a small ridge present at +1.5 to +1.8 m C.D. (Figure 5.18), there has been no noticeable on or offshore movement of this ridge. The depth of closure is deeper than 0.0 m C.D.

Profile 4, closer to the tip of Marsden Spit, exhibits a more consistent cross-section with minimal envelopes of change and standard deviations across much of the profile (Figure 5.19). There is no noticeable response of the profile to the storm episodes previously described. Between 1996 and 2003 the dune face has been retreating consistently at a rate of <1.0 my^{-1}. The beach face has been stable over the period 1996 to 2002 with slight lowering between November 2002 and August 2003. A small ridge present at +1.6 m C.D. has moved onshore between 1999 and 2002 at a rate of 2 my^{-1}. The development and onshore movement of features such as this is characteristic of beach accretion (CERC, 1984).

The ridge was not present during the 2003 survey. The stable profile results in a '*shallow*' closure depth of +1.0 m C.D. at profile 4.

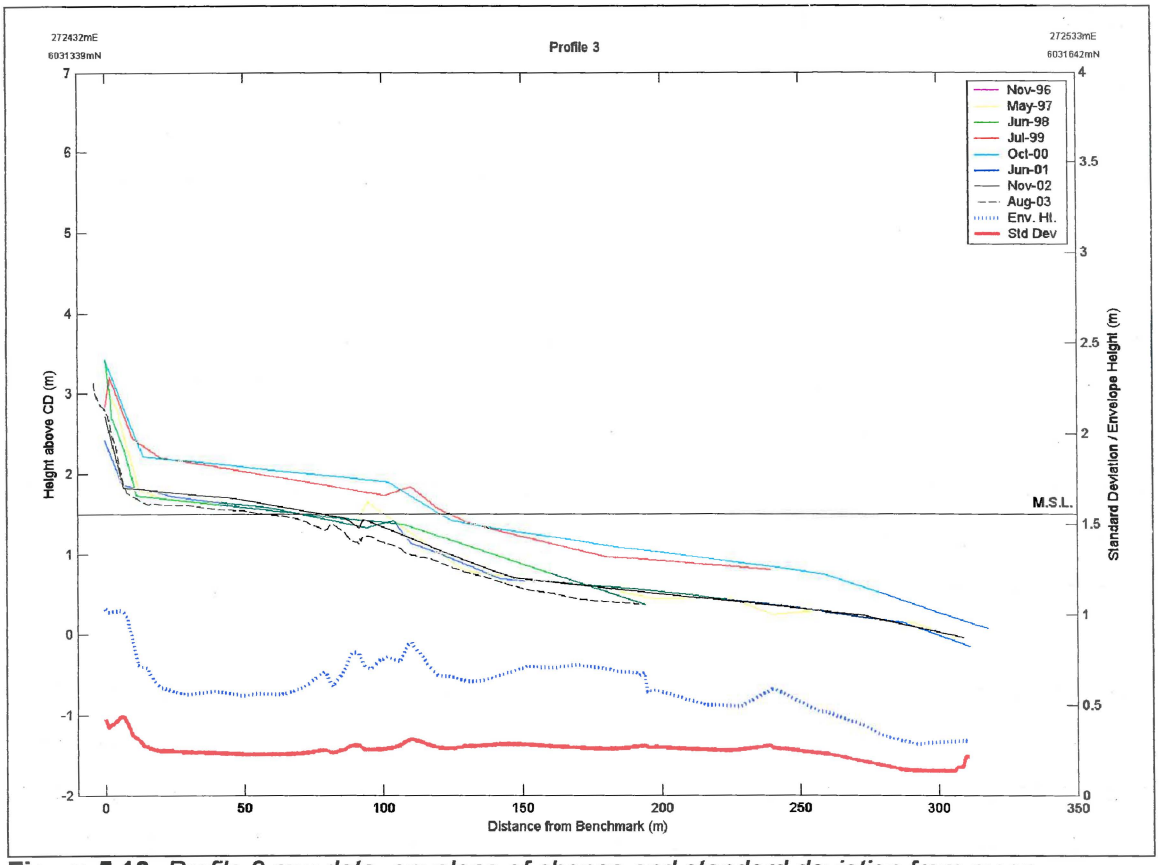


Figure 5.18- *Profile 3 raw data, envelope of change and standard deviation from mean.*

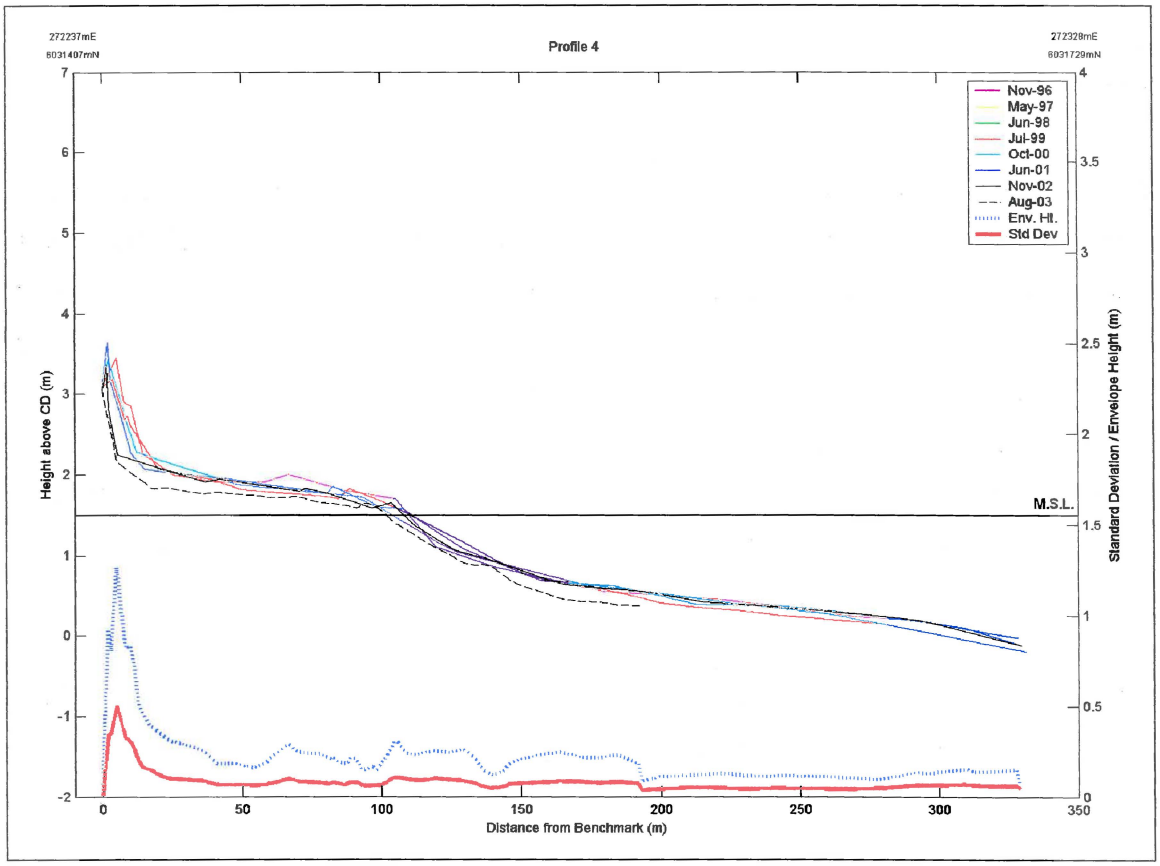


Figure 5.19 - *Profile 4 raw data, envelope of change and standard deviation from mean.*

5.4.3.5 Marsden Bay

Eastern Marsden Bay (Profile 5) underwent substantial changes during late 1999 (see Section 4.4.5) due to the reconfiguration of Blacksmiths Creek channel and the nourishment of the adjacent beach. Surveys of profile 5 document these changes well. Profiles of May 1997 and July 1999 show that the Blacksmiths Creek channel once cut a path much closer to the beach face than presently (Figure 5.20). The presence of Marsden Spit on the profile of May 1997 and its absence on the profile of July 1999 indicate that the reconfiguration of the spit commenced prior to the building of the training wall and roosting island. The inter-tidal terrace of profile 5 displays relatively small fluctuations with no consistent trend over the period from 1997 to 2003. However, an area more susceptible to change is a small ridge at the end of the inter-tidal flats, just below mean sea level (Figure 5.20).

Profile 6 is located immediately to the west of the boat ramp in the middle of Marsden Bay (Figure 5.1). The nourishment of the beach in 1999 consisted of sediment placement to the east of this boat ramp. The profile exhibits very little change from 1997 to 2003 (Figure 5.21). Standard deviations and envelopes of change are very small over the extent of the profile. No accretion has been noted over this profile following the nourishment of the beach nearby to the east.

Profile 7 also exhibits relative stability (Figure 5.22). The edge of the inter-tidal terrace exhibits a slight retreating trend over the period from 2001 to 2003. A small ridge at this location moved onshore between 1999 and 2001. It had disappeared in 2002. Field investigations have indicated there is no dry beach at profile 7 at high tide when any incident waves hit the seawalls directly.

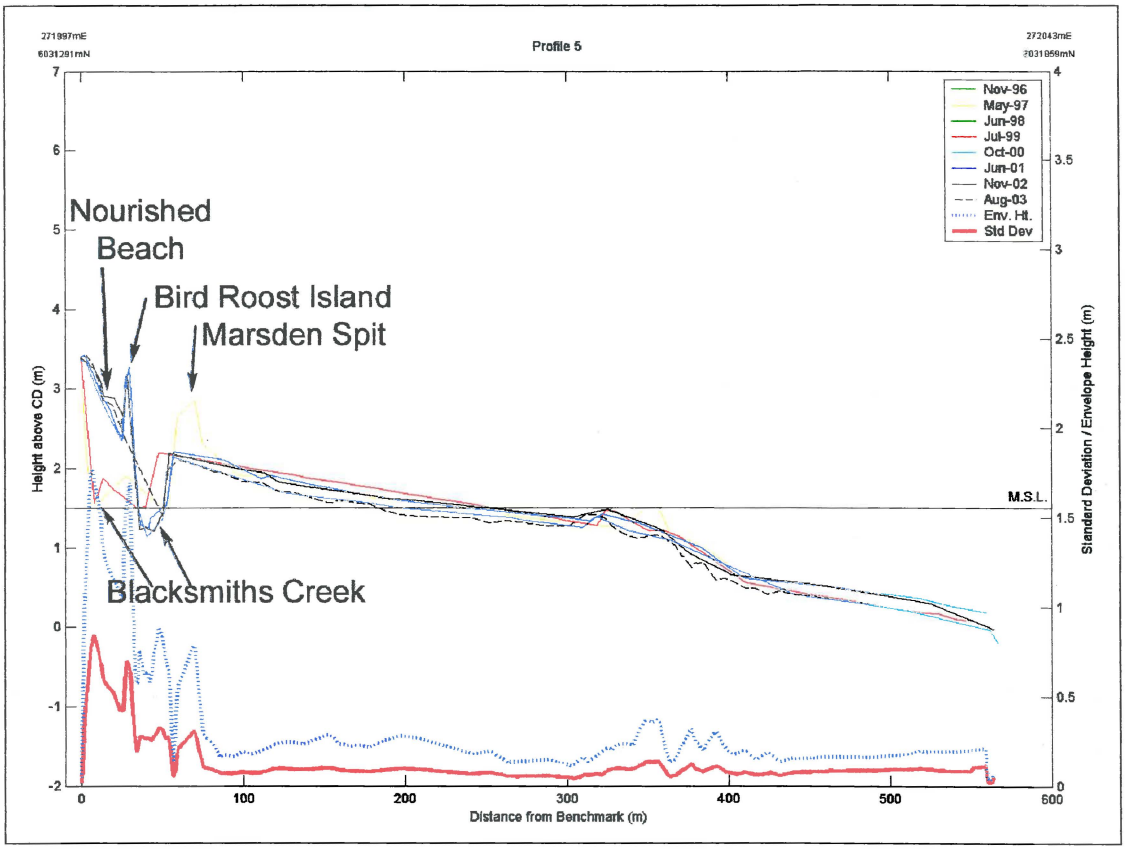


Figure 5.20 - *Profile 5 raw data, envelope of change and standard deviation from mean.*

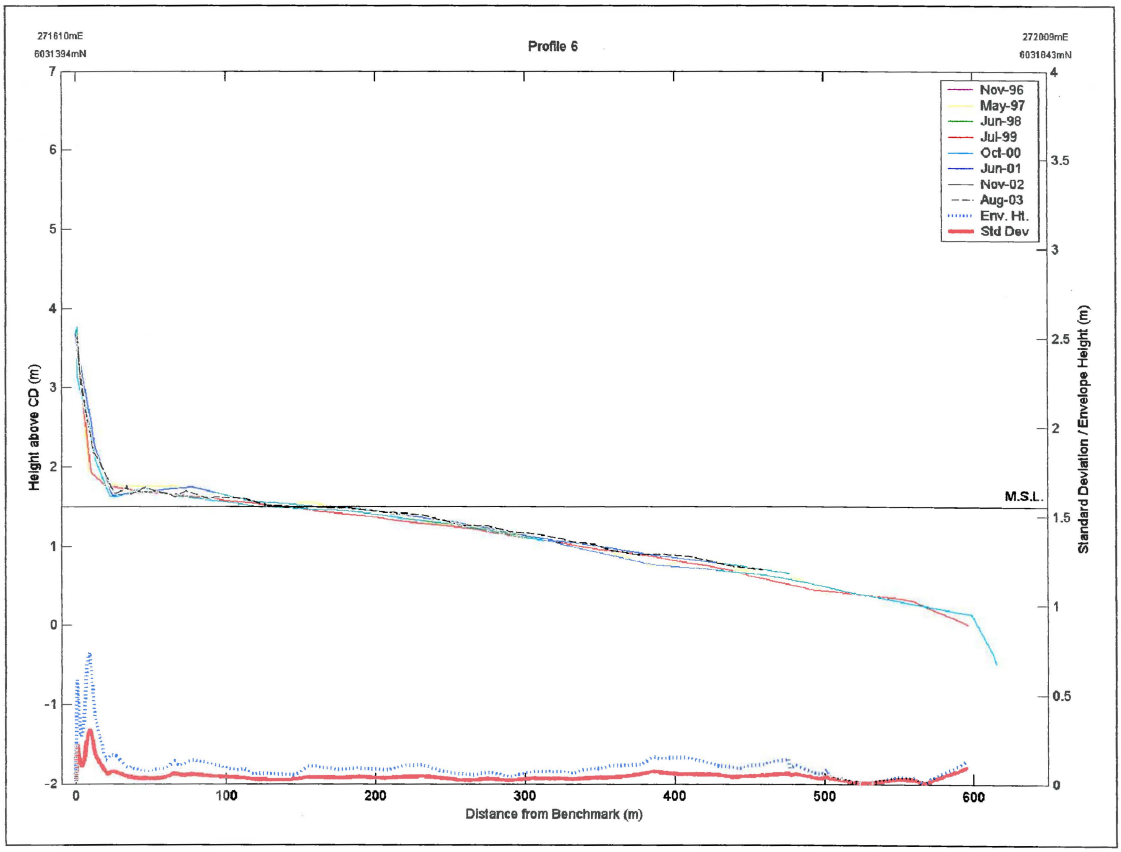


Figure 5.21 - *Profile 6 raw data, envelope of change and standard deviation from mean.*

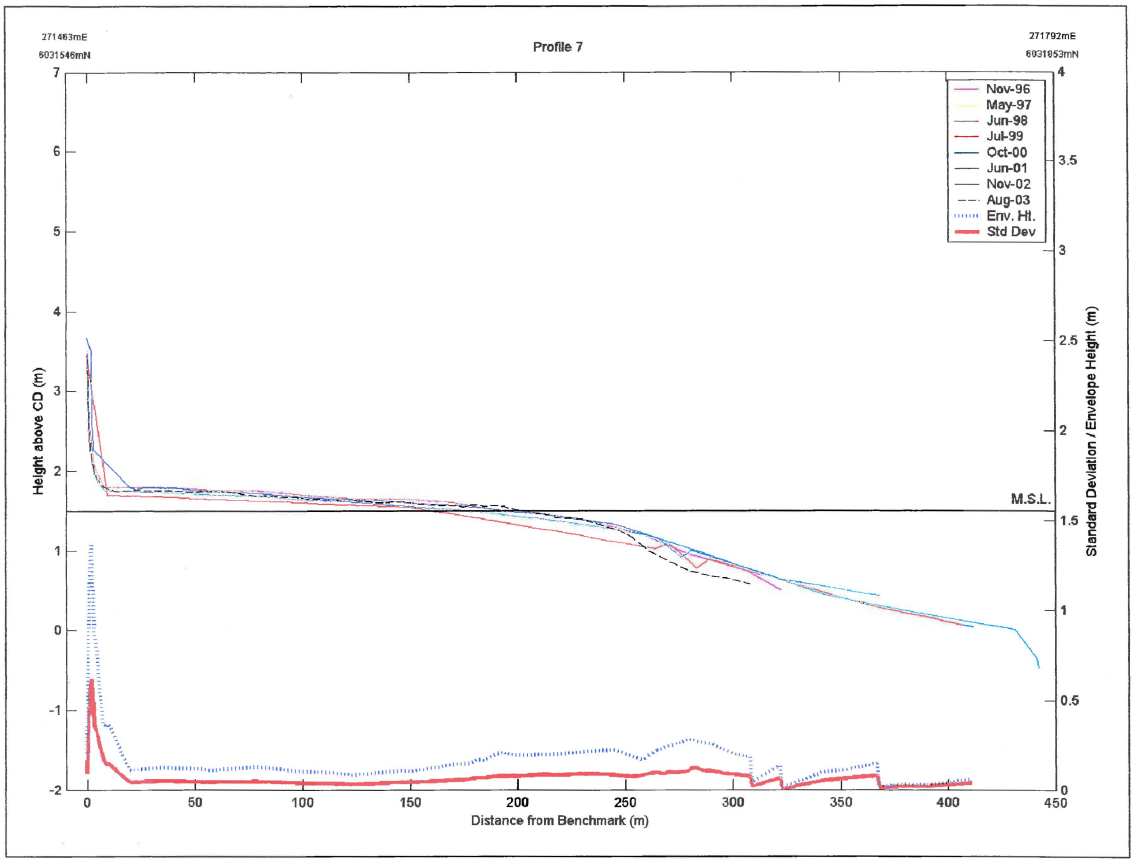


Figure 5.22 - *Profile 7 raw data, envelope of change and standard deviation from mean.*

5.4.3.6 One Tree Point Profiles

Profile 7-1, at Paradise Point exhibits stability with the exception of the 2003 profile near the cliff face (Figure 5.23). Concrete walls and protection structures have protected the cliffs at Paradise Point over the duration of these profiles (Gibb, 1998). Field observations between November 2002 and August 2003 have not revealed any evidence of cliff failure over this period. The profile data of August 2003 should be regarded as erroneous close to the benchmark and cliff edge.

Profile 8 (Figure 5.24) displays a consistently stable profile with very low standard deviations. Profile 9 (Figure 5.25) also shows great stability with a larger envelope of change at the beach face of ~0.2 m. Neither profile displays a ridge similar to that seen in several other profiles.

Profile 10 (Figure 5.26) exhibits a generally stable profile with likely erroneous data for 2003 at the cliff face that is not supported by field evidence over the period. Changes are greatest at the ridge located on the seaward edge of the inter-tidal terrace in depths of + 1.5 m C.D. The 0.2 – 0.3 m high ridge can be observed moving onshore at a rate of 6 my^{-1}.

Profile 11 (Figure 5.27) (again with erroneous 2003 data at the cliff face) shows greater variability than the profiles to the east along this section of coast (profiles 10 and 9). The greatest changes occur at the edge of the inter-tidal terrace where a 0.3 m high ridge moved onshore at a rate of 10 my^{-1} (2001-2003) and acted to narrow the width the inter-tidal zone. The ridge formed over the period 1998-1999 and moved onshore from 1999-2003 consistent with the CERC (1984) description of beach recovery and accretion.

Investigation of the data for profile 12 (Figure 5.28) revealed that the data of 2003 has been measured in the wrong location. While the benchmark for all previous surveys has been 817017 mN, 272319 mE (Mt Eden 1949) the 2003 data first point is located at 817089 mN, 272324 mE (Mt Eden 1949). The 2003 location is 72 m offset from the previous profiles. The offset is not in the direction of the profile transect. The 2003 data at profile 12 should be disregarded and is not used for further analysis. Remaining profiles exhibit relative stability, with no large-scale trends or changes and no large ridge similar to those observed at profiles 10 and.

Profile 13 (Figure 5.29) shows a stable profile over the period 1996 to 2003. The beach face in 1999 exhibited an eroded profile, however recovery occurred quickly. The winnowing blind channel can be seen 270 m from the benchmark, which is the trough feature seen in the profile.

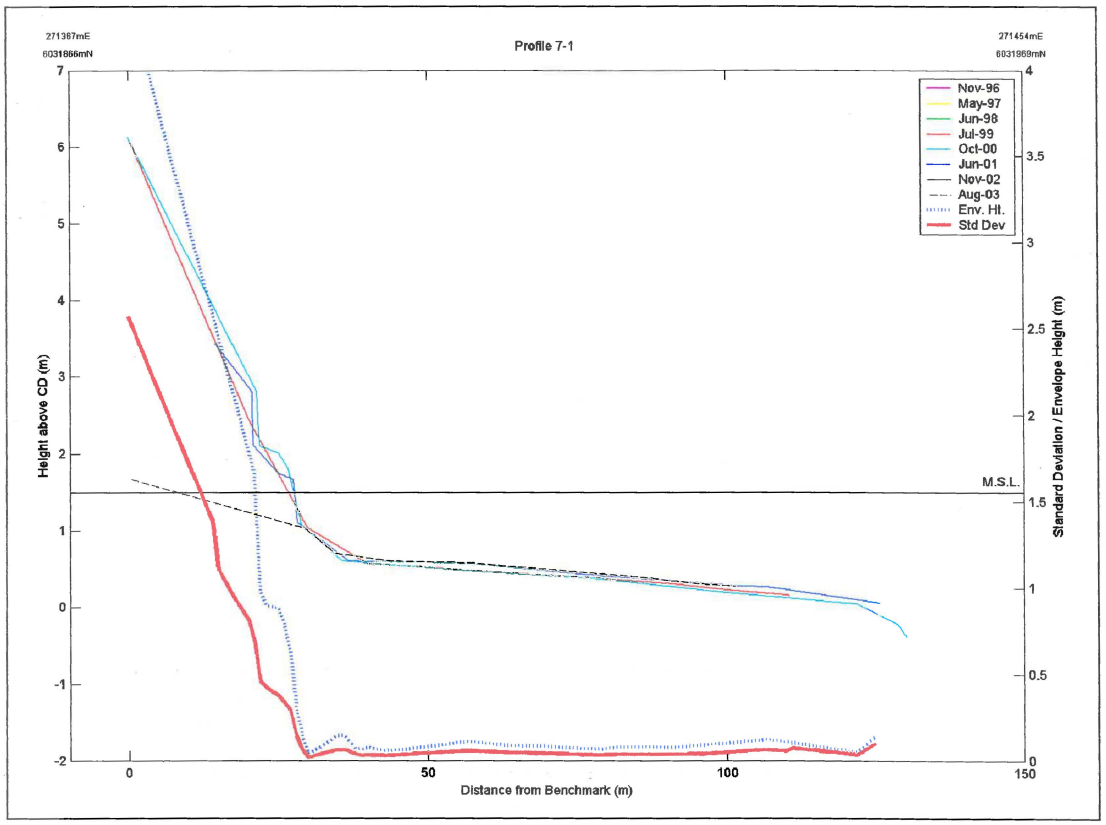


Figure 5.23 - *Profile 7-1 raw data, envelope of change and standard deviation from mean.*

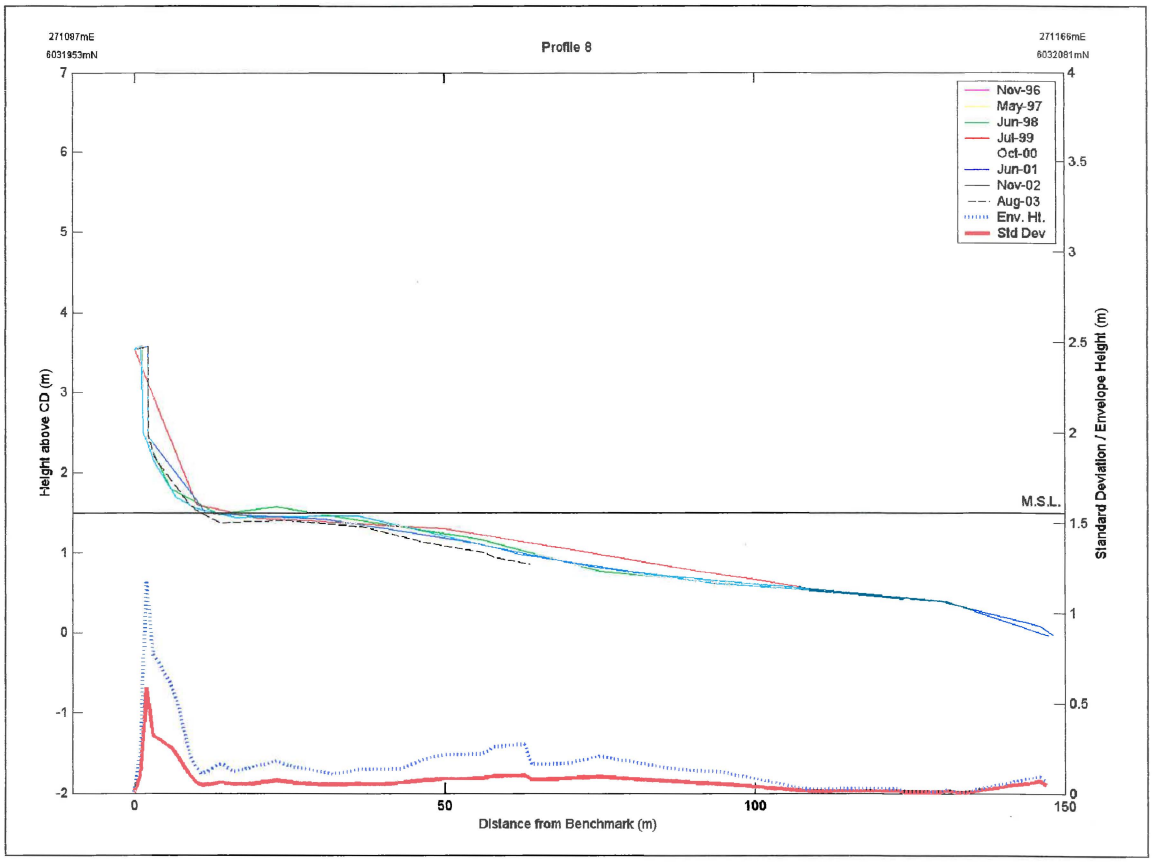


Figure 5.24 - *Profile 8 raw data, envelope of change and standard deviation from mean.*

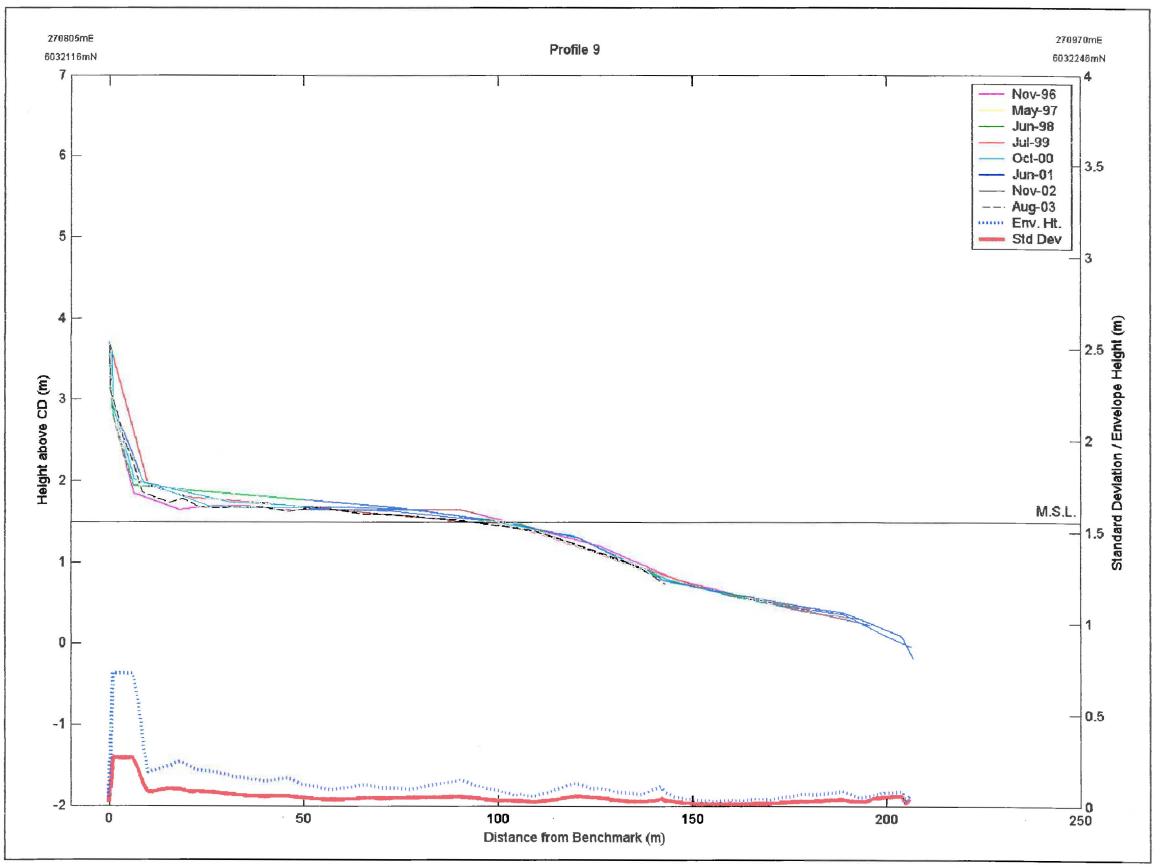


Figure 5.25 - *Profile 9 raw data, envelope of change and standard deviation from mean.*

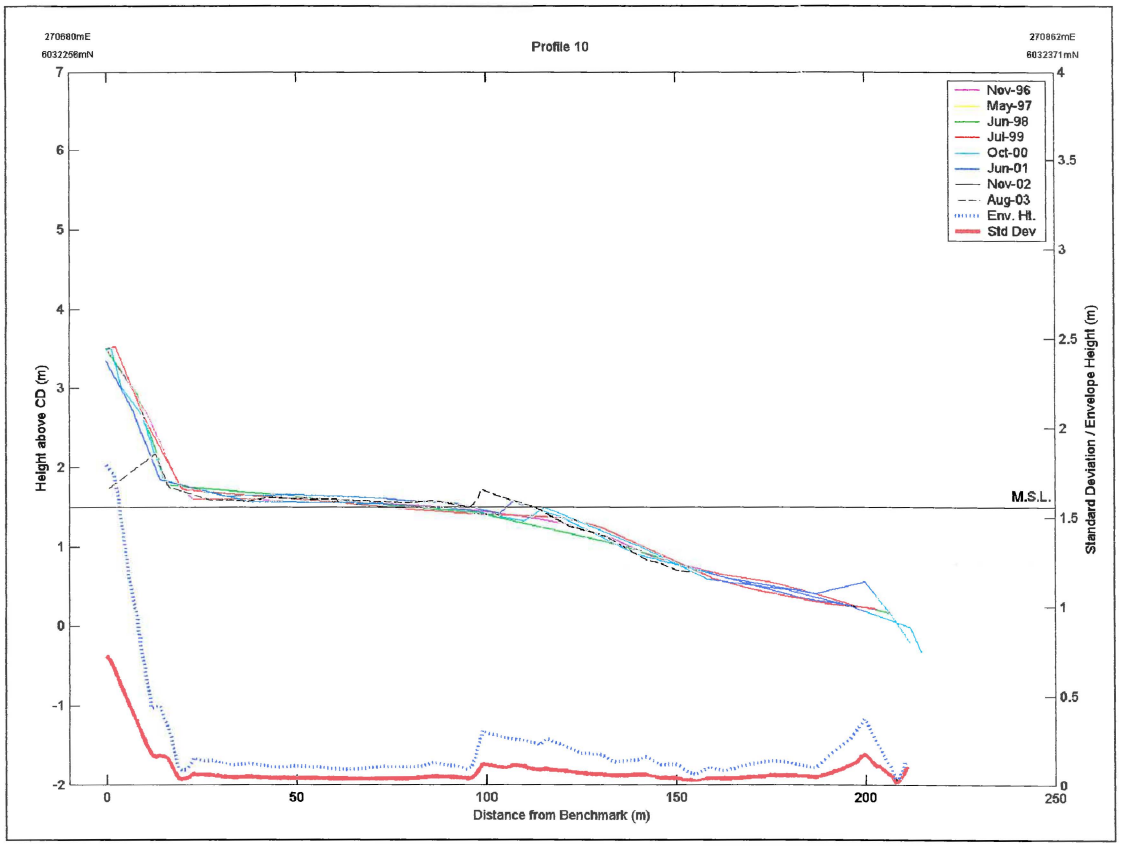


Figure 5.26 - *Profile 10 raw data, envelope of change and standard deviation from mean.*

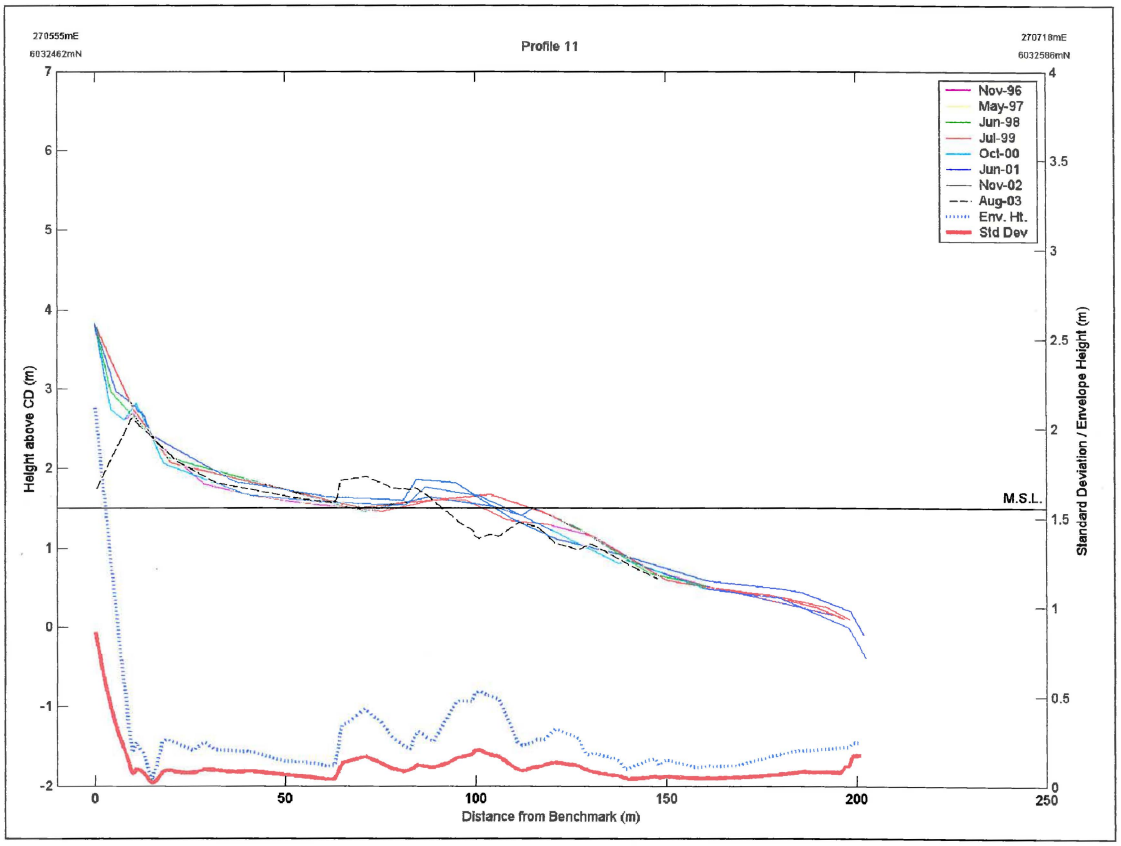


Figure 5.27 - *Profile 11 raw data, envelope of change and standard deviation from mean.*

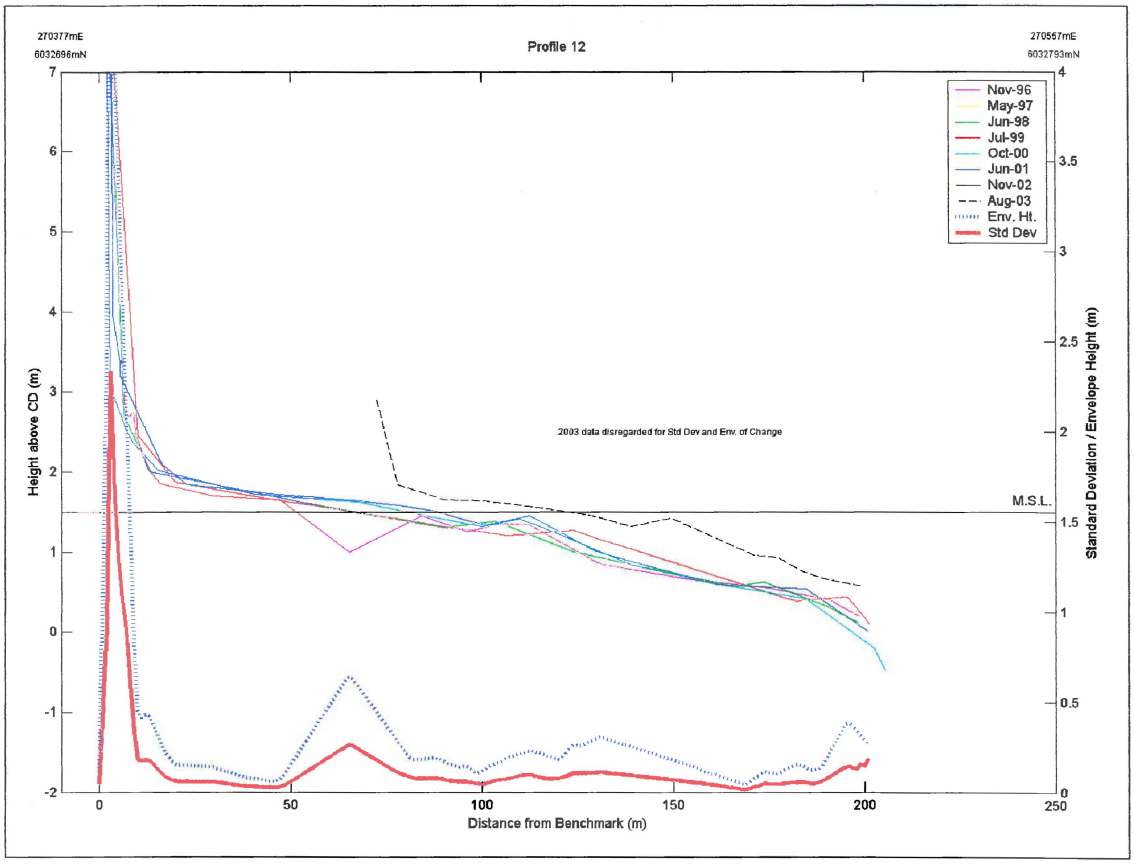


Figure 5.28 - *Profile 12 raw data, envelope of change and standard deviation from mean.*

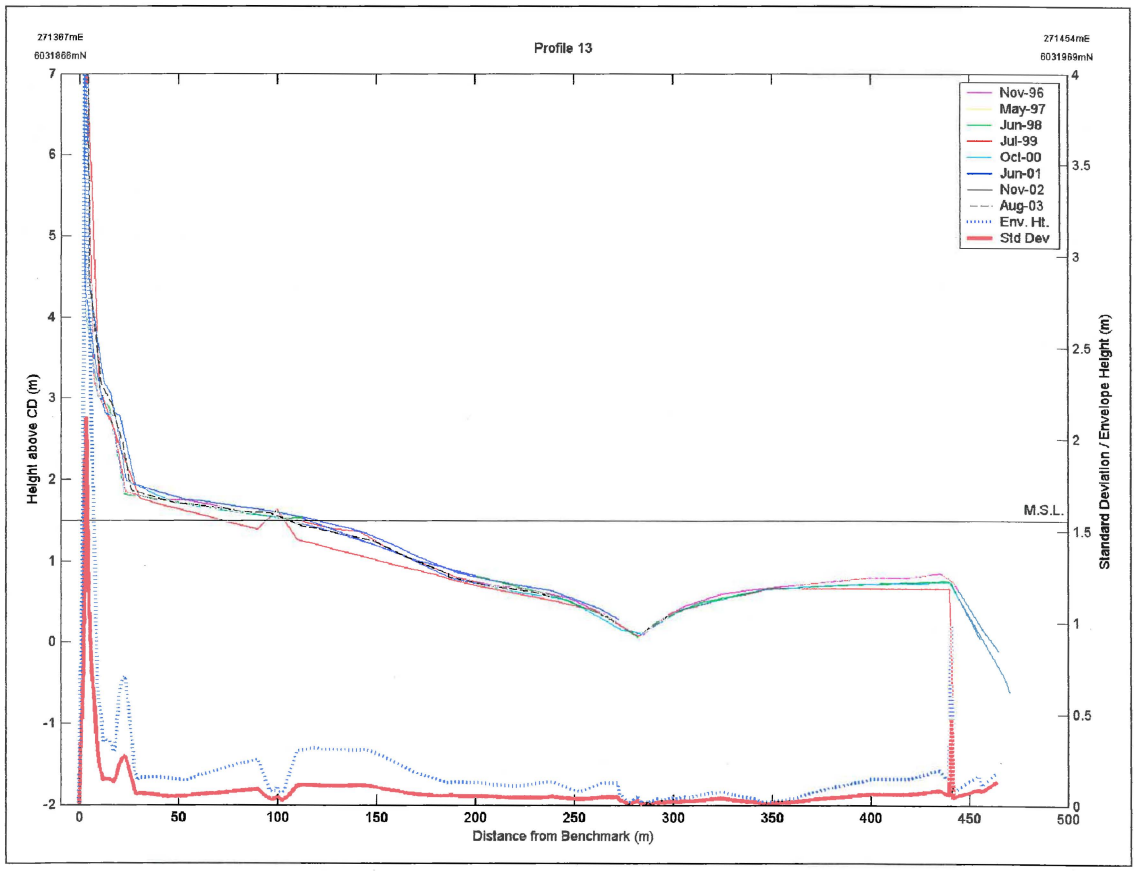


Figure 5.29 - *Profile 13 raw data, envelope of change and standard deviation from mean.*

5.5 Closure Depth From the Raw Profiles

5.5.1 Definition

The depth of closure is commonly defined as the minimum water depth at which no measurable or significant change in bottom depth occurs (Stauble et al., 1993; Gorman et al., 1998). This definition is however complicated as closure depth can vary with waves and hydrodynamic processes, various field studies have in fact verified that much sediment can move in deeper water (Schofield, 1975; Wright, 1991) (and also Chapter 6 of this thesis).

The depth of closure is a time-dependent quantity that may be predicted based on wave climatology or interpreted statistically using profile surveys (Stauble et al., 1993; Gorman et al., 1998). Two methods used to predict closure depth are:

i. Using predictive formulae based on wave and sediment characteristics (Hallermeier, 1981) and
ii. Empirically from observation of measured profiles (Kraus and Harakai, 1983; Stauble et al., 1993).

When surveys consisting of several years are available (as in the present case), closure is best determined empirically by plotting and analysing the profiles (Gorman et al., 1998). Closure depths determined in this manner contain the influence of higher wave energy events as well as typical waves that shape the profile into its dynamic equilibrium state. The depth of closure is identified as the minimum depth where the standard deviation in depth change decreases markedly to a near-constant value (Kraus and Harakai, 1983). Hallermeier (1981) defined the closure depth to be the initial depth at which the envelope of change was consistently smaller than 0.3 m.

Using this definition, the depth of closure is not necessarily the depth at which sediment transport ceases. Rather it is the depth at which observable morphologic changes due to sediment transport can no longer be detected. Sediment may still be transported onshore or offshore past the location of closure depth, however there is no (seasonal, or periodic) accumulation or removal of sediment (greater than the defined limits) at locations deeper than the depth of closure.

The landward section of the profile, where the standard deviation is larger is interpreted to be the active profile, influenced by gravity waves and storm driven water level changes. Lower frequency sediment transport processes such as shelf and oceanic currents primarily influence the offshore region of smaller standard deviation (Gorman et al., 1998).

5.5.2 Depth of Closure From Profile Changes at Marsden Point

The standard deviation of the surveys from the mean beach profile at each profile location has been calculated previously (Section 5.4.2.2). Using a technique based on that of Kraus and Harikai (1983) and also used by Stauble et al. (1993), the elevation of the mean profile and standard deviation of measured profile changes were obtained at each interpolated interval along the profile.

Profile lines were separated into three broad categories for the depth of closure analysis. Three groups were used as any further separation would lead to a scarcity of data points from which to draw conclusions from.

Profile lines A-G, adjacent the NZRC jetties lie in a more active wave environment than the other profiles (Black, 1983). A scatter plot of the standard deviations in the area show a sharp reduction of standard deviations at +0.5 m CD (Figure 5.30). Using the theory of Kraus and Harikai (1983) this can be deemed the empirically determined depth of closure for these profiles. The dip in deviations at elevations of +2.0 m C.D. indicates that there are relatively small changes at this elevation, potentially the beach pivots about this point. There are relatively large changes at elevations in the range +2.5 - +4.0 m C.D.

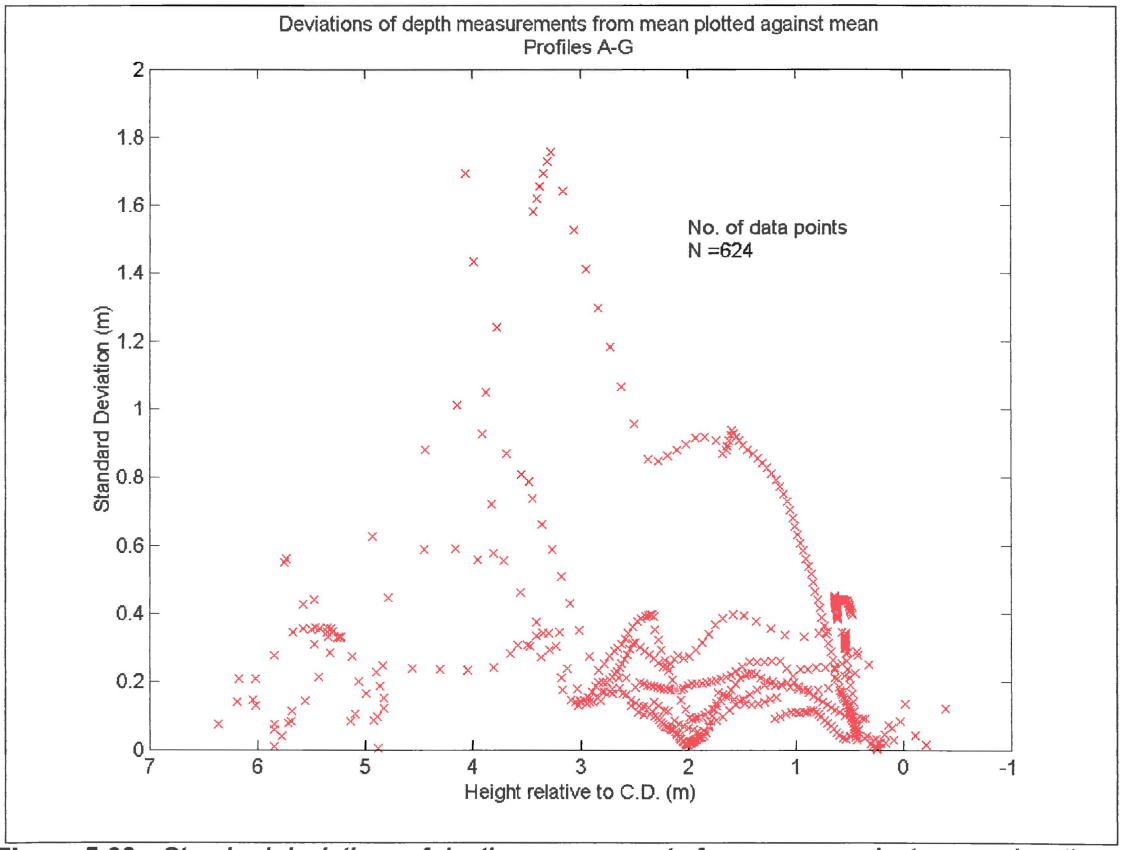


Figure 5.30 - *Standard deviations of depth measurements from mean against mean elevation at Profile lines A-G.*

The area extending from profile 1 to profile 4 is in general a lower energy environment. The area is inside the harbour entrance and profiles exhibit long inter-tidal terraces. Despite this, the depth of closure determined from the profile lines (Figure 5.31) appears deeper than that for profiles A-G (Figure 5.30). A closure depth of +0.2 m CD can be interpreted from the scatter plot (Figure 5.31). It must be noted however that for these locations the profile lines do not extend far enough to record a *'near constant'* standard deviation. A dip can be observed in the standard deviations, similar to that for profiles A-G (Figure 5.30) at +1.8 m C.D. The more elevated sections of the profiles (+2 - +4 m C.D.) are less changeable than similar elevations at profiles of A-G.

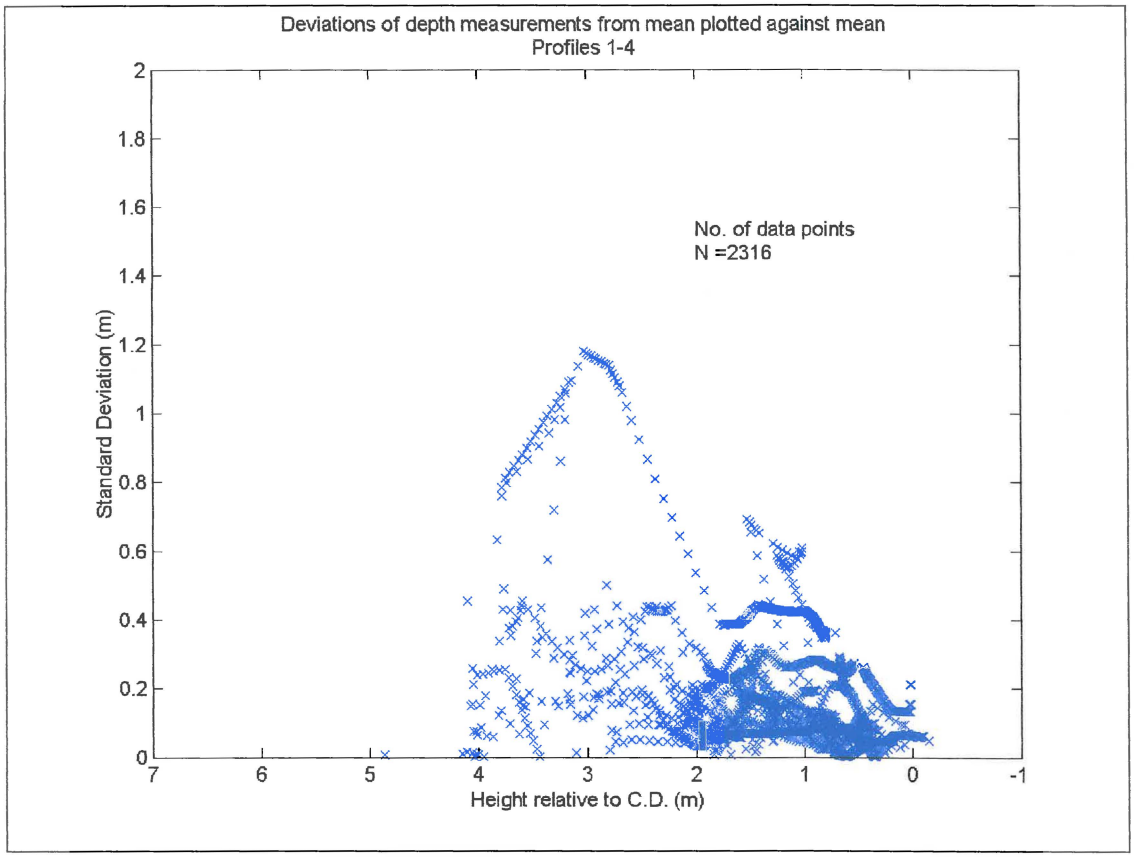


Figure 5.31 - *Standard deviations of depth measurements from mean against mean elevation at Profile lines 1-4 (incl. 215E-215W).*

One Tree Point and Marsden Bay beach profiles exhibit much smaller changes in comparison with the other areas (Figure 5.32). The standard deviations of the changes fall close to the limit of the measurement accuracy of the surveys (± 0.003 m). The uniformly low standard deviation values prevent the unambiguous specification of a closure depth at these locations.

It can be noted that the entire profile for this section of coast is more stable than the two areas considered previously. The changes occurring on the upper beach are of much less magnitude than farther down harbour. There is no observable '*dip*' in the standard deviations that may represent an onshore-offshore rotation point.

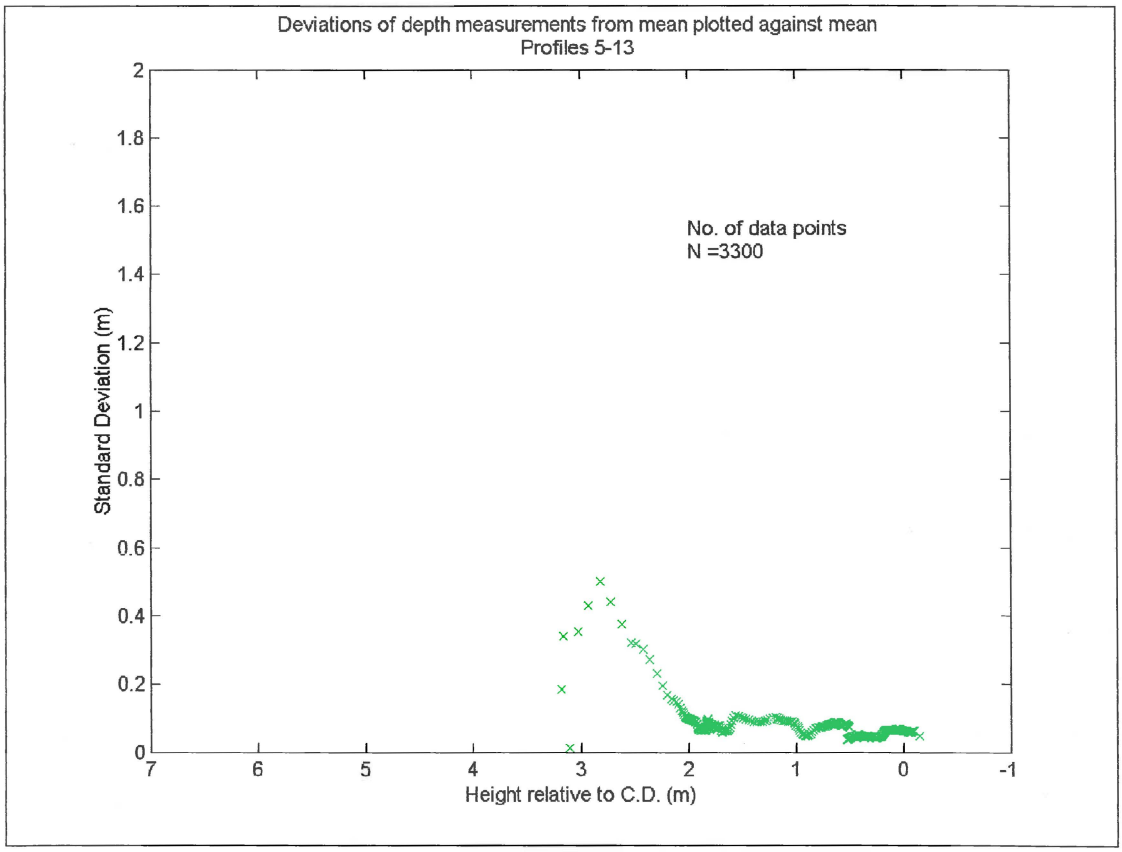


Figure 5.32 - *Standard deviations of depth measurements from mean against mean elevation at Profile lines 5-13.*

5.6 Volumetric Changes

5.6.1 Analytic Techniques and Methods

Volumetric changes are a commonly determined and useful descriptor of beach profile data (Stauble et al., 1993; Gorman et al., 1998; Dean and Dalrymple, 2002).

An arbitrary vertical datum was chosen (0.0 C.D. [0.5 m below mean low water springs]). The datum is suitable as it is deeper than the observed depth of closure for all areas being considered (Section 5.5). Volumetric estimates based on a datum shallower than the depth of closure are biased due to potential seasonal on-off shore sediment movement.

To normalise volumetric changes between survey dates, calculations were made from the baseline (created from the benchmark points) to a distance offshore where the first profile intersected with the vertical datum (0.0 C.D.).

The volume of sand (per unit length along width of beach) at each profile was calculated by integrating the profile (trapezoidal method) over the vertical datum. Then, for all profiles of the same date, the volume of sand in the beach (above the datum) is obtained by integrating the area (volume per unit width) of the profiles along the beach with the distance between the profiles (with half the distance between profiles being used at each end). When carried out over several years a time history of the volume of beach sediment can be generated and the erosion or accretion viewed as a function of time.

As there were odd periods in the data where one profile line may not have been surveyed for some reason, a solution had to be found to allow the calculations to be undertaken. In this situation, the area (volume per unit width) of the profile above 0.0 C.D was calculated for the years prior to and post the missing survey.

The required data was then interpolated from these two values, based on when the prior, post and missing survey were undertaken (or not!).

A MATLAB® program was written by this author to undertake the analysis and plot the results. The core function of the program *'get_volumes.m'* is included in Appendix C.

The accuracy of the calculated volumes depends on the number of beach profile lines covering the fill area. Sensitivity analysis has indicated that optimal profile line spacing

(cost versus accuracy) is in the order of 1000 ft (305 m) (Stauble, 1993). As the spacing increases, variations in beach plan-form can create uncertainties in the volumetric change. While the spacing of the Marsden Point profiles varies, the average distance is ~150 m, with the main areas of interest (surrounding the port site and NZRC jetties) being more closely spaced than this.

With the survey elevation accuracy of ± 0.3 cm, the errors in a typical profile can be calculated. A 150 m long profile (average for Marsden Point) is subject to the elevation accuracy along its entire length, representing an error of ± 0.5 m^3/m in the calculation of the volume per unit width of beach estimates.

The area over which the volume is calculated and the spacing of the profile lines over this area will, of course influence the final error estimate. The error in the volumetric estimates is proportional to the length of the profile, the distance between profiles and inversely proportional to the number of profiles being considered:

$$\text{Volumetric Error } \alpha \frac{0.003 \times \text{length of profile} \times \text{distance between profiles}}{\text{number of profiles}}$$

Results of calculations of errors for each area under consideration are compiled in Table 5.1. It should be remembered that the values calculated are potential errors in the volumetric estimates, based solely on errors in the profile measurement. They are errors inherent in the volume created, not the difference between reality and the volumetric estimates.

As the same technique compares volumes calculated using the same method, the difference between the absolute volumes and reality is not an issue.

Area	Error in volumetric change estimate
Profiles A-G	± 2%
Profiles 1-2	± 6%
Profiles 215E – 15E	± 3%
Profiles 15W-215W	± 3%
Profiles 3-4	± 6%
Profiles 5-7	± 10%
Profiles 8-10	± 8%
Profiles 11-13	± 10%

Table 5.1- *Errors in volumetric change estimates of sediment from beach profile data at Marsden Point.*

5.6.2 Results and discussion

While the areas taken into consideration vary slightly in their spatial extent (Figure 5.33), normalising the volumetric change data (Figure 5.34) for these variations impacted little on the visualisation of trends. Thus Figure 5.34 is displayed in terms of *'change of cubic meters of sediment'* (easier to visualise when referring to volumes) rather than *'average vertical change of the spatial extent'* (m^3/m^2 =m).

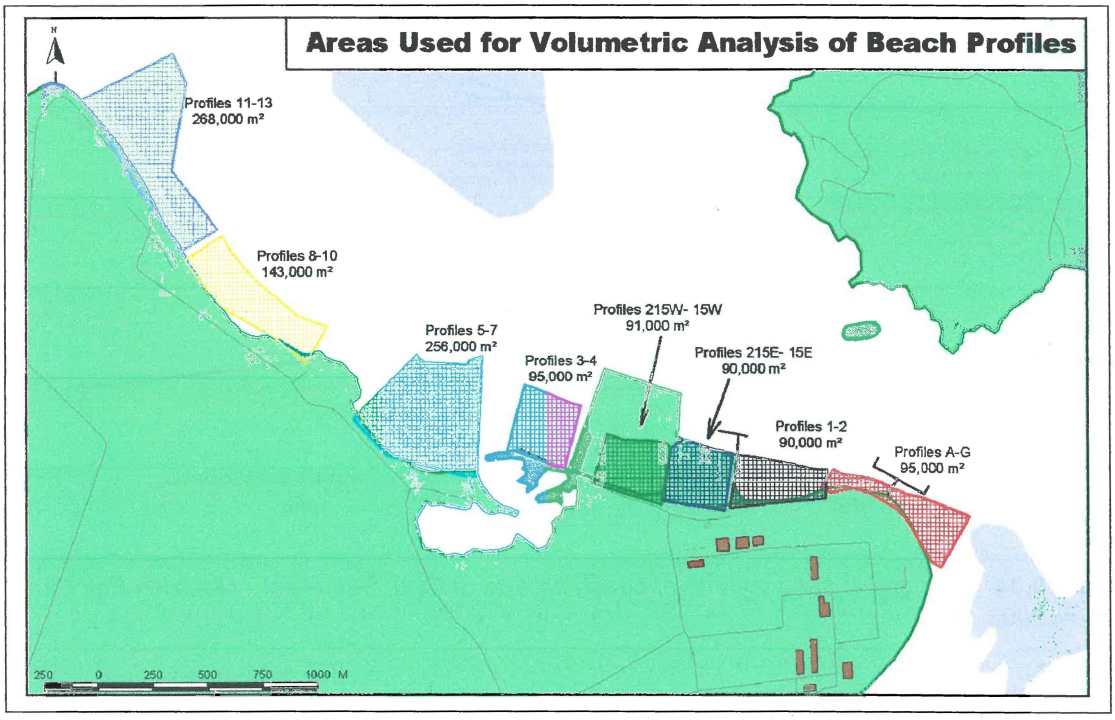


Figure 5.33- *Areas taken into consideration for volumetric analysis of beach sediments.*

It is apparent from Figure 5.34 that the area of beach adjacent to the NZRC jetty was steadily losing sediment from 1998 to late 2002. Balancing accretion could be seen to the west of this area (sum of the volumes of areas 1-2 and 15E –215E over 1998-1999). This trend did not change post-development of Northport. If the source of the accreting sediment at profiles 1-2 and 15E-215E is indeed the area of beach covered by profiles A-G, there is a westward directed longshore component of sediment transport at the tip of Marsden Point. It is likely that the westward directed sediment transport will be trapped against the rock-wall created adjacent to profile 2 as part of the Northport reclamation and accretion will occur. Note also that the erosive trend over profiles A-G has reversed and accretion has in fact occurred over the area between late 2002 and late 2003. Further monitoring of these profiles will reveal if the trend is a short-term fluctuation or longer term pattern.

The profiles to the west of the causeway (215W-15W) (where Northport is now located) were not monitored long enough to establish long term trends, however characteristic sediment transport volumes are of the order of 10,000 m^3y^{-1} for that extent of beach (Figure 5.34).

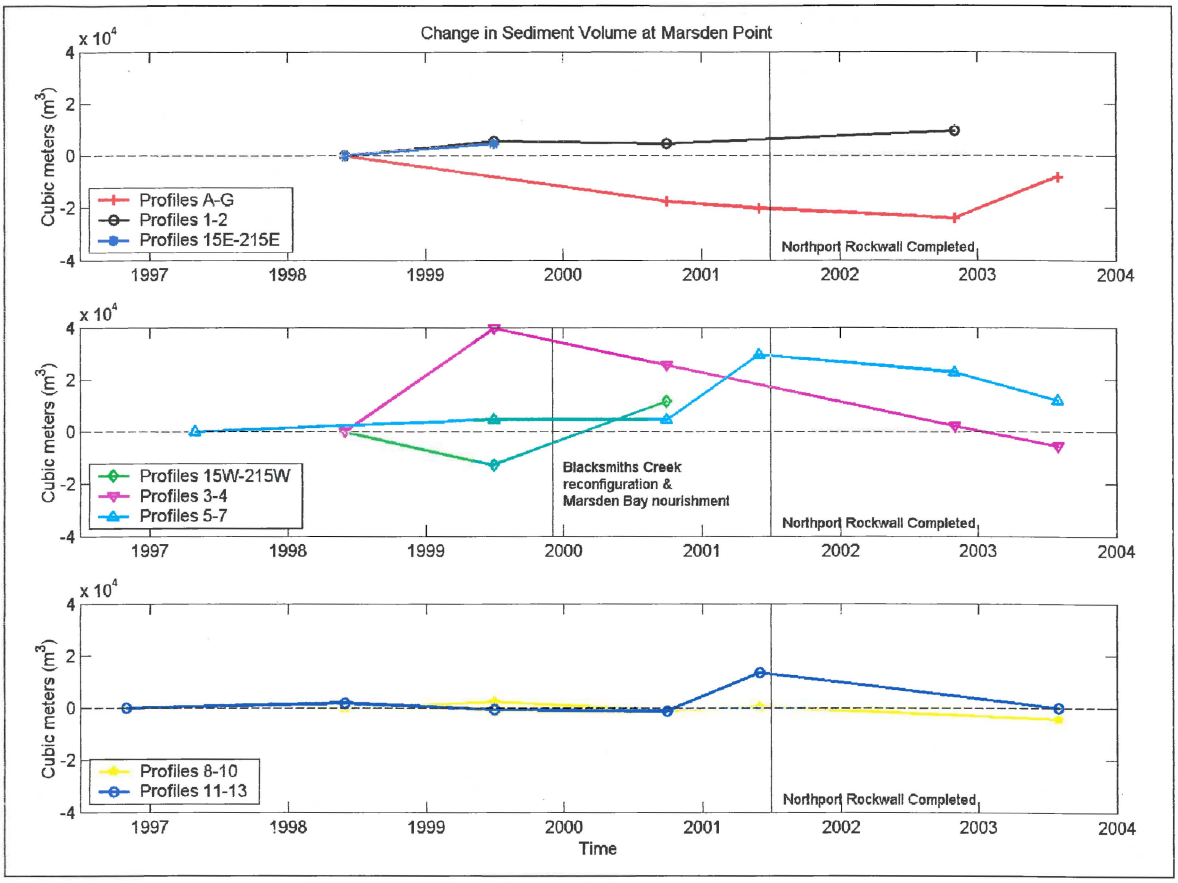


Figure 5.34- *Changes in sand volume of beach profiles at One Tree Point - Marsden Point from 1997 – 2003.*

Marsden spit (profiles 3 and 4) shows a large erosive trend post-construction of the rock-training wall and bird roosting island (Figure 5.34). The observed removal of sediment is in fact the realignment of Marsden Spit following the works (Chapter 4). Air photo analysis (Chapter 4) and other research (Gibb, 1998) has indicated a long-term retreat of the spit. The fixed nature of the profile benchmarks does not account for a large-scale morphologic realignment within the survey area. The observed removal of material is due to the retreat and realignment of the spit, following the works carried out in late 1999.

Marsden Bay sand volumes (profiles 5-7) remained relatively consistent from 1997 to 2000. While the beach was nourished in late 1999, the 2000 survey does not indicate an increase in sediment volume (Figure 5.34). An explanation for this is that the area under consideration also includes the *'old'* location of Marsden Spit (Figure 4.12). The increase in volume created by the nourishment has been balanced by the removal of sediment from the eroding Marsden Spit. The area has been in a slight erosive phase from 2001 – 2003, although overall sediment volumes are still greater than 1997-2000 levels.

The One Tree Point areas, covered by profiles 8-10 and 11-13, have exhibited much greater stability than other areas considered (Figure 5.34) despite covering relatively large spatial extents (Figure 5.33). Profiles 8-10 have shown almost no change in sediment volume at all, whilst the area covered by profiles 11-13, increased in sediment volume temporarily in 2001 before returning to *'normal'* levels in 2003 (Figure 5.34).

5.7 Even-Odd Analysis at the Northport site

5.7.1 Longshore Sediment Transport and Even-Odd Analysis

Even-Odd analysis (Berek and Dean, 1982; Work and Dean, 1990) is a method of determining the effects of a feature (e.g. inlet or coastal structure) that impacts on longshore sediment transport. Its purpose is to separate out those shoreline changes that are symmetric about a point on the coastline (and probably not due to the structure) and those that are due to the presence of the coastal structure (non-symmetric about the structure).

The method separates out net shoreline or volumetric (ΔV_N) changes into an even ($\Delta V_E(x)$) (symmetric) and odd function ($\Delta V_O(x)$) (non-symmetric) about the origin of a longshore coordinate system (Equation 5.1); the origin is placed at the feature being examined (Dean and Dalrymple, 2002).

The interruption of longshore sediment transport should contribute only to the odd component (Berek and Dean, 1982; Work and Dean, 1990; Dean and Dalrymple, 2002). Storms and sea level changes will tend to exert similar influences on both sides of the feature (origin) (+x and -x), leading to the even component. The odd function is by definition non-symmetric about the origin. This origin is therefore a pivot point about which alongshore shoreline or volumetric changes are measured.

$$\Delta V_N = \Delta V_E(x) + \Delta V_O(x) \qquad \textbf{(5.1)}$$

For negative values of x (one side of origin/feature), we have by definition

$$\Delta V_N(-x) = \Delta V_E(-x) + \Delta V_O(-x)$$

$$= \Delta V_E(x) - \Delta V_O(x) \qquad \textbf{(5.2)}$$

Solving the two equations (5.1 and 5.2) gives the formulae necessary to determine the even and odd functions:

$$\Delta V_E(x) = \frac{\Delta V_N(x) + \Delta V_N(-x)}{2} \quad \textbf{(5.3)}$$

$$\Delta V_O(x) = \frac{\Delta V_N(x) - \Delta V_N(-x)}{2} \quad \textbf{(5.4)}$$

Where the even function $V_E(x)$ is symmetric about the y-axis and the odd function $V_O(x)$ is asymmetric.

The odd function describes the changes to the shoreline or sediment volumes with the underlying common (+*x* and -*x*) trend removed (the even function).

Figure 5.35 (from Work and Dean [1990]) shows the results of an even-odd analysis applied to the shoreline adjacent to the St. Lucie Inlet, Florida. The inlet, cut in 1892, has caused severe erosion on Jupiter Island located down drift (south, to the right in the figure).

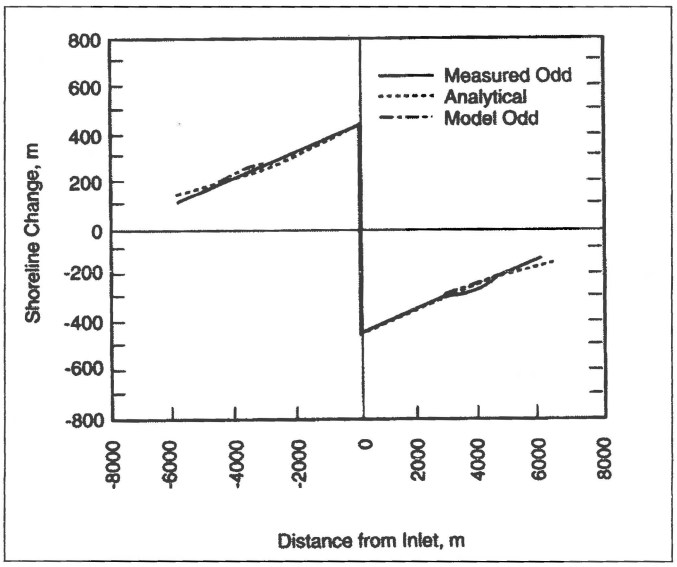


Figure 5.35 - *Even-Odd analysis of the St. Lucie Inlet, Florida (from Work and Dean, 1990). Data are for the period 1928-67.*

5.7.2 Even-Odd Analysis at the Port Site

Even-Odd analysis requires an even spacing of the data on either side of the origin. Repetitive surveys are also required in order to undertake the even-odd analysis on the changes to the profile over time. The impacts of the causeway previously present at the port site and more recently the impact of the Northport rock-walls on the nearby profiles is examined using the method. Even-Odd analysis of the changes in these profiles over time will reveal the impact of the structures on the longshore sediment transport in the area.

For the period June1998 – October 2000 the shoreline position (distance from benchmark line to MSL) and sediment volume (to CD) was calculated at each profile (215W, 55W, 15W, 15E, 55E, 215E). The change in shoreline position and sediment volume (ΔV_N) over the period was calculated at each profile location (alongshore [x]). The Even and Odd change functions were then calculated.

The change in shoreline position, sediment volume, even and odd functions was calculated in a MATLAB® program *'even_odd.m'*, written by this author contained in Appendix C.

Analysis of the changes in shoreline position is limited by the assumption that sand transported along a contour will remain at that contour. This essentially assumes that on-off shore sediment transport is negligible. To avoid the limitations of this assumption, analysis of the changes in sediment volumes about the causeway has also been undertaken.

The odd functions created using the causeway as the origin provide an insight to the longshore sediment transport at the port site prior to the port development. It is desirable to observe if the pattern observed prior to development is in fact continuing after post-development.

While the technique described by Berek and Dean (1982), Work and Dean (1990) and Dean and Dalrymple (2002) generally describes point type features such as groynes and the causeway used for the initial analysis, there is no reason why the analysis can not be carried out on a larger (wider) feature such as the Northport reclamation.

Profiles 1,2 and 3,4 are relatively evenly spaced on either side of the Northport reclamation (Figure 5.1). Even-Odd analysis can be carried out using the mid point between profiles 2 and 3 as the origin. It must be recognised that the function

generated over the area where the reclamation exists represents no physical pattern. Even-Odd analysis of the volumetric changes in these profiles was undertaken using the MATLAB® function *'even_odd.m'* (Appendix C). Data used include the changes in sediment volumes (to CD) of the profiles over the period October 2000 – November 2002.

5.7.3 Results and discussion

Over the period June 1998 – October 2000 the odd component of shoreline change centred on the causeway at the now Northport site (Figure 5.36) shows evidence of longshore sediment transport from west to east. The shoreline prograded seawards close to the causeway on the western side and retreated landwards on the eastern side. This effect is limited to 100 m either side of the causeway. Farther away from the causeway the pattern reversed and the shoreline retreated on the western side and advanced on the eastern side (Figure 5.36). Note these changes are not net changes but only those occurring as a result of the causeway. The shoreline was rotating in an anti-clockwise direction due to the effects of the causeway. The progradation of the shoreline on the eastern side (>100 m from causeway) could be evidence for sand bypassing the end of the causeway under a dominant west to east sediment transport regime.

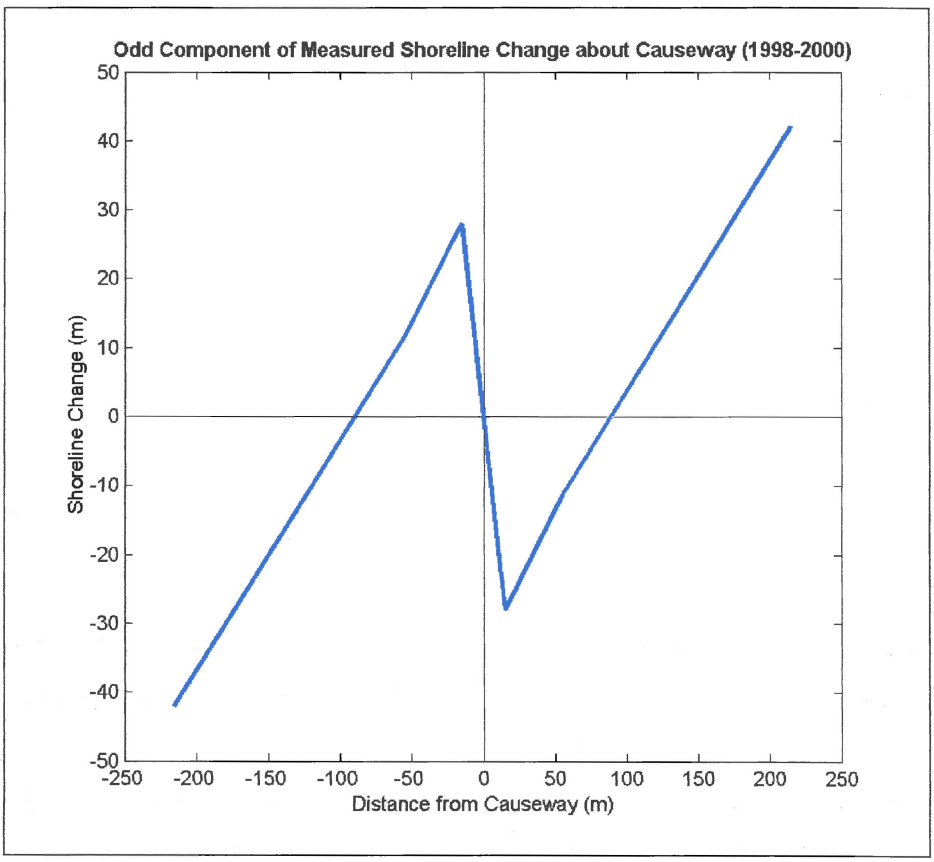


Figure 5.36- *Odd Component of shoreline change about causeway at Northport site 1996-2000. (West is to the left of the origin (causeway) and east to the right).*

Even-Odd analysis of the volumetric changes of the same area, over the same period (Figure 5.37) is not subject to the assumption of negligible onshore-offshore sediment transport.

Close to the causeway a similar pattern to the shoreline change data (Figure 5.36) is apparent. An increase in sediment volumes occurs on the western side, while the eastern side experiences a decrease as a result of the causeway (recall the odd function is only the non-symmetric changes about the origin). The effect of the causeway seems limited to between 50 and 100 m in the x direction (along the beach). The causeway was trapping sediment on its western side over the period 1998 – 2000. A sediment transport direction from west to east is inferred.

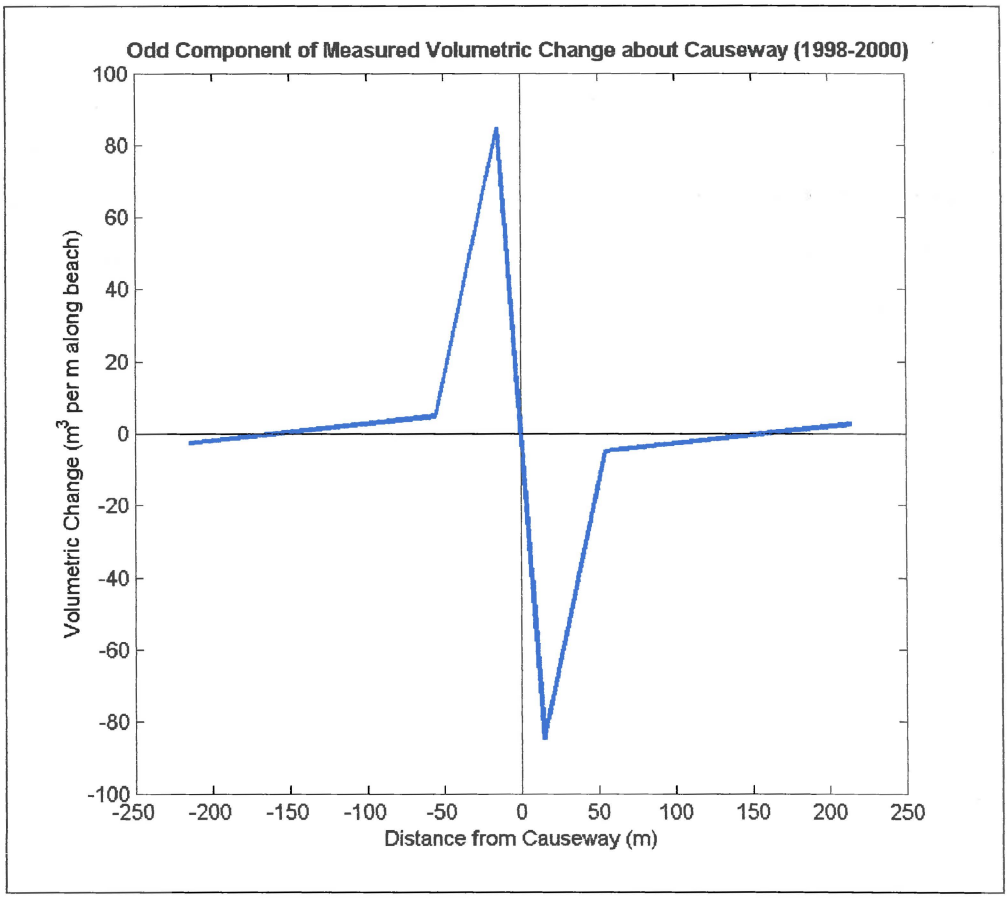


Figure 5.37- *Odd Component of volumetric sediment change about causeway at Northport site 1996-2000. (West is to the left of the origin (causeway) and east to the right).*

Post-construction (of Northport) profiles 1,2 and 3,4 have been analysed for non-symmetric changes in sediment volume. Results (Figure 5.38) indicate a non-symmetric (due to the rock-walls) pattern of an increase in sediment volume adjacent the western edge of the reclamation and a decrease adjacent the eastern edge. The odd component of volumetric change can be used to infer a sediment transport direction directed eastwards at the port site from 2000 to 2002. The direction is

consistent with that observed prior to port development. The magnitude of the odd-component (that due to the obstruction) post development (80 m^3/m) (Figure 5.38) is very similar to that caused by the causeway pre-construction (85 m^3/m) (Figure 5.37).

The Northport reclamation is acting as an 800 m wide groyne. Sediment moving in an easterly direction alongshore is trapped against its western edge. The process is no different to that observed about a causeway in the middle of the port site, prior to the reclamation.

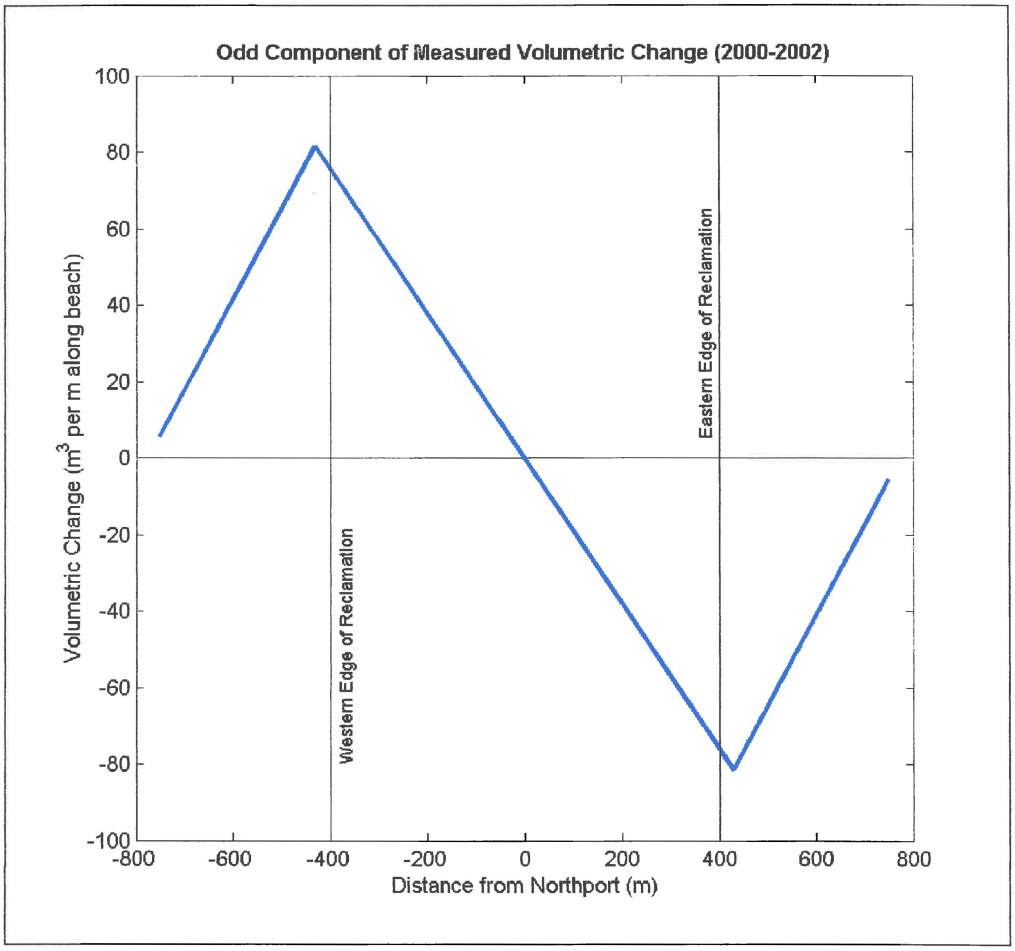


Figure 5.38- *Odd Component of volumetric sediment change about Northport reclamation 2000-2002. (West is to the left of the origin and east to the right).*

5.8 Principle Components Analysis

5.8.1 Background

Principle Components Analysis (PCA) is often alternately referred to in the coastal literature as Empirical Orthogonal Function (EOF) analysis. The empirical orthogonal eigenfunction method is a widely used statistical tool that can be applied to analyse beach profiles to determine their variation through time or along a beach. The statistical methodology was first introduced by meteorologists and has since been applied in many diverse scientific fields (Winant, Inman and Nordstrom, 1975).

The primary advantage of the method is that it can often identify underlying patterns within beach survey data that are typically highly variable and otherwise difficult to interpret. Eigenfunction analysis is an efficient way to describe beach profile changes, however it should be emphasised that it is a descriptive process and therefore does not reveal any information relating to the processes that shape the beach profile.

Previous studies using the method include those by Winant et al., (1975), Aubrey (1979) and Dick and Dalrymple (1984). Data required for the EOF analysis consist of multiple beach profiles, either over time at a fixed location or over distance at a fixed time.

The objective of the method is to separate the temporal and spatial dependence of the data so that it can be represented as a linear combination of corresponding functions of space and time. These functions then represent the variation of the beach profile configuration in terms of distance from fixed data points and in terms of temporal changes in profile configuration over the period of study (Winant et al., 1975). The method relies on the theory that the original profile (h_{xt}) can be described by the summation of multiple (eigen) functions (e_{nx}) each multiplied by its corresponding coefficient (c_{nt}). The weight of the coefficient defines the degree of variation from the statistical mean (Figure 5.39).

A schematic representation of the decomposition of a profile by the empirical eigenfunction method is contained in Figure 5.39.

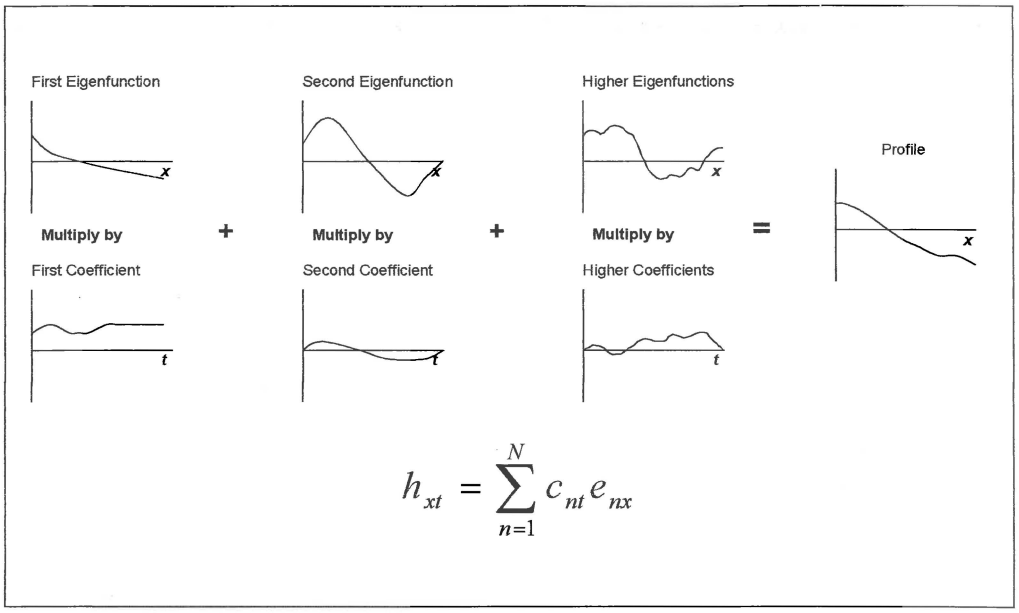


Figure 5.39- *Schematic decomposition of profiles using the eigenfunction method (after Dick and Dalrymple, 1984).*

5.8.2 Statistical method

The derivation of the eigenfunctions (eigenvectors) is explained following methods described by Winant et al. (1975) and Dean and Dalrymple (2002).

The method aims to represent the beach profile data (depth elevations h), as a linear combination of functions of distance normal to the beach (x) and functions of time (t).

Beach profile data is represented for a given profile location as h_{xt}, where x is an index ranging from 1 to n_x (the total number of points along the profile where data are given) and t is an index which varies between 1 and n_t (the total number of times at which the profile was surveyed).

The EOF method is based on assuming that the elevation h_{xt} (profile elevation at point x and time t) is explained by the summation of eigenfunctions multiplied by constants (Figure 5.39), a normal mode expansion of the form:

$$h_{xt} = \sum_{n=1}^{N} C_{nt} e_{nx} \qquad \textbf{(5.5)}$$

Where e_{nx} represents the n^{th} spatially varying empirical eigenfunction evaluated at the x^{th} location along the profile (there are N eigenfunctions and X profile data points). The constant C_{nt} represents the coefficient for the t^{th} survey and the n^{th} eigenfunction. (Similar to Fourier analysis, where the eigenfunctions are sines and cosines).

A property of the eigenfunctions is that they are independent of each other (orthogonal), that is,

$$\sum_{x=1}^{X} e_{nx} e_{mx} = \delta_{nm} \qquad \textbf{(5.6)}$$

Where δ_{nm}=1 if n=m and is zero otherwise. The e_{nx} form a set of normal modes, or eigenfunctions, which are normalised to unity.

To obtain the value of the unknown C_{nt}, we minimise the mean square error in the fit of h_{xt} by the eigenfunctions, the local error ε_{xt} is defined as,

$$\varepsilon_{xt} = h_{xt} - \sum_{n=1}^{N} C_{nt} e_{nx} \qquad \textbf{(5.7)}$$

The minimisation is carried out in the least squares sense by minimising the sum of the squares of the errors over the profile:

Minimise $\sum_{x=1}^{X} \varepsilon_{it}^2$ with respect to C_{mt} (where δ_{nm} =1 [eq.5.6]) **(5.8)**

or,

$$2\sum_{x=1}^{X}\left(h_{xt} - \sum_{n=1}^{N} C_{nt} e_{nx}\right) e_{mx} = 0 \qquad \textbf{(5.9)}$$

Using the orthogonality relationship [eq. 5.6], we have,

$$C_{mt} = \sum_{x=1}^{X} h_{xt} e_{mx} \qquad \textbf{(5.10)}$$

(C_{mt} is the coefficient C_{nt} that minimises the mean square in the fit of h_{xt}.)

This equation [5.10] allows us to determine the coefficients (C_{mt}) for a given survey once we know the eigenfunctions.

Following Dean and Dalyrumple (2002) the total mean square variance of the profile data σ^2 can be shown:

$$\sigma^2 = \frac{1}{XT}\sum_{t=1}^{T}\sum_{x=1}^{X} h_{xt}^2 = \frac{1}{XT}\sum_{t=1}^{T}\sum_{x=1}^{X}\left(\sum_{n=1}^{N} C_{nt} e_{nx}\right)\left(\sum_{m=1}^{N} C_{mt} e_{mx}\right) \qquad \textbf{(5.11)}$$

Which after repeated use of the orthogonality relationship [7.6] can be written as

$$\sigma^2 = \frac{1}{XT}\sum_{t=1}^{T}\sum_{n=1}^{N} C_{nx}^2 \qquad \textbf{(5.12)}$$

This is Parseval's theorem, i.e. the sum of the squares of the coefficients is equal to the square of the variance. The variance is composed of the sum of the squares of all the coefficients taken over all the surveys.

To find each eigenfunction, its contribution to the variance will be maximised. If we allow the eigenfunction to be large however, the coefficient can be made arbitrarily small. The size of the eigenfunction will therefore be restricted to unity in order to find a unique solution. This has in fact already been used previously in the orthogonality condition (eq. 5.6).

Therefore following Dean and Dalrymple (2002) we use the Lagrange multiplier approach to introduce the constraint to our maximisations problem. We maximise the following function,

$\frac{1}{XT}\sum_{t=1}^{T} C_{nt}^2 - \lambda\left(\sum_{x=1}^{X} e_{nx}^2 - 1\right)$ with respect to e_{nm}, where λ is the Lagrange multiplier. Differentiating, we obtain,

$$\sum_{x=1}^{X} e_{nx}\left(\frac{1}{XT}\sum_{t=1}^{T} h_{xt}h_{mt}\right) = \lambda e_{nm} \qquad \textbf{(5.13)}$$

If we form the **correlation matrix *A***, with elements

$$a_{xm} = \frac{1}{XT}\sum_{t=1}^{T} h_{xt}h_{mt} \qquad \textbf{(5.14)}$$

Like any square matrix, matrix *A* possesses a set of eigenvalues λ and a corresponding set of eigenfunctions e_n,

$$Ae_n = \lambda_n e_n \qquad \textbf{(5.15)}$$

If λ_1 and e_{1x} are the largest eigenvalue and its associated eigenfunction, respectively the function $e_{1x}(\lambda_1)^{0.5}$ is the best fit of the correlation matrix and hence the mean. Using equation 5.14 we have the symmetric matrix equation.

$$\sum_{x=1}^{X} a_{xm}e_{nx} = \lambda e_{nm} \qquad \textbf{(5.16)}$$

This is one equation for X unknowns, but by allowing m to vary from 1 to X we obtain X equations for X unknowns.

Equation 5.16 is an eigenvalue matrix equation consisting of a symmetric real coefficient matrix. There are as many eigenfunctions as there are points X in the profiles, therefore $N=X$ and each eigenfunction is associated with a distinct eigenvalue λ_n.

The diagonal terms of the correlation matrix A are

$$a_{xx} = \frac{1}{XT}\sum_t h_{xt}^2 \qquad \textbf{(5.17)}$$

These terms represent the mean square value of the data in time divided by X at the x^{th} point along the profiles. The sum of these values (the Trace of matrix A) is equal to the mean square value of all the data. Thus each eigenvalue can be thought of as being representative of a certain percentage of the mean square value of all the data.

5.8.3 Application to the Marsden Point Profiles

A MATLAB® program *'temporal_eigens.m'* was written by this author to undertake the preceding calculations on the Marsden Point profile data and calculate the eigenvalues and eigenfunctions of the profile data. The program is contained in Appendix C.

The eigenfunction method requires that the profile measurements to be compared be taken at consistent distances along the profile line (x). The raw data do not meet this criteria, thus profile measurements at regular intervals (0.5 m) in the x direction were interpolated from the raw data (lines 13 to 22 of *temporal_eigens.m*).

Next the correlation matrix (A) is formed from the matrix of beach elevations on the regular grid (H). This step forms the correlation matrix (A) described in equation 5.14, which is simply,

$$\frac{H^T H}{XT} \qquad \text{(Aubrey, 1979)}$$

Where X=the number of measurements in the x direction and T=the number of times the profile was surveyed. This step is undertaken on lines 26 to 28 of *temporal_eigens.m.*

The eigenvalues and eigenfunctions of the square correlation matrix were then calculated (line 30). The mean square error of the data (Trace of A) was evaluated (line 34), followed by the percentage of variance explained by the first three eigenfunctions (line 48). We now have the eigenvalues and eigenfunctions of the profile data.

The time variation of the eigenfunction coefficients was then determined using equation 5.10 in the MATLAB® program *'eigen_coeffs.m'*. The step required the nesting of three separate *'for'* loops to sum the required elements of the matrices, not an easy task to conceptualise in one's head. The function is called on line 62 of *'temporal_eigens.m'* and is also included in Appendix C.

5.8.4 Interpretation of Eigenfunctions

The first eigenfunction has been shown to represent the mean beach profile (eq. 5.15), while the corresponding eigenvalue represents the amount of variance explained by the eigenfunction (Winant et al., 1975; Aubrey, 1979; Dean and Dalrymple, 2002). The trend through time of this eigenfunction indicates net erosion or accretion (Aubrey, 1979).

The second eigenfunction accounts for the majority of the variation of the profile with the mean beach function removed. The maxima and minima of the second eigenfunction denote the locations of greatest change. Previous research (Winant et al., 1975; Aubrey, 1979; Dick and Dalrymple, 1984) has led to the term *'bar-berm function'* being used to describe the second eigenfunction. Temporal variation of this function generally shows a seasonal dependence, mimicking the building of the bar and berm.

The second eigenfunction should estimate of the pivotal point for seasonal profile changes (Aubrey, 1979). The onshore-offshore pivotal point is defined by the zero crossing of the second eigenfunction.

The third eigenfunction accounts for less variance in the data than the second function and has been referred to as the *'terrace'* function. It has been previously noted that variation in this function may take place over short time scales (less than months) (Winant et al., 1975; Aubrey, 1979; Dick and Dalrymple, 1984), which would mean a surveying scheme would need to be of a similar or greater frequency to observe changes in this function.

Further eigenfunctions can be calculated, each representing decreasing amounts of variance from the mean. It is generally accepted however (Winant et al., 1975; Aubrey, 1979), that the largest three eigenfunctions are sufficient to explain the major variations in beach profile data.

Due to the periodicity of the surveys at Marsden Point, the name given to the second eigenfunction by previous researchers might not be entirely appropriate. The *'bar-berm'* function was named based on analysis of monthly profile data (Winant et al., 1975; Aubrey, 1979). The current profiles under consideration were surveyed closer to annually (Appendix C). The second eigenfunction essentially represents the largest proportion of variations from the mean profile for the period the surveys cover. Due to the survey interval, the second eigenfunction may be subject to aliasing and any intra-annual (seasonal) pattern hidden.

5.8.5 Eigenfunctions at Marsden Point

The first three eigenfunctions, eigenvalues and the time variation of the eigenvalues were calculated for each profile line at Marsden Point and are included in Appendix C. A detailed analysis of eigenfunctions of all profile lines at Marsden Point would be an in depth and excessive exercise beyond the needs for the current study. Therefore the eigenfunctions of selected profiles only will be described.

The percentage of variance explained by each eigenfunction (Table 5.2) corresponds well with that found by Winant et al. (1975), who found the first eigenfunction usually accounted for 99% of the variance, the second ~>0.1% and the third ~0.06%.

Eigenfunctions at profile B (Figure 5.40) show that the eigenfunction with the largest eigenvalue represents over 99% of the mean square value of the data and signifies the mean beach profile. The time variation of the mean beach function displays a decreasing trend over time, indicating that the beach has experienced net erosion over the time period.

The second eigenfunction displays maxima at the foot of the dune, berm (HWL) and at the location of a bar (0.5 m below MWL) (Figure 5.40), indicating that these sites are the locations of greatest change in the profile.

Profile	Variance explained by 1st	Variance explained by 2nd	Variance explained by third
A	96.71%	3.00%	0.19%
B	99.22%	0.63%	0.12%
C	99.49%	0.37%	0.06%
E	99.90%	0.05%	0.03%
F	98.43%	1.33%	0.22%
G	99.82%	0.12%	0.04%
1	99.70%	0.13%	0.09%
2	99.74%	0.19%	0.05%
215E	99.75%	0.19%	0.06%
55E	97.44%	2.49%	0.05%
15E	99.79%	0.16%	0.04%
15W	98.41%	0.99%	0.60%
55W	99.21%	0.37%	0.25%
215W	99.44%	0.43%	0.10%
3	99.47%	0.34%	0.12%
4	99.77%	0.13%	0.05%
5	98.90%	0.86%	0.12%
6	99.92%	0.05%	0.02%
7	99.79%	0.14%	0.04%
8	99.60%	0.25%	0.14%
9	99.84%	0.11%	0.02%
10	99.41%	0.51%	0.04%
11	99.45%	0.44%	0.06%
12	98.57%	0.89%	0.35%
13	99.10%	0.58%	0.24%

Table 5.2- *Results of empirical eigenfunction analysis, percentage of variance explained by each eigenfunction.*

The shape of the second eigenfunction at profile B is similar to that observed by Aubrey (1979) at Indian Canyon Range, Torrey Pines Beach, California (Figure 5.41).

The second eigenfunction has a zero crossing at the mid point of the dune and also at a distance of 55 m from the benchmark, just above mean sea level (on the beach slope) on the mean profile. This indicates a periodic movement of sediment up and down the dune about the *'dune pivot point'* and also up and down the beach about the *'beach-slope pivot point'*. Pivot points found by Aubrey (1979) were generally in water depths of between 2 and 3 m below mean sea level. Pivot point can be coupled with a mean wave height for comparison between beaches. The Torrey Pines site (Aubrey, 1979) has an RMS wave height of 0.60 m, contrasting with the typical '*average*' wave heights of 0.4 m at Bream Bay Beach (Barnett, 2002), which is the likely cause of the shallower pivot point.

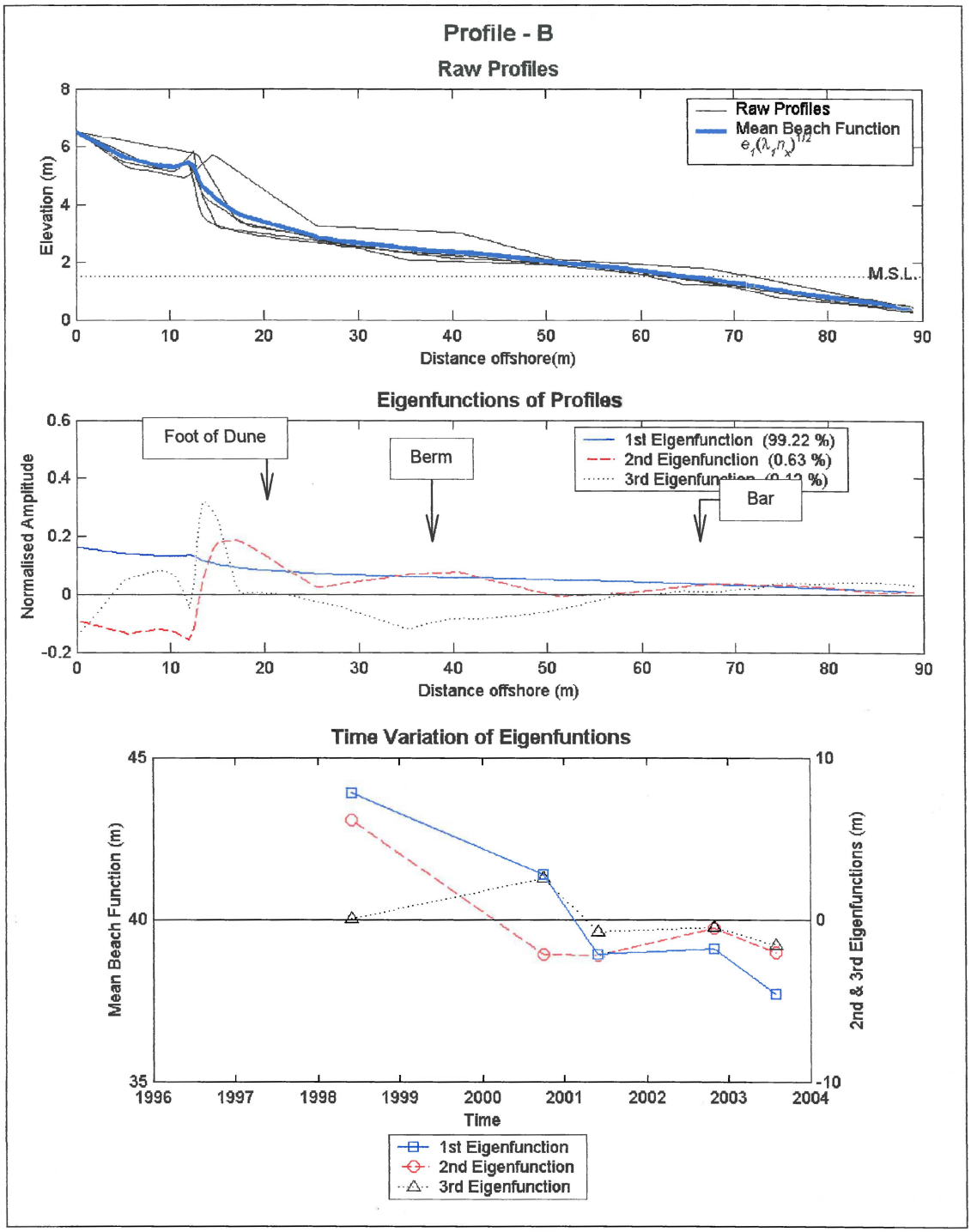


Figure 5.40 - *Eigenfunctions (and percentage of variance explained) and their temporal variation at profile B, Marsden Point.*

The foot of the dune is the site of the largest changes followed by the berm and then the bar. The time variation of this function cannot reveal any seasonality of these changes due to the frequency of the profiling interval.

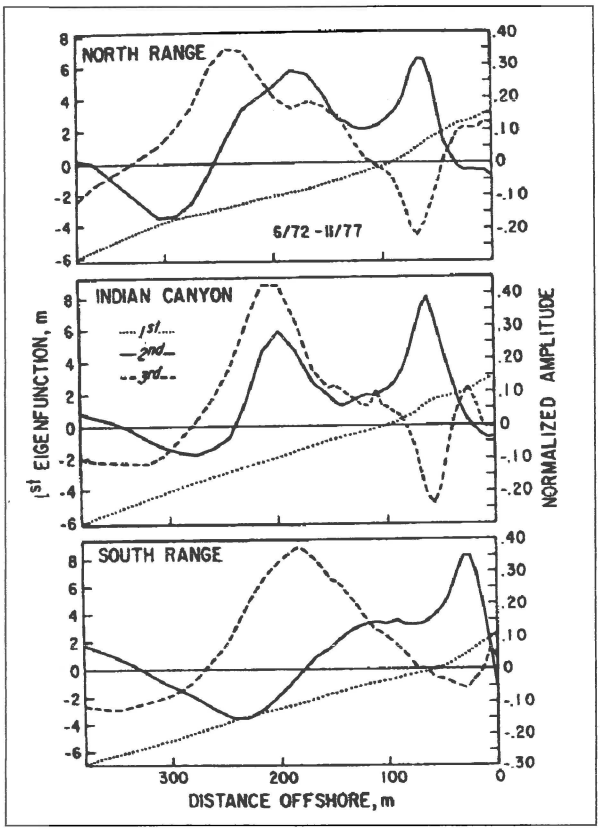


Figure 5.41- *Eigenfunctions for Torrey Pines Beach, California from June 1972 to November 1977 (Aubrey, 1979).*

The third eigenfunction at profile B is at a maximum at the top of the dune before crossing into negative values across much of the beach, then becoming positive again at mean sea level, again analogous to the data from Indian Canyon Range (Aubrey, 1979) (Figure 5.41).

Profile B has been subject to a general erosive trend between 1998 and 2003. The beach is subject to onshore-offshore sediment movement about two main pivot points along the profile. The first point, midway up the dune represents the changing shape of the dune and the dune slope. The second pivot point is located 55 m from the benchmark at an elevation of 0.5 m above mean sea level. The periodicity of sediment movement about these pivot points is on time scales of less than one year however, the exact interval cannot be gleaned from the data due to the survey interval.

Profile 2, close to the eastern edge of the port site displays some interesting results from the eigenfunction analysis (Figure 5.42). The mean beach function represents 99.74% of the mean square value of the data, indicating that the beach is more stable and less prone to change than profile B, which is farther around Marsden Point toward Bream Bay Beach.

The time variation of the first eigenfunction shows an increasing trend beginning in 2000 (Figure 5.42), when the Northport rock-wall was built nearby. An increasing coefficient of the first (mean) beach function has been interpreted as characteristic of accretion (Aubrey, 1979). Note this is a net pattern, not solely due to the rock-wall (c.f. even-odd analysis).

The second eigenfunction is at a maximum at the berm location (HWL) and also at the location of a ridge (bar) at MSL (Figure 5.42), indicating these are the locations of greatest change in the profile.

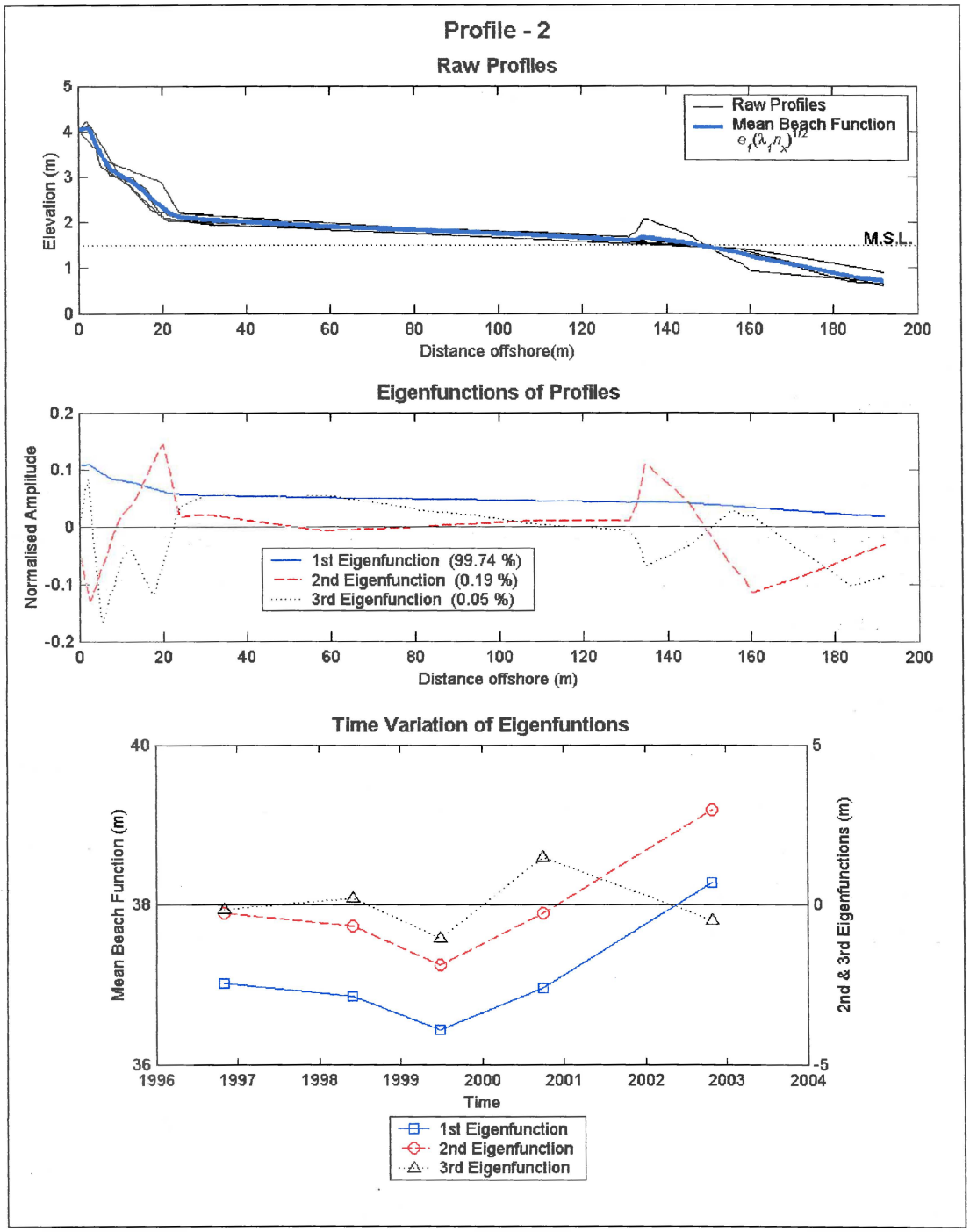


Figure 5.42- *Eigenfunctions (and % of variance explained) and their temporal variation at profile 2, Marsden Point.*

Zero crossings of the second eigenfunctions (pivot points) are located across a broad area of the inter-tidal terrace (50-90 m from benchmark), with a larger and better defined crossing at mean sea level, the location of bar formation.

The second eigenfunction fits the description of the *'bar-berm'* function well and is similar in shape to both the second eigenfunctions of North Range and Indian Canyon Range, Torrey Pines Beach, California (Aubrey, 1979) (Figure 5.41).

The trend through time of the second eigenfunction mimics the first (Figure 5.42), indicating that the accretion over the profile since the building of the rock-wall, has been concentrated mainly on the berm and at the ridge at MSL. The well defined zero crossing at the edge of the bar indicates that the sediment used for bar development is sourced immediately seaward and just below mean sea level. The bar development represents the onshore movement of sediment.

The third eigenfunction accounts for a relatively small amount of the variance from the mean (Table 5.2). The shape of the function is dissimilar to those observed by Aubrey (1979). The function shows a relatively low, broad maximum across the shore face and does not fit the description of a *'terrace'* function, as used by Winant et al. (1975) and Aubrey (1979).

Profile 2 has been experiencing a net accretionary trend since the development of the adjacent Northport rock-wall. Accretion has taken place at the berm and at a ridge located at the edge of the inter-tidal terrace at an elevation equal to mean sea level. The sediment for the ridge development has moved onshore from below mean sea level.

Profile 4, located near Marsden Spit and to the west of the Northport reclamation (Figure 5.1) is subject to only minor intra-annual changes. The second eigenfunction that describes these changes shows a strong minimum at the dune slope and no other distinct features (Figure 5.43). The time variation of the first eigenfunction indicates that the beach has experienced net erosion since 1997, with the trend accelerating in mid 2001 (Figure 5.43).

The second eigenfunction has a poorly defined zero crossing at the foot of the dune. The less distinct shape of the second eigenfunction indicates that onshore-offshore sediment movement is less dominant at profile 4 (Figure 5.43) than at profile 2 (Figure 5.42) and profile B (Figure 5.40). The dune is however subject to changes on an intra-annual scale (second eigenfunction minima).

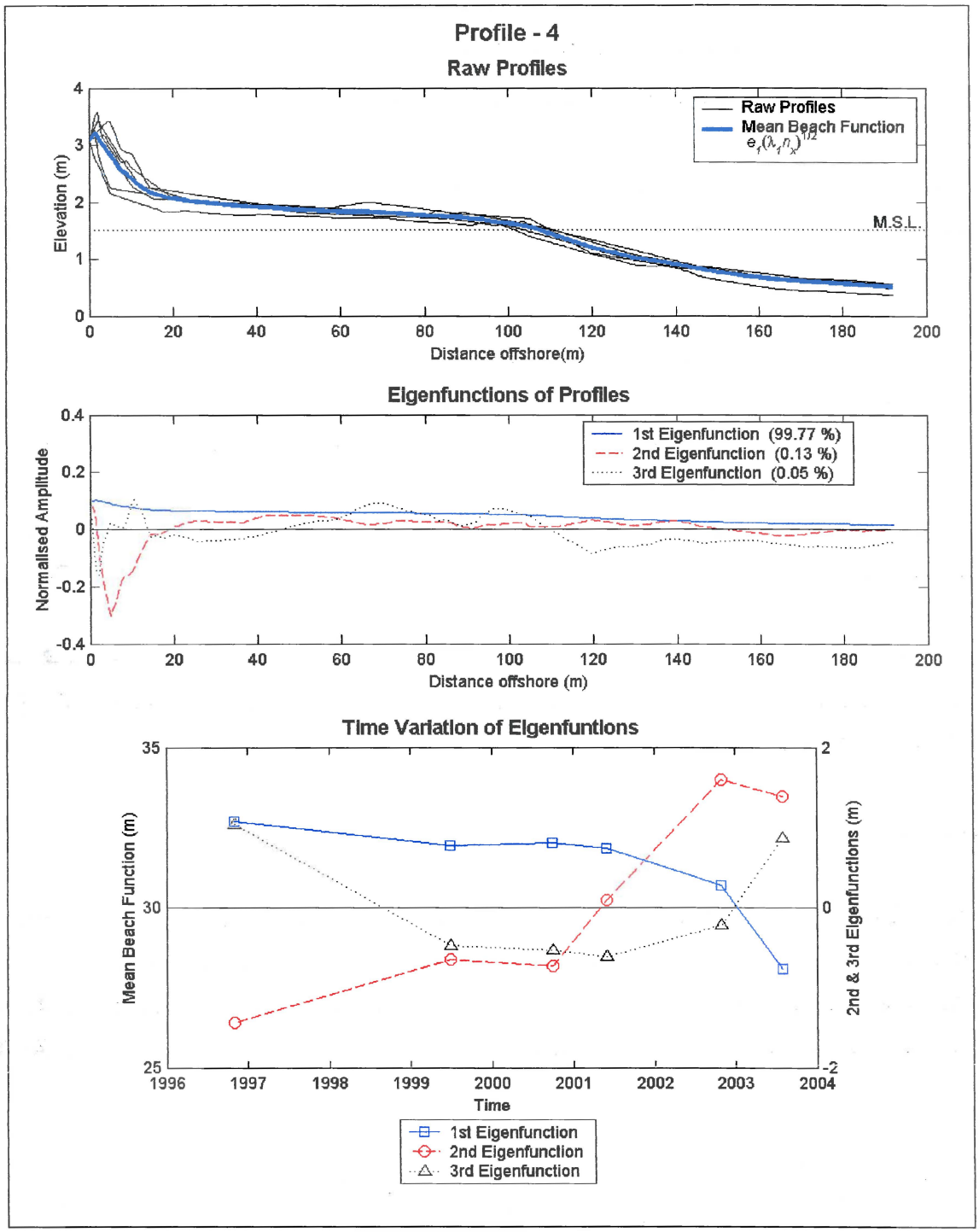


Figure 5.43 - *Eigenfunctions (and % of variance explained) and their temporal variation at profile 4, Marsden Point.*

5.9 An inter-tidal sediment budget

Using the results of the analysis of the beach profile data, a sediment budget is created for the inter-tidal areas of Marsden Point – One Tree Point (Figure 5.44). Values obtained from all analyses undertaken within this chapter were used in the compilation of the budget.

Sediment volumes described in Figure 5.44 relate to sediment movements over the dune/beach face, seawards to the depth of closure. Between 5,000 and 10,000 m^3y^{-1} of sediment has been transported around Marsden Point, past the refinery jetties towards Northport (Figure 5.44). Some of this sediment has accumulated against the eastern edge of the Northport reclamation. This transport pattern was occurring prior to the development of Northport.

A net southeasterly directed sediment transport pattern occurs in the area immediately west of Northport. This pattern also occurred prior to the Northport development and results in the accumulation of ~5,000 m^3y^{-1} of sediment against the western edge of the reclamation (Figure 5.44).

The spit in Marsden Bay (Marsden Spit) is retreating. The fixed nature of the survey lines results in a representation of a sediment loss from the area. It should be remembered however, that the spit is changing its morphology following the works carried out on Blacksmiths Creek in 1999. The data cannot be used to conclude a net sediment loss from the spit, only that the spit is retreating (it is possible the spit is retreating with a consistent sediment volume).

Marsden Bay has been steadily losing sediment (~1,000 m^3y^{-1}) since it was nourished with 8,000 m^3y^{-1} in 1999-2000 (Stevens, 1999). Currently (2003), sediment volumes remain above pre-nourishment levels.

The coastline from Paradise Point to One Tree-Point has maintained relatively stable sediment volumes.

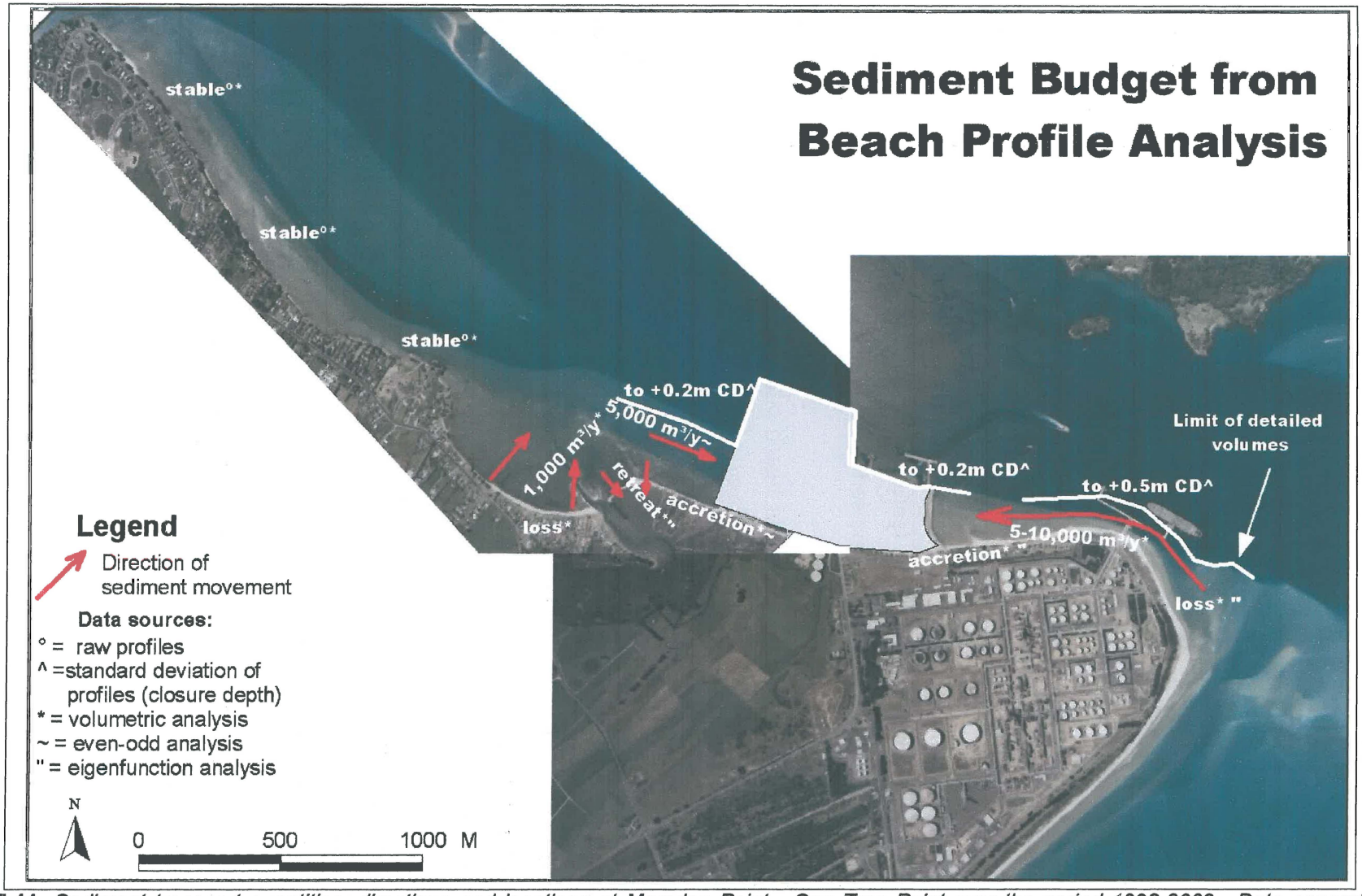


Figure 5.44- *Sediment transport quantities, directions and locations at Marsden Point - One Tree Point over the period 1998-2003. Data generated from beach profile analysis. (°=from raw profiles,^=from closure depth analysis,*=from volumetric analysis,~=from even-odd analysis,"=from eigenfunction analysis).*

5.10 Summary and conclusions

- Standard deviations of beach profile changes reveal that the beach surrounding the NZRC jetties is more variable than other locations under consideration farther up harbour.

- In the area surrounding the NZRC jetties, the beach profile is more variable closer to Bream Bay Beach and Mair Bank.

- Beach profiles are most stable at One Tree Point.

- The development of bars and ridges in the beach profiles has been observed across the study area from the NZRC jetties to One Tree Point. In general, the bars are located near mean sea level. The development and subsequent onshore movement of these features is characteristic of beach accretion under a wide range of wave, tide and sediment conditions (CERC, 1984).

- Standard deviation analyses of beach profile changes has revealed that the depth of closure is actually deeper surrounding Northport (+ 0.2 m CD) than adjacent to the NZRC jetties (+ 0.5 m CD). Closure depths are '*shallowest*' along the One Tree Point coastline.

- Sediment (~10,000 m^3y^{-1}) has moved in a westerly direction from adjacent to the NZRC jetties towards Northport from 1998 until at least late 2002. Since the building of the rock-wall for Northport development some of this sediment has been trapped here. It is expected the trapped sediment will act to prograde the MWL, until such time as the sediment begins being deposited on the batter slopes of the dredge basin near the old NHB jetty and water taxi berth. At a rate of 10,000 m^3y^{-1}, the average bed level can be expected to increase by ~ 0.1 my^{-1} (using the area defined in Figure 5.33), until such time as the sediment begins being deposited elsewhere. At this rate is expected that maintenance dredging will be required on these batter slopes in the time frame of 7-10 years.

- Works to train Blacksmiths Creek in late 1999, resulted in a large-scale realignment of Marsden Bay Spit. As a result of this realignment, the calculated volumetric sediment trends of the area are not entirely representative.

- Marsden Bay sediment volumes increased following nourishment in late 1999, since then sediment volumes have been slowly (~1,000 m^3y^{-1}) but steadily declining. Sediment volumes are still greater than pre-nourishment.

- Sediment volumes at Paradise Point and One Tree Point have shown very little change over the seven-year period 1996-2003.

- Prior to the development of Northport a causeway was impacting on sediment transport patterns at the port site. The influence of the causeway was to trap sediment on its western side and to shelter the eastern side (shallower closure depths c.f. western side). Beach profiles were more variable on the western side c.f. the eastern side. The impact of the causeway on sediment volumes was limited to around 50 m either side of the structure. The influence of the causeway on the profiles leads to the inference of an easterly-directed sediment transport pattern surrounding the causeway.

- Post-development of Northport, sediment has accreted against its western rock-wall. The pattern observed is no different in direction or magnitude to the pattern prior to development and is evidence of continued sediment transport along shore in a west to east direction at the port site.

- Onshore-Offshore sediment movement is not negligible surrounding the port site. This has been confirmed by even-odd analysis of shoreline and volumetric changes and also by orthogonal eigenfunctions of nearby profiles.

- The movement of sediment onshore can take the form of a bar or ridge feature, initially establishing itself at the edge of the inter-tidal terrace. The sediment is generally derived from immediately seaward of the inter-tidal terrace. The onshore movement of these ridges has been observed at several locations around Marsden Point.

- The most active and variable areas of the beach profiles at Marsden Point-One Tree Point coastline are the dune slopes, berm areas and bars or ridges, generally located at mean sea level. The berm area becomes less variable towards One Tree Point.

- Several profiles pivot about certain points in the profile, periodically transferring sediment onshore and offshore over time periods of less than one year.

- Raw profile, volumetric and eigenfunction analysis indicate an increase in sediment volumes and net accretion since 1997 immediately to the east of the Northport reclamation (profiles 2 and1). Even-odd analysis however, indicates that the effect of the reclamation is to block sediment transport from the west and cause the beach to lose sediment. This effect is however only the ODD component, with the even component (not due to the reclamation) resulting in the observed accretion. It can be stated that accretion is occurring more rapidly on the western side of Northport however, as this area experiences the combined effects of accretion due to even (common) and odd (due to rock-wall) components.

- Sediments have been transported around Marsden Point from Bream Bay Beach past the NZRC jetties and towards Northport along the beach face and seaward to 0.0 m C.D. This transport has caused the removal of sediment from adjacent to the NZRC jetties over the period 1998-2002. The rate of transport remained relatively constant over this time (~10,000 m^3y^{-1}). Over the same time period, sediment has been moving down harbour at the port site. The combined effect of these two opposing sediment transport vectors has led to accretion on both sides of the 800 m wide Northport reclamation. Accretion has occurred more rapidly against the western rock-wall due to the combined effects of onshore sediment movement and the groyne effect of the reclamation.

6 BATHYMETRY AND HYDROGRAPHY OF MARSDEN POINT

6.1 Introduction

'In many coastal studies, the analysis of topographic and bathymetric data is one of the fundamental tools used to evaluate historical morphological changes, patterns of erosion and sedimentation and shoreline response over time' (Gorman et al., 1998).

This chapter aims to document changes in the bathymetry of the lower Whangarei harbour in the region of Marsden Point in order to identify characteristic areas and volumes of sediment movement both prior to and post-port development.

This is achieved by:

i. an outline of previous investigations of the lower harbours seabed stability; and
ii. a comparison of more recent, detailed bathymetric surveys undertaken by the Ports of Auckland and Ports of Tauranga at the request of the Northland Port Corporation.

6.2 Previous Investigations

'Reviewing available historic bathymetric charts will assist in interpreting long-term trends as short-term changes are often larger than net changes.' (USACE, 2002).

The lower Whangarei harbour was first surveyed by Dumont D'Urville with L'Astrolabe in 1827. Since 1827 a variety of other surveys have been undertaken (major surveys are detailed in Appendix D). Other, more spatially restricted surveys, have been carried out for specific purposes such as offshore pipeline routes, e.g. Mair Bank in 1960 by Simpson Shaw and Co (Tonkin and Taylor, 1979a) and adjacent the Marsden Power Station 1976 by Morris and Wilson (Tonkin and Taylor, 1979a). These restricted surveys are of limited spatial and temporal extent, restricting their comparative value.

A variety of authors have analysed and compared previous bathymetric surveys for changes (Appendix D). Their findings have been summarised (Appendix D) and compiled into a graphic illustration (Figure 6.1). Many of these authors do not report on the accuracy of their comparisons, and others are based on digitised contours of questionable quality. It is prudent therefore to observe the general behaviour described, whilst remaining wary of specific details reported.

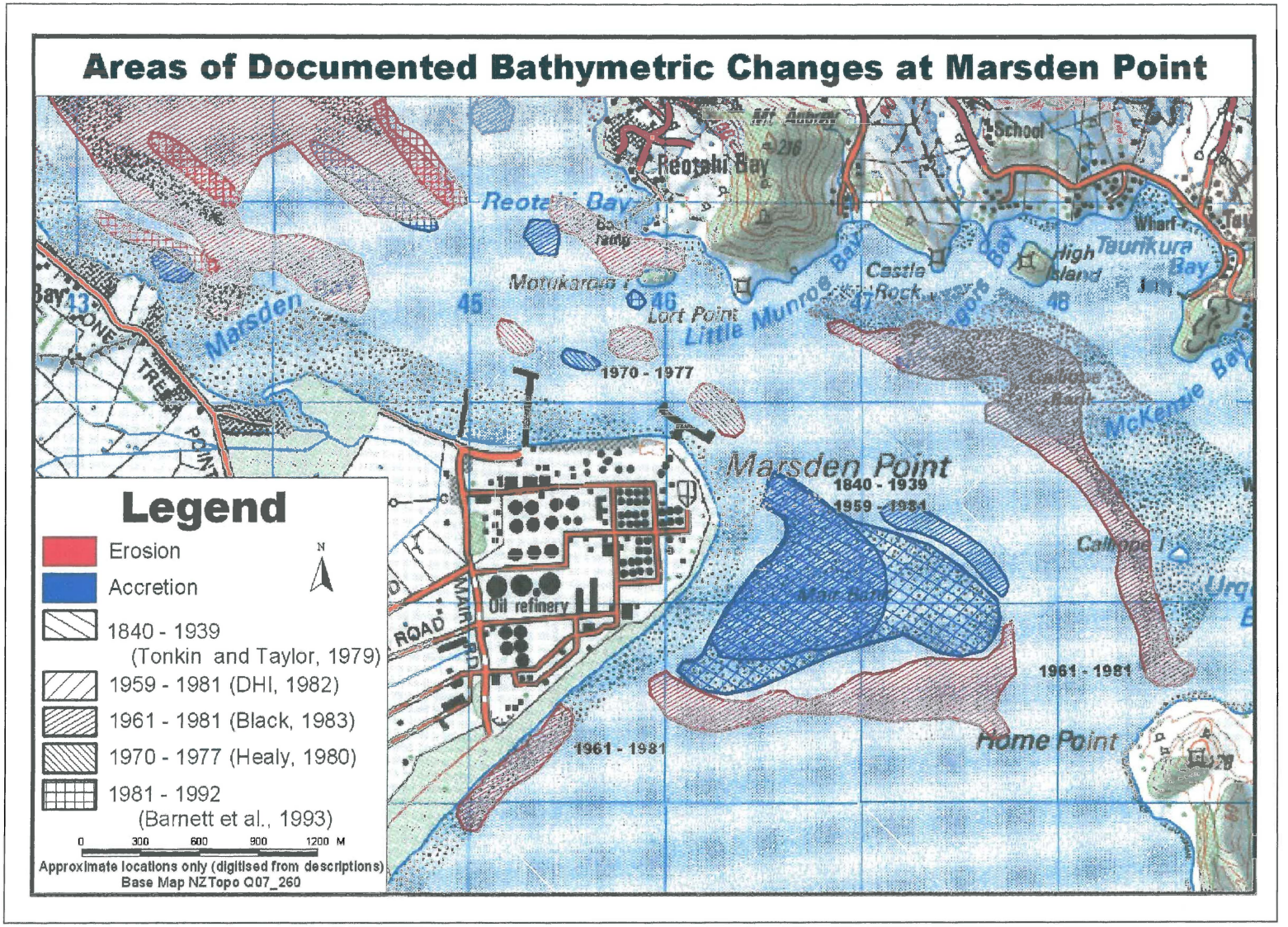


Figure 6.1 - *Bathymetric changes at Marsden Point observed by previous authors.*

Points of interest from previous investigations (Figure 6.1 and Appendix D) include:

i. Mair Bank was an accretionary feature between 1860 and 1981, although for the period of 1939 to 1959 no accretion was noted. During some periods of accretion, the Bream Bay Beach foreshore farther south has experienced erosion (Tonkin and Taylor, 1979a; DHI, 1982a);

ii. a redistribution of sediment occurred on Mair Bank between 1961 and 1981. Accretion was observed closer to the coast (Black, 1983). Concurrently the foreshore at northern Bream Bay beach experienced erosion, as did the extreme western edges of Calliope Bank adjacent to the main channel (Black, 1983);

iii. large areas surrounding Snake Bank experienced a net loss of sediment between 1961 and 1981. Only minor areas experienced accretion (Black, 1983);

iv. the sub-tidal extension of the ebb-tidal delta of Snake Bank (towards the harbour entrance) exhibited migration behaviour between 1981 and 1992 (Barnett et al., 1993);

v. the centre line of the Blind Channel adjacent to Marsden Bay moved 50 m shoreward between 1991 and 1992 (Barnett et al., 1993); and

vi. the channel margins, adjacent to the Northport site and NZRC jetties, were actively redistributing sediment between 1970 and 1978 (Healy, 1980).

6.3 Recent surveys

The Northland Port Corporation has been surveying the bathymetry of the lower Whangarei harbour regularly since 1995. Table 6.1 summarises and details the surveys. Details of areas covered by each survey are contained in Appendix D.

Date	Surve -yor	Avg. run-line separation(m) (and DEM resolution)	Avg. sampling interval (along run-line)(m) (and DEM resolution)	Equipment / Accuracy
May 1995	Ports of Auckland	19.2	5.2	Information unavailable, Conservatively estimated to be ± 0.1 m (positional) and ± 0.05 m (depth)
November 1995		19.2	6.1	
May 1996		19.2	3.6	
May 1997		19.6	6.9	
May 1998		19.6	7.0	
April 1999		19.1	3.7	
December 2000		19.2	1.9	
May 2001	Ports of Tauranga	18.5	7.6	Positional Information – Trimble 7600msi RTK GPS with 5Hz update: errors ± 0.05 m Depth Information – Knudsen 320m 200KHz Transducer errors ± 0.01 m to 100m depth (pers. comm. Owen Maynard 2003)
November 2001		19.5	6.7	
November 2002		19.2	1.9	

Table 6.1- *Recent bathymetric surveys at Marsden Point.*

The extent of the surveys is limited to the lower harbour and entrance, with the area centred on the Northport site and Marsden Point. Various factors have influenced the coverage of individual surveys, such as dredging operations, restricted areas, or equipment malfunction (e.g. November 1995 survey, Appendix D). This has led to variability in the areas covered by each survey. Appendix D details the extent of each survey undertaken.

The Northland Port Corporation provided the data in x-y-z ASCII text format for this study. Positional information was in the Mt Eden Grid Circuit (1969) projection, depths were in metres below the Marsden Point datum (Section 6.3.2 for an explanation of the datum at Marsden Point). Depths below datum were negative in all data files with the exception of the May 2001 survey. This data was imported to Microsoft Access® and a multiplication of the depth field by –1, created a new field of depths consistent with the scheme used for the other surveys.

6.3.1 Surveying Scheme and Resolution

The run-lines of the boat were regenerated in Arc View® GIS. This was achieved by using an avenue script (*Pt2Poly.ave*, Appendix D). The script took advantage of the fact that the depth values were recorded in the files sequentially, in the order they were measured. Pt2Poly essentially *'joins the dots'* of the locations at which the depth was recorded. A poly-line (a set of one or more line segments called parts, each line segment contains 2 or more points) is created, beginning at the first recorded value, then passing through the second, third and so on. Run-lines were driven in generally a northeast-southwest direction. Variations to this pattern occurred in the area south of Mair Bank, adjacent to Bream Bay Beach where an east-west direction was used for some surveys.

Run-line separation and along run line resolution was determined for each survey by averaging the number of points over a set distance (500 m and 100 m respectively) in each direction. Separation of the run-lines was of the order of 18-19 m (Table 6.1). There is some variation in the along run-line resolution between the surveys (Table 6.1).

6.3.2 Datum position at Marsden Point

There are two datum benchmarks in use at Whangarei Harbour (LINZ, 2002) (Table 6.2). The plane determined by the appropriate methods at each of these benchmarks is at different elevations, observation Department of Lands and Survey data indicates that the Port Whangarei Datum is of the order 0.15 – 0.20 m lower than that determined from the Marsden Point Bench mark (pers. comm. O. Maynard, 2003).

Location	Latitude (S) (WGS86)	Longitude (E) (WGS86)	Datum and Remarks
Port Whangarei	35°66'	176°21'	5.182 m below RNZN brass BM No. 1 1961 on the concrete coping near the root on the west side of Port Whangarei Wharf.
Marsden Point	35° 50'	176° 29'	6.816 m below the RNZN BM, an iron bolt in cement near the base of the light standard on the inshore east end of the Northland Harbour Board pier, near the launch steps.

Table 6.2 - *Datum Benchmarks at Marsden Point. Source (LINZ, 2002).*

The more recent surveys conducted by the Ports of Tauranga (Table 6.1) have all been registered relative to the Marsden Point Datum (pers. comm. O. Maynard, 2003). It has not been possible to definitively identify the datum used for the earlier Ports of Auckland surveys (pers. comm. J. Palmer, 2002). There is therefore a potential for error of the order ± 0.20 m in the comparison of survey results between the two data sources.

6.4 Digital Elevation Model (DEM) Generation

6.4.1 Error Checking

Raw data from each survey was imported to Microsoft Access® and queries written to check the data for erroneous values. Data with abnormal positional data, (data must fall within the following ranges 272636>x>278830 and 813931>y>817666) or abnormal depth data (data must be in range of – 60<z<6) was flagged in an *'error'* column and disregarded for any further analysis.

6.4.2 Gridding Operations

Gridding (surface modelling) is a mathematical process where a continuous surface is interpolated from a set of randomly distributed x, y and z data. A grid is an artificial structure, it is based on original data but the actual grid nodes (most likely) have not been surveyed.

A rectangular grid was established with nodes at 1 m intervals (in both x and y directions) in the Mt Eden Grid Circuit 1969 projection. On top of this grid a polygon, created from the shoreline of the Marsden Point area, was overlaid (Appendix D, Digital Elevation Model (DEM) boundaries). All values of the grid outside the polygon (i.e. land) were assigned null values.

Arc INFO® workstation GIS was used to interpolate depth values on to the grid for each of the bathymetric surveys. The gridding algorithm was based on a splining interpolator, which creates a minimum-curvature surface through the input points. The algorithm fits a mathematical function to multiple data points (depth values in data file) surrounding each node (grid point) (ESRI, 1996). The z value (depth) at the node can then be calculated. Output is in the form of an Environmental Systems Research Institute (ESRI) grid file.

The grid file is a raster type GIS image file. In this case the pixel size is 1 m x 1 m (the input grid resolution). Each pixel in the grid has attributed to it a value, which represents the depth relative to chart datum. The grid file can be displayed in GIS packages and operations (statistical summaries, spatial queries etc) carried out on the attribute information. The raw DEMs displayed according to attribute (depth) information are compiled in Appendix D.

Excessive irregularities existing in the data sets of the surveys of May 1997 and April 1999, prevented Arc Info® from being able to properly grid the data. These surveys are not considered further as grids could not be generated.

6.4.2.1 Spatial Extent of DEMs

Each bathymetric surveys coverage was influenced by a variety of factors e.g. dredging operations, restricted areas. Polygon coverages were created in the GIS from the data used to generate each DEM. These polygons represent the area over which data was surveyed and used to generate each DEM. By performing an intersection type operation with the entire grid area, an *'inverse'* polygon was created which could mask areas of the DEM where data is likely to be inaccurate due to the absence of surveyed points. When differences are calculated between the DEMs, the two '*inverse*' polygon coverages can be '*unioned*' to obtain the region over which valid conclusions can be drawn. The polygons are shown with the raw DEMs in Appendix D, while the intersected polygons mask non-valid areas in Figures 6.3 to 6.11.

6.4.3 Error Analysis of Gridded Bathymetry

Many DEMs used for mapping and spatial analyses are calculated from remotely sensed data e.g. LIDAR, SPOT and stereo pairs of air photographs. Estimation of errors in these images is a detailed and complex process (Carslile, 2000; Holmes et al., 2000; Lynch, 2002). The DEMs used for this study have been generated from *'true'* bathymetric data, in that the elevations (depths) were actually surveyed.

The gridding process ensures that the surface represented by the DEM *'travels through'* the surveyed points. This means the normal validation method utilising GPS points (location and elevation) and Root Mean Square Errors (RMSE) is redundant, as the DEM itself has been created from this data.

Two main factors will influence errors in the DEMs created from the bathymetry data:

i. errors inherent in the survey data (positional and depth); and
ii. the resolution of the survey data (spacing along and across run-line).

These are detailed in Table 6.1 for each survey.

The errors inherent in the survey data will carry directly through to the DEM and must be added to any subsequent errors.

With respect to the resolution of the surveyed data points, the situation is simplified by considering a rectangular co-ordinate system oriented in the along / across run-line direction. There are three different '*resolutions*' in the DEMs generated:

i. Those in the along run-line direction;
ii. The across run-line direction; and
iii. The depth.

Features in the DEMs at smaller scales than the along and across run-line resolutions in those directions should be disregarded as artefacts of the interpolation process.

It should be noted that the distance between run-lines and the spacing of points along run-lines varies slightly over the survey area. Values presented in Table 6.1 represent spatial averages.

Artefacts of the DEM generation process are apparent in several of the DEMs (e.g. linear features on the channel margins in the DEM of May 1998, Appendix D). The artefacts manifest themselves as linear features in the along run-line direction. The width (short axis) of the artefact features is less than or equal to the across run-line resolution of the DEM (of the order of 19 m). These features should be disregarded in a morphologic analysis as they are below the resolution of the raw data used to create the DEM (Table 6.1).

6.5 DEM Calculations

6.5.1 Calculating Bed Level Changes

The raw DEMs (Appendix D) are of limited use in isolation, other than as a graphic representation. Only large scale, major trends can be identified such as the deepening of the dredge basin adjacent Northport (compare DEMs from May 1998 to November 2002, Appendix D). Within a GIS however the DEMs become powerful tools that can be used for advanced analysis.

Arc View® 3.2a GIS with spatial and 3D analyst toolboxes was used for DEM calculations. The standard *'cut and fill'* command in Arc View's® 3D analyst was found to be inadequate in its determination of the amount of bed level rise or fall. The command operates by first finding all pixels (grid cells of the DEM) that have experienced a depth increase, then grouping them together and reporting the volume of change for all these pixels as one combined value. The same occurs for areas of depth decrease. This technique fails to provide information on the magnitude of bed level changes at various sites or at individual pixels, greatly restricting comparisons.

To create the output desired, an avenue script (*dem_diff_ave*) was written by this author utilising Arc Views® spatial analyst toolbox. The script calculates the change in bed level at each individual pixel in the DEM. Equation 6.1 shows the simple calculation undertaken at each pixel (total 25,171,696 pixels each DEM). Complexity arises while determining which pixel to subtract from which pixel.

$$z_{(x_i,y_i,t_2)} - z_{(x_i,y_i,t_1)} = \Delta z_{(x_i,y_i)} \qquad \textbf{(6.1)}$$

An output grid is created where the pixel attribute data represents the change in depth between the two surveys compared. Contours of the changes in bed level were then calculated and are contained in Appendix D.

6.5.2 Removing Artefacts of the Gridding Process

Artefacts of the gridding process have a characteristic shape (Section 6.4.3). They are generally linear shaped features, with their long axis in the along run-line direction, the width of the short axis is less than the across run-line resolution. Contour plots of changes in bed level elevations (Appendix D) show many such features, they are artefacts of the gridding process and bear no reflection on *'real'* physical changes at Marsden Point.

The contours of bed level change for each period were examined and measured using GIS software. The width of linear features orientated in the along run-line direction was measured. Any features exhibiting widths less than the across run-line resolution of the two surveys being compared, was tagged in the GIS attribute file as being an artefact of the gridding process. These features were then removed from display and any further calculations. The resulting contour plots are shown in Figures 6.3 to 6.10. Contour intervals were generated at 0.25 m (Figure 6.10) and 0.5 m (Figures 6.3 to 6.9). These levels were chosen as they best represent the data without reproducing other artefacts and very small-scale changes.

6.5.3 Volume calculations

Estimations of the volume of material deposited or eroded have been made using the non-artefact bed level change contours (Figures 6.3 to 6.10). The estimations were made by converting the contours of bed level change to polygons, calculating the area of each polygon, then multiplying by the change in bed level.

The volumetric estimations (Figures 6.3 to 6.9) consider only the amount of sediment accretion or erosion in excess of 0.5 m in vertical extent. Where changes greater than 0.5 m were experienced, multiple polygons were created at each contour level and the volumes from each added. The estimates are conservative due to the 0.5 m vertical threshold and the assumption of vertically walled *'stepping'* polygons, rather than sloping surfaces where changes exceed 0.5 m.

It is crucial to know how much confidence can be placed in growth rates based on bathymetric data. The Maximum Likely Error (MLE) method (Gorman et al., 1998) estimates errors in volumetric differences between surveys.

$$MLE = \frac{2 \times \Delta z}{\Delta z_{ave}} \qquad \textbf{(6.2 Gorman et al., 1998).}$$

Where:

MLE	=	Maximum Likely Error
Δz	=	Vertical accuracy of survey
Δz_{ave}	=	Average depth change in polygon

For coastal surveys this method assumes that errors in positioning (Δx and Δy) are random and have insignificant effects on the volumes compared with possible systematic errors in water depth measurements, tide correction and data reduction (Gorman et al., 1998). Older historical surveys (without accurate GPS), where positioning errors are important, require a much more complicated analysis procedure.

Using the vertical accuracy of each survey (Δz) from Table 6.1 (± 0.05 m Ports of Auckland and ± 0.01 m Ports of Tauranga) and the contours used to generate the polygons at 0.5 m vertical intervals (Δz_{ave}), the MLE was calculated for each comparison.

Volumes obtained from bed level changes using the Ports of Auckland surveys (Table 6.1) have a MLE of 20%, while those using the Ports of Tauranga data (Table 6.2) have a MLE of 6%.

Gorman et al. (1998) noted that more research is needed to quantify errors associated with various types of offshore surveys and to identify how these errors are passed through to the computed quantities.

6.6 Bathymetry Changes Prior to Port Development

The development of Northport commenced in December 2000, with the construction of a rock-wall to enclose the reclamation. Dredging operations began in January 2001. The reclamation area was completely enclosed in July 2001 and dredging completed in April 2003 (Figure 6.2).

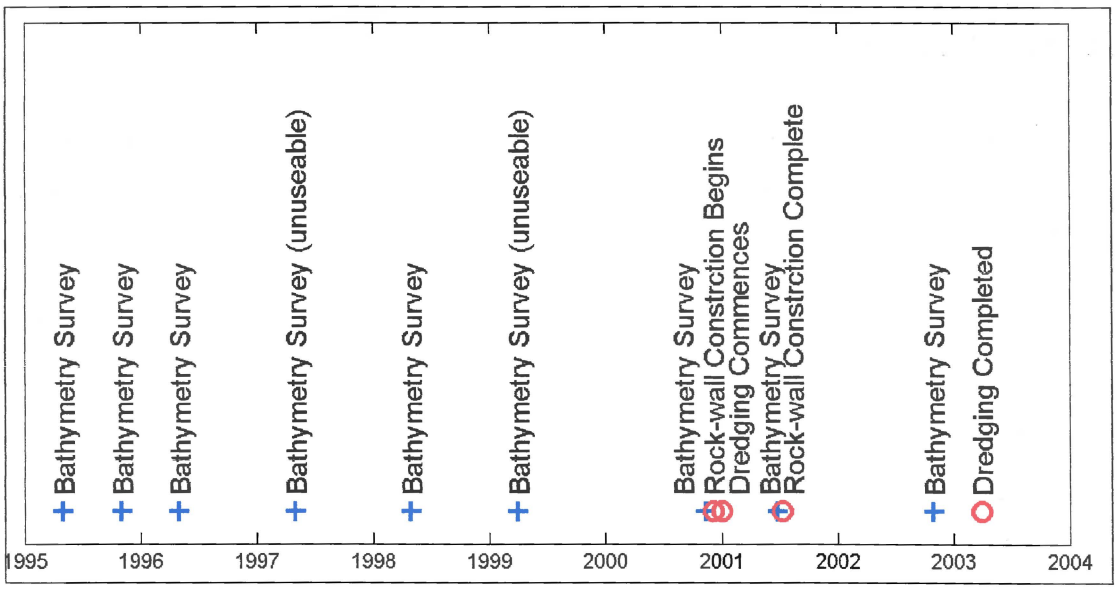


Figure 6.2 - *Time line of bathymetric surveys and development works.*

The surveys from May 1995 to December 2000, will be considered the 'prior to development' surveys, while those after this are considered the during and post construction surveys.

6.6.1 May 1995 to November 1995 (Figure 6.3)

Minor accretion (~6,300 m^3y^{-1}) can be observed on the northern edge of the ebb tidal delta (Mair Bank), near the NZRC jetties (Figure 6.3). This accretion took place in depths ranging from 2 to 5 m below CD.

The removal of sediment from the channel bottom / edge on the western flank of the other ebb tidal delta (Calliope Bank) is also noticeable, with this occurring at a rate of ~19,000 m^3y^{-1}. These changes took place in depths of 17 to 20 m below CD.

Remaining areas were relatively stable, with only localised areas of small changes in bed level.

It is noted that these surveys were conducted in different seasons (early winter and early summer). This has the potential to influence results due to variations in forcing mechanisms e.g. different wave climates. The changes observed on Mair Bank occur at depths greater than the observed closure depth (~+0.5 m C.D., from regular beach profiles, Figure 5.30, Section 5.5.2) and are thus not affected by seasonal changes in wave character. The erosion in the channel, at depths greater than 17 m is too deep to be influenced by variations in the wave climate.

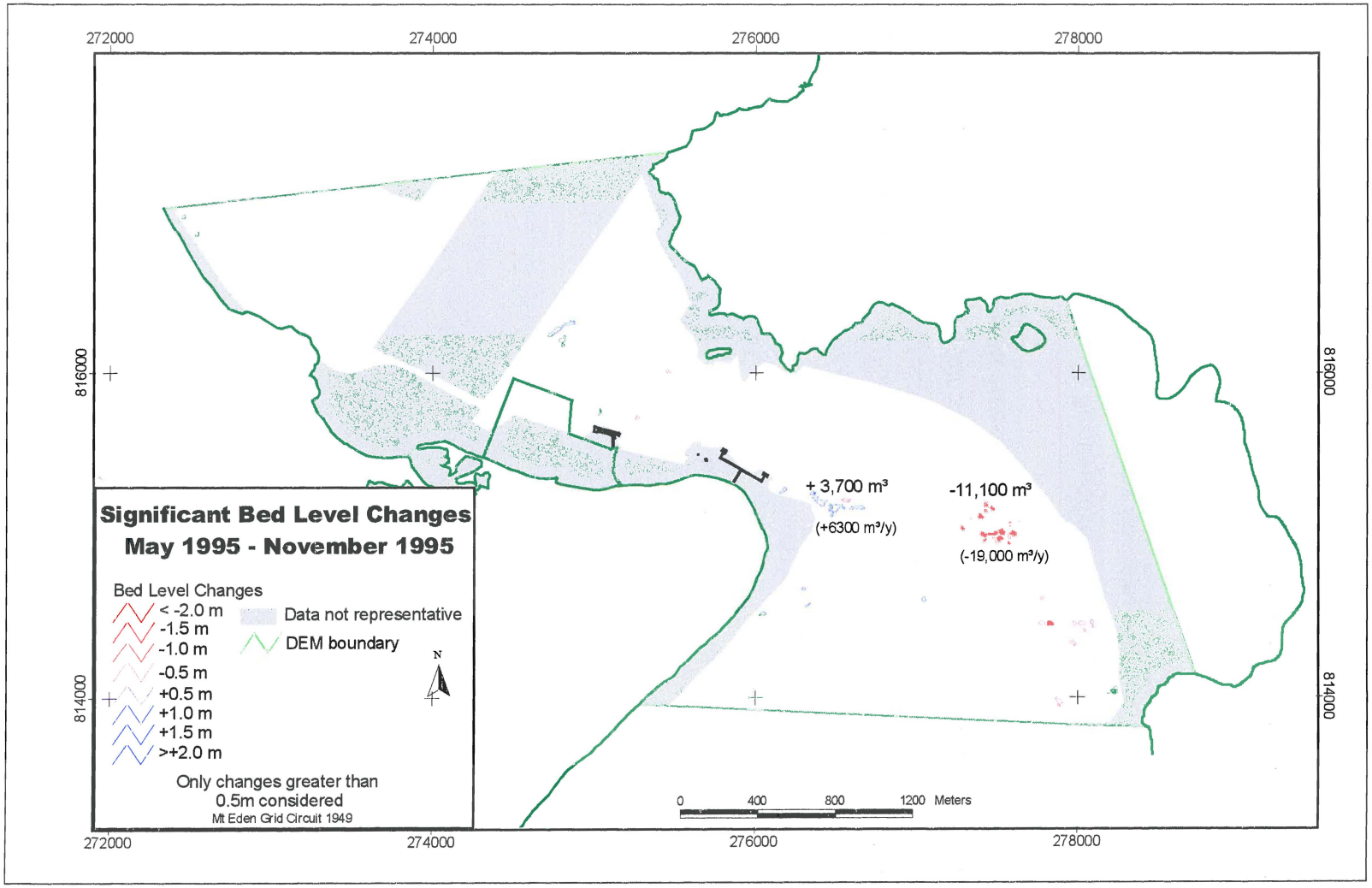


Figure 6.3 - *Bed level changes, minus gridding artefacts, for the period May 1995 to November 1995. Volumetric estimates have MLE of 20%.*

6.6.2 November 1995 to May 1996 (Figure 6.4)

The Mair Bank ebb tidal delta was actively moving sediment over its surface during this period. The sediment was being redistributed over depths ranging from 1 m above to 0.5 m below CD.

There is no evidence of a continuation of the erosive trend in the main channel (Section 6.6.1), observed in the prior 6 months.

The rest of the harbour remained relatively stable, with a small area in front of the NHB wharf (at the edge of the Northport site) experiencing a small redistribution of sediment.

Surveys were again conducted in different seasons, which could account for some changes observed at Mair Bank. The changes occurred within the depth of closure observed from beach profile analysis (~+0.5 m C.D.)

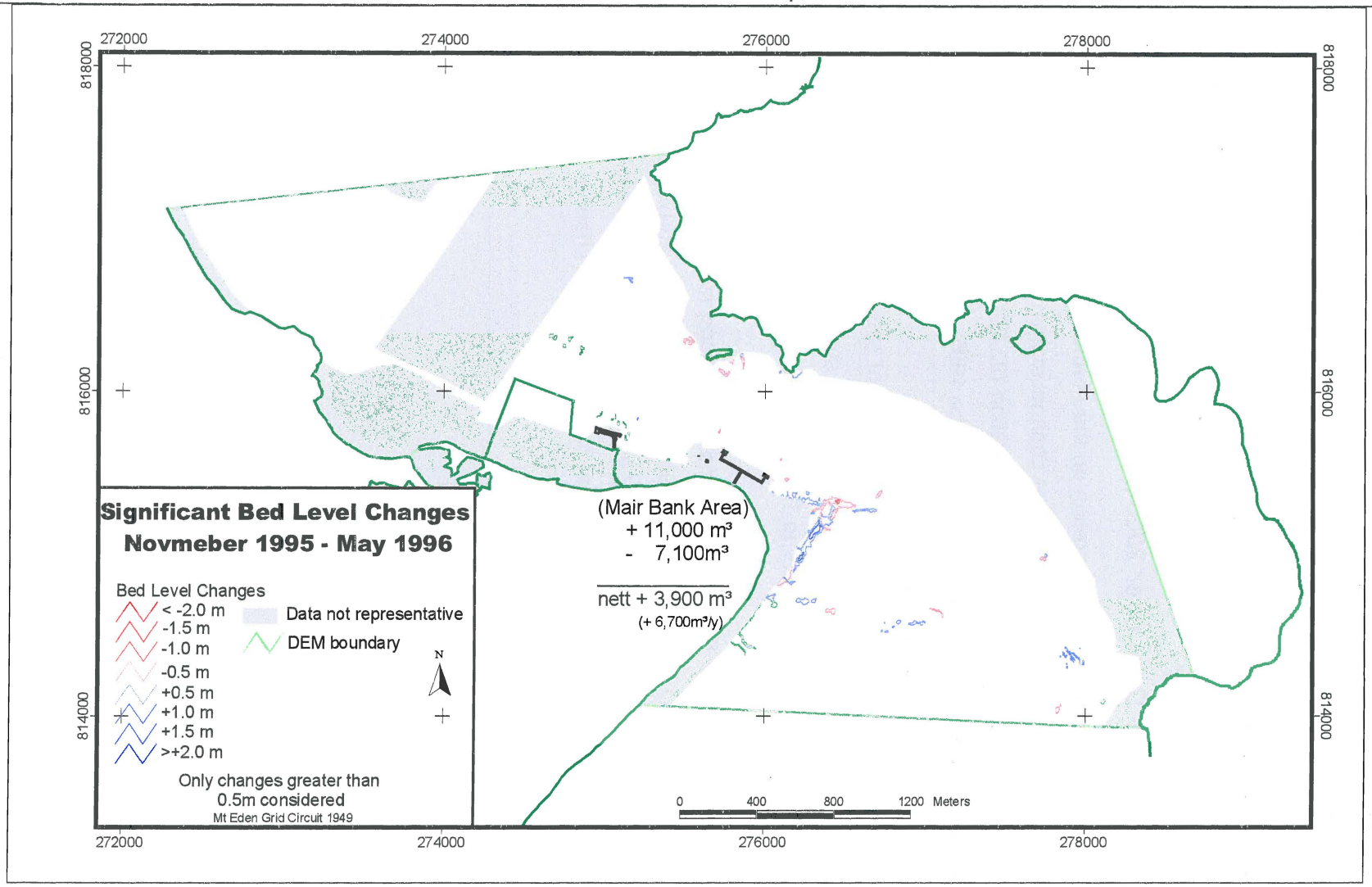


Figure 6.4 - *Bed level changes, minus gridding artefacts, for the period November 1995 to May 1996. Volumetric estimates have MLE of 20%.*

6.6.3 May 1996 to May 1998 (Figure 6.5)

Only very limited areas of minor accretion and erosion (< ± 3,000 m^3) (Figure 6.5) are apparent through this period. In general the harbour exhibited great stability. Areas that have experienced changes in bed level are shallower areas, on the flanks of the ebb tidal delta (Mair Bank) and on the sub-tidal extension of the flood tidal delta (Snake Bank) that extends towards the NHB wharf.

6.6.4 May 1998 to December 2000 (Figure 6.6)

Figure 6.6 shows a large area of accretion on the northern edge of Mair Bank, to the east of the NZRC jetties. The area is on the channel margin and in depths of 10 to 13 m below CD. The rate of accretion at this location (22,000 m^3y^{-1}) is faster than has been observed anywhere in the lower harbour since 1995.

The southern area of Mair Bank experienced a loss of sediment, although at a much slower rate of 6,100 m^3y^{-1}. This loss occurred in the shallower regions of Mair Bank, with depths ranging from 0.5 m above to 1 m below CD.

Accretion was observed in the area surrounding Passage Island, in depths ranging from 7 to 20 m below CD. The accretion is relatively wide spread and represents a rise in bed level of between 0.5 and 1.0 m. Minor accretion can also be observed along the sub-tidal extension of Snake Bank and on the flanks of the blind channel.

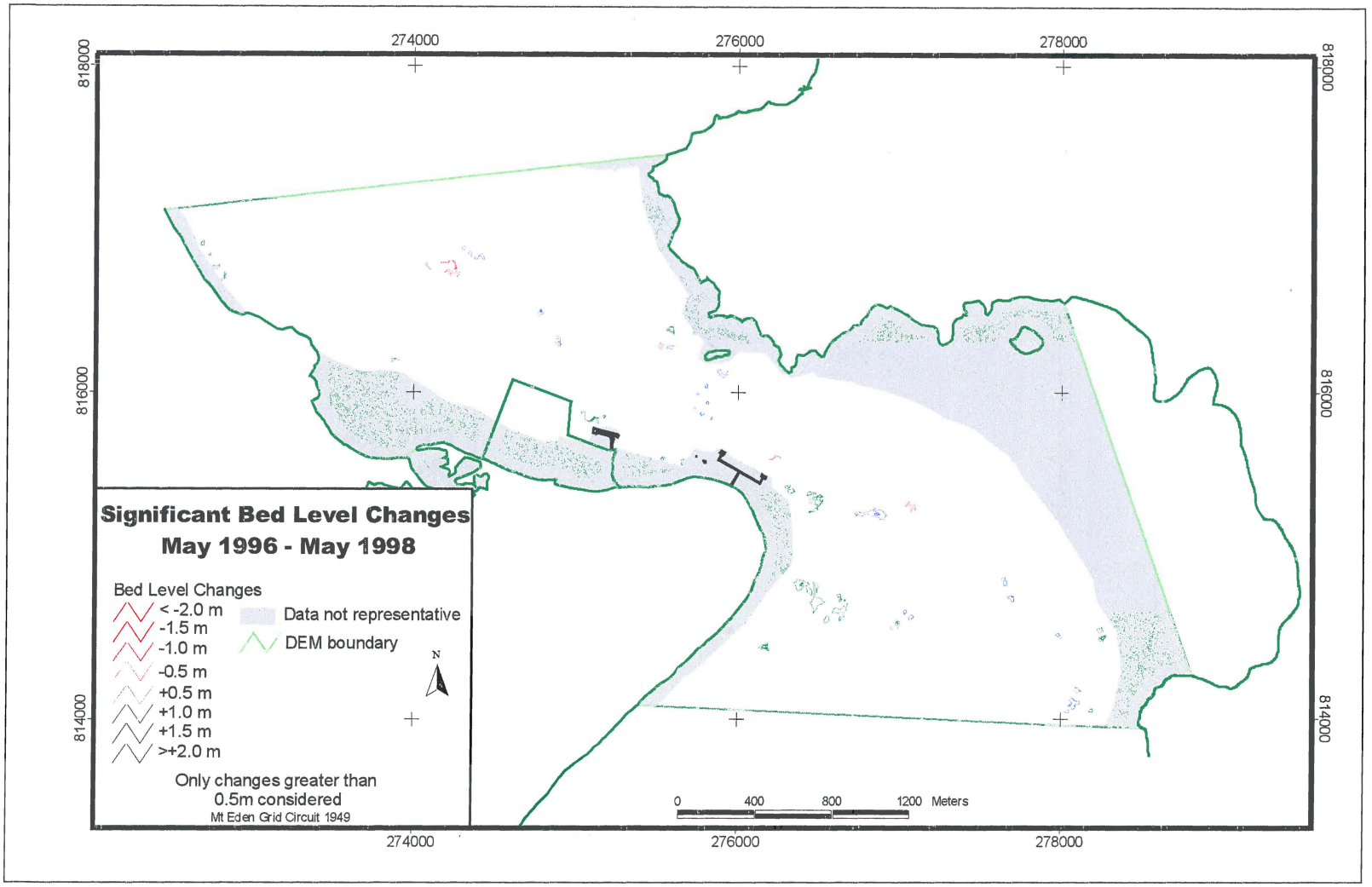


Figure 6.5 - *Bed level changes, minus gridding artefacts, for the period May 1996 to May 1998. Volumetric estimates have MLE of 20%.*

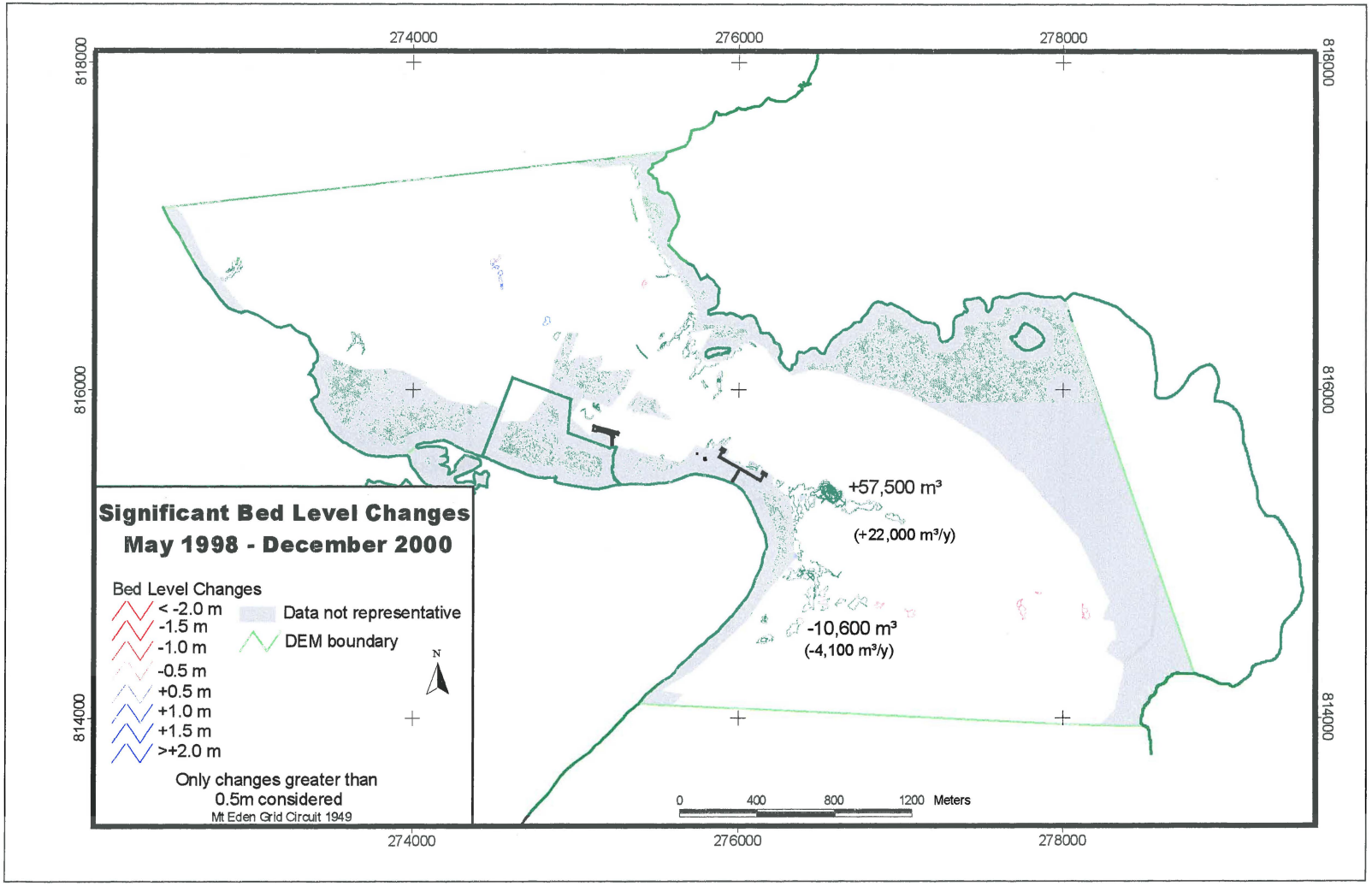


Figure 6.6 - *Bed level changes, minus gridding artefacts, for the period May 1998 to December 2000. Volumetric estimates have MLE of 20%*

6.6.5 Pre-Construction trends

Bathymetric surveys undertaken from 1995 to 2000, prior to the development of Northport indicate:

i. the Mair Bank ebb tidal delta is a variable feature that has experienced both erosion and accretion. Accretion has predominantly occurred on the northern flanks, while erosion has been dominant on the southern. These trends are consistent with those observed by Black et al. (1981) (Figure 6.1).

   The erosion/accretion pattern led Black et al. (1981) to conclude that over the period 1959 to 1981, the bank was shifting its longitudinal axis to be aligned east – west rather than northeast – southwest. The current data (Figures 6.3 to 6.6) indicate that this trend was continuing from 1995 to 2000.

   The rates of accretion calculated over Mair Bank (Figures 6.3 to 6.6) are similar to those evaluated by the DHI (1982a). The DHI however treated the bank as a whole, without separating areas of erosion and accretion within the bank, thus concealing the erosion/accretion pattern noted above;

ii. the removal of material from the channel bottom and flank of the other ebb tidal delta (Calliope Bank) between the surveys of May 1995 and November 1995 is localised both spatially and temporally. Changes were not noted in other comparisons (Figures 6.4 to 6.6). Previous investigations have not identified changes in this region (Figure 6.1) and comparison of other surveys did not indicate a continuation of the process (Figures 6.4 to 6.6);

iii. minor localised accretion and erosion occurred in front of the NZRC jetties. Small amounts of erosion are apparent between May 1995 and May 1998 and accretion is evident from May 1998 to December 2000;

iv. the area surrounding Passage (Motukaroro) Island is susceptible to changes in bed level. Black et al. (1983) observed erosion here between 1959 and 1981, whilst Barnett et al. (1993) observed localised accretion between 1981 and 1992 (Figure 6.1). Accretion was observed over these areas between 1998 and 2000; and

v. the remainder of the harbour was generally stable between 1995 and 2000, with only localised accretion and erosion.

The sub-tidal extension of the flood tidal delta (Snake Bank), extending in a southeasterly direction towards the Northport site, exhibited greater occurrences of localised accretion and erosion than the remainder of the harbour.

6.7 Bathymetric Changes During and Post Port Construction

The bathymetric surveys ranging from December 2000 to November 2002 were analysed for changes in bathymetry during and post port construction.

6.7.1 December 2000 to May 2001 (Figure 6.7)

During this period both reclamation and dredging works were in progress. Works on both were ongoing throughout the duration of this phase (Figure 6.2).

Mair Bank again shows both erosion and accretion. The rates of erosion/accretion are larger (by a factor of 2) than those observed since 1995. The erosive *'spot'* at the north of Mair Bank (Figure 6.7), is in the same location as a similar sized accretionary feature observed between May 1998 and December 2000 (Figure 6.6). This could potentially be used as evidence of anomalous values in the December 2000 survey. Investigation of Figure 6.7 however shows that adjacent (south-easterly direction) the *'erosion spot'* is an accretionary feature, similar to that in Figure 6.6. It is proposed that a *'mound'* of sand, deposited between May 1998 and December 2000 (Figure 6.6) has moved in a southeasterly direction, creating the pattern shown in Figures 6.6 and 6.7. Depths where the movement occurred range from 15 to 16 m below CD.

Bed lowering is apparent to the northeast of Passage (Motukaroro) Island. These locations are in the middle of the channel at depths of 17 to 20 m below CD.

Erosion of a large amount of material (57,200 m^3) occurred on the eastern edge of the channel, adjacent the ebb tidal delta of Calliope Bank. The erosion is relatively wide spread, covering an area 500 m in length and 100 m in width.

The remainder of the harbour was stable, with minor localised erosion occurring in front of the NZRC jetties.

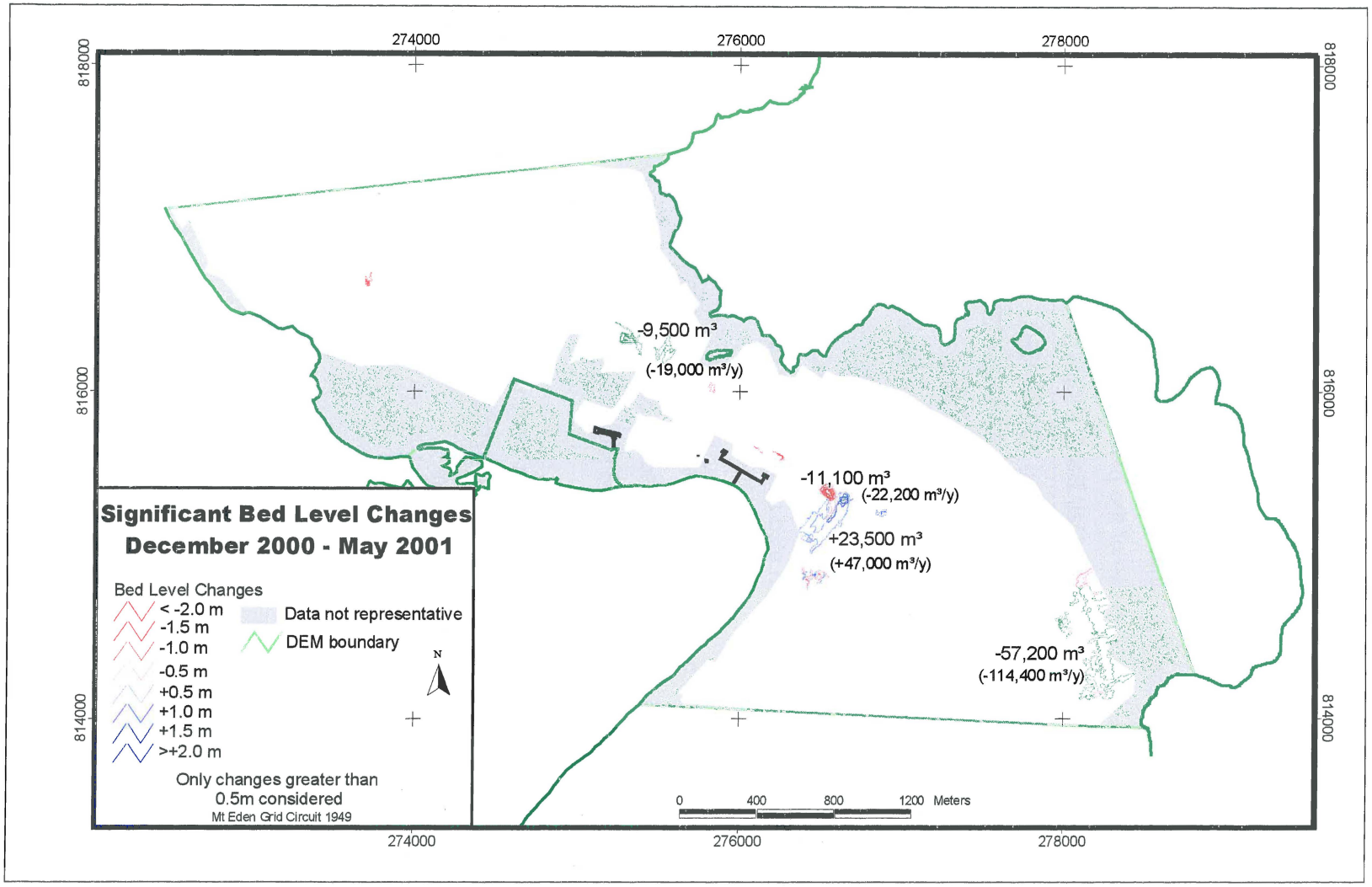


Figure 6.7 - *Bed level changes, minus gridding artefacts, for the period December 2000 to May 2001. Volumetric estimates have MLE of 20%.*

6.7.2 May 2001 to November 2001 (Figure 6.8)

The rock-wall enclosing the reclamation was completed (July 2001) during this period. Dredging operations continued (Figure 6.2).

The dominating feature during this period, is the appearance of the dredge basin adjacent Northport, with the removal of a significant amount of sediment (Figure 6.8).

Mair Bank continued to show variability, exhibiting both erosion and accretion. The rates of change are similar to those of the period December 2000 to May 2001 (Figure 6.7). Erosion at the northern end of Mair Bank shows the removal of a localised *'spot'* like feature, similar to that in Figure 6.7 and mentioned in Section 6.7.1. The location of the erosion during the period May 2001 to November 2001 (Figure 6.8) is the same as the accretion during the period December 2000 to May 2001 (Figure 6.7). During December 2000 – May 2001 (Figure 6.7) there is matching accretion to the southeast of the erosive *'spot'* (Figure 6.8). This provides further evidence for the southeasterly transport of a *'mound'* of sediment as proposed in Section 6.7.1. The western edge of Mair Bank, near Bream Bay beach also accumulated material (Figure 6.8).

Small areas of accretion occurred in the channel adjacent to Calliope Bank, at depths of 20 –23 m below CD (Figure 6.8). The accretion occurred in deeper water than the nearby erosion observed in the preceding 6 months (Figure 6.7).

Accretion occurred in the main channel, in front of the NZRC jetties. Some of this accretion has occurred in the same location as the erosion that occurred here between December 2000 and May 2001 (Figure 6.7).

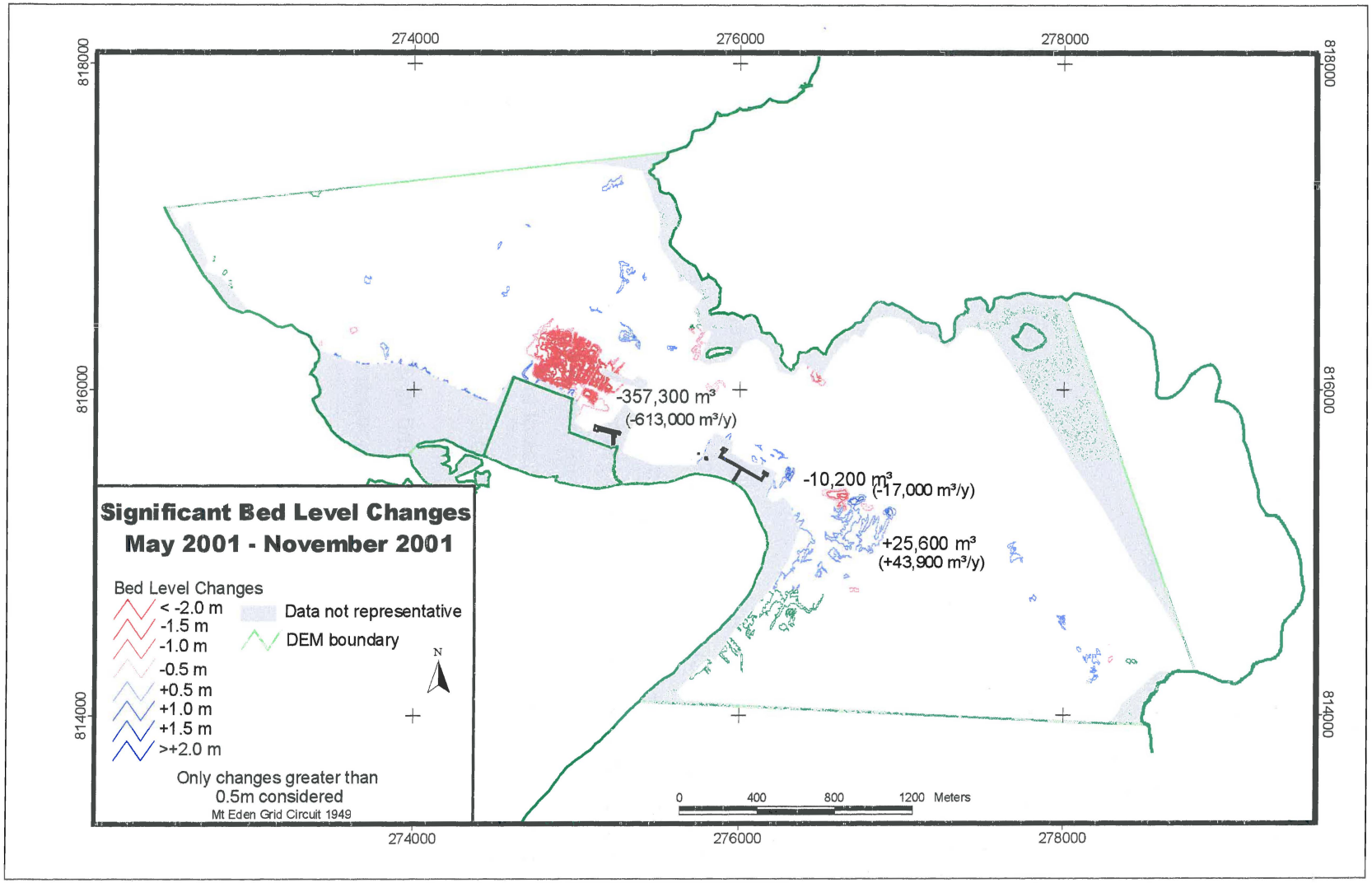


Figure 6.8 - *Bed level changes, minus gridding artefacts, for the period May 2001 to November 2001. Volumetric estimates have MLE of 6%.*

6.7.3 November 2001 to November 2002 (Figure 6.9)

The rock-wall enclosing the reclamation was completed prior to this period, dredging operations were ongoing throughout.

The dredge basin adjacent to the reclamation again dominates the bathymetry changes over this period (Figure 6.9).

The northern edge of Mair Bank exhibits net erosion. The rate of this erosion is less than the preceding 18 months.

Erosion occurred on the channel bottom adjacent the southern areas of Calliope Bank (Figure 6.9). This occurred in depths of 20 – 26 m below CD. These areas are similar to those that experienced accretion between May 2001 and November 2001.

In front of the NZRC jetties, minor erosion (6,900 m^3y^{-1}) occurred in depths of 18 – 21 m below CD.

Balancing quantities of erosion and accretion are apparent between the NZRC jetties and Northport (Figure 6.9). The movement occurred on the edge of the inter-tidal zone, in depths of 0.5 – 1.5 m below CD. The accretion occurred nearer Northport and the erosion closer to the NZRC jetties. It is logical to assume that given the balancing quantities and close proximity, that sediment has been transported from nearer the NZRC jetties towards Northport. The quantities of sediment being transported here are relatively small (~1,000 m^3y^{-1}).

Small quantities of accretion (~1,000 m^3y^{-1}) and larger amounts of erosion (~10,000 m^3y^{-1}) occurred to the northeast of Passage (Motukaroro) Island.

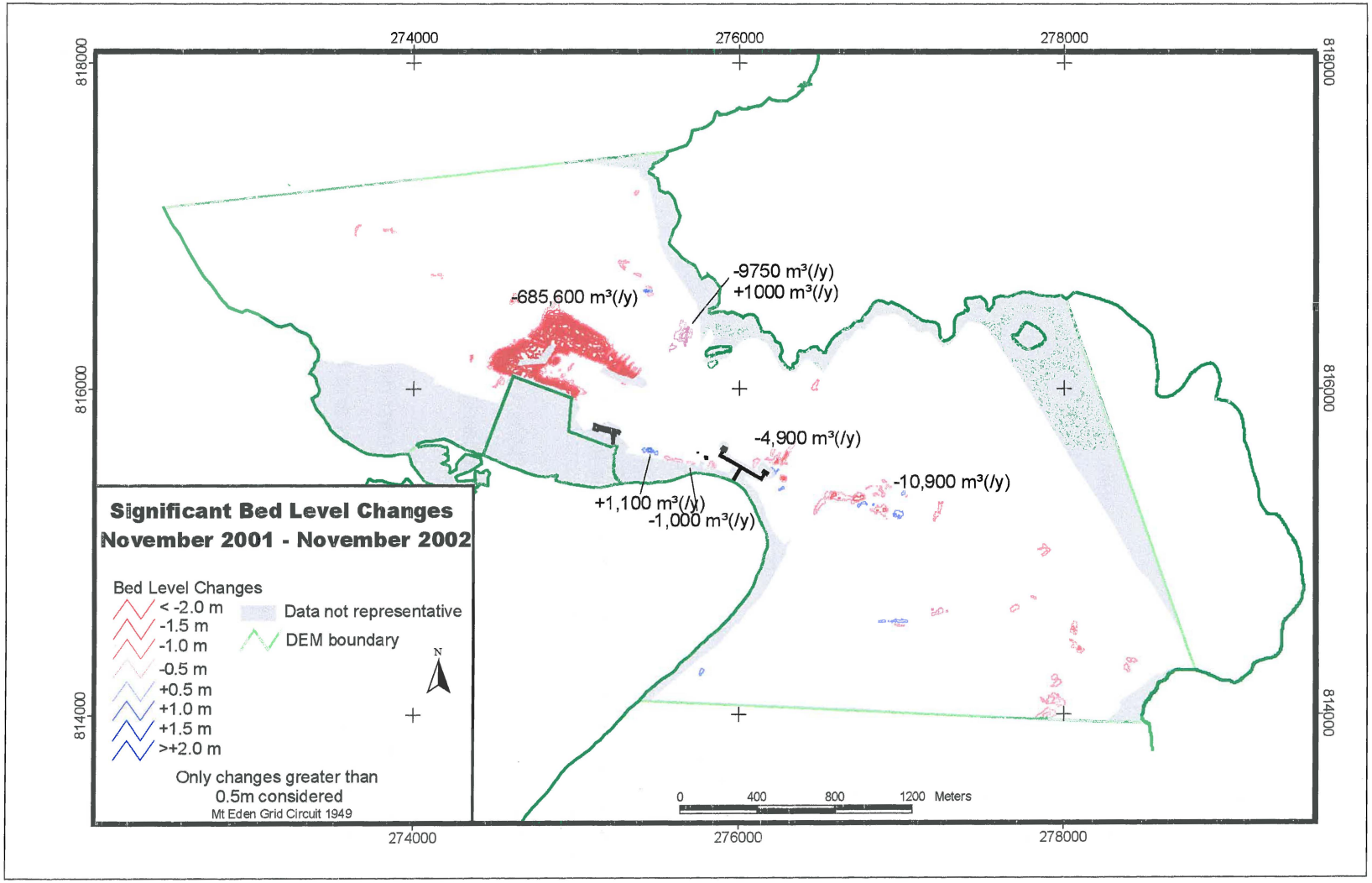


Figure 6.9 - *Bed level changes, minus gridding artefacts, for the period November 2001 to November 2002. Volumetric estimates have MLE of 6%.*

6.7.4 During and Post-Construction Trends

i. The ebb-tidal delta of Mair Bank experienced both erosion and accretion. A net trend of accretion is observed from December 2000 to November 2001 (Figures 6.7 and 6.8). Rates of sediment movement were larger by a factor of two - three than those of May 1995 to May 1998. There is evidence of the southeasterly movement of a *'sediment mound'* on the channel margin located at the northern edge of Mair Bank.

ii. The eastern edge of the channel, adjacent to and south of Calliope Bank (ebb-tidal delta) experienced the loss of a large amount of sediment between December 2000 and May 2001 (Figure 6.7). There are no indications as to where this sediment was transported. Erosion (>1,000 m^3y^{-1}) has not been observed here post May 2001 (through to the last survey considered). Minor volumes of accretion and erosion are noticeable in the middle of the channel adjacent this location from May 2001 to November 2002.

iii. In front of the NZRC jetties, both erosion and accretion has occurred. The volumes being transported were relatively small between December 2000 and November 2001 (Figures 6.7 and 6.8), whilst an increase in the transport rate occurred during the November 2001 and November 2002 period (Figure 6.9). The rate of sediment movement is less than 5,000 m^3y^{-1}.

iv. Areas to the northeast of Passage (Motukaroro) Island have experienced both erosion and accretion, with erosion being dominant.

v. Sediment is moving in an east-northeast direction along the edge of the inter-tidal terrace between the NZRC jetties and Northport.

vi. Remaining areas of the lower harbour were stable over the period. Areas where changes are more prevalent include the sub-tidal extension of Snake Bank towards Northport and the margins of the Blind Channel.

Accretionary features dominate between May 2001 and November 2001 (Figure 6.8), while erosive features are prevalent November 2001 and November 2002 (Figure 6.9).

6.8 Comparison of Pre and Post Construction Trends

For simplification the region is divided into separate areas of interest:

1) **Mair Bank (ebb-tidal delta)**

Prior to construction, Mair Bank experienced both erosion and accretion. This pattern continued during the construction of the reclamation and dredge basin. The volume of sediment being redistributed increased during 2001, then returned to more typical levels. There has been no consistent pattern to the accretion and erosion occurring at Mair Bank since December 2000 (Figures 6.7 to 6.9). Prior to this, accretion was dominant on the northern flanks and erosion on the southern, this pattern was initially observed between 1959 and 1981 (Black, 1983). The majority of Mair Bank exhibited stability between November 2001 and November 2002 (Figure 6.9).

With a documented history of variability (Tonkin and Taylor, 1979a; DHI, 1982a; Black, 1983) and also the variability shown between 1995 and 2000 (Figures 6.3 to 6.6), it would be questionable to attempt to attribute any changes in trends to the construction of Northport. Rates of erosion and accretion in the post construction phase are no greater or lesser than those experienced prior to development. The increase in magnitude, observed between December 2000 and May 2001 (Figure 6.7), occurred at a time when the construction of the rock wall was in its infancy. Impacts from the wall construction could be expected to have a lag time greater than 6 months.

There is no significant evidence from the bathymetric surveys of a change to the pattern or magnitude of the variability of Mair Bank since the construction of Northport.

2) **The eastern channel flank adjacent and to the south of Calliope Bank**

Minor changes occurred from 1995 to 2000, a significant amount of material was removed in early 2001. This location has a history of erosion, with bed level lowering of up to 6.7 m occurring between 1976 and 1981 (Black, 1983). Relatively minor, localised changes were experienced after May 2001, similar to those observed between 1995 and 2000.

The removal of a large amount of material from this region occurred early in 2001. At this stage the rock-wall construction and dredging operations had just begun. In light of the amount of material moved (~57,200 m^3), the timing of the change in relation to the development of Northport and the distance from where the development was occurring (3.3 km) (Figure 6.7), it is difficult to associate the changes to the development.

It is likely that the changes would have occurred with or without the development inside the harbour.

3) **In front of the NZRC Jetties**

Small areas of localised accretion and erosion are evident both prior to and during port development.

Surveys of November 2001 and November 2002 (after rock-wall completion but during dredging operations) indicate an increase of sediment movement in this location. The removal of ~6,900 m^3y^{-1} (Figure 6.9) occurring during this period, is greater than that moved in the small areas of localised accretion and erosion prior to 2001 (~1,000 m^3y^{-1}, Figures 6.3 to 6.8).

Healy (1980) observed significant erosion in this area between 1976 and 1978. During this time the erosion rate was ~26,700 m^3y^{-1}, much greater than anything observed between 1995 and November 2002. This places the November 2001 to November 2002 rates into perspective. With a history of changes of this magnitude, it would be somewhat erroneous to attribute a change of less than 5,000 m^3y^{-1} to port development.

Typical depths in front of the NZRC jetties are 16-18 m below CD. Ships that use these jetties have characteristic draughts of 16-15 m (Longdill et al., 2003a) and water lines of around 150 m. There have been periods in the past where accretion at the eastern most jetty has been a concern to the NZRC and the area surveyed (prior to ship berthing) to determine dredging requirements. Subsequent surveys (post ship berthing) revealed depth increases, eliminating the need for any dredging (pers. comm. J. Palmer, 2003).

The ships that use these jetties represent significant obstacles to current flows as a result of their length and draft relative to depth. The increased velocities that would be expected as a result of the '*obstacles*' presence will undoubtedly impact on the movement and removal of sediment from this location. The timing of the bathymetric surveys considered in this chapter relative to the shipping movements at these berths could significantly impact the *'observed'* patterns of sediment movement in the DEMs. While the volumes of sediment movement calculated will be representative of typical changes, attempts to attribute the changes either to underlying processes or to the effects of berthed ships at this location would be flawed without detailed analysis of the timing of when depths in this area were surveyed and detailed records of shipping

movements over the 8 year period. Neither were immediately available for this study, thus no conclusions can be accurately drawn as to the cause of changes in this area.

4) **Passage Island and surrounding areas**

Minor volumes of localised accretion and erosion existed from November 1995 to May 1998 (Figures 6.6 and 6.5). The accretion was more wide spread from May 1998 to December 2000 (Figure 6.6). After December 2000, a similar trend of minor localised accretion and erosion continued. It appears though that erosion is more prevalent than accretion (Figures 6.7 to 6.9).

Black (1983) has previously observed both accretion (up to 0.5 m rise) and erosion (up to 6 m lowering) in the areas surrounding Passage Island between 1959 and 1981. The areas identified in Black's (1983) comparisons (Figure 6.1) are larger in extent than those shown in Figures 6.3 to 6.9.

It is however noted that these larger areas were calculated by examining a longer time period (22 years) than the current surveys (7 years), which may account for the greater physical extent. Barnett et al. (1993) identified the '*filling of an existing hole*' between 1981 and 1992 in the area.

Recent trends (November 1995 to December 2000 and December 2000 to November 2002) in this area do not appear different from those observed by previous authors (Black, 1983; Barnett et al., 1993).

5) **The area between Northport and the NZRC jetties**

Prior to the Northport development this area was relatively stable. Previous studies have not identified any changes in the region (Figure 6.1).

Surveys from May 1995 to November 2001 indicated only very small-scale changes (Figures 6.3 to 6.8). Larger scale changes were identified between November 2001 and November 2002 (Figure 6.9), after the completion of the Northport reclamation. Accretion occurred on the edge of the inter-tidal area, close to the Northport rock-wall / reclamation, whilst balancing erosion occurred farther along to the east. The rate of movement is of the order 1,000 m^3y^{-1}. Accretion was predicted close to the reclamation here due to the expected formation of a large-scale eddy during the ebb tide (Healy, 1980).

6) **Remaining Areas**

The remainder of the harbour has remained stable, with only isolated pockets of erosion and accretion.

The occurrence of small areas of bed level change along the blind channel margins and the sub-tidal extension of the flood tidal delta (Snake Bank), has been consistent from May 1995 to November 2002 (Figures 6.3 to 6.9). These specific areas have previously been identified due to their variability between 1959 and 1992 (Black, 1983; Barnett et al., 1993). Changes found during this period were also relatively minor, with maximum changes in bed levels not exceeding ± 0.7 m (Black, 1983). Figures 6.3 to 6.9 show that since May 1995 the spatially limited bed level changes in these areas have not exceeded ± 1.0 m. The more recent data indicate no change to these trends.

The long-term stability of many areas of the lower harbour is not necessarily indicative of low sediment transport in these areas. It is possible that sediment is being transported through the area, or moving in a closed loop in balancing quantities without actively altering the bed level.

Table 6.3 provides a summary of sediment movement volumes at key locations in the lower harbour over the period of time covered by each survey.

Period	Mair Bank	In front of NZRC Jetties	Between NZRC and Northport	Flank of Calliope Bank	Passage Island	Dredge Basin
5/95 - 11/95	+ 6,300			-19,000		
11/95 – 5/96	+6,700	- <1,000				
5/96 – 5/98	+<3,000	- <1,000				
5/98 – 12/00	+22,000 (northern) -6,100 (southern)	+<1,000			+<1,000	
Start of Northport Reclamation (12/00)						
12/00 – 5/01	+25,000	- <1,000		-116,600	-19,000	
5/01 – 11/01	+26,900	+<1,000		+<1,000	-<1,000	-613,000
11/01 – 11/02	-10,900	-6,900	-1,000 (east) +1,000 (west)	- <1,000	-8,750	-685,600

Table 6.3 - *Summary of characteristic volumes of sediment movement at key locations in the Lower Whangarei Harbour from analysis of bathymetric data. All values normalised to* m^3y^{-1}.

6.9 Predictions of sediment transport models

Hydrodynamic model studies investigating sediment transport and its effects on the bathymetry have been undertaken by the DHI (1982a), Black (1983), Barnett et al., (1993) and Barnett (1997). The studies by the DHI (1982a), Barnett (1993) and Barnett (1997) are effectively successions of the same model. Modifications and improvements were made at each stage in order to improve the modelling technique, update the bathymetry being modelled and to alter the shape of the dredge basin and reclamation to the actual plans being considered. As a result of this, the findings of Barnett (1997) are the most pertinent to consider. This model is the only study that has been able to use the most recent plans of the dredge basin. Attempts to compare the predictions of the other models would be a rather pointless exercise, as they used rather different port and dredge basin layouts to that actually built (DHI, 1982a; Black, 1983; Barnett et al., 1993).

Sediment transport models are generally somewhat less robust than the hydrodynamic models they are based upon (Davies et al., 2002; Hass and Hanes, 2003). Hydrodynamic models are calibrated with *'real'* water velocity data. While the calibrated hydrodynamic model output is used to *'drive'* the sediment transport model, they are not generally calibrated with real data (DHI, 1982a).

Sediment transport models also tend to provide *'initial potential changes'* rather than final morphologic equilibriums, as they do not continually update the bathymetry and its effects on the water velocities (Barnett et al., 1993).

The predictions of erosion and accretion of Barnett (1997) have been rectified and georeferenced (Figure 6.10). Note that predictions of bed lowering are coloured BLUE and bed level rise is coloured RED.

The most appropriate surveys on which to make comparisons with the model predictions are the surveys of November 2001 and November 2002 (Figure 6.9). These surveys represent the time when the rock-wall / reclamation was complete and the dredge basin nearing the *'as modelled'* configuration.

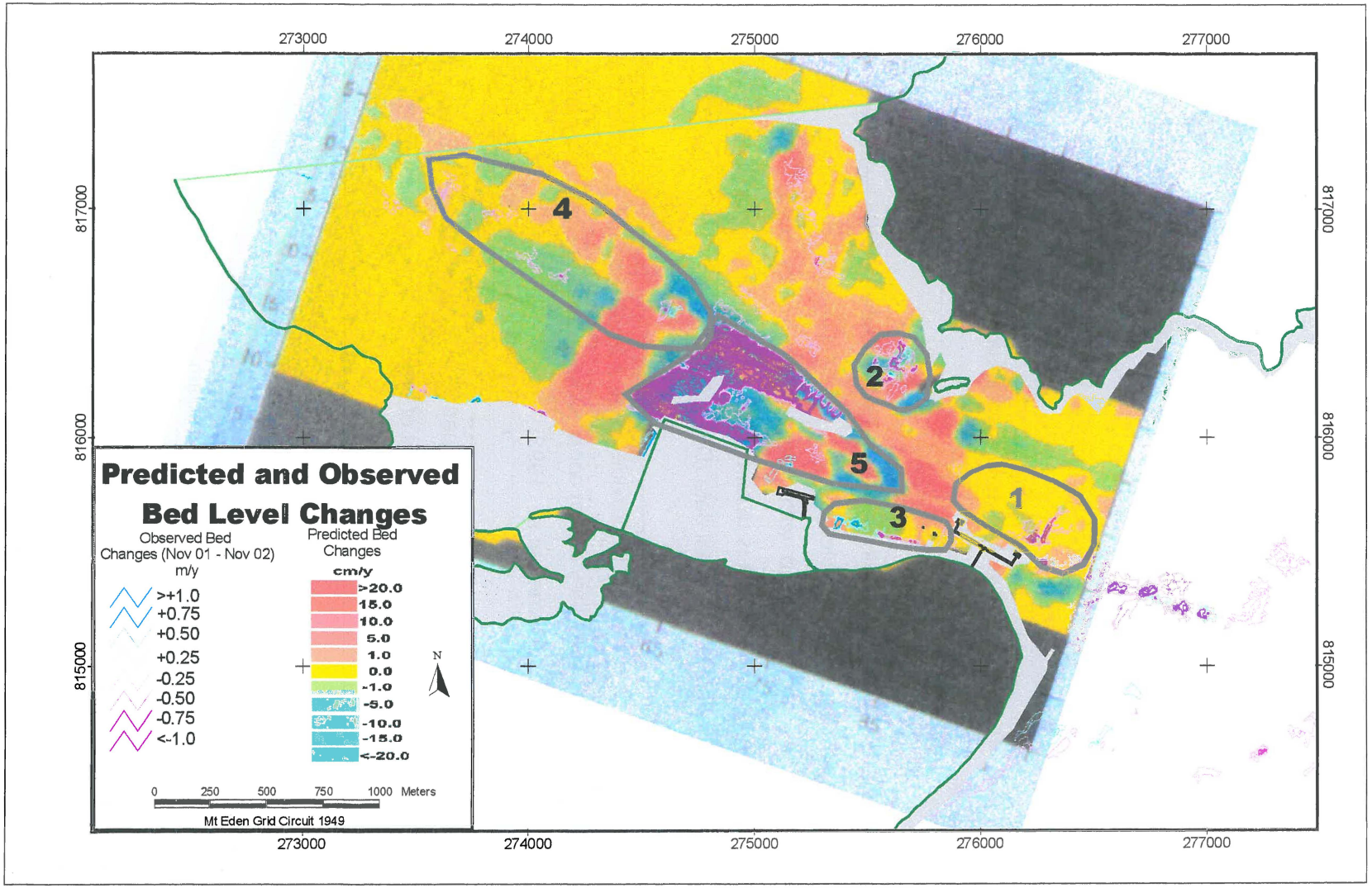


Figure 6.10 - *Observed and Predicted changes in bed level. Predicted changes from sediment transport model predictions (Barnett, 1997)*

The region has been broken down into smaller areas for comparisons (Figure 6.10). All predictions are based on Barnett (1997):

1) **In front of the NZRC Jetties**

This area experienced erosion (~5,000 m^3yr^{-1}) between November 2001 and November 2002 (Figure 6.9). The sediment transport model predicted minor levels of both erosion and accretion (Figure 6.9), with erosion being dominant. Calculations based on the number of grid cells and predicted bed level change give predicted eroded volumes of around 10,500 m^3yr^{-1} in the same area as the erosion experienced during 2002.

The slight discrepancy between the volumes predicted and observed could potentially be attributed to the partially completed nature of the dredge basin. Some of this area is also close to the jetties, where *'flow obstacle'* effects due to berthed ships may have influenced the surveyed data (Section 6.8).

The model predicted the location of the erosion well and the magnitude reasonably well given the limitations of the survey data.

2) **Passage Island and surrounding areas**

Between November 2001 and November 2002, both erosion and accretion occurred in localised areas (Figure 6.9). Model predictions are based on grid cells 50 m x 50 m. The extent of the accretion observed between November 2001 and November 2002 (Figure 6.9) is such that it will not be revealed on a 50 m x 50 m grid as it occurs at a smaller scale than this resolution.

The net removal rate of sediment for the period was 8,750 m^3y^{-1}. Calculations based on the grid cell size and predicted bed-lowering show a predicted removal rate of around 6,600 m^3y^{-1}.

The model predicted these changes accurately.

Minor accretion, predicted in the surrounding area (Area 2 in Figure 6.10), is not shown by the contours of the observed data. The predicted accretion here is of the order of 0.01 – 0.05 my^{-1}, on the limits of the accuracy of the bathymetric surveying methods (Table 6.1) and below the resolution of the 0.25 my^{-1}contours in Figure 6.10.

3) **The area between Northport and the NZRC jetties**

A pattern of accretion near Northport and erosion closer to the NZRC jetty was observed here in 2002 (Figure 6.9). The sediment transport model (Barnett, 1997) predicted similar patterns here (Figure 6.10), although erosion was also predicted farther out into the harbour.

The predicted changes are of a greater spatial extent and lesser magnitude than the observed changes.

4) **Sub-tidal extension of Snake Bank**

Model predictions in this area were for a complex pattern of alternating areas of bed level lowering and bed level increase (Figure 6.10). The magnitude of these changes was predicted to be small ($\pm$ 0.1 my^{-1}). Changes of this magnitude are below the resolution of the contours plotted in Figures 6.3 to 6.10. Contours at this level were filled with survey artefacts and on the limits of the accuracy of the survey data (Table 6.1). Observed changes in this region are between 0.25 and 0.50 my^{-1}.

The model identified the general area as being susceptible to change, which is validated by the observed changes.

5) **Dredge Basin**

Erosion and accretion predicted within and nearby the dredge basin (Figure 6.10) is not apparent in any of the bathymetric surveys. Dredging was ongoing throughout the survey period. The patterns predicted will only be able to be compared to *'real'* observations when using bathymetric surveys undertaken once all dredging is complete, thus at the time of writing no conclusions can be drawn regarding this region.

6) **Other areas**

Accretion at rates greater than 0.2 my^{-1} were predicted in the main channel between areas 1 and 5 (Figure 6.10). No changes greater than 0.25 my^{-1} were observed here during 2002. Possible reasons for this include:

i. the incomplete nature of the dredge basin; and
ii. the armouring effect of the shell lag which covers the bed in this region (Chapter 3).

Northeast of area 2, near Darch Point (Figure 6.10) bed level rise was predicted. The opposite was observed during 2002, with a lowering of the bed by 0.25 my^{-1} occurring (Figure 6.10). The model (Barnett, 1997) is not predicting changes accurately in this region.

note on the sediment transport model predictions:
The sediment transport model (Barnett, 1997) calculates sedimentation rates based on hydrodynamic equations and the sedimentary characteristics of the bed. It is widely acknowledged that these models have limitations. It is therefore somewhat dubious that in the plot of Barnett (1997) (Figure 6.10) there are contours of change plotted at the 0.01 my^{-1} level.

It is perhaps more logical to consider these predictions in terms of general areas of accretion and erosion, rather than place too much weight on the magnitude of changes predicted at this extremely fine level.

Plotting contours at these levels can have the effect of *'hiding'* more representative patterns in the predictions and should be kept in mind when considering Figure 6.10.

Estimates of the magnitude of errors in the predictions are not reported.

Box 6-1 *Note on the sediment transport predictions of Montgomery and Watson (1997)*

6.10 Sediment budget for Marsden Point

Using areas identified from the analysis of bathymetric surveys and the volumes calculated, a *'bathymetry based'* sediment budget has been created based on Table 6.3. The budget is *'primitive'* in that it attempts not to describe exactly where sediment is moving to-and-from. The data used to compile it does not disclose this. Analysis of bathymetric data does however identify typical magnitudes of sediment movement at various sites in the lower harbour.

By compiling the data presented in Figures 6.6 to 6.9, a sediment budget has been developed (Figure 6.11). In general, directions of movement could not be established, but where inferred, the transport direction is labelled. Maximum likely errors in the estimations range from 20 to 6%, as the errors from the volumetric calculations are carried through.

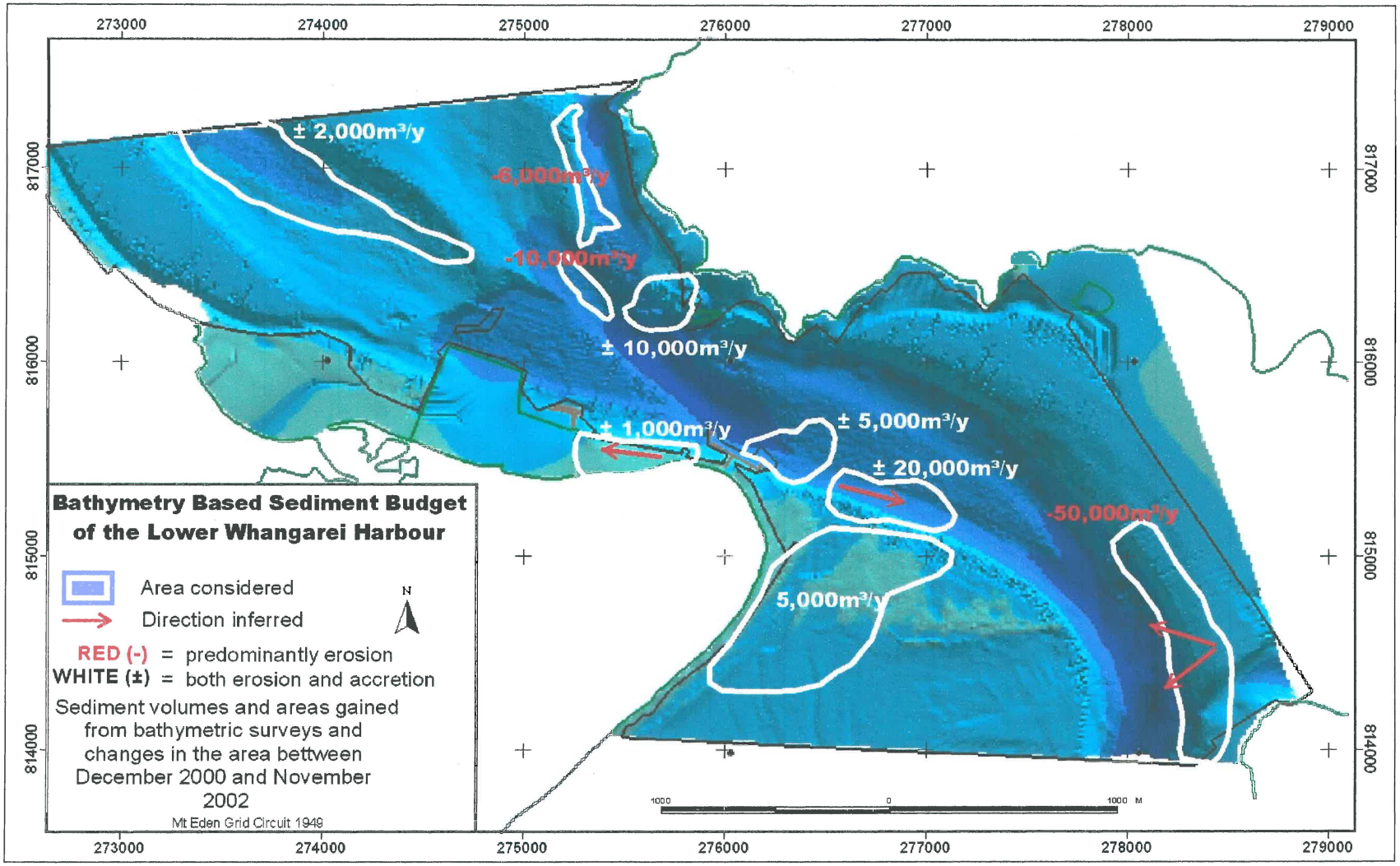


Figure 6.11 – *Bathymetry based sediment budget for the lower Whangarei Harbour, from Northport development to November 2002. Areas indicate zones prone to sediment movement and observed volumes moving. Bathymetry from November 2002.*

6.11 Summary

Using surveys undertaken by Northport from 1995 to 2002, bathymetric stability and bed level changes of the lower Whangarei harbour have been examined.

Irregularly x, y, z data has been interpolated to fit a 1 m resolution grid and DEMs of the surveys created. Differences in elevations between surveys have been examined.

Major findings include:

- The ebb tidal delta (Mair Bank) has been a variable feature of the harbour. It has exhibited accretion and erosion both prior to and post port development. There is no evidence of a major change in the volume of sediment being redistributed on Mair Bank. Volumes of movement are typically ~5,000 m^3y^{-1}, with larger amounts moving on the banks northern edge (up to 20,000 m^3y^{-1}).

- The flank of the lower channel, adjacent to the other ebb tidal delta (Calliope Bank), has experienced periods of significant erosion in the past and confirms that large-scale sediment fluxes occur in this location. The removal of material appears to be periodic and short lived. There are no attributable links between this process and the development of Northport.

- Sediment is being actively redistributed adjacent to the NZRC jetties. The volumes of sediment moving between 1999 and 2002 were of the order of 5,000 m^3y^{-1}. Previous investigations during the 1970's discovered volumes of sediment movement five times this amount in the same location. The development of Northport has not affected the rate of sediment transport in this area to date. *'Obstacle effects'* of berthed ships potentially influence sediment movement at this location. Whilst the volumes of movement are representative, the driving mechanisms could be underlying processes, increased velocities due to berthed ships, or a combination of these.

- The seabed surrounding Passage Island is continually changing and adjusting in form. This has been observed by previous researchers and again by the current study.

- The inter-tidal zone between the NZRC jetties and Northport has experienced a redistribution of sediment since the completion of the Northport reclamation. Accretion is occurring close to the Northport rock-wall, while balancing erosion is occurring nearer the refinery jetties. Changes in this region have not been identified previously and have only been observed since November 2001. Accretion in this region was predicted by Healy (1980)

- The remainder of the harbour exhibits remarkable stability both prior to and post development. Much of this stability is attributable to the effects of a shell lag layer armouring the main channel.

- The sediment transport model of Barnett (1997) has been shown to be predicting changes well in some areas. The model, somewhat limited by its 50 m grid cell resolution, predicts many of the general trends.

- A bathymetry based sediment budget has been created for the lower Whangarei harbour (Figure 6.11). The budget outlines characteristic volumes of sediment moving at various locations within the harbour. Assumptions are not made regarding the transport processes, sources or sinks of various sediments.

7 MORPHODYNAMICS OF THE LOWER HARBOUR

7.1 Introduction

Sediment character and the nature of the seabed adjacent to Northport is investigated through the use of a Side-Scan Sonar (SSS) system. The SSS image (sonograph) enables differentiation of bottom signals to identify sediment facies, bedforms, and active sediment pathways throughout the dredge basin, inlet gorge, ebb and flood tidal deltas. The character of the bottom inferred from the SSS record is used to relate hydrologic and sedimentologic conditions required for their formation. The spatial variation of bottom sediment facies links hydrologic processes to the transport of sediments. The chapter aims to map patterns of sediment movement surrounding Northport from the seabed character and orientation of bedforms.

7.2 Instrumentation

Side-Scan Sonar is a system of imaging underwater objects and the sea floor using high frequency acoustic signals. SSS collects a continuous swath of seafloor imagery from a towed *'fish'*, typically between 100-400 m in depths less than 100 m, it provides an underwater analogy of a continuous oblique aerial photograph. A basic system consists of a transducer (mounted inside a tow-fish) which is towed at a depth behind the survey boat and a data acquisition unit onboard the survey vessel (Figure 7.1). Surveys undertaken for this study used a Klein 595 data acquisition unit with a 100 / 500 kHz dual frequency transducer. Data was recorded electronically onboard the university research vessel *Taitimu* using an Isis V3.24 (Triton Elics, 1998a) on a PC operating under Windows 95. Post processing of the data was undertaken using Isis and maps of sonar mosaics were created in Geotiff form using DelphMap (Triton Elics, 1998b).

SSS operates by transmitting a narrow beam of acoustic energy (sound) from the tow fish out across the seabed. The transducer emits single pulses and waits for the sound to be reflected back. Imaging range is determined by the length of time the transducer *'listens'* before emitting a new pulse, this is a function of the water depth and frequency (of pulsing) used. The image is thus built up one line at a time as the transducer records reflections from the 100 – 400 m range obliquely beneath the transducer.

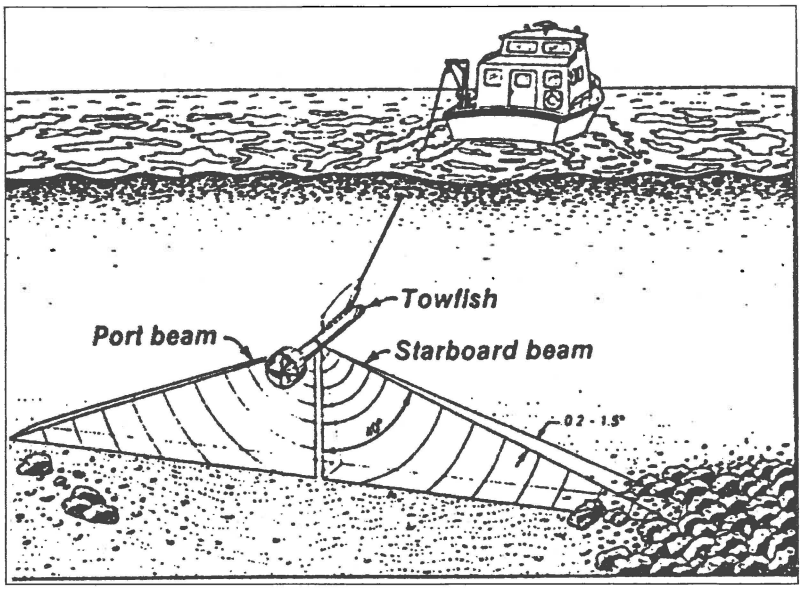


Figure 7.1- *A side scan sonar system operated from a small vessel (Morang et al. 1997). The system consists of a tow-fish towed behind the vessel using an electromechanical cable. The tow-fish insonifies a swath of seafloor using acoustic energy. Backscatter is recorded by an onboard computer and output as an acoustic image (sonograph) of the seafloor. Note the narrow horizontal and wide vertical beamwidth. Acoustic energy is denser immediately underneath the tow-fish, rather than farther along the beam due to the angle of incidence.*

Hard objects reflect more energy causing a dark signal on the image (e.g., rocks). Soft objects that do not reflect energy as well (e.g. mud, kelp) show as lighter signals, while certain phenomena that induce signal quenching show as a white shadow effect in the imagery.

7.3 Methods

7.3.1 Side Scan Sonar Survey

An initial side scan sonar survey was carried out on December 6th 2002, with a subsequent survey undertaken upon completion of dredging on October 16th 2003. During both surveys a Klein 595 side scan sonar system was operated from the University of Waikato research vessel *Taitimu*. An onboard computer running Isis® V3.24 under Windows 95® recorded the analogue reflected signal from the tow-fish and converted it to digital format. Analogue output was printed in real time during data collection.

The position of the survey vessel was determined in WGS 84 using a Real-Time Kinematic Global Positioning System (Trimble® RTKGPS) updated at 2 Hz by radio from a static shore position. This system provided positional information with horizontal accuracies in the order of 0.1 m (Chisolm, 1998). An offset was applied to the positional information received by the boat's GPS antenna to correct for the tow-fish position behind the boat. The distance applied was the length of the SSS cable deployed behind the boat plus the distance from the cable spool to the GPS antenna. Positional information was fed to the computer running the Isis software and tagged to the digitised reflected signals. Vessel speed averaged 2 ms^{-1} and the swath range was set at 200 m.

Weather conditions deteriorated during the initial survey (December 2002) resulting in the appearance of an amorphous boundary between water and bed in the recorded data due to sediment movement and interference from surface bubbles leading to a reduction in data quality. The second survey (October 2003) was undertaken out of a desire to obtain higher quality data and an image of the dredge basin upon completion of the capital dredging.

Details regarding to the SSS data processing are provided in Appendix E.

7.3.2 Sonograph Interpretation Methods

SSS technology is largely limited to qualitative studies. While this is changing somewhat with the advent of multi-beam systems, the interpretation of sonographs is still largely a subjective exercise (Morang et al., 1997). Accurate interpretation of SSS images requires an understanding of the operation and geometry of SSS systems and of the physics of sound in water (Appendix E). The need to check on interpretations by ground-truthing has been stressed by many authors (Morang and McMaster, 1980; Black and Healy, 1983; Green, 1986; Morang et al., 1997). Results from sediment grain size analysis (Chapter 3) are used as reliable ground truthing data for the sonograph.

In total, five different mapping units were identified based on their degree of sound reflectivity (shades of grey). These form the basic map units of Table 3.1.

Map Unit	Acoustic Return	General Setting
Rock	Strong, dark grey to black, shadows	Uncommon, isolated spots and near passage island.
Shell Lag	Strong, dark grey to black	On the main channel floor in front of Northport and the NZRC jetties.
Coarse Sand	Strong, dark grey to black	Can be mixed with fine sand (with decreased quantities of medium sands) in parts of the dredge basin.
Medium Sand	Moderate, light to dark grey	Common in front of Northport and on margins of the Blind Channel.
Fine Sand	Weak, light grey to white	Very common over entire area, where no shell lag exists. Makes up the sub-tidal extension of Snake Bank.

Table 7.1 - *Characteristics of the basic map units used in the interpretation of the side-scan sonographs.*

Composite mapping units (Figure 7.2) are used to classify the imagery of the sonograph following a method used by (Barnhardt et al., 1989). Schemes such as this are necessary for areas that are texturally complex. The sonograph was interpreted using this classification scheme with the areas selected digitised into Arc View® GIS as polygons with the appropriate attribute information. Figure 7.3 shows an example of the differing regions on the sonograph, used in conjunction with the sediment sampling results to classify the region.

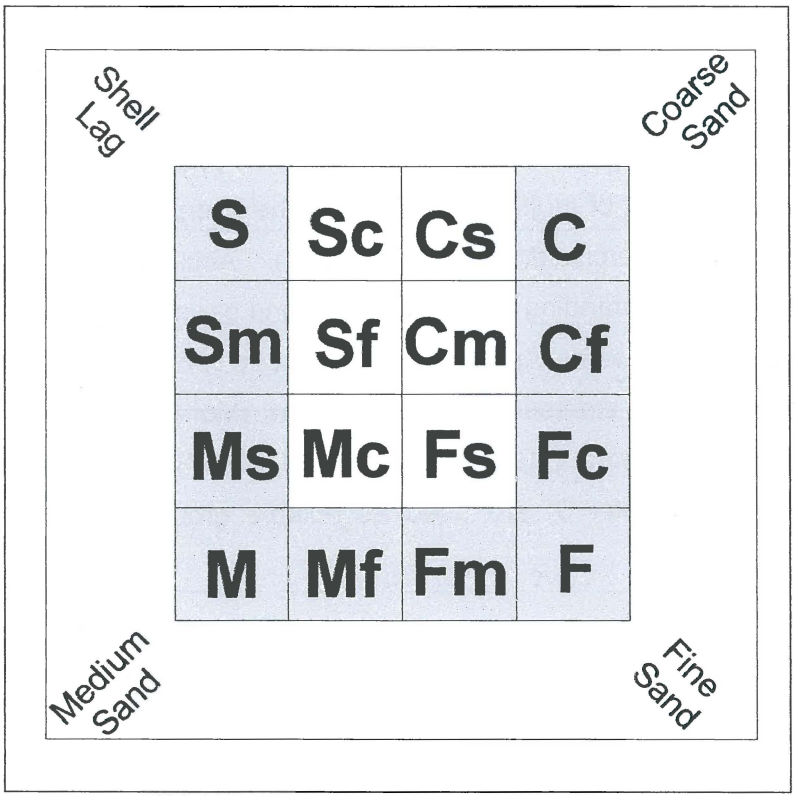


Figure 7.2- *Classification scheme based on four end-member units (S=Shell Lag, C = Coarse Sand, M = Medium Sand, F = Fine Sand) (after Barnhardt et al. 1989). The composite units are combinations of the end-members with the dominant unit taking the upper case letter. Only the shaded units are discernable on the SSS record.*

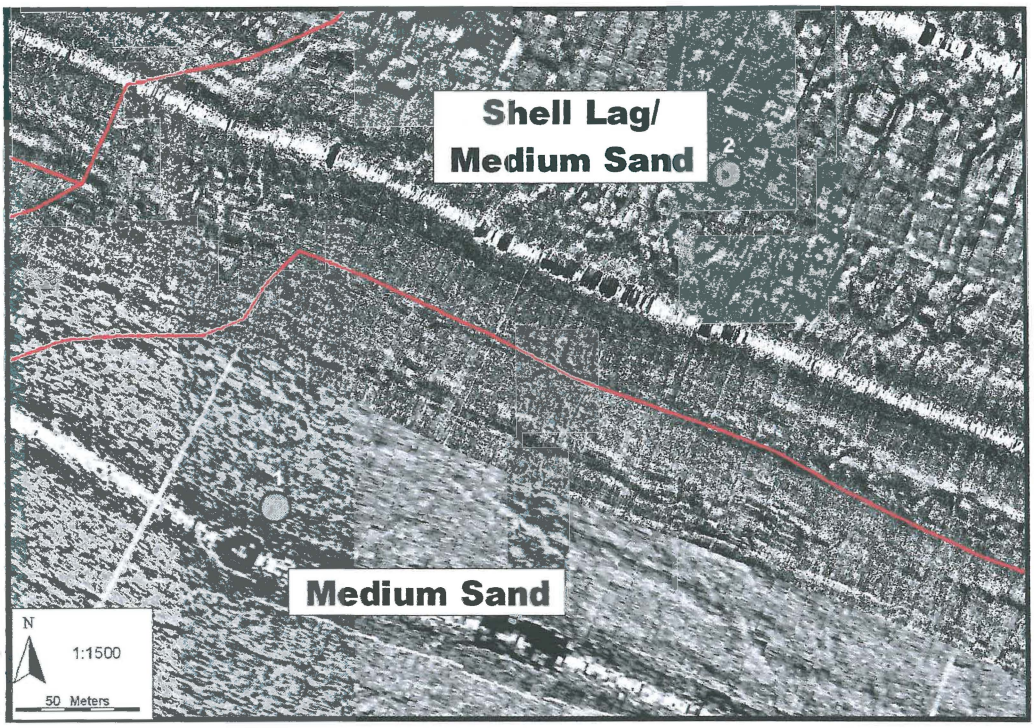


Figure 7.3 - *Rectified and mosaiced side scan sonar record showing differences between shell lag and medium sand zones. Sediment sample 1 had a mean grain size of 1.83 Φ, while sample 2 contained ~72% of shell material with the sand portion having a mean grain size of 1.78 Φ.*

7.3.4 Bedform Classification

Flowing water generally organises individual grains into morphological elements termed bedforms. Bedform orientation is an indicator of sediment transport pathways. The classification of bedforms from the sonograph has been undertaken using the scheme proposed by the Society for Sedimentary Geology, Bedforms and Bedding Structures Group in 1987 (Ashley, 1990). This classification scheme has been deemed suitable for all sub-aqueous bedforms (USACE, 2002). Bedforms may take the form of:

i. ripples — Small bedforms (wavelength $\lambda < 0.6$ m), (height H < 0.03 m). Formed under low shear stresses. Can be subdivided into groups based on the shape of the crestline: straight, sinuous, catenary, lingoid and lunate. Due to their size these features are not observable on sonographs;

ii. dunes — Wavelengths from under 1 m to over 1000 m. Flow transverse features which develop under unidirectional flows. Ubiquitous in sandy environments with water depths > 1 m, sediments coarser than 0.15 mm (very fine sand) and current velocities > 0.4 ms^{-1}. Subdivided into:

a. small 0.6 m < λ < 5 m;
b. medium 5 m < λ < 10 m;
c. large 10 m < λ < 100 m;
d. very Large 100 m < λ;

These features have been termed *'megaripples'* in previous investigations of the Whangarei Harbour (Black, 1983; Black and Healy, 1983);

iii. plane beds — May occur under two hydraulic conditions:

a. the transition zone between the region of no movement and the initiation of dunes and
b. the transition zone between ripples and anti-dunes, at mean flow velocities between about 1 and 2 ms^{-1};

iv. anti-dunes — Bedforms that are in phase with water surface gravity waves. Height and wavelength is dependent on the scale of the system and characteristics of the fluid and bed material. May migrate upstream, downstream, or remain stationary.

(Allen, 1969; Ashley, 1990; USACE, 2002)

The occurrence of the various bedform types is dependent on the velocity – grain size relationship. Bedforms are only stable under certain flow conditions. Figure 7.4 illustrates the zones where ripples, dunes, planar beds and anti-dunes are found. The figure summarises laboratory studies conducted by various researchers. The experiments support the common belief that large flow-transverse bedforms (dunes) are a distinct entity separate from smaller current ripples (USACE, 2002).

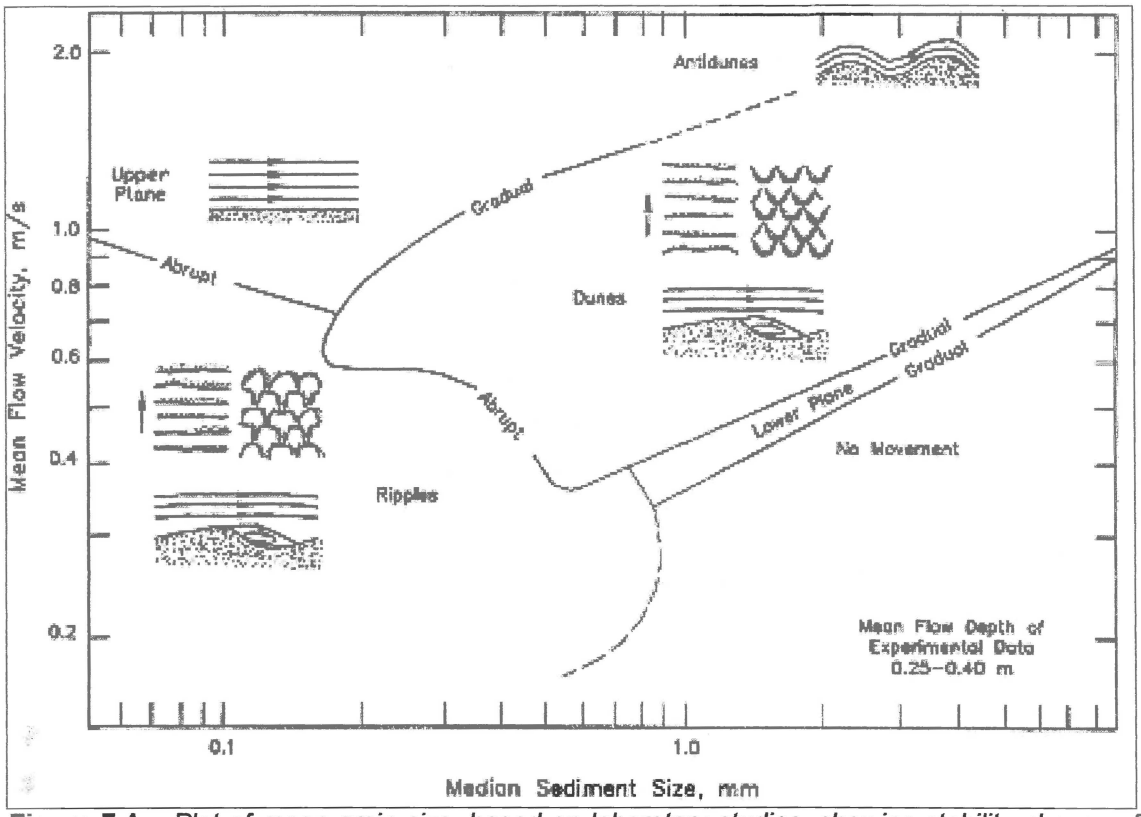


Figure 7.4 – *Plot of mean grain size, based on laboratory studies, showing stability phases of subaqueous bedforms (modified from Ashley, 1990). If the flow pattern remains relatively unchanged perpendicular to the flows overall direction and there are no eddies or vortices, the resulting bedform will be straight crested and 2 dimensional. If vortices present are capable of scouring the bed a 3 dimensional bedform is produced.*

Bedform location within the area covered during the SSS surveys is mapped from observations of the variation in reflection of the lee (slipface) and stoss slopes of the bedform. The assumed direction of net sediment transport can be determined from the orientation of the lee sides of the observed dunes with transport assumed to be perpendicular to the general direction of the crests.

7.4 Side Scan Sonar Survey Results

7.4.1 Sediment Facies Units

The sonograph (Figure 7.5) was interpreted (along with sediment sampling results, Chapter 3) using the classification scheme detailed in Figure 7.2 and Table 7.1. Bottom sediment facies units were created in Arc View® (polygons) based on the acoustic return signal strength and given appropriate attribute information (Figure 7.6). Figures 7.7 and 7.8 detail the proportions of bottom sediment types observed and the characteristic depths in which they were observed.

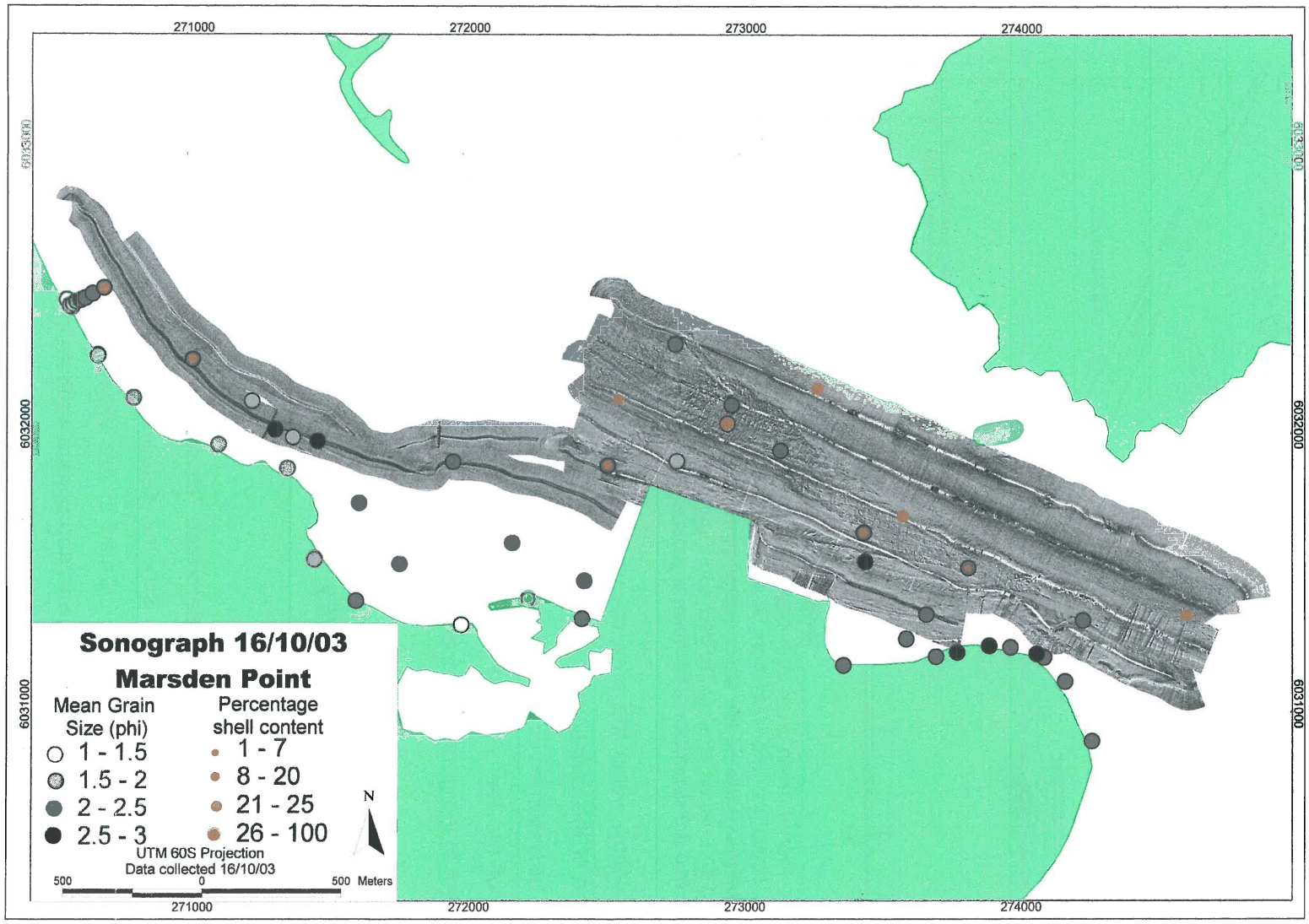


Figure 7.5- *Corrected, geocoded and mosaiced sonograph of the lower Whangarei Harbour. Positioning by RTK GPS, image has 0.25 m pixel resolution. Mean grain sizes from RSA analysis of surficial sediment samples. Percentage shell content shown where found in sediment samples.*

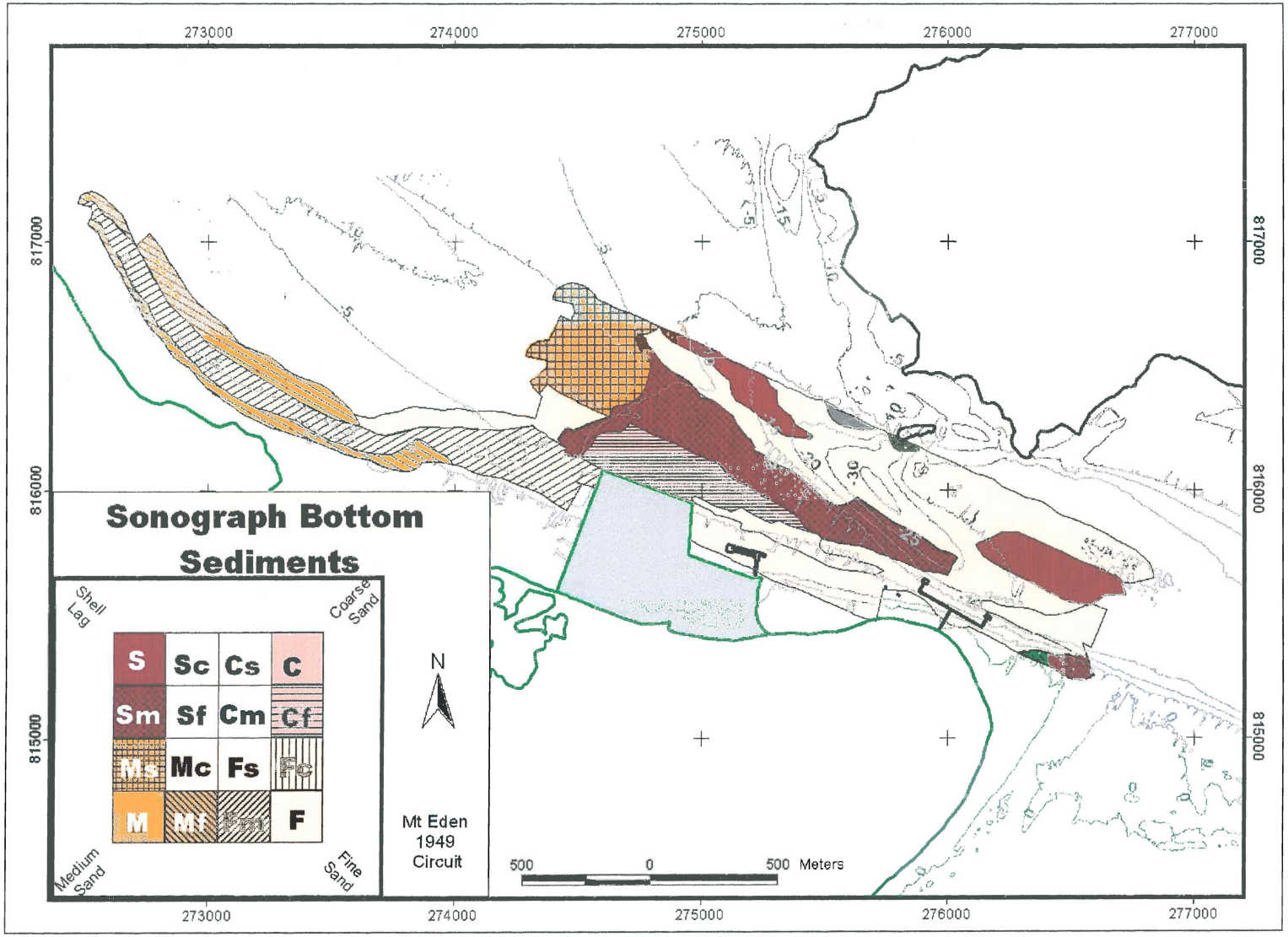


Figure 7.6 - *Bottom sediments interpreted from sonograph and sediment samples. Bathymetry at 5 m contours from November 2002 survey. Classifications scheme after Barnhardt et al.(1998).*

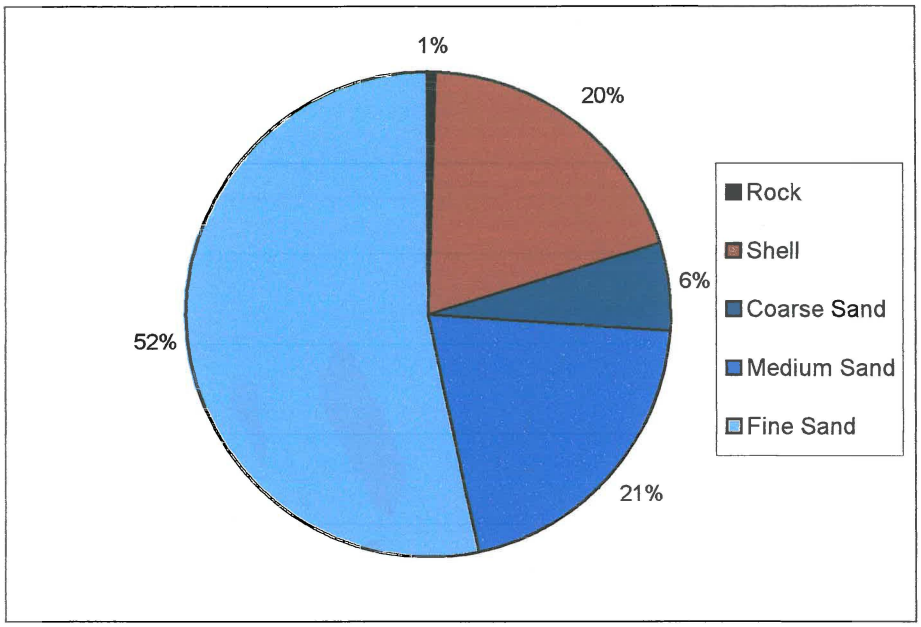


Figure 7.7- *Summary pie chart of dominant bottom types from side scan sonar survey. Total coverage was 2.236 km^2.*

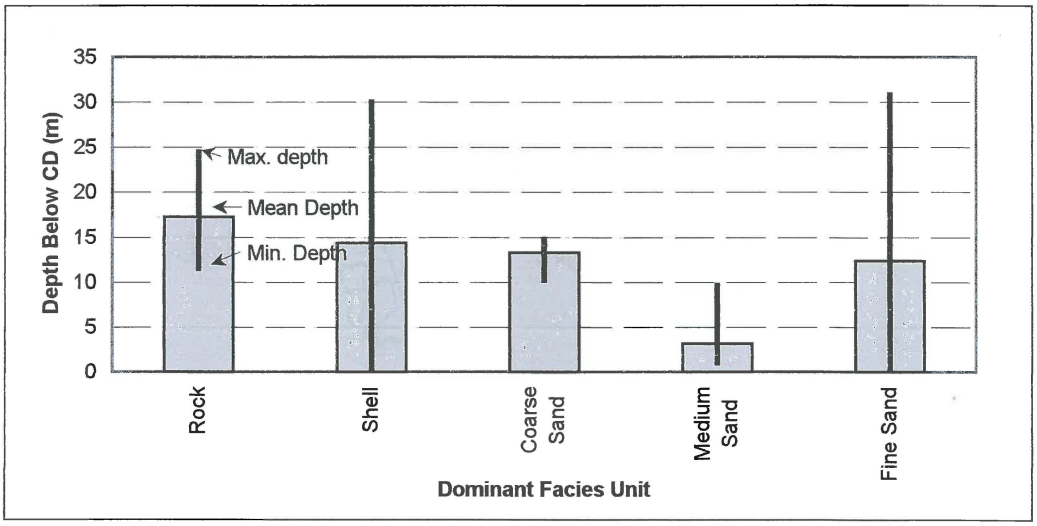


Figure 7.8- *Mean water depth and depth range of the dominant facies units. Depth in meters below chart datum, from Nov 2002 bathymetry grid.*

7.4.2 Bedform Orientation

Sediment transport directions were inferred from the bedform orientation on the sonograph. It is assumed that sediment movement can be determined from dunes whose lee slopes are orientated in the direction of net transport. Wavelengths of bedforms were calculated from the average of at least 15 bedform structures and results shown in Figure 7.9.

The orientation of asymmetrical bedforms (λ = 6-12 m) indicates a general direction of northwesterly transport in the northern parts of the dredge basin (Figure 7.9). Immediately to the east of the Northport quay wharf, adjacent the old NHB wharf, similar asymmetric bedforms (λ = 10-13 m) indicate sediment transport into the dredge basin. These bedforms, observed on the batter slopes of the dredge basin, are thought to reflect down slope movement into the deeper dredge basin.

At the eastern edge of the dredge basin, bedforms indicate sediment transport directed both out of the harbour and also in a more southerly direction in the deeper parts of the channel. In front of the NZRC jetties, bedforms are oriented in a southeasterly direction (out of the harbour) and in a southwesterly direction toward the jetties and shoreline (Figure 7.9).

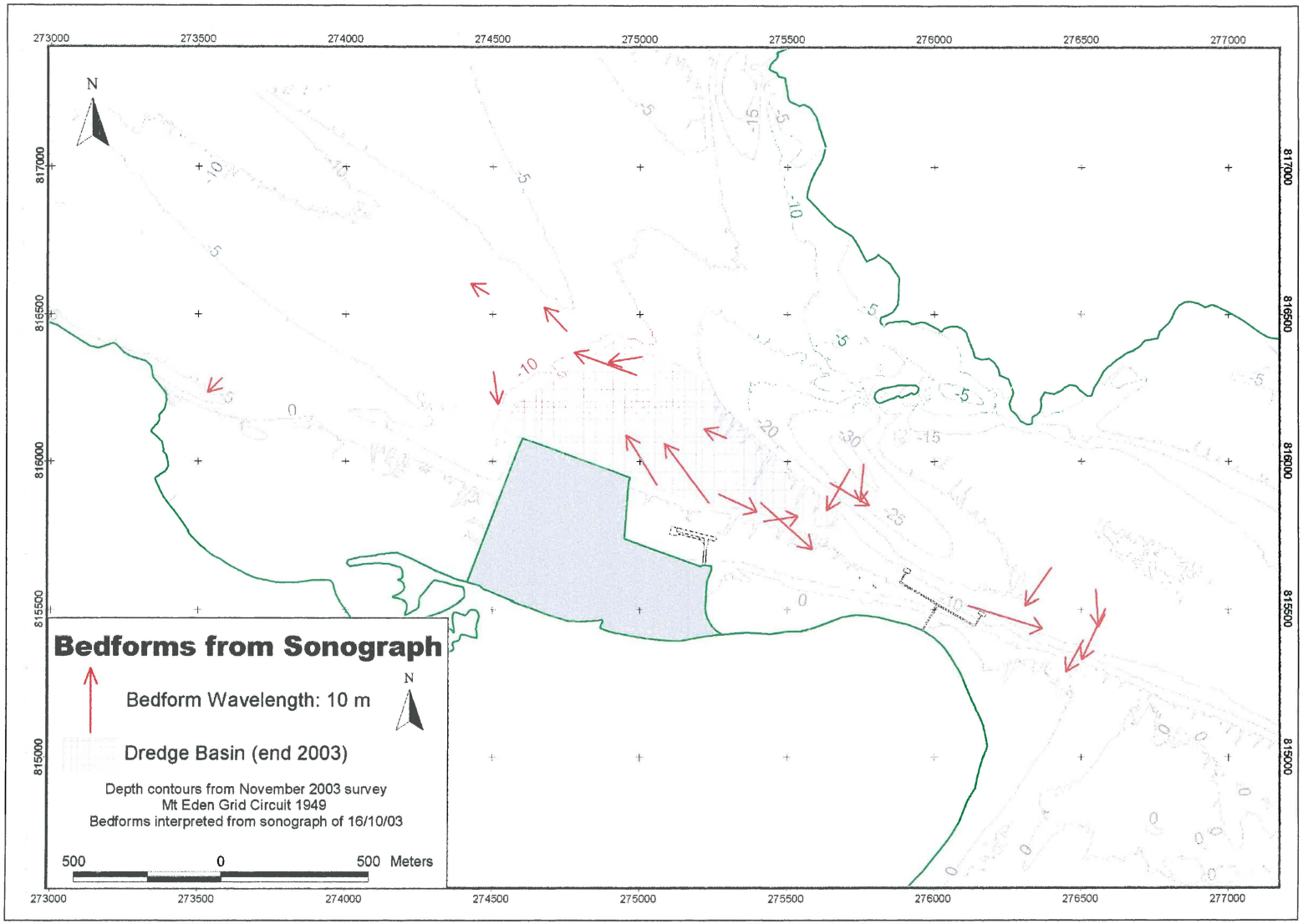


Figure 7.9- *Bed from orientation and wavelength as interpreted from sonograph (16/10/03).*

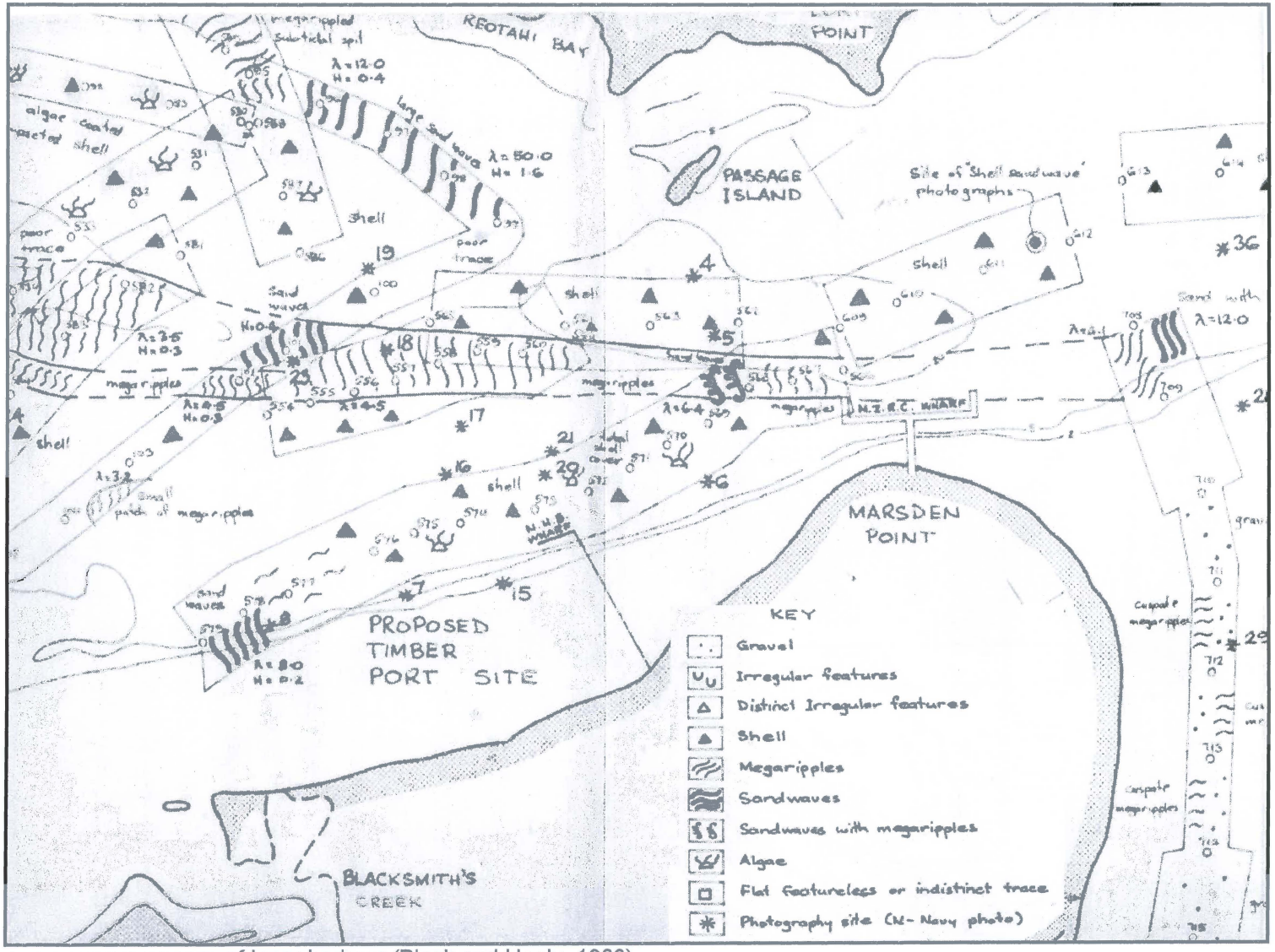


Figure 7.10 - Side-scan sonar summary of inner harbour (Black and Healy, 1983).

7.5 Discussion

The bottom sediment facies map (Figure 7.6) shows the abundance of fine sands across the region. The dredge basin comprises a mixture of coarse and fine sands with some shell content. Shelly lag sediments exist across the northern parts of the dredge basin and extend toward the NZRC jetties. There is also evidence of shelly lag sediments in the middle of the channel to the northeast of the NZRC jetties (Figure 7.6). Comparison with SSS records from 1983 (Figure 7.10, Black and Healy, 1983) indicates that these shelly lag sediments occurred in identical locations in 2003 to those in 1983.

Shelly lag sediments, observed immediately adjacent to the *'proposed timber port site'* in 1983 (Figure 7.10) have not been observed in more recent data (Figure 7.6). It is concluded that the dredging of the Northport turning basin has removed this shell lag cover.

Black and Healy (1983) noted an absence of the shell lag cover over the sub-tidal extension of the flood tide delta (Snake Bank), immediately northwest of the *'proposed'* dredge basin location (Figure 7.10), identified by a *'slither'* of bedforms separating areas of shell lag. A similar region of *'non-lag sediments'* was found in 2003 (Figure 7.6). The occurrence of dune/*'megaripple'* bedforms (λ=3.5 m and 4.0 m in 1983 and λ=5.5 m, 5.9 and 11.25 m in 2003, Figures 7.9 and 7.10) over this sub-tidal extension is also very similar in both 1983 (Figure 7.10) and 2003 (Figure 7.9).

The presence of bedforms over the sub-tidal extension led Black and Healy (1982) and Black (1983) to the conclusion that the region is an active sediment pathway. Tidal cycle residual distances calculated from model output however revealed that the sediment ridge is in fact dominated by neutral net flows (Black et al., 1989). The sub-tidal extension of Snake Bank separates zones of flood-dominated currents (to the north of the extension) and ebb-dominated currents (to the south of the extension) (Black et al., 1989). Opposing net sediment transport potentials on either side of the extension are the likely cause of periodic sediment movement, bedforms and the absence of shelly lag sediments (Black et al., 1989).

The northwesterly-directed asymmetric bedforms immediately east of the Northport quay (Figure 7.9) have not been identified previously (Figure 7.10). This provides more evidence supporting the conclusion that these features are due to down slope movement on the dredge basin batter slope, which did not exist during the 1983 survey.

A zone of "*megaripples*" (λ = 0.6 – 6.0 m), analogous with small-medium dunes, was identified extending in an east-west direction from the proposed dredge basin to in front of the NZRC jetties in 1983 (Figure 7.10). Comparison with the 2003 survey (Figure 7.9) reveals evidence of similar features, implying that the sediment transport in 2003 is in the same direction (west to east) as that observed in 1983.

Bedforms observed in 2003 adjacent to the eastern edge of the NZRC jetties and directed out of the harbour (Figure 7.9) were not present in 1983 (Figure 7.10). While a zone of "*megaripples*" (small-medium dunes), delineated by a dashed line (Figure 7.10), does extend past this region, the report of Black and Healy (1983) does not indicate any large-scale bedforms at this location similar to those observed in 2003 (Figure 7.9).

Bedforms (λ = 4.1 – 12.0 m) were observed immediately to the east of the NZRC jetties in 1983 (Figure 7.10). Similar features (λ = 6.0 – 10.0 m) were observed were in 2003. These bedforms indicate sediment movement that could explain changes in bathymetry observed both prior to and post port construction in this area (Chapter 6).

7.6 Conclusions

- The dredge basin, close to the reclamation, is made of a mixture of coarse and fine sediments.

- Dredging has removed shelly lag sediments from the areas immediately adjacent to the Northport quay wall.

- Sediment is moving down slope on the margins of the dredge basins southern extent, adjacent the old NHB wharf.

- Shelly lag deposits exist on the channel floor at the northern edge of the Northport turning basin and extend out toward the NZRC jetties. The same pattern was present in the early 1980's.

- A *'sediment ridge'* consisting of fine sands extends from the flood tidal delta (Snake Bank) towards the Northport dredge basin. This ridge separates areas of shelly lag deposits. The ridge (in 2003) is essentially identical to that observed in the early 1980's.

- The *'sediment ridge'* separates areas of opposing dominant flows, sand waves are often found on the ridge, indicative of active sediment transport.

- Between the old NHB wharf and the NZRC jetties the dominant transport direction is from west to east. Sand moves through this region in sand waves with wavelengths from 5 - 10 m. This is identical to patterns observed in 1983.

- Bedforms to the east of the NZRC jetties are of a similar scale, and cover a similar region as those observed in 1983. These bedforms provide a mechanism for the periodic transport of sand and changes in bathymetry.

- Bedforms indicate sediment transport out of the harbour in front of the easternmost NZRC jetty. Data from 1983 does not specifically identify such features there although the area is included in a *'zone of bedforms'*.

8 SEDIMENT TRANSPORT AT MARSDEN POINT

8.1 Introduction

The transport of mobile sediments plays a large role in coastal morphodynamic environments such as Marsden Point. Alterations to sediment transport patterns are likely to have morphologic implications and often result in either erosion or accretion, which can be both positive and negative.

With knowledge of sediment transport processes and patterns, coastal structures can be built and works undertaken which are less likely to have unforeseen impacts and more likely to have the desired effect on the natural environment.

In this chapter, sediment transport patterns are investigated using a variety of techniques, including residual velocities, residual distances, excess velocities, wave energy fluxes and combined wave-current transport formulations for the purposes of determining characteristic volumes and directions of sediment fluxes in the channels, channel margins and inter-tidal areas in the lower Whangarei Harbour surrounding Marsden Point and Northport.

8.2 Instrumentation

8.2.1 Autonomous ADP Surveys

Two Acoustic Doppler Current Profilers (ADCPs) were deployed in the lower Whangarei Harbour between October 21, 2002 and November 22, 2002. ADCP set-up details are summarised in Table 8.1. The instruments were deployed and retrieved by National Institute of Water and Atmospheric research (NIWA) technicians. Analyses of hydrodynamic data from Sites 1 and 2 (Table 8.1 and Figure 8.1) are reported in Longdill et al. (2003a,b,c), comparisons with previous measurements are summarised in Longdill et al. (2003d).

	Site 1	Site 2	1994 ADCPs
Location (Mt Eden 1949)	N815760, E275745	N815948, E275513	Same sites as 2002.
Location (UTMZone60S)	N6031499, E273832	N6031700, E273596	
Depth (Rel.CD)	-15.34m	-13.76m	-16.15m (Site 1) -12.95m (Site 2)
Instrument Type	Sontek (1500Hz) Serial No. 4028	RDI (1228.8Hz) Firmware Ver. 16.21	Not Available
Bin size	1.0 m	0.5 m	0.5 m
No. of Bins	18	30	44
Time between profiles	10 mins	5 mins	10 mins
Profile Averaging interval	60 seconds	60 seconds	Not Available
Velocity Uncertainty	$\pm 0.0026 ms^{-1}$	$\pm 0.002 ms^{-1}$	
Blanking Distance	0.4 m	0.44 m	Not Available
Number of Profiles (good)	4559	9178 (4589 used for analysis)	4465 (Site 1) and 4773 (Site 2)
Profiles Used for Analysis	1 - 4559	222 – 9400 (every 2nd profile used)	
Recording Duration (good data)	21/10/02 18:00:00 - 22/11/02 9:40:00	21/10/02 13:15:00 - 22/11/02 10:05:00	27/9/94 10:28:55 - 28/10/94 11:08:56 (site1) 27/9/94 10:19:20 - 30/10/94 14:59:25 (Site2)

Table 8.1 – *ADCP set-up information. 1994 data from Barnett (1995a). Error Values calculated from Sontek (1997a) and RDI (2001).*

Figure 8.1 displays the locations of the ADCPs in relation to Northport and Marsden Point.

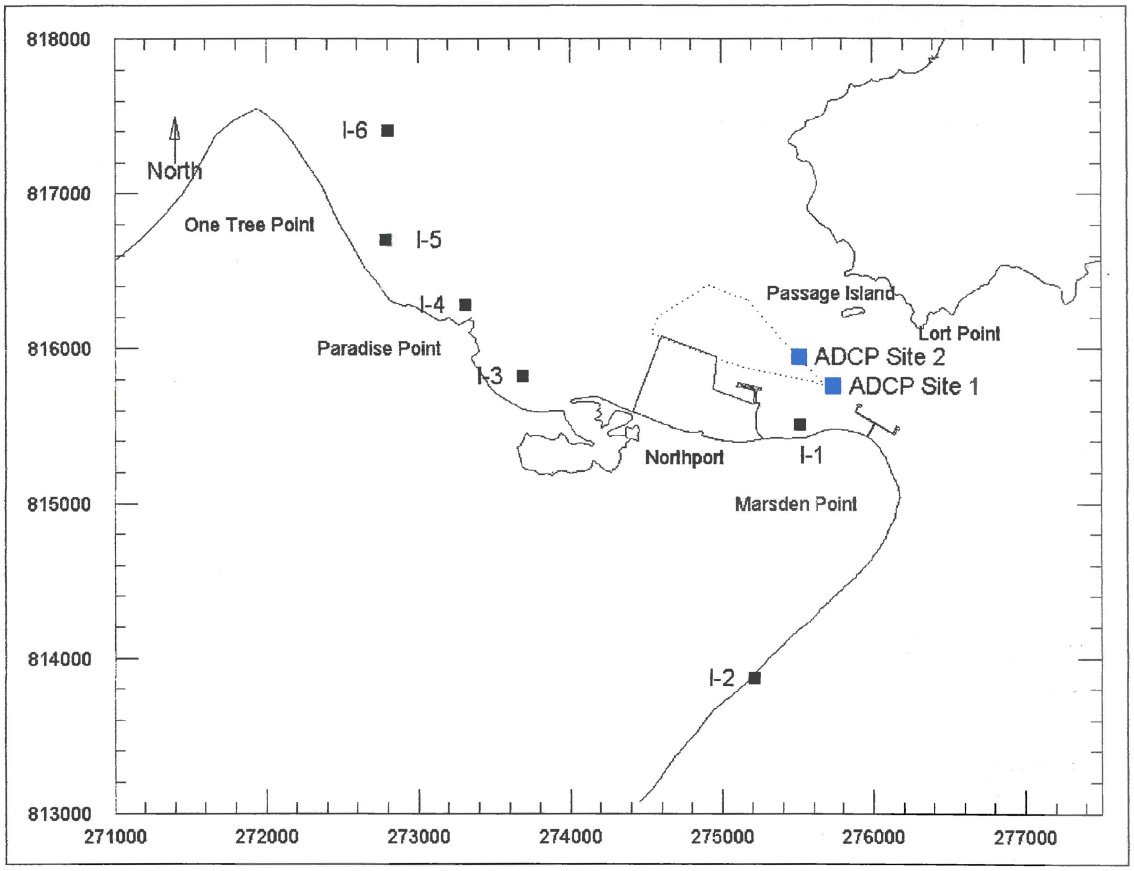


Figure 8.1 - *Location of instruments deployed at Marsden Point for the study of hydrodynamics and sediment movement. ADCP sites (Blue Squares) measured autonomous deployment of October and November 2002. Intertidal sites I-1 to I-4 (Black squares) sampled with a FSI current meter, Dobie Wave gauge and an OBS sensor from 5-8 July 2003. Intertidal sites I-5 and I-6 (Black squares) monitored from 10-13 November 2003 with a FSI current meter. Dotted line represent Northport Dredge basin. Grid references in Mt Eden Grid Circuit 1949.*

The ADCP instruments had three (Site 1, SONTEK ADCP) and four (Site 2, RDI ADCP) acoustic transducers oriented at 25° (Site 1) and 20° (Site 2) from the vertical, each emitting and receiving an acoustic pulse. These transducers obtained estimates of the water velocity profile, signal to noise ratio and standard deviation over the water column for each averaging interval. Internal sensors obtained information on the instrument tilt and orientation on the frame.

Data was collected and stored internally relative to magnetic north and in binary format by both SONTEK and RDI ADCPs.

Other data obtained for the duration of the deployment included:

i. tide gauge data from the Marsden Point Wharf (digitised at 15 minute intervals, from a hard copy pen on paper trace);
ii. ship berthing information for the NZRC jetties (times tied up);
iii. passing ship information (draughts and times passing ADCPs); and
iv. weather records from Whangarei Airport.

The uncertainty in the velocity measurements is a function of the acoustic frequency, depth cell size and number of samples averaged to calculate the mean velocity profile (Sontek, 1997a), specific estimates are provided in Table 8.1.

Water level elevations (tide height) at Marsden Point were digitised (15 min resolution) for the duration of the survey (Figure 8.2).

Only every second profile was extracted at Site 2, due to the 5 min gap between profiles recorded by this instrument and the desire to maintain consistency with the Site 1 instrument and the 1994 data (Table 8.1).

Further details regarding the two deployments can be found in Barnett (1995a) and Longdill et al. (2003a).

8.2.2 Shipboard, Downward-Looking ADP Survey

A 1500 kHz ADP manufactured by Sontek, mounted on the University of Waikato research vessel *Taitimu* (MSA12878) measured water velocity data in the Lower Whangarei Harbour during two full tidal cycles on December 4th, 2002 and December 5th, 2002. A field program was established to obtain water velocity profiles over two transect lines and three fixed sites (Table 8.2). Sites were chosen in order to compare water velocities with hydrodynamic model output (DHI, 1982a; Barnett et al., 1993) and with previous current measurements (DHI, 1982a; Black, 1983). Details of the ADP set-up and field program are provided in Table 8.2.

The sampling program was designed such that each location was sampled approximately hourly. Each survey began an hour after high tide and finished an hour before the next high tide. A break of two hours was taken during the time of slack water at low tide. The pattern used was as follows: Transect J=81 (South to North)→ Site 1→ Site 2→ Transect J=63 (South to North) then finally the Blind Channel measurement (Table 8.2). *Taitimu* then motored slowly back to the start for the next hours measurements. The vessel was restricted in its ability to motor at any speed between the sites as the ADP was mounted below the surface of the water.

ADP data collection details and initial data processing techniques are described in Appendix F. Water level elevations recorded by the Marsden Point tide gauge for the duration of the two boat-mounted surveys are contained in Figure 8.3.

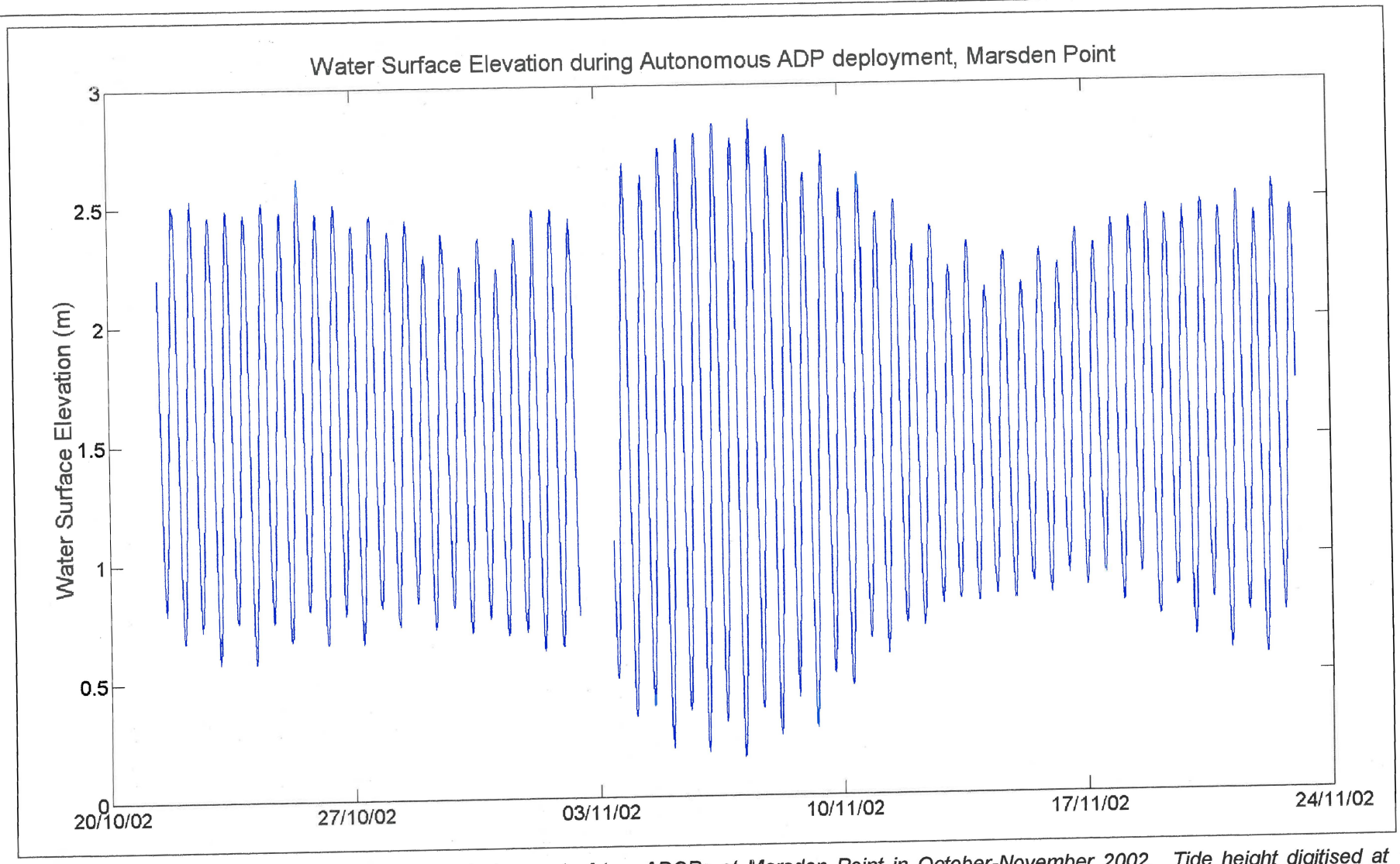


Figure 8.2 – *Tidal elevation during the autonomous deployment of two ADCPs at Marsden Point in October-November 2002. Tide height digitised at 15 min intervals from pen on paper trace of Marsden Point tide gauge. Data not recorded by tide gauge over 2/11/02-4/11/02.*

	Variable	Setting
Sontek 1500khz ADP Serial No. 4028	Sensor Orientation	DOWN
	Number of Bins	20
	Bin Size	1.0 m
	Averaging Interval	30s
	Ping Interval[1]	0.0s
	Blanking Distance	0.4 m
	Bottom Track	ON
	GPS Logging	ON
	Temperature Mode	Measured
	Velocity Precision[2]	± 0.085 ms^{-1}

		Mt Eden 1949	UTM Zone 60S
Survey Circuit	Waypoint 1 (J=81 start)	275589.60 mE 815595.24 mN	273680.59 mE 6031348.77 mN
	Waypoint 2 (J=81 finish)	275736.12 mE 816020.76 mN	273816.88 mE 6031777.13 mN
	Waypoint 3 (Site 1)	275745.00 mE 815760.00 mN	273832.3 mE 6031498.9 mN
	Waypoint 4 (Site 2)	275513.00 mE 815948.00 mN	273595.6 mE 6031699.6 mN
	Waypoint 5 (J=63 start)	274803.68 mE 816077.40 mN	272883.52 mE 6031812.83 mN
	Waypoint 6 (J=63 finish)	274901.36 mE 816361.08 mN	272974.03 mE 6032099.07 mN
	Waypoint 7 (Blind Channel)	273887.52 mE 816181.32 mN	271965.08 mE 6031895.90 mN

4/12/2002	First Profile	08:41:49 4/12/2002
4/12/2002	Last Profile	18:43:20 4/12/2002
5/12/2002	First Profile	09:31:16 5/12/2002
5/12/2002	Last Profile	19:47:39 5/12/2002

Table 8.2 - *Set-up parameters for Boat-mounted ADP survey. [1]A ping-interval of 0.0s causes the ADP to ping as rapidly as possible, about 9Hz in this case (Sontek, 1997a). [2]Calculated from formulae provided in Sontek (1997a).*

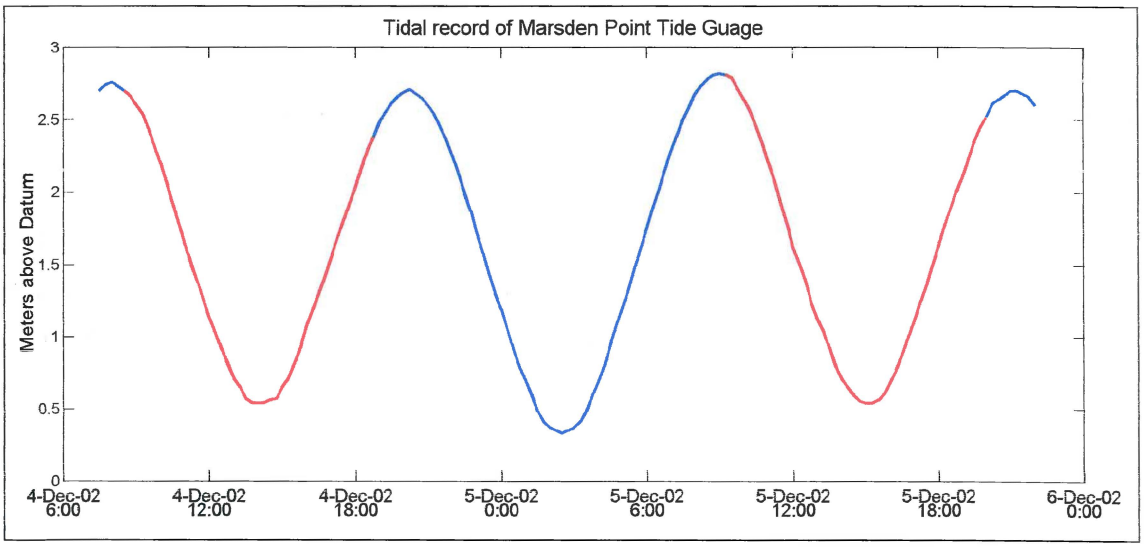


Figure 8.3 - *Tide height during boat mounted ADCP surveys. Red line indicates time over which measurements were actually taken on the two days.*

8.2.3 Current Velocity Measurements Over the Inter-tidal Zone

Measurements of water velocities were conducted on July 5th, 6th and 7th 2003 and November 10th, 11th and 12th 2003 at sites I-1, I-2, I-3, I-4 (July) and sites I-5 and I-6 (November). Site locations are shown in Figure 8.1. A mobile frame (Figure 8.4) used for the July measurements was equipped with:

i. Falmouth Scientific Incorporated (FSI) 3DACM97 (Wave);
ii. Dobie Wave Gauge manufactured by NIWA (NZ); and
iii. optical Backscatter Sensor (OBS) manufactured by D & A Instruments and connected to the Dobie.

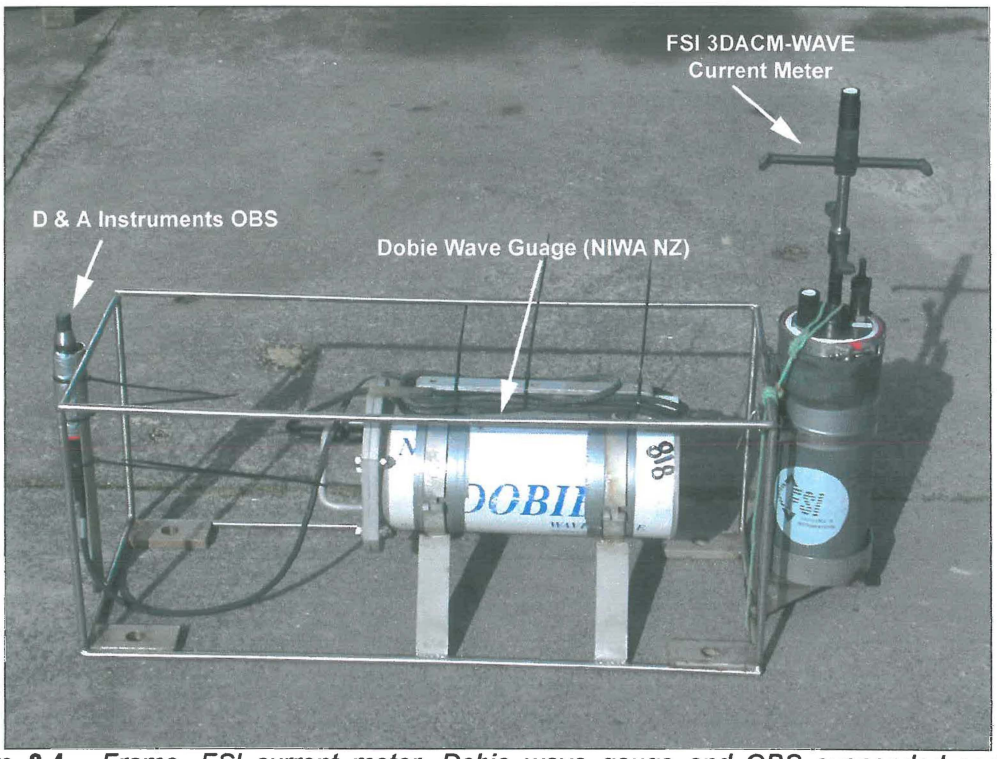


Figure 8.4 - *Frame, FSI current meter, Dobie wave gauge and OBS suspended sediment sensor used at intertidal locations on July 5th, 6th and 7th, 2003 at Marsden Point, Northland.*

The same frame (Figure 8.4) was used at Sites I-5 and I-6 in November 2003, without the Dobie and OBS. The same FSI current meter was used at all sites, with an identical sampling strategy and set-up (Table 8.3). Table 8.4 details the location and deployment times of the instruments.

FSI	Model	3DWAVE
	Serial No.	1589AW
	Firmware Ver	4.7
	Calibration Date	16/04/02
	Sampling Frequency	5Hz
	Interval Time	5 mins
	Average On Time	4 mins
	Burst On Time	3 min 25 secs
	Averaging Interval	1 min
	No. of averages before burst	5
	Start time	05:35:00 5/7/2003 (13:00:00 8/11/03)
	Mode	Average + Burst
	Speed Precision	± 2% of reading (max value ± 1cms^{-1})
	Direction Precision	± 2.5°
	Temperature Precision	± 0.5°C
	Pressure Precision	± 0.01% full scale
Dobie (incl OBS)	Dobie SerialNo.	818
	OBS serial No.	
	Sampling Frequency	5Hz
	Points per Burst	1024
	Burst Length	3 mins 24.8 secs
	Burst Interval	30 mins
	Total Bursts	1000
	Sensor Elevation	0.15m
	Spectral Estimates to Merge	16
	Max Period	30 secs
	Min Period	0.8 secs
	Start Time	05:30:00 5/7/03

Table 8.3 - *Set-up information for FSI current/wave meter for sites I-1 to I-6, Dobie wave gauge and OBS suspended sediment meter for sites I-1 to I-4.*

Site	Location Mt Eden 1949	Start time	Stop time	Tidal Range (m)
I-1	275514mE, 815510mN	05:07 5/7/03	17:10 5/7/03	1.60
I-2	275208mE, 813875mN	17:15 5/7/03	05:51 6/7/03	1.81
I-3	273686mE, 815821mN	05:59 6/7/03	18:02 6/7/03	1.59
I-4	273310mE, 816281mN	18:08 6/7/03	06:45 7/7/03	1.79
I-5	272785mE, 816701mN	13:45 8/11/03	02:07 9/11/03	1.6
I-6	272796mE, 817411mN	15:06 10/11/03	03:21 11/11/03	1.65

Table 8.4 - *Deployment locations, times and tidal ranges for inter-tidal series of current, wave and suspended sediment measurements.*

The FSI current/wave meter measures water velocity (in 3-dimensions), temperature and pressure. The Dobie also samples the water pressure, outputting these data in a more useful format. The OBS records an analogue voltage, related to the scattering of infrared (IR) light by suspended matter. Later, the output voltage is calibrated to provide an estimate of the suspended sediment concentration.

The FSI current / wave meter was set up to provide two types of data, averaged and burst. The instrument sampled currents (and pressure) in three dimensions, relative to magnetic north, at a frequency of 5 Hz. During the 5 min interval time (Table 5.3), the instrument provided vector averages of the currents over one-minute periods (Table 5.3). The instrument ran in average mode for 5 consecutive intervals (25 minutes) before switching to burst mode for a single interval. The timing of this burst was specified to begin on every half hour in order to coincide with the Dobie bursting time. The bursting FSI collected data at 5 Hz for a period of 3 minutes 25 seconds, sat idle for the remainder of the 5 minute interval time before beginning the cycle again by running in average mode for 5 intervals.

The timing of the Dobie (and OBS) bursts was designed to be identical to the burst time of the FSI. This not provides a back up record of the pressure data (in the FSI).

The frame (and instruments) was manually deployed at each site near the time of low tide, where it remained collecting data throughout the tidal cycle, to be retrieved and placed at a new location for the next tidal cycle. The frame was weighted to the bottom with a 20 kg chain placed around the base supports. A rope tied to the frame was run to diving belt weight, a buoy indicating the position of the frame was connected to this weight.

Sediment samples were obtained from each site (with the exception of Site I-6) and analysed in the RSA. Where present, rippled bedforms were measured for both height and wavelength.

8.3 Sediment Transport Over the Channels and Channel Margins

8.3.1 Introduction

The strength and duration of velocities exceeding a critical threshold are of prime importance when considering sediment transport potentials in the channels and margins of Whangarei Harbour (Black et al., 1989). Sediment transport is considered in terms of the strengths and durations of both flood and ebb velocities exceeding a critical threshold. Previous studies (DHI, 1982a; Black, 1983; Poynter, 1993) have confirmed that suspended sediment transport in the lower harbour is low. Potential sediment transport can be measured in terms of a residual distance (Black et al., 1989). Residual distances are calculated at various sites surrounding Northport and compared with values obtained in 1981. Comparisons of these vectors provide evidence for only minor changes in the sediment transport potentials in these areas between 1981 and 2002.

8.3.2 Sediment Thresholds

The determination of sediment threshold values under steady, unidirectional flows over non-cohesive, bedformed sediments has been greatly enhanced by investigations undertaken at Whangarei Harbour (Black and Healy, 1982, 1986; Black et al., 1989). While thresholds had historically been determined from laboratory data (e.g. Miller et al., 1977), Black's series of papers provided a method for the determination of threshold values over bedforms and shelly lag layers. The reader is referred to these for a detailed derivation of sediment thresholds in Whangarei Harbour. Data relating to sediment thresholds from these extensive peer reviewed papers is put to use here.

Characteristic values of the sediment threshold (velocities measured at 1 m above the bed) for the lower Whangarei harbour are (Black and Healy, 1982, 1986; Black, 1983; Black et al., 1989):

i. plane bed $U_{1cr} = 0.39$ ms^{-1};
ii. bedform $U_{1cr} = 0.33$ ms^{-1}; and
iii. shell armoured $U_{1cr} = 0.92 - 1.18$ ms^{-1}.

Mehta et al. (1980) measured the fall velocity of some disarticulated common bivalve shells. *Chione cancellata* (*Chione stuchburyi* is found in the Whangarei Harbour [WHS, 1984]) was found to have a mean fall velocity of 0.24 ms^{-1}. This compares with 0.032 ms^{-1} for sand with diameter D = 0.0003 m (Raudkivi, 1976). The shell's stability is ensured by its larger fall velocity.

As the velocity measurements under consideration (ADP surveys) relate only to the channels and channel margins of the lower harbour (> 10 m C.D) sediment entrainment by waves is considered negligible.

Black (1983) and Black and Healy (1989), based on detailed field observations and flume measurements with natural Whangarei Harbour sediments, found a general harbour threshold of U_{1cr} = 0.33 ms^{-1}. Following this work and the realisation that many of the bedforms in this region are similar in morphology to those observed in 1981 (Chapter 7), this threshold value is once again used in the calculation of excess velocities.

8.3.3 Residual Velocity Definition

Under the action of reversing tidal currents, sediment transport rates are constantly adjusting to the governing water speeds. Thus, the residual velocity integrated over the complete tidal cycle which accumulates these velocity variations, may reflect the net movement of sediment (Black, 1983).

Residual velocities ascertain degrees of ebb and flood dominance, which can be examined with respect to regional sediment transport vectors.

Definition:

The residual is the area under the velocity-time curve and is defined as

$$\overline{V}_r = \frac{1}{t_2 - t_1} \int_{t_1}^{t_2} \overline{V}\, dt \qquad \textbf{(8.1)}$$

Where the velocities (V) are treated as vectors. This definition can only be considered a residual when the integration is undertaken over an entire tidal cycle i.e. t_2-t_1=T.

In discrete form, taking the orthogonal components separately and considering the excess velocity (velocity exceeding a critical threshold) the equations (from Black, 1983) are:

- x-velocity: $$u_r = \frac{1}{N}\sum_{i=i}^{N}(v_i - v_{cr})^q \cos\theta_i \quad \text{for } v_i > v_{cr} \qquad \textbf{(8.2)}$$
- y-velocity: $$v_r = \frac{1}{N}\sum_{i=i}^{N}(v_i - v_{cr})^q \sin\theta_i \quad \text{for } v_i > v_{cr} \qquad \textbf{(8.3)}$$
- Magnitude: $$V_r = \left(\sqrt{u_r^2 + v_r^2}\right)^q \qquad \textbf{(8.4)}$$
- Direction: $$\vartheta_r = \tan^{-1}\left(\frac{v_r}{u_r}\right) \qquad \textbf{(8.5)}$$

Where v_i is the i^{th} speed and θ_i is its direction in a right handed, horizontal orthogonal axis system. v_{cr} is the critical water speed which can be equal to zero and q is a chosen power (v_i - v_{cr} is the excess velocity). If q=1 and v_{cr} =0, the equations define the average velocity over the period. $T=N\Delta t$, where Δt is the time increment between N discrete velocities. Values of q greater than 1 are introduced to recognise the fact that sediment transport potentials are a non-linear function of the water speed. Various investigators (e.g. Gadd et al., 1978, Black and Healy, 1982, and van Rijn, 1993) have shown that the sediment transport rate is proportional to the excess velocity cubed. Calculating the residual with $q=3$ and v_{cr} equal to the threshold velocity allows the reflection of this. Black (1983) found a statistically significant correlation between the excess velocity cubed ($q=3$) and the sediment transport rate at Whangarei Harbour. Therefore for the determination of residual distances (proportional to potential sediment transport rates) the excess velocity cubed will be used i.e. q=3.

When summed over the tidal cycle, the residual velocity represents the Eulerian resultant flux of velocity past the measurement point.

Velocities taken into consideration are located 1 m above the bed, characteristic depths of the lower harbour are 16-30 m below CD, hence the effects of any wind or gravity wave generated currents will be small in comparison to the tidal currents under question.

8.3.4 Residual Distance Definition and Calculation

The **residual distance** (proportional to the sediment transport potential) is defined as the residual velocity multiplied by the time for which the current velocity exceeded the threshold (ms^{-1} *x* s = m) (Black et al., 1989). The residual distance is an indicator of potential sediment transport rates. It should be noted that the residuals indicate transport potentials and do not take into account sediment availability. With a zero threshold speed, the time multiplier is constant (12 hrs 25 m in semi diurnal tides) and the residual distance and residual velocity are equivalent (Black et al., 1989).

Residual distances are calculated at sites in the lower harbour, following the work of Black (1983) and Black et al. (1989). The residual distance provides a better indication of net bed-load sediment movement than the residual velocity (Black, 1983; Black et al., 1989). The residual distance is a more accurate measure, as it reflects not only the velocities above the threshold but also the time that the velocities exceeded the threshold.

Residual distances were calculated using MATLAB® programs contained in "*find_residual_distance.m*" written specifically for this purpose by this author (Appendix F). The program finds the excess velocity to the power 3 at each time step in the tidal cycle (Equations 8.2 – 8.5), determines the residual velocity (Equation 8.1) and then multiplies this by the time over which the velocities were above the selected threshold to calculate the residual distance.

8.3.5 Morphologic and Erosional / Depositional Implications

For simplicity we can assume that the residual distance is linearly proportional to the bed load sediment transport potential (Black et al., 1989). Sediment transport rates have been shown to be proportional to the cube of the excess velocity (Gadd et al., 1978; Black and Healy, 1982; van Rijn, 1993). The residual distance, defined using the cube of the velocity excess, has also given results that are very similar to the linear situation (Black, 1983). As the linearity between residual distance and sediment transport potential has been identified at Marsden Point (Black, 1983) and used in the scientific literature (Black et al., 1989) it will again be assumed here.

Application of the conservation of mass argument to a *'box'* with vectors (residual distances) representing sediment inputs and outputs allows the realisation of the implications of variations in magnitude of the residual distances. Scour / erosion will occur at a location if residuals are greater than those *'upstream'* (with respect to sediment transport). Deposition will result if the residuals are of lesser magnitude than those *'upstream'*.

Black et al. (1989) note that the presence of shell lags is likely to reflect erosive conditions; sand cannot settle because the potential for output from the region, as indicated by the residual distances, is greater than the input potential. Sandy beds are to be expected where residual distances are neutral or decreasing in the down-transport direction.

It is emphasised that the residual distances do not necessarily reflect actual sediment transport, but rather sediment transport potentials or capacity. The calculation of the residuals does not take into consideration the availability of sediments for transport. It is possible that pre-existing shell lags will reduce the availability of sediments for transport. Hence, it should be restated that residual distances (and in fact any transport evaluated from flow conditions) represent sediment transport potentials rather than actual sediment transport volumes.

8.3.6 Spring-Neap tide differences

Using data from Sites 1 and 2 obtained during the autonomous ADP deployment of October / November 2002, both spring and neap tides were examined for their differences in sediment transport potential.

Figure 8.2 shows the tidal heights for the entire ADP deployment. The maximum and minimum tidal ranges experienced were chosen to represent spring and neap tides respectively. The tides occurred on:

- spring tide - November 7th, 2002, tidal range 2.69 m and
- neap tide - November 14th, 2002, tidal range 1.32 m.

Tidal cycle residual distances were calculated for each tide using velocities from 1 m above the bed (u_1) and a sediment entrainment threshold of u_{1cr} = 0.33 ms^{-1} (Figure 8.5).

It is clear there is a much greater potential for sediment transport during spring tides than neap tides (Figure 8.5). Black (1983) found the spring tide's potential for transport to be between 8 and 300 times the neap tide's. Data from 2002 (Figure 8.5) indicates potentials at Site 1 to be ~1,000 times larger and those at Site 2 to be 7.5 times larger during spring tides than those during neap tides. The magnitudes of residual distances during spring and neap tides at Site 2 are within a range (although at the lower end) calculated by Black (1983). The difference in residual distances of spring and neap tides at Site 1 is larger than any found by Black (1983).

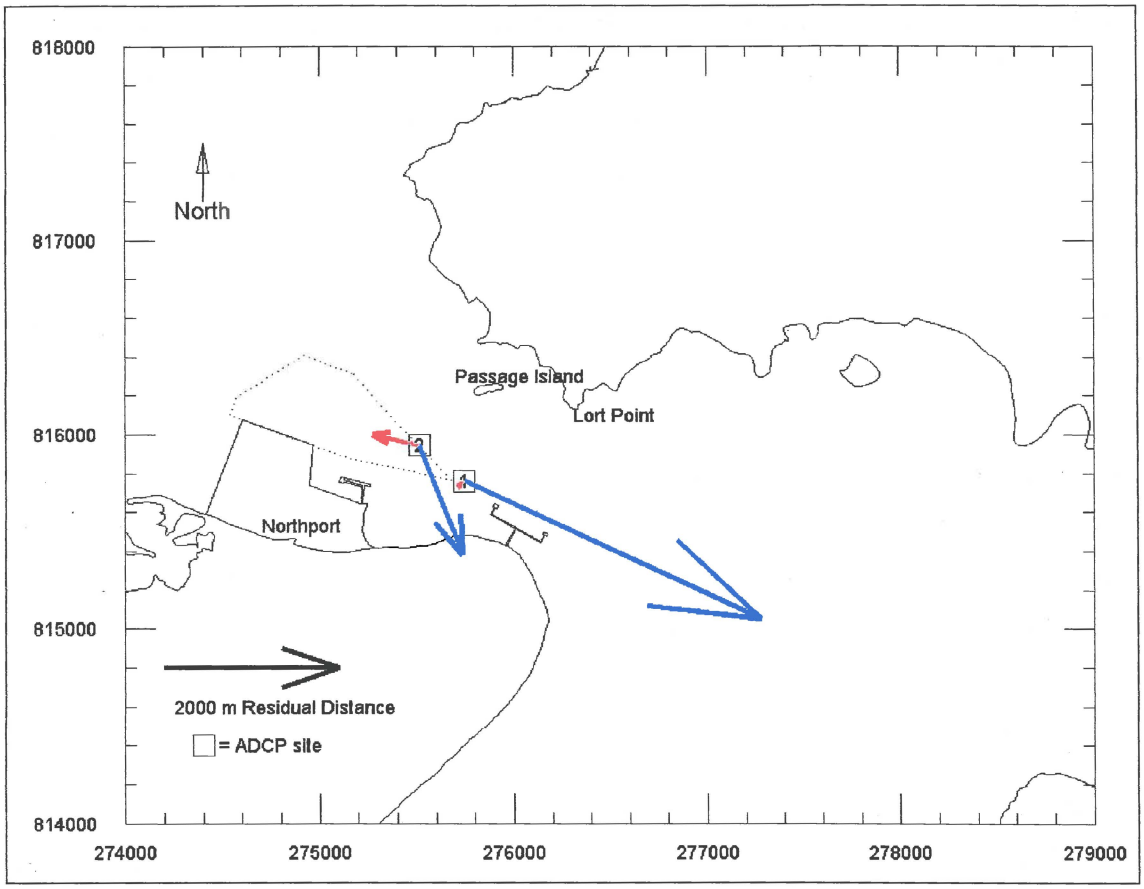


Figure 8.5 - *Spring (blue) and neap (red) tidal cycle residual distances at 1 m above the bed for periods when the speed exceeded 0.33 ms^{-1}. Data obtained from ADP deployment of October / November 2002. The Northport dredge basin is shown as the dotted line.*

Tidal current velocities at Site 1 increased by 3% between 1994 and 2002 during ebb flows and 1% during flood flows, those at Site 2 were unchanged (Longdill et al., 2003a; Longdill et al., 2003d).

While the increase in velocities at Site 1, especially during ebb flows could be expected to lead to an increase in transport potentials (in the ebb direction), the current velocity data do not cover a long enough period to determine velocity changes specific to spring or neap tides. Without these data it cannot be reliably concluded that the observed increase in velocities at Site 1 have lead to a change in the transport potentials of spring and neap tides.

It should be noted that Black's (1983) values (8-300 times) were based on tidal ranges of 2.2 m (spring) and 1.6 m (neap), compared with the 2002 data of 2.69 m (spring) and 1.32 m (neap). The variation in tidal ranges reduces slightly the strength of any comparisons between the values. A following section (8.3.7.2) addresses this by normalising the residuals to a constant tidal range.

Black (1983) found generally small differences in the directions of the residual distances between spring and neap tides. Differences in direction of the residuals at Site 1 are relatively unimportant, due the almost negligible magnitude of the neap tide residual (Figure 8.5). At Site 2, the neap tide residual is directed westerly whilst the spring tide residual is directed southeasterly (Figure 8.5). No explanation is offered for the difference in directions of residual distances at Site 2 between spring and neap tides. Velocity data from 1994 and 2002 do not cover long enough periods to determine any differences specific to spring or neap tides over these times. Tidal current velocities (monthly averages) at two the sites have not changed significantly in velocity or direction between 1994 and 2002 (Longdill et al., 2003a; Longdill et al., 2003d).

8.3.7 Tidal Cycle Residual Distances

8.3.7.1 Un-scaled Residuals

Tidal cycle residual distances at Sites 1 and 2 were determined from these velocity data (1 m above bed bin) using a sediment threshold of $u_{1cr} = 0.33$ ms^{-1}.

Residuals were initially calculated without any corrections for variations in tidal range (Figures 8.6 and 8.7).

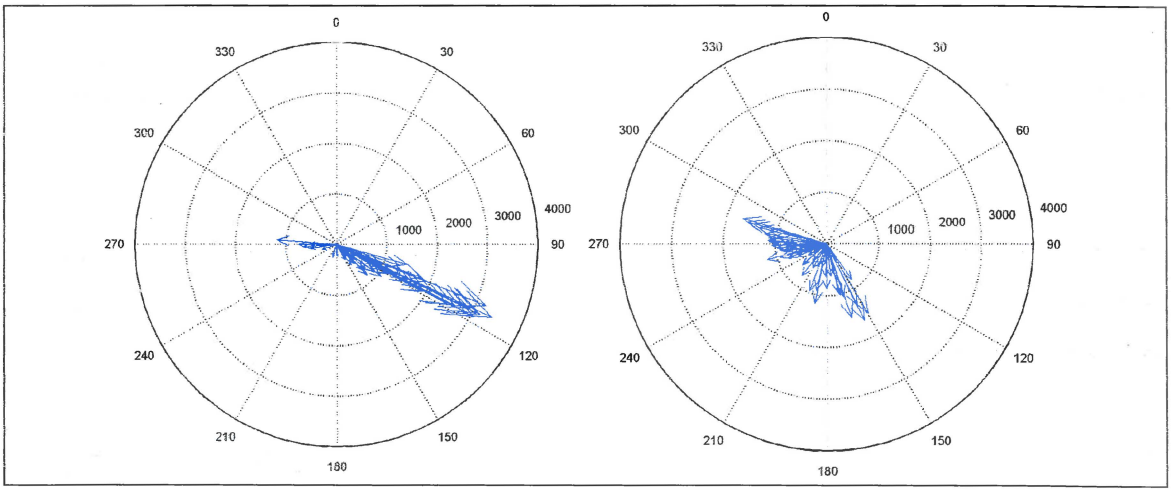


Figure 8.6 – *Tidal cycle residual distances (m) at 1 m above the bed for periods when the speed exceeded 0.33 ms^{-1} at Site 1 (left) and Site 2 (right) October – November 2002. No tidal range correction.*

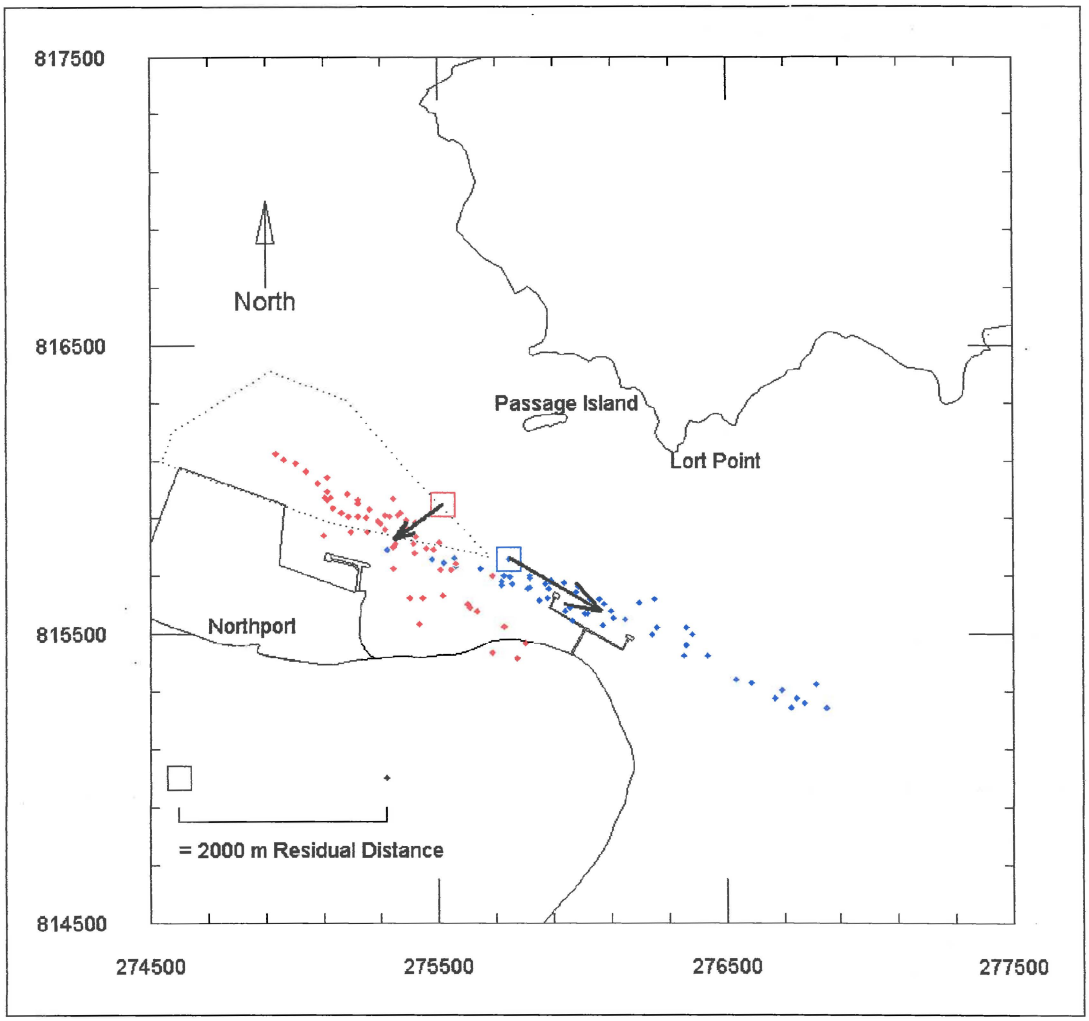


Figure 8.7 – *Tidal cycle residual distances at 1 m above the bed for periods when speed exceeded 0.33 ms^{-1} at Site 1 (blue) and Site 2 (red). Monthly average residual distances marked as black arrows. No tidal range corrections. Northport dredge basin is shown as the dotted line.*

Residual distances, indicative of sediment transport potentials, show considerable differences between the two sites examined. Site 1 residual distances display a strong concentration of residuals oriented at ~110° (Figure 8.6), roughly along the direction of ebb flows at this point (Longdill et al., 2003a; Longdill et al., 2003d).

Site 2 residual distances show much more variation in their direction (Figure 8.6). The magnitudes are less than at Site 1 and the dominant direction of the residual is in neither the general flood or ebb flow current direction. The mean residual distance direction at Site 2 is directed toward the southern shoreline and Northport. Further details are investigated after scaling the velocities to a constant tidal range.

8.3.7.2 Residual Distances Scaled to a Constant Tidal Range

In order to remove the effects of variations in tidal range and to enable more accurate comparisons with previous work (e.g. Black et al., 1989), tidal current velocities are required to be scaled to a constant tidal range.

Using methods described in Black (1983) and also used in Black et al. (1989) tidal current velocities were scaled to a constant tidal range of 2.2 m. Black (1983) found that tidal velocities at Whangarei Harbour could be related to the tidal range by both:

i. a Linear relationship (through the origin) $V_{\max} = b.\Delta H$ and **(8.6)**

ii. a Power relationship $V_{\max} = a(\Delta H)^b$ **(8.7)**

Where *a* and *b* are unknown constants and ΔH is the tidal range. Both curves have significant, similar correlation coefficients.

Black (1983) remarks that the linear equation (Equation 8.6) can be used to scale velocities according to tidal range without regard to site location. If $u=b.\Delta H$, where *b* is an unknown constant, then

$$u_2 = u_1 . \frac{\Delta H_2}{\Delta H_1} \quad \textbf{(8.8)}$$

Where u_2 is the velocity scaled to the range ΔH_2 and u_1 was measured at the same site when the tidal range was ΔH_1. As *b* is not included, the relationship is not site specific.

Every current velocity measurement during each tidal cycle at each site (~10,000 velocities) was scaled to a constant tidal range of 2.2 m, as used by both Black (1983) and Black et al. (1989), using the MATLAB® program "*scale_to_constant_tr.m*" written by this author (Appendix F). Scaled velocities were then subjected to the same program used to calculate residual distances previously "*find_residual_distance.m*" (Appendix F). This allows a direct comparison in terms of residual distance magnitude and direction with residual distances calculated and described in Black et al. (1989). Residual distances after this scaling are shown in Figures 8.8 and 8.9.

Mean residual distances are 1600 m at Site 1 and 750 m at Site 2 (Figure 8.9). Directions of the individual tidal cycle are more concentrated at Site 1 (generally 110°-125°) than at Site 2 (generally 150°-270°). The direction of the monthly mean residual is along the axis of flow (ebb tide) and out of the harbour at Site 1 and toward Northport's dredge basin at Site 2.

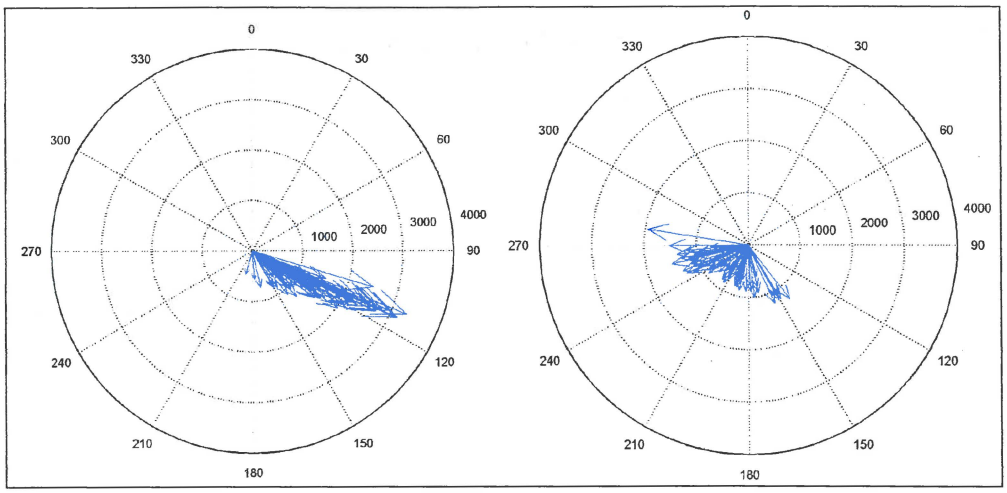


Figure 8.8 - *Tidal cycle residual distances (m) at 1 m above the bed for periods when the speed exceeded 0.33 ms^{-1} at Site 1 (left) and Site 2 (right) October – November 2002. Individual velocities scaled to 2.2 m tidal range prior to calculating excess velocities.*

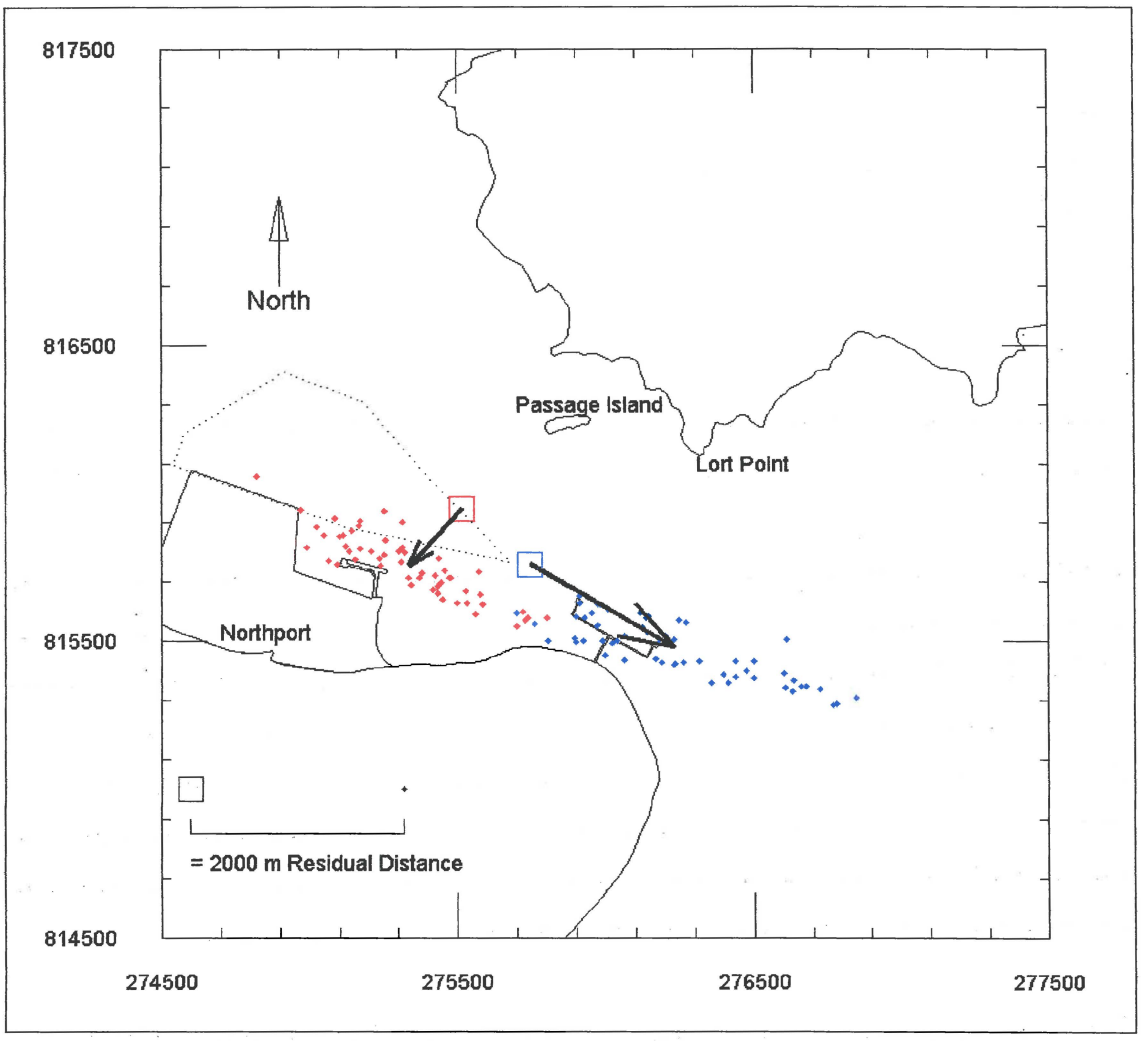


Figure 8.9 -*Tidal cycle residual distances at 1 m above the bed for periods when speed exceeded 0.33 ms^{-1} at Site 1 (blue) and Site 2 (red). Monthly average residual distances marked as black arrows. Individual velocities scaled to 2.2m tidal range prior to calculating excess velocities. Northport dredge basin is shown as the dotted line.*

8.3.7.3 Residuals From Boat Mounted Survey

Tidal current velocity data, obtained from the boat mounted ADP surveys of December 4th and 5th, 2002 were analysed and residual distances calculated after scaling the velocities to a constant tidal range (2.2 m). Water level elevations during the surveys are shown in Figure 8.3. Locations were selected along the path of the boat-mounted surveys, velocity profiles centred within 25 m of these locations selected to represent velocities at the selected sites.

Residual velocities were calculated by interpolation of measured velocities (~8 per tidal cycle), along with an assumption of zero excess velocity at the time of high and low tides, at 10 min intervals over the entire tidal cycle. This was conducted within the MATLAB® program "*bm_residuals.m*" written specifically for the purpose by this author (Appendix F). The program also uses "*find_residual_distance.m*" to determine the residual distances in the same manner as those at sites 1 and 2 previously.

As the boat mounted residuals are based on a single tidal cycle (the same as those detailed in Black (1983) and Black et al. (1989)), and the monthly average residuals from Site 1 and 2 being based on 60 tidal cycles, the residuals of sites 1 and 2 should be considered *'more representative'* of mean conditions than the residuals obtained from the boat mounted ADP surveys. That is not to say the boat-mounted residuals do not reflect the general conditions, but rather that there is greater potential for them to differ from the mean pattern as they are based on single tidal cycles rather the average of many such cycles.

Tidal cycle residual distances for both the boat mounted survey and the mean residual distances from the autonomous deployments at sites 1 and 2 are shown in Figures 8.10 and 8.11, the Figures show the residuals from December 4th, 2002 and December 5th, 2002 respectively.

The two surveys, undertaken on consecutive days, show strong replication of tidal cycle residual distances. In general, directions and magnitudes of residual distance vectors are consistent between the two independent surveys. One location not exhibiting this consistency is that nearest Passage Island. On December 4th, 2002 the residual was directed toward the dredge basin and into the harbour (Figure 8.10), however on December 5th, 2002 the residual was directed out of the harbour (Figure 8.11).

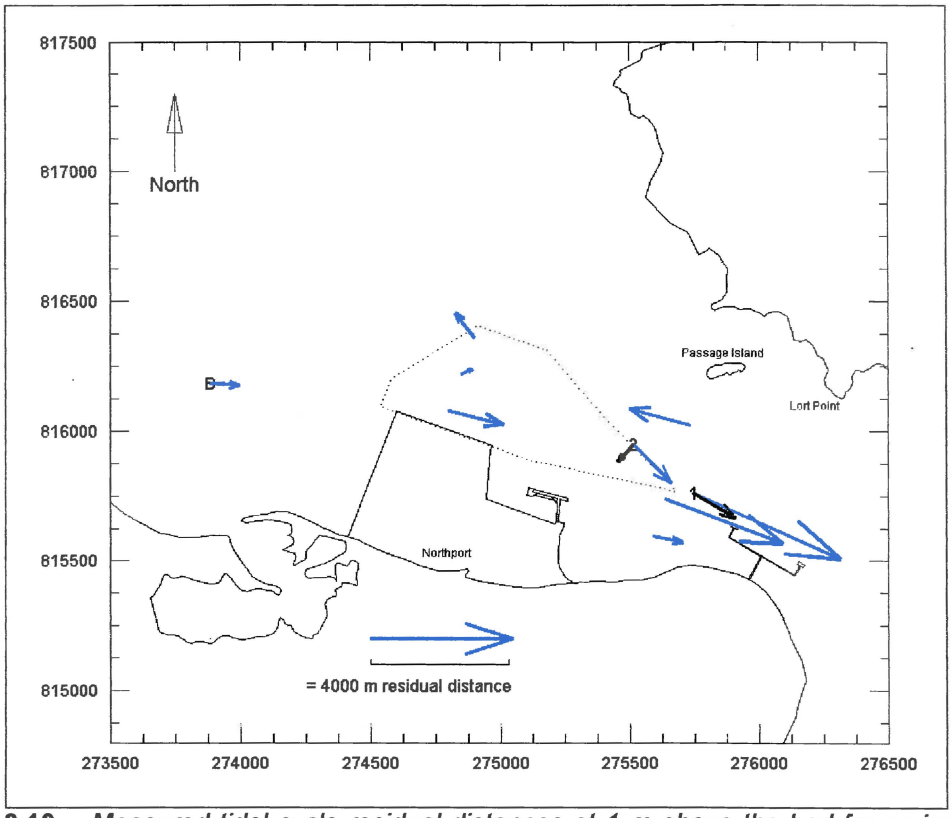


Figure 8.10 – *Measured tidal cycle residual distances at 1 m above the bed for periods when the speed exceeded 0.33 ms^{-1}. Data from boat mounted ADP survey of December 5 2002. Black arrows represent monthly mean residuals from autonomous ADCP deployment and hence reflect the mean of 60 tidal cycles compared with a single tidal cycle represented by the blue arrows. Northport dredge basin is shown as the dotted line.*

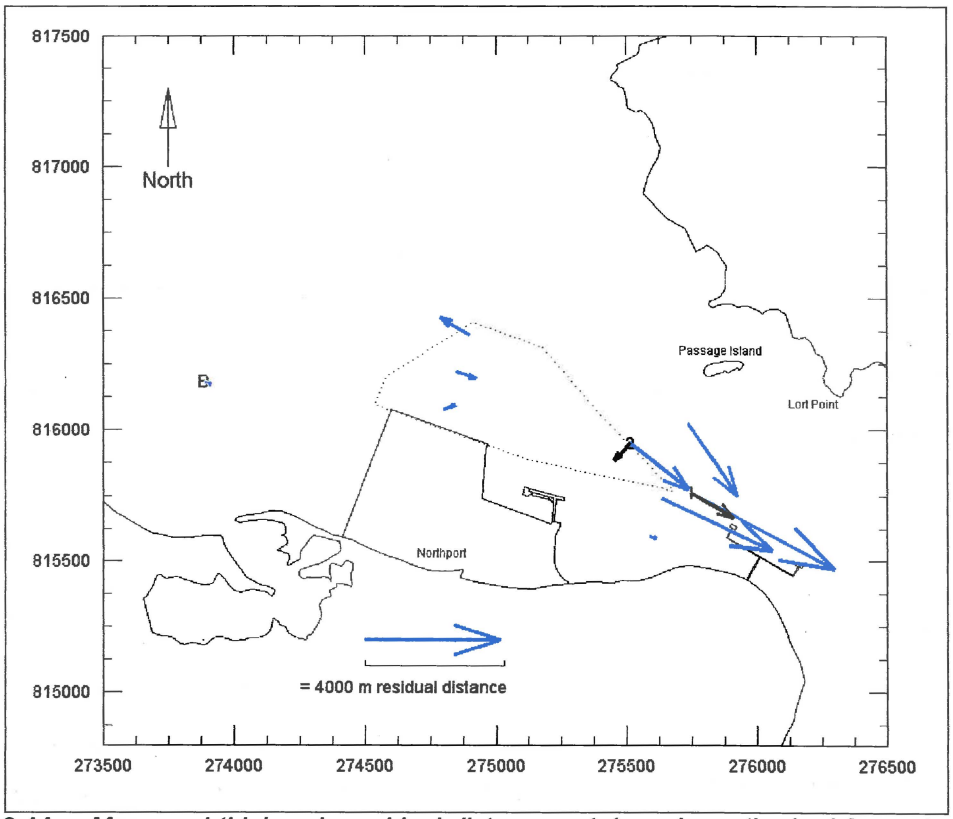


Figure 8.11 – *Measured tidal cycle residual distances at 1 m above the bed for periods when the speed exceeded 0.33 ms^{-1}. Data from boat mounted ADP survey of December 5, 2002. Black arrows represent monthly mean residuals from autonomous ADCP deployment and hence reflect the mean of 60 tidal cycles compared with a single tidal cycle represented by the blue arrows. Northport dredge basin is shown as the dotted line.*

Residual distances indicate an up-harbour movement of sediment in the northern areas of the dredge basin and a down-harbour movement in the southern parts, closer to the quay wall. The magnitude of the down harbour movement increases in an easterly (down-transport) direction, towards the NZRC jetties. The sediment transport potential is greater in the deeper water of the channel and its margins than nearer the shoreline (tidal currents only under consideration, no wave action).

Single tidal cycle residual distances at Site 1, calculated from velocities scaled to a standard tidal range, show agreement in terms of directions but magnitudes that are almost double the monthly mean residuals calculated from 60 tidal cycles (also scaled to the standard tidal range) in the month prior to the boat mounted, single tidal cycle survey. At Site 2, directions differ by ~90°, although magnitudes are closer than those at Site 1 (Figures 8.10 and 8.11).

Single tidal cycle residual distances found at Sites 1 and 2 (Figures 8.10 and 8.11) do however, lie within the range of residual distances calculated from the independently collected data from the autonomous deployment of ADCPs at the same two sites (Figures 8.8 and 8.9), indicating the validity of the method. It is apparent that directions and magnitudes of single tidal cycle residual distances at Sites 1 and 2 vary by amounts alluded to in Figures 8.8 and 8.9 even after the scaling of velocities to a constant tidal range. This variation should be kept in mind when using single tidal cycle residuals to characterise sediment transport potentials at specific locations.

Tidal cycle residuals at Marsden Point indicate a potential for sediment to be transported up-harbour in a northwesterly direction on the northern edge of the dredge basin. There is limited evidence of this up-harbour sediment transport potential closer to the harbour entrance adjacent Passage Island (Figures 8.10 and 8.11).

At the entrance to the Blind Channel, sediment transport potentials are directed easterly toward the Northport dredge basin, magnitudes of these potentials are relatively low.

Within the southern region of the dredge basin, sediment transport potentials indicate a net easterly movement. This transport potential maintains its direction and increases in magnitude towards the NZRC jetties, indicating either the existence of a shell lag or potential scouring to ultimately form a shell lag over this area. An observed increase in bed level (0.5 m) at Site 1 between 1994 and 2002 (Longdill et al., 2002d; Chapter 6) is not expected to be maintained in light of sediment transport potentials calculated (Figures 8.10 and 8.11).

While the two *'single tidal cycle calculated'* residual distance vectors at Site 2 indicate a potential sediment transport parallel with the dredge basin (Figures 8.10 and 8.11), the direction of potential transport at this location is subject to some variation (Figures 8.8 and 8.9) and is often directed into the dredge basin, perhaps to form a loop as it enters the zone of potential transport directed southeasterly and out of the harbour (Figures 8.10, 8.11 and 8.12).

A summary of the transport directions inferred is provided in Figure 8.12. The pattern indicates opposing transport directions, with leakage between the two pathways in the area surrounding Site 2. The increase in magnitude of the residual distance vectors indicates the potential for scour and/or the development of a shell lag between the dredge basin and the NZRC jetties (Figures 8.10, 8.11 and 8.12). Site 2 experienced scour of 0.5 m between 1994 and 2002 whilst Site 1 experienced an increase in bed level of a corresponding amount (Longdill et a., 2003d).

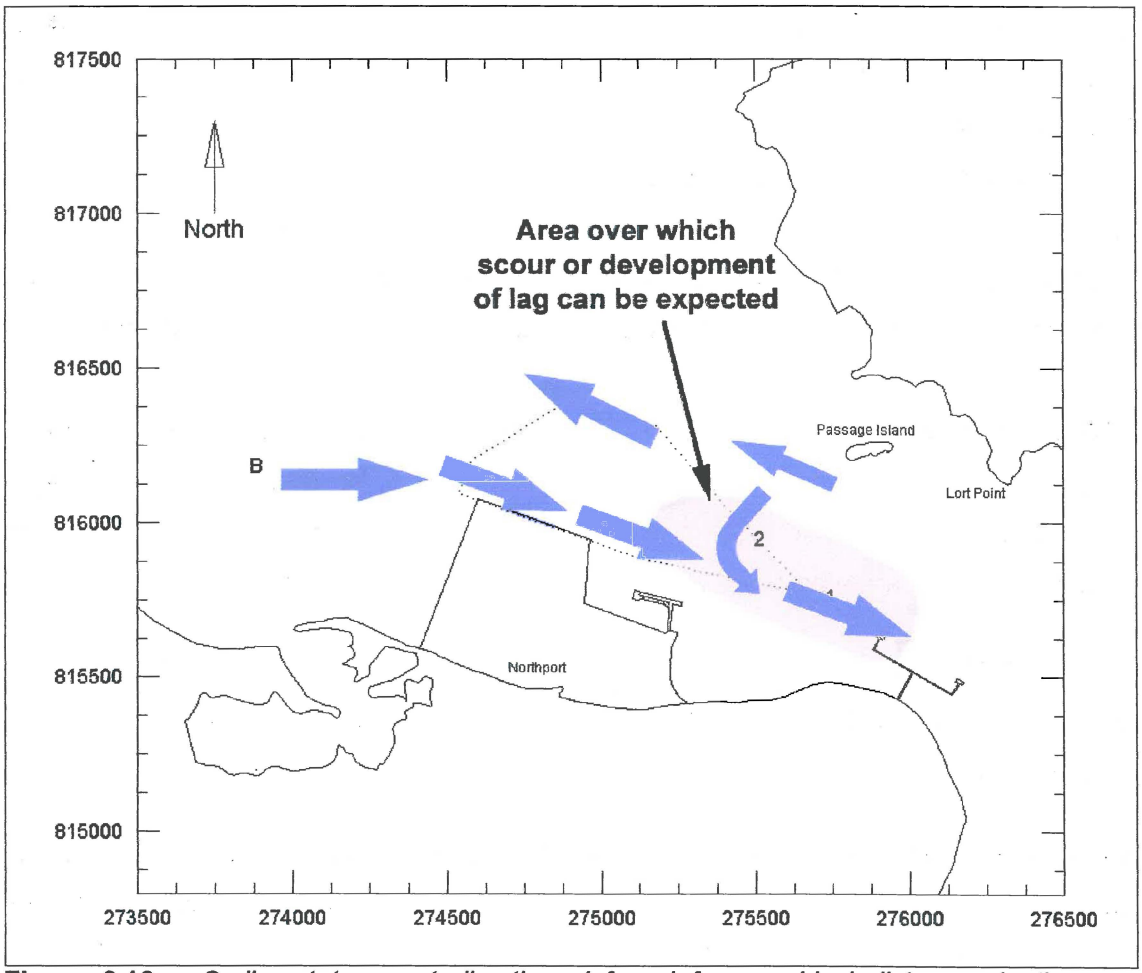


Figure 8.12 – *Sediment transport directions inferred from residual distances in the area surrounding Northport Ltd's dredge basin. Data obtained from October – December 2002. Scour expected where sediment transport potentials increase in magnitude in a 'downstream' direction. Arrow lengths / sizes do not reflect magnitudes.*

8.3.8 Comparison with Previous Sediment Transport Investigations

8.3.8.1 Tidal Cycle Residual Distances

Comprehensive investigations into the sediment transport potential of tidal currents adjacent to Northport have been undertaken by Black (1983) and have largely been summarised in Black et al. (1989). Techniques used in determining residual distances in this Chapter, have followed those used in these two publications; hence a direct comparison is possible.

In order to allow ease of comparison, Figures 8.10 and 8.11 are replicated in Figure 8.13 along with the residual distances described in Black et al. (1989).

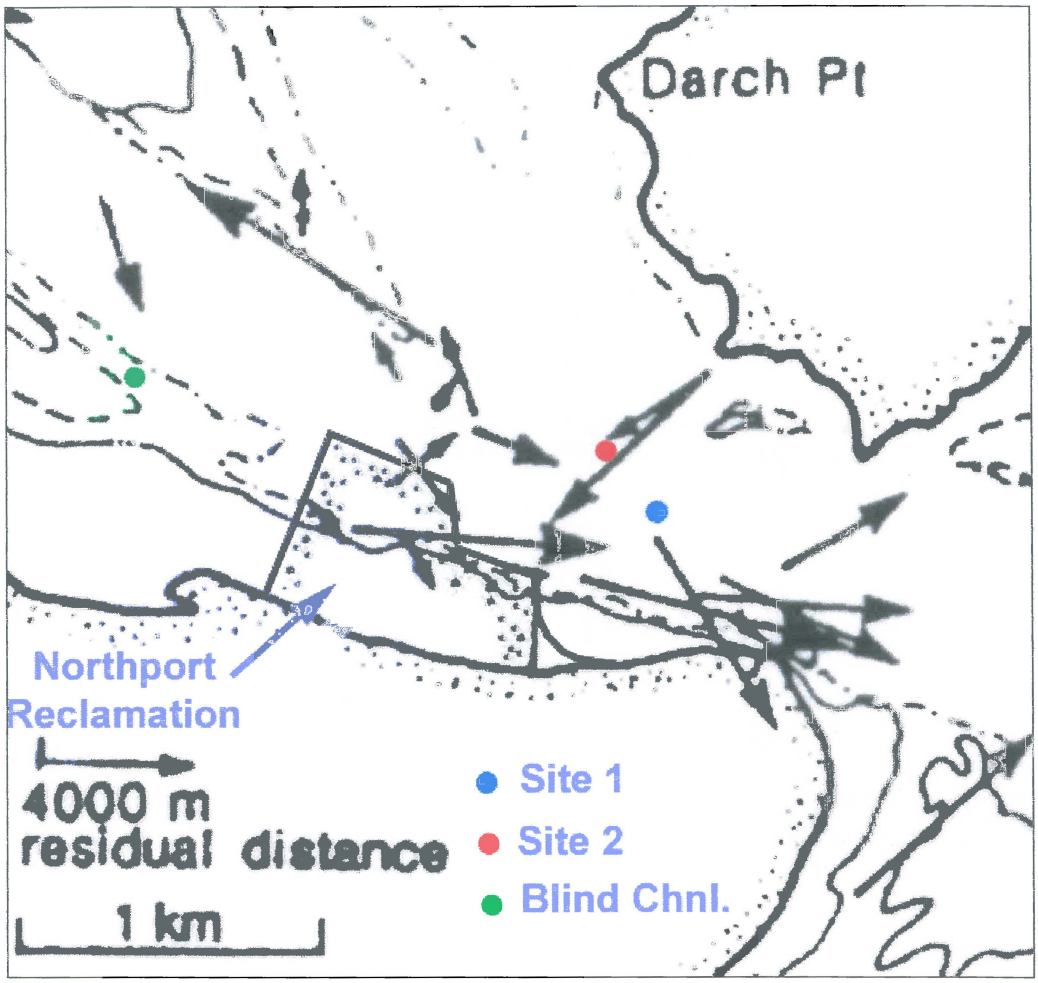


Figure 8.13a - *Tidal cycle residual distances at 1 m above the bed for periods when the speed exceeded 0.33 ms^{-1}. Compiled from 1981 data (after Black et al., 1989), also shown is the location of Northport and sites 1, 2 and Blind Channel to aid comparisons.*

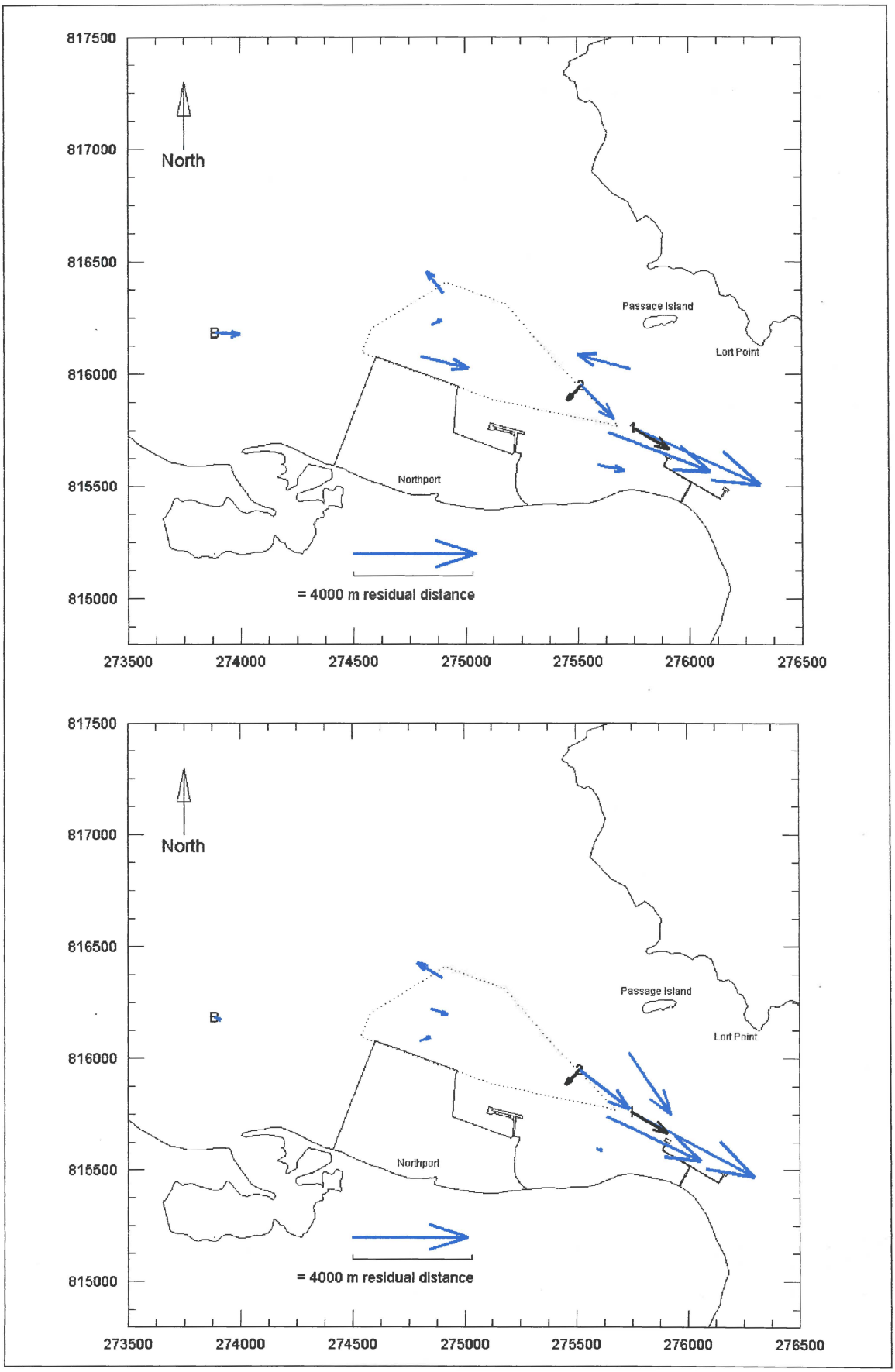


Figure 8.13b and c - *Tidal cycle residual distances at 1 m above the bed for periods when the speed exceeded 0.33 ms^{-1}. Top plot from 2002 data Dec 4th, 2002 and lower plot from Dec 5th, 2002 , black vectors on these plots indicate monthly mean residual distance vectors, dotted line is dredge basin.*

Tidal cycle residual distances calculated from water velocity measurements during October – December 2002 are very similar to those calculated from water velocity measurements in 1981 (Figure 8.13).

The largest variation between the residuals of 1981 and 2002 is the magnitude of the northeasterly-directed residual at the northern extent of the dredge basin. While the directions are similar in both 1981 and 2002, the 1981 residual distance is ~8000 m in length whilst the 2002 value in a similar location is a much smaller 1200 m in both independent surveys (Figure 8.13). The length of the residual distance is linearly proportional to the bedload sediment transport potential (Black, 1983). This would indicate reduced northeasterly-directed sediment transport capacity surrounding the northern extent of the Northport dredge basin. It is probable that the reduced transport potentials are a function of locally reduced water velocities due to the increased depth from dredging.

While no residual distances were actually calculated at Site 2 in 1981, there is evidence of southwesterly-directed residuals nearby. These residuals are in the same direction as the mean residual distance in 2002 (Figure 8.13). The direction of transport, indicated by the mean residual at Site 2 (into the Northport dredge basin), has not changed since 1981.

At Site 1 and near the NZRC jetties, residuals from 1981 and 2002 are similar in both magnitude and direction (Figure 8.13). It is apparent that the sediment transport potential in this region during October – December 2002 (post Northport development) is relatively unmodified from the pattern present in 1981.

Residual distances, indicative of sediment transport potentials, have changed little between 1981 and 2002 in the lower Harbour adjacent to Northport. The most notable variation is a reduction in potential transport in the northern parts of the dredge basin; directions remain constant.

8.3.8.2 Transport Pathways

Sediment transport directions inferred from residual distances in 2002 are consistent with the larger scale patterns reported using 1981 velocity data and 2-dimensional model output (Black et al., 1989) (Figure 8.14).

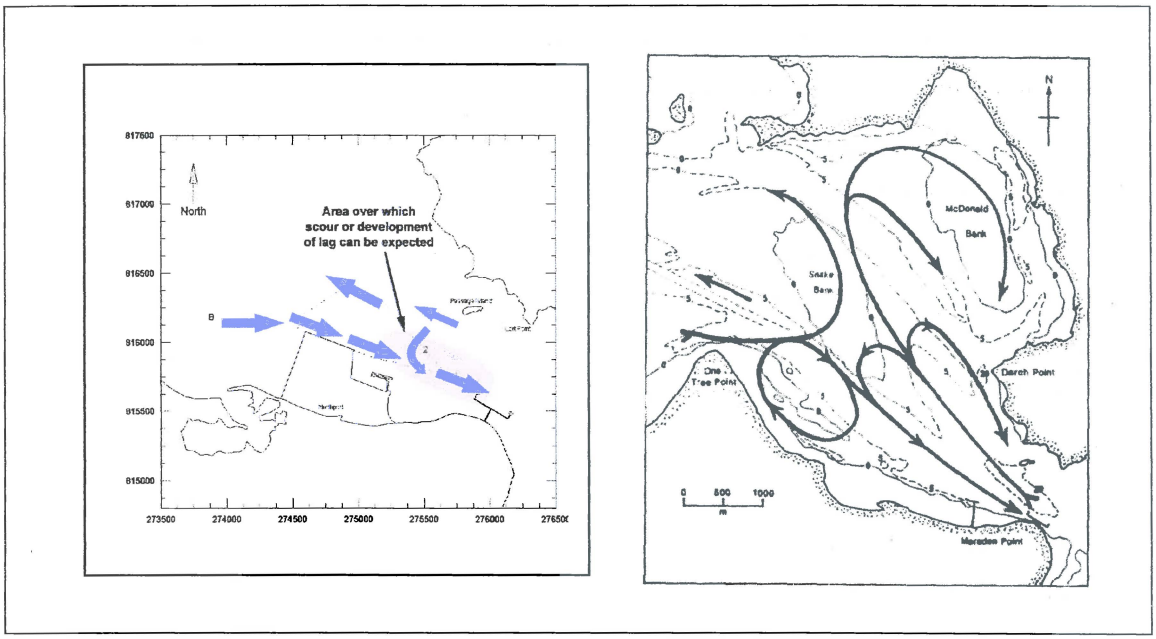


Figure 8.14 –*Sediment transport pathways inferred from tidal cycle residual distances and 2 dimensional model output (1981 only). 2002 results on left and 1981 results on right (Black et al., 1989).*

The 2002 measurements cover a smaller area in greater detail than that described in the plot of 1981 (Figure 8.14, Black et al., (1989)). Both the 1981 and 2002 results indicate a northwest movement of sediment through the deeper area of the harbour entrance and an opposing southeast directed transport closer to the southern shoreline (Figure 8.14). The greater detail of the 2002 data allows refinement of the 1981 patterns in the area surrounding Northport. More precise directions of potential movement alongside Northport have been evaluated using the 2002 data. Some leakage between the two opposing pathways has been observed in 2002, near the eastern edge of the dredge basin, the leakage is directed to the south (Figure 8.14). The 1981 pathways are not detailed enough to reveal this partial loop.

8.4 Transport by Tidal Currents Over Inter-tidal Zones

8.4.1 Introduction

Sediment transport due solely to tidal/*'uniform'* currents is calculated at six sites in the lower Whangarei Harbour. The term *'uniform currents'* is used to characterise those currents that influence one-minute, vector averaged velocities. Sediment transport is calculated over the inter-tidal zones using these currents and neglects the effects of wave induced sediment entrainment.

Sediment transport volumes calculated in this manner are somewhat un-realistic in that they do not take into account the effect of wave induced sediment transport and entrainment, they do however represent an attempt to separate the mechanisms of sediment transport over the inter-tidal areas at Marsden Point and assess the relative influence of these mechanisms.

8.4.2 Limitations and Assumptions

Longshore currents can be generated by a variety of mechanisms such as tidal flows, wind stress, oblique wave attack and longshore variations in set-up. In this section *'uniform'* currents alone are considered over the inter-tidal zones. The currents are considered *'uniform'* as one-minute average velocities are assumed to largely negate the periodic velocity bursts and changes in direction created by wave orbital motions, though it is noted that partially closed wave orbits may bear some influence on the results calculated in this manner.

The influence of obliquely breaking waves on the longshore current velocity cannot be entirely determined. No measurements were made of wave angle during the deployments, thus it is possible that the one-minute averaged velocities may contain influences due to an oblique wave approach. It should be noted also that short waves (such as locally generated wind waves) do not refract easily and thus influences due to these will be small. With the exception of Site I-2, all sites are located within the harbour entrance (Figure 8.1) where wave generation will be fetch limited. Wind records from the deployments (Appendix F) indicate that the wind direction was in general *'offshore'* at the sites measured, for the length of the deployments.

Site I-2 is likely to suffer the greatest inaccuracies due to its location on Bream Bay Beach. The site is exposed to swell waves from the Pacific Ocean (Black, 1983) without the sheltering effect offered by the Whangarei Heads and the harbour entrance to the other sites.

Wind induced longshore currents are assumed to be small in comparison to those created by the tidal movement of water in and out of the harbour. Wind induced surface currents are generally of the order of 1-2% of the wind speed measured at 10 m above MSL (Duxbury and Duxbury, 1997). This assumption is justified when comparison of characteristic wind velocities during the deployments (~5.5 ms^{-1} [Wind rose, Appendix F]) have the ability (after a sustained period of time [Dean and Dalrymple, 1991]) to generate currents of ~0.055 ms^{-1} at the surface.

The logarithmic velocity profile created (Dean and Dalrymple, 1991) will result in even lower velocities closer to the bed. Potential wind induced currents near the bed are small compared with measured near bed velocities (Appendix F), which are of the order 0.1 to 0.5 ms^{-1}.

It is assumed that tidal flows dominate the *'uniform'* currents over the inter-tidal zone. Throughout the chapter reference is made to *'tidal currents'*, this however should be read to incorporate all processes influencing the one-minute average velocity, as their influence is present in the results.

The propagation of errors (from measurements and relationships used) through the calculations is estimated to result in a final volume flux which is of an appropriate order of magnitude, and accurate within ± 50%.

8.4.3 Methods

Water velocities, averaged over minute long intervals, were obtained for full tidal cycles at each of the inter-tidal sites I-1, I-2, I-3, I-4, I-5 and I-6 (Figure 8.1 and Table 8.4, raw velocities in Appendix F). Velocities were corrected to reflect true directions rather than magnetic.

8.4.3.1 Sediment Thresholds

Sediment entrainment thresholds at each of the sites (I-1 to I-6) are required to accurately predict sediment transport. Prediction of the initiation of sediment transport over plane beds of non-cohesive grains is described by Miller et al. (1977). The critical speed (entrainment velocity) at 1 m above the bed in water of 20°C can be expressed by the following relationship:

$$u_{1cr} = 0.63D^{0.29} \qquad \textbf{(8.9 Millar et al., 1977)}$$

The grain size, D, has units of mm and the speed is in ms^{-1}. For D=0.3 mm, the critical 1 m speed is 0.44 ms^{-1}. Black and Healy (1986) observe that this speed is an overestimate of the threshold over rippled bedforms as it does not account for form drag. The Miller et al. (1977) equation (8.9) is applicable only to plane beds.

Black (1983) (also reported in Black and Healy (1986)) measured fluid velocities at the initiation of entrainment (critical velocity) over bedformed regions and developed a new method for determining the critical velocity at 1 m over bedformed regions:

$$u_{1cr} = 5.75u_{*cr}\log_{10}\left(\frac{1}{z_o}\right) \qquad \textbf{(8.10 Black, 1983)}$$

Where u_{*cr} is the sediment threshold friction velocity (ms^{-1}) and z_o is the roughness length (m), with z_o being calculated by Lettau's (1969) equation, referenced in Dyer (1980):

$$z_o = \frac{\Delta^2}{2\Lambda} \qquad \textbf{(8.11)}$$

Where Δ is the bedform height (m) and Λ is the bedform wavelength (m).
u_{*cr} is the subject of a long and detailed derivation and the reader is referred to Black (1983) and Black and Healy (1986) for details. It is dependent on the roughness length (z_o), depth (d) and flow velocity (u).

Threshold velocities were evaluated at each Site (I-1 to I-6) using either the Miller et al. (1977) relationship (equation 8.9) where the bed was planar or the Black and Healy (1986) equation where bedforms are present (Table 8.5). Critical thresholds for the bedformed regions were read from a table published in both Black (1983) and Black and Healy (1986) designed to determine the 1 m critical velocity from the roughness length and median sediment size (D_{50}). Black's (1983) and Black and Healy's (1986) method was developed using data from the Whangarei Harbour.

Site	Bedform height (m)	Bedform wavelength (m)	D_{50} (mm)	Z_o (m)	Equation used	U_{1cr} (ms^{-1})
I-1	0.01	0.1	0.17	0.0005	Black and Healy	0.36
I-2	0.01	0.1	0.15	0.0005	Black and Healy	0.36
I-3	N/A	N/A	0.25		Miller et al.	0.42
I-4	0.005	0.07	0.27	0.00018	Black and Healy	0.47
I-5	N/A	N/A	0.15		Miller et al.	0.36
I-6	N/A shell	N/S shell	Shell		Mehta et al. (1980)	0.96

Table 8.5 – *Threshold velocity at inter-tidal sites (I-1 to I-6) at 1 m above the bed. Where bedforms are present, both form and skin friction is taken into consideration (Black and Healy, 1986). Planar bed thresholds determined using Miller et al.'s (1977) equation. Thresholds for bedformed regions read from table in Black and Healy (1986) using values of D_{50} and z_o. Site I-6 threshold from Mehta et al. (1980) for a shell lagged bed (similar shells to Whangarei Harbour).*

8.4.3.2 Calculation of Tidal Cycle Sediment Transport

Many bed load equations provide an estimate of the sediment transport by utilising the excess shear stress (Bagnold 1963, Yalin, 1963, Sternberg 1972). Bagnold's (1963) bed load equation expresses the bed load transport rate (q_m) in terms of the stream power (ω) and an efficiency factor (K):

$$q_m = \frac{\rho_s}{(\rho_s - \rho)g} \cdot K\omega \qquad \textbf{(8.12 Bagnold, 1963)}$$

Where ρ_s is the sediment density and ρ is the fluid density. While K was originally thought to depend only on sediment characteristics (Bagnold, 1963), it has since been shown (Kachel and Sternberg, 1971 in Heathershaw, 1981) that K not only depends on grain size but also on the excess shear stress $(\tau - \tau_{cr})/\tau_{cr}$, where τ_{cr} is the threshold shear stress (that stress at which initial motion occurs).

Gadd et al. (1978) modified the Bagnold equation (8.12) using flume data to express the transport rate (q_m) in terms of the current velocity at 1 m above the bed (u_1) and a threshold velocity (u_{1cr}) to arrive at:

$$q_m = \beta(u_1 - u_{1cr})^3 \qquad \textbf{(8.13 Gadd et al., 1978)}$$

Where β is an empirically derived constant representing all the other coefficients (from equation 8.12) with units $kgm^{-4}s^2$.

Black (1983) found a statistically significant ($\alpha = 0.05$, $r^2 = 0.8$) relationship between the bed load mass transport rate (q_m) and the cube of the excess velocity at Whangarei Harbour:

$$q_m = 0.145(u_1 - u_{1cr})^3 \qquad \textbf{(8.13 Black, 1983)}$$

The bed load mass transport rate (q_m) from equation 8.13 has units of $kgm^{-1}s^{-1}$.

The bed load mass transport rate (in vector form) can be found for each velocity record (1 min averaged) over the tidal cycle. When each of these transport rates (vectors) are multiplied by the averaging time and summed over the tidal cycle the net tidal cycle transport is obtained:

$$Q_m = \int_{T=0}^{T=12.42\,hrs} 0.145(u_{1(t)} - u_{1cr})^3\, dt \qquad \textbf{(8.14)}$$

Where Q_m is the tidal cycle bed load transport rate ($kgm^{-1}tidalcyle^{-1}$) and dt is the time over which the velocities are averaged. When velocities are below threshold, no transport is assumed for that time period. The tidal cycle bed load sediment transport rate was converted to a volumetric representation assuming a sediment density of 2650 kgm^{-3} and a porosity of 0.45.

The preceding calculations were undertaken at each of the sites I-1 to I-6 (Figure 8.1) using the critical velocities detailed in Table 8.5. The calculations were performed in MATLAB® using the program "*tidal_cycle_transport.m*" written by this author specifically for the purpose (Appendix F).

8.4.3.3 Distribution of Tidal Ranges

It is desirable to estimate the annual bed load sediment transport flux from values obtained over a single tidal cycle measurements.

Black (1983) summarised seven months of typical tides at Marsden Point (during the year 1982) and found the tidal range cumulative probability curve was best represented by the normal distribution with a standard density function. Tides had a mean range of 1.87 m and a standard deviation of 0.347 m; unfortunately Barnett's (2002) thesis, in its analysis of long term tidal data at Marsden Point, did not update these values.

A normally distributed tidal probability curve with mean 1.87 m and standard deviation of 0.347 m is used to replicate the occurrence of various tidal ranges at Marsden Point.

8.4.3.4 Annual Sediment Transport Rates

The net sediment transport fluxes over a single tidal cycle were found for a low Neap range of 1.4 m, a mean tidal range of 1.9 m and a high Spring range of 2.4 m, using the procedure of linear velocity scaling according to tidal range (Section 8.3.7.2, equation 8.8). This process was performed in the MATLAB® program "*scale_to_constant_tr.m*" (Appendix F) written by this author specifically for the purpose.

With tidal velocities for each of the three tidal ranges at each site, the tidal cycle bed load transport was calculated (Section 8.4.3.2), providing an estimate of the sediment transport at each site, under the influence of the three different tidal ranges.

The MATLAB® program "*weighted_mean.m*" (Appendix F) was written (by this author) to calculate the annual bed load sediment transport rate. Methods undertaken by the program to calculate an annual rate area as follows:

1) To determine the annual fluxes at each site, a mean rate weighted with the probability that each tidal range will occur was derived. A span of tidal ranges from 1.1 m to 2.7 m (the extreme range of tidal ranges observed at Marsden Point by Black (1983)) was divided into 100 increments and the probability of each tidal range occurring found from the normal distribution of tidal ranges (Section 8.4.3.3).

2) The transport rate for each increment was found by interpolating or extrapolating using the three known transport rates (for the tidal ranges of 1.2 m, 1.9 m and 2.4 m). Black (1983) notes that the transport rate (q_m) is not linearly related to tidal range, but is better approximated by a power curve of the form:

$$q_m = a(\Delta H)^b \qquad \textbf{(8.15 Black, 1983)}$$

Where ΔH is the tidal range and a and b are constants. Taking the logarithm of both sides gives:

$$\log_{10 q_m} = \log_{10} a + b \log_{10} \Delta H \qquad \textbf{(8.16 Black, 1983)}$$

which is now a linear relationship. The gradient and intercept of this straight line was found from two of the three known transport rates, for ΔH = 1.1 m to 1.9 m or for ΔH = 1.9 m to 2.4 m. Transport rates were found by interpolating or extrapolating along these linear curves. The choice of curve was made depending on where the tidal range in question lay relative to the ranges used to determine the coefficients.

3) The tidal cycle transport for each of the 100 tidal ranges was multiplied by the probability of that tidal range occurring during the year (Section 8.4.3.3). When summed and multiplied by the number of tidal cycles in a year an estimation of the annual sediment transport flux is created.

8.4.4 Results

Annual net bed load sediment transport rates due to the action of tidal currents alone (assuming no effects from gravity-waves and wind generated currents) over the inter-tidal terraces surrounding Marsden Point are summarised in Table 8.6 and in Figure 8.15.

Site	D_{50} (mm)	Annual sediment transport magnitude (m^3y^{-1}/m)	Annual sediment transport direction (° True)
I-1	0.17	0.123	81.3
I-2	0.15	0.084	26.9
I-3	0.25	0.878	41.9
I-4	0.27	0.001*	336.8
I-5	0.15	0.136	296.6
I-6	Shell	0.000	N/A

Table 8.6 – *Annual tidal current (in isolation) induced sediment transport rates and directions at six inter-tidal sites surrounding Marsden Point. (Effects of gravity-waves and wind not taken into consideration). *Magnitude not considered to be above the errors of the equations used to calculate it.*

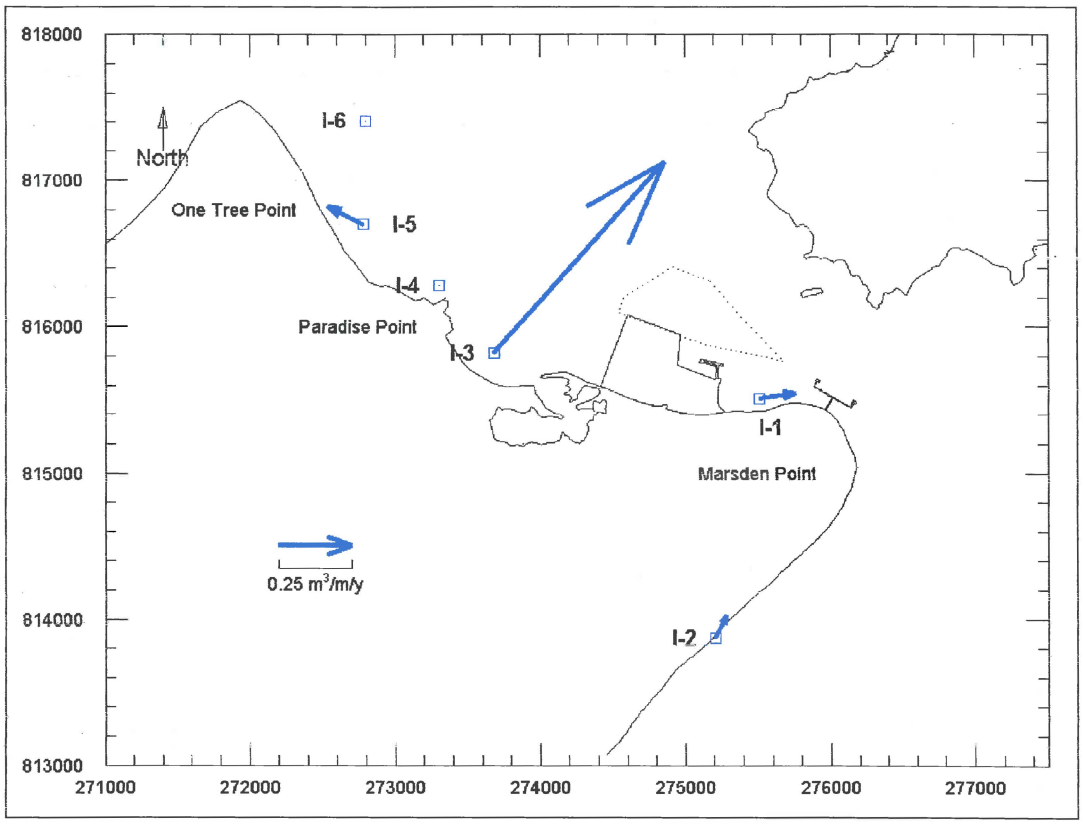


Figure 8.15 – *Annual tidal current (in isolation) induced sediment transport rates at six sites surrounding Marsden Point. (Effects of gravity-waves and wind not taken into consideration). Accuracy estimate ± 50%.*

Sediment transport under tidal flows only (assuming no wave action) is relatively limited at all sites under consideration. The largest magnitude observed is 0.878 m^3yr^{-1}/m (~350 m^3yr^{-1} for characteristic length) at Site I-3 in an off shore direction and is potentially influenced by water exiting Blacksmiths Creek (Figure 8.15).

Tidal current induced sediment transport (neglecting any influence of surface gravity-waves) indicates longshore sediment transport along Bream Bay Beach toward Marsden Point and Mair Bank (Site I-2, Figure 8.15). The direction of sediment transport found here is consistent with that of Gibb (1979), Tonkin and Taylor (1979a,c) and the DHI (1982). While the magnitude of the transport is much less (~168 m^3y^{-1}), assuming a 2 km length of beach with the present values (compared with the 19,000 – 150,000 m^3y^{-1} of Gibb [1979] and Tonkin and Taylor [1979a,c]), it must be recognised that the present calculations relate only to the tidal currents operating alone to entrain and transport sediment. The addition of wave effects to entrain sediment will likely result in greater transport volumes.

Tidal currents acting in isolation provide the potential to transport sediment in an easterly direction across the inter-tidal terrace between Northport and the NZRC jetties (Site I-1, Figure 8.15) at a rate of ~86 m^3y^{-1} (assuming 700 m distance). Observed accretion (Sections 4.4.2, 5.6.2, 6.7.3, 6.8 and Figures 5.34 and 6.9) against the eastern edge of the Northport reclamation is in contradiction to this transport direction. This issue is revisited once sediment transport resulting from wave action is also taken into account.

The solely tidal current driven transport at Site I-3 is much larger than those at the other sites and is directed toward the main channel of the harbour (Figure 8.15 and Table 8.6). The inter-tidal terrace here did not display bedforms and thus had a relatively high critical velocity (Table 8.5). One-minute averaged velocities at this site exhibit large ebb dominance (Appendix F). It is generally only ebb flows at this location that exceed the critical threshold. This is potentially due to the effects of water exiting Blacksmiths Creek contributing to increased ebb velocities whilst reducing flood velocities.

Site I-4, at Paradise Point (Figure 8.15), combines a reasonably high threshold (0.47 ms^{-1}, Table 8.5) with relatively balanced ebb and flood flows (Appendix F), resulting in a very low net transport. The magnitude of the transport is not considered to be above the accuracy of the calculations. Further toward One Tree Point, Site I-5 (Figure 8.15) indicates a tidally generated sediment transport toward One Tree Point, in a northwesterly direction.

If the transport is assumed to act over a distance of 1000 m (appropriate for this location) potential volumes of sand being transported are 140 m^3y^{-1} due to tidal currents alone, if acting in isolation.

Site I-6 showed no potential for tidally generated sediment transport. This is entirely due to the nature of the bottom at this location. Shells present here have a very high threshold velocity (Table 8.5). Even though the site displayed greater velocities of any of the other inter-tidal sites (Appendix F), they did not exceed the shell threshold at any predicted tidal range, thus no tidally generated transport is predicted to occur.

8.4.5 Comparison to Previous Calculations

Black (1983) estimated annual sediment transport fluxes using a similar method. Sites in common (± 50 m) include Sites I-1 (Black's Site B1) and I-6 (Black's Site C1).

The estimated transport flux at Site I-1 in 2003 was 0.123 m^3y^{-1}/m, whilst in 1983 it was 0.03 m^3y^{-1}/m. Directions were reasonably similar (81° in 2003 and 100° in 1983). It is important to note that even though sediment has been observed accumulating recently (2001-2002) against the eastern edge of the Northport reclamation, that the tidally generated (acting in isolation) sediment transport is directed in a similar direction to that observed in 1983. The magnitude of the tidally generated annual sediment transport flux is larger in 2003 than in 1983. This can be partially explained through Black's (1983) use of a higher critical velocity. While the critical velocity is not specifically documented by Black (1983), a D_{50} of 0.21 mm was used, compared with the present value of D_{50} = 0.15 mm. The influence of this on the critical velocity and then on the tidal cycle transport could be a major component of the difference in magnitudes. The reduction in mean grain size could be expected from recent sediment accretion.

Black's (1983) calculations indicate a tidal current induced sediment transport of 24.42 m^3y^{-1}/m near Site I-6, based on a bed composed of sandy mega-ripples. The difference in bed types (sandy mega-ripples [1983] and shell lag [2003]) and hence the threshold velocities employed explain the large difference in magnitudes. The difference also illustrates the importance of the shell lag in providing a stabilising influence on sections of the harbour. It can not be determined if the shell lag has developed at the site since 1983, a more likely explanation is due to spatial variations in bottom types and the fact that the instrument locations were only within 50 m of each other.

8.5 Longshore Transport by Waves at the Beach Face

8.5.1 Introduction

Waves and currents in the nearshore combine to transport sediment. An oblique wave approach generates longshore currents near the beach face (Bowen, 1969; Longuett-Higgins, 1970a, 1970b in Komar, 1998). The longshore currents generated, in combination with the velocity *'bursts'* of wave orbital velocities create an efficient mechanism for sediment transport.

In this section local wind generated waves are considered for their potential to transport sediment along the beach face at sites in the lower Whangarei Harbour.

8.5.2 Methods

A standard right-hand co-ordinate system is used throughout this thesis for work on longshore currents. Positive values offshore (i.e. +ve V_o is directed offshore) and to the right along-shore (i.e. +ve V_l is directed to the right) (Figure 8.16).

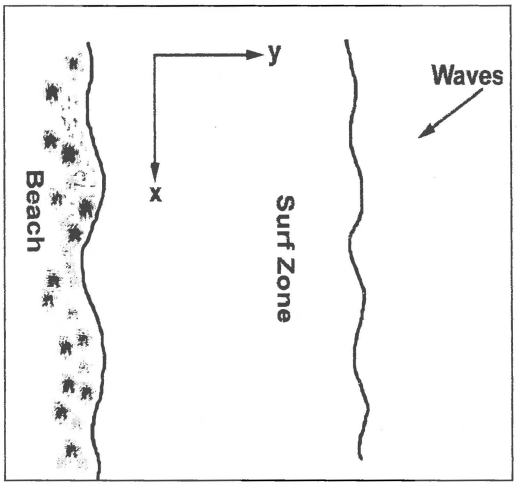


Figure 8.16– Longshore (x) and cross-shore (y) directions used. Positive longshore directions are to the right for an observer looking seawards. Positive cross-shore directions are offshore.

8.5.2.1 Longshore Wave Power and Transport

The energy flux method of determining longshore sediment transport relates the immersed weight longshore transport rate (I_l) to the longshore component of wave energy (P_l).

The longshore component of wave power can be evaluated relatively simply from the wave height, velocity and angle to the shoreline using a well established relationship:

$$P_l = (EC_g)_b \sin\alpha_b \cos\alpha_b \qquad \textbf{(8.17 CERC,1984)}$$

Where $(EC_g)_b$ is the wave energy flux or power evaluated at the breaker zone (E is the total wave energy at the breaker line per unit crest width (Nm) (= $\rho g H_b^2/8$), C_g is the group velocity of the waves (ms^{-1}) and approximately equal to the shallow water wave speed) and α_b is the wave breaker angle.

The immersed weight transport rate I_l (Ns^{-1}) can be found from the wave power relationship:

$$I_l = KP_l \qquad \textbf{(8.18 CERC, 1984)}$$

Where K is a dimensionless proportionality coefficient.

The value of K is a subject of some debate. Initially, it is dependent on the value used for the wave energy density (E) in the formulation of P_l ($H_{rms} \rightarrow K \approx 0.77$ [Komar and Inman, 1970], $H_s \rightarrow K \approx 0.39$ or K from H_{rms} divided by 2 [CERC, 1984]). The value of K has also been shown vary with median grain size and orbital velocities (Bailard, 1984) and the surf similarity parameter (Kampuis, 1991). USACE (2002) tested six different models for their evaluation of K and compared the results to long-term field data of sediment movement at Santa Barbara and Torrey Pines. They concluded that Bailard's (1984) equation performed the best:

$$K = 0.05 + 2.6 \sin^2 2\alpha_b + 0.007 \frac{u_b}{w_f} \qquad \textbf{(8.19 Bailard, 1984)}$$

Where α_b is the wave breaker angle as before, w_f is the sediment fall velocity (from RSA analysis in this case) and u_b is the maximum oscillatory velocity magnitude, from shallow water wave theory $u_{mb} = \frac{\gamma}{2}\sqrt{gh_b}$, in which $\gamma \approx 0.78$ at break point (Komar, 1998), g is the acceleration due to gravity and h_b is the water depth at wave breaking. While Bailard (1984) developed his equation for K with H_{rms} in mind, H_s can be used provided Bailard's (1984) K is divided by 2 prior to insertion (CERC, 1984).

The immersed weight transport rate (I_l) can be converted to a volumetric transport rate (m^3/time):

$$Q_l = \frac{I_l}{(\rho_s - \rho) g (1-n)} \qquad \textbf{(8.20 CERC,1984)}$$

Where ρ_s is the sediment density (2650 kgm^{-3} for quartz), ρ is the fluid density (1025 kgm^{-3} for seawater, g is the acceleration of gravity (9.81 ms^{-2}) and n is the in-place sediment porosity (≈ 0.4 dimensionless [USACE, 2002]).

8.5.2.2 *Limitations and assumptions*

The area of interest for these calculations is the beach face adjacent Sites I-1, I-3, I-4 and I-5 (Figure 8.1).

Location I-2 has not been used as its wave climate is influenced not only by local winds but also by the more general New Zealand, northeast coast swell regime due to its location on Bream Bay Beach. The sites within the harbour are not influenced to any great degree by these swells (Tonkin and Taylor, 1981). While Black (1983) found that southeasterly swells (those most likely to reach the lower harbour) can impact Mair Bank (in contrast to Tonkin and Taylor, 1981), they were still expected to have limited capacity to transport sediment once they had refracted around Marsden Point and reached the lower Harbour.

In calculating the potential longshore sediment transport using the energy flux method, the only longshore currents considered are those generated by the oblique wave approach. No consideration is given to any other longshore currents that may be present due to other forcing mechanisms. Transport rates calculated therefore relate to that transport resulting from the oblique wave approach only. While it is a reasonable assumption that tidal velocities at the *'top'* of the inter-tidal terrace (the beach face), which is covered for only part of the tidal cycle (Table 8.8), will be small, this has not been tested.

It is assumed that the wind data recorded at Marsden Point from 1 January 1983 to 31 December 1987 (Figure 2.5, Tabulated data in Appendix F) represents the *'typical'* Marsden Point wind climate.

Sediment transport rates calculated do not take into account sediment availability and hence represent transport potentials, rather than absolute values.

The energy flux formulae / relationships are based on the compilation of many years of research and testing and are entirely empirical. There has been little consideration of the physical processes involved in longshore sediment transport during their derivation; nonetheless the method has proved very successful at numerous sites around the world (Komar, 1998).

The propagation of errors (from measurements and relationships used) through the calculations is estimated to result in a final volume flux which of the appropriate order of magnitude, and accurate within ± 50%.

8.5.2.3 Wave Hindcasting

To use the energy flux method of determining longshore sediment transport, knowledge of wave heights, period and direction are required. To obtain accurate yearly figures of wave heights within the fetch limited environment of the lower harbour, wave hindcasting was performed.

8.5.2.3.1 Fetch Lengths

Fetch lengths were determined for each wind band direction at each Site (Table 8.7).

		Fetch Lengths (m)							
Direction (°)		0	45	90	135	180	225	270	315
Site	beach angle (°)								
I-1	86	1700	1000	-	-	-	-	-	6000
I-3	124	4300	3500	600	-	-	-	-	6000
I-4	129	4000	3800	3000	-	-	-	-	7500
I-5	146	3500	4200	3000	900	-	-	-	-

Table 8.7 – *Fetch lengths and beach angles for the wave hindcasting sites.*

8.5.2.3.2 Water Depths

Characteristic depths are required for wave hindcasting. The elevations of both landward and seaward edges of the inter-tidal terrace were obtained from beach profiles adjacent to the five sites (I-1, I-3, I-4 and I-5). A sharp change in profile gradient was used to define the landward and seaward extent of the terrace. Inter-tidal terrace lengths and slopes were determined (Table 8.8).

Site	Intertidal terrace elevation, landward (m C.D.)	Intertidal terrace elevation, seaward (m C.D.)	Intertidal terrace length (m)	Average intertidal slope	Foreshore contact time (hrs/tidalcyle)	Water depth [MHW] at foreshore toe (m)	Sediment fall velocity (D_{50}) w (ms^{-1})
I-1	2.0	0.5	185	0.008	5	0.58	0.0312
I-3	1.7	0.5	480	0.0025	6	0.88	0.0042
I-4	1	0.3	100	0.003	10	1.58	0.0526
I-5	1.6	0.9	130	0.005	6.5	0.98	0.0312

Table 8.8 – *Elevations of intertidal terrace from beach profiles. Foreshore contact time is the time that the foreshore is in contact with the water during each tidal cycle (mean TR=1.87). Sediment fall velocities of D_{50} grain size from RSA analysis. MSL at Marsden Point is 1.65 m C.D.*

Depths over the inter-tidal terraces range between 0.5 m and 2.2 m during a normal tidal cycle. A water depth of 1 m is used in the wave hindcasting calculations, reflecting an attempt to represent characteristic water depths over the inter-tidal area.

8.5.2.3.3 Wave Heights

Estimates of wave heights in the lower harbour were calculated using wind records obtained from NIWA via Northport of wind velocities and directions measured at Marsden Point between 1 January 1983 and 31 December 1987 (Figure 2.5 and Appendix F) and the JONSWAP equations (Hasselmann et al., 1973 in CERC, 1984).

The Shore Protection Manual (CERC, 1984) provides nomograms for the estimation of waves based on fetch lengths, wind strengths and wind duration. Also provided are the equations used to plot the curves in the nomograms, which are used here to estimate wave heights and periods at the Marsden Point sites. The shallow water, fetch limited equations are:

$$\frac{gH}{U_A^2} = 0.283 \tanh\left(\frac{gd}{U_A^2}\right)^{0.75} \tanh\left(\frac{0.065\left(\frac{gF}{U_A^2}\right)^{0.5}}{\tanh\left(0.530\left(\frac{gd}{U_A^2}\right)^{0.75}\right)}\right)$$ **(8.21 CERC, 1984) and**

$$\frac{gT}{U_A} = 7.54 \tanh\left(0.833\frac{gd}{U_A^2}\right)^{0.375} \tanh\left(\frac{0.0379\left(\frac{gF}{U_A^2}\right)^{0.33}}{\tanh\left(0.833\left(\frac{gd}{U_A^2}\right)^{0.375}\right)}\right)$$ **(8.22 CERC, 1984)**

Where H is Estimated wave height (m),

T is Estimated wave period (s),

U_A is Wind stress factor (U_A=0.71$U_s^{1.23}$ where U_s is the 10 m wind speed [ms^{-1}], CERC, 1984),

g is Acceleration of gravity (9.81 ms^{-2}),

d is Characteristic depth (assessed as 1 m) and

F is Fetch length (m).

A series of spreadsheets were set up to calculate the wave height and period for each wind band with an effective fetch at each of the sites. Wind and wave directions are considered coincident. Spreadsheets for each Site and each wind direction with an effective fetch length are compiled in Appendix F. An example spread sheet is shown in Table 8.9.

Site	1
fetch (m)	1700
wind/crest angle	0
beach angle	86
time on beach face (hrs)	5
% time on beach face	40%
no. of wind records	1000
D_{50} (mm)	0.17
w=fall velocity (D_{50}) (m/s)	0.0442
water depth (m)	1
breaker angle (α_b)	-86
$\sin(\alpha_b)*\cos(\alpha_b)$	-0.070

U_s= Surface wind Speed (Kts)	3	8	13	18	23	28	33
Wind occurrence (per 1000)	18	50	28	12	2	1	0
Wind % Occurrence	1.80%	5.00%	2.80%	1.20%	0.20%	0.10%	0.00%
U_s= Surface wind Speed (ms^{-1})	1.5	4.1	6.7	9.3	11.8	14.4	17.0
U_A = wind stress factor	1.2	4.0	7.4	11.0	14.8	18.9	23.1
gd/U^2=	6.692	0.599	0.182	0.082	0.045	0.027	0.018
gF/U^2=	11376	1019	309	139	76	47	31
$\tanh[0.530\{gd/U^2\}^{0.75}]$=	0.9760	0.3461	0.1463	0.0807	0.0514	0.0358	0.0264
gH_{sd}/U^2= $[0.0016\{gF/U^2\}^{0.5}]$	0.1707	0.0511	0.0281	0.0188	0.0139	0.0109	0.0089
H_{sd}=Sig. wave height deep (m)	0.03	0.09	0.15	0.23	0.31	0.40	0.49
gH_{ss}/U^2=	0.1517	0.0469	0.0245	0.0155	0.0108	0.0080	0.0062
H_{ss}=Sig. wave height shal. (m)	**0.02**	**0.08**	**0.13**	**0.19**	**0.24**	**0.29**	**0.34**
$\tanh[0.833\{gd/U^2\}^{0.375}]$	0.9353	0.5964	0.4131	0.3144	0.2538	0.2131	0.1839
gT/U=	5.0901	2.5385	1.7166	1.3128	1.0707	0.9084	0.7916
T=wave period (s)	**0.63**	**1.05**	**1.29**	**1.47**	**1.62**	**1.75**	**1.87**
L_d=deepwater=$gT/2\pi$	0.9807	1.6344	2.0081	2.2916	2.5267	2.7306	2.9122
L_s=shallow water = $T(gd)^{0.5}$	1.9677	3.2791	4.0289	4.5977	5.0694	5.4785	5.8428
h/L_d	1.0196	0.6119	0.4980	0.4364	0.3958	0.3662	0.3434
$d_b=0.78*H_{ss}$	0.02	0.06	0.11	0.15	0.19	0.23	0.26
C_{sg}=Shal. water grp wave speed	0.4165	0.7736	1.0152	1.2049	1.3616	1.4948	1.6105
U_{mb} (linear wave theory)	0.1624	0.3017	0.3959	0.4699	0.5310	0.5830	0.6281
K (Bailard, 1984)/2	0.8065	0.9168	0.9914	1.0500	1.0984	1.1395	1.1752
$(EC_g)_b=pgH_{sb}^2/8$	0.2692	5.9468	23.14	54.52	100.47	160.22	232.54
$P_l=(EC_g)_b\sin\alpha_b\cos\alpha_b$	-0.018	-0.41	-1.61	-3.79	-6.99	-11.14	-16.18
$Q_l=K*P_l/((p_s-p)ga')$ (m^3/yr^{-1})	-50	-1251	-5265	-13135	-25320	-41890	-62704
Q_{lw}=wtd (wind&time/tide)(m^3/yr^{-1})	-0.36	-25.18	-59.35	-63.46	-20.39	-16.86	0.00

Table 8.9 –*Example spreadsheet of wave height, wave period, energy and longshore sediment transport obtained from wind hindcasting using CERC (1984) formulae. This example for Site I-1 and winds from the North (0°).*

Data input to the spreadsheet required for calculation includes:

i. fetch length (measured in GIS);
ii. wind direction (wind records);
iii. time of water on foreshore (per tidal cycle) (Table 8.8);
iv. D_{50} (median) grain size (RSA analysis, Table 8.5);
v. fall velocity of D_{50} grain size (RSA analysis, Appendix A); and
vi. wind occurrence (per 1000) for wind bands (wind records).

Using equations 8.21 and 8.22 the significant wave height and wave period are estimated. K is calculated using Bailard's (1984) equation (Eq. 8.19). The longshore sediment transport rate is calculated for each wind band with Equation 8.20 (CERC, 1984).

8.5.2.4 Time Averaging of Wave Energy

The longshore sediment transport rate (Q_l) calculated for a given wind condition was multiplied by the probability of experiencing a certain wind condition to represent the typical duration of winds from this direction over a year long period. As wave transport at the foreshore is the purpose for the calculations, the transport rate was multiplied by the proportion of time that waves can act on the foreshore (Table 8.8) to represent the tidal cover time producing breaking / broken waves over the beach face. A weighted transport rate (Q_{lw}) was obtained for each wind strength and direction at each Site (Table 8.9).

8.5.3 Results

Variation in wind direction results in variation in sediment transport rates. Wave driven longshore sediment transport rates under characteristic wind conditions is shown in Figure 8.17 for four sites in the lower Whangarei Harbour. Positive longshore sediment transport rates reflect transport to the right and negative to the left (of an observer looking seaward, Figure 8.16).

Summation of the weighted transport rates at each location reveals net longshore wave driven transport magnitudes and directions at the beach face (Table 8.10 and Figure 8.18).

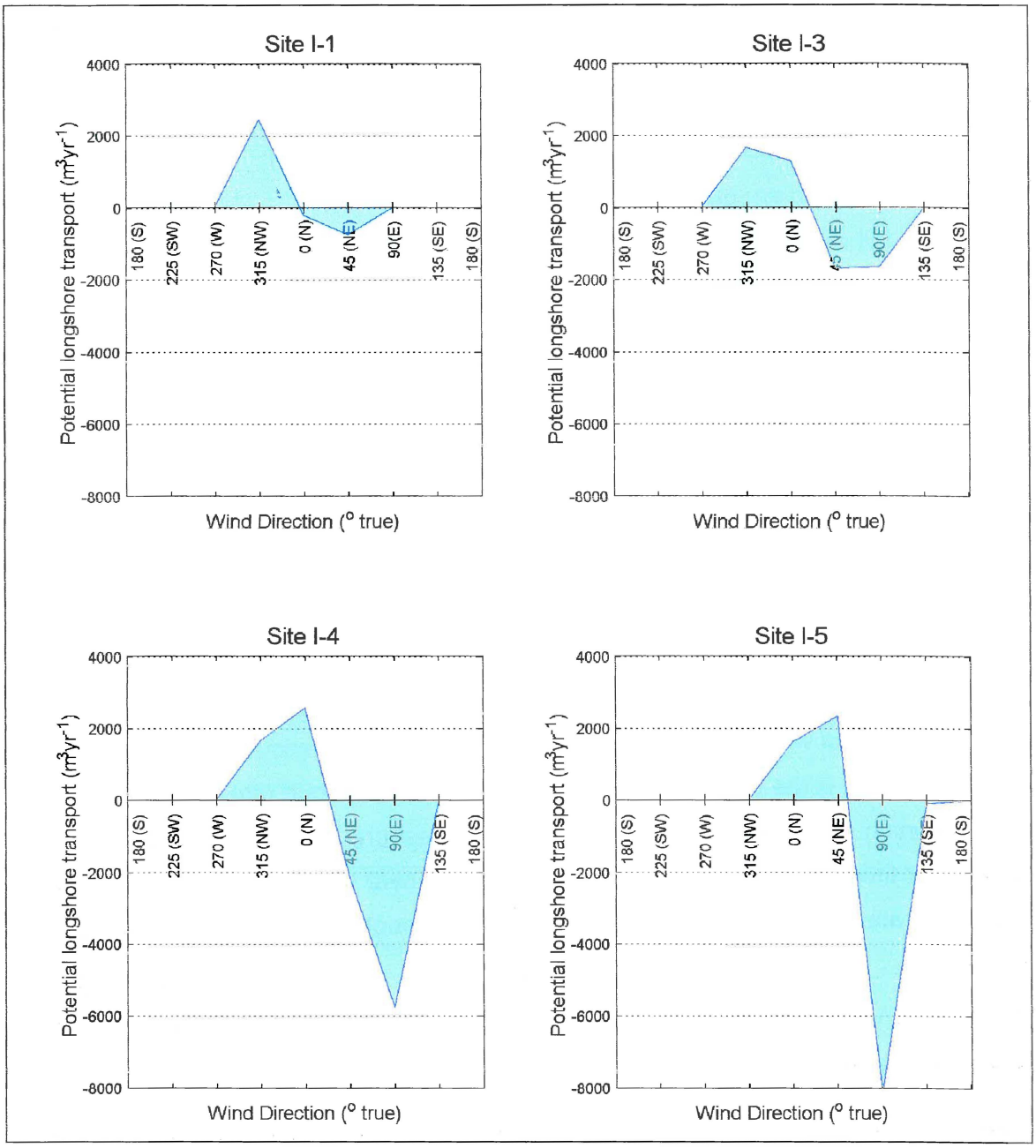


Figure 8.17 – *Mass curves showing potential longshore sediment transport at sites I-1,I-3,I-4 and I-5. Negative values indicate transport up-harbour (toward the left of an observer standing on the beach looking seaward). Transport rates are weighted by the probability of the specific wind direction (and strength).*

Site	Q_{lw}(net), Weighted yearly transport rate (m^3yr^{-1})
I-1	1500 (down-harbour)
I-3	-400 (up-harbour)
I-4	-3700 (up-harbour)
I-5	-4200 (up-harbour)

Table 8.10 – *Weighted net yearly transport rates at the foreshore due to wind generated waves. Weighted transport calculated from probability of specific wind speed and direction occurring and time of wave action on foreshore.*

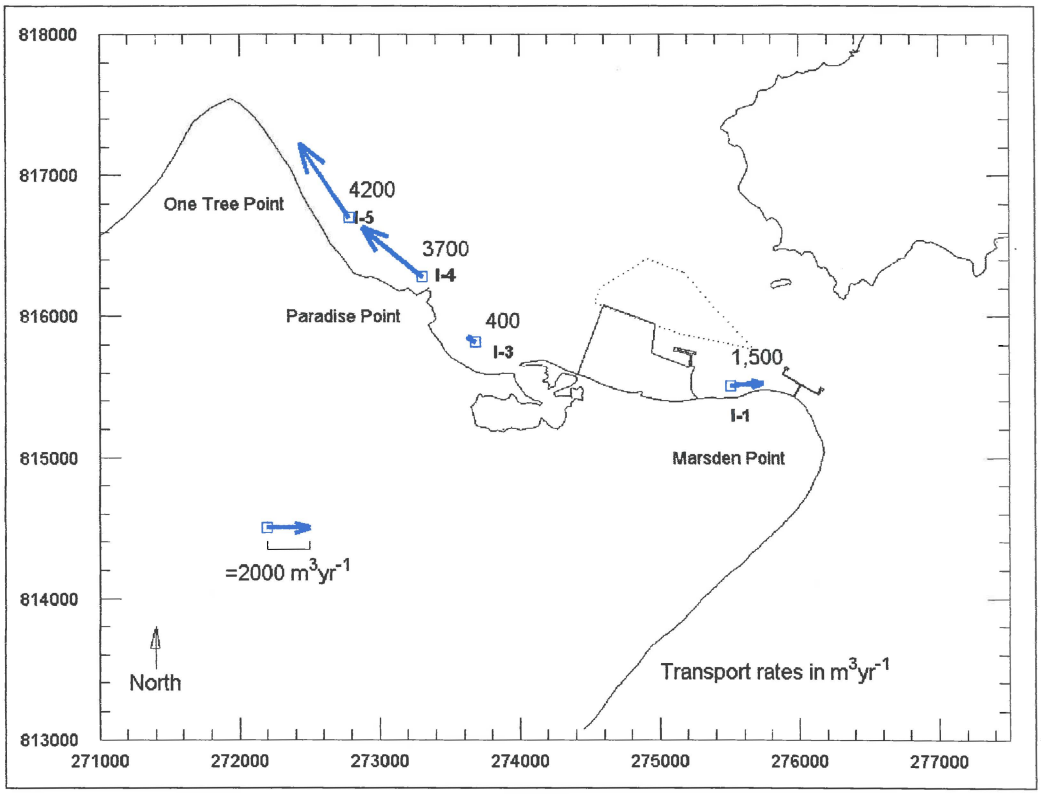


Figure 8.18 – *Assessed yearly longshore transport vectors due to wave action on the beach face. Accuracy estimate ± 50%.*

Wind generated waves and their associated currents provide the potential for the transport of ~1,500 m^3yr^{-1} of sediment toward the NZRC jetties on the beach face between Northport and the NZRC jetties (Figure 8.18). Pre-development, this location (Site I-1) would have had a greater fetch to the west (Figure 8.18), resulting in a larger wind-wave generated transport in the easterly direction and a larger magnitude than that observed with the present situation.

An observed pattern of accretion of the order of 1,000 m^3yr^{-1} of sediment adjacent the eastern edge of the Northport reclamation (Sections 5.6.2 and 6.7.3, Figures 5.34 and 6.9) is in conflict with this transport direction.

The potential wave generated transport rates at the foreshore between Sites I-3 and I-5 are of a consistent direction, toward One Tree Point. The magnitude of the transport increases in the same direction as the transport (Figure 8.18). The net potential wave driven sediment transport rate, along the foreshore of eastern One Tree Point, accelerates towards One Tree Point. Accelerating (i.e. increasing magnitudes) sediment transport vectors imply the progressive removal of material over the area of acceleration; there is the potential for more sediment to leave the *'box'* than to enter it, suggesting that eventually the sea floor over this area will become shell lagged.

Beach profiles (Chapter 5) and aerial photographs (Chapter 4) in this area show narrow, sediment starved beaches. The direction of sediment movement (in a northeast direction toward One Tree Point) that is suggested by the calculations is consistent with directions inferred from morphologic examination of beach widths in the area (Figure 4.7 and 4.8).

8.6 Longshore Transport by Waves and Currents Over the Inter-tidal Zone

8.6.1 Introduction

Longshore sediment transport in the nearshore and over inter-tidal areas occurs due to the combined effects of waves and currents. Variations or alterations in longshore sediment transport rates can cause local erosion or accretion. With sound knowledge of longshore sediment transport directions and magnitudes coastal structures can be designed accordingly, to have the desired effect and minimal undesirable results.

This section assesses the longshore sediment transport surrounding Marsden Point from measurements of both waves and currents. Results are compared with previous findings to estimate changes and predict sediment impoundment (accretion) or erosion by coastal structures in the region.

8.6.2 Methods

Tidal currents are expected to have an influence over longshore current velocities over the inter-tidal terraces of the measurement sites (I-1 to I-4, Figure 8.1). The longshore current method (Inman and Bagnold, 1963) does not discriminate between potential causes of longshore currents (e.g. oblique wave attack, tidal currents, wind generated currents, cell circulation), making it applicable to the inter-tidal terraces surrounding Marsden Point.

The equations of the longshore current method (Inman and Bagnold, 1963) were derived on the basis of considerations of the processes of sand transport is broader in its potential applications and should be viewed as more fundamental than the empirical correlations with longshore wave power (energy flux method, Section 8.5) (Komar, 1998).

The longshore current method is used to determine potential sediment transport rates at the sites of concurrent wave and current measurements (Sites I-1 to I-4) surrounding Marsden Point.

8.6.2.1 *Longshore Current Method*

Early workers such as Grant (1943) (in USACE, 2002) stressed that sand transport results from the combined effects of waves and currents i.e. waves entrain the sediment while the longshore current provides the transport mechanism. Inman and Bagnold (1963) in Komar (1998) formulated the relationship:

$$I_l = K'\left(EC_g\right)_b \frac{\bar{v}_l}{u_{mb}} \qquad \textbf{(8.23 Inman and Bagnold, 1963)}$$

Where $\bar{v}_l$ is the longshore current velocity, in practice measured at the mid-surf position and u_{mb} is the maximum horizontal orbital velocity of the waves evaluated at the breaker zone. $(EC_g)_b$ is the wave energy flux or power evaluated at the breaker zone and K' is a dimensionless coefficient generally accepted to equal 0.25, following a summary of measurements from several studies (Kraus et al., 1982).

Taking $E_b=(1/8)\rho g H_b^2$ for the wave energy density and

$u_{mb} = \sqrt{2E_b / \rho h_b} = 0.5\sqrt{\gamma g H_b}$ for the orbital velocity (from linear wave theory), (γ is the ratio of wave height to water depth ≈ 0.78 at break point), Komar (1998), used the accepted K' value of 0.25 to develop the relationship:

$$I_l = 0.044 \rho g H_{bs}^2 \bar{v}_l \qquad \textbf{(8.24 Komar, 1998)}$$

Where the breaker height (H_{bs}) is the significant wave height. The use of equation 8.20 along with 8.24 in order to obtain the volume transport rate (Q_l) led Komar (1998) to the equation (using quartz-density sand):

$$Q_l = 0.044 \rho g H_{bs}^2 \bar{v}_l \qquad \textbf{(8.25 Komar, 1998 [eq 9.10b p394])}$$

Komar (1998) noted "*The equivalence of the coefficients in equation [8.24] and [8.25] is fortuitous and results from* $(\rho_s-\rho)a'/\rho_s \approx 1$ *for quartz density sand in seawater with* $a'=0.6$." Here a' is the pore-space factor equal to $1-n$ (Equation 8.20).

The equivalence of equations 8.24 and 8.25 (9.10b and 9.10a in Komar, 1998) noted by Komar (1998) is considered incorrect. Simple substitution into Komar's (1998) own statement of "$(\rho_s-\rho)a'/\rho_s \approx 1$" with the common values of ρ_s = 2650 kgm^{-3}, ρ = 1025 kgm^{-3} and a' = 0.4 gives 0.369, a long way off ≈ 1.

By substituting equation 8.25 into 8.20, a more correct expression for the volume transport rate is obtained:

$$Q_l = \frac{0.0733\rho H_{bs}^2 \overline{v}_l}{(\rho_s - \rho)} \qquad \textbf{(8.26)}$$

Assuming a pore space factor of 0.6, as Komar (1998) had earlier in the derivation. Equation 8.26 should be considered the correct equation for the volume transport rate rather than Komar's (1998) equation (Equation 8.25). This error has been corrected in subsequent printings of Komar's (1998) book (pers. comm. P. Komar, 2004)

Equations 8.24 and 8.26 have several advantages over the longshore component of wave power formulations of equation 8.17 in the preceding section. It is often easier and more accurate to measure the longshore current $\overline{v}_l$ than it is to determine the breaker angle α_b needed in the wave power formulation (Komar, 1998). Equation 8.23 was derived from Bagnold (1963) and Inman and Bagnold (1963) on the basis of considerations of the processes of sand transport, and accordingly should be viewed as more fundamental than the empirical correlations with P_l (Section 8.5) (Komar, 1998). The original longshore current $\overline{v}_l$ in Inman and Bagnold's (1963) equation (Equation 8.23), also present in equations 8.24 and 8.26, was never specified (Komar, 1998) and so its generation could be due to an oblique wave approach, tidal currents, cell circulations or driven by local winds.

8.6.2.2 *Methods of Calculation*

Shoreline orientations relative to true north were obtained from Northport data files (Table 8.7). One-minute average velocities from the FSI current meter deployments at Sites I-1 to I-4 (Figure 8.1, Tables 8.3 and 8.4) were decomposed into longshore (V_l) and on/off-shore (V_o) components relative to the orientation of the coast at the site.

Significant wave heights were measured by Dobie wave gauges concurrently with the water velocities at Sites I-1 to I-4 (Table 8.3). Wave heights were sampled over a 3 m 24.8 s period every half hour (Table 8.3). Significant wave heights measured during this period were assigned to the one-minute velocities for the 15 mins either side of the wave height sampling time, resulting in a matrix of one-minute averaged velocities in one column and the assigned wave heights in a second column. This was performed by the MATLAB® program "*waveH2V.m*" written by this author (Appendix F).

Potential longshore sediment transport estimates for each velocity measurement was calculated using equation 8.26 in the MATLAB® program "*getQl.m*" written by this author (Appendix F). Sediment density was assumed to be that of quartz (2650 kgm^{-3}) and the water density that of seawater (1025 kgm^{-3}).

Both the net and gross sediment transport over the tidal cycle can be found by numerical integration of the time varying potential transport:

$$Q_{lNET} = \int_{T=0}^{T=12.42\,hrs} Q_l(t).dt \qquad \textbf{(8.27)}$$

and

$$Q_{lGROSS} = \int_{T=0}^{T=12.42\,hrs} |Q_l(t)|.dt \qquad \textbf{(8.27)}$$

The trapezoidal method of numerical integration was employed in the MATLAB® program "*net_gross_transport.m*", written by tise author (Appendix F), to determine the volume of potential sediment movement during the deployments. Transport rates were converted to units of m^3yr^{-1} for ease of comparison and consistency with other measurements (rather than $m^3tidalcyle^{-1}$). It should be remembered however, that the rates reflect measurements from a single tidal cycle and cannot be accurately extrapolated due to potential variations in wave conditions.

8.6.2.3 Limitations and Assumptions

Applying calculated sediment transport rates to a field site assumes the availability of sediment for transport. Should there be some factor limiting the availability of sediment, calculated sediment transport rates will not be realised. Calculated sediment transport rates should therefore be thought of as potential sediment transport rates rather than absolutes.

Only one tidal cycle has been monitored for wave heights and longshore water current velocities. Any estimated sediment transport rates calculated from this data will bear the influence of the conditions occurring during that tidal cycle e.g. tidal range and wave conditions. While it is possible to correct velocities (and therefore longshore velocities) for variations in the tidal range, such an exercise would be redundant in this case as the results would still be influenced by a single tidal cycle's wave conditions.

In order to mitigate the effect of the wave conditions on the calculated sediment transport rates, a time when weather conditions reflected *'typical'* conditions at

Marsden Point was selected for the deployment. *'Typical'* conditions at Marsden Point consist of winds generally less than 5 ms^{-1} (10 knots) from the west (20%) or southwest (13%) (Figure 2.5, Section 2.7), calm wave conditions within the harbour and a waves of average height ~0.4 m with periods of 5-7 s at the coast (near Site I-2) (Barnett, 2002). Wind conditions during the deployments are shown in Appendix F and are similar to those *'typical'* of the region. The incident wave climate at Site I-2 is similar to that described by Barnett (2002) (Figure 8.19) and wave conditions within the harbour were relatively calm (Figure 8.19).

While this is all that can be done to mitigate the effects of the wave climate apparent at the time of measurement, it should be taken into consideration that the estimated sediment transport rates reflect the wave conditions from the deployment and that changes to these conditions will affect the transport rates.

The propagation of errors (from measurements and relationships used) through the calculations is estimated to result in a final volume flux which of an appropriate order of magnitude, and accurate within ± 50%.

8.6.3 Results

Longshore velocities, on/offshore velocities, significant wave heights, mean spectral periods and the potential longshore sediment transport rates over tidal cycles at each site are shown in Figure 8.19.

Site I-1, located between Northport and the NZRC jetties (Figure 8.20) displayed very low on/off shore velocities and faster ebb flows than flood flows (Figure 8.19). Sediment is estimated to be transported only when waves were present in order to entrain the material. Sediment was transported toward Northport on the flood tide and in the opposite direction during ebb flows. The net tidal cycle transport rate was ~1,600 m^3yr^{-1} and directed toward the NZRC jetties (Table 8.7, Figure 8.20). A much larger amount of sediment (~5,100 m^3yr^{-1}) is mobilised during the tidal cycle.

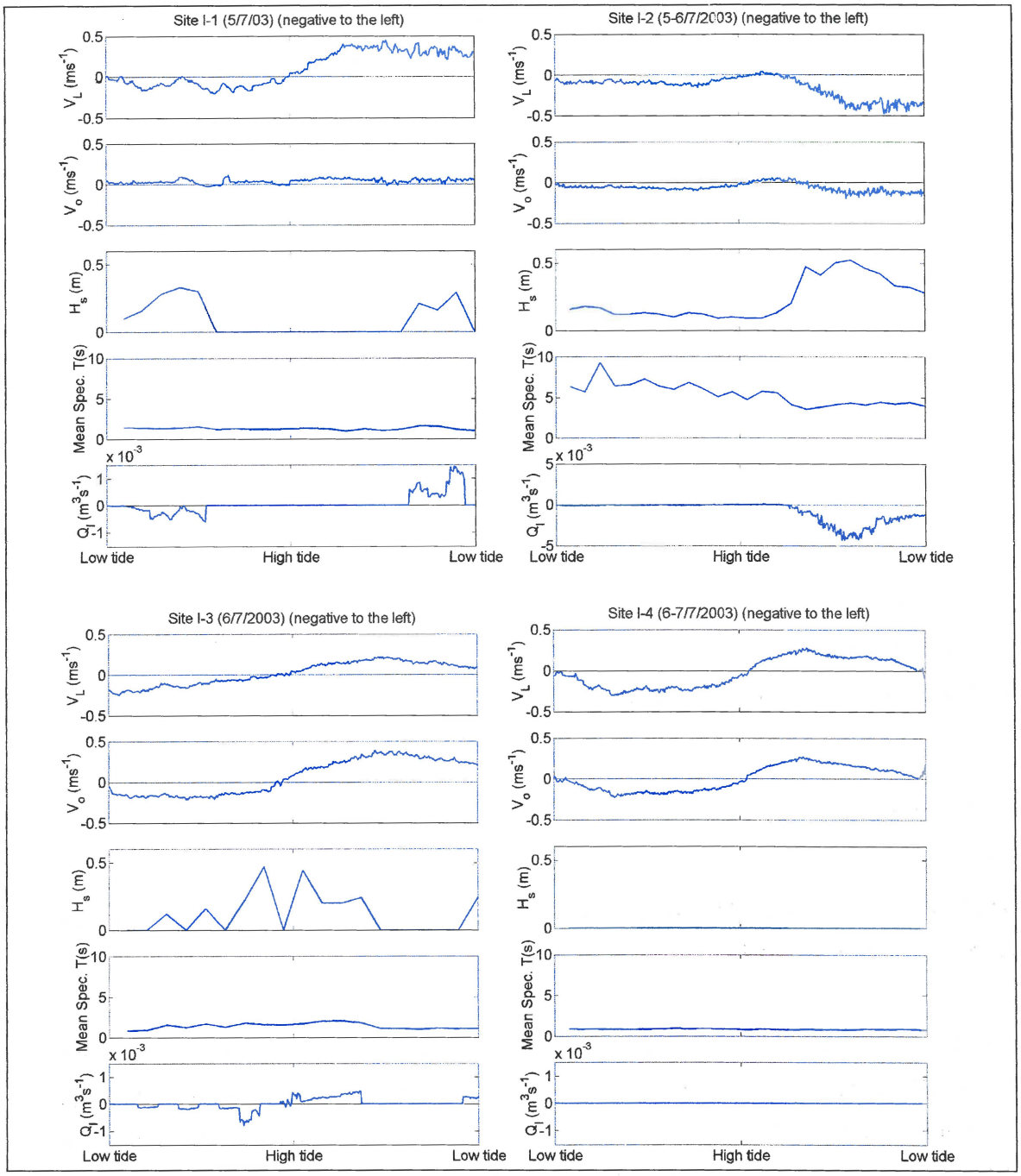


Figure 8.19 – *Longshore velocity (V_L), on/offshore velocity (V_o), significant wave height (H_s), mean spectral period of waves and the calculated longshore sediment transport over tidal cycles at sites I-1 to I-4. Note the change in scale for the plot of Q_l at Site I-2. Velocity measurements taken every minute and wave statistics every half hour. Positive longshore velocities are directed down-harbour and positive on / offshore velocities are directed offshore. * No waves present at Site I-4 during deployment.*

Site	Net potential transport (m^{3}yr^{-1})	Gross potential transport (m^{3}yr^{-1})
I-1	1,600 (down-harbour)	5,100
I-2	-25,500 (up-harbour)	25,600
I-3	300 (down-harbour)	3,600
I-4	0*	0*

Table 8.11 – *Net and Gross potential sediment transport rates at Sites I-1 to I-4. Negative values for Net transport indicate transport directed up-harbour, positive values indicate transport directed down-harbour. Note that while expressed as m^{3}yr^{-1}, the measurements reflect only a single tidal cycle. *No waves present during instrument deployment.*

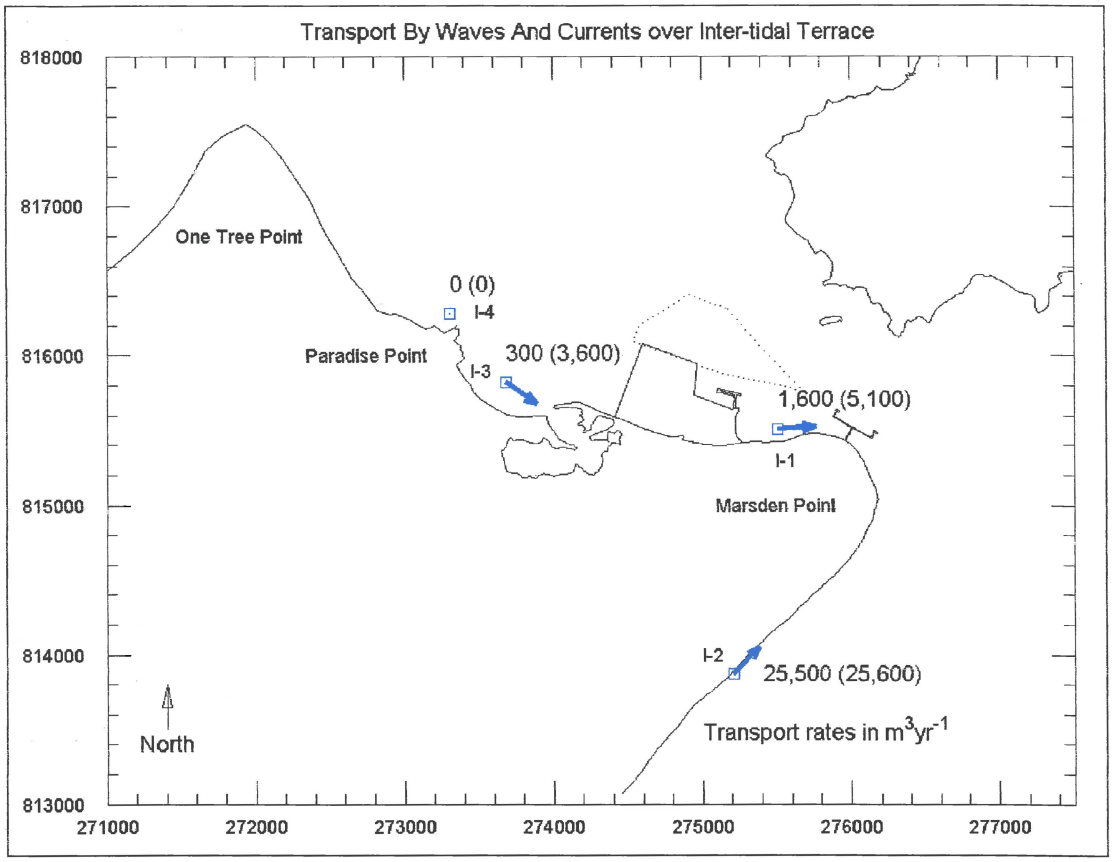


Figure 8.20 – *Net (and Gross) sediment transport over individual (separate) tidal cycles as assessed using equation 8.25. Care must be taken using the values to represent year long patterns as the rates were determined from individual tidal cycles. * No waves present at Site I-4 during deployment. Accuracy estimate ± 50%.*

Site I-2, along Bream Bay Beach was subject to waves of longer mean period than other sites (Figure 8.19). On/offshore velocities were small. The longshore velocity is consistently directed towards Marsden Point and Mair Bank during both flood and ebb flows. The magnitude of potential sediment transport closely mimics the change in significant wave heights (Figure 8.19). The potential sediment transport increased during the ebb tide, however it is likely that this was the result of an increase in wave heights occurring at the same time (Figure 8.19). Due to the asymmetry of the longshore velocity here almost all of the sediment transport is directed toward Marsden Point and is evident from the very small difference between the net and gross transport rates (Table 8.7, Figure 8.20).

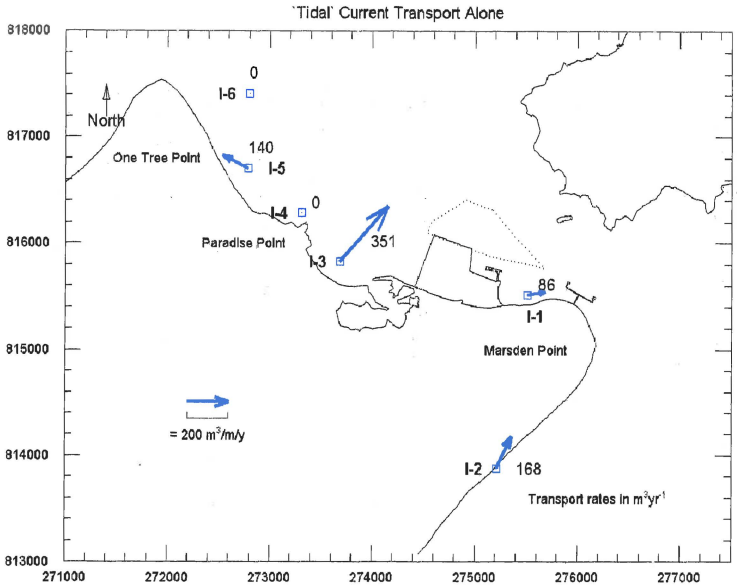
The rate of potential sediment transport measured at this site is much larger than those measured inside the harbour (Table 8.7). Reasons for this are likely due to the greater exposure of the site to swell waves and also the dominance of a northerly longshore current throughout the tidal cycle.

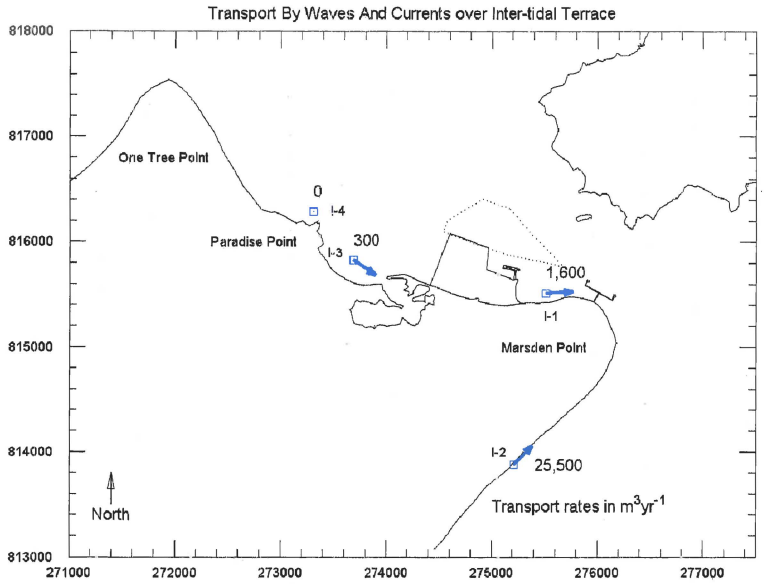
Site I-3, situated over a more expansive inter-tidal terrace, exhibits larger on-offshore velocities through the tidal cycle (Figure 8.20); these may be influenced by the close proximity of Blacksmiths Creek channel. Mean spectral periods of the waves are low (~1-2 s), consistent with local wind generated waves with limited fetch area. Longshore sediment transport is directed up-harbour during flood flows and out of the harbour, toward Northport during ebb flows. Net tidal cycle transport is directed alongshore toward Northport at a rate of ~300 m^3yr^{-1} (Table 8.7, Figure 8.20). The net sediment transport rate is much less than that mobilised during the entire tidal cycle (~3,600 m^3yr^{-1})(Table 8.7).

At Site I-4, located off Paradise Point, no waves were measured. The equation used to calculate the potential longshore sediment transport (Equation 8.26), while not relying on waves to create a longshore current (as in the energy flux method), does require waves to entrain sediment and initiate the sediment motion. The predicted sediment transport at this location is zero as no waves were measured which were capable of entraining the sediment.

8.7 Discussion of Northport – One Tree Point Inter-tidal Area Sediment Transport

Consideration of the various mechanisms contributing to the overall sediment transport over the inter-tidal area allows a more complete understanding of the sediment transport system present. Figure 8.21 shows the potential sediment transport vectors generated from one minute averaged water currents, local wind generated waves and waves and currents in combination.





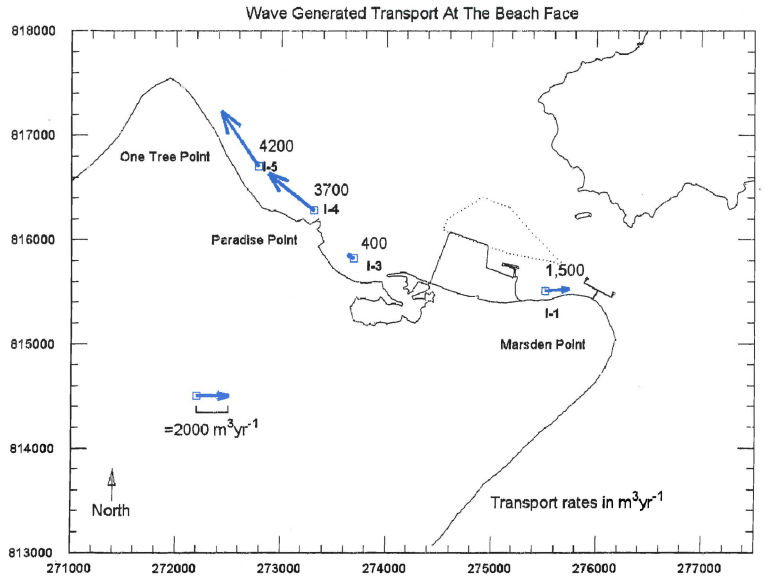


Figure 8.21- *Sediment transport vectors over the inter-tidal areas surrounding Northport. Tidal current transport from one -minute average excess velocities cubed. Wave generated transport at the beach face from longshore component of wave power (hindcast wave data) and transport by combined waves and currents from the longshore current method (extrapolated from single tidal cycle). Volumetric rates for tidal current transport estimated by multiplication of 'per unit width' measures by characteristic widths at the specific location. Both transport by waves and by waves and currents refer to longshore components only. Accuracy estimate ± 50%.*

8.7.1 Inter-tidal Transport at Site I-1 (Marsden Point)

At Site I-1, the direction of sediment transport obtained using the three different methods is similar, from Northport toward the NZRC jetties (Figure 8.21). Predicted volumes of transport by tidal currents over the inter-tidal area (86 m^3yr^{-1}) and by local wind generated waves over the beach face (~1,500 m^3yr^{-1}) relate well to the value of 1,600 m^3yr^{-1} obtained using a method incorporating both tidal current and wave current influences (Figure 8.21). There is thorough evidence of a potential net sediment transport along the beach at Site I-1 toward the NZRC jetties, the magnitude of which is ~1,600 m^3yr^{-1}.

The direction of transport at Site I-1 is consistent with a pattern of observed sediment accumulation against a causeway located in the center of the now Northport reclamation (Poynter, 1993). Sediment accumulation was noted between 1983 and 1993 although no estimations of transport volumes were made.

The general longshore transport direction is also consistent with that indicated by even-odd analysis of beach profile volumes and shorelines (Chapter 5, Figures 5.36, 5.37 and 5.38).

With the potential sediment transport directed along the beach, away from the reclamation, it would be expected that the beach at Site I-1 would show signs of sediment depletion, being down drift of an impoundment structure (Northport). Both beach profiles (Chapter 5, Figure 5.34) and sediment textural properties (Chapter 3) adjacent Site I-1 however, indicate recent deposition and accretion of sediment.

This raises the question "*Why is the beach here accreting if the net sediment transport is directed away from the reclamation?*".

It can be safely stated, in light of the present data, that the accretion of sediment against the western edge of Northport is not due to longshore transport generated by tidal currents, local wind generated waves or a combination of the two. The cause of the accumulation and source of the sediment can be speculated with reference to Figure 8.14, a map of sediment transport pathways adjacent to the site. It is interpreted that sediment from the southeasterly-directed pathway, immediately offshore, is being deposited in a *'current transport shadow zone'*, and of course at times when transport from the east (Marsden Point) (Figures 5.34 and 5.44) moves sediment there.

The magnitude of this deposition is expected to be equal to the rate of transport out of the area (~1,500 m^3yr^{-1}, Figure 8.17) added to the rate of observed sediment accumulation (~ 5 - 600 m^3yr^{-1}, Figure 5.34); that is, of the order of 2,000 m^3yr^{-1}.

The direction of sediment transport in this region implied from beach profiles alone (Chapter 5), has been shown to be incorrect (Section 5.9, Figure 5.44) and a more substantiated direction of longshore sediment movement established.

8.7.2 Inter-tidal Transport at Site I-2 (Bream Bay Beach)

Tidal currents alone at Site I-2 have the capacity to transport only a very limited volume in comparison to tidal currents and waves working together (Figure 8.21)

Previous estimates of longshore sediment transport along northern Bream Bay Beach (Site I-2) have been consistent in their direction while varying greatly in their magnitude (Table 8.12).

Study	Technique	Date under consideration	Direction	Magnitude (m^3yr^{-1})
Tonkin and Taylor (1979a)	Wave Hindcasting	Sth Pacific wind data 1945-1965	north	140,000*
Gibb (1979) in Tonkin and Taylor (1981)	N/A	N/A	north	<100,000
Tonkin and Taylor (1981)	CERC – Longuet-Higgins (energy flux)	1978 - 1980	north and south	19,000 north 45,000 south
	Bijker	1978 - 1980	north and south	9,000 north 13,000 south
DHI (1982a)	Beach Profiles, Air Photos and soundings	1959 - 1981	north	100,000 to 150,000
Present Measurements	Longshore current method	7/2003	north	26,000

Table 8.12 – *Previous estimations of longshore sediment transport at northern Bream Bay Beach (Site I-2). *Qualified by the statement "could be off by as much as a factor of three".*

Site I-2 was not used for the calculation of local wind wave generated transport rates at the beach face as the wave climate is influenced by a greater range of factors than just the local winds in isolation (Black 1983).

The potential sediment transport estimated using both the tidal currents and waves occurring at the time of instrument deployment (~25,500 m^3yr^{-1} to the north) is consistent in direction with previous values calculated for the area (Table 8.12).

All the previous studies of sediment transport in this area have used *'remote'* methods to determine the sediment flux. They have not measured any influencing mechanisms *'in-situ'* (e.g. wave height, wave direction and water currents). Estimates have instead been based on assessments of wave climates from wind roses, offshore wave climates or beach profile and air photo analysis (Table 8.12). Transport rates in this chapter at Site I-2 (Figure 8.21) have been calculated from the measurement two major influences on sediment transport (wave height and water velocity).

While the present estimate is in the same direction and of similar order of magnitude to many previous measurements, the effects of annual variations in the wave climate have not been taken into account.

Net sediment transport at Site I-2 is directed northwards toward Marsden Point and Mair Bank (Table 8.12, Figure 8.21). Mair Bank, actively accreting sediment between 1950 and 1981 (DHI, 1982a; Black and Healy, 1982; Black, 1983; Venus, 1984; Chapter 2) has been relatively stable (*c.f.* 1950 – 1981) in recent times (1981 to 1992, Barnett et al., 1993; 1995 to 2002, Chapter 6). Transport estimates of the DHI (1982a), Tonkin and Taylor (1979a, 1981) (Table 8.12) are influenced by the driving mechanisms resulting in the observed accretion at Mair Bank over these periods. This is reflected in their relatively large sediment transport rates. More recent estimates (including those calculated here) indicate a reduced capacity for transport, which is supported by the observed relative stability of Mair Bank.

8.7.3 Inter-tidal Transport at Site I-3 (Marsden Bay)

Sediment transport at Site I-3 consists of relatively equal contributions from both tidal currents along the inter-tidal terrace and wave induced transport at the beach face (Figure 8.21). There no consistent pattern to the direction of transport with the three methods employed indicating three different orientations. Net potential fluxes are relatively small (< 400 m^3yr^{-1}) compared with other sites.

The only previous work somewhat relating to sediment transport at this location is that of Poynter (1993) and Gibb (1998) who took into consideration sediment impoundment by a structure (causeway) with no volumetric estimates being made. Both Poynter (1993) and Gibb (1998) concluded that net sediment transport was from west to east (Figure 2.3) over the inter-tidal area.

Volumetric analysis of beach profiles along with even-odd analysis of the shoreline and profile volumes indicated a net sediment transport rate of ~ 5,000 m^3yr^{-1} directed eastwards towards the western edge of the Northport reclamation between 1997 and 2002 (Chapter 5, Figures 5.36, 5.37 and 5.38). This pattern did not change post-Northport construction.

Magnitudes of net potential sediment transport calculated at Site I-3 are an order of magnitude less than observed accretion against the western edge of Northport. The gross volumes calculated moving due to both waves and tides (~3,600 m^3yr^{-1}, Figure 8.20) are closer to volumes of observed accretion. Figure 8.13 indicates a sediment transport pathway immediately offshore of the inter-tidal zone directed toward the western edge of Northport, where the accretion is taking place. The solely tidal generated sediment transport is directed offshore at Site I-3 (Figure 8.21). Neither the wave generated transport at the beach face, nor the combined wave / current transport across the inter-tidal terrace can reflect this movement as they consider only longshore sediment movement. It is possible that the assumption of minimal on / offshore sediment transport maybe invalid at Site I-3.

Beach profiles near Site I-3 (Marsden Bay) have experienced a regular decline in sediment volumes at a rate of approximately 600 m^3yr^{-1} since nourishment in 1999 / 2000 (Figure 5.34). It is likely that this sediment is being moved offshore by *'tidal'* currents (which may include influences from Blacksmiths Creek flows). The sediment then joins the *'pathway'* directed toward Northport and results in both accretion against Northport's eastern rock wall and accretion of sediment in the dredge basin.

Implications of this transport are that initially sand will accumulate against the western edge of Northport (this has been observed already); concurrently some sediment is being transported into the Northport dredge basin on its western side. The proportion of the sediment that is transported into the dredge basin will increase as the beach and inter-tidal area here becomes more *'sediment rich'* and the bathymetry and profile created diverts more of the flow to deeper areas. Maintenance dredging requirements resulting from sediment inputs at the western edge of the dredge basin will increase over time until the beach against the western edge of Northport reaches its capacity. This is expected to occur in a time frame of 5-10 years.

8.7.4 Inter-tidal Transport at Sites I-4, I-5 and I-6 (Paradise Point to One Tree Point

No previous work has alluded to sediment transport near Sites I-4, I-5 or I-6.

Beach profile analysis indicated that the inter-tidal terraces are reasonably stable with very little change in profile volumes between 1997 and 2003 (Figure 5.34, profile 8), leading to the conclusion that there was very little net longshore sediment transport in the area (Chapter 5, Figure 5.44).

There is however, considerable potential for transport along the beach face of this shoreline (eastern One Tree Point) as a result of locally generated wind waves (Figure 8.21). The acceleration of the potential flux in a northeasterly direction leads to erosive conditions. The beach face is already relatively sediment starved (Chapter 4, Figure 4.6) having experienced erosion between 1984 and 2001 (Chapter 4, Figures 4.6 and 4.7). It is likely that this sediment has been transported along the beach face in a northeasterly direction. This direction of movement is consistent with morphologic patterns of beach narrowing (Chapter 4, Figures 4.7 and 4.8).

8.8 Summary of Sediment Transport, Debits and Credits at Marsden Point

Sediment transport rates determined within this chapter along with volumetric changes determined from beach profiles (Figure 5.44, Chapter 5) and bathymetry changes (Figure 6.11, Chapter 6) have been compiled in Figures 8.22 and 8.23 to provide an overall summary of potential sediment transport and implied areas of accretion and erosion.

The figures indicate that the likely source of the accumulating sediment against Northport's western rock wall is Marsden Bay – East, with both an offshore and alongshore sediment transport vectors present over the inter-tidal terrace (Figures 8.22 and 8.23).

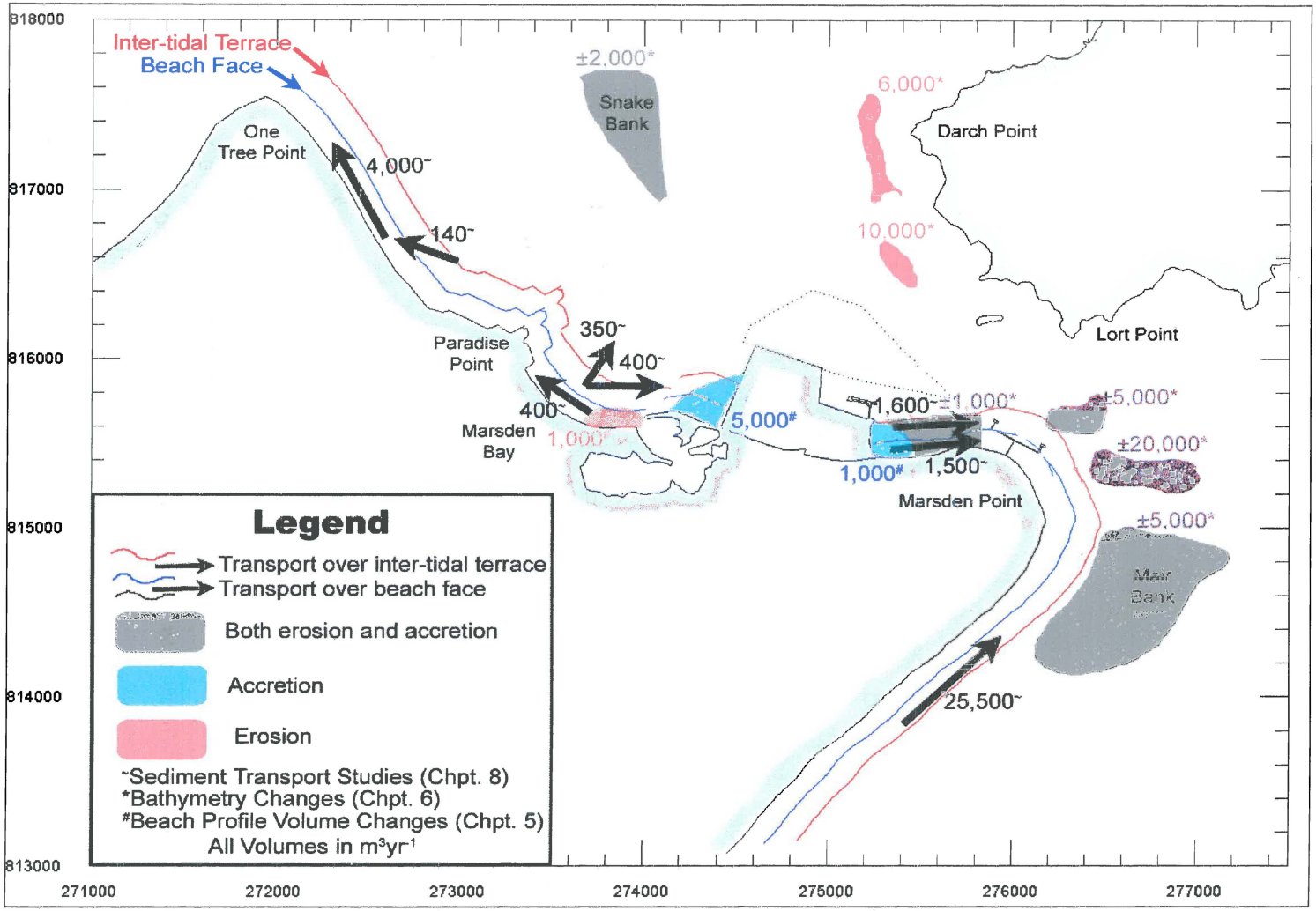


Figure 8.22–*Observed (areas) and potential (arrows) sediment transport, credits (accretion) and debits (erosion) for all sediments. Sediment transport evaluated July/November 2003 [Accuracy est ± 50%]. Erosion and accretion from beach profiles [± 10%] (1996 –2003) and bathymetry surveys [± 20%] (1995 – 2003).*

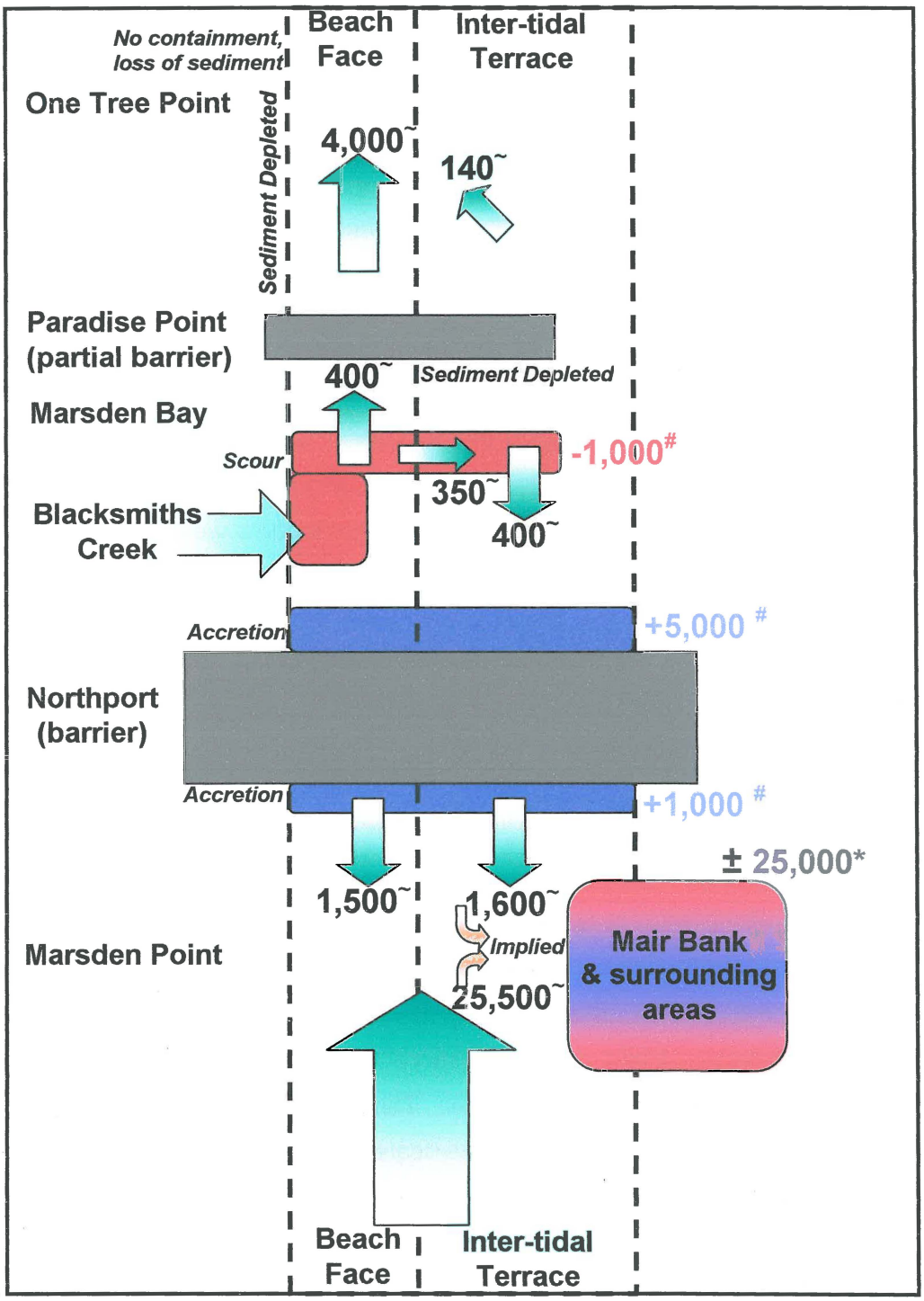


Figure 8.23 – *Schematic diagram of potential sediment transport, debits and credits in the Marden Point – One Tree Point region. All volumes are on an annual basis (m^3yr^{-1}) and are calculated from: ~sediment transport investigations [est. ± 50%] (Chapter 8), *bathymetric changes [± 20%] (Chapter 6), #beach profile volumetric changes [± 10%] (Chapter 5).*

The variability of Mair Bank and areas adjacent to the NZRC jetties, observed from bathymetric changes, is likely to be the result of the opposing sediment transport vectors directed towards Marsden Point (and the general area of Mair Bank) along both Bream Bay Beach and from between Northport and the NZRC jetties, on the other side of Marsden Point (Figures 8.22 and 8.23).

8.9 Implications of Sediment Transport

One Tree Point - Any sediment present along the One Tree Point shoreline will be transported in a northwesterly direction. As there is no structure to retain the sediment it will ultimately be lost to the system. The beach face will be sediment depleted, with narrow dry beach widths, as has been identified by both aerial photographs (Chapter 4) and beach profiles (Chapter 5).

Marsden Bay – There is potential for sediment is being moved in a northwesterly direction along the beach face toward Paradise Point, however some morphologic evidence indicates periods of transport in the other direction (Chapter 4). Over the inter-tidal terrace sediment is being transported off shore and down harbour toward Northport. This sediment is accumulating against Northport's western rock wall at a rate of $400m^3y^{-1}$ (± *50%)*. Beach profiles have shown an increase in sediment at a faster rate than this due to the contributions from a sediment transport pathway directed down harbour on the channel margins here (Figures 8.12 and 8.14). It is predicted that once this area becomes *full* of sediment (estimated 5 - 10 years) that the bathymetry and cross-section of the profile will result in increasing volumes of sediment being deposited in the dredge basin.

Northport, Marsden Point, Bream Bay Beach and Mair Bank – While there is sediment accumulating against Northport's eastern rock wall, the potential sediment transport vectors over the beach face and inter-tidal terrace are directed toward Marsden Point. Accretion is occurring in a *'current transport shadow zone'*. Also directed toward Marsden Point is the longshore transport along the beach face at Bream Bay Beach (Figures 8.22 and 8.23). These co-incident sediment transport vectors would be expected to result in large-scale accretion at Marsden Point. The meeting of the opposing longshore transport vectors has caused the ebb tidal delta (Mair Bank) to become *'welded'* to the shoreline (Figure 4.5). Progradation has been has been observed between 1984 and 2001 (Table 4.2). It is inferred that Mair Bank plays a significant role in the transfer of the sediment along these beaches, evidenced by the changes in bathymetry observed (± 25,500 m^3yr^{-1} Figure 8.23), the transfer of sediment to Mair Bank prevents the large scale and continuing progradation of Marsden Point due to the opposing sediment transport directions.

Dredge Basin – The dredge basin is being in filled with sediment due to downward movement on the batter slopes, the effect of this is greatest immediately to the east of the Northport quay wharf (Figure 7.9). At the eastern most tip of the dredge basin sediment is being moved down harbour (Figures 7.9 and 8.12) and a *'lagged'* or *'armoured'* bed is predicted to develop. Maintenance dredging requirements are expected to increase to the order of 15-20,000 m^3yr^{-1} over the next 5 to 10 years as the beach profile to the west of Northport becomes more *'sediment rich'*.

8.10 Conclusions

- Equations 9.10a and 9.10b in Komar's (1998) book "*Beach Processes and Sedimentation 2nd ed.*" should be considered incorrect, with a more accurate formulation being that of equation 8.26 of this Chapter.

- There is potential for sediment to be transported into the harbour in the center of the harbour entrance, a balancing return sediment pathway exists nearer the southern shoreline, close to the Northport dredge basin.

- There is some degree of leakage between the two opposing sediment transport pathways in the region surrounding the eastern extent of the Northport dredge basin.

- Potential for scour and the development of a shell lag (armoured bottom) exists at the southeastern extent of the Northport dredge basin. Limited scour has already occurred at this location.

- Sediment transport patterns in the lower harbours channel and channel margins surrounding Northport are very similar to those existing in 1983, prior to the Northport development. There is however, reduced sediment transport capacity in an up-harbour direction at the northern extent of the Northport dredge basin.

- The rate of sediment accumulation in the dredge basin is expected to increase to 15-20,000 m^3yr^{-1} over the next 5 – 10 years as the beach to the west of Northport fills with sediment.

- Sediment transport over the inter-tidal zones due to tidal currents only is relatively limited surrounding Marsden Point.

- Locally generated wind waves provide a much more effective mechanism for the entrainment and transport of sediment over the beach face and inter-tidal areas than tidal currents in isolation.

- Sediment transport along northern Bream Bay Beach is directed northward at a rate of approximately 26,000 m^3yr^{-1}. Rates of movement have been much larger at times in the past (late 1970's).

- Sediment is transported toward the NZRC jetties over the inter-tidal terrace and beach face between Northport and the NZRC jetties at a rate of approximately 1,600 m^3yr^{-1}. The direction of this longshore transport is consistent with patterns observed prior to the development of Northport. The addition of sediment to the area at a greater rate than the longshore transport however, has resulted in local accretion.

- These opposing longshore sediment transport directions meet where the ebb tidal delta (Mair Bank) is '*welded*' to the shore and there is significant transfer of sediment from the beach to the ebb tidal delta.

- Sediment accumulating against Northport's eastern rock wall is predicted to be sourced from the southeasterly-directed transport pathway immediately adjacent.

- Sediment is being moved offshore at a rate of ~4 – 600 m^3yr^{-1} over the inter-tidal terrace of Marsden Bay. This movement is not as a result of locally generated wind wave action.

- Accelerating sediment transport potentials in a northwest direction along the eastern One Tree Point inter-tidal areas have caused the movement and erosion of sediment. The overall beach width has narrowed and thins in a southeasterly direction as a result.

9 POTENTIAL BEACH RENOURISHMENT, MARSDEN POINT – ONE TREE POINT

9.1 Introduction

"*In New Zealand, as at many other sites around the world, beach renourishment has been carried out ancillary to major coastal engineering works (such as harbour reconstruction, channel maintenance or extension) rather that for primary goals of arresting coastal erosion or enhancing beaches*" (Healy et al., 1990)

The potential use of material dredged from the Northport dredge basin as sediment for beach nourishment has been identified previously (NPC, 2000). No previous studies however, have analytically identified potential nourishment locations, compared dredge basin sediments with potential site sediments or developed a nourishment plan.

In this chapter a site for nourishment is identified, a nourishment plan developed utilising sediments originated from the Northport dredge basin, maintenance requirements and economic costs area also assessed.

9.2 The Case for Renourishment

The use of dredged material as fill for beach nourishment has precedent in New Zealand (Pohara Beach - Golden Bay, Pilot Bay Beach – Tauranga Harbour and Marsden Bay-East in 1999) and throughout the world (Healy et al., 1990). These schemes are attractive as dual benefits (dredging and renourishment) are realised at considerably less cost than if each process was undertaken individually.

The beach face, from mid-way along Marsden Bay to One Tree Point is '*sediment depleted*', exhibiting narrow dry-beach widths (Chapter 4) and reduced recreational potential compared with wider beach faces in the area.

Estimated maintenance dredging requirements from Northport's dredge basin result in the potential availability of between 10 and 50,000 m^3yr^{-1} of sediment (DHI, 1982a; Black, 1983; Montgomery Watson, 1997; Chapter 9).

Sediment sourced from the maintenance dredging of Northport's dredge basin may be used in reclamation projects or other developments as Northport sees fit. There is however, potential for the sediment (or some proportion of it) to be available for beach nourishment projects (pers. comm. J. Palmer 2003).

This potential provides a case for the Marsden Point – One Tree Point shoreline to be assessed for its renourishment suitability. Site characterisation has been undertaken within the previous chapters of this thesis (e.g. sediment characteristics, long-medium term coastal change patterns, beach volumetric analysis and sediment transport directions and magnitudes). A nourishment plan requires this information to be considered in order to assess the suitability of various locations for nourishment with the dredged sediment.

There is precedence for artificial beach replenishment in the lower Whangarei Harbour, with Marsden Bay – East being supplied with 8,000 m^3 of sediment in 1999 (Stevens, 1998, 1999). Sediment was placed to the east of the boat ramp in Marsden Bay and is detailed in Section 4.4.5 of this thesis.

9.3 Potential Sites for Renourishment

Long-medium term analysis of beach face changes (Chapter 4) found the following sites (Figure 9.1) had experienced narrowing of the dry beach width between 1981 and 2001:

i. One Tree Point – Central;
ii. One Tree Point – South;
iii. Marsden Bay – West; and
iv. Marsden Bay – Central.

Table 9.1 summarises the decrease in beach width over the medium term and also highlights the narrow dry beach present in the four areas.

The four sites, One Tree Point (Central and South) and Marsden Bay (West and Central) are identified as being locations that would benefit from additional sediment inputs. Additional sediment inputs would act to widen the dry beach (back to or exceeding previous levels), provide additional erosion resistance to the eroding sea cliffs along One Tree Point (Gibb, 1998), protect archaeological sites in the area (Gibb, 1998) and enhance the recreational opportunities of the coastline.

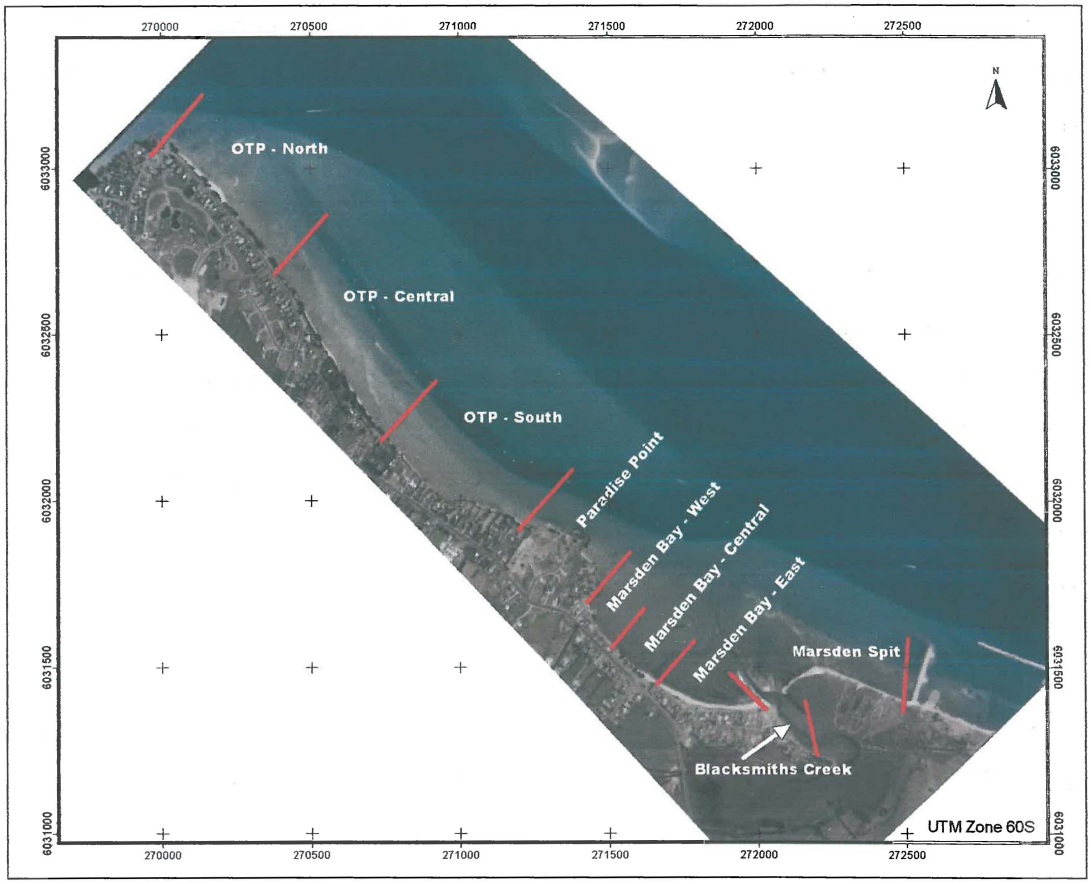


Figure 9.1 – *Area boundaries used for analysis of aerial photographs. Specific locations detailed in Appendix B. Narrowing of the dry beach width between 1981 and 2001 was observed at locations OTP-Central, OTP-South, Marsden Bay-West and Marsden Bay-Central. Note the comparably wide dry-beach at Marsden Bay-East, which was artificially nourished in 1999.*

Site	Profiles (Chapter 5)	Dry Beach Width (2001) (m)	Beach Narrowing (1981 – 2001) (m)	Source
One Tree Point – Central	P-10, P-11	8.2	4.1	Table 4.3, Figure 4.6
One Tree Point – South	P-8, P-9	9.8	1.2	Table 4.5, Figure 4.7
Marsden Bay – West	P-7	0	0	Table 4.7, Figure 4.10
Marsden Bay - Central	P-6	7.6	3.2	Table 4.7, Figure 4.10

Table 9.1 – *Dry-beach width and beach narrowing from analysis of aerial photographs interpretation.*

These areas are similar to those recommended by Gibb (1998) in his very brief appraisal of potential renourishment. A key difference however, is that Gibb (1998) recommended replenishment along the entire One Tree Point coastline. Both beach face sediment transport vectors (Figure 8.18) and patterns of beach narrowing (Figures 4.7 and 4.8) along the One Tree Point coastline indicate sediment transport directed up-harbour, towards the *'tip'* of One Tree Point. It is anticipated that sediment placed along central or southern One Tree Point will be transported in this direction. Sediment placed along the One Tree Point–North coastline would likely be transported out of the system relatively quickly.

This study provides a more complete understanding of the processes enabling effective beach nourishment along the One Tree Point – Marsden Point shoreline than that of Gibb (1998).

9.4 Suitability of Available Sediments

"*The single most important borrow material characteristic is the sediment grain size*" (USACE, 2002). The grain size distribution of the borrow material (dredge basin sediments) will affect the cross-shore shape of the nourished beach profile, the rate at which fill material is eroded, and how the beach will respond to storms (USACE, 2002).

Particle size distributions for the four sites and dredge basin are shown in Figure 9.2, whilst Table 9.2 contains a summary of selected particle size fractions.

Site	Mean (M_φ)	Mean (mm)	Standard Deviation (sorting) (σ_φ)	$\frac{\sigma_{\varphi b}}{\sigma_{\varphi n}}$	$\frac{M_{\varphi b} - M_{\varphi n}}{\sigma_{\varphi n}}$
One Tree Point-Central* ($_n$)	1.50	0.35	0.44	1.80	1.89
One Tree Point – South* ($_n$)	2.08	0.24	0.31	2.55	0.81
Marsden Bay – West# ($_n$)	1.96	0.26	0.39	2.03	0.95
Marsden Bay – Central# ($_n$)	2.09	0.23	0.52	1.52	0.46
Dredge Basin (5 sites)* ($_b$)	**2.33**	**0.20**	**0.79**	**N/A**	**N/A**

Table 9.2 – *Mean sediment sizes and standard deviations (sorting) for potential nourishment sites and dredge basin sediments. Values required for the calculation of James' (1975) overfill factor (R_A) evaluated from equations 9.1 and 9.2. #Data from RSA analysis of single sample. *Data from RSA analysis of multiple samples with mean and standard deviation (sorting) recalculated from average values (9.1 and 9.2).*

Nourishment can be effective if the borrow material does not exactly match native beach particle size distributions. James (1975) developed a method to calculate an overfill factor (R_A) and renourishment factor (R_J). The overfill factor (R_A) evaluates the volume of borrow material required to produce a stable unit of useable fill material with the same characteristics as the native beach sediments. The renourishment factor (R_J) addresses the higher alongshore transportability of the of the finer grain sizes in the borrow sediment and provides an estimate of renourishment needs. The United States Army Corps of Engineers (USACE) has since recommended that the renourishment factor (R_J) is no longer used in beach fill design calculations (USACE, 2002) and is thusly not evaluated in this case.

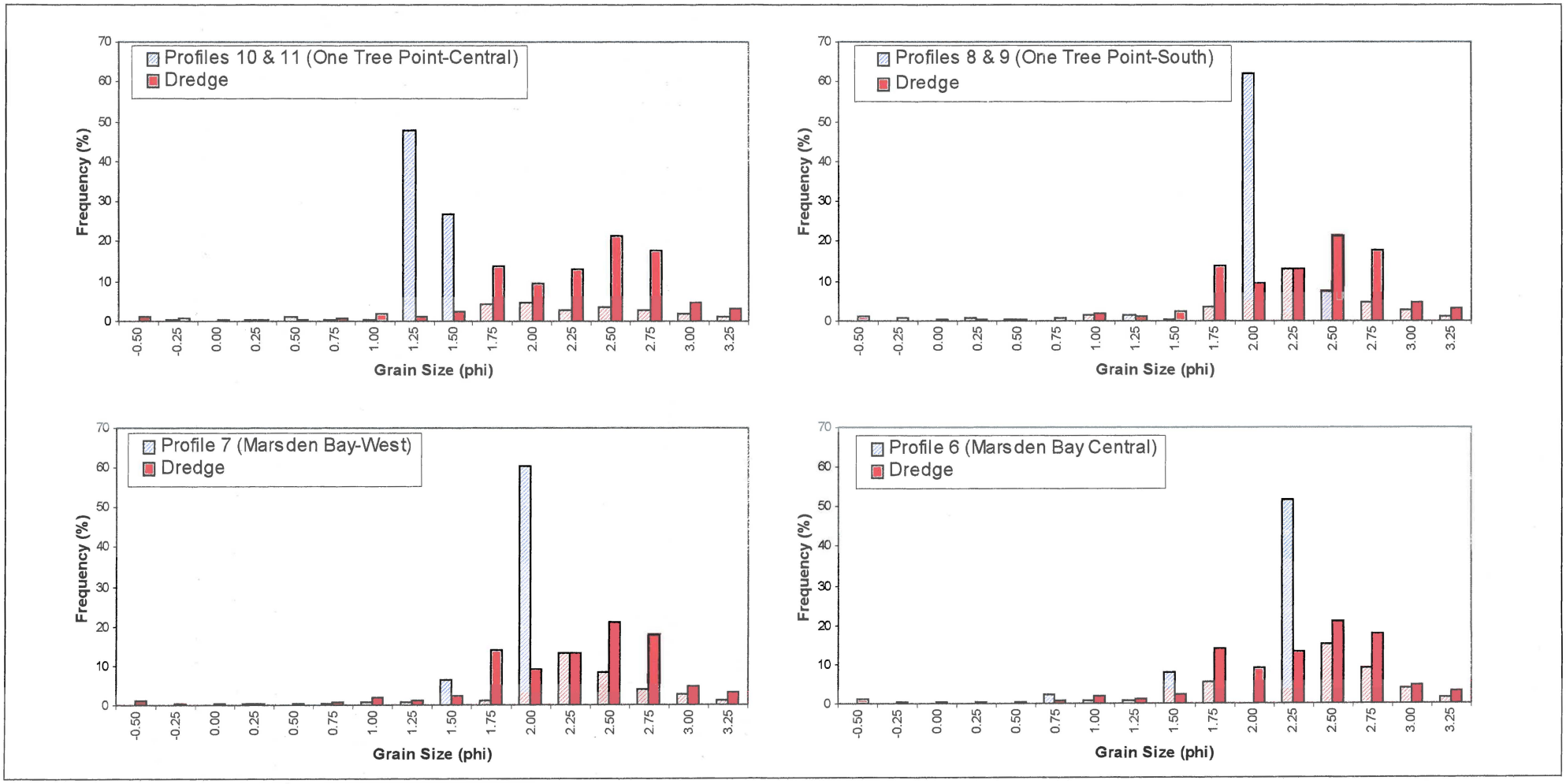


Figure 9.2 – *Particle size distribution for the prenourished 'native' beach face at potential nourishment sites and the dredge basin sediments (average of 5 sites). Tabulated data in Appendix G.*

9.4.1 Calculation of the Overfill Factor

The overfill factor (James, 1975) is calculated by comparing the mean sediment diameter and sorting values of the native beach and borrow sediments (in phi units, Table 3.1).

The following relationships between the borrow and native beach material are evaluated:

$$\frac{\sigma_{\varphi b}}{\sigma_{\varphi n}} = \frac{\left[\frac{(\varphi_{84}-\varphi_{16})}{4}+\frac{(\varphi_{95}-\varphi_{5})}{6}\right]_b}{\left[\frac{(\varphi_{84}-\varphi_{16})}{4}+\frac{(\varphi_{95}-\varphi_{5})}{6}\right]_n} \qquad \textbf{(9.1, CERC, 1984)}$$

and

$$\frac{M_{\varphi b}-M_{\varphi n}}{\sigma_{\varphi n}} = \frac{\left[\frac{(\varphi_{16}+\varphi_{50}+\varphi_{84})}{3}\right]_b - \left[\frac{(\varphi_{16}+\varphi_{50}+\varphi_{84})}{3}\right]_n}{\left[\frac{(\varphi_{84}-\varphi_{16})}{4}+\frac{(\varphi_{95}-\varphi_{5})}{6}\right]_n} \qquad \textbf{(9.2, CERC, 1984)}$$

Where $\sigma_{\varphi b}$ = standard deviation (sorting) of borrow material,
$\sigma_{\varphi n}$ = standard deviation (sorting) of native material,
$M_{\varphi b}$ = mean sediment diameter of borrow material and
$M_{\varphi b}$ = mean sediment diameter of native material. (all phi units)

These relationships have been calculated using the Marsden Point data (Table 9.2).

Values obtained (9.1 and 9.2) are then plotted on the graph presented in Figure 9.3 (CERC, 1984).

Overfill ratios for the four sites are (Figure 9.3):

i. One Tree Point – Central → R_A = 3.5 – 4.0,
ii. One Tree Point – South → R_A = 1.75 – 2.0,
iii. Marsden Bay – West → R_A = 1.75 – 2.0 and
iv. Marsden Bay – Central → R_A = 1.5 .

The compatibility of the dredge sediments with the native sand varies between the potential nourishment locations. The overfill ratios suggest that the dredged sediments, if used as beach '*fill*' will be more efficient at Marsden Bay – Central, where 1.5 units of dredge sediment will result in 1 unit of stable beach material, than at One Tree Point – Central, where 3.5 to 4.0 units of dredge sediment are required for each unit of stable beach material (Figure 9.3).

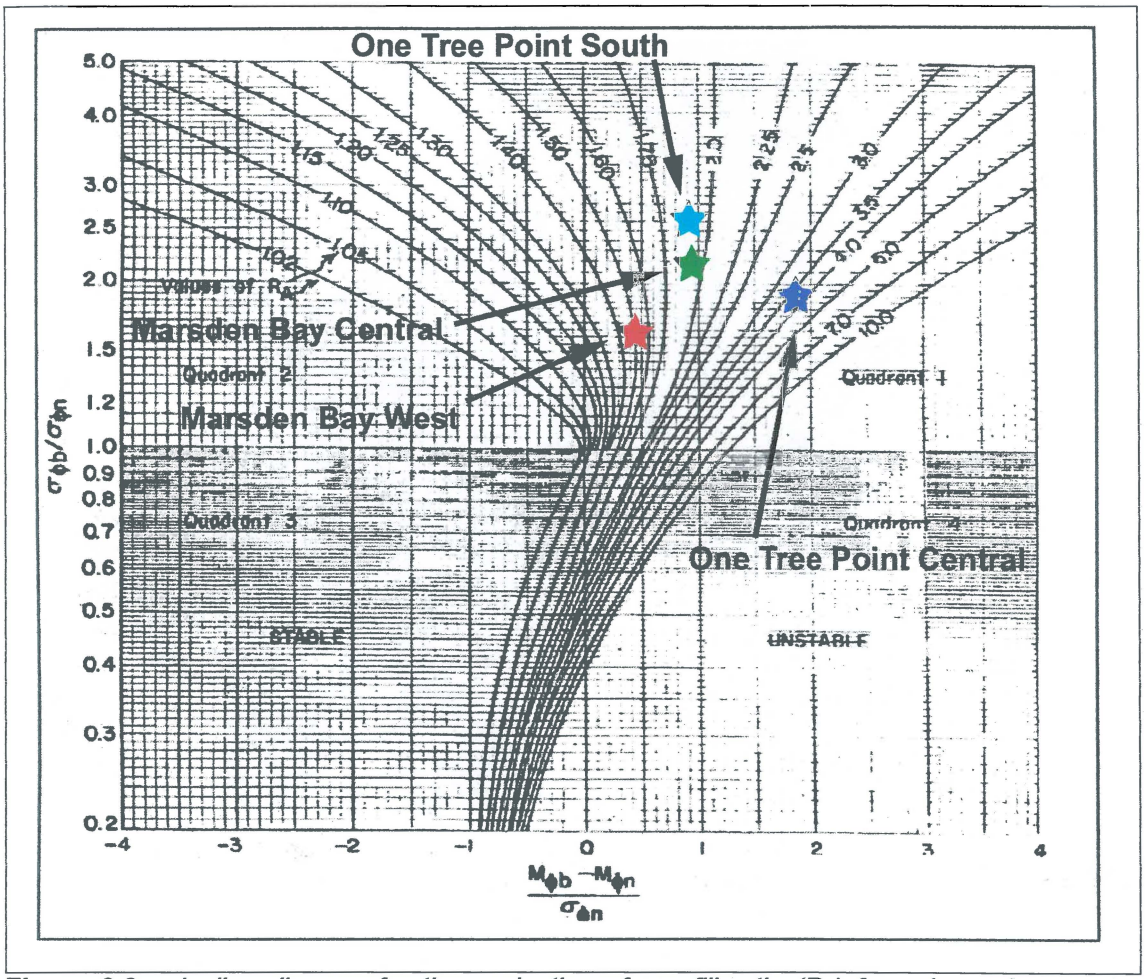


Figure 9.3 – *Isoline diagram for the evaluation of overfill ratio (R_A) for values of mean (φ) difference and sorting (φ) ratio of borrow sediments and native beach sediments (CERC, 1984). Values from prospective Marsden Point sites plotted as stars, values calculated in Table 9.2.*

It is clear that the most effective location for nourishment, with respect to volumes of sediment retained on the beach face only, is Marsden Bay – Central, followed by Marsden Bay – West and One Tree Point – South.

9.5 Selection of Nourishment Site

Both beach face sediment transport vectors (Figure 8.18) and patterns of beach narrowing (Figures 4.7 and 4.8) along the One Tree Point coastline indicate sediment transport directed up-harbour, toward the *'tip'* of One Tree Point. Overfill ratios (James, 1975) also increase toward One Tree Point (Figure 9.4).

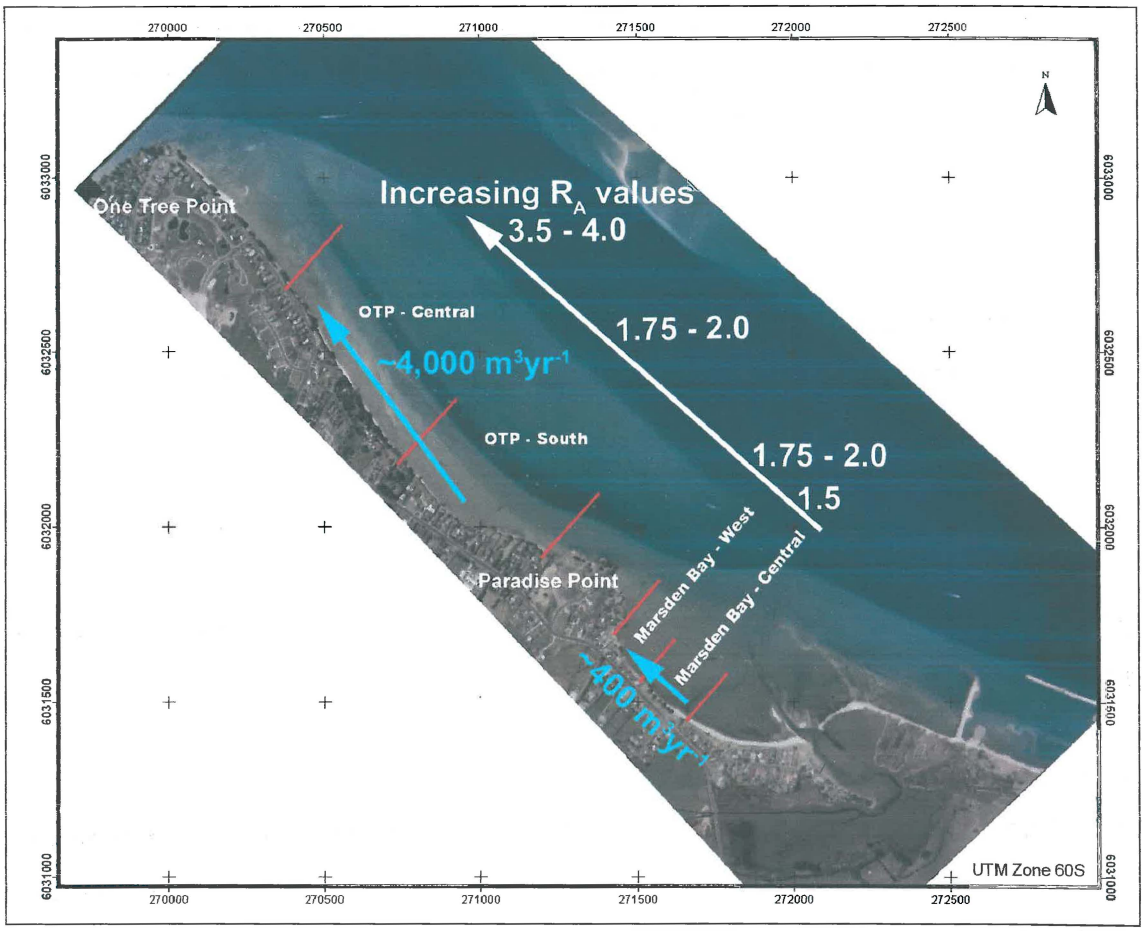


Figure 9.4 –B*each face sediment transport vectors and James' (1975) overfill ratios at potential nourishment sites. Beach face sediment transport from energy flux method (Section 8.5), James' (1975) overfill ratios from Figure 9.3.*

Marsden Bay-West presently (2003/4) has no dry beach face at high tide (Chapter 4), whilst Marsden Bay-Central has an average dry beach width of 7.6 m (Table 9.1).

Beach face sediment transport vectors indicate that sediment placed on Marsden Bay–West and Marsden Bay–Central would be transported toward Paradise Point at a rate of ~400 m^3yr^{-1} (Figure 9.4). Paradise Point is a prominent headland, down-drift of this transport that would act to trap much of the placed sediment in the Marsden Bay area.

Beach face sediment transport vectors (and beach morphology, Chapter 4) indicate that sediment placed on the One Tree Point (South or Central) beach face would be transported towards One Tree Point at a rate of ~4,000 m^3yr^{-1}. There are no natural or artificial (e.g. groyne) features present in this area that could act to impede this transport. Without such features or structures, there is the potential for sediment to be transported along the beach face to One Tree Point and ultimately *'lost'* to the system. It is recommended that:

> "*should beach nourishment be undertaken along the One Tree Point coastline, a groyne, groyne field, or other such structure(s) should be built to impede the longshore transport of sand in a north-westerly direction along the beach face*".

The Marsden Bay shoreline, with its relatively low magnitude of longshore sediment transport (~400 m^3yr^{-1}), natural impoundment feature (Paradise Point), narrower dry beach widths and more efficient overfill ratios (R_A = 1.5 – 2.0) is recommended as the most appropriate site for any initial beach face nourishment using sediments from the Northport dredge basin.

The Marsden Bay beach face is expected to utilize the *'fill'* more efficiently (lower R_A ratios) and have a longer life expectancy (smaller longshore transport magnitudes and impoundment feature) than any equivalent placement along the One Tree Point beach face.

Additional works required, should nourishment proceed along the Marsden Bay–Central and West beach face, include the lengthening or relocation of a stormwater pipe discharging at Marsden Bay–Central. Seawalls currently present along Marsden Bay–West could be either removed or retained behind the nourished beach as a last line of defence.

9.6 A Plan for Nourishment

The Marsden Bay (Central and West) coastline proposed for nourishment is 310 m long (Figure 9.5). Only the beach face is intended to be nourished, not the entire inter-tidal terrace. There are no natural dunes present along Marsden Bay and it is not proposed to create any in the nourishment plan.

9.6.1 Volumes of Sediment

A desirable beach profile (in keeping with other, more sediment rich profiles in the region) at Marsden Bay would include sand reaching, in a vertical extent, to the top of the seawalls (~+3.5 m C.D. Figure 9.6) and a dry beach width of between 15 and 20 m at high tide. This configuration represents 10,500 m^3 of sediment above MSL in the profile. Presently, there is approximately 2,900 m^3 of sediment above MSL. Using an overfill factor (R_A) conservatively estimated at 2.0 (Figure 9.4), the volume of dredge basin sediments required for placement is 15,200 m^3.

The constructed beach contains both the design fill and the advanced-fill (erodible portion of dredge sediments) quantities. The construction profile should be significantly wider and have steeper slopes than the design cross-section due to the allowance of the advanced-fill and construction limitations (NRC, 1995; USACE, 2002)

A construction profile has been developed (Figure 9.6), allowing for the advanced fill quantities.

9.6.2 The Construction Profile

Sediment should be placed horizontally outwards from the top of the sea walls (+3.5 m C.D) for a distance of 17 meters (Figures 9.5 and 9.6) based on calculations of sediment volumes and the *'overbuilding method'* (USACE, 2002). A consistent slope of 3.3° (USACE, 2002) should then be achieved where the profile drops to MSL at a distance of 50 m from the edge of the seawall.

The excess sediment (advance-fill) volume in the construction profile is 7,600 m^3 (7,600 m^3 required for design profile and R_A = 2, therefore advance-fill = 7,600 m^3). Wave action will cause an adjustment of the construction profile to a flatter equilibrium slope (NRC, 1995; Houston, 1991). The design profile is expected to take shape within 1.5 years of sediment placement. The *'advance-fill'* portion (7,600 m^3) of the placed sediment will be removed at a more rapid rate than the ~400 m^3yr^{-1} beach face longshore sediment transport would suggest as the sediment being eroded consists of only the finer grain sizes of the overall placement sediment (15,200 m^3).

9.6.3 Methods of Placement

As the dredging operation is in reasonable proximity (~800 m) to the proposed nourishment site, the most economic method of transporting and depositing sediment is direct pumping and placement.

The fill would be pumped as a slurry onto the beach via a hydraulic pipeline, then reworked into the desired construction profile by earth moving equipment. The temporary construction of a sand dike behind the discharge point will reduce the loss of fines and provide better water quality in the area (USACE, 2002).

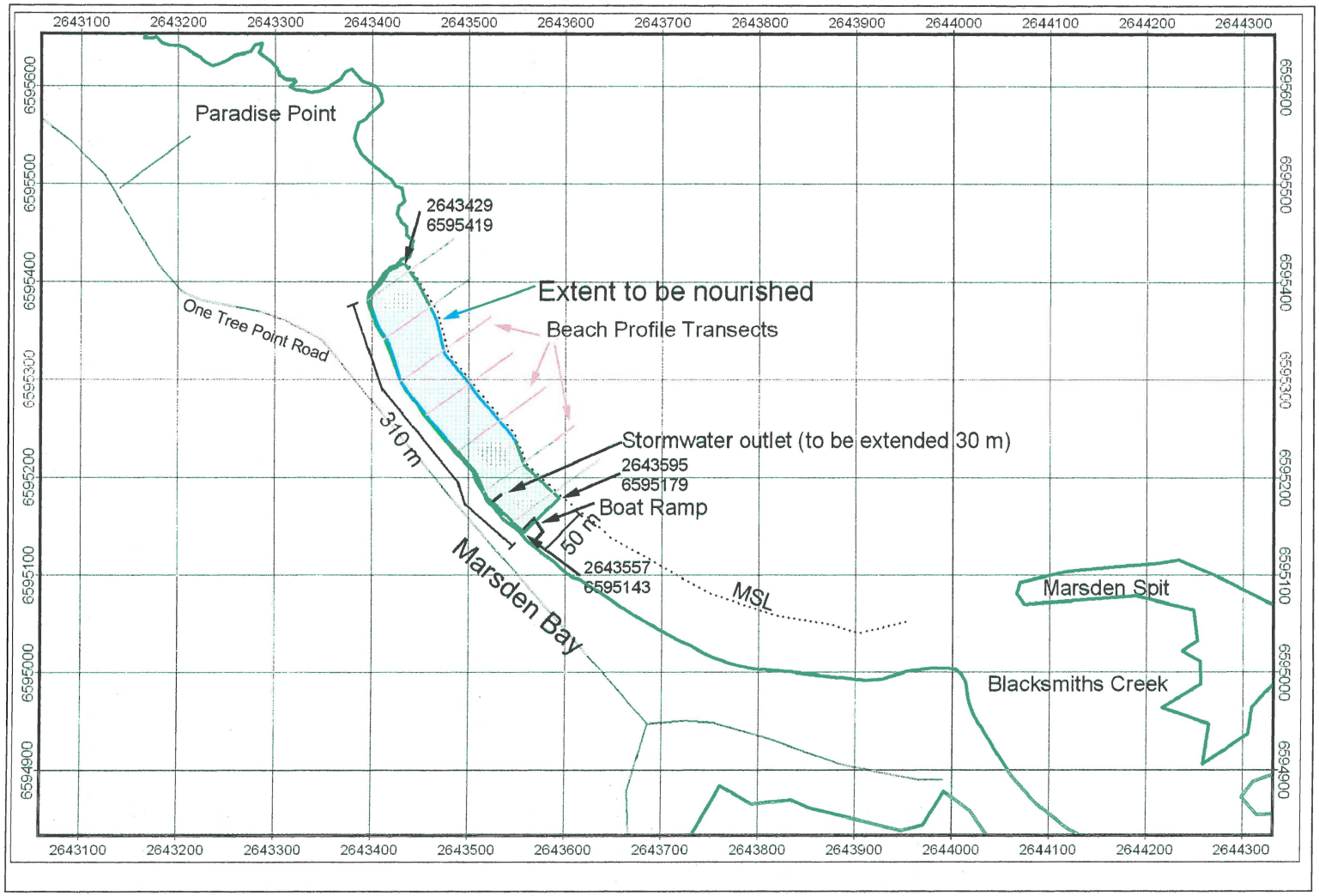


Figure 9.5 – *Planform and extent of proposed beach nourishment at Marsden Bay. Locations of transects detailed in Appendix G. Grid references in NZMG.*

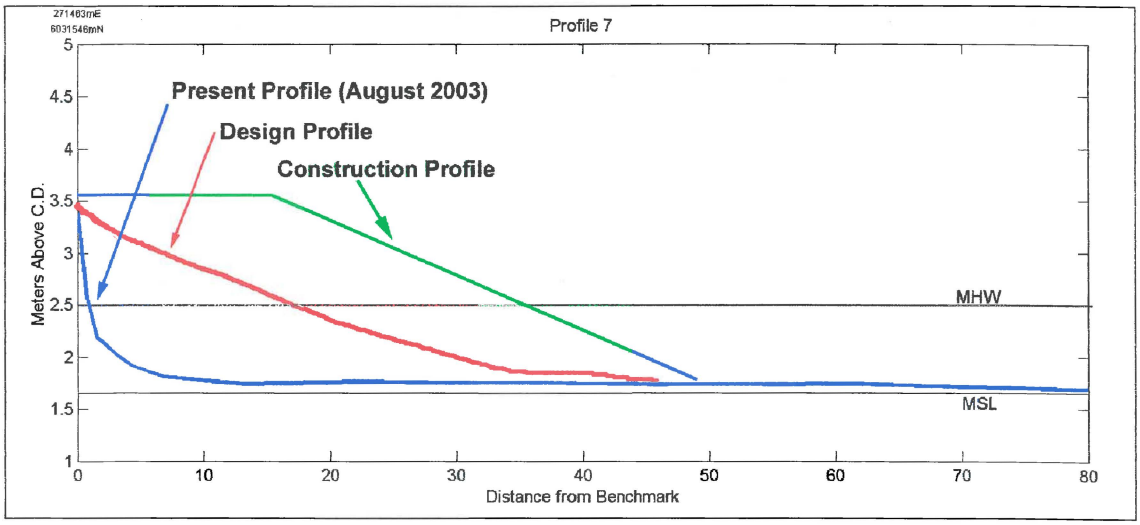


Figure 9.6 – *Typical beach profile, proposed design and construction profiles at Marsden Bay.*

9.6.4 Life Expectancy

The longevity of a beach nourishment project is primarily determined by the degree to which to the placed sand volume addresses any pre-project volume deficit and the rate at which fill material is transported out of the project domain in the alongshore direction (USACE, 2002). Annual losses will likely vary from year to year because of the dependency on storm activity (NRC, 1995).

Sediment transport vectors in the area have characteristic magnitudes of 400 m^3yr^{-1} and are directed both alongshore and offshore (influenced by Blacksmiths Creek) (Figure 8.22). The natural barrier to alongshore transport in the up-harbour direction, Paradise Point, will act to trap some sediment in the Marsden Bay area, though there will inevitably be some leakage.

Estimated life expectancies of the renourished beach (volume = 7,600 m^3) are expected to be of the order of 10 to 19 years, considering the magnitude of potential sediment transport over the beach face (400 m^3yr^{-1}) and inter-tidal terrace (350 m^3yr^{-1}) (Figure 8.21).

9.6.5 A Monitoring Program

Beach nourishment is a "*soft-structure*" which will respond dynamically to changing waves and water levels. Physical responses of a beach-fill include post-construction adjustment of the placed sand, seasonal variation and storm-induced changes of the beach profile, and seasonal and long-term change of the project planform (USACE, 2002).

Monitoring the physical elements of beach nourishment projects provides a means for determining the projects actual performance versus its predicted performance (NRC, 1995). Monitoring also provides data needed to identify and correct any problems associated with the project and help guide maintenance renourishment programs.

Pre-construction monitoring has been detailed within this thesis, although updated values of beach volume changes and sediment transport vectors may be useful if nourishment is not planned until some time in the future (post 2005).

During-construction monitoring should consist of:

i. placement sediment textural analysis and
ii. beach profiles.

Analyses of placement sediments *'insitu'* will allow a check on overfill ratios and potential readjustment of either volumes required or life expectancy. Surveying of regularly spaced profiles (50 m intervals, Appendix G) along the nourishment site allows a check on the construction profile being created and determination of sediment volumes being placed on the beach face.

Post-construction monitoring involves the systematic collection of data to determine the projects performance. Monitoring should include:

i. beach profiles surveys;
ii. beach face sediment samples;
iii. aerial photography (immediately post nourishment, then regularly every 5 years);
iv. wave and current monitoring; and
v. biological monitoring.

Beach Profiles – beach profiles (50 m intervals, Appendix G) should be surveyed bi-monthly for the year following nourishment. Surveys should also be conducted along pre-existing profile lines adjacent to Marsden Bay (Profiles 5, 6, 7 and 7-1, Chapter 5). Following this, profiles should be surveyed annually. Estimates of beach sediment volume should be made for each survey and compared with both pre-nourishment and immediately post-nourishment volumes (methods described in Chapter 5). Changes in beach profiles should be documented. In addition to this timetable of profile monitoring, transects should ideally be surveyed immediately after severe storm activity. Ideally, the need for any maintenance renourishment will be determined by this monitoring.

Sediment Samples – sediment samples should be collected annually from profile transects. Sediment sampling should consist of shallow grab samples from the beach face, MSL, MLW and 2 samples along the inter-tidal terrace (Larson et al., 1997). This sampling scheme documents cross-shore variability of the median grain size and size distribution, which can influence profile shape (USACE, 2002). Sediment sampling should be performed concurrently with beach profile surveying.

Aerial Photography – aerial photographs provide a visual record of shoreline position, variations in planform and beach width (Chapter 4). Aerial photographs provide a *'total-project'* perspective that cannot be obtained by ground photography and beach profile surveys alone (USACE, 2002). Vertical aerial photographs of the area should be taken immediately following nourishment and at 5-yearly intervals thereafter. Photographs should be taken around midday and near the time of low tide. Photographs should be rectified and geo-referenced for comparison with past photographs (Chapter 4).

Wave and Current measurements – waves, currents and water levels are the principle forcing parameter controlling beach-fill evolution (NRC, 1995). Waves and water currents should be monitored throughout Marsden Bay. Instruments should be deployed bi-annually, the data analysed for sediment transport potentials and compared with values presented in Chapter 8.

Biological Monitoring – The placement of sediment will impact the biology of the local area. Biological impacts may also be created in adjacent areas due to turbidity created by moving sediment about the beach. Pre-nourishment, immediately post-nourishment and annually thereafter, biological surveys should be performed at Marsden Bay and surrounding areas. Surveys should include an assessment of shellfish populations, bird-nesting areas and other beach organisms. Data analysis should evaluate any fluctuations of flora and fauna. Results should be compared with previous surveys conducted by Bioresearches (1980), WHSWC (1988) and Poynter (1993).

9.6.6 Estimated Costs of Nourishment

Initial costs (estimates only):

i. Sediment for fill (15,200 m^3) = courtesy of Northport;
ii. Extension of stormwater pipe (30 m) = $5,000;
iii. Contribution towards transport of sediment from dredge basin to Marsden Bay (~ 800 m) = $30,000;
iv. Earthmoving machinery to form sediment into the construction profile (~$1.00 per m^3) =$15,000.

Monitoring costs (estimates only):

i. First year = $30,000;
ii. Subsequent years = $10,000 per year.

This results in an expected initial cost of **NZ$80,000** with an ongoing cost of $10,000 for environmental monitoring, data analysis and reports.

These are the costs required for nourishment works to be undertaken. Costs not considered include:

i. Engineers drawings for contractors;
ii. Costs associated with gaining resource consent;
iii. Consultation with local iwi etc.

9.7 Summary

- Marsden Bay (West and Central) has been identified as the preferred site for any potential beach nourishment using sediments sourced from the Northport dredge basin.

- The nourishment of Marsden Bay (West and Central) with 15,200 m^3 of dredge sediments, in accordance with the construction profile outlined, would widen the dry beach width and provide enhanced recreational opportunities at Marsden Bay.

- The most economic and sensible method of sediment transport from the dredge basin to Marsden Bay is by hydraulic pipeline, with earthmoving machinery configuring the sediment along the beach face.

- A monitoring plan has been created in order to measure the success of the project and environmental conditions following nourishment.

- A structure(s) should be built to trap longshore sediment transport along the One Tree Point coastline if any nourishment is carried out there. The structure would inhibit the longshore transport of sediment along the beach face and out of the system.

10 SUMMARY AND CONCLUSIONS

10.1 Introduction

This study has undertaken a site characterisation of the lower Whangarei Harbour and Marsden Point, with respect to the Northport reclamation, dredge basin, and potential beach renourishment within the lower harbour. A literature review, sediment textural analyses, medium-long term coastal changes, beach profile volumetric changes, bathymetric and morphologic changes, and sediment flux patterns have been investigated to assess sediment transport patterns and changes in morphology of the lower harbour and also to evaluate the suitability of dredge basin sediments for the effective nourishment of sediment depleted from lower harbour beaches. This chapter outlines the key findings of the study.

10.2 General Summary

Based upon beach profile volumetric changes, sediment transport vectors and observed bedforms, sediments are expected to be deposited in the dredged basin at an increasing rate over the next 5 to 10 years, to reach volumes of 15-20,000 m^3yr^{-1}. This material will need to be removed to maintain dredge basin depth and vessel access. The sediments dredged could be put to use as effective beach nourishment fill at Marsden Bay (West and Central). The use of the dredged sediments would improve recreational opportunities and increase the dry beach width at Marsden Bay.

The Northport reclamation and dredge basin has evidently not modified the medium – large-scale sediment transport patterns in the area. Local/small-scale changes to sediment transport include the creation of a barrier to the longshore sediment transport (western rock wall) and the creation of a *'current transport shadow zone'* close to the eastern rock wall. Both changes have resulted in local accretion of sediment (400 – 5,000 m^3yr^{-1} [west] and 1,000 m^3yr^{-1} [east] ± 50%).

10.3 Grain Size Patterns

Analyses of sediment grain size distributions over the beach faces and inter-tidal terraces of the lower Whangarei Harbour have found:

- Sediments of the lower harbour are consistent with Schofield's (1975) Hauraki (B) facies;
- the areal distribution and extent of shelly lag sediments in 2003 is very similar to that in 1983;
- sediment textural patterns indicate transport of sediments toward the western edge of Northport, and a northwesterly transport direction along the Marsden Bay – Paradise Point – One Tree Point shoreline; and
- dredging activities have '*stirred*' up sediments in the dredge basin resulting in very poorly sorted sediments.

The general grain size characteristics and distributions of the lower Whangarei Harbour have not changed greatly since a previous investigation by Millar (1980). There have been local changes within the dredge basin and immediately either side of the Northport reclamation where sediments indicate recent deposition.

10.4 Medium – Long Term Coastal Change

Thirteen vertical aerial photographs of Marsden Point and the lower Harbour were scanned, rectified and geo-referenced to be investigated for morphologic coastal shoreline changes between 1984 and 2001, resulting in the following findings:

- The dry beach width of the One Tree Point shoreline has narrowed at an average rate of 0.26 my^{-1} between 1984 and 2001;
- beach width variations are consistent with a net longshore drift toward One Tree Point along the One Tree Point – Paradise Point beach face;
- the beach at Marsden Bay-West completely disappeared between 1984 - 2001, and seawalls now (2003) front the sea at high tide;
- Marsden Bay-Central has experienced a reduction in dry beach width of 0.4 my^{-1} between 1984 and 2001. This value is in agreement with the 0.13 - 0.44 my^{-1} obtained by Gibb (1998) using independent data;

- artificial beach nourishment of Marsden Bay-East in 1999 increased the local dry beach width, and associated '*training*' of Blacksmiths Creek channel has improved the likelihood of nourished sediment remaining on the beach face;

- Marsden Spit, enclosing Blacksmiths Creek experienced rapid retreat rates (5 – 7.5 my^{-1}) between 1984 and 1999, especially following breaches caused by storms in 1996, 1997 and 1998. Small (750 m^3) nourishment efforts have not had any significant impacts on this trend; and

- the shoreline of Marsden Point adjacent to the ebb tidal delta of Mair Bank has prograded between 1984 and 2001.

Analysis of the aerial photographs provided morphologic evidence for a northwesterly-directed longshore drift over the beach face at One Tree Point – Paradise Point. The narrowing of beach widths between 1984 and 2001 over the entire Marsden Bay – One Tree Point area has been observed, with the exception of the artificially nourished Marsden Bay-East. This nourishment has successfully widened the dry beach and the associated relocation of Blacksmiths Creek channel has prevented the sand being quickly moved away. Marsden Spit is in a state of readjustment to the new position of Blacksmiths Creek. Accretion and progradation has been observed at Marsden Point adjacent to Mair Bank.

10.5 Beach Profile Analysis

Beach profiles of the shoreline surrounding Marsden Point were examined, providing information on closure depths, variations in sediment volume, longshore sediment transport and patterns of profile change. Findings included:

- The beach surrounding the NZRC jetties is more variable than other locations farther up harbour. The beach adjacent to the ebb tidal delta of Mair Bank showed the greatest variation of any location surveyed;
- beach profiles near One Tree Point are relatively depleted of sediment and stable in the short term;
- small (<0.5 m heights) ridges and bars have been seen to develop (within 0.5 m vertically of MSL) on the inter-tidal terrace and move onshore;
- sediment volumes at the Marsden Bay-East beach face increased in 1999 following nourishment, since then volumes have declined at a rate of ~1000 m^3yr^{-1};
- sediment volumes along the One Tree Point – Paradise Point shoreline have remained relatively steady between 1996 and 2003;
- sediment is accreting against both western and eastern rock walls of the Northport reclamation:
    - Prior to Northport development sediment transport was directed from west to east over the site. This has not changed post-development, with accretion being observed against Northport's western rock wall (~5,000 m^3yr^{-1}), and
    - beach profile data indicate sediment has moved from the beach adjacent to the NZRC jetties toward Northport at a rate of approximately 10,000 m^3yr^{-1} between 1998 and 2002;
- several beach profiles pivot about certain points in the profile over time periods of less than one year.

Investigation of beach profiles indicated sediment actively accreting against both eastern and western rock walls of the Northport reclamation. Patterns of longshore sediment transport present prior to the Northport development, were unchanged post-development. The beach adjacent to the NZRC jetties was found to be more variable in cross-section than profiles father up harbour and closer to One Tree Point. The greater variability is associated with the much larger magnitudes of longshore sediment transport present along Bream Bay Beach, near the NZRC jetties.

10.6 Bathymetry and Hydrography

A summary of previously documented bathymetric changes and a comparison of recently surveyed bathymetric data was compiled to evaluate the stability of the lower Whangarei Harbour and changes in morphology. Findings were:

- The ebb tidal delta of Mair Bank has been a highly variable feature of the lower harbour. Volumes of sediment movement over and immediately surrounding Mair Bank range from 5-20,000 m^3yr^{-1}. Typical volumes of erosion and accretion have not changed post Northport development;

- volumes of sediment movement adjacent to the NZRC jetties (~5,000 m^3yr^{-1}) have not altered post Northport development. It is possible that these changes are the result of increased local water current velocities due to ships being berthed at the NZRC jetties and the timing of the bathymetry surveys (Section 6.8);

- sediment is being actively redistributed surrounding Passage Island, in patterns similar to those observed by Black (1983) and Barnett et al. (1993);

- accretion has been observed since 2001 over the inter-tidal terrace next to Northport's eastern rock wall (~1,000 m^3yr^{-1}); and

- the majority of the lower harbour has remained stable post Northport development. This stability is attributed to the armouring effects of a shell lag in the harbour channel off Marsden Point and adjacent to the dredge basin.

Bathymetric surveys of the lower Whangarei Harbour have identified locations and volumes of characteristic changes. It has been found that the Northport reclamation and dredge basin has thus far influenced only a local area (immediately east of the reclamation) and has not altered or modified patterns of change elsewhere in the lower harbour. Mair Bank has been found to be a variable feature (Chapter 6) supporting the findings of the DHI (1982a), Black and Healy (1982), Black (1983), Venus (1984) and Barnett (1997).

10.7 Morphodynamics of the Lower Harbour

The sediment character and morphology of the seabed has been investigated through the use of Side Scan Sonar. Seabed character, sediment pathways, and bedforms were interpreted from the sonograph record. The investigation revealed:

- Shelly lag sediments in the vicinity of Northport and the NZRC jetties exist in very similar patterns to those in the early 1980's;

- an active sediment transport pathway consisting of fine sands, extends from the flood tidal delta of Snake Bank toward the Northport dredge basin. The ridge separates areas of opposing dominant flows and is essentially identical to that observed in the early 1980's;

- sediment moves down harbour between Northport and the NZRC jetties. The movement can be observed from sand waves of wavelengths ranging from 5 to 10 m. This pattern is identical to that observed in 1983;

- bedforms observed adjacent to the NZRC jetties indicate sediment transport directed out of the harbour. Similar bedforms were also observed here in 1983;

- dredging has removed some shell lag cover from immediately adjacent to the Northport quay wall; and

- sediments are moving down the batter slopes of the dredge basin on its southern edge. It remains to be seen whether these sediments accumulate in the dredge basin or are transported through with little or no accretion.

Large-scale patterns of sediment transport and shell lag cover appear to have been unaffected by the Northport development. The development has modified sediment textural properties within and immediately surrounding the dredge basin, as would be expected. Bedforms, indicative of sediment transport, elsewhere in the harbour exist in patterns very similar to those observed in 1983.

10.8 Sediment Transport at Marsden Point

Sediment transport patterns and fluxes have been determined from current meter data and hindcast wave data over the channels, channel margins, inter-tidal terraces, and beach faces of the lower harbour. Potential sediment transport vectors have, where possible, been compared with previous estimates. Findings have included:

- Sediment is likely transported up harbour in the middle of the entrance, with a return flow down harbour closer to the southern shoreline (and the dredge basin);

- increasing potential sediment transport vectors in the direction of transport indicate the potential for scour at the eastern extent of the dredge basin;

- in general, potential sediment transport vectors over the channel and channel margins adjacent to Northport in 2002 are very similar to those calculated in 1983. There is however, less potential for up-harbour transport at the northern extent of the dredge basin in 2002 than in 1983;

- sediment accretion in the Northport dredge basin is expected to increase to 15-20,000 m^3yr^{-1} over the next 5 to 10 years;

- sediments over the inter-tidal terrace and beach face are transported by a combination of locally generated wind waves and tidal currents much more effectively than by tidal currents alone;

- between the Northport and NZRC jetties sediment transport is directed toward Marsden Point, away from Northport. The accretion observed here is due to a *'current transport shadow zone'*;

- opposing longshore sediment transport vectors meet at a location where the ebb tidal delta (Mair Bank) is *'welded'* to the shoreline. This location has displayed a highly variable beach profile cross-section as well as bathymetry farther offshore;

- potential sediment transport vectors indicate an accretion of sediment (~400 m^3yr^{-1}) against Northport's western rock wall. A similar accretion pattern has been alluded to by beach profile "even-odd" analysis and sediment textural properties. Accretion has been observed in beach profiles at this location; and

- potential sediment transport vectors over the One Tree Point – Paradise Point shoreline indicate accelerating transport vectors toward One Tree Point, implying that beach faces will be sediment depleted. Beach profiles verify this and aerial photographs also indicate a net medium-term transport direction over the beach face towards One Tree Point.

A medium-scale sediment transport pathway diagram presented by Black et al. (1989) has been verified for the area surrounding Northport, with the addition of potential leakage from one pathway to another and the potential for scour or development of a shell lag at the easternmost edge of the dredge basin.

Accretion observed against Northport's western rock wall has been shown to be a result of longshore sediment transport patterns. Accretion observed against Northport's eastern rock wall has been shown to be a result of a *'current transport shadow zone'* rather than longshore sediment transport.

The meeting of opposing longshore sediment transport vectors at Marsden Point has resulted in the '*welding*' of the ebb tidal delta (Mair Bank) to the shoreline and represents a highly variable beach profile and ebb tidal delta.

10.9 Potential Beach Renourishment

The potential use of dredge basin sediments as beach nourishment fill has been examined. Dredge basin sediments have been compared with several locations for their compatibility as nourishment fill. A suitable site for beach nourishment has been identified and a nourishment plan developed:

- Marsden Bay (West and Central) is the most suitable site for beach nourishment using dredge basin sediments;

- a hydraulic pipeline delivering 15,200 m^3 of dredge basin sediments to the beach face, to be spread by earthmoving machinery, provides the most economic nourishment method and would act to increase the dry beach width and enhance recreational opportunities in the area;

- appropriate monitoring should be undertaken during and following nourishment; and

- any nourishment of the One Tree Point – Paradise Point shoreline should be accompanied by structures to impede the longshore transport of sediments.

10.10 Aims Achieved

In review, this study aimed to:

1) identify and characterise sediment transport patterns and changes in the geomorphology of the lower Whangarei Harbour; and
2) assess the suitability of sediments, and create a plan for the effective artificial nourishment of adjacent beach areas with sediment dredged from Northport's turning basin.

These aims have been achieved within the preceding chapters and are largely summarised within this chapter. *'Special Condition No. 9'* within Northport's Land Use Consent No.2 has been fulfilled through this study with the acknowledgement of Marsden Bay (West and Central) as locations suitable for artificial nourishment using dredge basin sediments.

The impacts of Northport and its dredge basin on the physical environment have been evaluated. This thesis also provides as excellent benchmark on which to measure future changes in the region.

10.11 Suggestions for Further Research

This study has suggested an active pathway transports sediments between the beach face of Marsden Point and the ebb tidal delta of Mair Bank. Further investigation of the links between the sediment movements of the tidal inlet delta system including Bream Bay Beach, Marsden Point and Mair Bank will assist in the understanding of beach movements and bathymetry changes in this critical area.

The development and onshore movement of sediment ridges has been observed at several beach profiles monitored within this study. Further investigation could be undertaken to determine the actual mechanism of this transport, and its implications for beach nourishment.

The calculation of sediment transport vectors over the beach face and inter-tidal terrace resulting from local wind generated waves, tidal currents, and both local wind waves and tides in combination has revealed an interesting technique for the separation of the components of the overall transport resultant. Further study is required to determine the applicability, scope and limitations of this technique.

It has not been determined wether sediments transported into the dredged basin will actually accumulate in the basin or be subsequently transported out of the dredged basin via an alternate pathway. Further research could identify precisely how much of the sediment transported into the dredged basin is expected to stay there, and how much is expected to be moved from the basin by natural processes.

RMA, 1991. *Resource Management Act, NZ Act of Parliament.*

Allen, J.R.L., 1968. *Current Ripples: Their Relation to Patterns of Water and Sediment Movement*, North Holland, Amsterdam, Netherlands, 433 pp.

Allen, J.R.L., 1985. *Principles of Physical Sedimentology*. Allen and Unwin, London, 272 pp.

Ashley, G.M., 1990. Classification of Large-Scale Subaqueous Bedforms: A New Look at an Old Problem. *Journal of Sedimentary Petrology*, 60(1): 363-396.

Aubrey, D.G., 1979. Seasonal Patterns of Onshore/Offshore Sediment Movement. *Journal of Geophysical Research*, 84(C10): 6347-6354.

Bagnold, R.A., 1963. Mechanics of Marine Sedimentation. In: M.N. Hill (Editor), *The Sea*. Wiley-Interscience, New York, pp. 507-582.

Bailard, J.A., 1984. *A Simplified Model for Longshore Sediment Transport.* Proceedings, 19th international coastal engineering conference, 1454-1470

Barnett, A.G., Joynes, S.A. and Madsen, P.R., 1993. *Marsden Point Port Development - Hydrodynamic Study*, Barnett Consultants Ltd & Danish Hydraulic Institute: for the Northland Port Corporation, March.

Barnett, A.G., 1995a. *Report on ADCP Data Processing*, Barnett Consultants Ltd for Northport Ltd, June, 1995.

Barnett, A.G., 1995b. *Report on ADCP Data Processing (Harmonic and Extreme Value Analysis)*, Barnett Consultants Ltd for Northport Ltd, August, 1995.

Barnett, A.G., 1997, Montgomery Watson Ltd. *Marsden Point Port Development Hydrodynamic Study: Addendum G to Original Report: Sediment Accretion/Erosion Quantities*, Montgomery Watson N.Z. Ltd, May 1997, Hamilton, New Zealand.

Barnett, K.M.C., 2002. *Behaviour of Storm Surges in Whangarei Harbour and Bream Bay, Northland, New Zealand.* MSc Thesis, University of Waikato, Hamilton.

Barnhardt, W.A., Kelley, J.T., Dickson, S.M. and Belknap, D.F., 1989. Mapping the Gulf of Maine with Side-Scan Sonar: A New Bottom-Type Classification for Complex Seafloors. *Journal of Coastal Research*, 14(2): 646-659.

BCHF, 1992, Beca Carter Hollings and Ferner Ltd. *Geotechnical Investigation: Proposed Marsden Point Port Development. In, Den Ouden Associates, Marsden Point Terminal Draft EIA, Volume 2*, Northland Port Corporation.

BCHF, 1999, Beca Carter Hollings and Ferner Ltd. *Marsden Point Port Development: Estimation of Wave Climate for Bund Design*, Northland Port Corporation, November 1999.

Berek, E.P. and Dean, R.G., 1982. *Field Investigation of Longshore Transport Distribution.* Eighteenth Coastal Engineering Conference, Cape Town, South Africa, 1620-1639

Bioresearches, 1976. *Surface Water Currents in the Marsden Point Region*, New Zealand Refining Company Ltd, August 1976.

Bioresearches, 1978. *The Monitoring of Marine Habitats in the Vicinity of Marsden Point Oil Refinery: Report No.1*, New Zealand Refining Company Ltd, June 1978.

Bioresearches, 1979. *The Monitoring of Marine Habitats in the Vicinity of Marsden Point Oil Refinery: Report No.2*, New Zealand Refining Company Ltd., March 1979.

Bioresearches, 1980. *The Ecological Impact of the Proposed Forestry Wharf at Marsden Point, Northland. : Northland Forestry Port Environmental Impact Report Supplementary Appendices*, Northland Harbour Board.

Bioresearches, 1981. *Assessment of the Hydrological and Biological Impacts of the Proposed Temporary Offloading Ramp at Marsden Point*, New Zealand Refining Company Ltd, June 1981.

Black, K., Healy, T., Venus, G., Stoakes, J. and Hunter, M., 1981. *Marsden Point Forestry Port Investigation, Sea Floor Photographic Survey*, Northland Harbour Board.

Black, K. and Healy, T., 1982. *Sediment Transport Investigations in a New Zealand Tidal Inlet*. Proceedings of the Eighteenth Coastal Engineering Conference, Cape Town, Republic of South Africa, 2436-2457.

Black, K., Beazley, M. and Hunter, M., 1982. *Marsden Point Forestry Port Investigation, Channel Drogue Tracking*, Northland Harbour Board, April 1982.

Black, K., 1983. *Sediment Transport and Tidal Inlet Hydraulics*. PhD Thesis, University of Waikato, Hamilton, 331 pp.

Black, K. and Healy, T., 1983. *Northland Forestry Port, Marsden Point,Side-Scan Sonar Survey*, Northland Harbour Board, January 1983.

Black, K. and Healy, T., 1986. The Sediment Threshold over Tidally Induced Megaripples. *Marine Geology*, 69: 235-249.

Black, K., Healy, T. and Hunter, M., 1989. Sediment Dynamics in the Lower Section of a Mixed Sand and Shell-Lagged Tidal Estuary, New Zealand. *Journal of Coastal Research*, 5(3): 503-521.

Boak, E. and Turner, I., 2003. *A Process Based Analysis of the 'Shoreline' as Detected in Digital Images*. Coasts and Ports Australasian Conference, Auckland, Paper No. 16

Bowen, A.J., 1969. The Generation of Longshore Currents on a Planar Beach. *Journal of Marine Research*, 27: 206-215.

Bridgewater, G.D., 1986. Littoral Sediment Transport at Mangatawhiri Spit, New Zealand. *New Zealand Journal of Marine and Freshwater Research*, 20: 147-151.

Carslile, B., 2000. *The Highs and Lows of Digital Elevation Model (Dem) Error - Developing a Spatially Distributed Dem Error Model.* Proceedings of the 5th International Conference on GeoComputation, University of Greenwich, United Kingdom,

CERC, 1984, United States Coastal Engineering Research Center. *Shore Protection Manual*. U.S. Government Printing Office, Washington D.C.

CFTE, 1976, Commission for the Environment. *The Implications of Forestry Development for Port Needs in Northland: Whangaroa Harbour as a Possible Port Location, Unpublished Report*, Wellington.

CFTE, 1981, Commission for the Environment. *Northland Forestry Port Proposal, Marsden Point Environmental Impact Audit*, Commission for the Environment, July, Wellington.

CFTE, 1994, Commission for the Environment. *Marsden Point Terminal Proposal : Technical Review Panel Report*, Office of the Parlimentary Commissioner for the Environment, December 1994.

Chisolm, G., 1998. Kinematic (RTK) GPS: What Is It and What Are Its Uses in Hydrography. *Port Engineering*, 15(6): 13 - 16.

Crowell, M., Leatherman, S. and Buckley, M., 1991. Historical Shoreline Change: Error Analysis and Mapping Accuracy. *Journal of Coastal Research*, 7(3): 839-852.

Crowell, M., Leatherman, S. and Buckley, M., 1993. Shoreline Erosion Rate Analysis - Long Term Versus Short Term Data. *Shore and Beach*, 61(2): 13-20.

Davies, A.G., van Rijn, L.C., Damgaard, J.S., Van De Graaff, J. and Ribberink, J.S., 2002. Intercomparison of Research and Practical Sand Transport Models. *Coastal Engineering*, 46: 1-23.

de Lange, W.P. and Healy, T.R., 1990. Renourishment of a Flood-Tidal Delta Adjacent Beach, Tauranga Harbour, New Zealand. *Journal of Coastal Research*, 6(3): 627-639.

de Lange, W.P., Healy, T. and Darlan, Y., 1997. Reproducibility of Sieve and Settling Tube Textural Determinations for Sand-Sized Beach Sediment. *Journal of Coastal Research*, 13(1): 73-80.

Dean, R.G. and Dalrymple, R.A., 1991. Water Wave Mechanics for Engineers and Scientists. *World Scientific*: 157-158.

Dean, R.G. and Dalrymple, R.A., 2002. *Coastal Processes with Engineering Applications*. University of Cambridge, Cambridge, 475 pp.

DHI, 1982a, Danish Hydraulic Institute. *Proposed Forestry Terminal, Hydraulic Model Studies - Text*, Northland Harbour Board, September 1982.

DHI, 1982b, Danish Hydraulic Institute. *Proposed Forestry Terminal, Hydraulic Model Studies - Drawings*, Northland Harbour Board, September 1982.

Dick, J.E. and Dalrymple, R.A., 1984. *Coastal Changes at Bethany Beach, Delaware*. Nineteenth Coastal Engineering Conference, Houston, Texas, 1650-1667

Dolan, R., Hayden, B., May, S. and May, P., 1980. The Reliablitiy of Shoreline Change Measurements from Aerial Photographs. *Shore and Beach*, 48(4): 22-29.

Dolan, R., Fenster, M. and Holme, S., 1991. Temporal Analysis of Shoreline Recession and Accretion. *Journal of Coastal Research*, 7(3): 723-744.

Duxbury, A.C. and Duxbury, A.B., 1997. *An Introduction to the World's Oceans*. Wm.C. Brown Publishers, Dubuque, Indiana, 504 pp.

Dyer, K.R., 1980. Velocity Profiles over a Rippled Bed and the Threshold of the Movement of Sand. *Estuarine and Coastal Marine Science*, 10: 181-199.

El-Ashry, M.T. (Editor), 1977. Air Photography and Coastal Problems. *Benchmark Papers in Geology*, 38. Dowden, Hutchiinson & Ross, Inc., Pennsylvania, 425 pp.

Engelund, F. and Fredsoe, J., 1976. A Sediment Trasnsport Model for Straight Alluvial Channels. *Nordic Hydrology*, 7(5).

ESRI, 1996, Environmental Systems Research Institute Inc. *Arcview Spatial Analyst: Advanced Spatial Analysis Using Raster and Vector Data*. Environmental systems Research Institute, Redlands, California.

Fenster, M. and Dolan, R., 1993. Historical Shoreline Trends Along the Outer Banks, North Carolina: Processes and Responses. *Journal of Coastal Research*, 9(1): 172-188.

Ferrar, H.T., 1925. The Geology of the Whangarei - Bay of Islands Subdivision. *New Zealand Geological Survey (NZGS)*, Bulletin 27.

Ferrar, H.T., 1934. The Geology of the Dargaville - Rodney Subdivision. *New Zealand Geological Survey (NZGS)*, Bulletin 34.

Folk, R.L., 1966. A Review of Grain Size Parameters. *Sedimentology*, 6: 73-93.

Gadd, P.E., Lavelle, J.W. and Swift, D.J.P., 1978. Estimates of Sand Transport on the New York Shelff Using near-Bottom Current-Meter Observations. *Journal of Sedimentary Petrology*, 48: 239-252.

Gibb, J.G., 1979. *Aspects of Beach Sediments and Their Transport Along the New Zealand Coast*. Workshop on Physical Aspects of Coastal Problems, Hamilton.

Gibb, J.G., 1998. *Coastal Hazards and Solutions for Eastern One Tree Point, Whangarei Harbour, Whangarei District*, Whangarei District Council.

Gibb, J.G., 1999. *Coastal Hazard Management Strategy for the One Tree Point - Marsden Bay Area, Whangarei Harbour, Whangarei District*, Whangarei District Council, June 1999.

Gibbs, R.J., M.D., M. and Link, A.D., 1971. The Relationship between Sphere Size and Settling Velocity. *Journal of Sedimentary Petrology*, 41(1): 7-18.

Glover, D., 1997. *Holocene Infill of an Incised Valley System: Blacksmiths Creek*. M.Sc Thesis, University of Auckland, Auckland.

Godfrey, P.J. and Godfrey, M.M., 1973. Comparison of Ecological and Geomprohic Interactions between Altered and Unaltered Barrier Systems in North Carolina. In: M.T. El-Ashry (Editor), *Air Photography and Coastal Problems*. Benchmark Papers in Geology. Dowden, Hutchinson & Ross Inc, pp. 341-360.

Gorman, L., Morang, A. and Larson, R., 1998. Monitoring the Coastal Environment; Part Iv: Mapping, Shoreline Changes, and Bathymetric Analysis. *Journal of Coastal Research*, 14(1): 61-92.

Grant, U.S., 1943. Waves as a Transporting Agent. *American Journal of Science*, 241: 117-123.

Green, M., 1986. Side-Scan Mosaic of a Sand Ridge Field: Southern Mid-Atlantic Bight. *Geo-Marine Letters*, 6: 35-40.

Haas, K.A. and Hanes, D.M., 2003. Process Based Modeling of Total Longshore Sediment Transport. *Journal of Coastal Research*, In Press: Revision 1, 11 July 2003.

Hallermeier, R.J., 1981. A Profile Zonation for Seasonal Sand Beaches from Wave Climate. *Coastal Engineering*, 4: 253-277.

Hasselmann, K.D. et al., 1973. Measurements of Wind-Wave Growth and Swell Decay During the Joint North Sea Wave Project (Jonswap). *Deutschen Hydrographischen Zeitschrift, Supplement A.8.*, 12: 95.

Healy, T., 1980. *Sediments and Hydraulics in the Vicinity of the Proposed Timber Port at Marsden Point: A Contribution to the Environmental Impact Report for the Northland Harbour Board*, University of Waikato.

Healy, T.R., Kirk, R.M. and de Lange, W.P., 1990. Beach Renourishment in New Zealand. *Journal of Coastal Research*(Special Issue 6): 77-90.

Healy, T.R., Cole, R. and de Lange, W.P., 1996. Geomporphology and Ecology of New Zealand Shallow Estuaries and Shorelines. In: K.F. Nordstrom and C.T. Roman (Editors), *Estuarine Shores: Evolution, Environments and Human Alterations*. John Wiley & Sons Ltd, West Sussex, England, pp. 486.

Heathershaw, A.D., 1981. Comparisons of Measured and Predicted Sediment Transport Rates in Tidal Currents. *Marine Geology*, 42: 75-104.

Holmes, K., Chadwick, O. and Kyriakidis, P., 2000. Error in a Usgs 30-Meter Digital Elevation Model and It's Impact on Terrain Modelling. *Journal of Hydrology*, 233: 154-173.

Houston, J.R., 1991. Beachfill Performance. *Shore and Beach*, 59: 15-24.

Hume, T.M. and Herdendorf, C.E., 1988. A Geomorphic Classification of Estuaries and Its Application to Coastal Resource Management: A New Zealand Example. *Ocean and Shoreline Management*, 11: 249-274.

Hume, T.M., Bell, R.G., Black, K.P., Healy, T.R. and Nichol, S.L., 2000. *Mangawhai-Pakiri Sand Study: Module 6 Final Report, Sand Movment and Storage and Nearshore Sand Extraction in Teh Mangawhai-Pakiri Embayment.*, National Institute of Water And Atmpospheric Research Ltd (NIWA), Revised March 2000, Hamilton.

Hwang, D., 1981. *Beach Changes Onoahu as Revealed by Aerial Photographs*. Hawaii Institute of Geophysics, Honolulu, 146 pp.

Inman, D.L. and Bagnold, R.A., 1963. Littoral Processes. In: M.N. Hill (Editor), *The Sea*. Wiley-Interscience, New York, pp. 529-553.

Inman, D.L., 1971. Nearshore Processes, *Encyclopedia of Science and Technology*. McGraw-Hill, New York, pp. 26-33.

James, J.R., 1975. *Techniques in Evaluating Suitability of Borrow Material for Beach Nourishment*, Technical Memorandum No. 60, Coastal Engineering Research Center, U.S. Army Engineer Waterways Experiment Station, Vicksburg, M.S.

Kachel, N.V. and Sternberg, R.W., 1971. Transport of Bedload as Ripples During Ebb Current. *Marine Geology*, 10: 229-244.

Kampuis, J.W., 1991. *Alongshore Sediment Transport Rate Distributions*. Coastal Sediments '91, 170-183

King, C.A.M., 1972. *Beaches and Coasts 2nd Ed.* St Martin's Press, New York, 570 pp.

Klein Associates, 1985. *Side Scan Sonar Training Manual*. Klein, New Hampshire, 89 pp.

Komar, P.D. and Inman, D.L., 1970. Longshore Sand Transport on Beaches. *Journal of Geophysical Research*, 75(30): 5514-5527.

Komar, P.D., 1998. *Beach Processes and Sedimentation*. Prentice-Hall, New Jersey, 544 pp.

Komar, P.D., 2004. *Emails Regarding Errors in Longshore Sediment Transport Equations within "Beach Processes and Sedimentation, 2nd Ed."* to P. Longdill.

Kraus, N.C., Isobe, M., Igarashi, H., Sasaki, T.O. and Horikawa, K., 1982. *Field Experiments on Longshore Sediment Transport in the Surf Zone*. Proceedings of the 18th Coastal Engineering Conference, 969-988

Kraus, N.C. and Harakai, S., 1983. Numerical Model of the Shoreline Change at Oariai Beach. *Coastal Engineering*, 7(1): 1-28.

Kraus, N.C., 1988. The Effects of Seawalls on the Beach: An Extended Literature Review. *Journal of Coastal Research* (Special Issue 4): 1-28.

Kraus, N.C. and McDougal, W.G., 1996. The Effects of Seawalls on the Beach: Part 1, an Updated Literature Review. *Journal of Coastal Research*, 12(3): 691-701.

Krumbein, W.C. and Pettijohn, F.J., 1938. *Manual of Sedimentary Petrography*. Appleton-Century-Crofts, New York.

Larson, R., Morang, A. and Gorman, L., 1997. Monitoring the Coastal Environment; Part Ii: Sediment Sampling and Geotechnical Methods. *Journal of Coastal Research*, 13(2): 308-330.

Lettau, H., 1969. Note on Aerodynamic Roughness-Parameter Estimation on the Basis of Rougness-Elemnt Description. *Journal of Applied Meteorology*, 8: 828-832.

Levin, N. and Ben-Dor, E., 2002. *Monitoring of Sand Dune Movement Along the Coastal Dunes of Ashdod-Nizanim, Israel, over Half a Century (1945-2000)*. Proceedings of the 29th International Symposium on Remote Sensing of Environmental Information for Sustainability and Development, Buenos Aires, Argentina, 54-57.

LINZ, 2002, Land Information New Zealand. *Nz5213, Whangarei Harbour & Approaches to Marsden Point*. Royal New Zealand Navy, Auckland.

Longdill, P., Healy, T. and Barnett, A.G., 2003a. *Post Dredging Monitoring for Northport Ltd, Adcp Data Processing*, University of Waikato, February, 2003.

Longdill, P., Healy, T. and Barnett, A.G., 2003b. *Post Dredging Monitoring for Northport Ltd, Harmonic Analysis of Tides and Currents*, University of Waikato, February, 2002.

Longdill, P., Healy, T. and Barnett, A.G., 2003c. *Post Dredging Monitoring for Northport Ltd, Analysis of Short Term Boat Mounted Adcp Measurements*, University of Waikato, February, Hamilton.

Longdill, P., Healy, T., Barnett, A.G. and Palmer, J., 2003d. *Post Development, Post Dredging Tidal Current Changes at Marsden Point, Northland, New Zealand.* Coasts and Ports Australasian Conference, Auckland, New Zealand.

Longuett-Higgins, M.S., 1970a. Longshore Currents Generated by Obliquely Incident Waves, 1. *Journal of Geophysical Research*, 75: 6778-6789.

Longuett-Higgins, M.S., 1970b. Longshore Currents Generated by Obliquely Incident Waves, 2. *Journal of Geophysical Research*, 75: 6790-6801.

Lynch, S., 2002. Digital Elevation Models and Spatial Resolution. *South African Journal of Science*, 98: 219-222.

MAF, 1979, Ministry of Agriculture and Fisheries. *Aspects of the Ecology of Whangarei Harbour: A Report Commissioned by the Northland Harbour Board and the Ministry of Agriculture and Fisheries*, Fisheries Management Division, Ministry of Agriculture and Fisheries, December 1979, Whangarei.

Markham, G.S., 1981. *New Zealand Land Inventory, Nzms 290 Sheet Q06/07 Partsheet R 06/07*. New Zealand Geological Survey, Department of Scientific and Industrial Research (DSIR), Wellingotn, New Zealand.

McLaren, P., 1981. An Interpretation of Trends in Grain Size Measures. *Journal of Sedimentary Petrology*, 51(2): 611-624.

McLaren, P. and Bowles, D., 1985. The Effects of Sediment Transport on Grain Size Distributions. *Journal of Sedimentary Petrology*, 55(4): 457-470.

McLaren, P., Cretney, W.J. and Powys, R.I., 1993. Sediment Transport Pathways in a British Columbia Fjord and Their Relationship with Particle-Associated Contaminants. *Journal of Coastal Research*, 9(4): 1026-1042.

Mehta, A.J., Lee, J. and Christensen, B.A., 1980. Fall Velocity of Shells as a Coastal Sediment. *Journal of the Hydraulics Division (ASCE)*: HY11:1727-1744.

Millar, A.S., 1980. *Hydrology and Surficial Sediments of Whangarei Harbour*. M.Sc Thesis, University of Waikato, Hamilton, 212 pp.

Miller, M.C., McCave, I.N. and Komar, P.D., 1977. Threshold of Sediment Motion under Uni-Directional Currents. *Sedimentology*, 24: 507-527.

Morang, A. and McMaster, R., 1980. Nearshore Bedform Patterns Along Rhode Island from Side-Scan Sonar Surveys. *Journal of Sedimentary Petrology*, 50(3): 831-840.

Morang, A., Larson, R. and Gorman, L., 1997. Monitoring the Coastal Environment: Part Iii: Geophysical and Research Methods. *Journal of Coastal Research*, 13(4): 1064-1085.

MOWD, 1974, Ministry of Works and Development. *Preliminary Investigation of Port Locations for the Shipment of Timber from Northland, Unpublished Report.*, Ministry of Works and Development, Wellington.

Mulloly, G., 2003. *Emails and Meetings Regarding Marsden Bay Nourishment and Works*. In: P. Longdill (Editor), Whangarei District Council.

NFPWC, 1980, Northland Forestry Port Working Committee. *Northland Foresty Port Study*, Northland Forestry Port Steering Committee, February.

NFPWC, 1982, Northland Forestry Port Working Committee. *Northland Forestry Port, Marsden Point : Comments on the Audit of the Environmental Impact Report*, Northland Forestry Port Steering Commitee.

NHB, 1981, Northland Harbour Board. *Northland Forestry Port, Marsden Point: Environmental Impact Report.*, Northland Harbour Board, April.

Nichol, S.L., 1997. *Ground Penetrating Radar Stratigraphy of Relict Coastal Deposits, Whangarei Harbour, New Zealand*. Pacific Coasts and Ports '97. 13th Asutralasian Coastal and Ocean Engineering conference and 6th Australasian Port and Harbour Conference, Christchurch, New Zealand.

Nichol, S.L., 2002. Morphology, Stratigraphy and Origin of Last Interglacial Beach Ridges at Bream Bay, New Zealand. *Journal of Coastal Research*, 20(1): 149-159.

NIWA, 1988, National Institute of Water and Atmospheric Research. *Brief Interpretation of Marsden Point Wind Data*, NIWA.

NIWA, 2000, National Institute of Water and Atmospheric Research. *Dobie Wave Gauge Operators Manual*, Version 3.1. National Institute of WAter and Atmospheric Research Ltd, Christchurch, New Zealand.

Novak, K., 1992. Rectification of Digital Imagery. *Photogrammetric Engineering and Remote Sensing*, 58(3): 339-344.

NPC, 1994, Northland Port Corporation. *Marsden Point Terminal Proposal : Draft Environmental Impact Assessment (3 Volumes)*, Northland Port Corportation (NZ) Ltd.

NPC, 2000, Northland Port Corporation. *Information Memorandum on the Proposal to Establish a Deepwater Port at Marsden Point*, Northland Port Corporation (NZ) Ltd, June 2000.

NRC, 1995, National Research Council - Committee on Beach Renourishment and Protection. *Beach Nourishment and Protection*. National Academy Press, Washington D.C, 334 pp.

NRC, 1999, Northland Regional Council. *Land Use Consent for Northport Ltd.*

O'Regan, P. and Chalmers, L., 1993. *Shoreline Change Analysis Using Digital Mapping Techniques*, University of Waikato, November, 1993, Hamilton.

Palmer, J., 2003a. *Meeting at Northport - Discussions Re: Bathymetric Changes Adjacent Nzrc Jetties*. to P. Longdill.

Palmer, J., 2003b. *Northport Development: The Consent Process in the New Zealand Coastal Environment*. Coasts and Ports Australasian Conference, Auckland, New Zealand, Paper no.10

Palmer, J., 2003c. *Talks Regarding Use of Sediment from Dredge Basin*. to P. Longdill.

Palmer, J., Orange, A. and Tucker, S., 2003. *Marsden Point Deepwater Port Development*. Coasts and Ports Australasian Conference, Auckland, New Zealand, Paper no. 158.

Pethick, J., 1984. *An Introduction to Coastal Geomoprphology*. Edward Arnold, 260 pp.

Poynter, M., 1993. *Marsden Point Forestry Port : Environmental Impact Report, Ecology and Water Qualtiy*, Marine Biological Consultant, for Northland Port Corportation, 18 March 1993, Whangarei.

Price, M., 2002. *Registering Images in Arcgis*, ArcUser, pp. 48-51.

Raudkivi, A.J., 1976. *Loose Boundary Hydraulics*. Pergamon Press, 397 pp.

RDI, 2001, RDI Instruments. *Winadcp*1.1.0 ADCP Programming, Download and Analysis Software for RD Instuments,

Rogers, N.C., 1959. *Hydraulic Model Study*, Whangarei Harbour Board.

Ross, M.A. and Mehta, A.J., 1989. On the Mechanics of Lutoclines and Fluid Mud. *Journal of Coastal Research*(Special Issue 5): 51-61.

Schofield, J.C., 1970. Coastal Sands of Northland and Whangarei. *New Zealand Journal of Geology and Geophysics*, 13(3): 767-824.

Schofield, J.C., 1975. Sea-Level Fluctuations Cause Periodic, Post-Glacial Progradation, South Kaipara Barrier, North Island, New Zealand. *New Zealand Journal of Geology and Geophysics*, 18: 295-316.

Shepard, F.P., 1950. *Beach Cycles in Southern California*, U.S. Army Corps of Engineers, Beach Erosion Board, Technical Memo No.20.

SONTEK, 1997a. *Acoustic Doppler Profiler (ADP) Principles of Operation*, San Diego, CA, 12 pp.

SONTEK, 1997b. *ADPS.exe* Data Aquisition Software,

Stauble, D.K., Garcia, A.W., Kraus, N.C., Grosskopf, W.G. and Bass, G.P., 1993. *Beach Nourishment Project Response and Design Evaluation: Ocean City, Maryland*, US Army Corps of Engineers, Waterways Experiment Station, Vicksburg, Mississippi.

Stevens, R., 1998. *Resource Consent Application: Assessment of Effects: Proposed Foreshore Protection - Eastern One Tree Point*, Richard Stevens Consultants Ltd, November, 1998, Whangarei.

Stevens, R., 1999. *One Tree Point Protection Works - Stage 2*, Richard Stevens Consultants Ltd, August 1999, Whangarei.

Sunamura, T. and Horikawa, K., 1972. *Improved Method for Inferring the Direction of Littoral Drift from Grain Size Properties of Beach Sands. In Annual Report of the Engineering Research Institute, Faculty of Engineering, University of Tokyo 31*, Tokyo.

Tanner, W.F., 1995. *Environmental Clastic Granulometry.* Florida Geological Survey Special Publication No.40, Tallahassee, 164 pp.

Thompson, B.N., 1961. *Sheet 2a, Whangarei. (1st Edition) Geological Map of New Zealand.* Department of Scientific and Industrial Research (DSIR), Wellington, New Zealand.

Tonkin-Taylor, T.T., 1979a. *New Zealand Electricity Report on Foreshore Erosion Marsden Power Stations, Bream Bay*, New Zealand Electricity, March 1979.

Tonkin-Taylor, T.T., 1979b. *New Zealand Electricity Report on Foreshore Erosion Marsden Power Station, Bream Bay Appendicies*, New Zealand Electricity, March 1979.

Tonkin-Taylor, T.T., 1979c. *New Zealand Electricity, Marsden Power Stations, Coastal Erosion Investigations, Phase 1 Report.*, New Zealand Electricity, December 1979.

Tonkin-Taylor, T.T., 1980. *New Zealand Electricity, Marsden Power Stations, Coastal Erosion Investigation, Foreshore Protection Trial.*, New Zealand Electricity, November 1980.

Tonkin-Taylor, T.T., 1981. *New Zealand Electricity, Marsden Power Stations, Coastal Erosion Investigations, Wave Studies*, New Zealand Electricity, February 1981.

Triton Elics, 1998a. *Isis Sonar User's Manual*, Version 3.22. Triton Elics International, 414 pp.

Triton Elics, 1998b. *Using Delph Map, Users Manual*, Version 2.0. Triton Elics International, 26 pp.

Tucker, M.E., 1991. *Sedimentary Petrology: An Introduction to the Origin of Sedimentary Rocks, 2nd Ed.* Blackwell Scientific Publications, Cambrigde, 260 pp.

Turner, I. et al., 2000. *Predicted and Observed Coastline Changes at the Gold Coast Artificial Reef.* Proceedings of the 27th International Conference on Coastal Engineering, Sydeny, Auastralia, 1836-1847.

USACE, 2002, United States Army Corps of Engineers. *Coastal Engineering Manual (Em 1110-2-1100).*

van Rijn, L.C., 1993. *Principles of Sediment Transport in Rivers, Estuaries and Coastal Seas.* Aqua Publications, Amsterdam.

Venus, G., 1984. *Whangarei Harbour Study :Technical Report No.1. Physical Oceanography*, Northland Harbour Board.

White, B., 1998. *Spinnaker Strand and Waimanu Bay Reserve, Coastal Protection, Technical Report*. 2022, Wood and Partners Consultants Ltd, CDL Land New Zealand Ltd, Waitakere City Council, April, 1998, Auckland.

WHSWSC, 1988, Whangarei Harbour Study Working and Steering Comittees. *Whangarei Harbour Study*, Northland Harbour Board, May 1988.

Winant, C.D., Inman, D.L. and Nordstrom, C.E., 1975. Description of Seasonal Beach Changes Using Empirical Eigenfunctions. *Journal of Geophysical Research*, 80(15): 1979-1986.

Work, P.A. and Dean, R.G., 1990. *Even/Odd Analysis of Shoreline Changes Adjacent to Florida's Tidal Inlets*. Twenty-Second Coastal Engineering Conference, Delft, The Netherlands, 2522-2535

Wright, L.D., Boon, J.D., Kim, S.C. and List, J.H., 1991. Modes of Cross-Shore Sediment Transport on the Shoreface of the Mid Atlantic Bight. *Marine Geology*, 96: 19-51.

Yallin, M.S., 1963. An Espression for Bed-Load Transportation. *Journal of the Hydraulics Div. (ASCE)*, 89(HY3): 221-250.

Appendix A

SEDIMENT DETAILS AND DISTRIBUTIONS

Moment measures: (Krumbein and Pettijohn, 1938)

The first moment is also the mean. Given by:

$$m_1 = \frac{\sum fx}{n}$$

Where x = grain size class midpoint (Φ)

f= class frequency (%)

$n = \sum f$

The higher orders of moments are calculated by:

$$m_p = \frac{\sum f(x - m_1)^p}{n-1}$$

Where p is an integer

m_p is the p^{th} moment about the mean.

The first four moments are required to calculate the sorting, skewness, and kurtosis of a grain size distribution:

$$sorting, \sigma_\phi = \sqrt{m_2}$$

$$skewness, Sk_\phi = \frac{m_3}{(m_2)^{1.5}}$$

$$kurtosis, K_\phi = \frac{m_4}{(m_2)^2}$$

Verbal descriptors

Verbal descriptors for moment measures of the grain size distribution (after Larsen et al. 1997).

Sorting Range (Φ)	Description of Sorting
< 0.35	Very well sorted
0.35 – 0.50	Well sorted
0.50 – 0.71	Moderately well sorted
0.71 – 1.00	Moderately sorted
1.00 – 2.00	Poorly sorted
2.00 – 4.00	Very poorly sorted
> 4.00	Extremely poorly sorted

Skewness Range	Description of Skewness
+1.0 - +0.3	Very fine skewed
+0.3 - +0.1	Fine skewed
+0.1 - -0.1	Near symmetrical
-0.1 - -0.3	Coarse skewed
-0.3 - -1.0	Very coarse skewed

Percent abundances of sediment fractions.

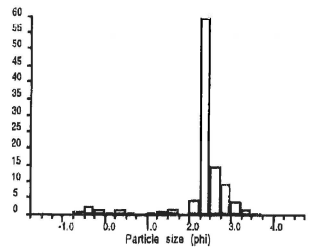
		Mt Eden 1949		Percent Abundance				Cumulative Weights (g)			
Site			E	-1 - 1 phi	1 - 2 phi	2 - 3 phi	> 3 phi	1 phi	2 phi	3 phi	Total
				Coarse/V. Coarse	Medium	Fine	Very Fine				
Profile A	1	815130	276179	5.9%	2.4%	86.7%	4.9%	1.07	1.5	17.13	18.02
Profile B	2	815344	276087	2.7%	2.9%	90.8%	3.6%	0.62	1.28	22.22	23.05
Profile C	3	815432	276013	0.3%	3.4%	89.1%	7.2%	0.03	0.43	10.89	11.74
Profile D	4	815446	275987	0.8%	1.0%	87.9%	10.3%	0.11	0.25	13.01	14.51
Profile E	5	815471	275892	0.5%	1.8%	91.9%	5.8%	0.05	0.24	9.83	10.44
Profile F	6	815478	275815	0.1%	3.3%	87.9%	8.7%	0.01	0.58	15.56	17.05
Profile G	7	815458	275699	0.2%	1.2%	85.5%	13.1%	0.02	0.14	8.65	9.95
Profile 1	8	815444	275622	0.2%	2.7%	97.0%	0.0%	0.05	0.69	23.37	23.37
Profile 2	9	815420	275285	0.1%	15.1%	82.0%	2.8%	0.01	2.3	14.73	15.15
Profile 3	10	815608	274342	1.3%	34.6%	64.1%	0.0%	0.24	6.69	18.64	18.64
Profile 4	11	815684	274150	0.6%	25.9%	71.3%	2.2%	0.16	6.56	24.18	24.72
Profile 5	12	815596	273905	18.1%	74.2%	6.0%	1.8%	2.09	10.67	11.36	11.57
Profile 6	13	815691	273526	3.8%	14.5%	80.1%	1.6%	0.63	3.04	16.32	16.58
Profile 7	14	815844	273379	1.8%	68.6%	28.2%	1.4%	0.31	12.16	17.04	17.28
Profile 7-1	15	816170	273287	3.1%	73.0%	22.3%	1.6%	0.69	17.17	22.21	22.57
Profile 8	16	816261	273040	4.2%	58.6%	35.1%	2.0%	0.87	12.94	20.16	20.58
Profile 9	17	816435	272736	2.1%	75.9%	21.6%	0.4%	0.3	11.04	14.09	14.15
Profile 10	18	816591	272610	3.0%	78.0%	15.2%	3.7%	0.45	11.97	14.22	14.76
Profile 11	19	816791	272502	3.0%	88.9%	7.3%	0.9%	0.44	13.43	14.49	14.62
Profile 12	20	817107	272322	1.0%	72.9%	24.2%	1.9%	0.19	14.02	18.61	18.97
Profile 13	21	817346	272168	1.0%	85.2%	12.5%	1.3%	0.15	13.15	15.06	15.26
Dredge Basin A	22	816164	274699	27.6%	9.5%	40.8%	22.2%	2.39	3.21	6.74	8.66
Dredge Basin B	23	816293	274885	4.0%	74.8%	20.5%	0.7%	0.88	17.44	21.98	22.14
Dredge Basin C	24	816194	275075	9.5%	9.3%	77.7%	3.5%	1.15	2.27	11.63	12.05
Dredge Basin D	25	815893	275370	5.6%	8.9%	84.0%	1.6%	0.74	1.92	13.12	13.33
Consent Area E	26	816584	274703	1.2%	23.3%	73.9%	1.6%	0.13	2.69	10.8	10.98
Consent Area F	27	816154	274448	1.3%	17.0%	70.9%	10.8%	0.12	1.74	8.49	9.52
Intertidal 1	28	815510	275515	0.1%	3.9%	91.1%	4.9%	0.01	0.78	18.68	19.65
Intertidal 2	29	813875	275208	0.9%	18.2%	75.3%	5.6%	0.11	2.35	11.61	12.3
Intertidal 3	30	815821	273686	2.2%	51.8%	42.2%	3.9%	0.48	11.7	20.84	21.68
Intertidal 4	31	816281	273310	7.4%	56.7%	29.6%	6.3%	1.54	13.4	19.59	20.91
Intertidal 5	50	816701	272785	0.0%	3.6%	74.8%	21.6%	0	0.7	15.1	19.26
45,14	33	816181	273887	9.9%	18.7%	52.4%	18.9%	1.38	3.98	11.26	13.88
81,14	34	815595	275590	2.4%	1.9%	84.1%	11.6%	0.32	0.58	11.84	13.39
63,24	35	816362	274901	0.4%	6.3%	91.0%	2.2%	0.04	0.61	8.82	9.02
SS2 - site 1	36	815760	275745	2.5%	2.5%	93.6%	1.4%	0.43	0.86	16.95	17.19
SS2 - D	37	815790	275373	1.6%	5.0%	84.4%	8.9%	0.25	1.04	14.26	15.66
SS2 - E	38	815561	276157	3.8%	0.0%	89.6%	6.5%	0.17	0.17	4.15	4.44
SS2 - H	39	815931	274363	0.0%	4.3%	89.7%	6.1%	0	0.78	17.23	18.34
SS2 – I	40	815885	274095	1.1%	11.0%	87.8%	0.0%	0.19	2.03	16.7	16.7
SS2 – J	41	816040	273544	0.0%	5.4%	84.5%	10.2%	0	1.07	17.96	19.99
SS2 - K	42	816266	273399	2.6%	1.4%	70.8%	25.2%	0.21	0.32	6.07	8.12
SS2 - L	43	816414	273164	27.5%	22.5%	46.0%	4.0%	4.16	7.55	14.49	15.1
SS2 - M	44	816569	272954	14.5%	20.1%	45.2%	20.1%	1.74	4.15	9.56	11.97

PARTICLE SIZE ANALYSIS

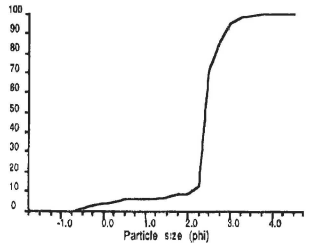
Earth Sciences - University of Waikato

Sample: PROFILE A - MARSDEN POINT, NORTHPORT

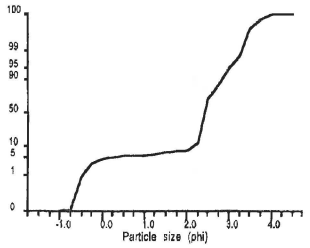
Size distribution histogram



Cumulative frequency



Cumulative frequency



Results summary

Textural size classes

Gravel= 0.00% Sand= 99.94% Silt= 0.06% Clay= 0.00%

Gravel free detrital sediment

Sand

Moment method parameters (phi)

Mean= 2.32 Sorting= 0.69 Skewness= -2.77 Kurtosis= 11.43

Graphical method parameters (phi)

Mean= 2.46 Sorting= 0.52 Skewness= -0.10 Kurtosis= 4.38

Median= 2.41 C= -0.49 D35= 2.34 D65= 2.47

Textural description:

Moderately well sorted, Near symmetrical, Extremely leptokurtic

Raw data summary

Size (phi)	Size (mm)	Cumulative weight (g)	Interval frequency (%)	Cumulative frequency (%)
-1.50	2.8284	0.00	0.00	0.00
-1.25	2.3784	0.00	0.00	0.00
-1.00	2.0000	0.00	0.00	0.00
-0.75	1.6818	0.02	0.11	0.11
-0.50	1.4142	0.16	0.78	0.89
-0.25	1.1892	0.57	2.28	3.16
0.00	1.0000	0.78	1.17	4.33
0.25	0.8409	0.85	0.39	4.72
0.50	0.7071	1.01	0.89	5.60
0.75	0.5946	1.06	0.28	5.88
1.00	0.5000	1.07	0.06	5.94
1.25	0.4204	1.11	0.22	6.16
1.50	0.3536	1.22	0.61	6.77
1.75	0.2973	1.50	1.55	8.32
2.00	0.2500	1.50	0.00	8.32
2.25	0.2102	2.26	4.22	12.54
2.50	0.1768	12.98	59.49	72.03
2.75	0.1487	15.54	14.21	86.24
3.00	0.1250	17.13	8.82	95.06
3.25	0.1051	17.75	3.44	98.50
3.50	0.0884	17.95	1.11	99.61
3.75	0.0743	17.99	0.22	99.83
4.00	0.0625	18.01	0.11	99.94
4.25	0.0526	18.01	0.00	99.94
4.50	0.0442	18.02	0.06	100.00

Total weight = 18.02 g

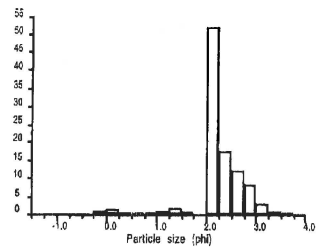
University of Waikato
Rapid Sediment Analyser
Operating System Version 7.1

PARTICLE SIZE ANALYSIS

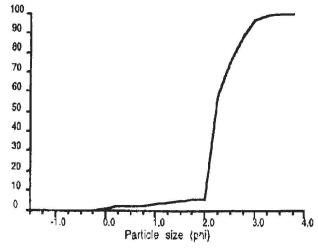
Earth Sciences - University of Waikato

Sample: Profile B, MARSDEN POINT, NORTHPORT

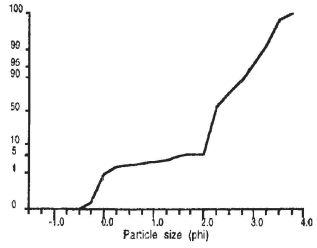
Size distribution histogram



Cumulative frequency



Cumulative frequency



Results summary

Textural size classes

Gravel= 0.00% Sand= 100.00% Silt= 0.00% Clay= 0.00%

Gravel free detrital sediment

Sand

Moment method parameters (phi)

Mean= 2.26 Sorting= 0.49 Skewness= -2.05 Kurtosis= 12.22

Graphical method parameters (phi)

Mean= 2.31 Sorting= 0.37 Skewness= 0.27 Kurtosis= 1.44

Median= 2.21 C= 0.03 D35= 2.14 D65= 2.35

Textural description:

Well sorted, Fine skewed, Leptokurtic

Raw data summary

Size (phi)	Size (mm)	Cumulative weight (g)	Interval frequency (%)	Cumulative frequency (%)
-1.25	2.3784	0.00	0.00	0.00
-1.00	2.0000	0.00	0.00	0.00
-0.75	1.6818	0.01	0.04	0.04
-0.50	1.4142	0.02	0.04	0.09
-0.25	1.1892	0.05	0.13	0.22
0.00	1.0000	0.20	0.65	0.87
0.25	0.8409	0.45	1.09	1.95
0.50	0.7071	0.50	0.22	2.17
0.75	0.5946	0.55	0.22	2.39
1.00	0.5000	0.62	0.30	2.69
1.25	0.4204	0.77	0.65	3.34
1.50	0.3536	1.11	1.48	4.82
1.75	0.2973	1.28	0.74	5.56
2.00	0.2500	1.28	0.00	5.56
2.25	0.2102	13.38	52.52	58.07
2.50	0.1768	17.46	17.71	75.78
2.75	0.1487	20.31	12.37	88.15
3.00	0.1250	22.22	8.29	96.44
3.25	0.1051	22.86	2.78	99.22
3.50	0.0884	22.99	0.56	99.79
3.75	0.0743	23.05	0.26	100.05

Total weight = 23.04 g

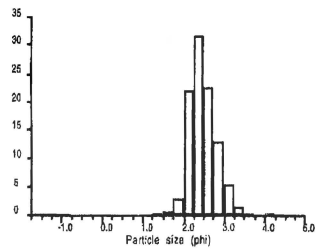
University of Waikato
Rapid Sediment Analyser
Operating System Version 7.1

PARTICLE SIZE ANALYSIS

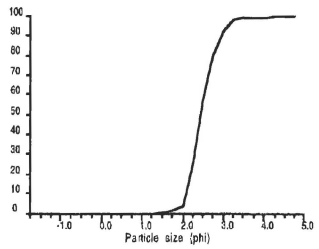
Earth Sciences - University of Waikato

Sample: Profile C - MARSDEN POINT, NORTHPORT

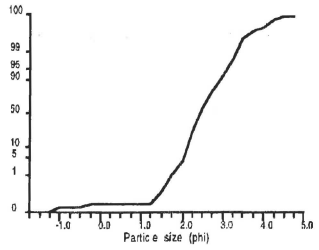
Size distribution histogram



Cumulative frequency



Cumulative frequency



Results summary

Textural size classes

Gravel= 0.17% Sand= 99.49% Silt= 0.34% Clay= 0.00%

Gravel bearing detrital sediment

Slightly Gravelly Sand

Moment method parameters (phi)

Mean= 2.47 Sorting= 0.38 Skewness= -1.35 Kurtosis= 20.60

Graphical method parameters (phi)

Mean= 2.47 Sorting= 0.34 Skewness= 0.17 Kurtosis= 0.99

Median= 2.44 C= 1.74 D35= 2.32 D65= 2.59

Textural description:

Very well sorted, Fine skewed, Mesokurtic

Raw data summary

Size (phi)	Size (mm)	Cumulative weight (g)	Interval frequency (%)	Cumulative frequency (%)
-1.50	2.8284	0.00	0.00	0.00
-1.25	2.3784	0.01	0.09	0.09
-1.00	2.0000	0.02	0.09	0.17
-0.75	1.6818	0.02	0.00	0.17
-0.50	1.4142	0.02	0.00	0.17
-0.25	1.1892	0.03	0.09	0.26
0.00	1.0000	0.03	0.00	0.26
0.25	0.8409	0.03	0.00	0.26
0.50	0.7071	0.03	0.00	0.26
0.75	0.5946	0.03	0.00	0.26
1.00	0.5000	0.03	0.00	0.26
1.25	0.4204	0.03	0.00	0.26
1.50	0.3536	0.06	0.26	0.51
1.75	0.2973	0.12	0.51	1.02
2.00	0.2500	0.43	2.64	3.66
2.25	0.2102	3.01	21.96	25.62
2.50	0.1768	6.72	31.57	57.19
2.75	0.1487	9.38	22.64	79.83
3.00	0.1250	10.89	12.85	92.68
3.25	0.1051	11.52	5.36	98.04
3.50	0.0884	11.68	1.36	99.40
3.75	0.0743	11.70	0.17	99.57
4.00	0.0625	11.71	0.09	99.66
4.25	0.0526	11.73	0.17	99.83
4.50	0.0442	11.74	0.09	99.91
4.75	0.0372	11.74	0.00	99.91

Total weight = 11.75 g

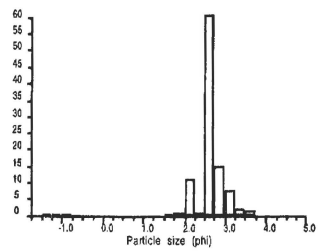
University of Waikato
Rapid Sediment Analyser
Operating System Version 7.1

PARTICLE SIZE ANALYSIS

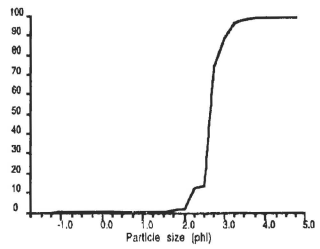
Earth Sciences - University of Waikato

Sample: PROFILE D - MARSDEN POINT, NORTHPORT

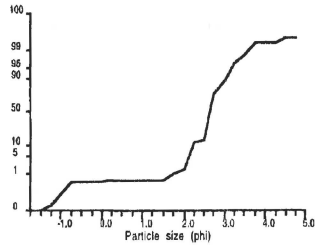
Size distribution histogram



Cumulative frequency



Cumulative frequency



Results summary

Textural size classes

Gravel= 0.41% Sand= 98.92% Silt= 0.67% Clay= 0.00%

Gravel bearing detrital sediment

Slightly Gravelly Sand

Moment method parameters (phi)

Mean= 2.62 Sorting= 0.43 Skewness= -4.40 Kurtosis= 40.86

Graphical method parameters (phi)

Mean= 2.69 Sorting= 0.27 Skewness= 0.14 Kurtosis= 2.15

Median= 2.65 C= 1.68 D35= 2.59 D65= 2.71

Textural description:

Very well sorted, Fine skewed, Very leptokurtic

Raw data summary

Size (phi)	Size (mm)	Cumulative weight (g)	Interval frequency (%)	Cumulative frequency (%)
-1.50	2.8284	0.00	0.00	0.00
-1.25	2.3784	0.03	0.21	0.21
-1.00	2.0000	0.06	0.21	0.41
-0.75	1.6818	0.10	0.27	0.69
-0.50	1.4142	0.10	0.00	0.69
-0.25	1.1892	0.10	0.00	0.69
0.00	1.0000	0.10	0.00	0.69
0.25	0.8409	0.11	0.07	0.75
0.50	0.7071	0.11	0.00	0.75
0.75	0.5946	0.11	0.00	0.75
1.00	0.5000	0.11	0.00	0.75
1.25	0.4204	0.11	0.00	0.75
1.50	0.3536	0.11	0.00	0.75
1.75	0.2973	0.16	0.34	1.10
2.00	0.2500	0.25	0.62	1.71
2.25	0.2102	1.87	11.10	12.81
2.50	0.1768	1.98	0.75	13.56
2.75	0.1487	10.85	60.77	74.33
3.00	0.1250	13.01	14.80	89.13
3.25	0.1051	14.10	7.47	96.59
3.50	0.0884	14.35	1.71	98.31
3.75	0.0743	14.50	1.03	99.33
4.00	0.0625	14.50	0.00	99.33
4.25	0.0526	14.50	0.00	99.33
4.50	0.0442	14.51	0.07	99.40
4.75	0.0372	14.51	0.00	99.40

Total weight = 14.60 g

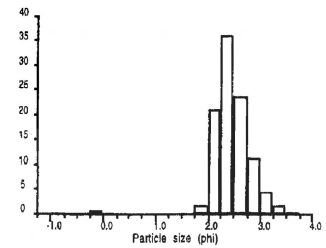
University of Waikato
Rapid Sediment Analyser
Operating System Version 7.1

PARTICLE SIZE ANALYSIS

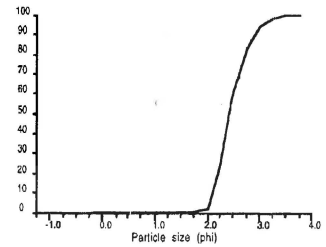
Earth Sciences - University of Waikato

Sample: PROFILE E - MARSDEN POINT, NORTHPORT

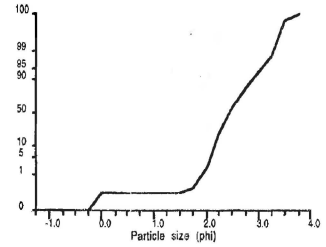
Size distribution histogram



Cumulative frequency



Cumulative frequency



Results summary

Textural size classes

Gravel= 0.00% Sand= 100.00% Silt= 0.00% Clay= 0.00%

Gravel free detrital sediment

Sand

Moment method parameters (phi)

Mean= 2.47 Sorting= 0.35 Skewness= -1.42 Kurtosis= 16.11

Graphical method parameters (phi)

Mean= 2.46 Sorting= 0.31 Skewness= 0.16 Kurtosis= 1.03

Median= 2.44 C= 1.81 D35= 2.33 D65= 2.56

Textural description:

Very well sorted, Fine skewed, Mesokurtic

Raw data summary

Size (phi)	Size (mm)	Cumulative weight (g)	Interval frequency (%)	Cumulative frequency (%)
-1.00	2.0000	0.00	0.00	0.00
-0.75	1.6818	0.00	0.00	0.00
-0.50	1.4142	0.00	0.00	0.00
-0.25	1.1892	0.00	0.00	0.00
0.00	1.0000	0.05	0.48	0.48
0.25	0.8409	0.05	0.00	0.48
0.50	0.7071	0.05	0.00	0.48
0.75	0.5946	0.05	0.00	0.48
1.00	0.5000	0.05	0.00	0.48
1.25	0.4204	0.05	0.00	0.48
1.50	0.3536	0.05	0.00	0.48
1.75	0.2973	0.06	0.10	0.57
2.00	0.2500	0.24	1.72	2.30
2.25	0.2102	2.42	20.88	23.18
2.50	0.1768	6.19	36.11	59.29
2.75	0.1487	8.65	23.56	82.85
3.00	0.1250	9.83	11.30	94.16
3.25	0.1051	10.28	4.31	98.47
3.50	0.0884	10.42	1.34	99.81
3.75	0.0743	10.44	0.19	100.00

Total weight = 10.44 g

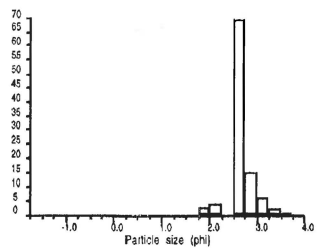
University of Waikato
Rapid Sediment Analyser
Operating System Version 7.1

PARTICLE SIZE ANALYSIS

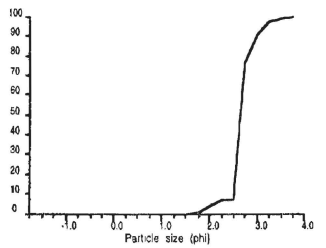
Earth Sciences - University of Waikato

Sample: PROFILEGD F - MARSDEN POINT, NORTHPORT

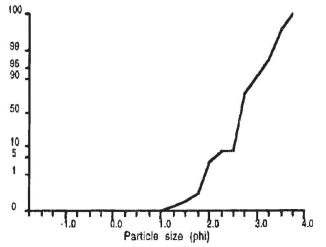
Size distribution histogram



Cumulative frequency



Cumulative frequency



Results summary

Textural size classes

Gravel= 0.00% Sand= 100.00% Silt= 0.00% Clay= 0.00%

Gravel free detrital sediment

Sand

Moment method parameters (phi)

Mean= 2.67 Sorting= 0.28 Skewness= -1.29 Kurtosis= 15.06

Graphical method parameters (phi)

Mean= 2.69 Sorting= 0.24 Skewness= 0.12 Kurtosis= 2.37

Median= 2.65 C= 1.80 D35= 2.60 D65= 2.71

Textural description:

Very well sorted, Fine skewed, Very leptokurtic

Raw data summary

Size (phi)	Size (mm)	Cumulative weight (g)	Interval frequency (%)	Cumulative frequency (%)
-1.50	2.8284	0.00	0.00	0.00
-1.25	2.3784	0.00	0.00	0.00
-1.00	2.0000	0.00	0.00	0.00
-0.75	1.6818	0.00	0.00	0.00
-0.50	1.4142	0.00	0.00	0.00
-0.25	1.1892	0.01	0.06	0.06
0.00	1.0000	0.01	0.00	0.06
0.25	0.8409	0.01	0.00	0.06
0.50	0.7071	0.01	0.00	0.06
0.75	0.5946	0.01	0.00	0.06
1.00	0.5000	0.01	0.00	0.06
1.25	0.4204	0.03	0.12	0.18
1.50	0.3536	0.05	0.12	0.29
1.75	0.2973	0.08	0.18	0.47
2.00	0.2500	0.58	2.93	3.40
2.25	0.2102	1.24	3.87	7.28
2.50	0.1768	1.25	0.06	7.34
2.75	0.1487	13.05	69.25	76.58
3.00	0.1250	15.56	14.73	91.31
3.25	0.1051	16.64	6.34	97.65
3.50	0.0884	16.97	1.94	99.59
3.75	0.0743	17.05	0.47	100.06

Total weight = 17.04 g

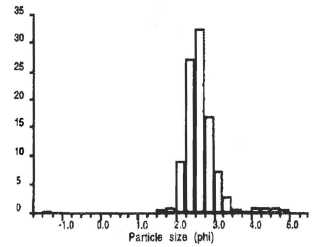
University of Waikato
Rapid Sediment Analyser
Operating System Version 7.1

PARTICLE SIZE ANALYSIS

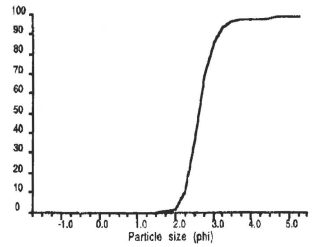
Earth Sciences - University of Waikato

Sample: PROFILE G - MARSDEN POINT, NORTHPORT

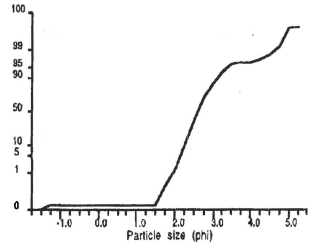
Size distribution histogram



Cumulative frequency



Cumulative frequency



Results summary

Textural size classes

Gravel= 0.20% Sand= 96.80% Silt= 3.00% Clay= 0.00%

Gravel bearing detrital sediment

Slightly Gravelly Sand

Moment method parameters (phi)

Mean= 2.64 Sorting= 0.47 Skewness= 0.40 Kurtosis= 18.22

Graphical method parameters (phi)

Mean= 2.62 Sorting= 0.36 Skewness= 0.16 Kurtosis= 1.18

Median= 2.60 C= 1.87 D35= 2.48 D65= 2.71

Textural description:

Well sorted, Fine skewed, Leptokurtic

Raw data summary

Size (phi)	Size (mm)	Cumulative weight (g)	Interval frequency (%)	Cumulative frequency (%)
-1.50	2.8284	0.00	0.00	0.00
-1.25	2.3784	0.02	0.20	0.20
-1.00	2.0000	0.02	0.00	0.20
-0.75	1.6818	0.02	0.00	0.20
-0.50	1.4142	0.02	0.00	0.20
-0.25	1.1892	0.02	0.00	0.20
0.00	1.0000	0.02	0.00	0.20
0.25	0.8409	0.02	0.00	0.20
0.50	0.7071	0.02	0.00	0.20
0.75	0.5946	0.02	0.00	0.20
1.00	0.5000	0.02	0.00	0.20
1.25	0.4204	0.02	0.00	0.20
1.50	0.3536	0.02	0.00	0.20
1.75	0.2973	0.06	0.40	0.60
2.00	0.2500	0.14	0.80	1.40
2.25	0.2102	1.02	8.81	10.21
2.50	0.1768	3.73	27.13	37.34
2.75	0.1487	6.97	32.43	69.77
3.00	0.1250	8.65	16.82	86.59
3.25	0.1051	9.36	7.11	93.69
3.50	0.0884	9.62	2.60	96.30
3.75	0.0743	9.67	0.50	96.80
4.00	0.0625	9.69	0.20	97.00
4.25	0.0526	9.76	0.70	97.70
4.50	0.0442	9.84	0.80	98.50
4.75	0.0372	9.91	0.70	99.20
5.00	0.0312	9.95	0.40	99.60
5.25	0.0263	9.95	0.00	99.60

Total weight = 9.99 g

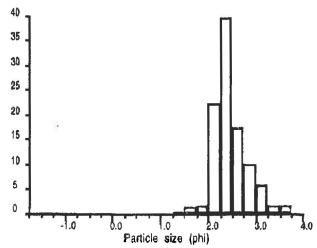
University of Waikato
Rapid Sediment Analyser
Operating System Version 7.1

PARTICLE SIZE ANALYSIS

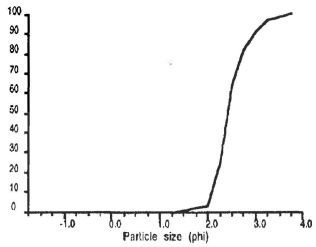
Earth Sciences - University of Waikato

Sample: Profile 1 - MARSDEN POINT, NORTHPORT

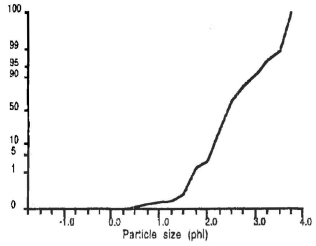
Size distribution histogram



Cumulative frequency



Cumulative frequency



Results summary

Textural size classes

Gravel= 0.04% Sand= 99.96% Silt= 0.00% Clay= 0.00%

Gravel bearing detrital sediment

Slightly Gravelly Sand

Moment method parameters (phi)

Mean= 2.48 Sorting= 0.37 Skewness= -0.23 Kurtosis= 11.05

Graphical method parameters (phi)

Mean= 2.45 Sorting= 0.34 Skewness= 0.26 Kurtosis= 1.15

Median= 2.41 C= 1.62 D35= 2.31 D65= 2.51

Textural description:

Very well sorted, Fine skewed, Leptokurtic

Raw data summary

Size (phi)	Size (mm)	Cumulative weight (g)	Interval frequency (%)	Cumulative frequency (%)
-1.50	2.8284	0.00	0.00	0.00
-1.25	2.3784	0.01	0.04	0.04
-1.00	2.0000	0.01	0.00	0.04
-0.75	1.6818	0.01	0.00	0.04
-0.50	1.4142	0.02	0.04	0.09
-0.25	1.1892	0.02	0.00	0.09
0.00	1.0000	0.02	0.00	0.09
0.25	0.8409	0.02	0.00	0.09
0.50	0.7071	0.03	0.04	0.13
0.75	0.5946	0.04	0.04	0.17
1.00	0.5000	0.05	0.04	0.22
1.25	0.4204	0.06	0.04	0.26
1.50	0.3536	0.09	0.13	0.39
1.75	0.2973	0.38	1.25	1.63
2.00	0.2500	0.69	1.33	2.97
2.25	0.2102	5.82	22.06	25.03
2.50	0.1768	14.99	39.44	64.47
2.75	0.1487	19.01	17.29	81.76
3.00	0.1250	21.32	9.94	91.70
3.25	0.1051	22.61	5.55	97.24
3.50	0.0884	22.99	1.63	98.88
3.75	0.0743	23.37	1.63	100.51

Total weight = 23.25 g

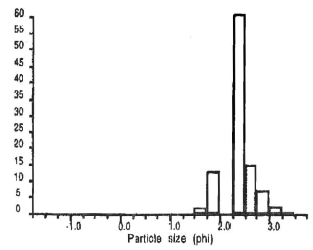
University of Waikato
Rapid Sediment Analyser
Operating System Version 7.1

PARTICLE SIZE ANALYSIS

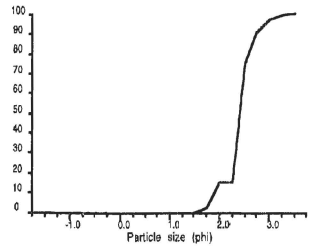
Earth Sciences - University of Waikato

Sample: PROFILE 2 - MARSDEN POINT, NORTHPORT

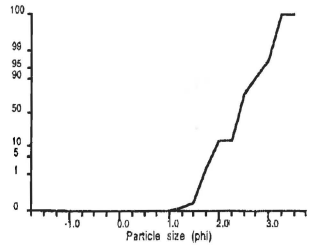
Size distribution histogram



Cumulative frequency



Cumulative frequency



Results summary

Textural size classes

Gravel= 0.07% Sand= 99.93% Silt= 0.00% Clay= 0.00%

Gravel bearing detrital sediment

Slightly Gravelly Sand

Moment method parameters (phi)

Mean= 2.39 Sorting= 0.31 Skewness= -1.35 Kurtosis= 17.22

Graphical method parameters (phi)

Mean= 2.43 Sorting= 0.26 Skewness= 0.10 Kurtosis= 2.19

Median= 2.39 C= 1.60 D35= 2.33 D65= 2.45

Textural description:

Very well sorted, Fine skewed, Very leptokurtic

Raw data summary

Size (phi)	Size (mm)	Cumulative weight (g)	Interval frequency (%)	Cumulative frequency (%)
-1.50	2.8284	0.00	0.00	0.00
-1.25	2.3784	0.01	0.07	0.07
-1.00	2.0000	0.01	0.00	0.07
-0.75	1.6818	0.01	0.00	0.07
-0.50	1.4142	0.01	0.00	0.07
-0.25	1.1892	0.01	0.00	0.07
0.00	1.0000	0.01	0.00	0.07
0.25	0.8409	0.01	0.00	0.07
0.50	0.7071	0.01	0.00	0.07
0.75	0.5946	0.01	0.00	0.07
1.00	0.5000	0.01	0.00	0.07
1.25	0.4204	0.02	0.07	0.13
1.50	0.3536	0.04	0.13	0.26
1.75	0.2973	0.31	1.79	2.05
2.00	0.2500	2.30	13.18	15.23
2.25	0.2102	2.30	0.00	15.23
2.50	0.1768	11.47	60.73	75.96
2.75	0.1487	13.69	14.70	90.66
3.00	0.1250	14.73	6.89	97.55
3.25	0.1051	15.09	2.38	99.93
3.50	0.0884	15.15	0.40	100.33

Total weight = 15.10 g

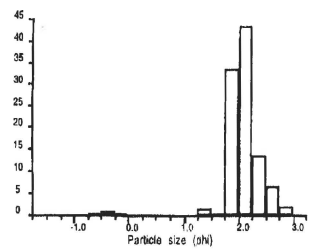
University of Waikato
Rapid Sediment Analyser
Operating System Version 7.1

PARTICLE SIZE ANALYSIS

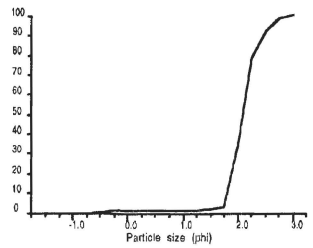
Earth Sciences - University of Waikato

Sample: PROFILE 3 - MARSDEN POINT, NORTHPORT

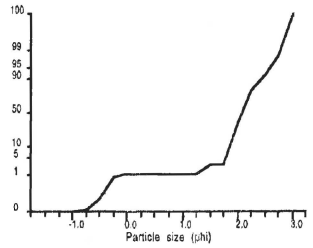
Size distribution histogram



Cumulative frequency



Cumulative frequency



Results summary

Textural size classes

Gravel= 0.05% Sand= 99.95% Silt= 0.00% Clay= 0.00%

Gravel bearing detrital sediment

Slightly Gravelly Sand

Moment method parameters (phi)

Mean= 2.09 Sorting= 0.38 Skewness= -3.49 Kurtosis= 26.99

Graphical method parameters (phi)

Mean= 2.09 Sorting= 0.25 Skewness= 0.16 Kurtosis= 1.12

Median= 2.08 C= -0.15 D35= 1.99 D65= 2.17

Textural description:

Very well sorted, Fine skewed, Leptokurtic

Raw data summary

Size (phi)	Size (mm)	Cumulative weight (g)	Interval frequency (%)	Cumulative frequency (%)
-1.50	2.8284	0.00	0.00	0.00
-1.25	2.3784	0.01	0.05	0.05
-1.00	2.0000	0.01	0.00	0.05
-0.75	1.6818	0.02	0.05	0.11
-0.50	1.4142	0.07	0.27	0.38
-0.25	1.1892	0.17	0.54	0.92
0.00	1.0000	0.21	0.22	1.13
0.25	0.8409	0.22	0.05	1.19
0.50	0.7071	0.22	0.00	1.19
0.75	0.5946	0.22	0.00	1.19
1.00	0.5000	0.24	0.11	1.29
1.25	0.4204	0.25	0.05	1.35
1.50	0.3536	0.49	1.29	2.64
1.75	0.2973	0.52	0.16	2.80
2.00	0.2500	6.69	33.26	36.06
2.25	0.2102	14.67	43.02	79.08
2.50	0.1768	17.11	13.15	92.24
2.75	0.1487	18.29	6.36	98.60
3.00	0.1250	18.64	1.89	100.49

Total weight = 18.55 g

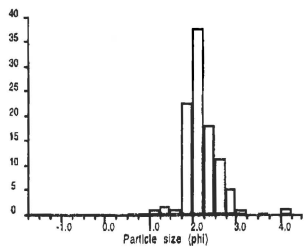
University of Waikato
Rapid Sediment Analyser
Operating System Version 7.1

PARTICLE SIZE ANALYSIS

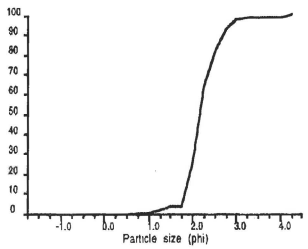
Earth Sciences - University of Waikato

Sample: PROFILE 4 - MARSDEN POINT, NORTHPORT

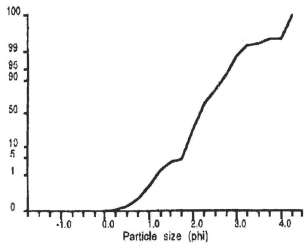
Size distribution histogram



Cumulative frequency



Cumulative frequency



Results summary

Textural size classes

Gravel= 0.08% Sand= 99.35% Silt= 0.57% Clay= 0.00%

Gravel bearing detrital sediment

Slightly Gravelly Sand

Moment method parameters (phi)

Mean= 2.21 Sorting= 0.42 Skewness= 0.31 Kurtosis= 11.52

Graphical method parameters (phi)

Mean= 2.19 Sorting= 0.33 Skewness= 0.21 Kurtosis= 1.05

Median= 2.15 C= 1.09 D35= 2.06 D65= 2.26

Textural description:

Very well sorted, Fine skewed, Mesokurtic

Raw data summary

Size (phi)	Size (mm)	Cumulative weight (g)	Interval frequency (%)	Cumulative frequency (%)
-1.50	2.8284	0.00	0.00	0.00
-1.25	2.3784	0.01	0.04	0.04
-1.00	2.0000	0.02	0.04	0.08
-0.75	1.6818	0.02	0.00	0.08
-0.50	1.4142	0.02	0.00	0.08
-0.25	1.1892	0.02	0.00	0.08
0.00	1.0000	0.02	0.00	0.08
0.25	0.8409	0.03	0.04	0.12
0.50	0.7071	0.04	0.04	0.16
0.75	0.5946	0.09	0.20	0.37
1.00	0.5000	0.16	0.28	0.65
1.25	0.4204	0.39	0.94	1.59
1.50	0.3536	0.82	1.75	3.33
1.75	0.2973	1.04	0.89	4.23
2.00	0.2500	6.56	22.45	26.68
2.25	0.2102	15.84	37.74	64.42
2.50	0.1768	20.22	17.81	82.23
2.75	0.1487	22.98	11.22	93.45
3.00	0.1250	24.18	4.88	98.33
3.25	0.1051	24.41	0.94	99.27
3.50	0.0884	24.42	0.04	99.31
3.75	0.0743	24.45	0.12	99.43
4.00	0.0625	24.45	0.00	99.43
4.25	0.0526	24.72	1.10	100.53

Total weight = 24.59 g

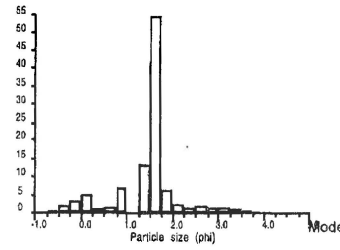
University of Waikato
Rapid Sediment Analyser
Operating System Version 7.1

PARTICLE SIZE ANALYSIS

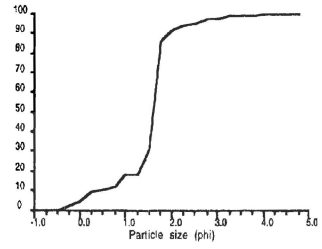
Earth Sciences - University of Waikato

Sample: PROFILE 5 - MARSDEN POINT, NORTHPORT

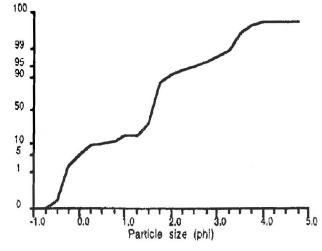
Size distribution histogram



Cumulative frequency



Cumulative frequency



Results summary

Textural size classes

Gravel= 0.00% Sand= 99.74% Silt= 0.26% Clay= 0.00%

Gravel free detrital sediment

Sand

Moment method parameters (phi)

Mean= 1.45 Sorting= 0.64 Skewness= -0.66 Kurtosis= 5.20

Graphical method parameters (phi)

Mean= 1.42 Sorting= 0.57 Skewness= -0.46 Kurtosis= 3.12

Median= 1.59 C= -0.39 D35= 1.52 D65= 1.65

Textural description:

Moderately well sorted, Strongly Coarse skewed, Extremely leptokurtic

Raw data summary

Size (phi)	Size (mm)	Cumulative weight (g)	Interval frequency (%)	Cumulative frequency (%)
-0.75	1.6818	-0.01	-0.09	-0.09
-0.50	1.4142	0.03	0.34	0.26
-0.25	1.1892	0.22	1.64	1.90
0.00	1.0000	0.55	2.84	4.74
0.25	0.8409	1.10	4.74	9.48
0.50	0.7071	1.19	0.78	10.26
0.75	0.5946	1.35	1.38	11.64
1.00	0.5000	2.09	6.38	18.02
1.25	0.4204	2.09	0.00	18.02
1.50	0.3536	3.62	13.19	31.21
1.75	0.2973	9.98	54.83	86.03
2.00	0.2500	10.67	5.95	91.98
2.25	0.2102	10.91	2.07	94.05
2.50	0.1768	11.06	1.29	95.34
2.75	0.1487	11.23	1.47	96.81
3.00	0.1250	11.36	1.12	97.93
3.25	0.1051	11.47	0.95	98.88
3.50	0.0884	11.54	0.60	99.48
3.75	0.0743	11.56	0.17	99.66
4.00	0.0625	11.57	0.09	99.74
4.25	0.0526	11.57	0.00	99.74
4.50	0.0442	11.57	0.00	99.74
4.75	0.0372	11.57	0.00	99.74

Total weight = 11.60 g

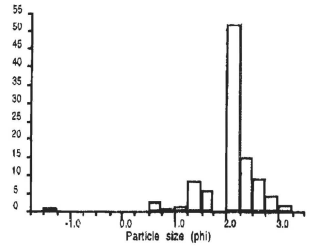
University of Waikato
Rapid Sediment Analyser
Operating System Version 7.1

PARTICLE SIZE ANALYSIS

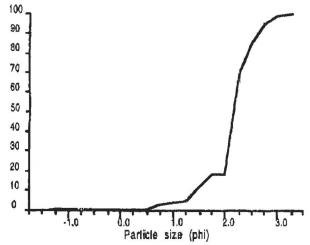
Earth Sciences - University of Waikato

Sample: PROFILE 6 - MARSDEN POINT, NORTHPORT

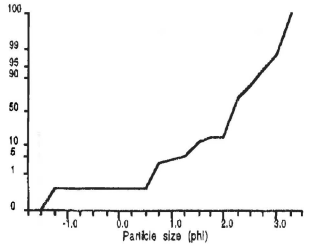
Size distribution histogram



Cumulative frequency



Cumulative frequency



Results summary

Textural size classes

Gravel= 0.54% Sand= 99.46% Silt= 0.00% Clay= 0.00%

Gravel bearing detrital sediment

Slightly Gravelly Sand

Moment method parameters (phi)

Mean= 2.09 Sorting= 0.52 Skewness= -2.17 Kurtosis= 13.24

Graphical method parameters (phi)

Mean= 2.09 Sorting= 0.44 Skewness= -0.20 Kurtosis= 2.10

Median= 2.15 C= 0.55 D35= 2.08 D65= 2.22

Textural description:

Well sorted, Coarse skewed, Very leptokurtic

Raw data summary

Size (phi)	Size (mm)	Cumulative weight (g)	Interval frequency (%)	Cumulative frequency (%)
-1.50	2.8284	0.00	0.00	0.00
-1.25	2.3784	0.09	0.54	0.54
-1.00	2.0000	0.09	0.00	0.54
-0.75	1.6818	0.09	0.00	0.54
-0.50	1.4142	0.09	0.00	0.54
-0.25	1.1892	0.09	0.00	0.54
0.00	1.0000	0.09	0.00	0.54
0.25	0.8409	0.09	0.00	0.54
0.50	0.7071	0.09	0.00	0.54
0.75	0.5946	0.51	2.54	3.08
1.00	0.5000	0.63	0.72	3.80
1.25	0.4204	0.79	0.97	4.77
1.50	0.3536	2.14	8.15	12.92
1.75	0.2973	3.04	5.43	18.36
2.00	0.2500	3.04	0.00	18.36
2.25	0.2102	11.63	51.87	70.23
2.50	0.1768	14.12	15.04	85.27
2.75	0.1487	15.64	9.18	94.44
3.00	0.1250	16.32	4.11	98.55
3.25	0.1051	16.58	1.57	100.12

Total weight = 16.56 g

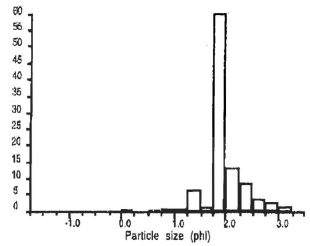
University of Waikato
Rapid Sediment Analyser
Operating System Version 7.1

PARTICLE SIZE ANALYSIS

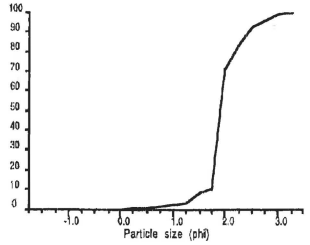
Earth Sciences - University of Waikato

Sample: Profile 7 - MARSDEN POINT, NORTHPORT

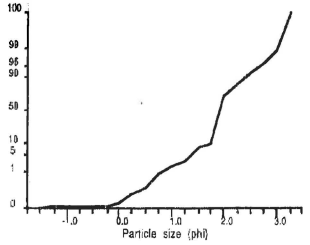
Size distribution histogram



Cumulative frequency



Cumulative frequency



Results summary

Textural size classes

Gravel= 0.12% Sand= 99.88% Silt= 0.00% Clay= 0.00%

Gravel bearing detrital sediment

Slightly Gravelly Sand

Moment method parameters (phi)

Mean= 1.96 Sorting= 0.39 Skewness= -0.78 Kurtosis= 11.80

Graphical method parameters (phi)

Mean= 1.98 Sorting= 0.32 Skewness= 0.28 Kurtosis= 2.00

Median= 1.92 C= 0.75 D35= 1.85 D65= 1.98

Textural description:

Very well sorted, Fine skewed, Very leptokurtic

Raw data summary

Size (phi)	Size (mm)	Cumulative weight (g)	Interval frequency (%)	Cumulative frequency (%)
-1.50	2.8284	0.00	0.00	0.00
-1.25	2.3784	0.02	0.12	0.12
-1.00	2.0000	0.02	0.00	0.12
-0.75	1.6818	0.02	0.00	0.12
-0.50	1.4142	0.02	0.00	0.12
-0.25	1.1892	0.02	0.00	0.12
0.00	1.0000	0.03	0.06	0.17
0.25	0.8409	0.07	0.23	0.41
0.50	0.7071	0.09	0.12	0.52
0.75	0.5946	0.17	0.46	0.99
1.00	0.5000	0.31	0.81	1.80
1.25	0.4204	0.46	0.87	2.67
1.50	0.3536	1.56	6.38	9.04
1.75	0.2973	1.76	1.16	10.20
2.00	0.2500	12.16	60.29	70.49
2.25	0.2102	14.45	13.28	83.77
2.50	0.1768	15.90	8.41	92.17
2.75	0.1487	16.58	3.94	96.12
3.00	0.1250	17.04	2.67	98.78
3.25	0.1051	17.28	1.39	100.17

Total weight = 17.25 g

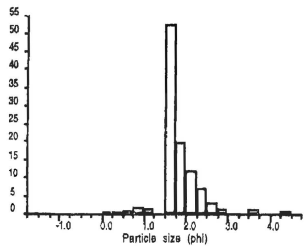
University of Waikato
Rapid Sediment Analyser
Operating System Version 7.1

PARTICLE SIZE ANALYSIS

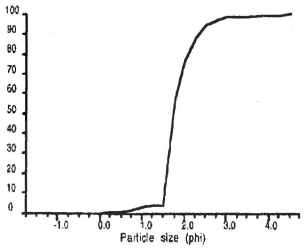
Earth Sciences - University of Waikato

Sample: PROFILE 7-1 - MARSDEN POINT, NORTHPORT

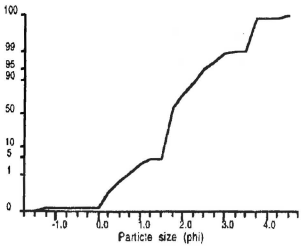
Size distribution histogram



Cumulative frequency



Cumulative frequency



Results summary

Textural size classes

Gravel= 0.13% Sand= 99.73% Silt= 0.13% Clay= 0.00%

Gravel bearing detrital sediment

Slightly Gravelly Sand

Moment method parameters (phi)

Mean= 1.83 Sorting= 0.45 Skewness= 0.86 Kurtosis= 13.31

Graphical method parameters (phi)

Mean= 1.81 Sorting= 0.30 Skewness= 0.52 Kurtosis= 1.06

Median= 1.72 C= 0.60 D35= 1.65 D65= 1.86

Textural description:

Very well sorted, Strongly fine skewed, Mesokurtic

Raw data summary

Size (phi)	Size (mm)	Cumulative weight (g)	Interval frequency (%)	Cumulative frequency (%)
-1.50	2.8284	0.00	0.00	0.00
-1.25	2.3784	0.03	0.13	0.13
-1.00	2.0000	0.03	0.00	0.13
-0.75	1.6818	0.03	0.00	0.13
-0.50	1.4142	0.03	0.00	0.13
-0.25	1.1892	0.03	0.00	0.13
0.00	1.0000	0.03	0.00	0.13
0.25	0.8409	0.11	0.36	0.49
0.50	0.7071	0.17	0.27	0.76
0.75	0.5946	0.31	0.62	1.38
1.00	0.5000	0.69	1.69	3.07
1.25	0.4204	0.88	0.85	3.91
1.50	0.3536	0.88	0.00	3.91
1.75	0.2973	12.73	52.71	56.63
2.00	0.2500	17.17	19.75	76.38
2.25	0.2102	19.85	11.92	88.30
2.50	0.1768	21.37	6.76	95.06
2.75	0.1487	21.99	2.76	97.82
3.00	0.1250	22.21	0.98	98.80
3.25	0.1051	22.24	0.13	98.93
3.50	0.0884	22.24	0.00	98.93
3.75	0.0743	22.45	0.93	99.87
4.00	0.0625	22.45	0.00	99.87
4.25	0.0526	22.45	0.00	99.87
4.50	0.0442	22.57	0.53	100.40

Total weight = 22.48 g

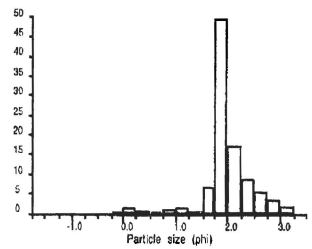
University of Waikato
Rapid Sediment Analyser
Operating System Version 7.1

PARTICLE SIZE ANALYSIS

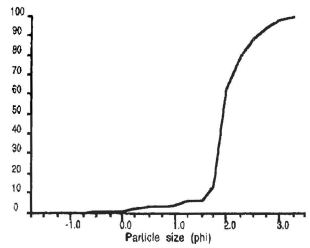
Earth Sciences - University of Waikato

Sample: Profile 8, MARSDEN POINT, NORTHPORT

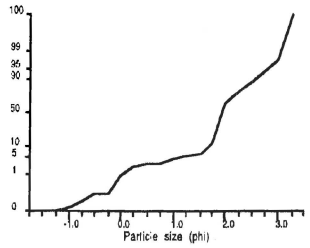
Size distribution histogram



Cumulative frequency



Cumulative frequency



Results summary

Textural size classes

Gravel= 0.15% Sand= 99.85% Silt= 0.00% Clay= 0.00%

Gravel bearing detrital sediment

Slightly Gravelly Sand

Moment method parameters (phi)

Mean= 1.97 Sorting= 0.51 Skewness= -1.56 Kurtosis= 10.23

Graphical method parameters (phi)

Mean= 2.02 Sorting= 0.40 Skewness= 0.23 Kurtosis= 1.85

Median= 1.93 C= 0.03 D35= 1.86 D65= 2.03

Textural description:

Well sorted, Fine skewed, Very leptokurtic

Raw data summary

Size (phi)	Size (mm)	Cumulative weight (g)	Interval frequency (%)	Cumulative frequency (%)
-1.50	2.8284	0.00	0.00	0.00
-1.25	2.3784	0.01	0.05	0.05
-1.00	2.0000	0.03	0.10	0.15
-0.75	1.6818	0.06	0.15	0.29
-0.50	1.4142	0.09	0.15	0.44
-0.25	1.1892	0.09	0.00	0.44
0.00	1.0000	0.17	0.39	0.83
0.25	0.8409	0.46	1.41	2.24
0.50	0.7071	0.58	0.58	2.82
0.75	0.5946	0.64	0.29	3.11
1.00	0.5000	0.87	1.12	4.23
1.25	0.4204	1.18	1.51	5.74
1.50	0.3536	1.31	0.63	6.37
1.75	0.2973	2.73	6.91	13.28
2.00	0.2500	12.94	49.66	62.93
2.25	0.2102	16.44	17.02	79.96
2.50	0.1768	18.25	8.80	88.76
2.75	0.1487	19.41	5.64	94.40
3.00	0.1250	20.16	3.65	98.05
3.25	0.1051	20.58	2.04	100.09

Total weight = 20.56 g

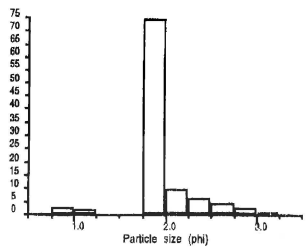
University of Waikato
Rapid Sediment Analyser
Operating System Version 7.1

PARTICLE SIZE ANALYSIS

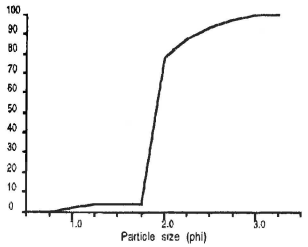
Earth Sciences - University of Waikato

Sample: PROFILE 9 - MARSDEN POINT, NORTHPORT

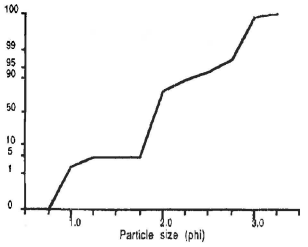
Size distribution histogram



Cumulative frequency



Cumulative frequency



Results summary

Textural size classes

Gravel= 0.00% Sand= 100.00% Silt= 0.00% Clay= 0.00%

Gravel free detrital sediment

Sand

Moment method parameters (phi)

Mean= 1.96 Sorting= 0.31 Skewness= 0.17 Kurtosis= 7.09

Graphical method parameters (phi)

Mean= 1.95 Sorting= 0.22 Skewness= 0.50 Kurtosis= 2.02

Median= 1.90 C= 0.88 D35= 1.85 D65= 1.96

Textural description:

Very well sorted, Strongly fine skewed, Very leptokurtic

Raw data summary

Size (phi)	Size (mm)	Cumulative weight (g)	Interval frequency (%)	Cumulative frequency (%)
0.75	0.5946	-0.04	-0.28	-0.28
1.00	0.5000	0.30	2.41	2.13
1.25	0.4204	0.58	1.98	4.11
1.50	0.3536	0.58	0.00	4.11
1.75	0.2973	0.58	0.00	4.11
2.00	0.2500	11.04	74.13	78.24
2.25	0.2102	12.37	9.43	87.67
2.50	0.1768	13.21	5.95	93.62
2.75	0.1487	13.79	4.11	97.73
3.00	0.1250	14.09	2.13	99.86
3.25	0.1051	14.15	0.43	100.28

Total weight = 14.11 g

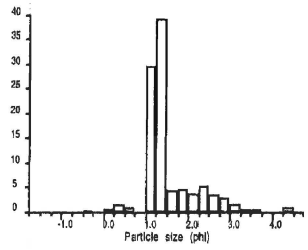
University of Waikato
Rapid Sediment Analyser
Operating System Version 7.1

PARTICLE SIZE ANALYSIS

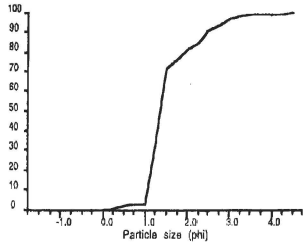
Earth Sciences - University of Waikato

Sample: PROFILE 10 - MARSDEN POINT, NORTHPORT

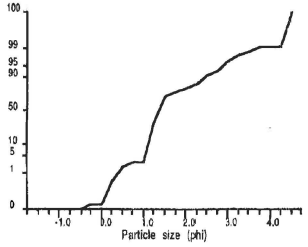
Size distribution histogram



Cumulative frequency



Cumulative frequency



Results summary

Textural size classes

Gravel= 0.07% Sand= 99.12% Silt= 0.81% Clay= 0.00%

Gravel bearing detrital sediment

Slightly Gravelly Sand

Moment method parameters (phi)

Mean= 1.55 Sorting= 0.64 Skewness= 1.53 Kurtosis= 6.78

Graphical method parameters (phi)

Mean= 1.55 Sorting= 0.55 Skewness= 0.58 Kurtosis= 1.56

Median= 1.36 C= 0.31 D35= 1.27 D65= 1.46

Textural description:

Moderately well sorted, Strongly fine skewed, Very leptokurtic

Raw data summary

Size (phi)	Size (mm)	Cumulative weight (g)	Interval frequency (%)	Cumulative frequency (%)
-1.50	2.8284	0.00	0.00	0.00
-1.25	2.3784	0.01	0.07	0.07
-1.00	2.0000	0.01	0.00	0.07
-0.75	1.6818	0.01	0.00	0.07
-0.50	1.4142	0.01	0.00	0.07
-0.25	1.1892	0.03	0.14	0.20
0.00	1.0000	0.03	0.00	0.20
0.25	0.8409	0.10	0.47	0.68
0.50	0.7071	0.30	1.36	2.04
0.75	0.5946	0.45	1.02	3.05
1.00	0.5000	0.45	0.00	3.05
1.25	0.4204	4.81	29.58	32.63
1.50	0.3536	10.60	39.28	71.91
1.75	0.2973	11.27	4.55	76.46
2.00	0.2500	11.97	4.75	81.21
2.25	0.2102	12.52	3.73	84.94
2.50	0.1768	13.32	5.43	90.37
2.75	0.1487	13.82	3.39	93.76
3.00	0.1250	14.22	2.71	96.47
3.25	0.1051	14.48	1.76	98.24
3.50	0.0884	14.54	0.41	98.64
3.75	0.0743	14.62	0.54	99.19
4.00	0.0625	14.62	0.00	99.19
4.25	0.0526	14.62	0.00	99.19
4.50	0.0442	14.76	0.95	100.14

Total weight = 14.74 g

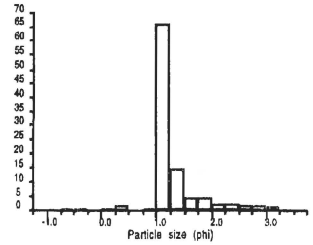
University of Waikato
Rapid Sediment Analyser
Operating System Version 7.1

PARTICLE SIZE ANALYSIS

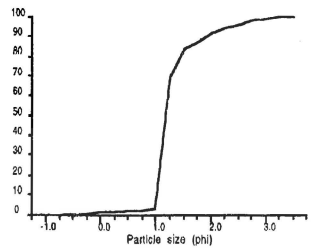
Earth Sciences - University of Waikato

Sample: PROFILE 11 - MARSDEN POINT, NORTHPORT

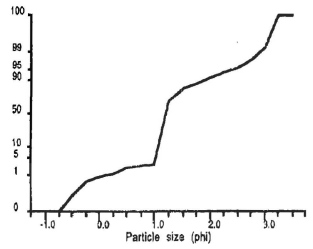
Size distribution histogram



Cumulative frequency



Cumulative frequency



Results summary

Textural size classes

Gravel= 0.00% Sand= 100.00% Silt= 0.00% Clay= 0.00%

Gravel free detrital sediment

Sand

Moment method parameters (phi)

Mean= 1.30 Sorting= 0.47 Skewness= 1.25 Kurtosis= 8.39

Graphical method parameters (phi)

Mean= 1.26 Sorting= 0.33 Skewness= 0.61 Kurtosis= 2.04

Median= 1.18 C= 0.10 D35= 1.12 D65= 1.23

Textural description:

Very well sorted, Strongly fine skewed, Very leptokurtic

Raw data summary

Size (phi)	Size (mm)	Cumulative weight (g)	Interval frequency (%)	Cumulative frequency (%)
-1.00	2.0000	0.00	0.00	0.00
-0.75	1.6818	0.01	0.07	0.07
-0.50	1.4142	0.06	0.34	0.41
-0.25	1.1892	0.11	0.34	0.75
0.00	1.0000	0.13	0.14	0.89
0.25	0.8409	0.17	0.27	1.16
0.50	0.7071	0.34	1.16	2.33
0.75	0.5946	0.35	0.07	2.40
1.00	0.5000	0.44	0.62	3.01
1.25	0.4204	10.08	66.03	69.04
1.50	0.3536	12.17	14.32	83.36
1.75	0.2973	12.75	3.97	87.33
2.00	0.2500	13.43	4.66	91.99
2.25	0.2102	13.75	2.19	94.18
2.50	0.1768	14.03	1.92	96.10
2.75	0.1487	14.30	1.85	97.95
3.00	0.1250	14.49	1.30	99.25
3.25	0.1051	14.60	0.75	100.00
3.50	0.0884	14.62	0.14	100.14

Total weight = 14.60 g

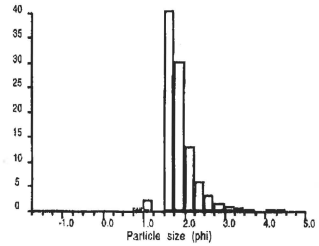
University of Waikato
Rapid Sediment Analyser
Operating System Version 7.1

PARTICLE SIZE ANALYSIS

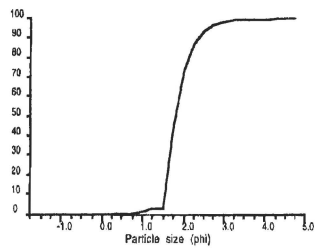
Earth Sciences - University of Waikato

Sample: PROFILE 12 - MARSDEN POINT, NORTHPORT

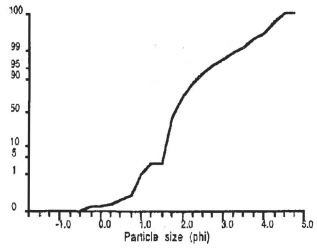
Size distribution histogram



Cumulative frequency



Cumulative frequency



Results summary

Textural size classes

Gravel= 0.11% Sand= 99.42% Silt= 0.47% Clay= 0.00%

Gravel bearing detrital sediment

Slightly Gravelly Sand

Moment method parameters (phi)

Mean= 1.88 Sorting= 0.42 Skewness= 0.95 Kurtosis= 12.83

Graphical method parameters (phi)

Mean= 1.86 Sorting= 0.32 Skewness= 0.38 Kurtosis= 1.19

Median= 1.80 C= 1.00 D35= 1.70 D65= 1.93

Textural description:

Very well sorted, Strongly fine skewed, Leptokurtic

Raw data summary

Size (phi)	Size (mm)	Cumulative weight (g)	Interval frequency (%)	Cumulative frequency (%)
-1.50	2.8284	0.00	0.00	0.00
-1.25	2.3784	0.02	0.11	0.11
-1.00	2.0000	0.02	0.00	0.11
-0.75	1.6818	0.02	0.00	0.11
-0.50	1.4142	0.02	0.00	0.11
-0.25	1.1892	0.03	0.05	0.16
0.00	1.0000	0.03	0.00	0.16
0.25	0.8409	0.04	0.05	0.21
0.50	0.7071	0.06	0.11	0.32
0.75	0.5946	0.08	0.11	0.42
1.00	0.5000	0.19	0.58	1.00
1.25	0.4204	0.60	2.16	3.16
1.50	0.3536	0.60	0.00	3.16
1.75	0.2973	8.29	40.52	43.68
2.00	0.2500	14.02	30.19	73.87
2.25	0.2102	16.54	13.28	87.14
2.50	0.1768	17.71	6.16	93.31
2.75	0.1487	18.30	3.11	96.42
3.00	0.1250	18.61	1.63	98.05
3.25	0.1051	18.75	0.74	98.79
3.50	0.0884	18.83	0.42	99.21
3.75	0.0743	18.87	0.21	99.42
4.00	0.0625	18.89	0.11	99.53
4.25	0.0526	18.94	0.26	99.79
4.50	0.0442	18.97	0.16	99.95
4.75	0.0372	18.97	0.00	99.95

Total weight = 18.98 g

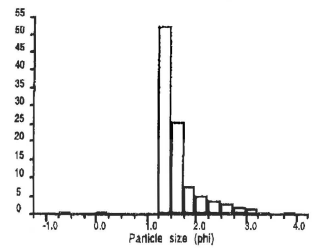
University of Waikato
Rapid Sediment Analyser
Operating System Version 7.1

PARTICLE SIZE ANALYSIS

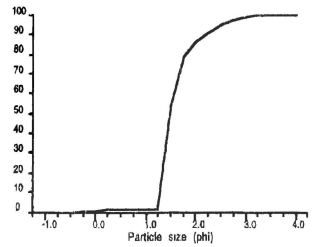
Earth Sciences - University of Waikato

Sample: PROFILE 13 - MARSDEN POINT, NORTHPORT

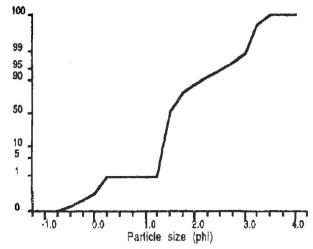
Size distribution histogram



Cumulative frequency



Cumulative frequency



Results summary

Textural size classes

Gravel= 0.00% Sand= 100.00% Silt= 0.00% Clay= 0.00%

Gravel free detrital sediment

Sand

Moment method parameters (phi)

Mean= 1.62 Sorting= 0.43 Skewness= 1.04 Kurtosis= 8.78

Graphical method parameters (phi)

Mean= 1.58 Sorting= 0.34 Skewness= 0.56 Kurtosis= 1.51

Median= 1.48 C= 1.25 D35= 1.41 D65= 1.61

Textural description:

Very well sorted, Strongly fine skewed, Very leptokurtic

Raw data summary

Size (phi)	Size (mm)	Cumulative weight (g)	Interval frequency (%)	Cumulative frequency (%)
-1.00	2.0000	0.00	0.00	0.00
-0.75	1.6818	0.00	0.00	0.00
-0.50	1.4142	0.03	0.20	0.20
-0.25	1.1892	0.05	0.13	0.33
0.00	1.0000	0.07	0.13	0.46
0.25	0.8409	0.14	0.46	0.92
0.50	0.7071	0.15	0.07	0.98
0.75	0.5946	0.15	0.00	0.98
1.00	0.5000	0.15	0.00	0.98
1.25	0.4204	0.15	0.00	0.98
1.50	0.3536	8.15	52.49	53.48
1.75	0.2973	12.01	25.33	78.81
2.00	0.2500	13.15	7.48	86.29
2.25	0.2102	13.91	4.99	91.27
2.50	0.1768	14.40	3.22	94.49
2.75	0.1487	14.80	2.62	97.11
3.00	0.1250	15.06	1.71	98.82
3.25	0.1051	15.20	0.92	99.74
3.50	0.0884	15.23	0.20	99.93
3.75	0.0743	15.23	0.00	99.93
4.00	0.0625	15.26	0.20	100.13

Total weight = 15.24 g

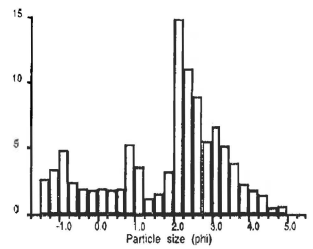
University of Waikato
Rapid Sediment Analyser
Operating System Version 7.1

PARTICLE SIZE ANALYSIS

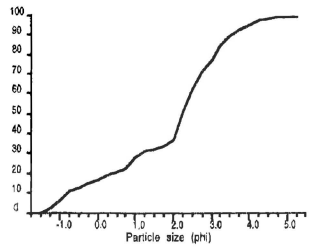
Earth Sciences - University of Waikato

Sample: DREDGE BASIN A, MARSDEN POINT, NORTHPORT

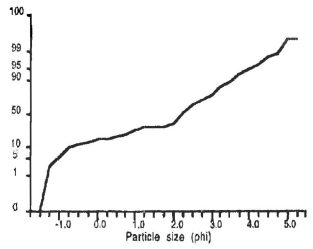
Size distribution histogram



Cumulative frequency



Cumulative frequency



Results summary

Textural size classes

Gravel= 5.86% Sand= 89.44% Silt= 4.71% Clay= 0.00%

Gravel bearing detrital sediment

Slightly Gravelly Sand

Moment method parameters (phi)

Mean= 1.83 Sorting= 1.51 Skewness= -0.59 Kurtosis= 2.49

Graphical method parameters (phi)

Mean= 1.79 Sorting= 1.60 Skewness= -0.35 Kurtosis= 1.03

Median= 2.22 C= -1.40 D35= 1.86 D65= 2.56

Textural description:

Poorly sorted, Strongly Coarse skewed, Mesokurtic

Raw data summary

Size (phi)	Size (mm)	Cumulative weight (g)	Interval frequency (%)	Cumulative frequency (%)
-1.50	2.8284	0.00	0.00	0.00
-1.25	2.3784	0.22	2.53	2.53
-1.00	2.0000	0.51	3.33	5.86
-0.75	1.6818	0.93	4.82	10.68
-0.50	1.4142	1.14	2.41	13.09
-0.25	1.1892	1.30	1.84	14.93
0.00	1.0000	1.45	1.72	16.65
0.25	0.8409	1.62	1.95	18.60
0.50	0.7071	1.77	1.72	20.32
0.75	0.5946	1.93	1.84	22.16
1.00	0.5000	2.39	5.28	27.44
1.25	0.4204	2.70	3.56	31.00
1.50	0.3536	2.80	1.15	32.15
1.75	0.2973	2.93	1.49	33.64
2.00	0.2500	3.21	3.21	36.85
2.25	0.2102	4.51	14.93	51.78
2.50	0.1768	5.48	11.14	62.92
2.75	0.1487	6.26	8.96	71.87
3.00	0.1250	6.74	5.51	77.38
3.25	0.1051	7.32	6.66	84.04
3.50	0.0884	7.77	5.17	89.21
3.75	0.0743	8.10	3.79	93.00
4.00	0.0625	8.30	2.30	95.29
4.25	0.0526	8.45	1.72	97.01
4.50	0.0442	8.57	1.38	98.39
4.75	0.0372	8.61	0.46	98.85
5.00	0.0312	8.66	0.57	99.43
5.25	0.0263	8.66	0.00	99.43

Total weight = 8.71 g

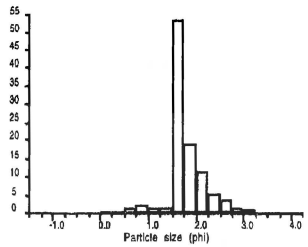
University of Waikato
Rapid Sediment Analyser
Operating System Version 7.1

PARTICLE SIZE ANALYSIS

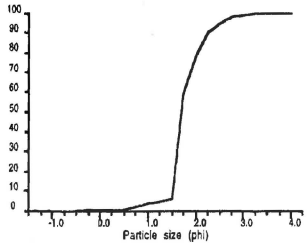
Earth Sciences - University of Waikato

Sample: DREDGE BASIN B, MARSDEN PT, NORTHPORT

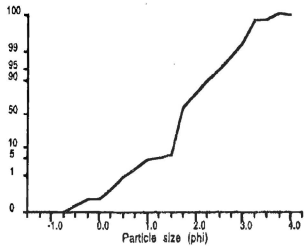
Size distribution histogram



Cumulative frequency



Cumulative frequency



Results summary

Textural size classes

Gravel= 0.00% Sand= 100.00% Silt= 0.00% Clay= 0.00%

Gravel free detrital sediment

Sand

Moment method parameters (phi)

Mean= 1.78 Sorting= 0.41 Skewness= -0.36 Kurtosis= 9.63

Graphical method parameters (phi)

Mean= 1.79 Sorting= 0.33 Skewness= 0.37 Kurtosis= 1.38

Median= 1.71 C= 0.54 D35= 1.63 D65= 1.82

Textural description:

Very well sorted, Strongly fine skewed, Leptokurtic

Raw data summary

Size (phi)	Size (mm)	Cumulative weight (g)	Interval frequency (%)	Cumulative frequency (%)
-1.25	2.3784	0.00	0.00	0.00
-1.00	2.0000	0.00	0.00	0.00
-0.75	1.6818	0.02	0.09	0.09
-0.50	1.4142	0.05	0.14	0.23
-0.25	1.1892	0.08	0.14	0.36
0.00	1.0000	0.08	0.00	0.36
0.25	0.8409	0.12	0.18	0.54
0.50	0.7071	0.19	0.32	0.86
0.75	0.5946	0.41	0.99	1.85
1.00	0.5000	0.88	2.12	3.98
1.25	0.4204	1.08	0.90	4.88
1.50	0.3536	1.38	1.36	6.24
1.75	0.2973	13.19	53.37	59.60
2.00	0.2500	17.44	19.20	78.81
2.25	0.2102	19.92	11.21	90.01
2.50	0.1768	21.07	5.20	95.21
2.75	0.1487	21.76	3.12	98.33
3.00	0.1250	21.98	0.99	99.32
3.25	0.1051	22.09	0.50	99.82
3.50	0.0884	22.09	0.00	99.82
3.75	0.0743	22.12	0.14	99.95
4.00	0.0625	22.14	0.09	100.05

Total weight = 22.13 g

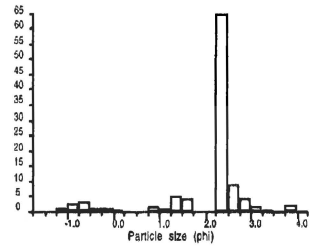
University of Waikato
Rapid Sediment Analyser
Operating System Version 7.1

PARTICLE SIZE ANALYSIS

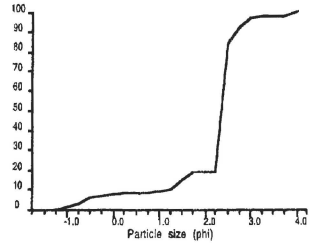
Earth Sciences - University of Waikato

Sample: DREDGE BASIN C, MARSDEN PT, NORTHPORT

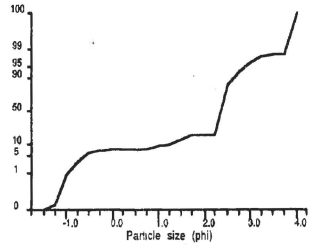
Size distribution histogram



Cumulative frequency



Cumulative frequency



Results summary

Textural size classes

Gravel= 0.92% Sand= 99.42% Silt= 0.00% Clay= 0.00%

Gravel bearing detrital sediment

Slightly Gravelly Sand

Moment method parameters (phi)

Mean= 2.11 Sorting= 0.93 Skewness= -2.11 Kurtosis= 7.32

Graphical method parameters (phi)

Mean= 2.14 Sorting= 0.76 Skewness= -0.71 Kurtosis= 7.44

Median= 2.37 C= -0.99 D35= 2.31 D65= 2.43

Textural description:

Moderately sorted, Strongly Coarse skewed, Extremely leptokurtic

Raw data summary

Size (phi)	Size (mm)	Cumulative weight (g)	Interval frequency (%)	Cumulative frequency (%)
-1.50	2.8284	0.00	0.00	0.00
-1.25	2.3784	0.02	0.17	0.17
-1.00	2.0000	0.11	0.75	0.92
-0.75	1.6818	0.38	2.25	3.16
-0.50	1.4142	0.75	3.08	6.24
-0.25	1.1892	0.86	0.92	7.16
0.00	1.0000	0.93	0.58	7.74
0.25	0.8409	0.96	0.25	7.99
0.50	0.7071	0.97	0.08	8.08
0.75	0.5946	0.98	0.08	8.16
1.00	0.5000	1.15	1.42	9.58
1.25	0.4204	1.22	0.58	10.16
1.50	0.3536	1.80	4.83	14.99
1.75	0.2973	2.27	3.91	18.90
2.00	0.2500	2.27	0.00	18.90
2.25	0.2102	2.27	0.00	18.90
2.50	0.1768	10.09	65.11	84.01
2.75	0.1487	11.15	8.83	92.84
3.00	0.1250	11.63	4.00	96.84
3.25	0.1051	11.79	1.33	98.17
3.50	0.0884	11.83	0.33	98.50
3.75	0.0743	11.83	0.00	98.50
4.00	0.0625	12.05	1.83	100.33

Total weight = 12.01 g

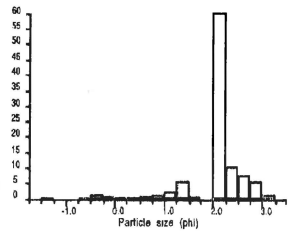
University of Waikato
Rapid Sediment Analyser
Operating System Version 7.1

PARTICLE SIZE ANALYSIS

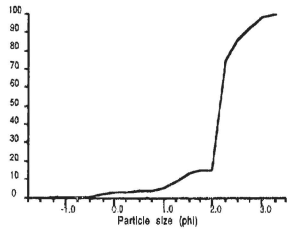
Earth Sciences - University of Waikato

Sample: DREDGE BASIN D, MARSDEN PT, NORTHPORT

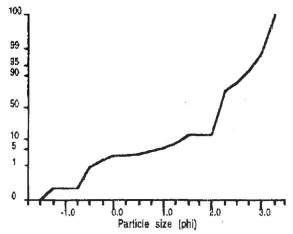
Size distribution histogram



Cumulative frequency



Cumulative frequency



Results summary

Textural size classes

Gravel= 0.38% Sand= 99.62% Silt= 0.00% Clay= 0.00%

Gravel bearing detrital sediment

Slightly Gravelly Sand

Moment method parameters (phi)

Mean= 2.06 Sorting= 0.62 Skewness= -2.35 Kurtosis= 10.91

Graphical method parameters (phi)

Mean= 2.20 Sorting= 0.41 Skewness= 0.05 Kurtosis= 3.81

Median= 2.15 C= -0.47 D35= 2.09 D65= 2.21

Textural description:

Well sorted, Near symmetrical, Extremely leptokurtic

Raw data summary

Size (phi)	Size (mm)	Cumulative weight (g)	Interval frequency (%)	Cumulative frequency (%)
-1.50	2.8284	0.00	0.00	0.00
-1.25	2.3784	0.05	0.38	0.38
-1.00	2.0000	0.05	0.00	0.38
-0.75	1.6818	0.05	0.00	0.38
-0.50	1.4142	0.11	0.45	0.83
-0.25	1.1892	0.28	1.28	2.10
0.00	1.0000	0.36	0.60	2.70
0.25	0.8409	0.41	0.38	3.08
0.50	0.7071	0.44	0.23	3.30
0.75	0.5946	0.54	0.75	4.05
1.00	0.5000	0.74	1.50	5.56
1.25	0.4204	1.08	2.55	8.11
1.50	0.3536	1.83	5.63	13.74
1.75	0.2973	1.92	0.68	14.41
2.00	0.2500	1.92	0.00	14.41
2.25	0.2102	9.98	60.51	74.92
2.50	0.1768	11.41	10.74	85.66
2.75	0.1487	12.39	7.36	93.02
3.00	0.1250	13.12	5.48	98.50
3.25	0.1051	13.33	1.58	100.08

Total weight = 13.32 g

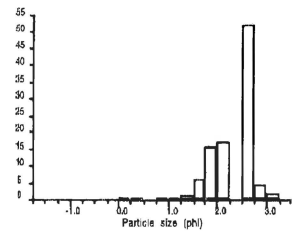
University of Waikato
Rapid Sediment Analyser
Operating System Version 7.1

PARTICLE SIZE ANALYSIS

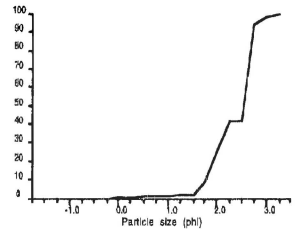
Earth Sciences - University of Waikato

Sample: CONSENT AREA E, MARSDEN POINT, NORTHPORT

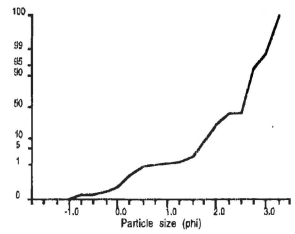
Size distribution histogram



Cumulative frequency



Cumulative frequency



Results summary

Textural size classes

Gravel= 0.09% Sand= 99.91% Silt= 0.00% Clay= 0.00%

Gravel bearing detrital sediment

Slightly Gravelly Sand

Moment method parameters (phi)

Mean= 2.33 Sorting= 0.46 Skewness= -1.84 Kurtosis= 10.38

Graphical method parameters (phi)

Mean= 2.37 Sorting= 0.39 Skewness= -0.59 Kurtosis= 0.75

Median= 2.54 C= 0.74 D35= 2.15 D65= 2.61

Textural description:

Well sorted, Strongly Coarse skewed, Platykurtic

Raw data summary

Size (phi)	Size (mm)	Cumulative weight (g)	Interval frequency (%)	Cumulative frequency (%)
-1.50	2.8284	0.00	0.00	0.00
-1.25	2.3784	0.00	0.00	0.00
-1.00	2.0000	0.01	0.09	0.09
-0.75	1.6818	0.02	0.09	0.18
-0.50	1.4142	0.02	0.00	0.18
-0.25	1.1892	0.03	0.09	0.27
0.00	1.0000	0.04	0.09	0.36
0.25	0.8409	0.07	0.27	0.64
0.50	0.7071	0.10	0.27	0.91
0.75	0.5946	0.11	0.09	1.00
1.00	0.5000	0.13	0.18	1.19
1.25	0.4204	0.17	0.36	1.55
1.50	0.3536	0.27	0.91	2.46
1.75	0.2973	0.95	6.20	8.66
2.00	0.2500	2.69	15.86	24.52
2.25	0.2102	4.58	17.23	41.75
2.50	0.1768	4.59	0.09	41.84
2.75	0.1487	10.35	52.51	94.35
3.00	0.1250	10.80	4.10	98.45
3.25	0.1051	10.98	1.64	100.09

Total weight = 10.97 g

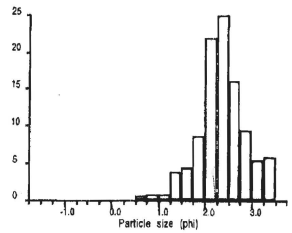
University of Waikato
Rapid Sediment Analyser
Operating System Version 7.1

PARTICLE SIZE ANALYSIS

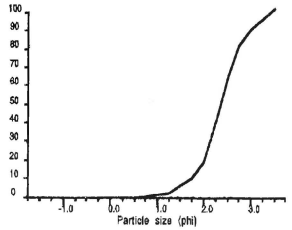
Earth Sciences - University of Waikato

Sample: CONSENT AREA F, MARSDEN POINT, NORTHPORT

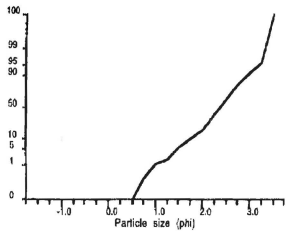
Size distribution histogram



Cumulative frequency



Cumulative frequency



Results summary

Textural size classes

Gravel= 0.00% Sand= 100.00% Silt= 0.00% Clay= 0.00%

Gravel free detrital sediment

Sand

Moment method parameters (phi)

Mean= 2.41 Sorting= 0.52 Skewness= -0.54 Kurtosis= 3.61

Graphical method parameters (phi)

Mean= 2.36 Sorting= 0.49 Skewness= 0.01 Kurtosis= 1.24

Median= 2.34 C= 0.90 D35= 2.19 D65= 2.49

Textural description:

Well sorted, Near symmetrical, Leptokurtic

Raw data summary

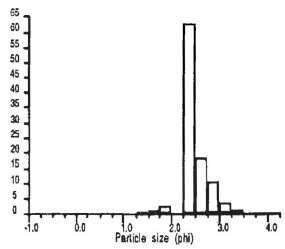
Size (phi)	Size (mm)	Cumulative weight (g)	Interval frequency (%)	Cumulative frequency (%)
-1.50	2.8284	0.00	0.00	0.00
-1.25	2.3784	0.00	0.00	0.00
-1.00	2.0000	0.00	0.00	0.00
-0.75	1.6818	0.00	0.00	0.00
-0.50	1.4142	0.00	0.00	0.00
-0.25	1.1892	0.00	0.00	0.00
0.00	1.0000	0.00	0.00	0.00
0.25	0.8409	0.00	0.00	0.00
0.50	0.7071	0.00	0.00	0.00
0.75	0.5946	0.05	0.54	0.54
1.00	0.5000	0.12	0.75	1.29
1.25	0.4204	0.19	0.75	2.04
1.50	0.3536	0.54	3.75	5.79
1.75	0.2973	0.94	4.29	10.08
2.00	0.2500	1.74	8.58	18.67
2.25	0.2102	3.78	21.89	40.55
2.50	0.1768	6.11	25.00	65.55
2.75	0.1487	7.61	16.09	81.64
3.00	0.1250	8.49	9.44	91.08
3.25	0.1051	8.98	5.26	96.34
3.50	0.0884	9.52	5.79	102.13

Total weight = 9.32 g

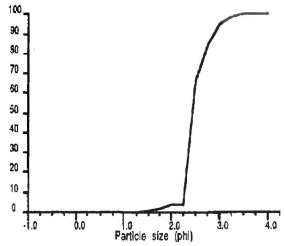
University of Waikato
Rapid Sediment Analyser
Operating System Version 7.1

Sample: Intertidal_1

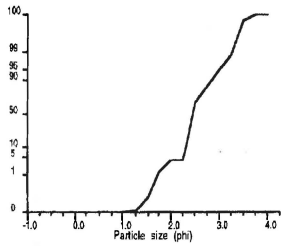
Size distribution histogram



Cumulative frequency



Cumulative frequency



Results summary

Textural size classes

Gravel= 0.00% Sand= 100.00% Silt= 0.00% Clay= 0.00%

Gravel free detrital sediment

Sand

Moment method parameters (phi)

Mean= 2.49 Sorting= 0.28 Skewness= -0.07 Kurtosis= 10.64

Graphical method parameters (phi)

Mean= 2.49 Sorting= 0.22 Skewness= 0.45 Kurtosis= 1.08

Median= 2.43 C= 1.67 D35= 2.37 D65= 2.49

Textural description:

Very well sorted, Strongly fine skewed, Mesokurtic

Raw data summary

Size (phi)	Size (mm)	Cumulative weight (g)	Interval frequency (%)	Cumulative frequency (%)
-0.75	1.6818	-0.01	-0.05	-0.05
-0.50	1.4142	0.01	0.10	0.05
-0.25	1.1892	0.01	0.00	0.05
0.00	1.0000	0.01	0.00	0.05
0.25	0.8409	0.01	0.00	0.05
0.50	0.7071	0.01	0.00	0.05
0.75	0.5946	0.01	0.00	0.05
1.00	0.5000	0.01	0.00	0.05
1.25	0.4204	0.02	0.05	0.10
1.50	0.3536	0.08	0.31	0.41
1.75	0.2973	0.25	0.87	1.27
2.00	0.2500	0.78	2.70	3.97
2.25	0.2102	0.78	0.00	3.97
2.50	0.1768	13.06	62.53	66.50
2.75	0.1487	16.66	18.33	84.83
3.00	0.1250	18.68	10.29	95.11
3.25	0.1051	19.38	3.56	98.68
3.50	0.0884	19.60	1.12	99.80
3.75	0.0743	19.63	0.15	99.95
4.00	0.0625	19.65	0.10	100.05

Total weight = 19.64 g

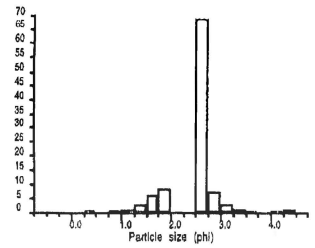
University of Waikato
Rapid Sediment Analyser
Operating System Version 7.1

PARTICLE SIZE ANALYSIS

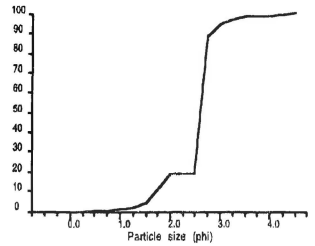
Earth Sciences - University of Waikato

Sample: INTERTIDAL SITE 2, MARSDEN POINT, NORTHP I-2

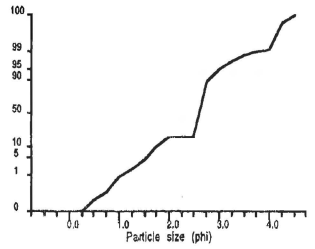
Size distribution histogram



Cumulative frequency



Cumulative frequency



Results summary

Textural size classes

Gravel= 0.00% Sand= 99.18% Silt= 0.82% Clay= 0.00%

Gravel free detrital sediment

Sand

Moment method parameters (phi)

Mean= 2.51 Sorting= 0.51 Skewness= -0.75 Kurtosis= 6.62

Graphical method parameters (phi)

Mean= 2.42 Sorting= 0.43 Skewness= -0.59 Kurtosis= 3.35

Median= 2.61 C= 1.03 D35= 2.56 D65= 2.67

Textural description:

Well sorted, Strongly Coarse skewed, Extremely leptokurtic

Raw data summary

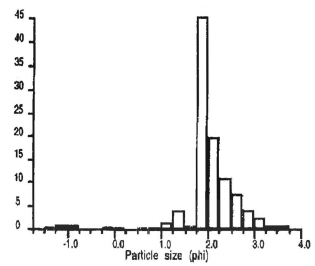
Size (phi)	Size (mm)	Cumulative weight (g)	Interval frequency (%)	Cumulative frequency (%)
-0.50	1.4142	0.00	0.00	0.00
-0.25	1.1892	0.00	0.00	0.00
0.00	1.0000	0.01	0.08	0.08
0.25	0.8409	0.01	0.00	0.08
0.50	0.7071	0.04	0.25	0.33
0.75	0.5946	0.06	0.16	0.49
1.00	0.5000	0.11	0.41	0.90
1.25	0.4204	0.22	0.90	1.80
1.50	0.3536	0.55	2.70	4.50
1.75	0.2973	1.32	6.30	10.79
2.00	0.2500	2.35	8.42	19.22
2.25	0.2102	2.35	0.00	19.22
2.50	0.1768	2.36	0.08	19.30
2.75	0.1487	10.77	68.77	88.06
3.00	0.1250	11.61	6.87	94.93
3.25	0.1051	11.96	2.86	97.79
3.50	0.0884	12.07	0.90	98.69
3.75	0.0743	12.11	0.33	99.02
4.00	0.0625	12.13	0.16	99.18
4.25	0.0526	12.20	0.57	99.75
4.50	0.0442	12.30	0.82	100.57

Total weight = 12.23 g

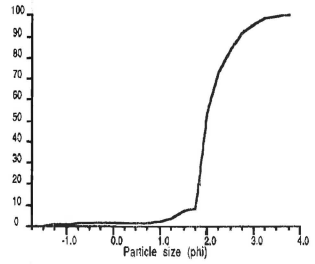
University of Waikato
Rapid Sediment Analyser
Operating System Version 7.1

Sample: intertidal_3 I-3

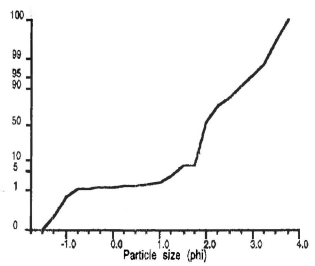
Size distribution histogram



Cumulative frequency



Cumulative frequency



Results summary

Textural size classes

Gravel= 0.74% Sand= 99.26% Silt= 0.00% Clay= 0.00%

Gravel bearing detrital sediment

Slightly Gravelly Sand

Moment method parameters (phi)

Mean= 2.04 Sorting= 0.57 Skewness= -1.94 Kurtosis= 14.41

Graphical method parameters (phi)

Mean= 2.09 Sorting= 0.42 Skewness= 0.33 Kurtosis= 1.50

Median= 1.98 C= -0.86 D35= 1.90 D65= 2.14

Textural description:

Well sorted, Strongly fine skewed, Leptokurtic

Raw data summary

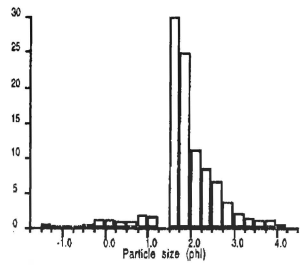
Size (phi)	Size (mm)	Cumulative weight (g)	Interval frequency (%)	Cumulative frequency (%)
-1.50	2.8284	0.00	0.00	0.00
-1.25	2.3784	0.07	0.32	0.32
-1.00	2.0000	0.16	0.42	0.74
-0.75	1.6818	0.26	0.46	1.20
-0.50	1.4142	0.27	0.05	1.25
-0.25	1.1892	0.29	0.09	1.34
0.00	1.0000	0.33	0.18	1.52
0.25	0.8409	0.36	0.14	1.66
0.50	0.7071	0.37	0.05	1.71
0.75	0.5946	0.40	0.14	1.85
1.00	0.5000	0.48	0.37	2.21
1.25	0.4204	0.79	1.43	3.64
1.50	0.3536	1.68	4.11	7.75
1.75	0.2973	1.82	0.65	8.39
2.00	0.2500	11.70	45.57	53.97
2.25	0.2102	15.99	19.79	73.75
2.50	0.1768	18.35	10.89	84.64
2.75	0.1487	19.93	7.29	91.93
3.00	0.1250	20.84	4.20	96.13
3.25	0.1051	21.37	2.44	98.57
3.50	0.0884	21.57	0.92	99.49
3.75	0.0743	21.68	0.51	100.00

Total weight = 21.68 g

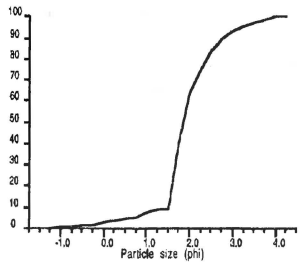
University of Waikato
Rapid Sediment Analyser
Operating System Version 7.1

Sample: intertidal_4 T-4

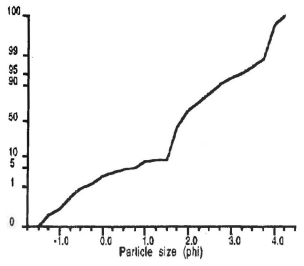
Size distribution histogram



Cumulative frequency



Cumulative frequency



Results summary

Textural size classes

Gravel= 0.43% Sand= 99.35% Silt= 0.22% Clay= 0.00%

Gravel bearing detrital sediment

Slightly Gravelly Sand

Moment method parameters (phi)

Mean= 1.92 Sorting= 0.73 Skewness= -0.58 Kurtosis= 6.37

Graphical method parameters (phi)

Mean= 1.98 Sorting= 0.62 Skewness= 0.19 Kurtosis= 1.71

Median= 1.86 C= -0.45 D35= 1.71 D65= 2.02

Textural description:

Moderately well sorted, Fine skewed, Very leptokurtic

Raw data summary

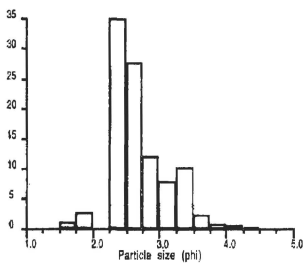
Size (phi)	Size (mm)	Cumulative weight (g)	Interval frequency (%)	Cumulative frequency (%)
-1.50	2.8284	0.00	0.00	0.00
-1.25	2.3784	0.06	0.29	0.29
-1.00	2.0000	0.09	0.14	0.43
-0.75	1.6818	0.14	0.24	0.67
-0.50	1.4142	0.19	0.24	0.91
-0.25	1.1892	0.29	0.48	1.39
0.00	1.0000	0.56	1.29	2.68
0.25	0.8409	0.77	1.01	3.69
0.50	0.7071	0.97	0.96	4.64
0.75	0.5946	1.16	0.91	5.55
1.00	0.5000	1.54	1.82	7.37
1.25	0.4204	1.89	1.68	9.05
1.50	0.3536	1.89	0.00	9.05
1.75	0.2973	8.20	30.21	39.26
2.00	0.2500	13.40	24.90	64.16
2.25	0.2102	15.74	11.20	75.36
2.50	0.1768	17.47	8.28	83.64
2.75	0.1487	18.84	6.56	90.20
3.00	0.1250	19.59	3.59	93.79
3.25	0.1051	20.04	2.15	95.95
3.50	0.0884	20.35	1.48	97.43
3.75	0.0743	20.60	1.20	98.63
4.00	0.0625	20.84	1.15	99.78
4.25	0.0526	20.91	0.34	100.11

Total weight = 20.89 g

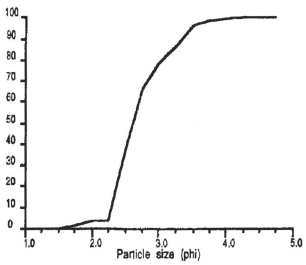
University of Waikato
Rapid Sediment Analyser
Operating System Version 7.1

Sample: dobie_blind_channel T-5

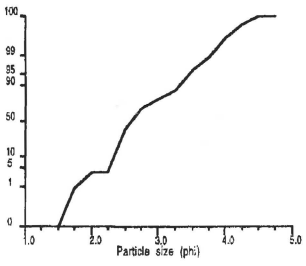
Size distribution histogram



Cumulative frequency



Cumulative frequency



Results summary

Textural size classes

Gravel= 0.00% Sand= 99.48% Silt= 0.52% Clay= 0.00%

Gravel free detrital sediment

Sand

Moment method parameters (phi)

Mean= 2.69 Sorting= 0.42 Skewness= 0.68 Kurtosis= 3.79

Graphical method parameters (phi)

Mean= 2.71 Sorting= 0.39 Skewness= 0.40 Kurtosis= 0.93

Median= 2.60 C= 1.75 D35= 2.47 D65= 2.74

Textural description:

Well sorted, Strongly fine skewed, Mesokurtic

Raw data summary

Size (phi)	Size (mm)	Cumulative weight (g)	Interval frequency (%)	Cumulative frequency (%)
1.25	0.4204	0.00	0.00	0.00
1.50	0.3536	0.01	0.05	0.05
1.75	0.2973	0.19	0.93	0.99
2.00	0.2500	0.70	2.65	3.63
2.25	0.2102	0.70	0.00	3.63
2.50	0.1768	7.43	34.94	38.58
2.75	0.1487	12.75	27.62	66.20
3.00	0.1250	15.10	12.20	78.40
3.25	0.1051	16.63	7.94	86.34
3.50	0.0884	18.60	10.23	96.57
3.75	0.0743	19.02	2.18	98.75
4.00	0.0625	19.16	0.73	99.48
4.25	0.0526	19.22	0.31	99.79
4.50	0.0442	19.26	0.21	100.00
4.75	0.0372	19.26	0.00	100.00

Total weight = 19.26 g

University of Waikato
Rapid Sediment Analyser
Operating System Version 7.1

SEIVE ANALYSIS TEST REPORT

Page 2

Project :	Northport Development
Location :	Auckland
Client :	Geotechnics Ltd. Auckland
Contractor :	Unknown
Sampled by :	Geotechnics Ltd. Auckland
Date sampled :	Unknown
Sampling method :	Unknown
Sample description :	See Below
Sample condition :	Damp

Project No :	2-68264.82
Lab Ref No :	01/264/003
Client Ref No :	Sample 1-4

Seive Analysis of Whole & Broken Shell Fragments

Sample	Seive Size	Percentages Retained: Sand	Whole Shells	Broken Shells	Pebbles/Stones
Sand (High Shell Content)	19.0mm	0%	46%	54%	0%
	13.2mm	0%	14%	67%	19%
	9.5mm	0%	39%	56%	5%
	6.7mm	0%	13%	83%	4%
	4.75mm	0%	6%	91%	3%
	2.36mm	0%	3%	92%	5%
	1.18mm	0%	1%	99%	0%
Sand (Moderate Shell Content)	19.0mm	0%	34%	66%	0%
	13.2mm	0%	11%	81%	8%
	9.5mm	0%	22%	78%	0%
	6.7mm	0%	17%	79%	4%
	4.75mm	0%	8%	90%	2%
	2.36mm	0%	4%	93%	3%
	1.18mm	0%	1%	74%	25%
Silty Sand	19.0mm	0%	0%	0%	0%
	13.2mm	0%	0%	100%	0%
	9.5mm	0%	51%	49%	0%
	6.7mm	0%	18%	82%	0%
	4.75mm	0%	14%	86%	0%
	2.36mm	0%	1%	67%	32%
	1.18mm	0%	2%	65%	33%
Silty Sand	19.0mm	0%	0%	0%	0%
	13.2mm	0%	0%	0%	0%
	9.5mm	0%	0%	0%	0%
	6.7mm	0%	0%	0%	0%
	4.75mm	0%	0%	0%	0%
	2.36mm	0%	0%	100%	0%
	1.18mm	0%	0%	100%	0%

Date tested : 14/06/01
Date reported : 20/06/01

Signatory
Designation : *Laboratory Manager*
Date : 20/06/01

CSF 2004 (1/01)

Opus International Consultants Limited
Hamilton Laboratory
Quality Management Systems Certified to ISO 9001

Fox Street
Private Bag 3057
Hamilton, New Zealand

Telephone +64 7 856 2670
Facsimile +64 7 856 2673
Website www.opus.co.nz

WET SIEVE ANALYSIS TEST REPORT

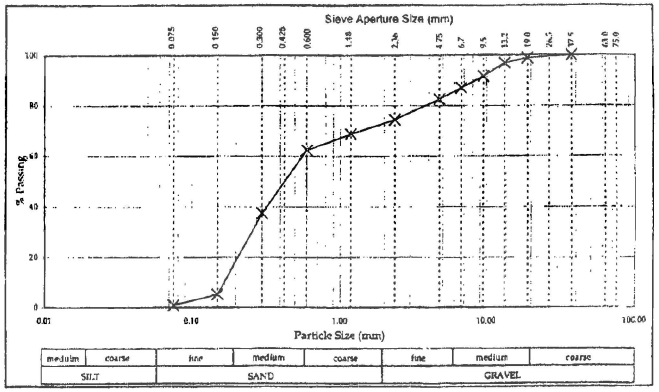
Page 2

Project :	Northport Development
Location :	Auckland
Client :	Geotechnics Ltd. Auckland
Contractor :	Unknown
Sampled by :	Geotechnics Ltd. Auckland
Date sampled :	Unknown
Sampling method :	Unknown
Sample description :	Sand (High Shell Content, Sample 1)
Sample condition	Damp

Project No :	2-68264.82
Lab Ref No :	01/264/003
Client Ref No :	Sample 1

Sieve Analysis

Size (mm)	% Passing	Size (mm)	% Passing	Size (mm)	% Passing	Size (mm)	% Passing
75.00	-	19.00	99	4.75	83	0.425	-
63.00	-	13.20	97	2.36	74	0.300	37
37.50	100	9.50	92	1.18	69	0.150	5
26.50	-	6.70	87	0.600	62	0.075	1



Test method :
NZS 4407 : 1991 Test 5.8.1

Notes :
History : Unknown
Fraction tested Whole

Fraction passing finest sieve is by difference.

Date tested : 14/06/01
Date reported : 20/06/01

Testing is covered by IANZ Accreditation
This report may only be reproduced in full

IANZ Approved Signatory
Designation : *Laboratory Manager*
Date : 20/06/01

20 Tests indicated as not accreditated are outside the scope of the laboratory's accreditation

CSF 2099 (1/01)

Opus International Consultants Limited
Hamilton Laboratory
Quality Management Systems Certified to ISO 9001

Fox Street
Private Bag 3057
Hamilton, New Zealand

Telephone +64 7 856 2670
Facsimile +64 7 856 2673
Website www.opus.co.nz

App III Page 3

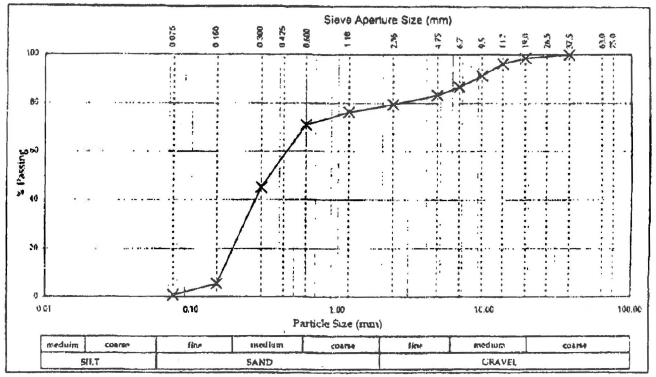
WET SIEVE ANALYSIS TEST REPORT

Project :	Northport Development
Location :	Auckland
Client :	Geotechnics Ltd. Auckland
Contractor :	Unknown
Sampled by :	Geotechnics Ltd. Auckland
Date sampled :	Unknown
Sampling method :	Unknown
Sample description :	Sand (Moderate Shell Content, Sample 2)
Sample condition	Damp

Project No :	2-68264.82
Lab Ref No :	01/264/003
Client Ref No :	Sample2

Sieve Analysis

Size (mm)	% Passing	Size (mm)	% Passing	Size (mm)	% Passing	Size (mm)	% Passing
75.00	-	19.00	99	4.75	83	0.425	-
63.00	-	13.20	96	2.36	79	0.300	45
37.50	100	9.50	91	1.18	76	0.150	5
26.50	-	6.70	87	0.600	71	0.075	1



Test method	Notes
NZS 4407 : 1991 Test 3.8.1	History : Unknown Fraction tested Whole *Fraction passing finest sieve is by difference*

Date tested : 14/06/01
Date reported : 20/06/01

Testing is covered by IANZ Accreditation
This report may only be reproduced in full

IANZ Approved Signatory

Designation : *Laboratory Manager*
Date : 20/06/01

Tests indicated as not accreditated are outside the scope of the laboratory's accreditation

CSF 2099 (1/01)

Opus International Consultants Limited
Hamilton Laboratory
Quality Management Systems Certified to ISO 9001
Fox Street
Private Bag 3057
Hamilton, New Zealand
Telephone +64 7 856 2670
Facsimile +64 7 856 2673
Website www.opus.co.nz

App III Page 4

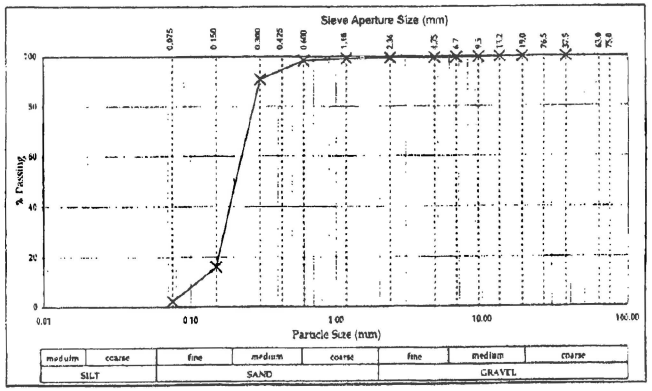
WET SIEVE ANALYSIS TEST REPORT

Project :	Northport Development
Location :	Auckland
Client :	Geotechnics Ltd. Auckland
Contractor :	Unknown
Sampled by :	Geotechnics Ltd. Auckland
Date sampled :	Unknown
Sampling method :	Unknown
Sample description :	Silty Sand (Sample 3)
Sample condition	Damp

Project No :	2-68264.82
Lab Ref No :	01/264/003
Client Ref No :	Sample 3

Sieve Analysis

Size (mm)	% Passing	Size (mm)	% Passing	Size (mm)	% Passing	Size (mm)	% Passing
75.00	-	19.00	100	4.75	100	0.425	-
63.00	-	13.20	100	2.36	99	0.300	91
37.50	100	9.50	100	1.18	99	0.150	16
26.50	-	6.70	100	0.600	98	0.075	0



Test method	Notes
NZS 4407 : 1991 Test 3.8.1	History : Unknown Fraction tested Whole *Fraction passing finest sieve is by difference.*

Date tested : 14/06/01
Date reported : 20/06/01

Testing is covered by IANZ Accreditation
This report may only be reproduced in full

IANZ Approved Signatory

Designation : *Laboratory Manager*
Date : 20/06/01

Tests indicated as not accreditated are outside the scope of the laboratory's accreditation

CSF 2099 (1/01)

Opus International Consultants Limited
Hamilton Laboratory
Quality Management Systems Certified to ISO 9001
Fox Street
Private Bag 3057
Hamilton, New Zealand
Telephone +64 7 856 2670
Facsimile +64 7 856 2673
Website www.opus.co.nz

App III Page 5

WET SIEVE ANALYSIS TEST REPORT

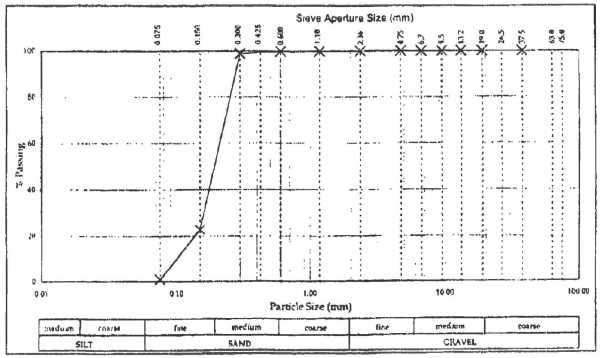
OPUS INTERNATIONAL CONSULTANTS

Project :	Northport Development
Location :	Auckland
Client :	Geotechnics Ltd. Auckland
Contractor :	Unknown
Sampled by :	Geotechnics Ltd. Auckland
Date sampled :	Unknown
Sampling method :	Unknown
Sample description :	Silty Sand (Sample 4)
Sample condition	Damp

Project No :	2-68264.82
Lab Ref No :	01/264/003
Client Ref No :	Sample 4

Sieve Analysis

Size (mm)	% Passing	Size (mm)	% Passing	Size (mm)	% Passing	Size (mm)	% Passing
75.00	-	19.00	100	4.75	100	0.425	-
63.00	-	13.20	100	2.36	100	0.300	99
37.50	100	9.50	100	1.18	100	0.150	23
26.50	-	6.70	100	0.600	100	0.075	1



Test method: NZS 4407 : 1991 Test 3.8.1

Notes
History : Unknown
Fraction tested Whole

Fraction passing finest sieve is by difference.

Date tested : 14/06/01
Date reported : 20/06/01

Testing is covered by IANZ Accreditation
This report may only be reproduced in full

IANZ Approved Signatory

Designation : Laboratory Manager
Date : 20/06/01

Tests indicated as not accredited are outside the scope of the laboratory's accreditation

Page 1 of 1

Opus International Consultants Limited
Hamilton Laboratory
Quality Management Systems Certified to ISO 9001

For Street
Private Bag 3057
Hamilton, New Zealand

Telephone +64 7 856 2879
Facsimile +64 7 856 2673
Website www.opus.co.nz

Sediment mean, sorting and skewness for sites for which could not be printed via the RSA system. (values from RSA data files).

Mt Eden 1949					
Site	**mN**	**mE**	**Mean**	**Sorting**	**Skewness**
45,14	816181	273887	2.20	1.00	-0.10
81,14	815595	275590	2.60	0.35	0.21
63,24	816362	274901	2.20	0.23	0.30
SS2 - Site 1	815760	275745	2.30	0.29	0.25
SS2 - D	815790	275373	2.70	0.28	0.04
SS2 - E	815561	276157	2.40	0.28	0.11
SS2 - H	815931	274363	2.50	0.26	0.29
SS2 - I	815885	274095	2.20	0.34	0.08
SS2 - J	816040	273544	2.40	0.42	0.41
SS2 - K	816266	273399	2.80	0.50	0.42
SS2 - L	816414	273164	1.70	1.10	-0.34
SS2 - M	816569	272954	2.2	0.99	-0.27

APPENDIX B

VERTICAL AIR PHOTOGRAPHS

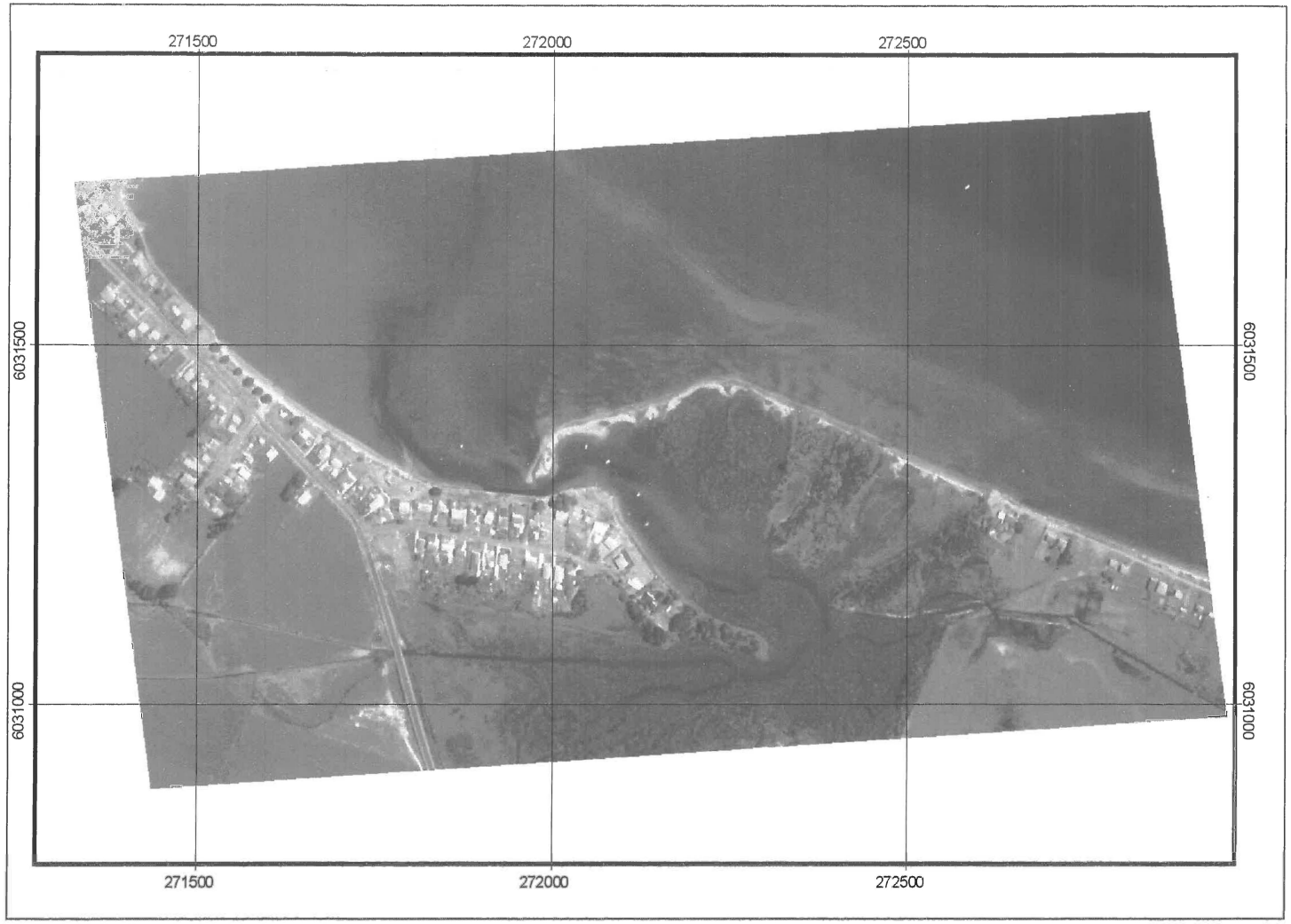


Figure B.1 - *20/2/84, Grayscale, Marsden Bay.*

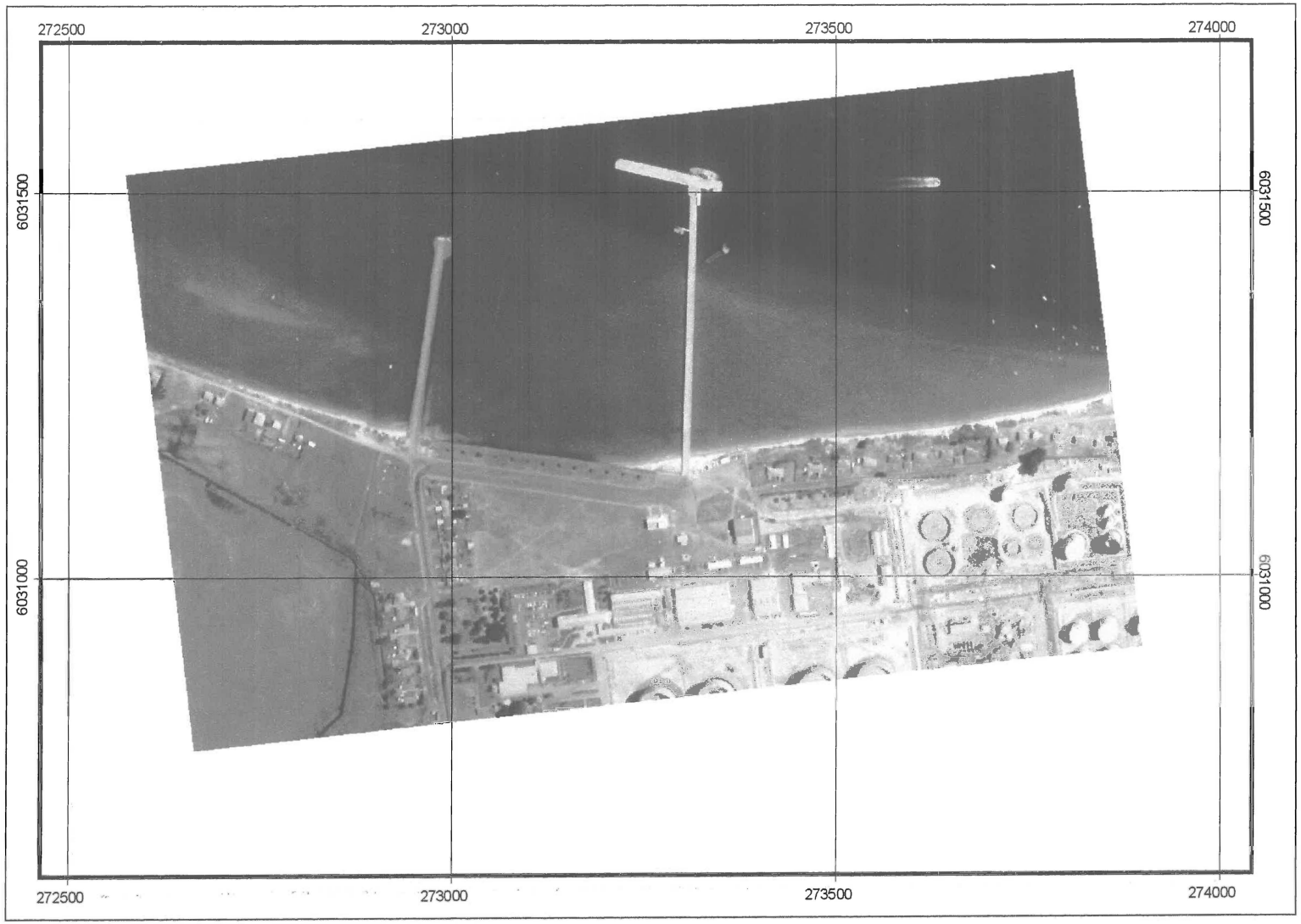


Figure B.2 - *20/2/84, Grayscale, Northport*

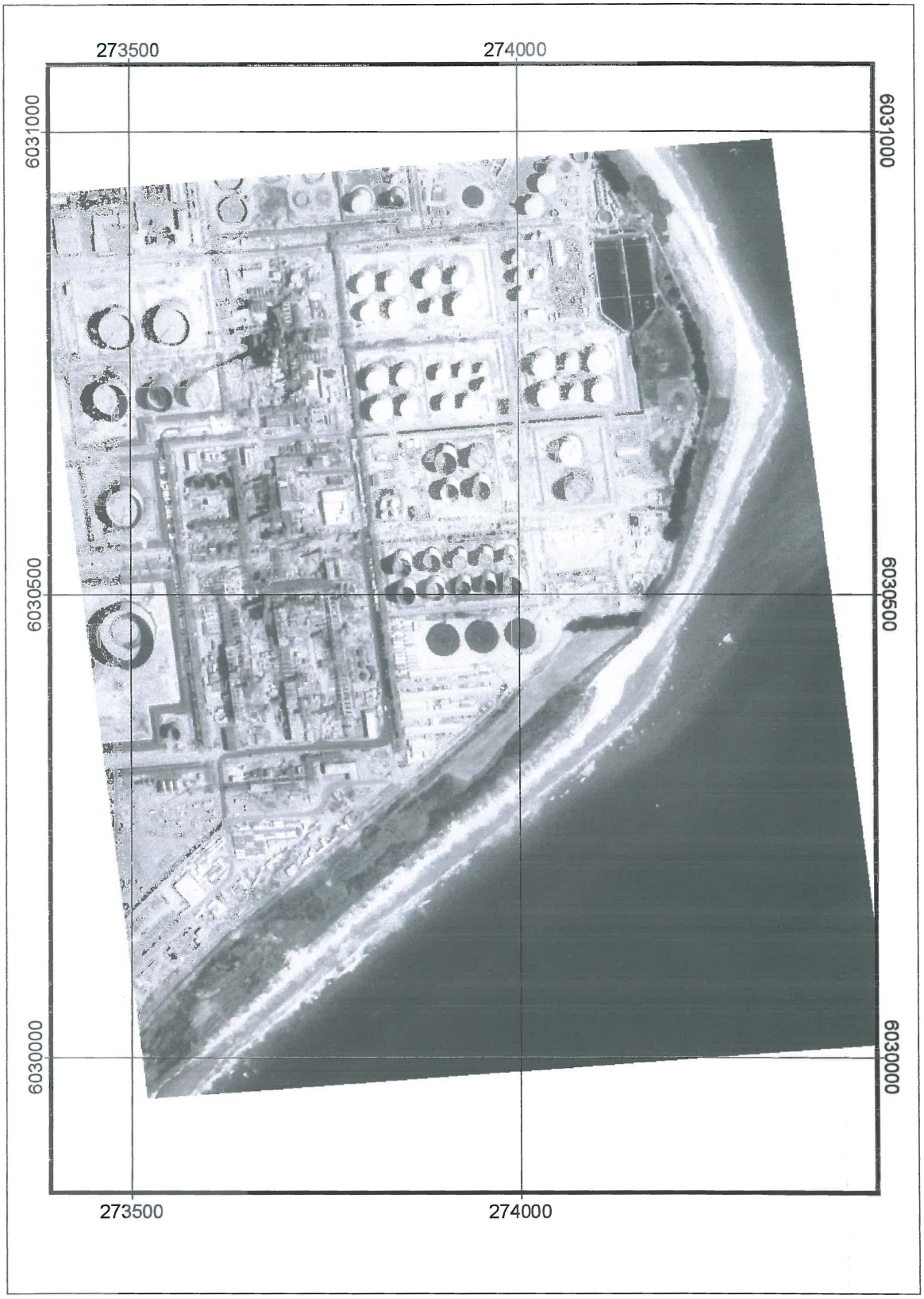


Figure B.3 - *20/2/84, Grayscale, Bream Bay Beach*

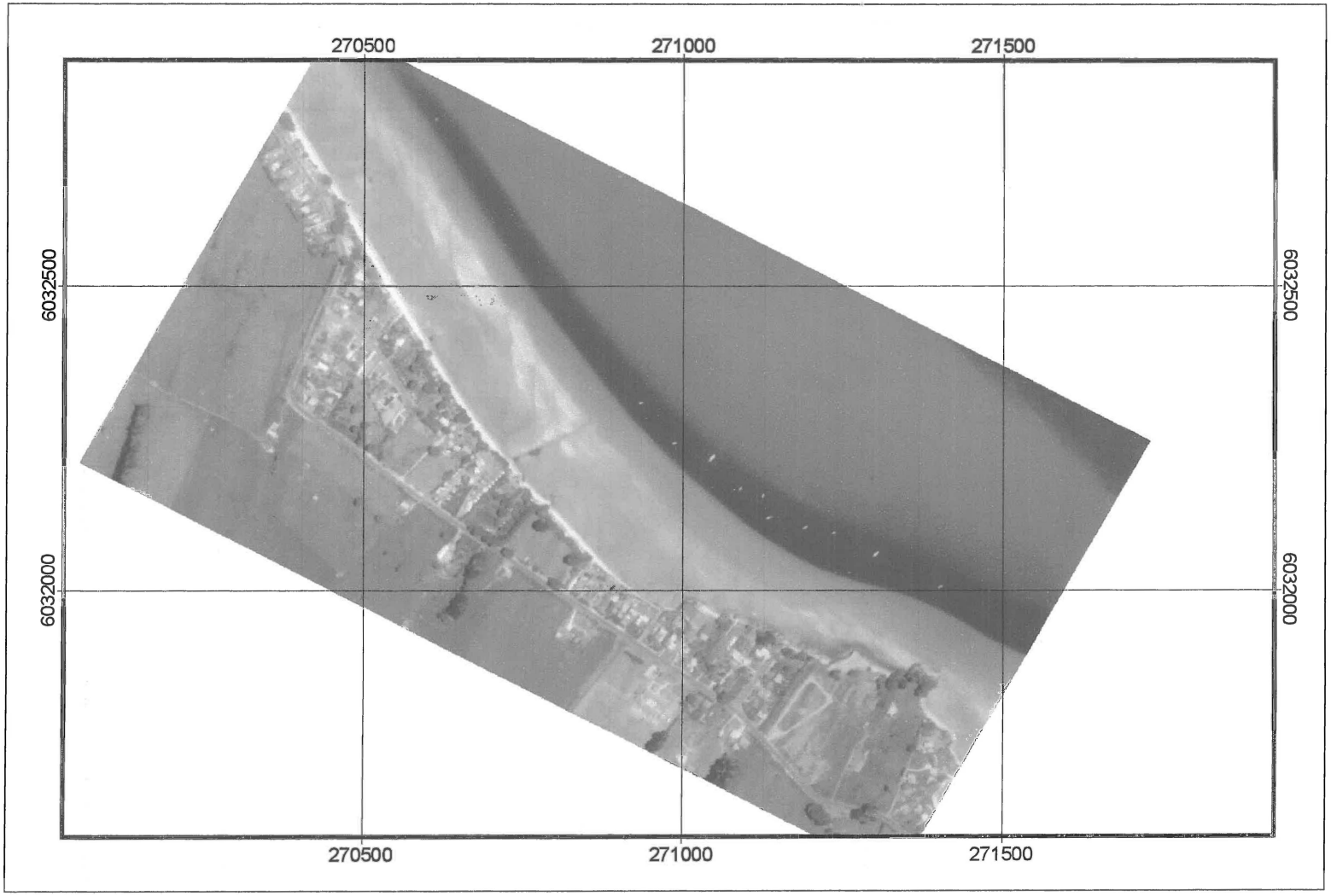


Figure B.4 - *19/12/84, Grayscale, One Tree Point*

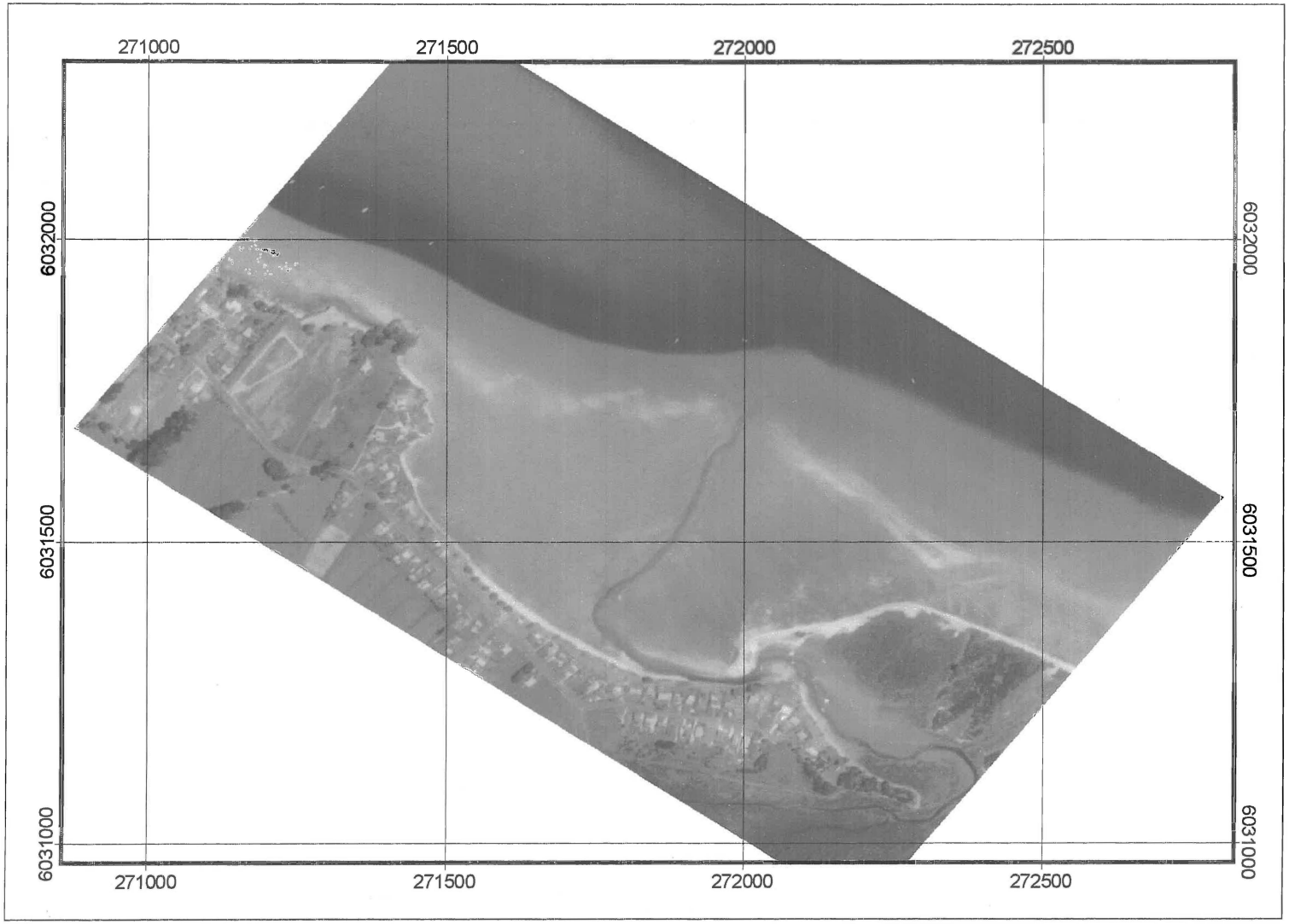


Figure B.5 - *19/12/84, Grayscale, Marsden Bay*

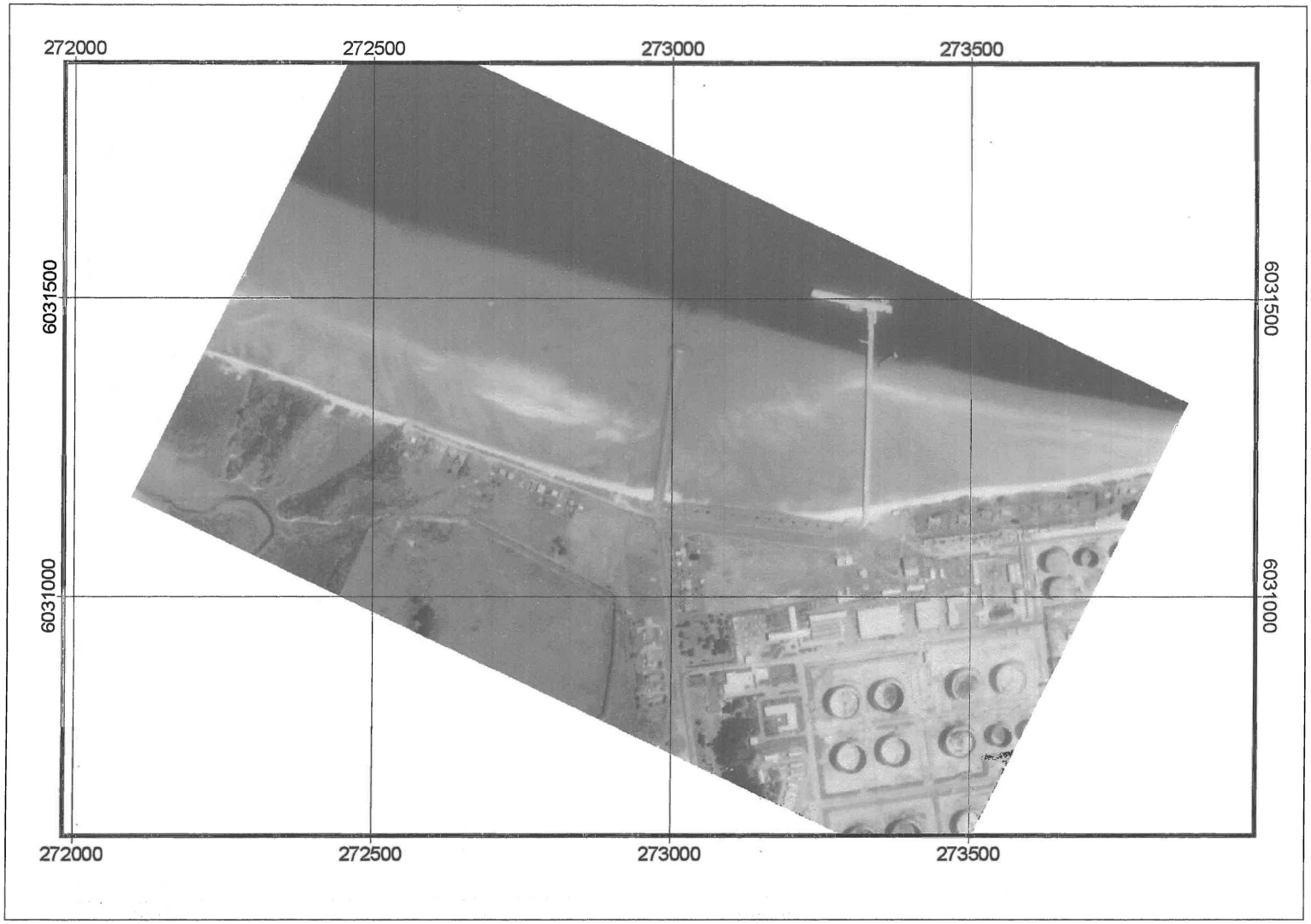


Figure B.6 - *19/12/84, Grayscale, Northport*



Figure B.7 - *9/12/00, 3250ft, RGB Colour, One Tree Point*



Figure B.8 - *9/12/00, 3250ft, RGB Colour, Blacksmiths Creek*

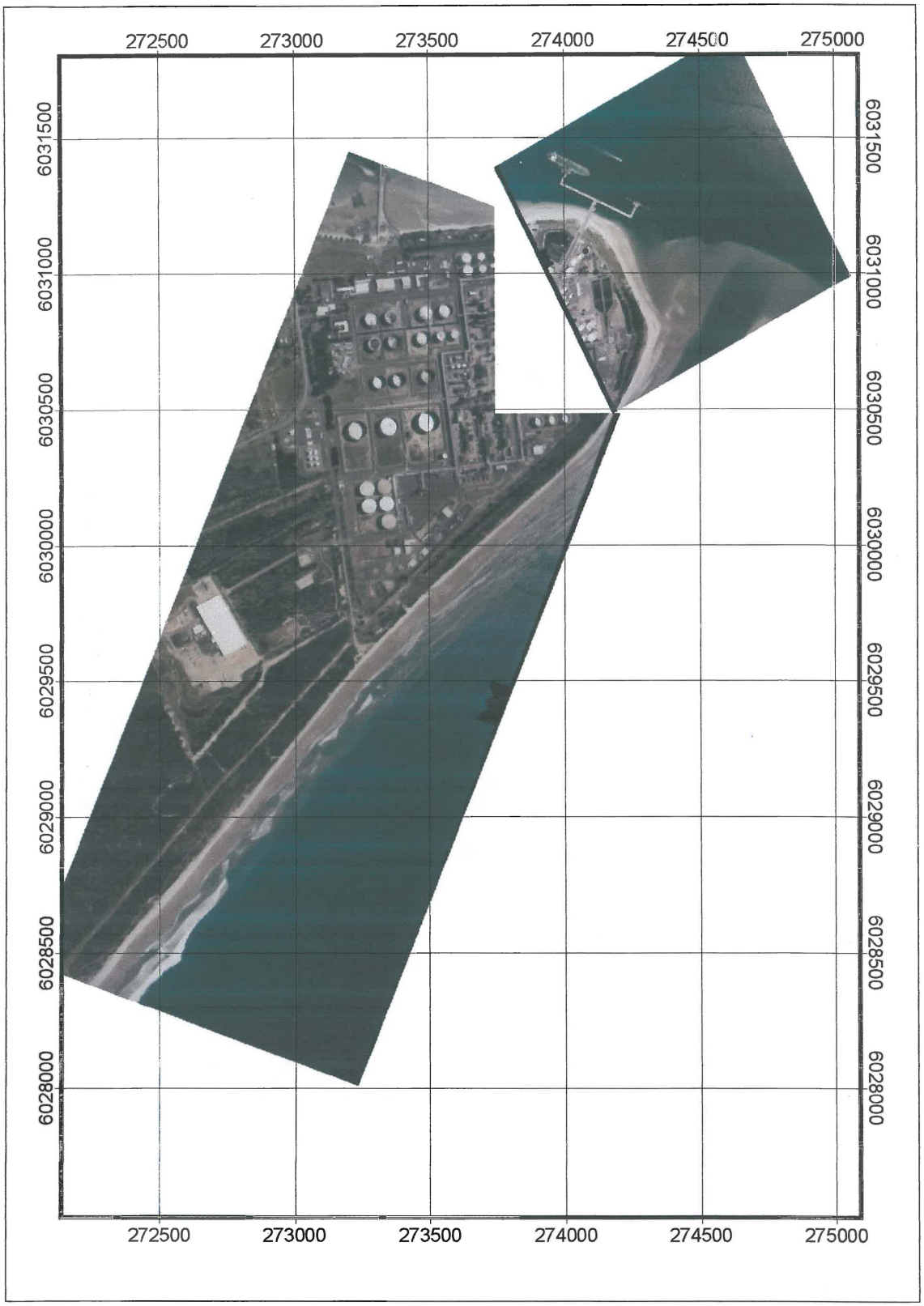


Figure B.9 - *9/12/00, 3250ft (Mair Bank), 7500ft (Bream Bay Beach), RGB Colour*

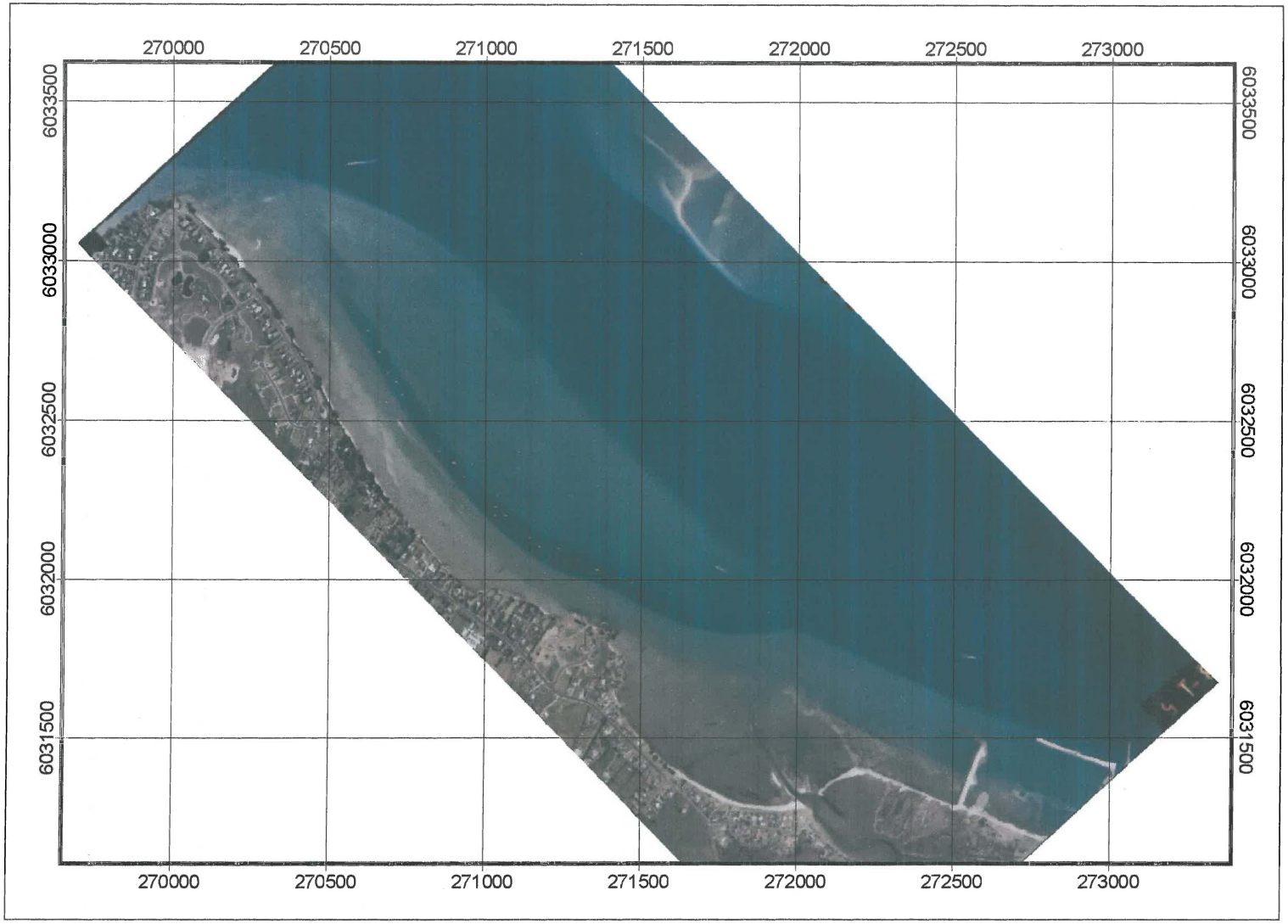


Figure B.10 - *5/1/01, 7500ft, RGB Colour, One Tree Point – Marsden Bay.*



Figure B.11 - *5/1/01, 7500ft, RGB Colour, Northport*

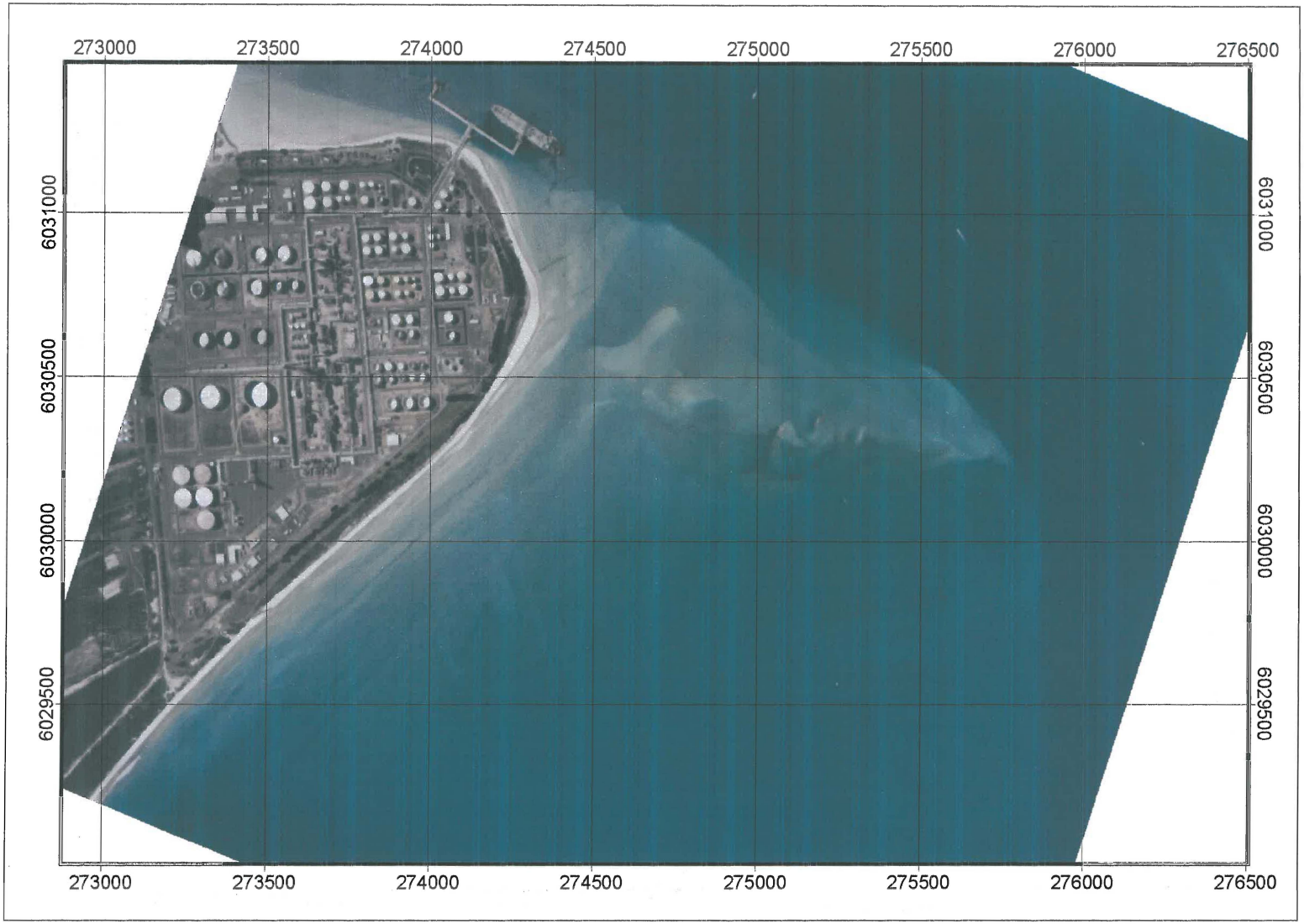


Figure B.12 - *5/1/01, 7500ft, RGB Colour, Bream Bay Bch – Mair Bank*

Ground Control Points used to rectify and geo-reference photographs.

Ground Control Point locations for registration and rectification of images.
Note for 2000 & 2001 images X and Y image refers to a previously referenced image (Draft)
Co-ordinates in UTM Zone 60S

20/2/84 - Marsden Bay

X- image	Y-image	X- LINZ	Y- LINZ
5.055949	10.915715	271416.57	6031534.1
3.611109	10.137166	271527.08	6031349.1
3.42853	9.714489	271573.93	6031348.6
3.119905	10.619305	271470.48	6031291.5
3.087939	11.051201	271409.76	6031287.2
4.846734	11.149378	271391.83	6031486
2.396559	8.690741	271719.62	6031225.9
1.816981	10.818349	271462.12	6031123.4
1.798163	8.181153	271776.52	6031133.5
0.736393	10.040935	271559.73	6030974.4
1.107659	8.450583	271767.94	6031079.3
1.114362	2.737828	272514.58	6031142.5
2.172634	2.008623	272584.45	6031269.4
0.081696	8.25681	271814.11	6030954.7

Points Used 14
Total RMS error 10.49
1st Order polynomial (affine) transformation

20/2/84 - Bream Bay Beach

X- image	Y-image	X- LINZ	Y- LINZ
1.681635	1.494915	274151.33	6030914.3
1.692535	2.670453	274157.9	6030746.4
4.338975	4.039758	273838.84	6030574.8
3.257993	4.334015	273978.04	6030537.8
4.327319	4.290516	273843.84	6030522.5
4.664254	4.526403	273810.06	6030470.9
3.041149	4.482786	274024.03	6030496.2
2.973274	2.685755	274002.47	6030733.7
3.762901	3.009962	273919.42	6030684.8
3.430396	3.013557	273960.31	6030688.9
3.746858	3.324209	273919.42	6030641.8
3.422595	3.300451	273961.69	6030642.5
2.452419	2.942502	274069.82	6030702.8
4.710522	2.703953	273790.27	6030720.8
4.850146	3.57715	273782.24	6030604.8
4.319847	1.169431	273812.68	6030918.4
3.367152	1.446984	273940.21	6030886.5
6.370581	1.399885	273569.4	6030859.4
6.648279	2.628054	273542.37	6030702.1
7.055461	3.270885	273482.76	6030616.9
7.432315	0.271396	273397.91	6030993.1
7.438986	0.623282	273400.05	6030945.7
7.190793	0.622661	273452.75	6030947.9
7.187712	0.272056	273450.81	6030995.6
6.489648	6.519318	273620.68	6030208.1
5.708551	5.726215	273689.04	6030325.4
5.710067	4.406779	273682.91	6030491.3
1.964827	0.907698	274098.88	6030986.6
1.419634	0.903994	274182.82	6030989.2

Points Used 29
Total RMS error 11.426
3rd Order polynomial transformation

20/2/84 - Northport

X-image	Y- image	X-LINZ	Y-LINZ
0.658073	5.549065	273328.53	6031492
3.872476	1.782664	272891.34	6031003.1
5.079398	2.539117	273008.45	6030881.2
4.310516	2.291543	272965.02	6030969.1
5.355805	1.963348	272945.12	6030834.1
4.309977	1.947376	272925.82	6030964.9
5.155433	3.098007	273078.73	6030869.5
5.151093	3.636698	273156.85	6030875.3
0.961486	3.014741	273012.59	6031412.2
2.786629	2.518513	272976.66	6031165.6
3.230171	2.552653	272995.18	6031103.8
3.394833	5.781625	273399.82	6031136.4
3.669022	5.763862	273399.2	6031112.6
4.318578	7.480789	273637.15	6031064.2
4.217767	8.397839	273744.19	6031077.1
4.614955	7.479932	273641.86	6031017.2
4.566853	8.863569	273802.9	6031036.6
5.433059	8.770356	273812.31	6030922.7
5.4661	9.050286	273855.32	6030920.2
4.929486	4.882291	273317.26	6030931.5
4.590446	4.869532	273315.38	6030988.3
4.937952	5.634481	273401.08	6030945
4.897727	5.899114	273450.99	6030948.7
4.572522	4.249146	273222.46	6030981.1
4.928216	4.638685	273285.87	6030920.5
0.404297	4.797363	273235.62	6031510.7
0.751831	5.803955	273370.59	6031483.3

Points Used 27
Total RMS error (I 9.09
2nd Order polynomial transformation

19/12/84 - Marsden Bay

X- image	Y-image	X- LINZ	Y- LINZ
0.30379	4.383168	271719.62	6031225.8
2.574354	10.433161	271222.06	6031867.9
1.591731	10.408071	271162.98	6031771
3.036917	9.978042	271278.97	6031896.7
1.330103	9.194035	271264.28	6031658.2
1.154903	8.440114	271327.91	6031601
1.597543	8.520217	271343.59	6031645.1
1.377516	11.326431	271045.69	6031804.9
1.300383	8.378643	271357.65	6031607.8
1.185547	8.890751	271291.13	6031631.1
0.56894	4.113515	271762.77	6031230.4
0.016254	4.051124	271740.36	6031174.2
0.06311	8.190995	271282.1	6031464.3
0.536978	5.478193	271610.11	6031309.2
1.386692	2.208428	272031.53	6031206.5
2.721764	8.771654	271415.16	6031780.4
2.61262	8.685849	271418.23	6031765.5

Points Used 17
Total RMS error (I 14.43
1st Order polynomial (affine) transformation

19/12/84 - Northport			
X- image	**Y-image**	**X- LINZ**	**Y- LINZ**
6.233791	4.179544	273328.76	6031492
1.30335	5.173879	272926.32	6030965.3
0.41021	4.568815	272945.46	6030834.1
0.984413	4.257049	273008.62	6030881.9
1.220774	3.746056	273078.91	6030869.6
1.507306	3.30699	273157.21	6030875.6
2.658615	2.603636	273314.95	6030988.4
2.947459	2.160928	273379.53	6030990.7
2.548774	2.812017	273283.8	6030983.6
3.21319	1.769457	273450.68	6030995.9
3.072634	1.985174	273405.25	6030992.7
4.074501	2.49525	273399.82	6031136.2
3.894848	2.368661	273399.25	6031112.2
0.344753	0.759829	273385.82	6030605.8
1.527752	2.275868	273280.66	6030830.4
0.939318	1.817306	273295.23	6030735
0.195938	1.920266	273228.08	6030643.2
1.855882	1.712343	273364.38	6030836.1
1.258173	1.340465	273375.81	6030748.1
3.737205	3.021308	273314.37	6031130.8
0.92414	8.671343	272514.78	6031142.2
2.27513	8.893036	272552.94	6031294.5
4.675234	6.131173	273012.62	6031412.1
2.564302	5.346785	272994.9	6031104.5
4.331144	0.577503	273638.3	6031068
5.487344	0.384745	273741.56	6031181.1
5.204478	0.249315	273736.65	6031139
3.971522	1.020868	273560.33	6031033.6
3.482908	0.446634	273615.82	6030945.1
2.540588	5.745758	272905.34	6031129.8
2.668945	0.464661	273567.31	6030857.5
2.372772	0.90799	273491.66	6030851
Points Used	32		
Total RMS error	11.47		
3rd Order polynomial transformation			

19/12/84 - One Tree Point		
X- image	**Y-image**	**X- LINZ**
3.361647	9.767017	270438.55
2.719949	8.242217	270564.28
4.565542	10.05358	270477.75
2.052688	9.067815	270452.07
1.949419	5.288554	270842.71
1.570432	5.348339	270817.42
1.074826	4.368358	270912.96
1.273521	6.075607	270730.06
0.920681	3.334578	271045.93
2.131618	2.320322	271222.04
1.084164	2.407118	271162.82
0.468802	0.463892	271327.8
0.843123	0.409612	271358.96
0.684901	1.194778	271264.17
2.5075	1.86165	271279.02
2.069188	0.649293	271415.1
Points Used	16	
Total RMS error	13.74	
2nd Order polynomial transformation		

9/12/00 - One Tree Point

X-Image	Y- Image	X - Map	Y - Map
269892.1263	6032981.3	269886.57	6032973.4
269995.9214	6033207	269984.67	6033217.2
269833.0486	6032330.6	269838.09	6032345.7
269570.2053	6032399.6	269554.79	6032387.2
269489.1319	6032474.5	269476.35	6032477.6
269807.4592	6031895.4	269801.18	6031888.9
269642.446	6031863.8	269657.22	6031858.4
269353.4405	6032321.9	269354.54	6032315.2
270392.3586	6031322.1	270396.92	6031307.9
270014.603	6031311.6	270007.16	6031298.8
269921.5511	6031400.2	269925.89	6031385.8
270108.3212	6031627.9	270097.55	6031628.8
270446.1149	6032445.3	270438.23	6032469.6
270262.7179	6032269.6	270254.19	6032272.7
270166.6593	6033036.1	270138.37	6033036.1
270005.5437	6033158.4	269998.58	6033147.9
270477.0434	6032594.3	270478.29	6032603.4
270683.7772	6032111.5	270667.15	6032129.2
270688.9109	6032124.2	270670.45	6032143.1
270707.3094	6032190.6	270684.99	6032204.1
270675.249	6032221.7	270653.05	6032235.4
270649.5993	6032261.8	270630.37	6032273.2
270638.9525	6032271.6	270617.81	6032282.1
270572.0047	6032407.3	270555.27	6032414.2
270404.2037	6032663.1	270400	6032679.2
270921.0443	6031883.5	270910.81	6031897.3
270979.576	6031858.3	270962.25	6031875.1
271102.7198	6031910.7	271084.43	6031914.2
271164.6437	6031769.7	271163.35	6031771.6
271221.3319	6031871	271220.64	6031868.1
271328.5642	6031579.7	271327.13	6031598.8
271402.4046	6031772.5	271415.23	6031781.5
271375.6245	6031688.6	271378.39	6031695.6
271604.2459	6031324.2	271620.13	6031315.6
271656.3173	6031340	271673.7	6031329.8
271560.8323	6031364.4	271573.27	6031355.7
271732.1277	6031278.4	271749.82	6031268.1
271714.0375	6031232.6	271720.82	6031225.2
271857.8907	6031215.3	271879.52	6031200.5

Points Used 39
Total RMS error 10.15
2nd Order polynomial transformation

9/12/00 - Blacksmiths Creek

X-Image	Y- Image	X - Map	Y - Map
271718.5758	6031233.1	271719.51	6031225.8
271596.3678	6031340.2	271609.82	6031308.9
272967.7604	6031145.3	272976.59	6031163.4
271873.4736	6030799.3	271855.23	6030881.2
271494.3531	6031372	271525.65	6031348.6
271356.718	6031540.6	271393.49	6031484.9
272396.0084	6030816.7	272371	6030903.5
272015.5851	6031202.7	272008.67	6031205.5
272031.3111	6031200.2	272030.83	6031206.6
272095.9671	6031103.3	272091.41	6031116.3
272973.6771	6031457.2	273012.48	6031411.5
271892.2941	6031260.5	271899.1	6031252.2
271728.3921	6031280.9	271740.58	6031276
271784.4216	6031269.8	271794.89	6031265.4
271829.1415	6031264.2	271835.52	6031260.6

Points Used 15
Total RMS error 5.87
2nd Order polynomial transformation

9/12/00 - Mair Bank

X-Image	Y- Image	X - Map	Y - Map
273993.8457	6031326.8	273998.1	6031338.1
274019.1569	6031370.5	274019.98	6031380.3
274272.2103	6031249.7	274268.25	6031243
274249.773	6031205.2	274244.85	6031203.8
274121.1612	6031266.3	274112.36	6031275.8
274153.1699	6030853.4	274150.55	6030864.4
274148.5165	6030899.3	274151.45	6030914.6
274096.9415	6030969.5	274099.23	6030986
274173.5181	6030987.5	274182.53	6030989.2
274104.983	6030891.1	274107	6030911.4
274154.7906	6030751.6	274158.04	6030746.4
274113.817	6030816	274106.35	6030847.4
274116.677	6030767.4	274115.93	6030791.9
274075.5925	6030805.2	274067.49	6030840.9
274028.1059	6031008.7	274016	6031024.6
274139.4945	6030978.5	274148.43	6030988.7

Points Used 15
Total RMS error 7.59
1st Order polynomial (affine) transformation
As the GCPs could only be on the land part of the image,
a 2nd order transform would cause distortion to parts.

5/1/01 Northport			
X-Image	**Y- Image**	**X - Map**	**Y - Map**
273232.7889	6031517	273236.16	6031511.5
271715.9028	6031228.8	271719.44	6031225.6
271129.0561	6031782.8	271163.54	6031770.9
271033.8537	6031621.3	271041.52	6031600.9
271109.5644	6031745.8	271125.32	6031739.1
270887.9232	6031900.4	270913.84	6031897.5
271321.1048	6031600.1	271327.51	6031598.6
271253.0842	6031421.1	271262.55	6031407.1
271133.9346	6031508.2	271151.21	6031501.8
271339.3724	6031634.7	271359.32	6031639.7
271248.8887	6031661.4	271264.54	6031660.9
271567.7156	6031045.5	271557.49	6031040.5
273044.574	6029971.9	273047.41	6029964.2
273053.9354	6029897	273051.38	6029890.6
273166.8468	6030018.6	273175.32	6030001.3
273346.537	6030085.4	273359.57	6030066.3
273620.6611	6030212.2	273620	6030207.9
273607.7467	6030295.5	273613.57	6030297.9
273827.3658	6030486.6	273808.49	6030469.7
274041.3887	6030520.6	274023.22	6030496.5
274095.3228	6030668.9	274073.02	6030647
273791.9045	6030728	273790.28	6030719.8
274110.987	6030995	274098.72	6030987.6
274161.4475	6030918	274150.66	6030913.7
274051.5369	6030827.8	274024.29	6030831.7
273638.8549	6031016.9	273642.49	6031017.5
273403.8375	6030951.5	273401.52	6030945.8
273305.5406	6030940.3	273317.45	6030931.3
273006.8212	6030885.3	273009.54	6030881
273279.6956	6030938.2	273286.39	6030920.6
273151.4165	6030888.2	273158.41	6030874
273329.3073	6031492.4	273328.38	6031491.4
273363.5956	6031487.7	273369.72	6031483.1
Points Used	33		
Total RMS error (	9.7		
2nd Order polynomial transformation			

5/1/01 - One Tree Point			
X-Image	**Y- Image**	**X - Map**	**Y - Map**
269884.1979	6032978.3	269886.05	6032971.8
269923.5883	6032876.4	269943.52	6032880.5
269991.6269	6033199.9	269985.22	6033217.5
270034.0224	6033180.5	270013.49	6033187.3
270000.513	6033149.5	269997.27	6033146.5
270148.3809	6033036.1	270140	6033034.9
270135.6335	6033026.8	270124.25	6033017.7
270433.9482	6032459.6	270438.91	6032469
270479.3046	6032587	270478.76	6032602.5
270568.2328	6032300.8	270564.03	6032302.2
271144.5965	6031772.5	271163.23	6031770.7
271213.9333	6031870.9	271220.69	6031867.1
271123.5022	6031735.3	271125.69	6031738.2
270902.8308	6031902.7	270910.66	6031893.9
271331.03	6031588.2	271328.2	6031599.7
271352.8007	6031629.2	271358.79	6031639.5
271408.1207	6031770.6	271418.1	6031765.6
271381.9091	6031508.2	271392.62	6031485.7
271515.9477	6031364.3	271526.54	6031348.5
271612.2861	6031322.1	271614.13	6031307.7
271722.3945	6031228	271719.79	6031225.2
272281.4509	6030804.3	272258.33	6030791.9
273052.3538	6031407.8	273013.15	6031409.3
272538.9117	6031273	272553.39	6031294.7
272012.0629	6031197.2	272008.08	6031205.1
270720.2477	6032027.1	270730.4	6032026.6
270650.1276	6032102.3	270656.48	6032111.3
Points Used	27		
Total RMS error (	11.3264		
2nd Order polynomial transformation			

5/1/01 - Marsden Bay			
X-Image	Y- Image	X - Map	Y - Map
273981.0259	6031350	273998.3	6031337
274241.0196	6031210	274245.8	6031203
273321.4367	6031483	273328.6	6031492
273229.0113	6031506	273235.5	6031511
273308.0645	6031116	273314.3	6031131
271728.6191	6031208	271719.5	6031226
272243.9547	6030066	272232.4	6030065
272322.0058	6029894	272308	6029897
273046.0296	6029961	273046	6029964
273060.3014	6029934	273060.9	6029940
273075.0301	6029857	273072.9	6029856
273055.3417	6029891	273051.2	6029890
273170.5598	6030009	273175.2	6030004
273606.9445	6030208	273619.3	6030207
274135.8357	6030916	274150.8	6030914
274140.9479	6030872	274150.3	6030865
273990.3447	6030751	274002.8	6030733
274137.442	6030773	274158.3	6030747
274059.3784	6030719	274069.5	6030704
274107.681	6030792	274115.7	6030791
274125.3638	6030996	274149.3	6030988
274094.2831	6030911	274107.1	6030911
274109.8796	6031275	274112.2	6031274
273616.7245	6031051	273635.7	6031066
273625.1751	6031005	273641.7	6031016
273394.3724	6030942	273400.5	6030946
273269.6238	6030928	273285.6	6030920
273299.8279	6030932	273317.7	6030932
273008.5289	6030874	273009.3	6030882
273276.5627	6030826	273286.6	6030828
Points Used	30		
Total RMS erro	8.34		
2nd Order polynomial transformation			

5/1/01 Mair Bank			
X-Image	Y- Image	X - Map	Y - Map
273993.7755	6031352	273998.6	6031338
274015.8742	6031391	274019.2	6031380
274119.3795	6031266	274111.8	6031276
274249.4706	6031184	274245.5	6031203
274269.8233	6031224	274267.6	6031243
274142.6636	6030835	274150.2	6030865
274130.9763	6030966	274148.5	6030988
274137.1152	6030884	274151.7	6030915
273624.3002	6031076	273637.1	6031067
273625.2983	6031031	273644.1	6031019
273411.528	6031138	273399.2	6031113
273407.8994	6031169	273399.4	6031136
273968.7818	6030976	273971	6030968
273798.9004	6030887	273820.2	6030876
273917.29	6030934	273936.1	6030928
274138.6759	6030736	274157.9	6030747
273992.0092	6030722	274003.1	6030733
274053.4933	6030683	274068	6030700
273544.3381	6030548	273550.3	6030547
273770.8744	6030587	273781.5	6030605
273809.3942	6030456	273809.7	6030470
274018.8352	6030470	274023.6	6030496
273971.9849	6030500	273977	6030540
273837.3459	6030487	273844.7	6030516
273594.8701	6030172	273620.6	6030208
273586.3105	6030272	273612.7	6030297
273160.675	6029997	273175.8	6030003
273402.2382	6029917	273430	6029956
273176.8858	6029703	273172.4	6029728
273035.4564	6029959	273047.2	6029964
273042.2488	6029879	273051	6029892
Points Used	31		
Total RMS erro	11.09		
2nd Order polynomial transformation			

Boundaries of regions used for analysis

Locations for Air Photo analysis - One Tree Point- Marsden Bay UTM 60S		
	Easting	Northing
One Tree Point - North	270010.7218	6033188.672
	270385.9142	6032746.174
One Tree Point - Central	270385.9142	6032746.174
	270745.3543	6032186.25
One Tree Point - South	270745.3543	6032186.25
	271205.0366	6031886.955
Paradise Point	271205.0366	6031886.955
	271424.1375	6031637.781
Marsden Bay – West	271424.1375	6031637.781
	271514.3555	6031487.418
Marsden Bay – Central	271514.3555	6031487.418
	271663.2869	6031362.831
Marsden Bay – East	271663.2869	6031362.831
	272024.159	6031276.909
Blacksmiths Creek	272024.159	6031276.909
	272201.731	6031120.818
Marsden Spit.	272201.731	6031120.818
	272491.0015	6031279.773

Locations and bearing of Transects used by Healy (1980) and at Marsden Point.

Transect	Easting	Northing	Bearing(° True)
A	273425	603114	0
2	273686	6031180	0
B	274247	6030955	63
7	274299	6030746	88
C	274144	6030431	126
8	273924	6030212	137

Appendix C

BEACH PROFILES

Profile ID	Profile Start Points		Direction (degrees true North)	Years Surveyed
	mN (Mt Eden 1949)	mE (Mt Eden 1949)		
A	815105.4	276183.1	30.08	1998,2001,2002,2003
B	815314.3	276064.3	30.08	1997,1998,2000,2001,2002,2003
C	815371.4	276012.8	30.08	1998,2000,2001,2002,2003
D	Along C.L of Wharf	Along C.L of Wharf	30.08	1998,2000
E	815452	275886	30.08	1998,2000,2002,2003
F	815473	275813.3	30.08	1998,2000,2001,2002
G	815452.6	275692	30.08	1998,2000,2001,2002,2003
1	815437.8	275623.3	1.5	1996,1998,1999,2000,2001,2002,2003
2	815404.4	275285.1	6.1	1996,1998,1999,2000,2002,2003
215E	815396.3	275073.2	10	1997,1998,1999
55E	815422.9	274915.4	10	1997,1998,1999,2000
15E	815429.6	274876	10	1998,1999,2000
15W	815410.8	274842.2	10	1998,1999.2000
55W	815426.6	274804.3	10	1997,1998,1999,2000
215W	815489.7	274653	10	1997,1998,1999,2000
3	815613.4	274342.5	18.4	1997,1998,1999,2000,2001,2002,2003
4	815686	274149.1	15.7	1996,1999,2000,2001,2002,2003
5	815575.4	273906.9	4.6	1997,1999,2000,2001,2002,2003
6	815687.8	273522.7	41.6	1997,1999,2000,2001,2003
7	815842.8	273378.8	47	1996,1999,2000,2001,2003
7-1	816164.4	273290.1	40	1999,2000,2001,2003
8	816258.7	273011.9	31.8	1998,1999,2000,2001,2003
9	816427.2	272734.5	51.5	1996,1998,1999,2000,2001,2003
10	816570.2	272612.6	57.5	1996,1998,1999,2000,2001,2003
11	816779.4	272491.8	53	1996,1998,1999.2000,2001,2003
12	817017.3	272319.5	61.7	1996,1998,1999,2000,2001,2003
13	817323.9	272155	62.2	1996,1998,1999,2000,2001,2003

Beach Profile Locations at Marsden Point - One Tree Point used for analysis. Locations in Mt Eden Grid Circuit (1949) co-ordinates.

profile_sd_eoc.m MATLAB® program to calculate standard deviation and envelope of change of multiple beach profiles

```
1   function []=profile_sd_eoc(profile_data)
2   [m,n]=size(profile_data);
3   identity=profile_data(1,:);
4   profile=profile_data(2:m,:);
5
6   %set x values for interpolated profiles (for Std Dev)
7   interp_xi=-10:1:max(max(profile));
8
9   %find the length in x direction that profile should extend
10  xlength=0:50:max(max(profile))+100;
11  xmax=xlength(min(find(xlength-(max(max(profile)))>0)));
12
13  figure
14  set(gcf,'papertype','A4','paperorientation','landscape','paperposition',[.25 .15 11.3 7.77])
15  %plot each profile
16    for i=1:2:length(identity)
17
18      %calculate 1m interpolation of each profile to work out Std Dev
19      yi(:,(i+1)/2)=interp1Q(profile(:,i),profile(:,i+1),interp_xi');
20
21      %plot each profile line - RAW DATA
22      h_p((i+1)/2)=line(profile(:,i),profile(:,i+1));
23
24      %set line colour depending on date of profile
```

```
25          [linecolour,linestyle,mark]=findcolour(identity(i));
26          set(h_p((i+1)/2),'color',linecolour,'linestyle',linestyle)
27          set(gca,'xlim',[-10 xmax],'fontsize',8)
28          ylabel('Height above CD (m)')
29          hold on
30        end
31      h=line(get(gca,'xlim'),[1.5,1.5]);
32      set(h,'color','k','linestyle','-')
33      h=text(max(get(gca,'xlim')),1.65,'M.S.L. ');
34      set(h,'horizontalalignment','right','fontsize',8)
35
36
37
38      [myi,nyi]=size(yi);
39      for i=1:myi;
40        env_of_change(i)=max(yi(i,:))-min(yi(i,:));
41      end
42      env_of_change(find(env_of_change==0))=NaN;
43
44      xlabel('Distance from Benchmark (m)')
45      %calculate std dev using nanstd.m -disregards NaN's and cretes std dev for as much of
        profile as possible
46      profile_stddev=nanstd(yi');
47      ax1=gca;
48      set(ax1,'ylim',[floor(min(min(yi))) ceil(max(max(yi)))]);
49      set(ax1,'ylim',[-2 7])
50      ax2=axes('Position',get(ax1,'position'),'xaxislocation','top','YAxisLocation','right','color','none');
51      set(ax2,'xlim',get(ax1,'xlim'),'xticklabel',{},'ylim',[0 4],'fontsize',8)
52      ylabel('Standard Deviation / Envelope Height (m)')
53      %plot std dev line
54      h_p(length(h_p)+1)=line(interp_xi,profile_stddev);
55      set(h_p(length(h_p)),'color','r','linewidth',2)
56
57      %plot env_of_change
58      h_eoc=line(interp_xi,env_of_change);
59      set(h_eoc,'color','b','linewidth',2,'linestyle',':')
60
61
62      %create legend
63      legend_linesx(1,1:10)=-100;
64      legend_linesx(2,1:10)=-101;
65      legend_linesy(1,1:10)=-10;
66      legend_linesy(2,1:10)=-11;
67      h_leg=line(legend_linesx,legend_linesy);
68      colours=['m','y','g','r','c','b','k','k','b','r'];
69      styles=['-','-','-','-','-','-','-','-',':',':','-'];
70      widths=[.5,.5,.5,.5,.5,.5,.5,.5,2,2];
71      for i=1:10
72        set(h_leg(i),'color',colours(i),'linestyle',styles(i),'linewidth',widths(i));
73      end
74      [LEGH,OBJH,OUTH,OUTM]=legend(h_leg,'Nov-96','May-97','Jun-98','Jul-99','Oct-00','Jun-
        01','Nov-02','Aug-03','Env. Ht.','Std Dev');
75      set(OUTH(8),'linestyle','--')
76      %**********************************************************************************************
        **************
77
78
79
80      %**********************************************************************************************
        **************
81      function [linecolour,linestyle,mark]=findcolour(profile_date)
82
83        if profile_date>datenum(1996,10,1,0,0,0) & profile_date<datenum(1996,12,1,0,0,0);
84          linecolour='m';linestyle='-';mark='s';
85          elseif profile_date>datenum(1997,4,1,0,0,0) & profile_date<datenum(1997,6,1,0,0,0);
86            linecolour='y';linestyle='-';mark='^';
87          elseif profile_date>datenum(1998,5,1,0,0,0) & profile_date<datenum(1998,7,1,0,0,0);
88            linecolour='g';linestyle='-';mark='+';
```

```
89          elseif profile_date>datenum(1999,6,1,0,0,0) & profile_date<datenum(1999,8,1,0,0,0);
90            linecolour='r';linestyle='-';mark='o';
91          elseif profile_date>datenum(2000,7,1,0,0,0) & profile_date<datenum(2000,11,1,0,0,0);
92            linecolour='c';linestyle='-';mark='*';
93          elseif profile_date>datenum(2001,5,1,0,0,0) & profile_date<datenum(2001,7,1,0,0,0);
94            linecolour='b';linestyle='-';mark='x';
95          elseif profile_date>datenum(2002,10,1,0,0,0) &
        profile_date(1,:)<datenum(2002,12,1,0,0,0);
96            linecolour='k';linestyle='-';mark='d';
97          elseif profile_date>datenum(2003,7,1,0,0,0) &
        profile_date(1,:)<datenum(2003,9,1,0,0,0);
98            linecolour='k';linestyle='--';mark='h';
99          else linecolour='k';linestyle='.';mark='p';
100       end
101
102     %*************************************************************************************************
        **************
103
104     function [f_std] = nanstd(data);
105     %
106     %   [f_std] = nanstd(data);
107     %
108     %Function which calculates the std (not NaN) of data containing
109     %NaN's.  NaN's are excluded completely from calculation.
110
111     [m,n] = size(data);
112
113     for index = 1:n;
114       not_nans = find(isnan(data(:,index)) == 0);
115         if length(not_nans) > 0;
116           f_std(index) = std(data(not_nans,index));
117         else
118           f_std(index) = NaN;
119         end
120     end
121
122     %added 11/11/03 - need to get rid of std = 0 values where there is only one value. convert to
        NaN
123     f_std(find(f_std==0))=NaN;
```

get_volume.m *MATLAB® program to calculate area and volume of beach sediments from beach profile data.*

```
1     function [volume]=get_volume(profiles_times)
2
3     [m,n]=size(profiles_times);
4     profileid=profiles_times(1,:);
5     profile_data=profiles_times(2:m,:);
6     for i=1:2:n
7       last_good_measure=max(find(isnan(profile_data(:,i))==0));
8       %get all profiles from bench mark to CD.
9       xi=0:.5:600;
10
        yi=interp1(profile_data(1:last_good_measure,i),profile_data(1:last_good_measure,i+1),xi,'linear');
17      %now find height = 0 and take volume from 0 to that
18      this=abs(yi);
19      CDi=find(this==min(this));
20      CDi=min(CDi);
21      volume((i+1)/2,1)=profileid(i);
22      volume((i+1)/2,2)=trapz(xi(1:CDi),yi(1:CDi));
23    end
```

even_odd.m *MATLAB(R) program to calculate shoreline change, volumetric change and even-odd functions as described by Berek and Dean (1982).*

```
msl_98_00(1,:)=[-215 -55 -15 15 55 215];
msl_98_00(2,:)=[98.00
msl_98_00(3,:)=[86.00

msl_diff_98_00(1,:)=msl_98_00(1,:);
msl_diff_98_00(2,:)=msl_98_00(3,:)-msl_98_00(2,:);

y(1,:)=msl_98_00(1,:);
for i=1:6
   y_minus_x=[6 5 4 3 2 1];
   %even function
   y(2,i)=(msl_diff_98_00(2,i)+msl_diff_98_00(2,y_minus_x(i)))/2;
   %odd function
   y(3,i)=(msl_diff_98_00(2,i)-msl_diff_98_00(2,y_minus_x(i)))/2;
end
figure
h=plot(y(1,:),y(3,:));
set(h,'linewidth',2)
xlabel('Distance from Causeway (m)')
ylabel('Shoreline Change (m)')
h=title('Odd Component of Measured Shoreline Change about Causeway (1998-2000)');
set(h,'fontweight','bold')
hl(1)=line([0 0],get(gca,'ylim'));
hl(2)=line(get(gca,'xlim'),[0 0]);
set(hl,'color','k')

clear all
vol_98_00(1,:)=[-215 -55 -15 15 55 215];
vol_98_00(2,:)=[272.07
vol_98_00(3,:)=[302.11

vol_diff_98_00(1,:)=vol_98_00(1,:);
vol_diff_98_00(2,:)=vol_98_00(3,:)-vol_98_00(2,:);

y(1,:)=vol_98_00(1,:);
for i=1:6
   y_minus_x=[6 5 4 3 2 1];
   %even function
   y(2,i)=(vol_diff_98_00(2,i)+vol_diff_98_00(2,y_minus_x(i)))/2;
   %odd function
   y(3,i)=(vol_diff_98_00(2,i)-vol_diff_98_00(2,y_minus_x(i)))/2;
end
figure
h=plot(y(1,:),y(3,:));
set(h,'linewidth',2)
xlabel('Distance from Causeway (m)')
ylabel('Volumetric Change (m^3 per m along beach)')
h=title('Odd Component of Measured Volumetric Change about Causeway (1998-2000)');
set(h,'fontweight','bold')
hl(1)=line([0 0],get(gca,'ylim'));
hl(2)=line(get(gca,'xlim'),[0 0]);
set(hl,'color','k')
clear all

vol_1_4_98_00(1,:)=[-750 -430 430 750];
vol_1_4_98_00(2,:)=[184.24
%the last value here for 215 East of 113 is the value from 1999 as no survey data in 2000.
vol_1_4_98_00(3,:)=[191.34

vol_1_4_diff_98_00(1,:)=vol_1_4_98_00(1,:);
vol_1_4_diff_98_00(2,:)=vol_1_4_98_00(3,:)-vol_1_4_98_00(2,:);

y(1,:)=vol_1_4_98_00(1,:);
```

```
64      for i=1:4
65        y_minus_x=[4 3 2 1];
66        %even function
67        y(2,i)=(vol_1_4_diff_98_00(2,i)+vol_1_4_diff_98_00(2,y_minus_x(i)))/2;
68        %odd function
69        y(3,i)=(vol_1_4_diff_98_00(2,i)-vol_1_4_diff_98_00(2,y_minus_x(i)))/2;
70      end
71      figure
72      h=plot(y(1,:),y(3,:));
73      set(h,'linewidth',2)
74      % hold on
75      % plot(y(1,3:4),y(3,3:4))
76      xlabel('Distance from Northport (m)')
77      ylabel('Volumetric Change (m^3 per m along beach)')
78      h=title('Odd Component of Measured Volumetric Change (2000-2002)');
79      set(h,'fontweight','bold')
80      hl(1)=line([-400 -400],get(gca,'ylim'));
81      hl(2)=line([400 400],get(gca,'ylim'));
82      hl(3)=line(get(gca,'xlim'),[0 0]);
83      set(hl,'color','k')
84      ht(1)=text(-370,-80,'Western Edge of Reclamation');
85      ht(2)=text(370,5,'Eastern Edge of Reclamation');
86      set(ht,'rotation',90,'fontsize',8)
```

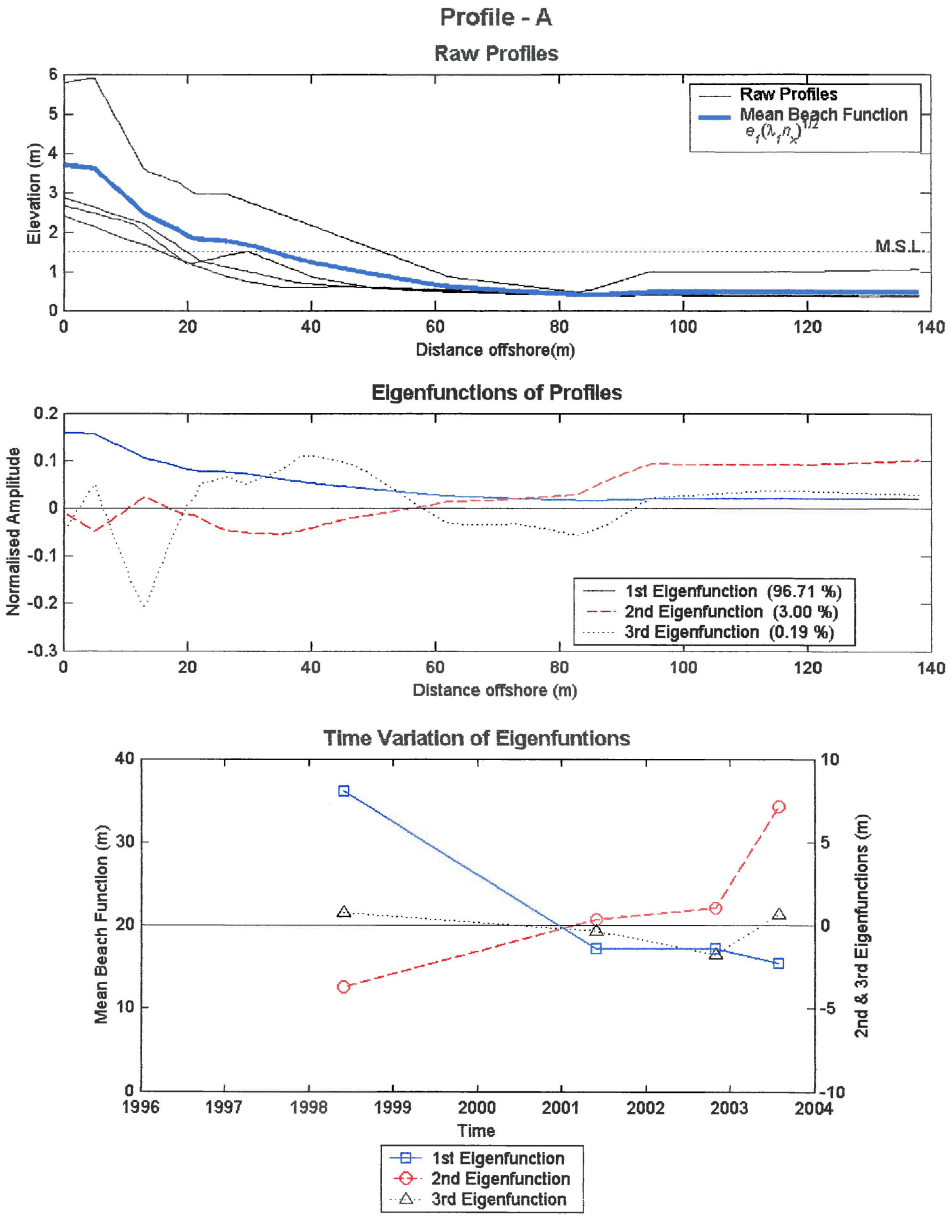
temporal_eigens.m *MATLAB(R) program to undertake empirical orthogonal eigenfunction analysis of beach profile data.*

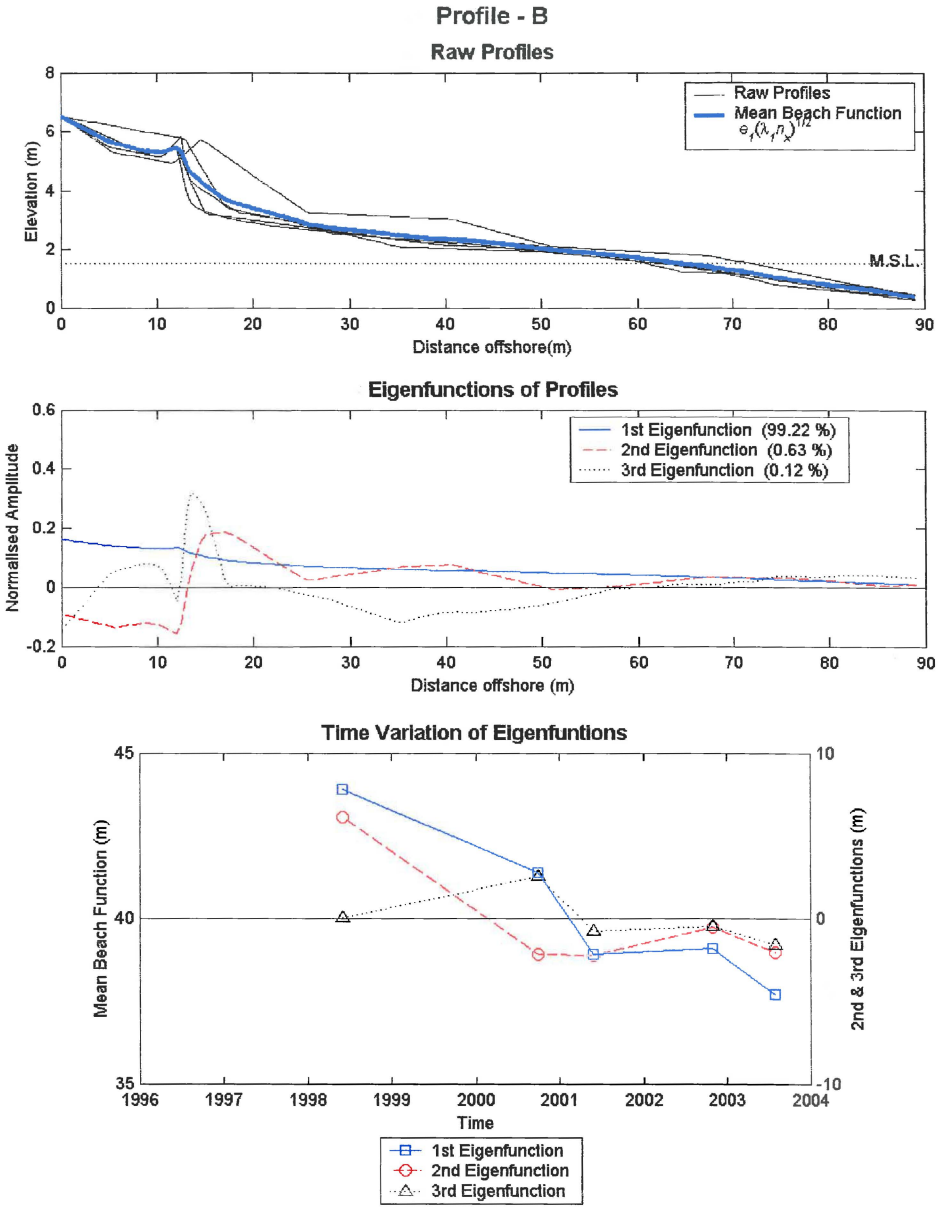
```
1       %temporal_eigens
2       function [eigen_vals_out]=temporal_eigens(profile,profile_name)
3
4       %definition of eigen_val_out
5       %Column1=mean_square,then eigen values.
6       %Column2=0, then %of variance explained
7       %column3=0, then number of eigenvalue
8
9       %find the times that profile lines were taken
10      profile_times=profile(find(profile > datenum(1995,1,1)));
11      [m,n]=size(profile);
12      length_all_profiles=min(max(profile(2:m,[1:2:n])));
13      x_interp=[0:.5:length_all_profiles];
14      %for temporal eigens all profiles are relative same Benchmark, no adjustments
        needed.
15      %need to interpolate all profiles onto a common Xgrid
16      for i=1:length(profile_times);
17        %find indcies of each profile line
18        [ii,jj]=find(profile==profile_times(i));
19        %interpolation will not work with nans present so remove them
20        [x,y]=profile_no_nan(profile(2:m,jj),profile(2:m,jj+1));
21        %interpolate each profile in series
22        [y_on_grid(i,:)]=interp1(x,y,x_interp);
23      end
24
25      %begin calculating correlation matrix
26      [m,n]=size(y_on_grid);
27      %calculate correlation matrix
28      y_correlation=(y_on_grid'*y_on_grid)/(m*n);
29      %calcualate eigen vectors and eigen values
30      [eigenvector,eigenvalue]=eig(y_correlation);
31
32      %calculate the mean square value of all the data from the diagonal elements in
        covariance matrix
33      %this is also equal to the sum of all eigenvalues from the matix by Ae_n=Y_ne_n
34      mean_square=trace(y_covariance);
35
36      %shape eigen vectors and take only the first 3
37      [m,n]=size(eigenvector);
38      eigenvect(1,:)=eigenvector(:,n)';
```

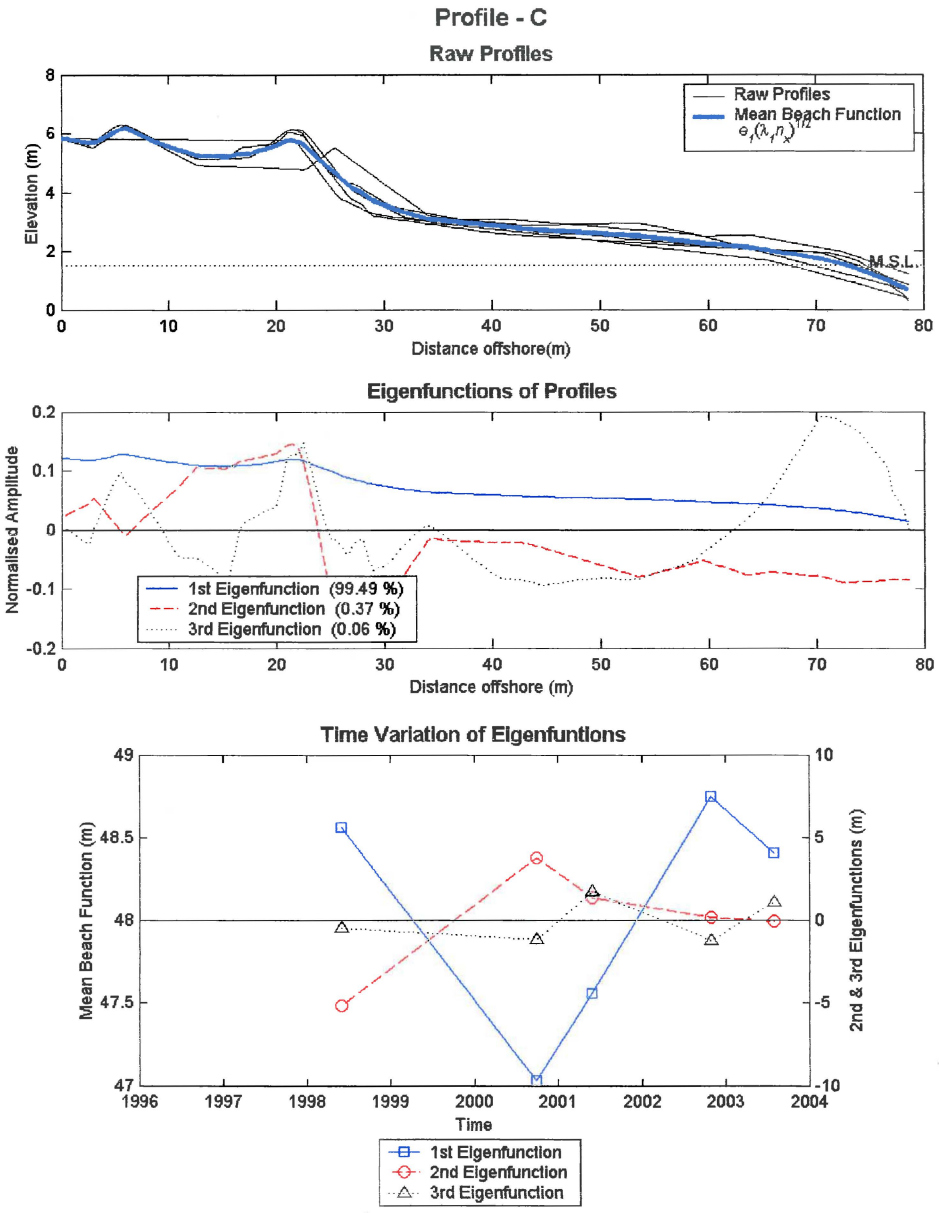
```
39  eigenvect(2,:)=eigenvector(:,n-1)';
40  eigenvect(3,:)=eigenvector(:,n-2)';
41
42  %isolate the eigen values for the associated eigen vectors
43  [m,n]=size(eigenvalue);
44  eigenval(1,1)=eigenvalue(m,n);
45  eigenval(2,1)=eigenvalue(m-1,n-1);
46  eigenval(3,1)=eigenvalue(m-2,n-2);
47
48  variance_explained=(eigenval./mean_square)*100;
49
50  %generate the out matrix of eigenvalues
51  %Column1=mean_square,then eigen values.
52  %Column2=0, then %of variance explained
53  %column3=0, then number of eigenvalue
54  eigen_vals_out(1,1:2)=[mean_square 0];
55  eigen_vals_out(2:4,1)=eigenval;
56  eigen_vals_out(2:4,2)=variance_explained;
57  eigen_vals_out(1:4,3)=[0:1:3]';
58
59
60  %now caculate variation in eigenvectors over the surveys
61  %this is the coefficient matrix - calls eigen_coeffs.m
62  [Coeff_nt]=eigen_coeffs(y_on_grid,eigenvect);
63  %remove the nan's from the data.
64  function [no_nan_x,no_nan_y]=profile_no_nan(input_x,input_y)
65  bad_indicies=find(isnan(input_x)==1);
66  if isempty(bad_indicies)==1
67     no_nan_x=input_x;
68     no_nan_y=input_y;
69  else
70  no_nan_x=input_x(1:min(bad_indicies)-1);
71  no_nan_y=input_y(1:min(bad_indicies)-1);
72  end
```

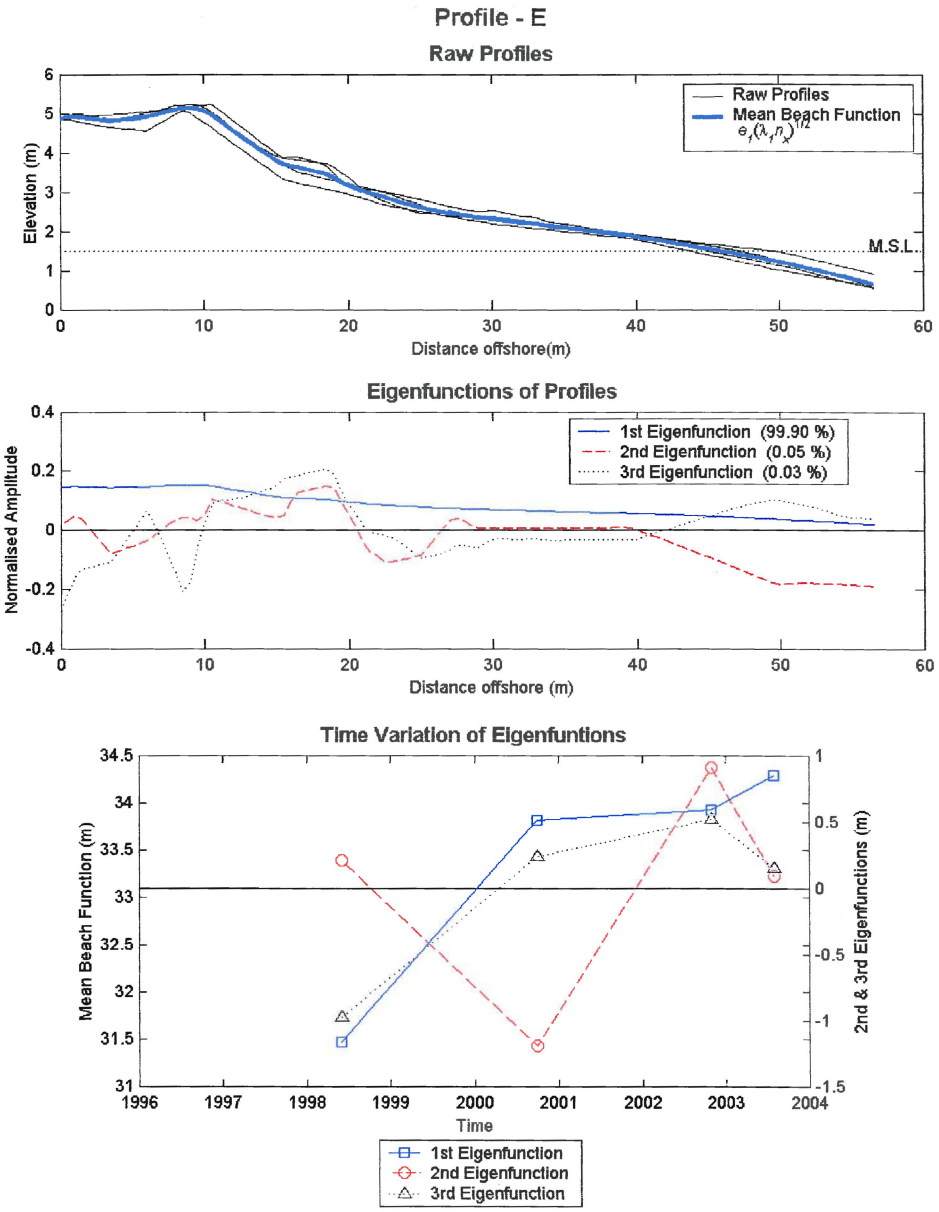
eigen_coeffs.m *MATLAB(R) program to calculate the variation of eigenvectors with each survey over time. From equation 7.10.*

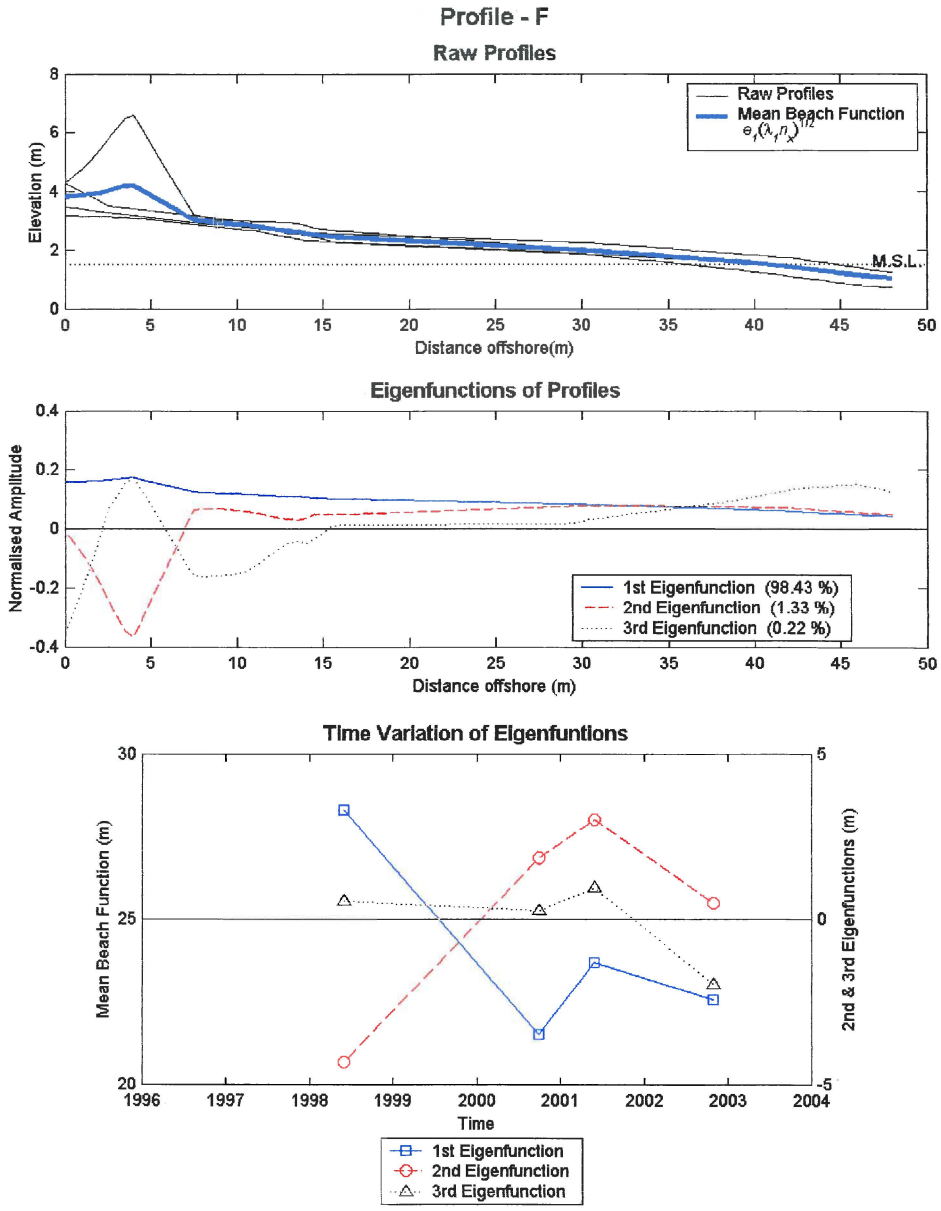
```
1   function [Coef_nt]=eigen_coeffs(Y_xt,eigenvect_nx)
2
3   [nT,nXy]=size(Y_xt);
4   [nN,nXe]=size(eigenvect_nx);
5
6   for i=1:nT
7      for ii=1:nN
8         for iii=1:nXe
9            vals_to_sum(iii)=(Y_xt(i,iii)*eigenvect_nx(ii,iii));
10        end
11        Coef_n_1t(ii)=sum(vals_to_sum);
12        clear vals_to_sum
13     end
14     Coef_nt(i,:)=Coef_n_1t;clear Coef_n_1t
15  end
```

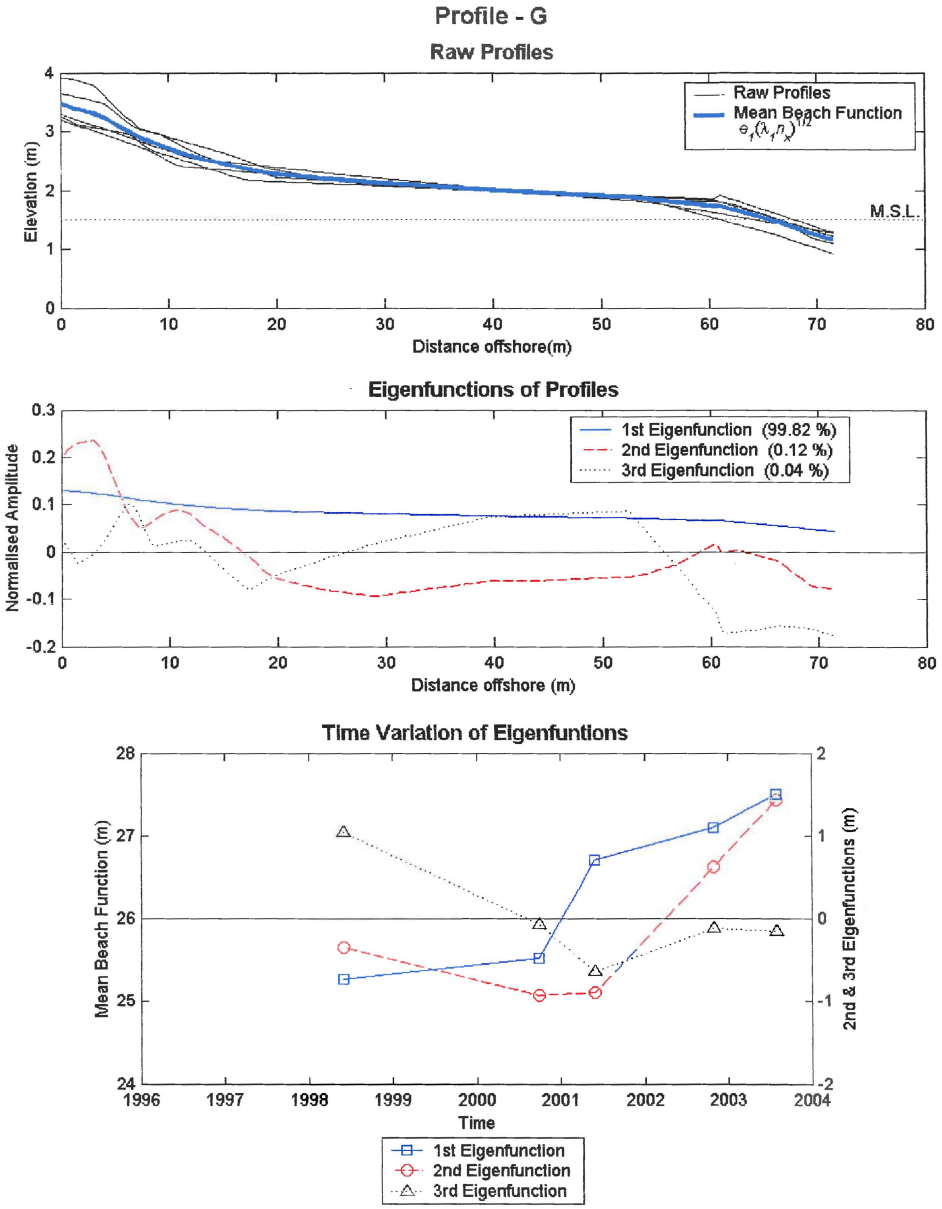

Profile - A
Raw Profiles
Raw Profiles
Mean Beach Function
$e_1(\lambda_1 n_x)^{1/2}$
M.S.L.
Elevation (m)
Distance offshore(m)
Eigenfunctions of Profiles
Normalised Amplitude
1st Eigenfunction (96.71 %)
2nd Eigenfunction (3.00 %)
3rd Eigenfunction (0.19 %)
Distance offshore (m)
Time Variation of Eigenfuntions
Mean Beach Function (m)
2nd & 3rd Eigenfunctions (m)
Time
1st Eigenfunction
2nd Eigenfunction
3rd Eigenfunction

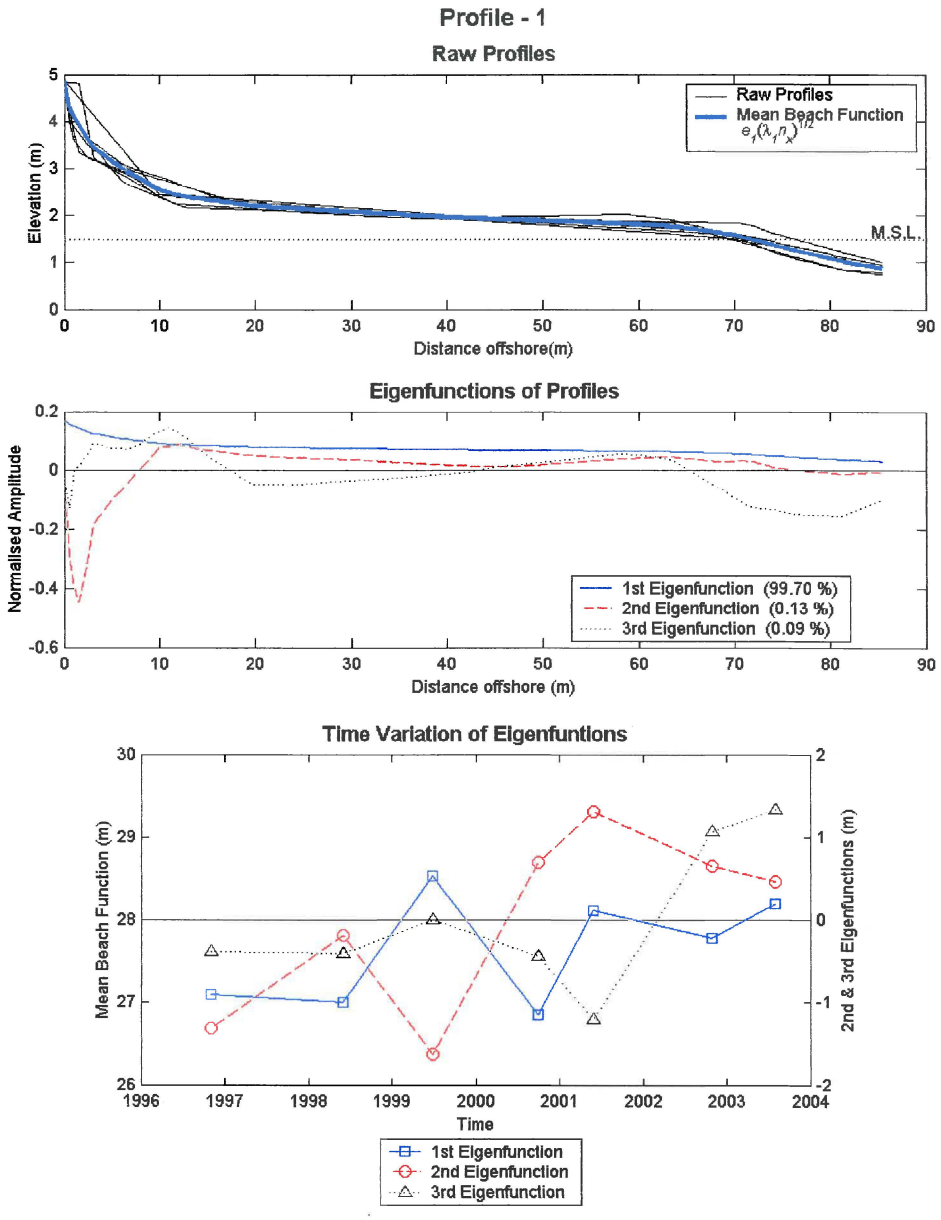

Profile - B
Raw Profiles
Raw Profiles
Mean Beach Function
$e_1(\lambda_1 n_x)^{1/2}$
Elevation (m)
M.S.L.
Distance offshore(m)
Eigenfunctions of Profiles
1st Eigenfunction (99.22 %)
2nd Eigenfunction (0.63 %)
3rd Eigenfunction (0.12 %)
Normalised Amplitude
Distance offshore (m)
Time Variation of Eigenfuntions
Mean Beach Function (m)
2nd & 3rd Eigenfunctions (m)
Time
1st Eigenfunction
2nd Eigenfunction
3rd Eigenfunction

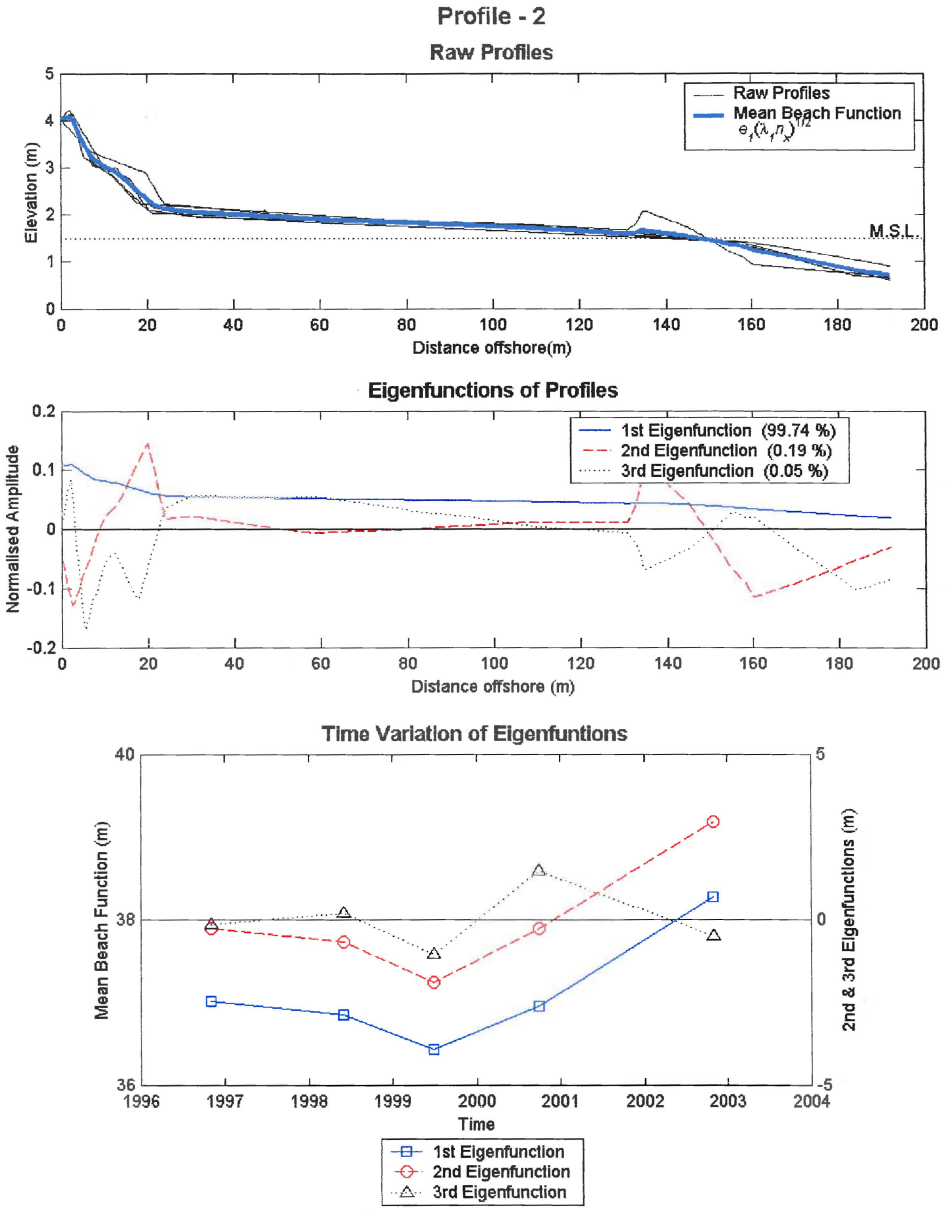

Profile - C
Raw Profiles
Raw Profiles
Mean Beach Function
M.S.L.
Elevation (m)
Distance offshore(m)
Eigenfunctions of Profiles
1st Eigenfunction (99.49 %)
2nd Eigenfunction (0.37 %)
3rd Eigenfunction (0.06 %)
Normalised Amplitude
Distance offshore (m)
Time Variation of Eigenfuntions
Mean Beach Function (m)
2nd & 3rd Eigenfunctions (m)
Time
1st Eigenfunction
2nd Eigenfunction
3rd Eigenfunction

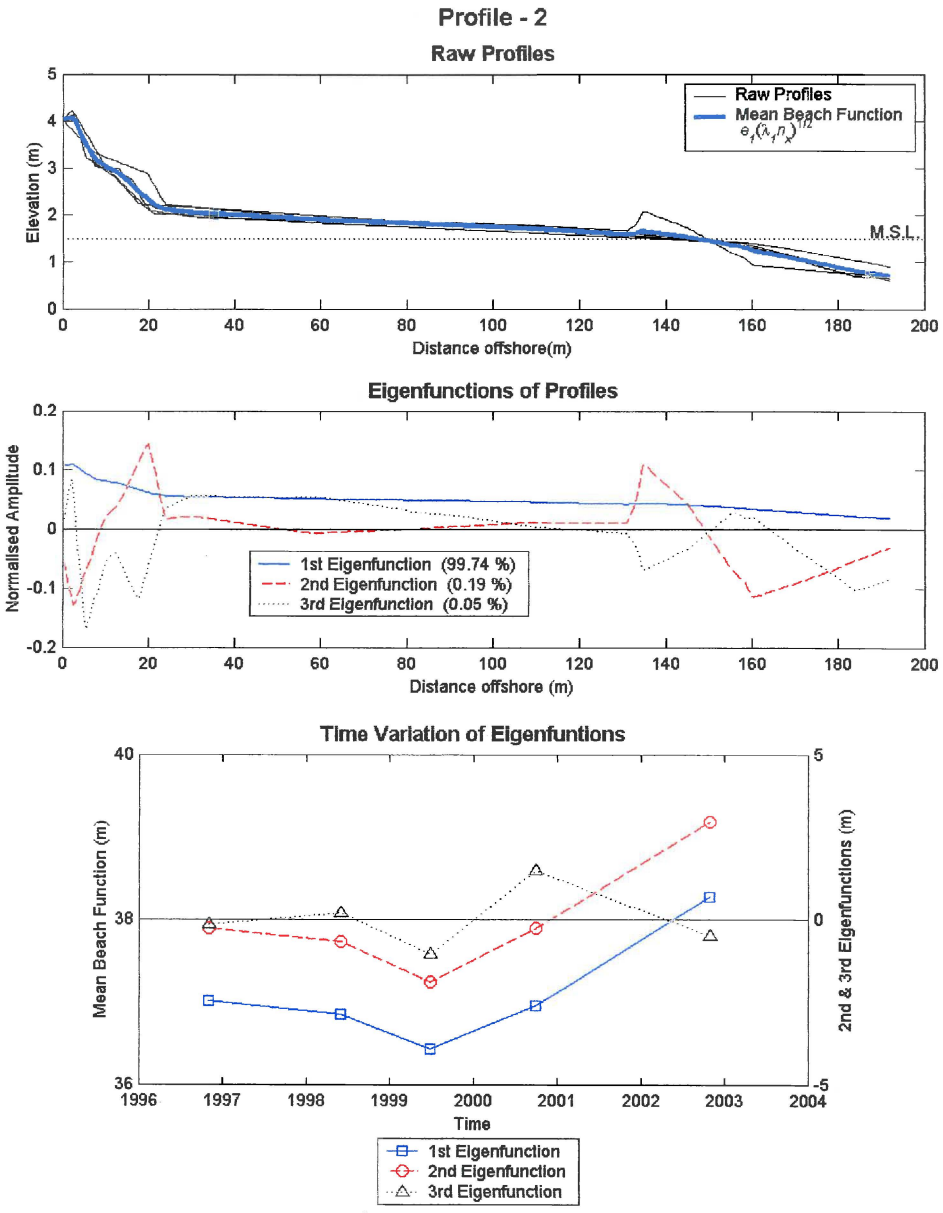

Profile - E
Raw Profiles
Raw Profiles
Mean Beach Function
M.S.L.
Elevation (m)
Distance offshore(m)
Eigenfunctions of Profiles
1st Eigenfunction (99.90 %)
2nd Eigenfunction (0.05 %)
3rd Eigenfunction (0.03 %)
Normalised Amplitude
Distance offshore (m)
Time Variation of Eigenfuntions
Mean Beach Function (m)
2nd & 3rd Eigenfunctions (m)
Time
1st Eigenfunction
2nd Eigenfunction
3rd Eigenfunction

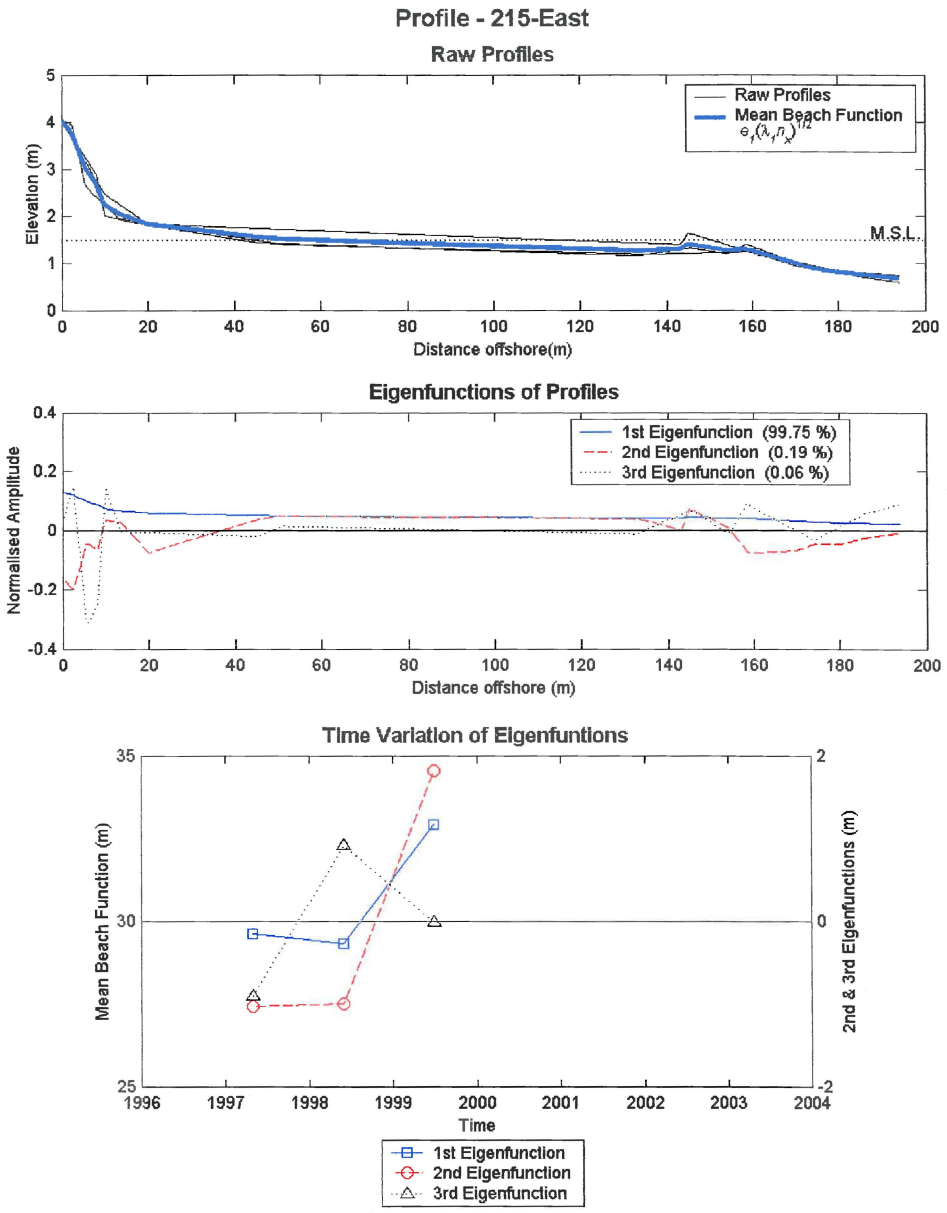

Profile - F
Raw Profiles
Raw Profiles
Mean Beach Function
M.S.L.
Elevation (m)
Distance offshore(m)
Eigenfunctions of Profiles
Normalised Amplitude
1st Eigenfunction (98.43 %)
2nd Eigenfunction (1.33 %)
3rd Eigenfunction (0.22 %)
Distance offshore (m)
Time Variation of Eigenfuntions
Mean Beach Function (m)
2nd & 3rd Eigenfunctions (m)
Time
1st Eigenfunction
2nd Eigenfunction
3rd Eigenfunction

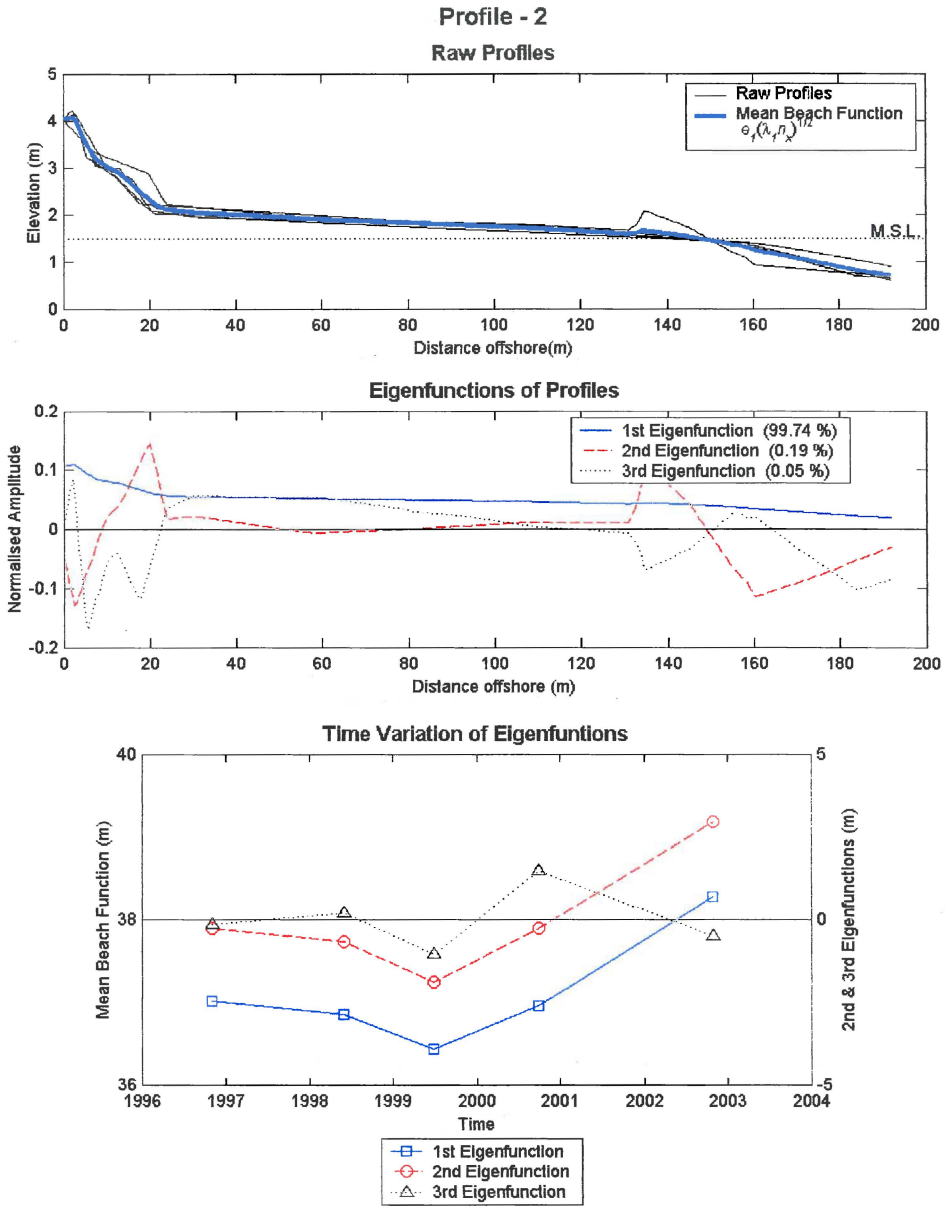

Profile - G
Raw Profiles
Raw Profiles
Mean Beach Function
M.S.L.
Elevation (m)
Distance offshore(m)
Eigenfunctions of Profiles
1st Eigenfunction (99.82 %)
2nd Eigenfunction (0.12 %)
3rd Eigenfunction (0.04 %)
Normalised Amplitude
Distance offshore (m)
Time Variation of Eigenfuntions
Mean Beach Function (m)
2nd & 3rd Eigenfunctions (m)
Time
1st Eigenfunction
2nd Eigenfunction
3rd Eigenfunction

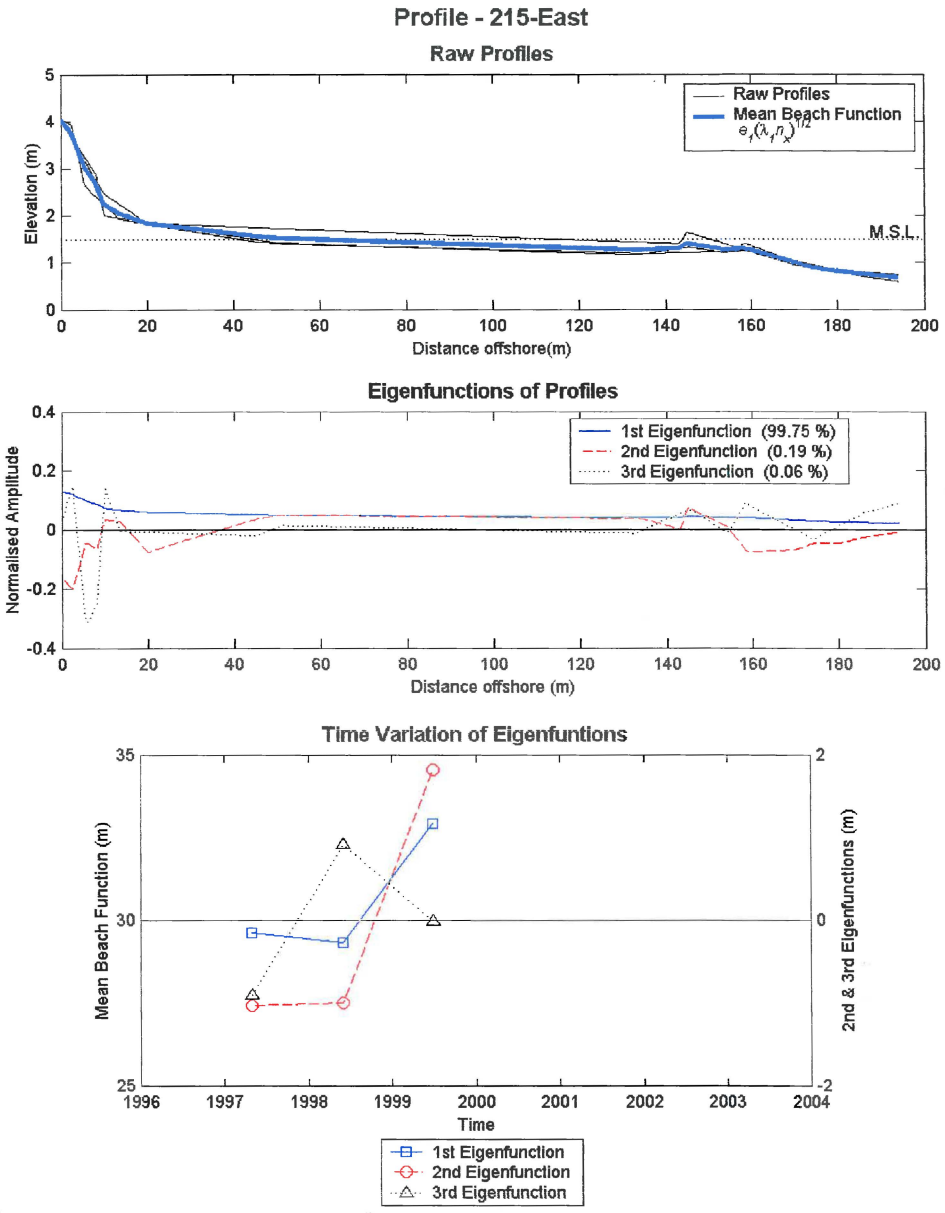

Profile - 1
Raw Profiles
Raw Profiles
Mean Beach Function
M.S.L.
Elevation (m)
Distance offshore(m)
Eigenfunctions of Profiles
Normalised Amplitude
1st Eigenfunction (99.70 %)
2nd Eigenfunction (0.13 %)
3rd Eigenfunction (0.09 %)
Distance offshore (m)
Time Variation of Eigenfuntions
Mean Beach Function (m)
2nd & 3rd Eigenfunctions (m)
Time
1st Eigenfunction
2nd Eigenfunction
3rd Eigenfunction

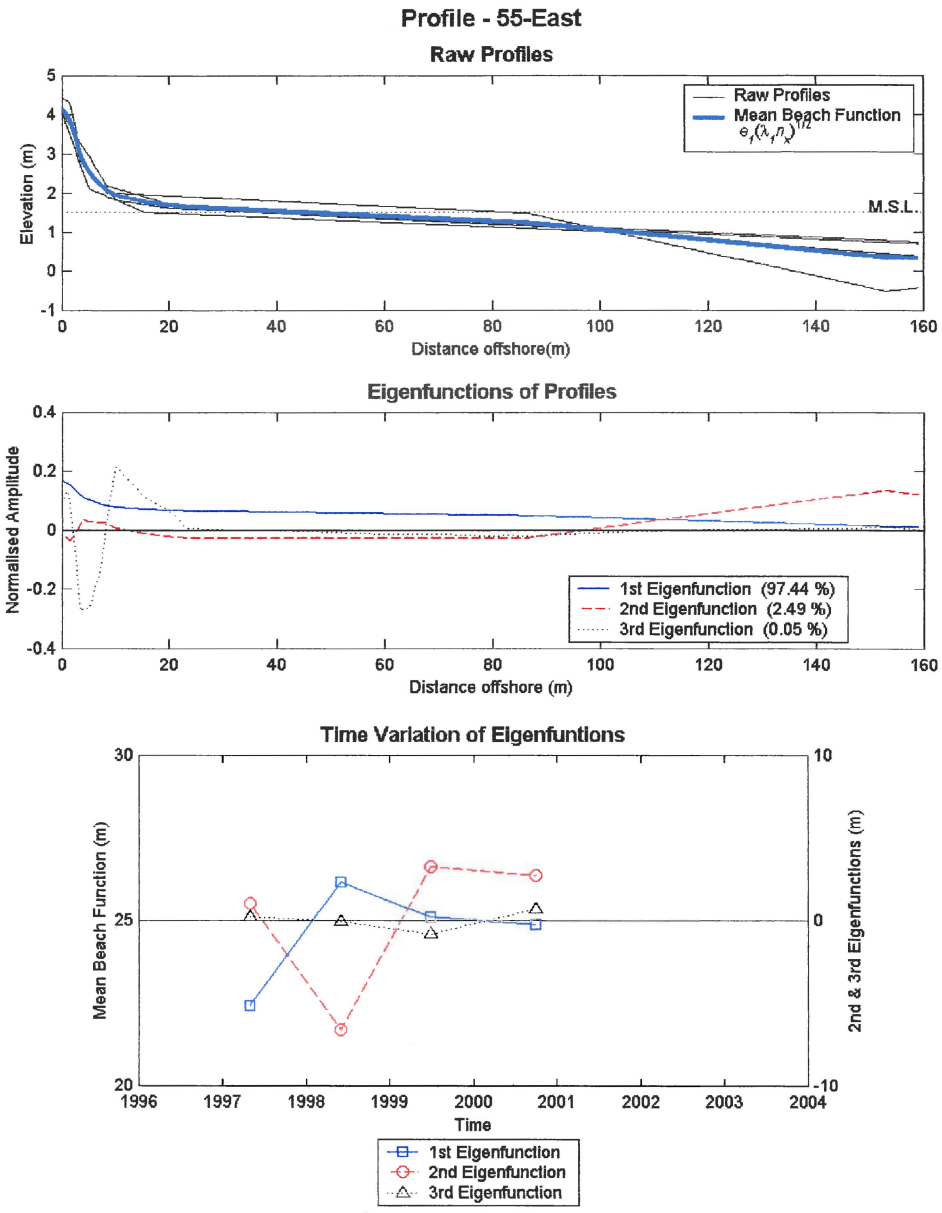

Profile - 2
Raw Profiles
Raw Profiles
Mean Beach Function
$e_1(\lambda_1 n_x)^{1/2}$
M.S.L.
Elevation (m)
Distance offshore(m)
Eigenfunctions of Profiles
1st Eigenfunction (99.74 %)
2nd Eigenfunction (0.19 %)
3rd Eigenfunction (0.05 %)
Normalised Amplitude
Distance offshore (m)
Time Variation of Eigenfuntions
Mean Beach Function (m)
2nd & 3rd Eigenfunctions (m)
Time
1st Eigenfunction
2nd Eigenfunction
3rd Eigenfunction

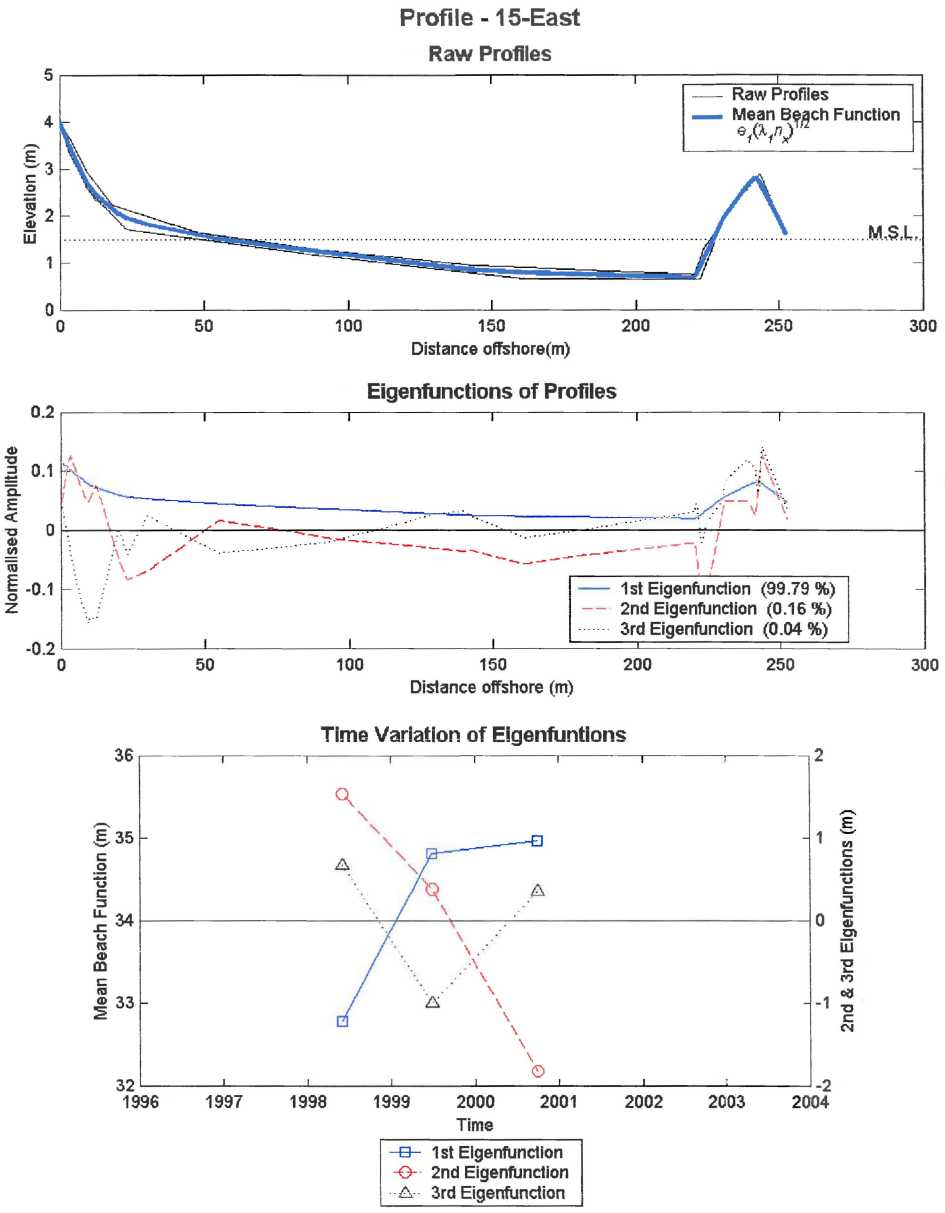

Profile - 2
Raw Profiles
Raw Profiles
Mean Beach Function
M.S.L.
Elevation (m)
Distance offshore(m)
Eigenfunctions of Profiles
1st Eigenfunction (99.74 %)
2nd Eigenfunction (0.19 %)
3rd Eigenfunction (0.05 %)
Normalised Amplitude
Distance offshore (m)
Time Variation of Eigenfuntions
Mean Beach Function (m)
2nd & 3rd Eigenfunctions (m)
Time
1st Eigenfunction
2nd Eigenfunction
3rd Eigenfunction

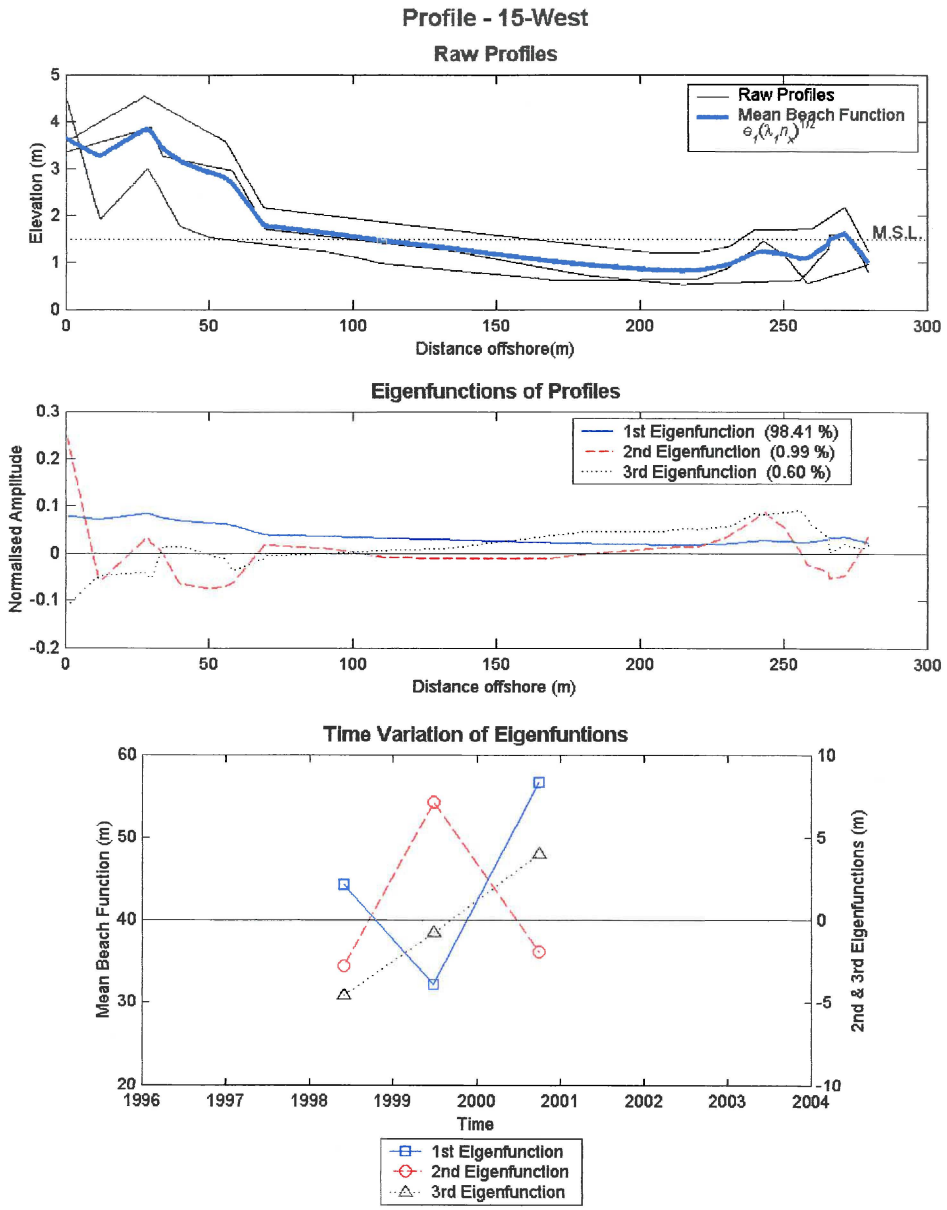

Profile - 215-East
Raw Profiles
Raw Profiles
Mean Beach Function
M.S.L.
Elevation (m)
Distance offshore(m)
Eigenfunctions of Profiles
1st Eigenfunction (99.75 %)
2nd Eigenfunction (0.19 %)
3rd Eigenfunction (0.06 %)
Normalised Amplitude
Distance offshore (m)
Time Variation of Eigenfuntions
Mean Beach Function (m)
2nd & 3rd Eigenfunctions (m)
Time
1st Eigenfunction
2nd Eigenfunction
3rd Eigenfunction

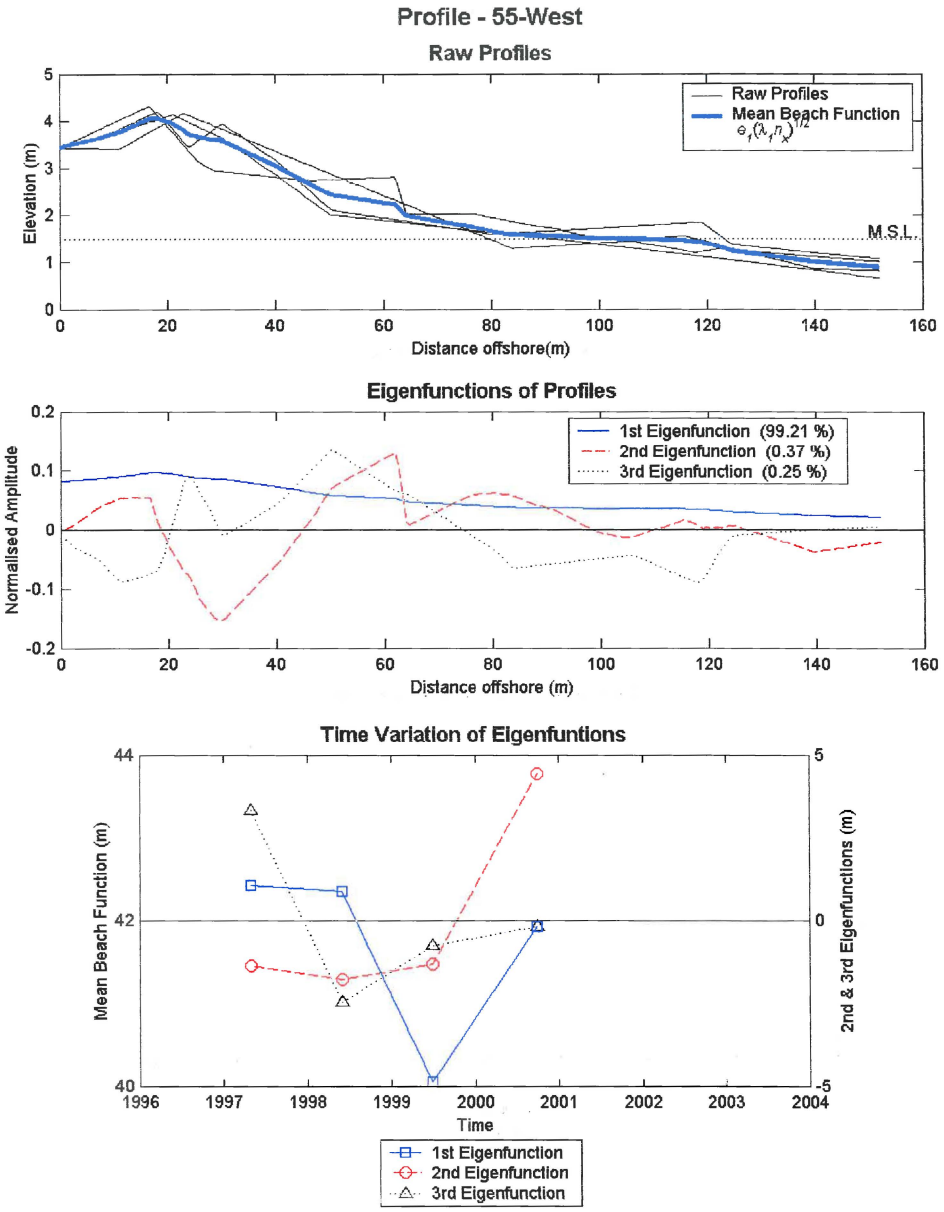

Profile - 2
Raw Profiles
Raw Profiles
Mean Beach Function
M.S.L.
Elevation (m)
Distance offshore(m)
Eigenfunctions of Profiles
1st Eigenfunction (99.74 %)
2nd Eigenfunction (0.19 %)
3rd Eigenfunction (0.05 %)
Normalised Amplitude
Distance offshore (m)
Time Variation of Eigenfuntions
Mean Beach Function (m)
2nd & 3rd Eigenfunctions (m)
Time
1st Eigenfunction
2nd Eigenfunction
3rd Eigenfunction

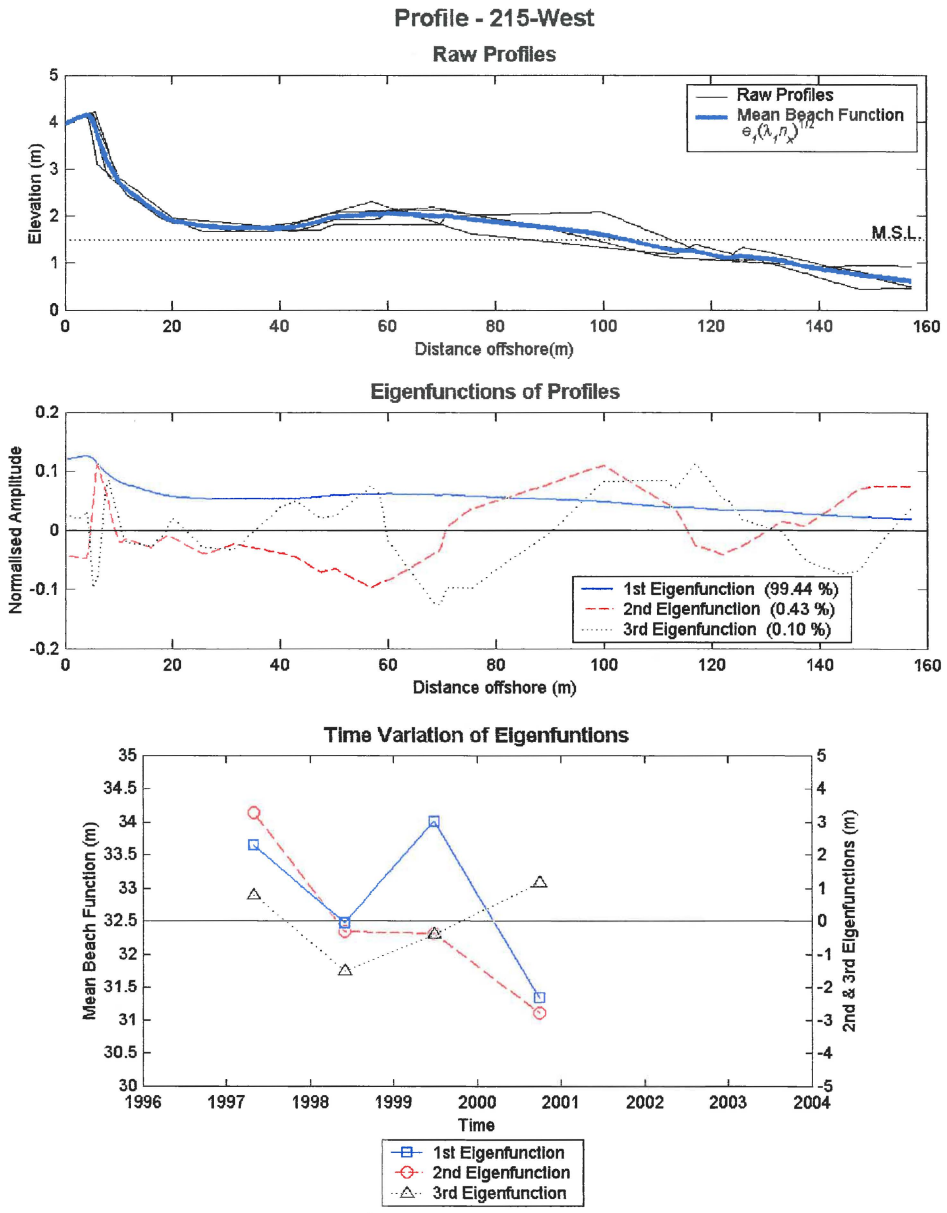

Profile - 215-East
Raw Profiles
Raw Profiles
Mean Beach Function
M.S.L.
Elevation (m)
Distance offshore(m)
Eigenfunctions of Profiles
1st Eigenfunction (99.75 %)
2nd Eigenfunction (0.19 %)
3rd Eigenfunction (0.06 %)
Normalised Amplitude
Distance offshore (m)
Time Variation of Eigenfuntions
Mean Beach Function (m)
2nd & 3rd Eigenfunctions (m)
Time
1st Eigenfunction
2nd Eigenfunction
3rd Eigenfunction

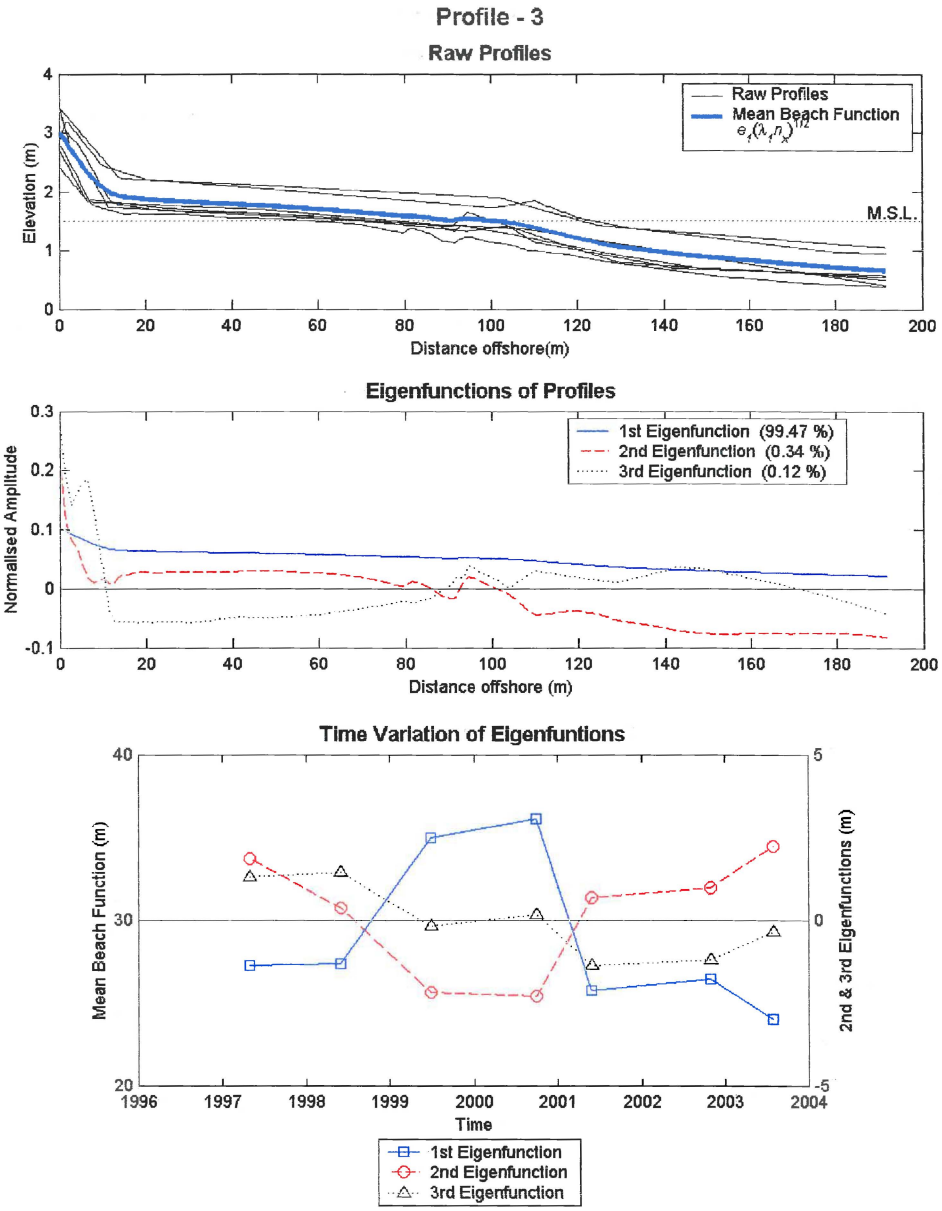

Profile - 55-East
Raw Profiles
Raw Profiles
Mean Beach Function
$e_1(\lambda_1 n_x)^{1/2}$
M.S.L.
Elevation (m)
Distance offshore(m)
Eigenfunctions of Profiles
Normalised Amplitude
1st Eigenfunction (97.44 %)
2nd Eigenfunction (2.49 %)
3rd Eigenfunction (0.05 %)
Distance offshore (m)
Time Variation of Eigenfuntions
Mean Beach Function (m)
2nd & 3rd Eigenfunctions (m)
Time
1st Eigenfunction
2nd Eigenfunction
3rd Eigenfunction

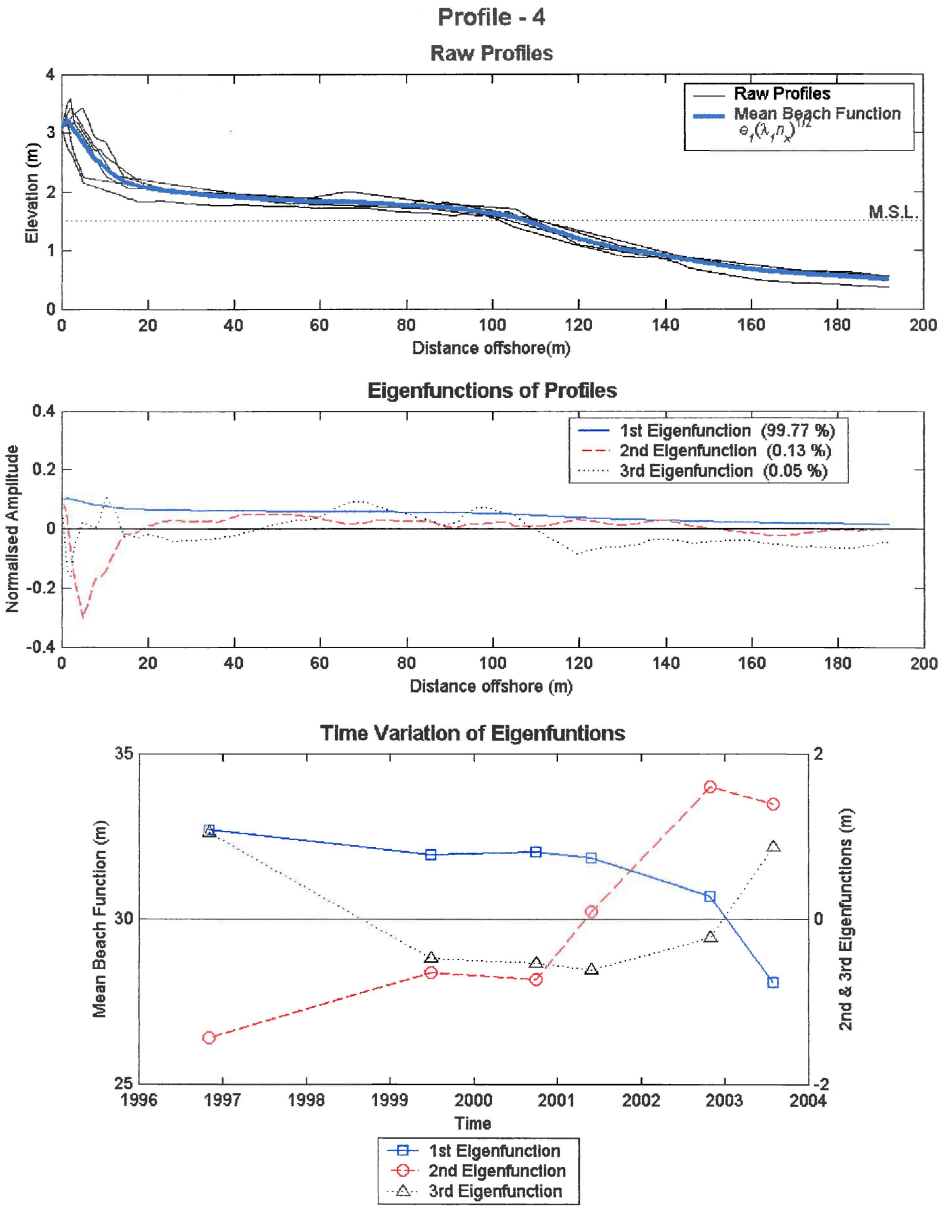

Profile - 15-East
Raw Profiles
Raw Profiles
Mean Beach Function
$e_1(\lambda_1 n_x)^{1/2}$
M.S.L.
Elevation (m)
Distance offshore(m)
Eigenfunctions of Profiles
Normalised Amplitude
1st Eigenfunction (99.79 %)
2nd Eigenfunction (0.16 %)
3rd Eigenfunction (0.04 %)
Distance offshore (m)
Time Variation of Eigenfuntions
Mean Beach Function (m)
2nd & 3rd Eigenfunctions (m)
Time
1st Eigenfunction
2nd Eigenfunction
3rd Eigenfunction

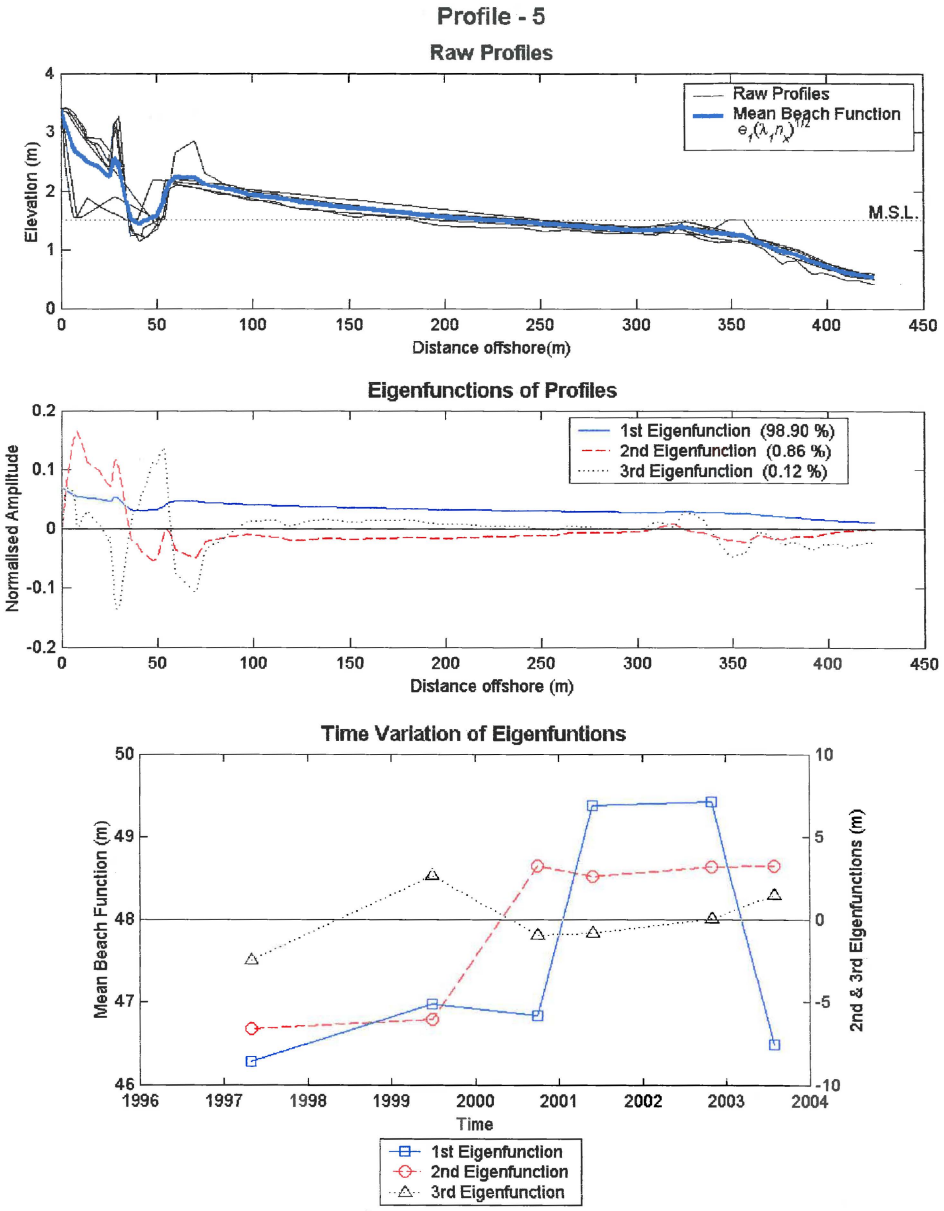

Profile - 15-West
Raw Profiles
Raw Profiles
Mean Beach Function
M.S.L.
Elevation (m)
Distance offshore(m)
Eigenfunctions of Profiles
1st Eigenfunction (98.41 %)
2nd Eigenfunction (0.99 %)
3rd Eigenfunction (0.60 %)
Normalised Amplitude
Distance offshore (m)
Time Variation of Eigenfuntions
Mean Beach Function (m)
2nd & 3rd Eigenfunctions (m)
Time
1st Eigenfunction
2nd Eigenfunction
3rd Eigenfunction


Profile - 55-West
Raw Profiles
Raw Profiles
Mean Beach Function
M.S.L.
Elevation (m)
Distance offshore(m)
Eigenfunctions of Profiles
1st Eigenfunction (99.21 %)
2nd Eigenfunction (0.37 %)
3rd Eigenfunction (0.25 %)
Normalised Amplitude
Distance offshore (m)
Time Variation of Eigenfuntions
Mean Beach Function (m)
2nd & 3rd Eigenfunctions (m)
Time
1st Eigenfunction
2nd Eigenfunction
3rd Eigenfunction

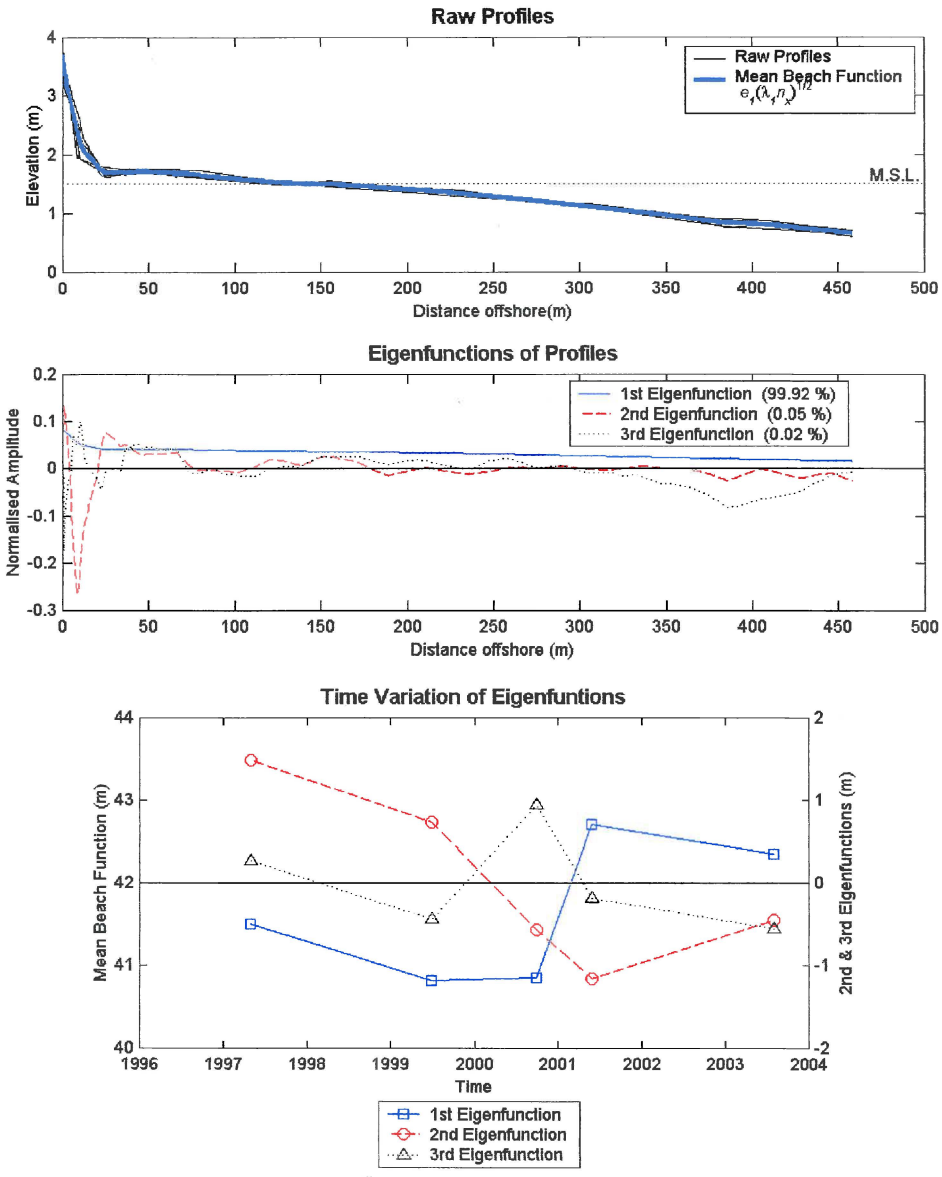

Profile - 215-West
Raw Profiles
Raw Profiles
Mean Beach Function
M.S.L.
Elevation (m)
Distance offshore(m)
Eigenfunctions of Profiles
Normalised Amplitude
1st Eigenfunction (99.44 %)
2nd Eigenfunction (0.43 %)
3rd Eigenfunction (0.10 %)
Distance offshore (m)
Time Variation of Eigenfuntions
Mean Beach Function (m)
2nd & 3rd Eigenfunctions (m)
Time
1st Eigenfunction
2nd Eigenfunction
3rd Eigenfunction

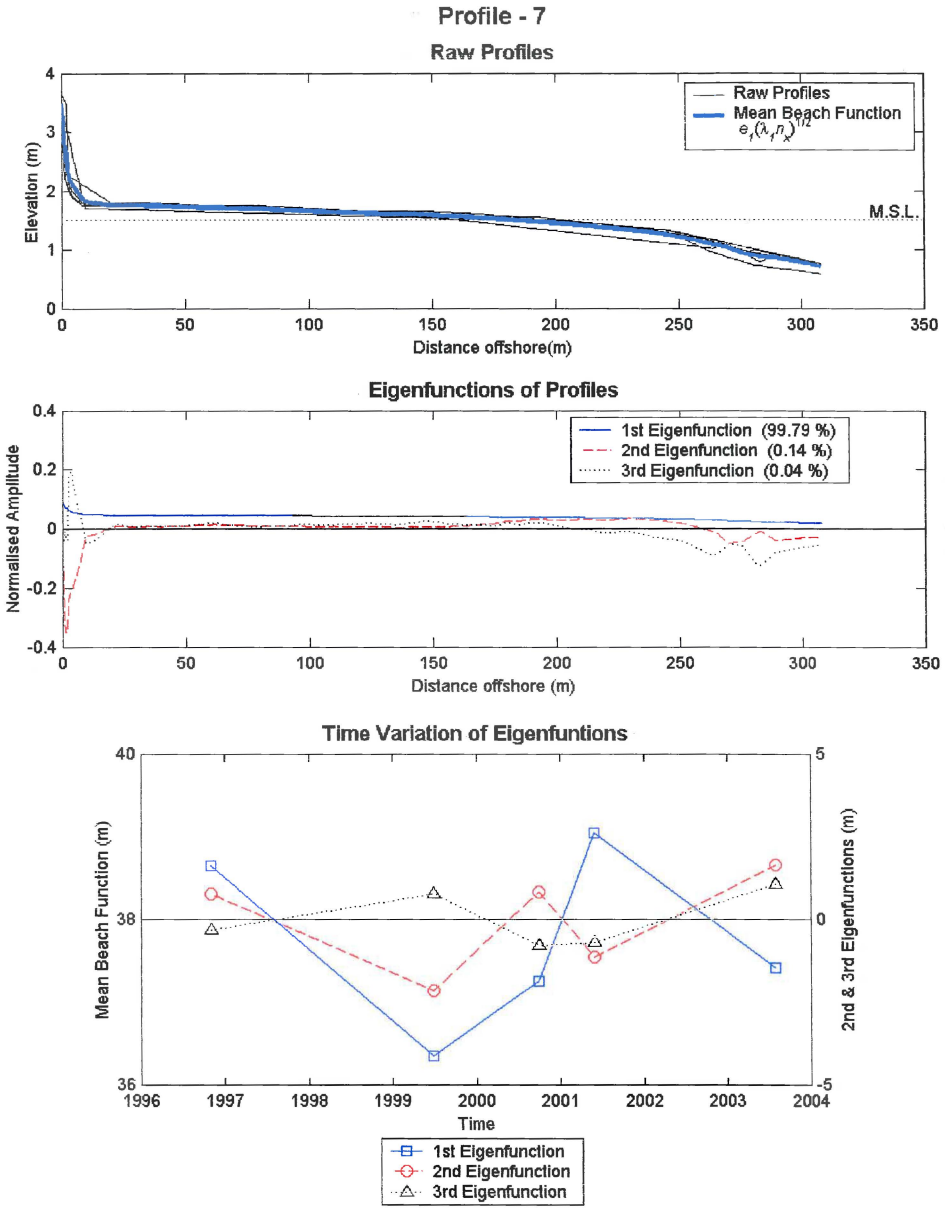

Profile - 3
Raw Profiles
Raw Profiles
Mean Beach Function
M.S.L.
Elevation (m)
Distance offshore(m)
Eigenfunctions of Profiles
1st Eigenfunction (99.47 %)
2nd Eigenfunction (0.34 %)
3rd Eigenfunction (0.12 %)
Normalised Amplitude
Distance offshore (m)
Time Variation of Eigenfuntions
Mean Beach Function (m)
2nd & 3rd Eigenfunctions (m)
Time
1st Eigenfunction
2nd Eigenfunction
3rd Eigenfunction

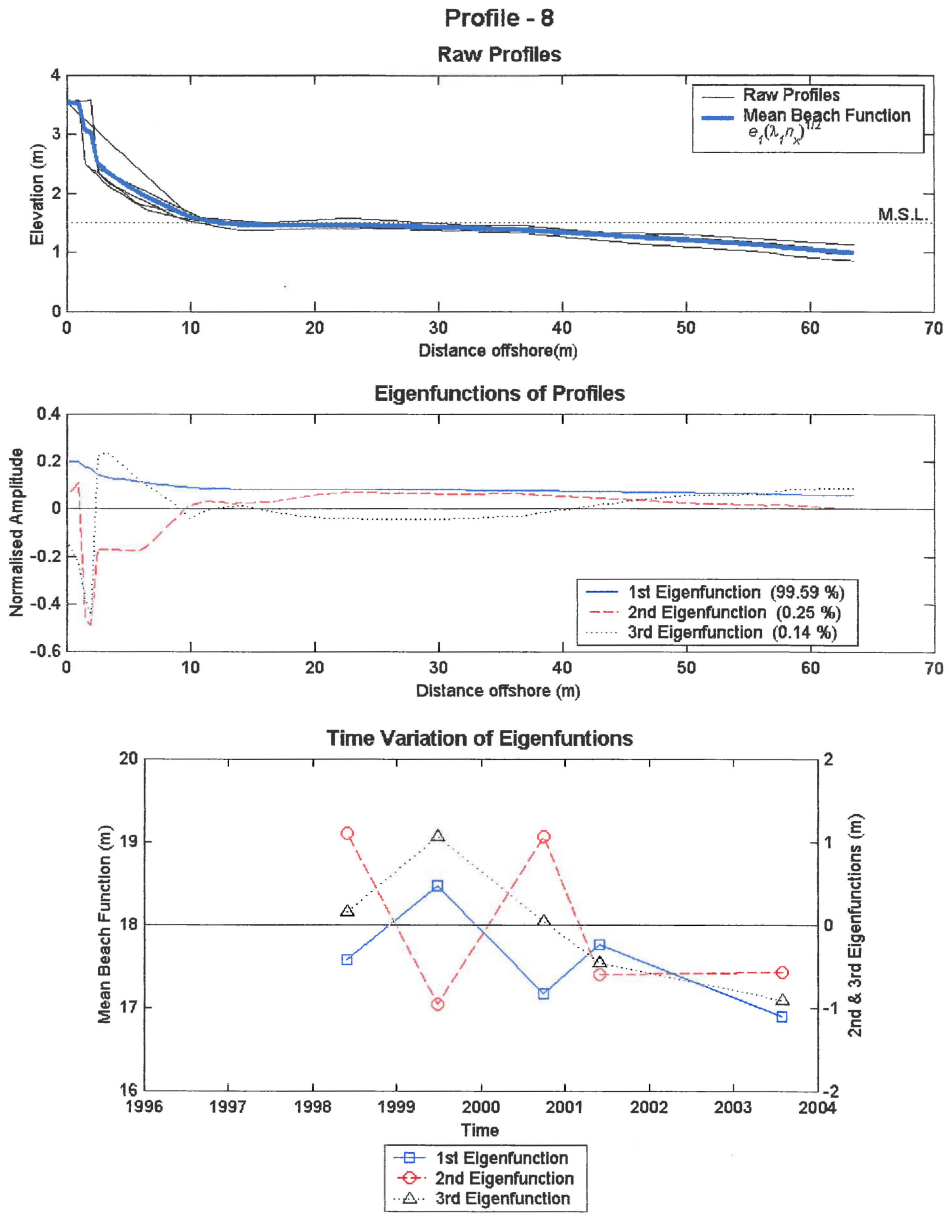

Profile - 4
Raw Profiles
Raw Profiles
Mean Beach Function
$e_1(\lambda_1 n_x)^{1/2}$
M.S.L.
Elevation (m)
Distance offshore(m)
Eigenfunctions of Profiles
1st Eigenfunction (99.77 %)
2nd Eigenfunction (0.13 %)
3rd Eigenfunction (0.05 %)
Normalised Amplitude
Distance offshore (m)
Time Variation of Eigenfuntions
Mean Beach Function (m)
2nd & 3rd Eigenfunctions (m)
Time
1st Eigenfunction
2nd Eigenfunction
3rd Eigenfunction

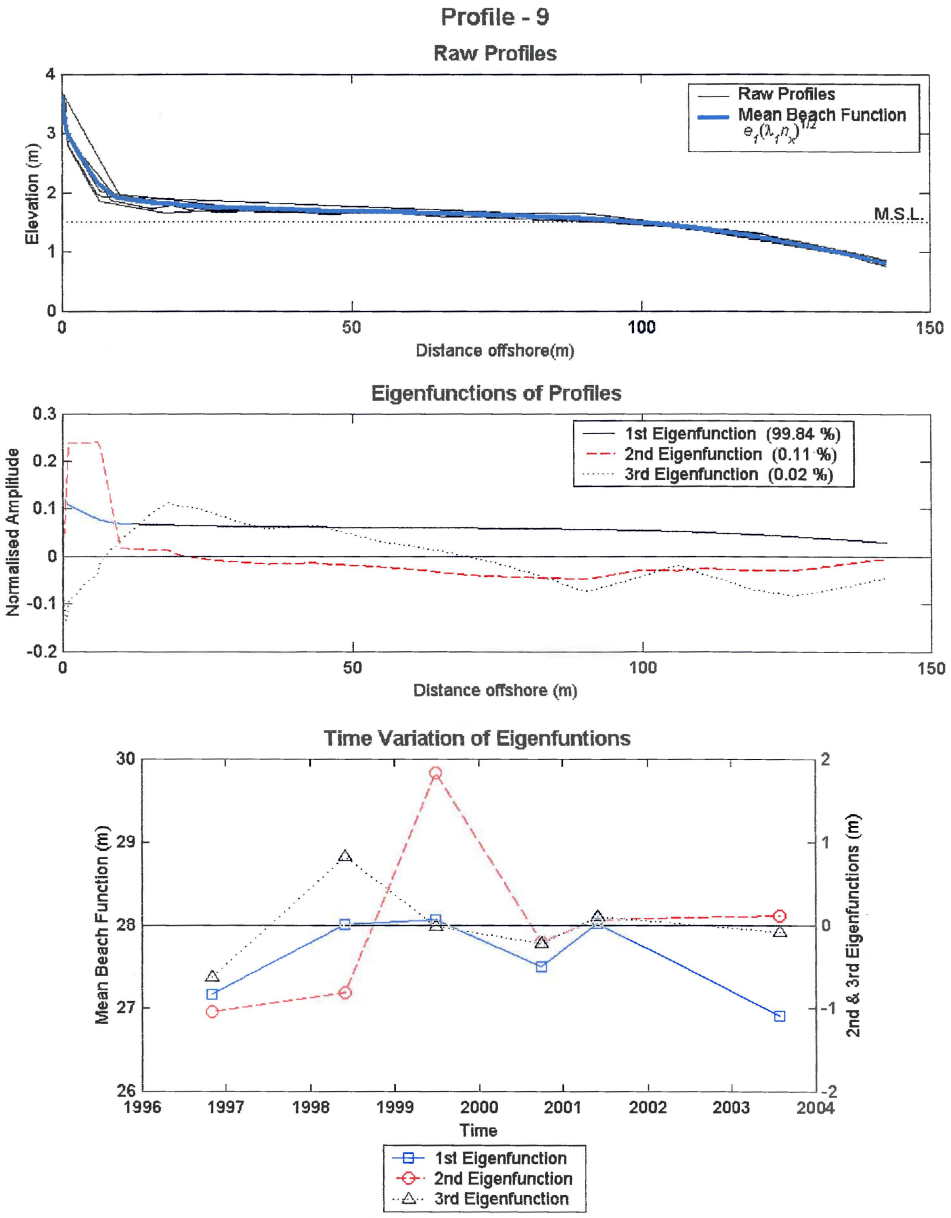

Profile - 5
Raw Profiles
Raw Profiles
Mean Beach Function
M.S.L.
Elevation (m)
Distance offshore(m)
Eigenfunctions of Profiles
1st Eigenfunction (98.90 %)
2nd Eigenfunction (0.86 %)
3rd Eigenfunction (0.12 %)
Normallsed Amplitude
Distance offshore (m)
Time Variation of Eigenfuntions
Mean Beach Function (m)
2nd & 3rd Eigenfunctions (m)
Time
1st Eigenfunction
2nd Eigenfunction
3rd Eigenfunction

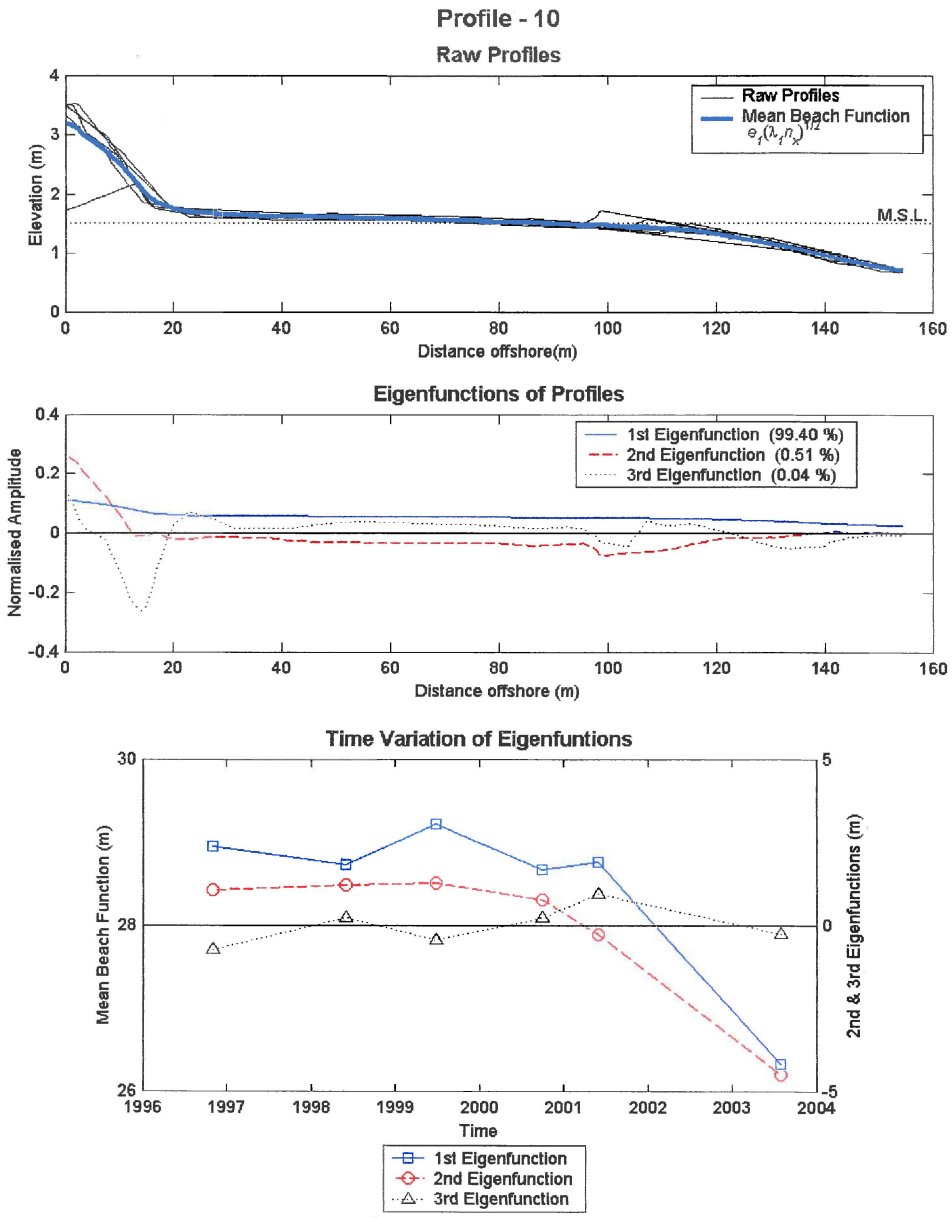
Profile - 6

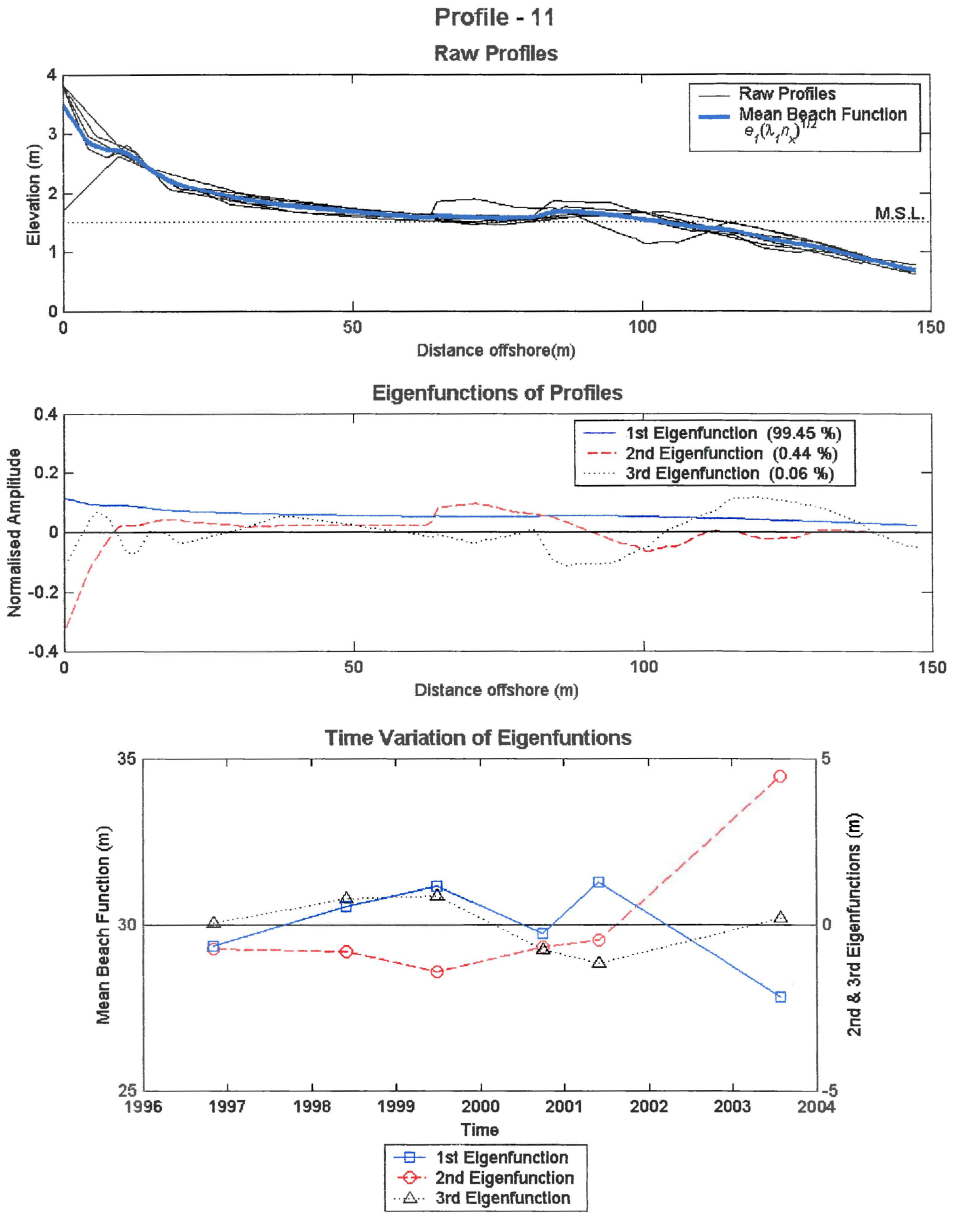

Raw Profiles
Raw Profiles
Mean Beach Function
$e_1(\lambda_1 n_x)^{1/2}$
M.S.L.
Elevation (m)
Distance offshore(m)
Eigenfunctions of Profiles
1st Eigenfunction (99.92 %)
2nd Eigenfunction (0.05 %)
3rd Eigenfunction (0.02 %)
Normalised Amplitude
Distance offshore (m)
Time Variation of Eigenfuntions
Mean Beach Function (m)
2nd & 3rd Eigenfunctions (m)
Time
1st Eigenfunction
2nd Eigenfunction
3rd Eigenfunction

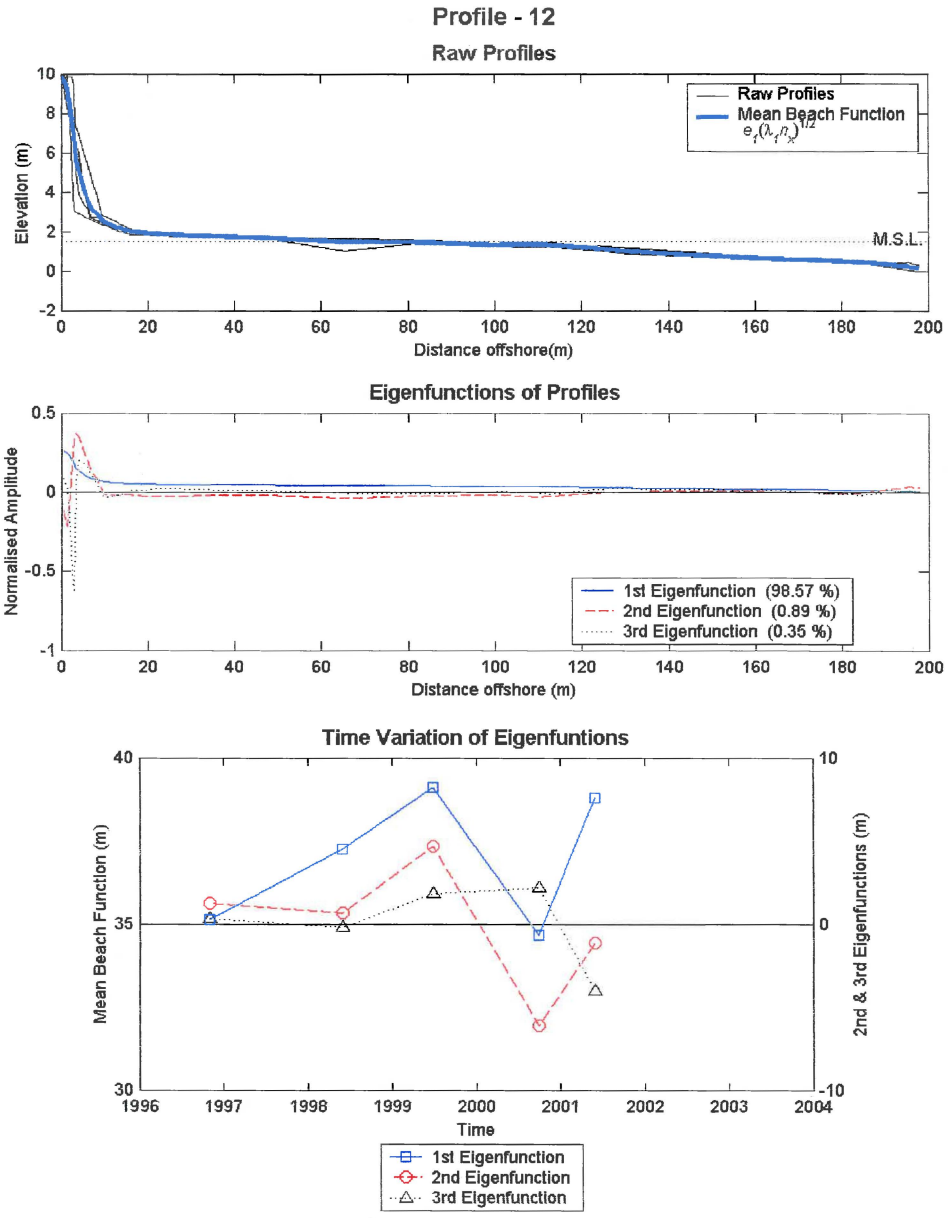

Profile - 7
Raw Profiles
Raw Profiles
Mean Beach Function
$e_1(\lambda_1 n_x)^{1/2}$
M.S.L.
Elevation (m)
Distance offshore(m)
Eigenfunctions of Profiles
1st Eigenfunction (99.79 %)
2nd Eigenfunction (0.14 %)
3rd Eigenfunction (0.04 %)
Normalised Amplitude
Distance offshore (m)
Time Variation of Eigenfuntions
Mean Beach Function (m)
2nd & 3rd Eigenfunctions (m)
Time
1st Eigenfunction
2nd Eigenfunction
3rd Eigenfunction

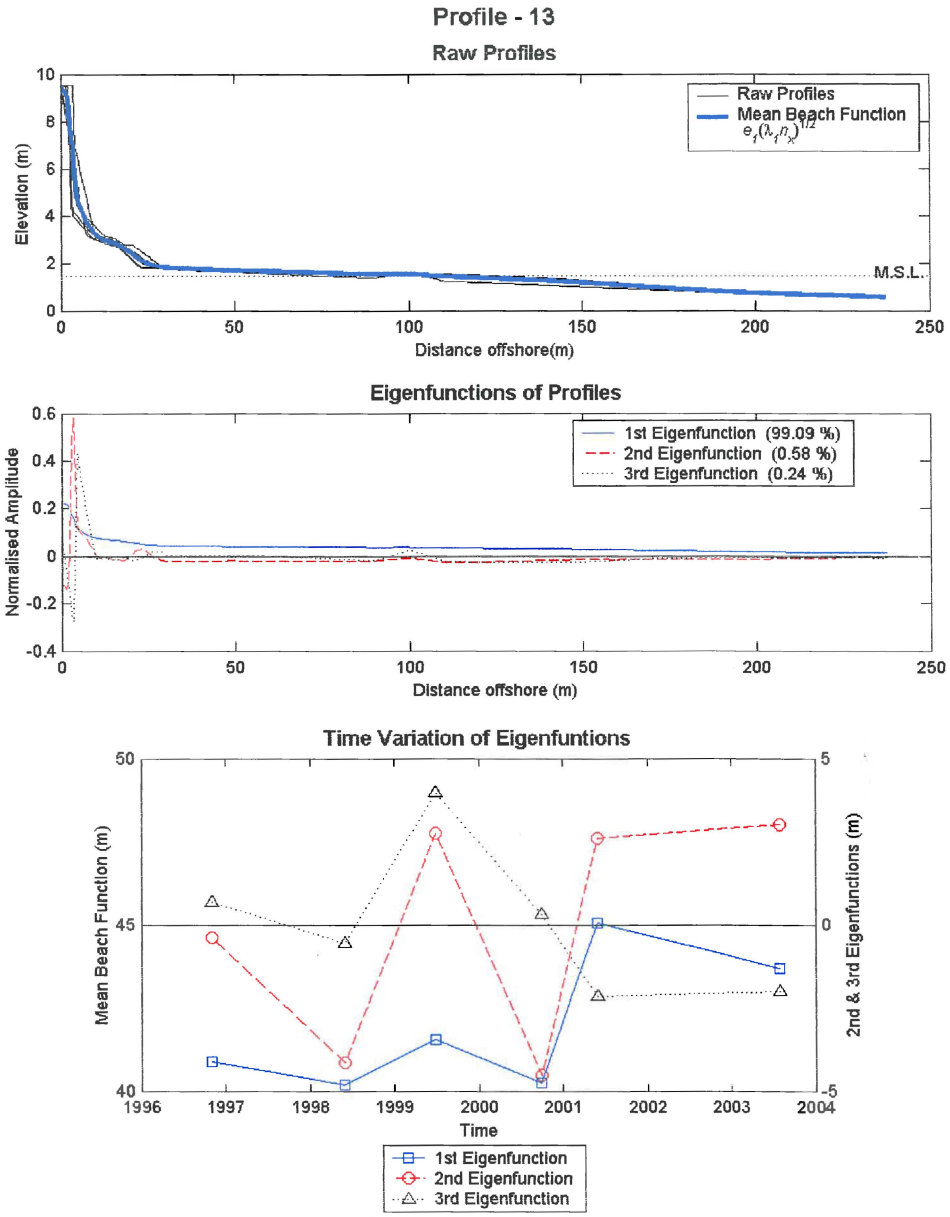

Profile - 8
Raw Profiles
Raw Profiles
Mean Beach Function
$e_i(\lambda_i/n_x)^{1/2}$
M.S.L.
Elevation (m)
Distance offshore(m)
Eigenfunctions of Profiles
Normalised Amplitude
1st Eigenfunction (99.59 %)
2nd Eigenfunction (0.25 %)
3rd Eigenfunction (0.14 %)
Distance offshore (m)
Time Variation of Eigenfuntions
Mean Beach Function (m)
2nd & 3rd Eigenfunctions (m)
Time
1st Eigenfunction
2nd Eigenfunction
3rd Eigenfunction


Profile - 9
Raw Profiles
Raw Profiles
Mean Beach Function
M.S.L.
Elevation (m)
Distance offshore(m)
Eigenfunctions of Profiles
1st Eigenfunction (99.84 %)
2nd Eigenfunction (0.11 %)
3rd Eigenfunction (0.02 %)
Normalised Amplitude
Distance offshore (m)
Time Variation of Eigenfuntions
Mean Beach Function (m)
2nd & 3rd Eigenfunctions (m)
Time
1st Eigenfunction
2nd Eigenfunction
3rd Eigenfunction


Profile - 10
Raw Profiles
Raw Profiles
Mean Beach Function
M.S.L.
Elevation (m)
Distance offshore(m)
Eigenfunctions of Profiles
1st Eigenfunction (99.40 %)
2nd Eigenfunction (0.51 %)
3rd Eigenfunction (0.04 %)
Normalised Amplitude
Distance offshore (m)
Time Variation of Eigenfuntions
Mean Beach Function (m)
2nd & 3rd Eigenfunctions (m)
Time
1st Eigenfunction
2nd Eigenfunction
3rd Eigenfunction


Profile - 11
Raw Profiles
Raw Profiles
Mean Beach Function
M.S.L.
Elevation (m)
Distance offshore(m)
Eigenfunctions of Profiles
1st Eigenfunction (99.45 %)
2nd Eigenfunction (0.44 %)
3rd Eigenfunction (0.06 %)
Normalised Amplitude
Distance offshore (m)
Time Variation of Eigenfuntions
Mean Beach Function (m)
2nd & 3rd Eigenfunctions (m)
Time
1st Eigenfunction
2nd Eigenfunction
3rd Eigenfunction


Profile - 12
Raw Profiles
Raw Profiles
Mean Beach Function
$e_i(\lambda_i n_x)^{1/2}$
Elevation (m)
M.S.L.
Distance offshore(m)
Eigenfunctions of Profiles
Normalised Amplitude
1st Eigenfunction (98.57 %)
2nd Eigenfunction (0.89 %)
3rd Eigenfunction (0.35 %)
Distance offshore (m)
Time Variation of Eigenfuntions
Mean Beach Function (m)
2nd & 3rd Eigenfunctions (m)
Time
1st Eigenfunction
2nd Eigenfunction
3rd Eigenfunction


Profile - 13
Raw Profiles
Raw Profiles
Mean Beach Function
$e_1(\lambda_1 n_x)^{1/2}$
Elevation (m)
M.S.L.
Distance offshore(m)
Eigenfunctions of Profiles
1st Eigenfunction (99.09 %)
2nd Eigenfunction (0.58 %)
3rd Eigenfunction (0.24 %)
Normalised Amplitude
Distance offshore (m)
Time Variation of Eigenfuntions
Mean Beach Function (m)
2nd & 3rd Eigenfunctions (m)
Time
1st Eigenfunction
2nd Eigenfunction
3rd Eigenfunction

Appendix D

BATHYMETRY DATA AND COMPUTED BATHYMETRIC CHANGES

Date	Surveyors	General Location	Depth Accuracy
1827	Dumont D'Urville L'Astrolabe	Whangarei Harbour	
1848	HMS Calliope		
1939	Royal Navy		
1959	RNZN	Mair bank	
1961	RNZN HMS Lachlan	One Tree Point to Marsden Point	
1974	*Bathymetric map published NZ5213*	*Whangarei Harbour and Approaches*	*±0.1 m (<18 m) ±1.0 m (>18 m)*
1981	RNZN HMNZS Monowai	Lower Harbour, and harbour entrance	±0.3 m
1992	C/- Northland Port Corporation	Lower Harbour	± 0.1m

Table D.1 – *Major bathymetric surveys of the lower Whangarei harbour and evnirons.*

Author	Surveys considered	Location	Brief Findings
Tonkin & Taylor (1979a)	1848,1939, 1959	Marsden Point – Mair Bank	1840's – 1939: Substantial growth of Mair bank (1.5 m rise of bed level) 9m contour position unchanged. 1939 – 1959: No marked changes from. 1960 – 1979: Other sources point to accretion of Mair bank
Millar (1980)	1848,1939, 1961 1967 upper harbour survey	Entire harbour	1848 – 1961: No change in main features of the harbour. 1939 – 1967: Increase of tidal foreshore in upper harbour due to Portland Cement washings.
Healy (1980)	NHB wharf: Drawings from 1970, 1977. NZRC jetties: Soundings 1974, 1978	NHB wharf NZRC jetties	NHB wharf 1970-1977: Erosion from channel edge to west of NHB wharf, corresponding accretion on channel edge 300m northeast of wharf. NZRC jetties 1974 – 1978: 100 000m^3 of sediment eroded. Channel floor lowered 4 m.
DHI (1982)	1959, 1981	Mair Bank	Mair bank accumulating sediment at a rate of 100-150 000 m^3y^{-1}
Black (1983)	1959, 1961, 1981. 1981 cross-section surveys.	Lower Harbour	1961 – 1981: Stability of entrance gorge and Northport site. Nett erosion of lower harbour. Erosion of southern end of Mair Bank, Bream Bay beach, Calliope Bank near main channel. Accretion on the western and northern flanks of Mair Bank, and between Mair Bank and Marsden Point
Barnett et al (1993)	1981(2), 1992	Lower Harbour	1981 – 1992: Meandering of sub-tidal extension of snake bank (towards Northport site), no net change in sediment volume. Blind channel centre-line moved 50 m southwards. Filling of a hole just south of Passage Island. Minor erosion of the south side of the channel. slow accretion to the southeast of NZRC jetties.

Table D.2 – *Findings of previous comparisons of bathymetry surveys at Whangarei Harbour.*

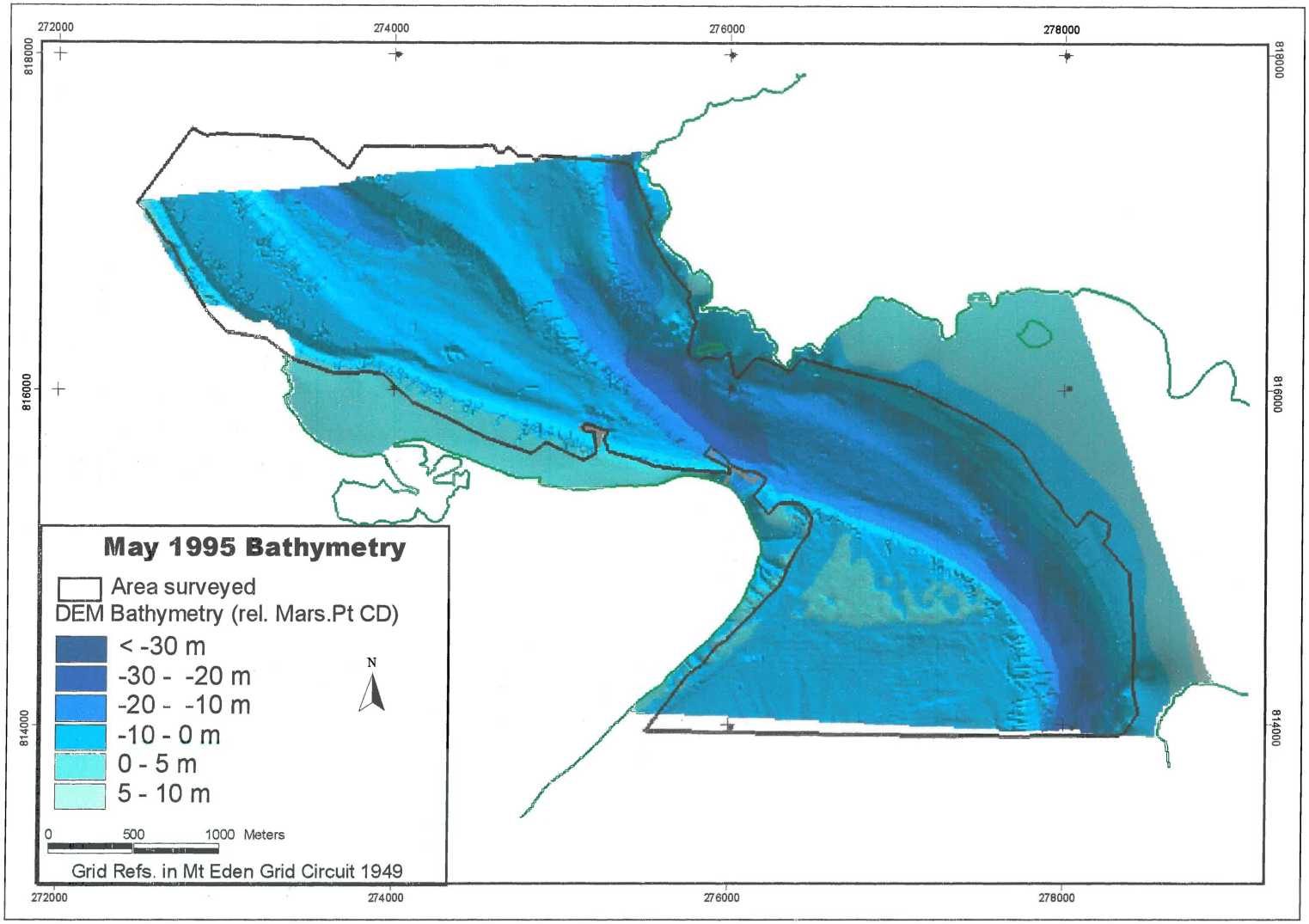


Figure D.1 - *DEM of the May 1995 Bathymetry Survey*

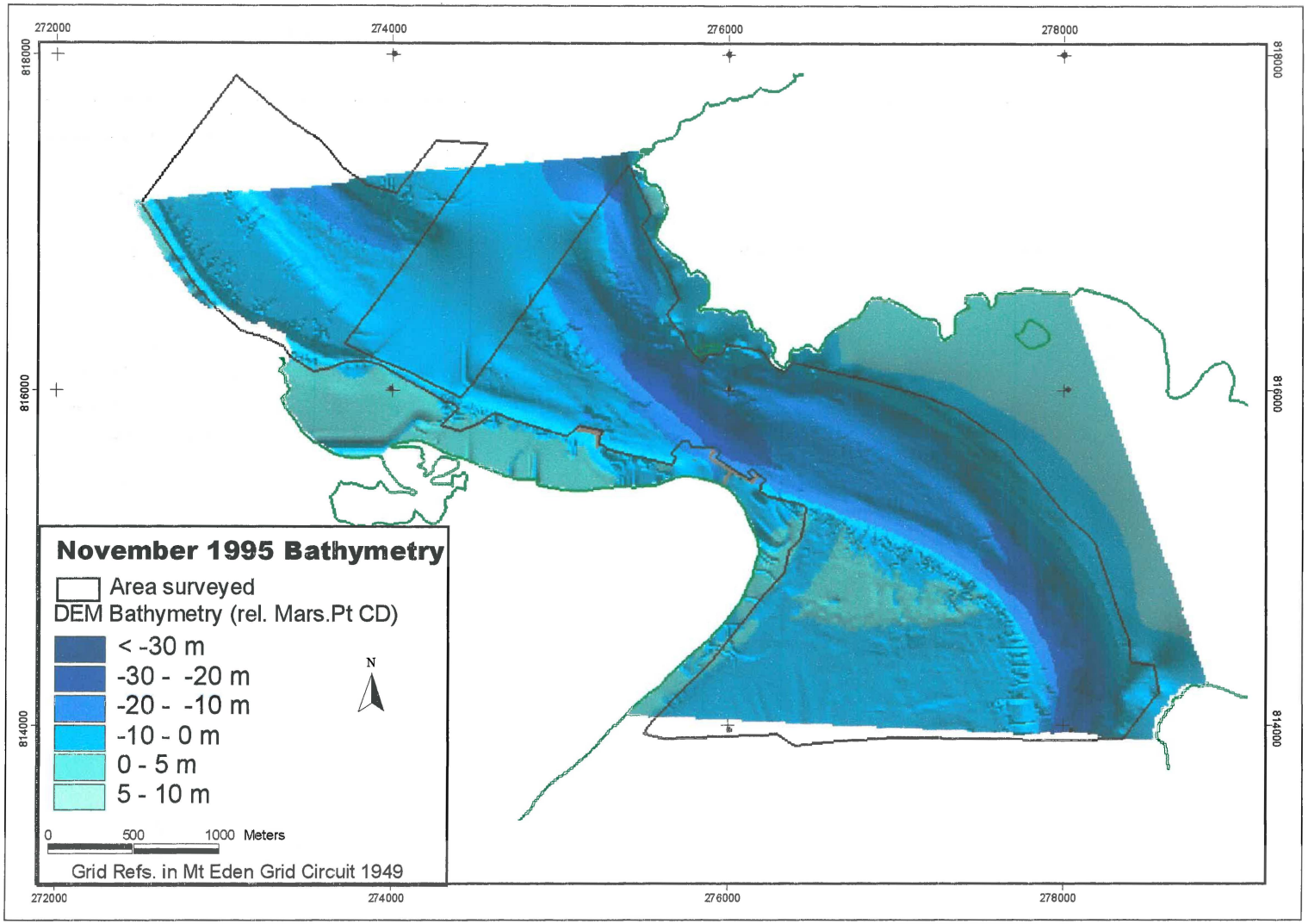


Figure D.2 - *DEM of the November 1995 Bathymetry Survey*

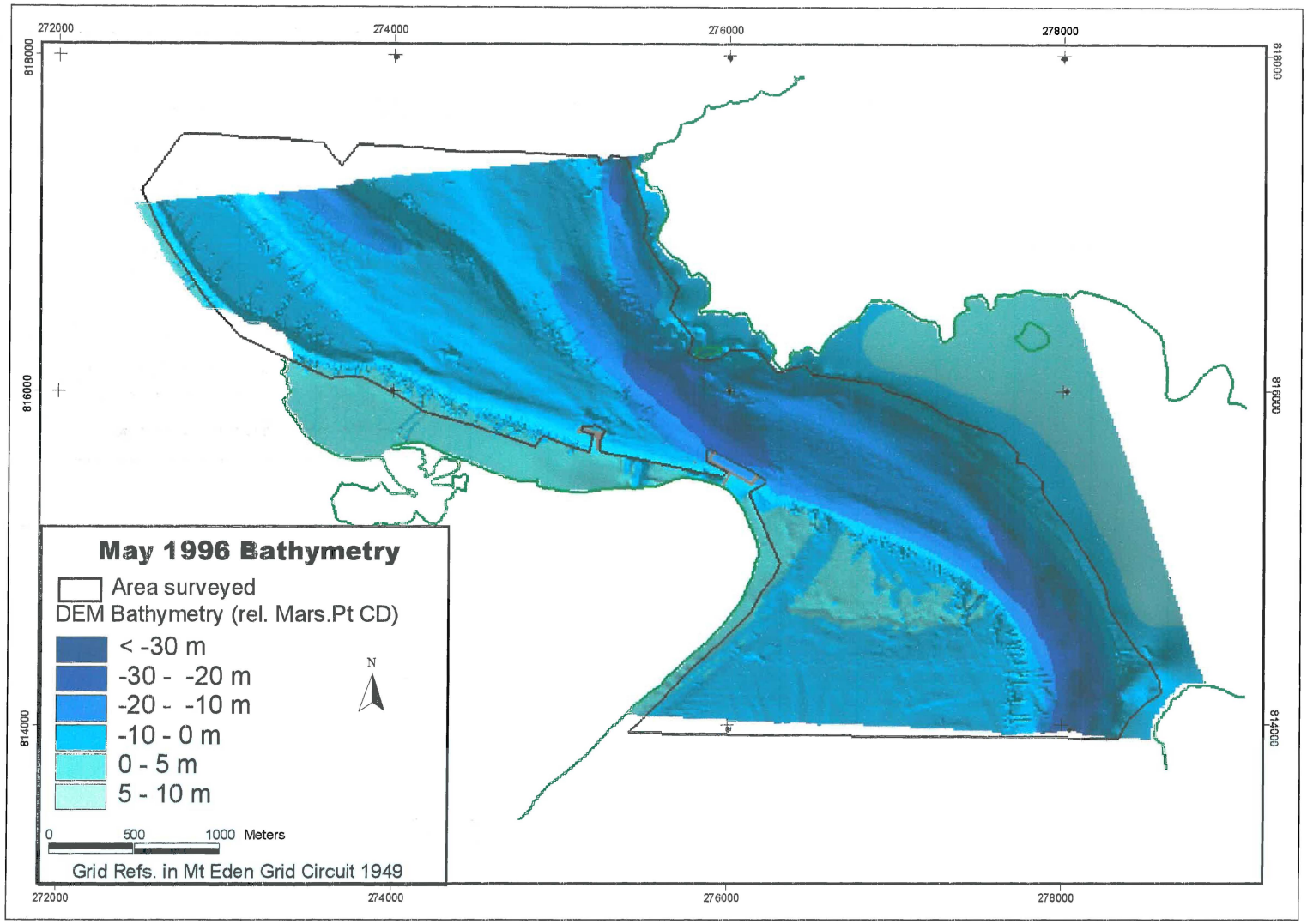


Figure D.3 - *DEM of the May 1996 Bathymetry Survey*

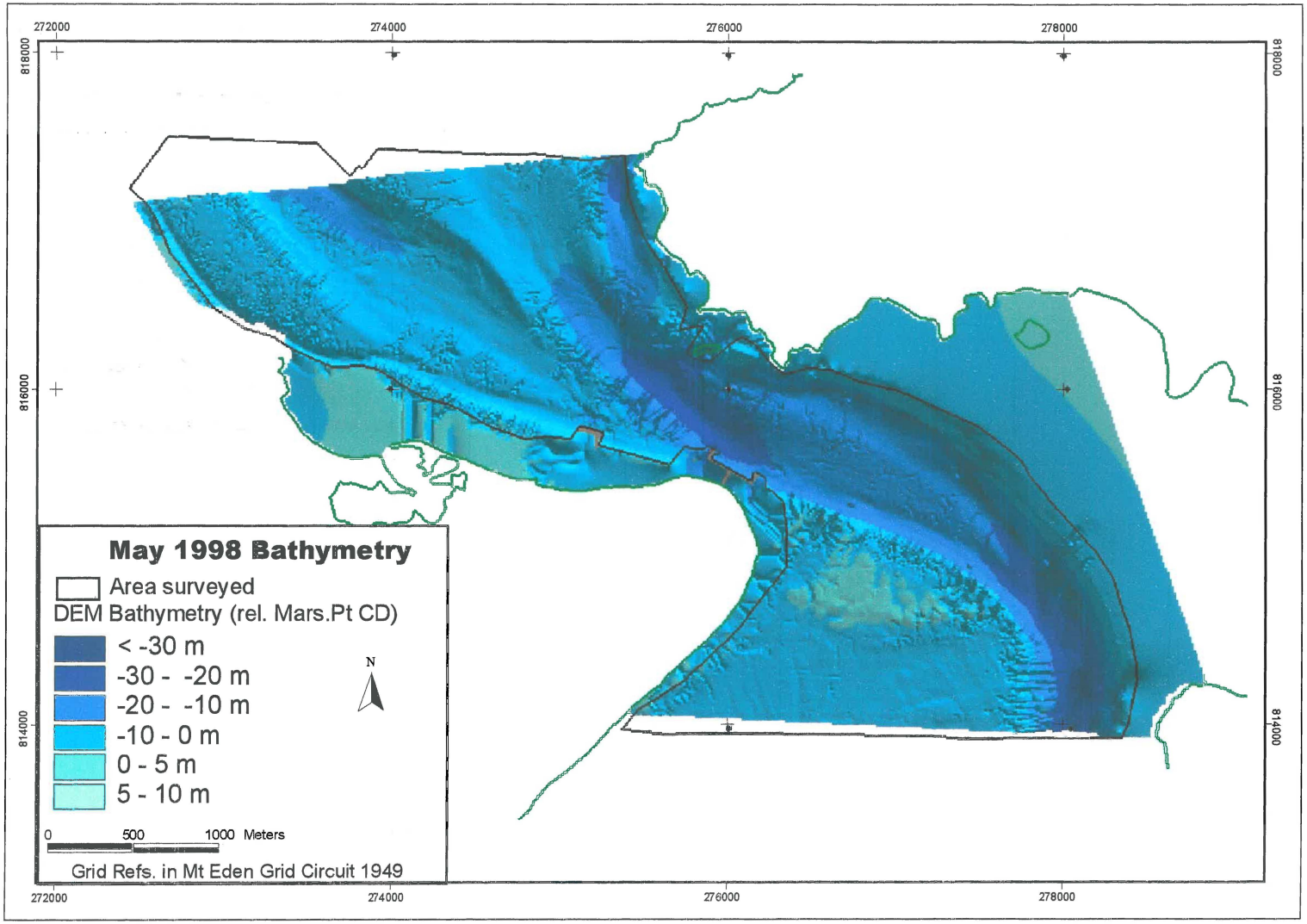


Figure D.4 - *DEM of the May 1998 Bathymetry Survey*

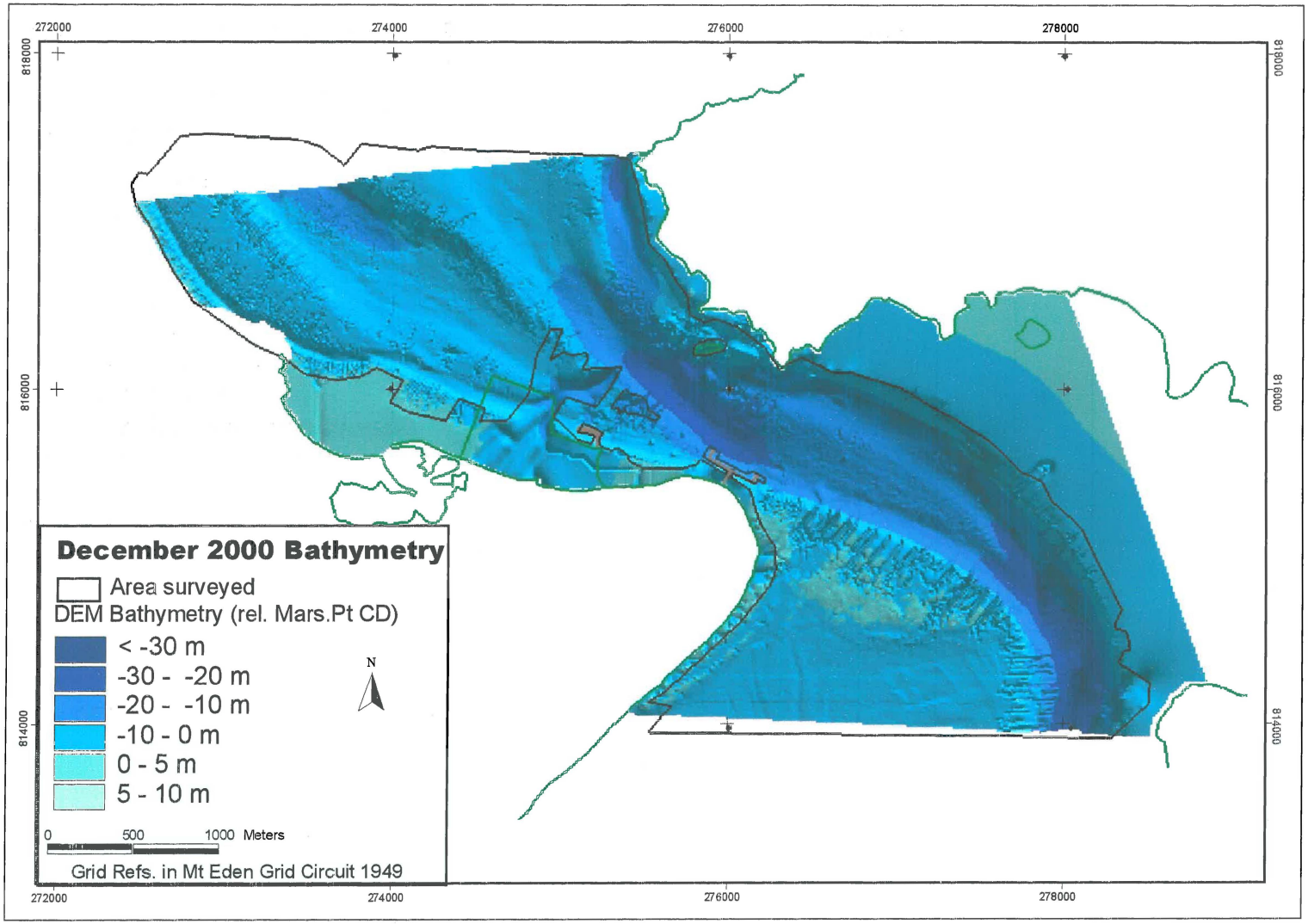


Figure D.5 - *DEM of the December 2000 Bathymetry Survey*

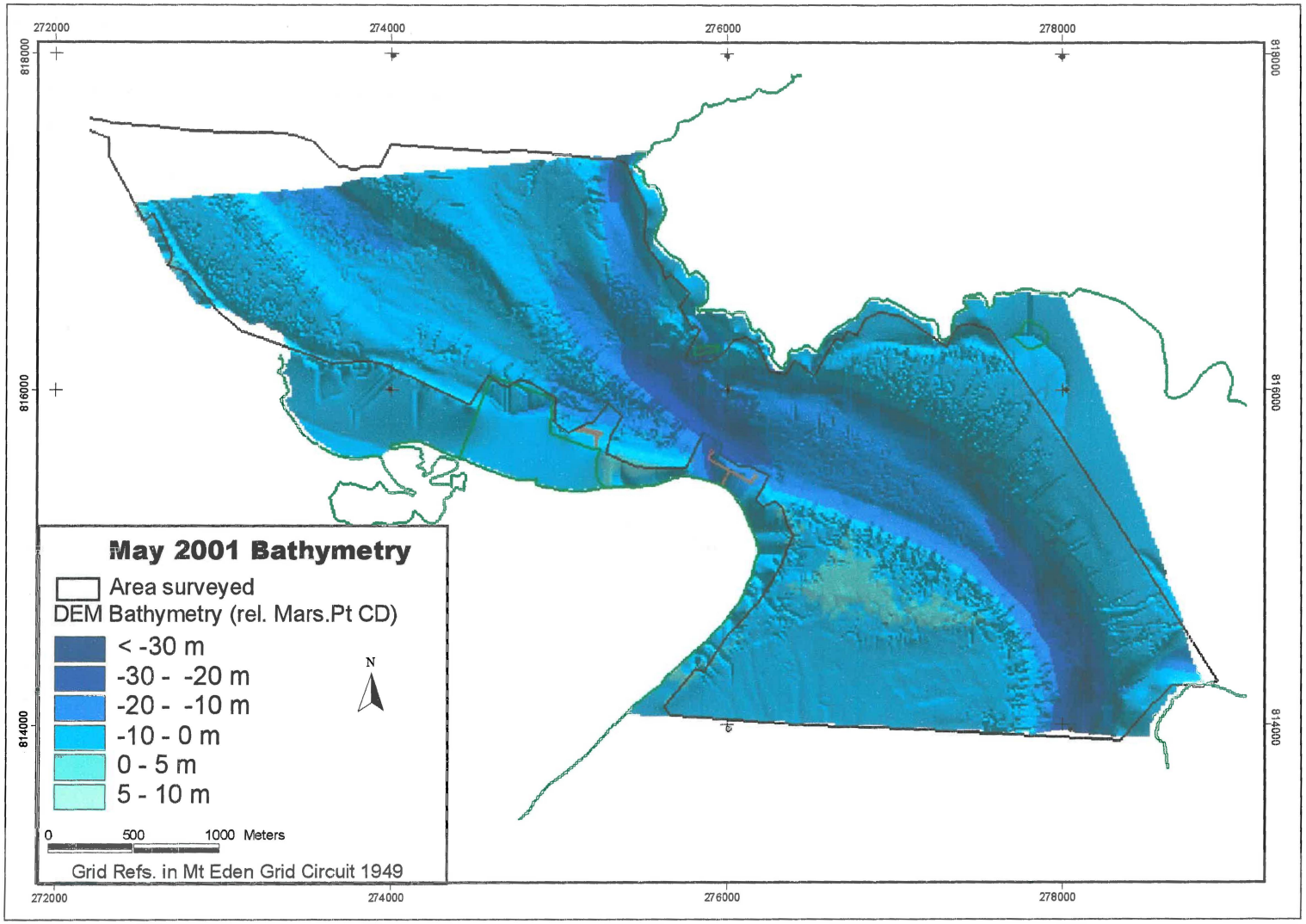


Figure D.6 - *DEM of the May 2001 Bathymetry Survey*

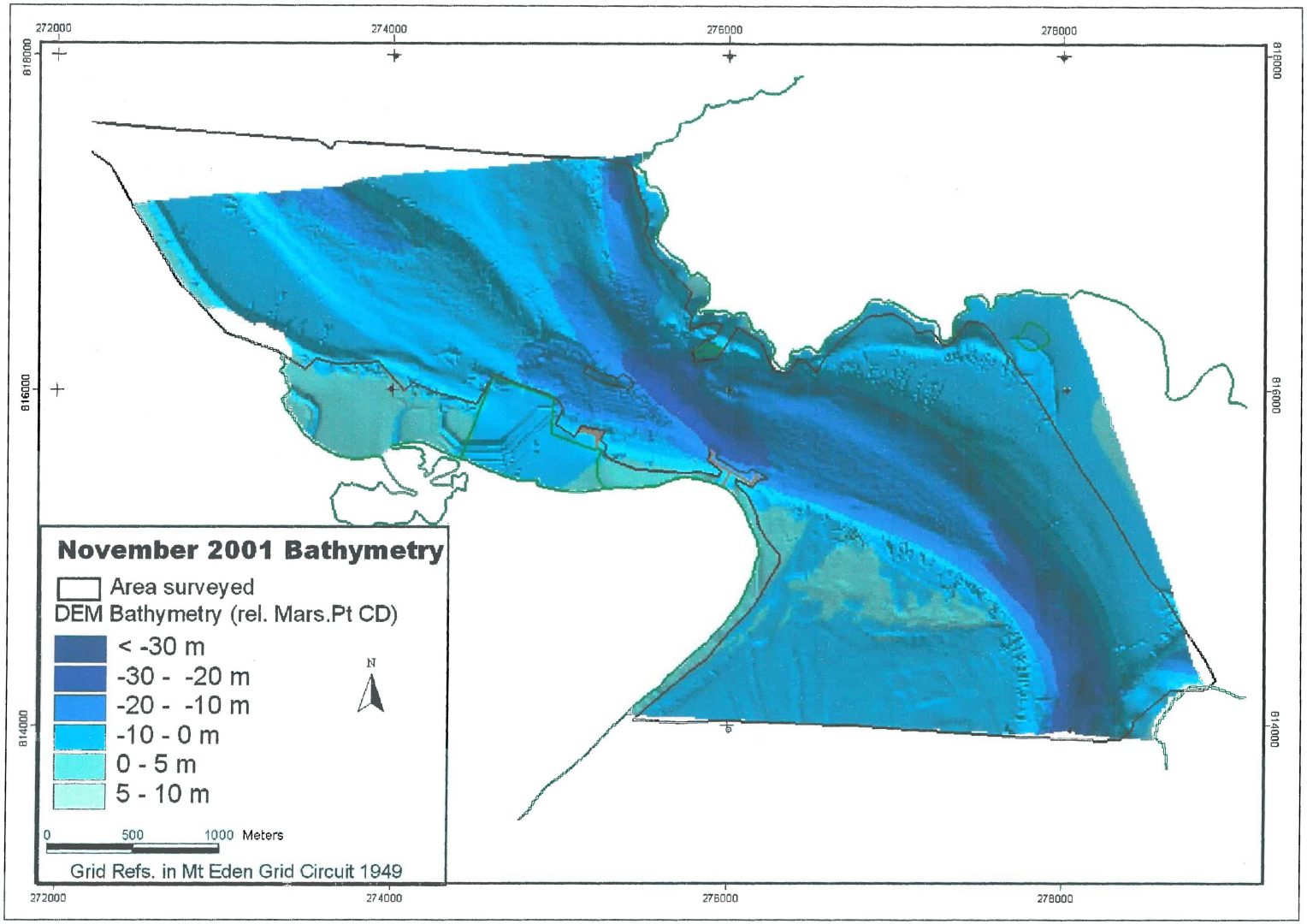


Figure D.7 - *DEM of the November 2001 Bathymetry Survey*

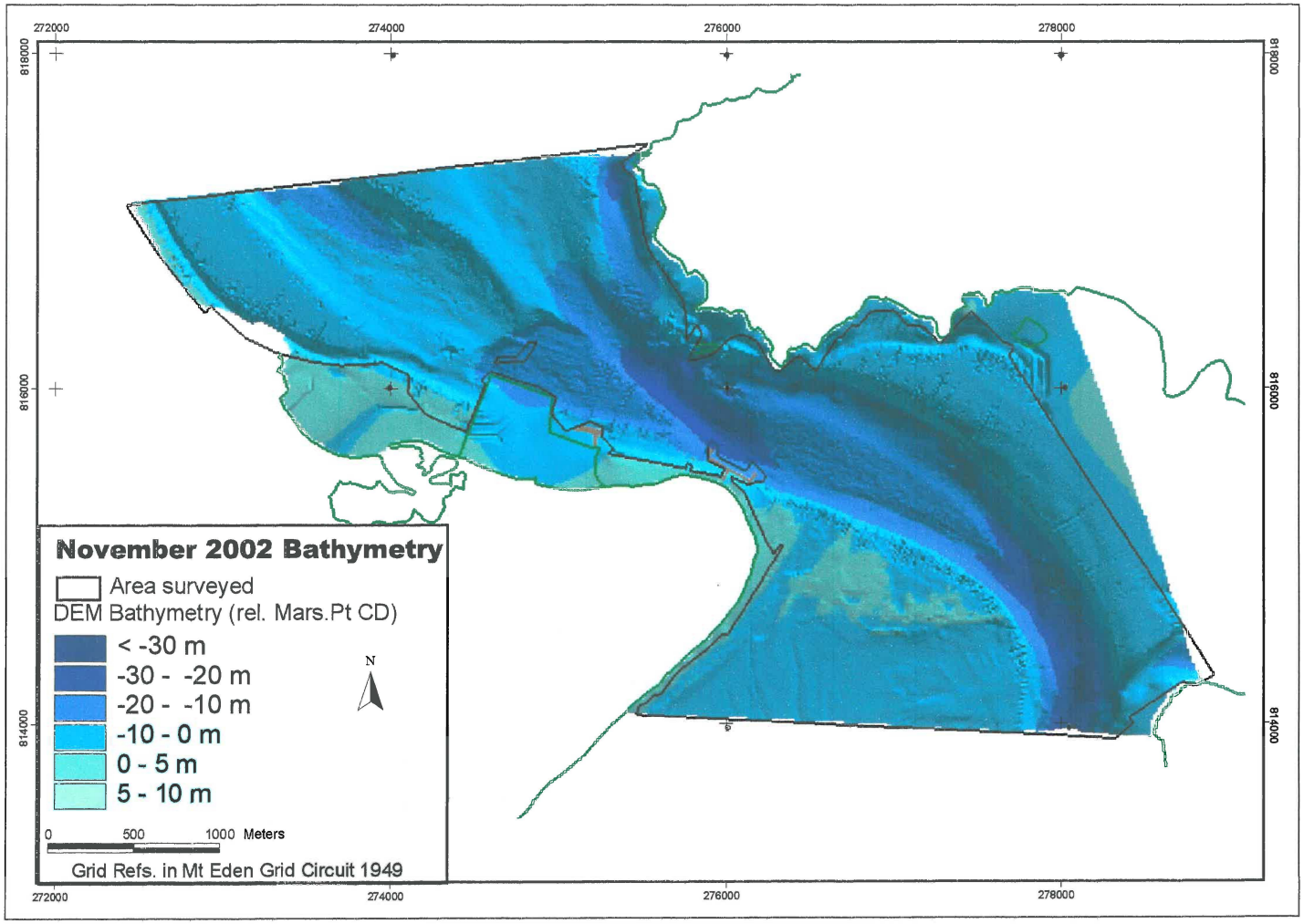


Figure D.8 - *DEM of the November 2002 Bathymetry Survey*

Script D.1 - *Pt2Poly (avenue for ArcView®)*

```
'Script Pt2Poly
'
' Convert a cluster of points to a polygon
'This script creates a polygon representing the
connection
'of the outermost points from a cluster of graphic
points.
v = av.GetActivedoc
pts = v.GetGraphics
if (pts.Count < 3) then
  msgbox.info("Please select at least 3 points to
make polygon","")
  exit
end
dicX = dictionary.make(11)
dicY = dictionary.make(11)
listPoly = {}
for each pt in pts
  pt = pt.GetShape
  if (pt.Is(Point)) then
    dicX.Add(pt.GetX,pt)
    dicY.Add(pt.GetY,pt)
  end
end
if (dicX.Count < 3) then
  msgbox.info("Please have least 3 graphic points
on view to make polygon","")
  exit
end
listX = dicX.ReturnKeys
listY = dicY.ReturnKeys
listX.Sort(true)
pt0 = dicX.Get(listX.Get(0))
listPoly.Add(pt0)
'msgbox.listasstring(listx,pt0.GetX.AsString,"")
listX.Remove(0)
for each X in listX
  pt = dicX.Get(X)
  if (pt.GetY < pt0.GetY) then
    pt0 = pt
    listPoly.Add(pt0)
'   msgbox.listasstring(listx,pt0.GetX.AsString,"")
  end
end
listY.Sort(true)
listY.Remove(0)
for each Y in listY
  pt = dicY.Get(Y)
    if (pt.GetX > pt0.GetX) then
    pt0 = pt
    listPoly.Add(pt0)
  end
end
listX.Sort(false)
listX.Remove(0)
for each X in listX
  pt = dicX.Get(X)
  if (pt.GetY > pt0.GetY) then
    pt0 = pt
    listPoly.Add(pt0)
  end
end
listY.Sort(false)
listY.Remove(0)
for each Y in listY
  pt = dicY.Get(Y)
    if (pt.GetX < pt0.GetX) then
    pt0 = pt
    listPoly.Add(pt0)
  end
end
listPoly.Add(listPoly.Get(0))
poly = polygon.make({listPoly})
v.GetGraphics.Add(GraphicShape.Make(poly))
```

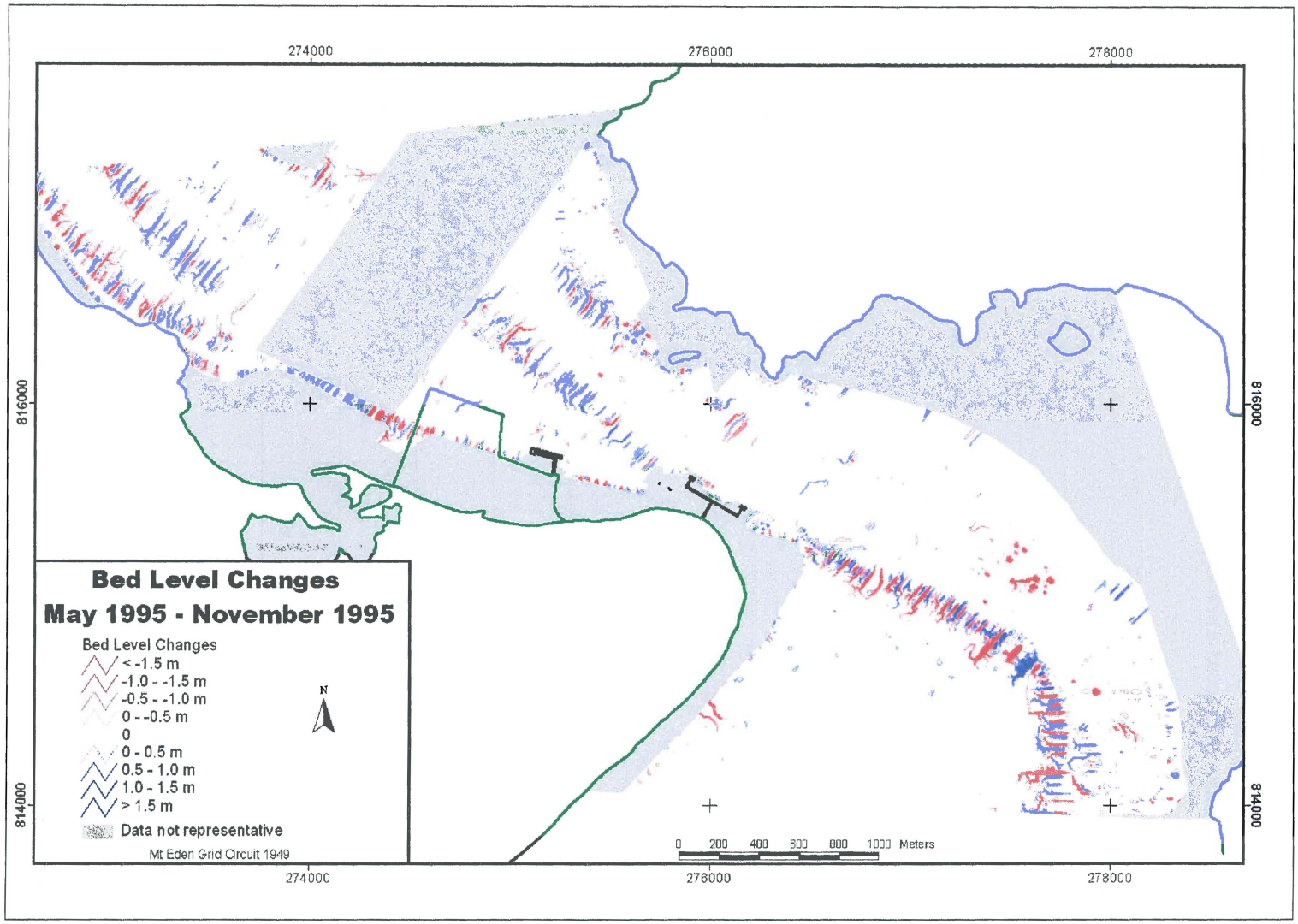


Figure D.9 - *Contours of bathymetric change at lower Whangarei Harbour, May 1995 to November 1995*

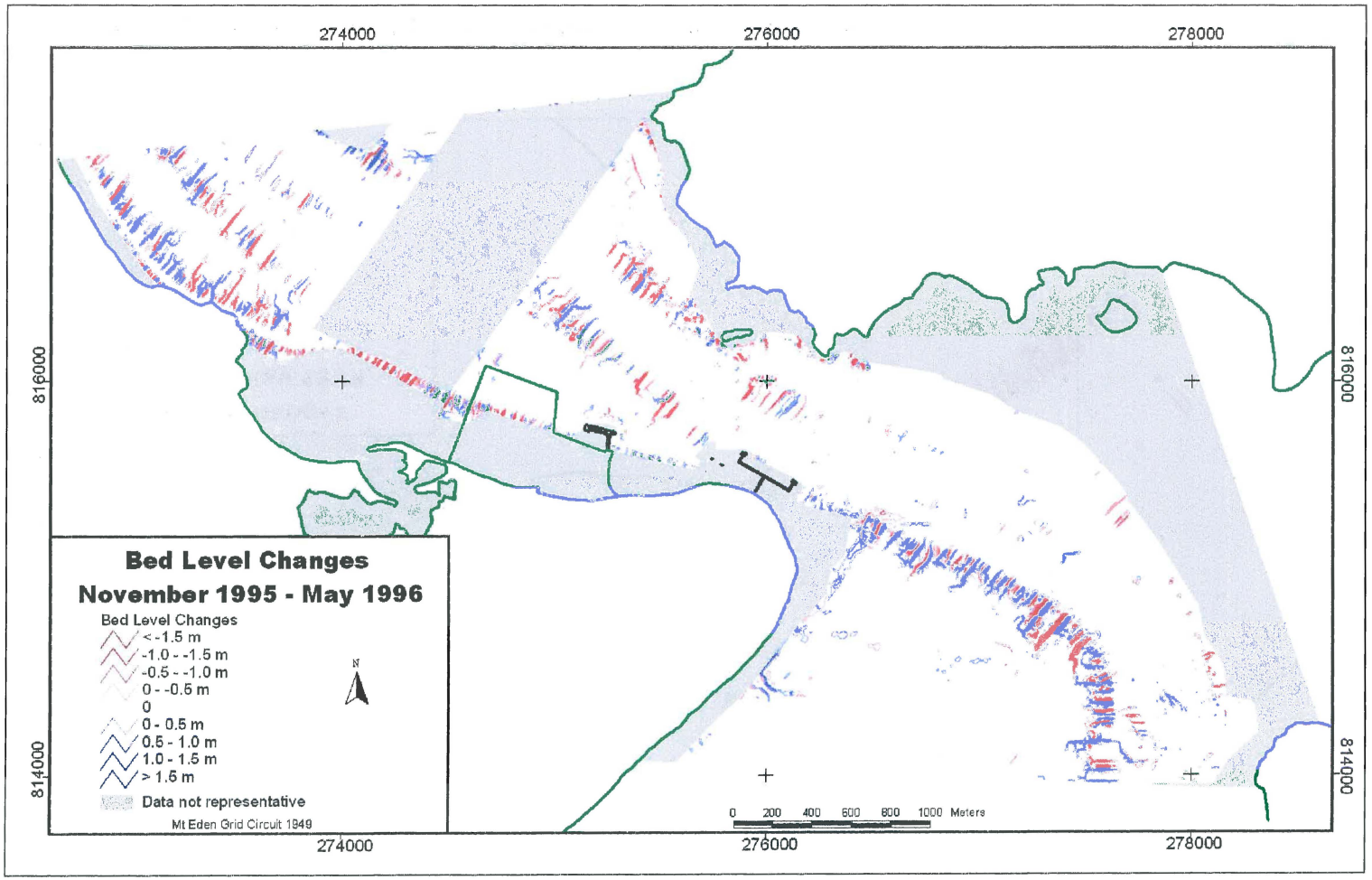


Figure D.10 - *Contours of bathymetric change at lower Whangarei Harbour, November 1995 to May 1996*

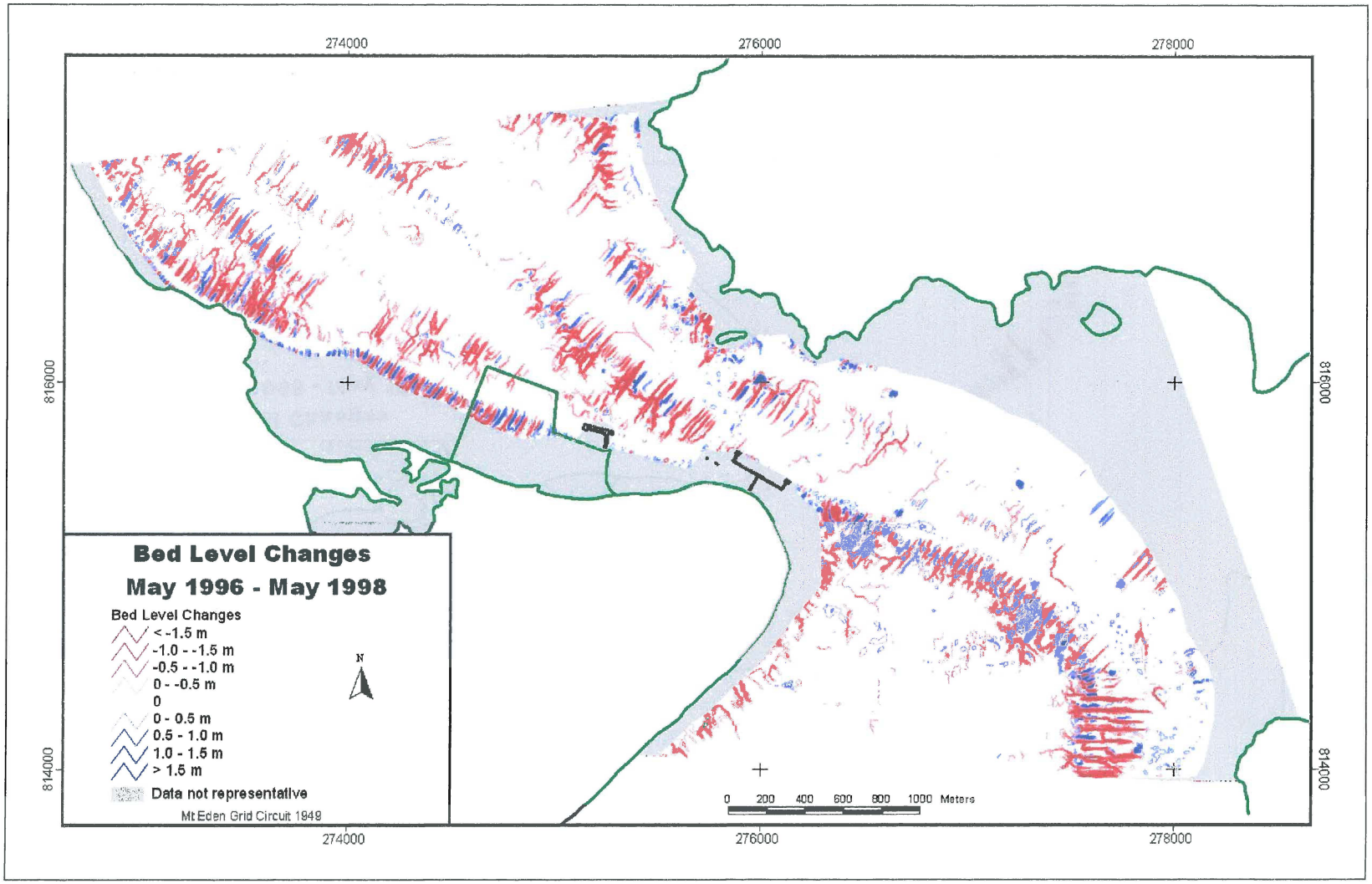


Figure D.11 - *Contours of bathymetric change at lower Whangarei Harbour, May 1996 to May 1998*

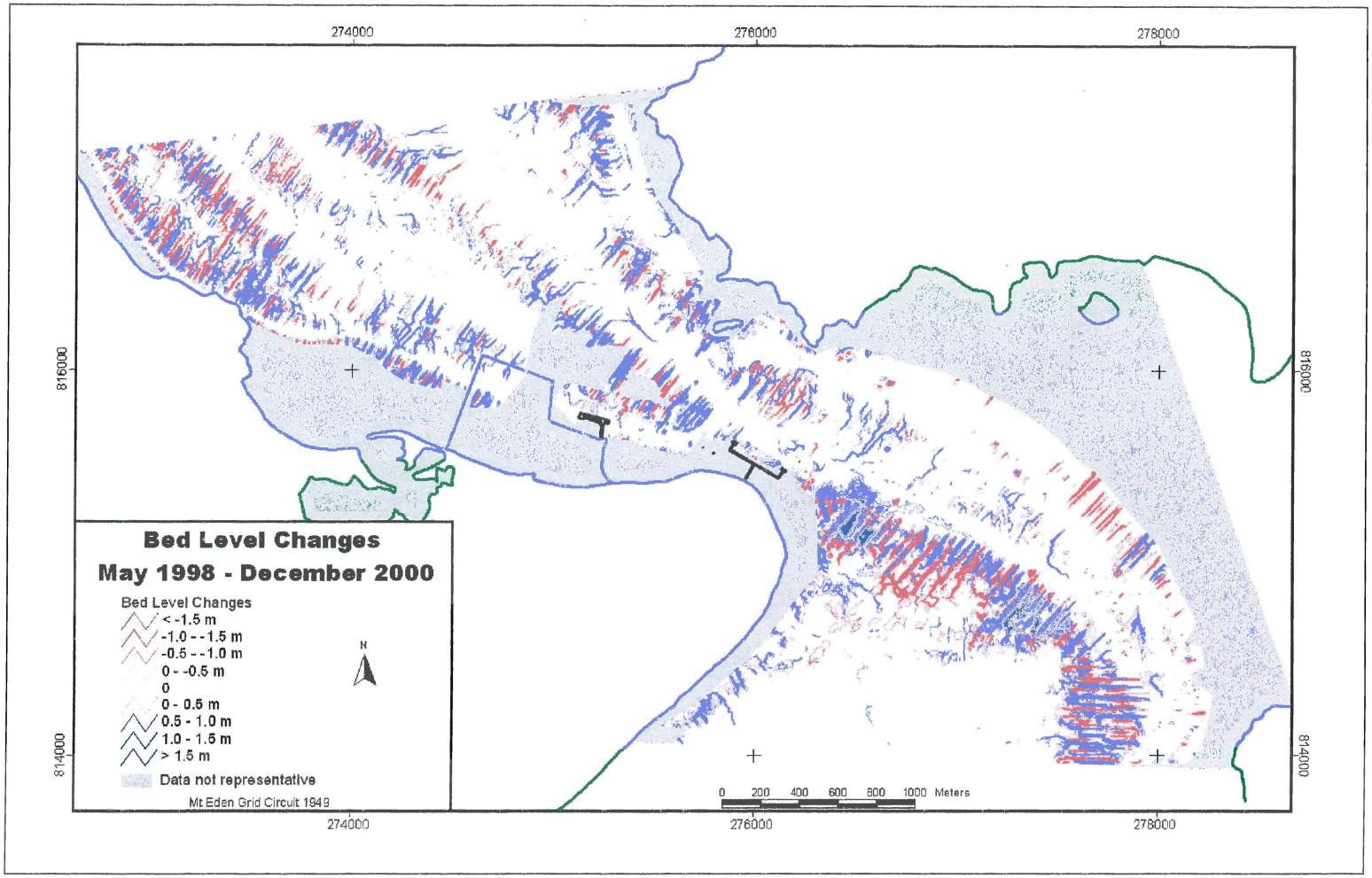


Figure D.12 - *Contours of bathymetric change at lower Whangarei Harbour, May 1998 to December 2000*

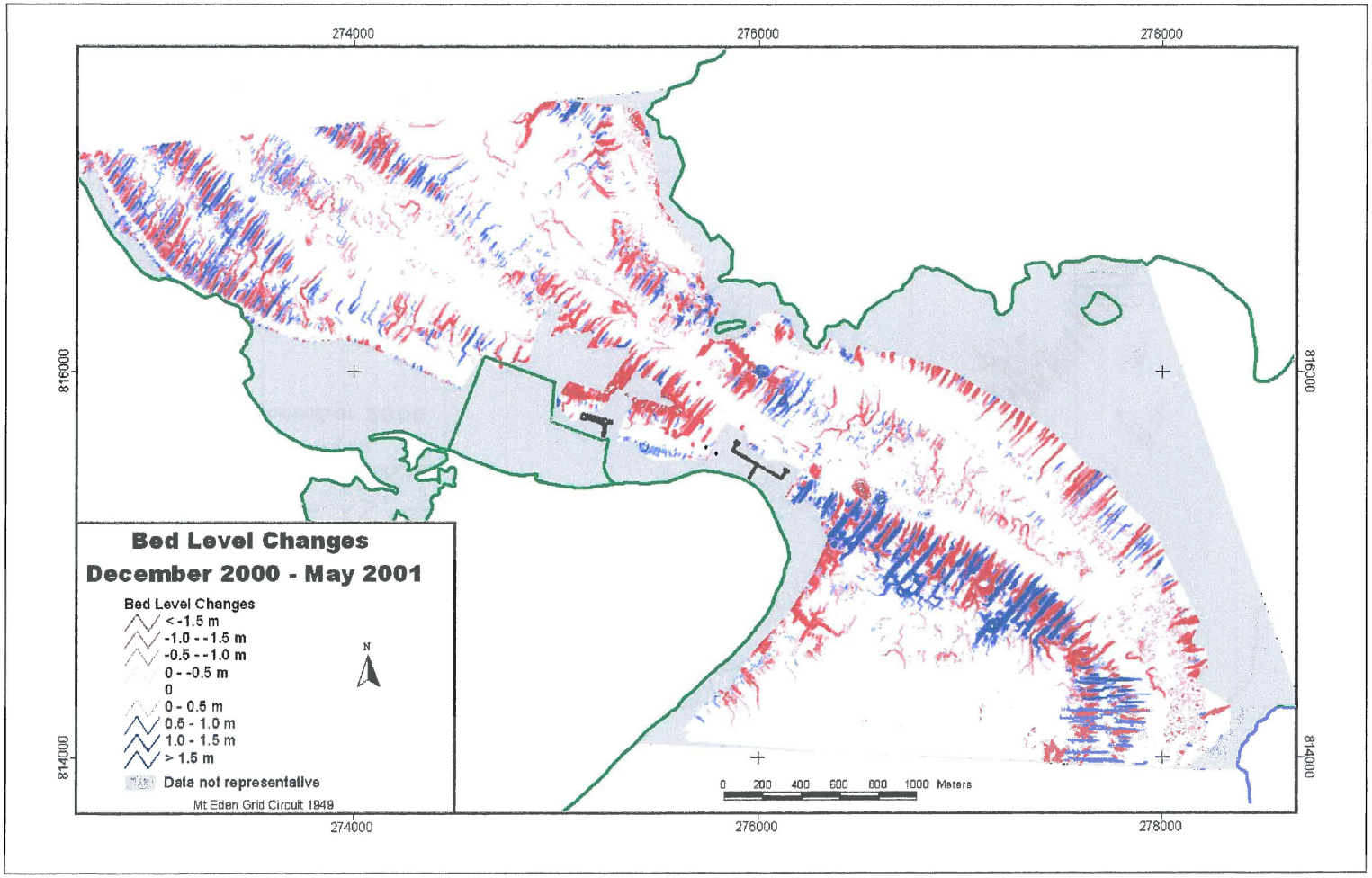


Figure D.13 - *Contours of bathymetric change at lower Whangarei Harbour, December 2000 to May 2001*

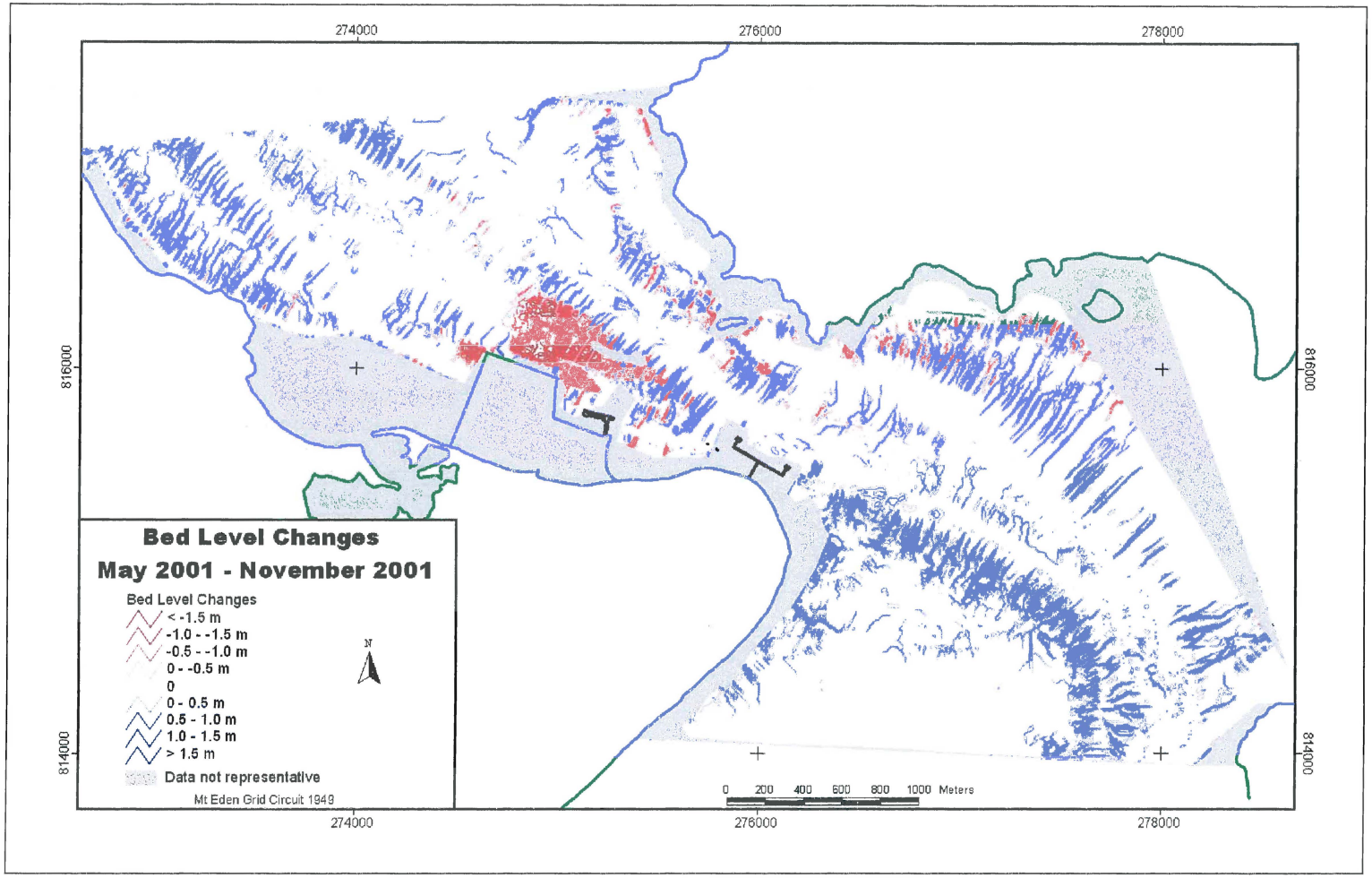


Figure D.14 - *Contours of bathymetric change at lower Whangarei Harbour, May 2001 to November 2001*

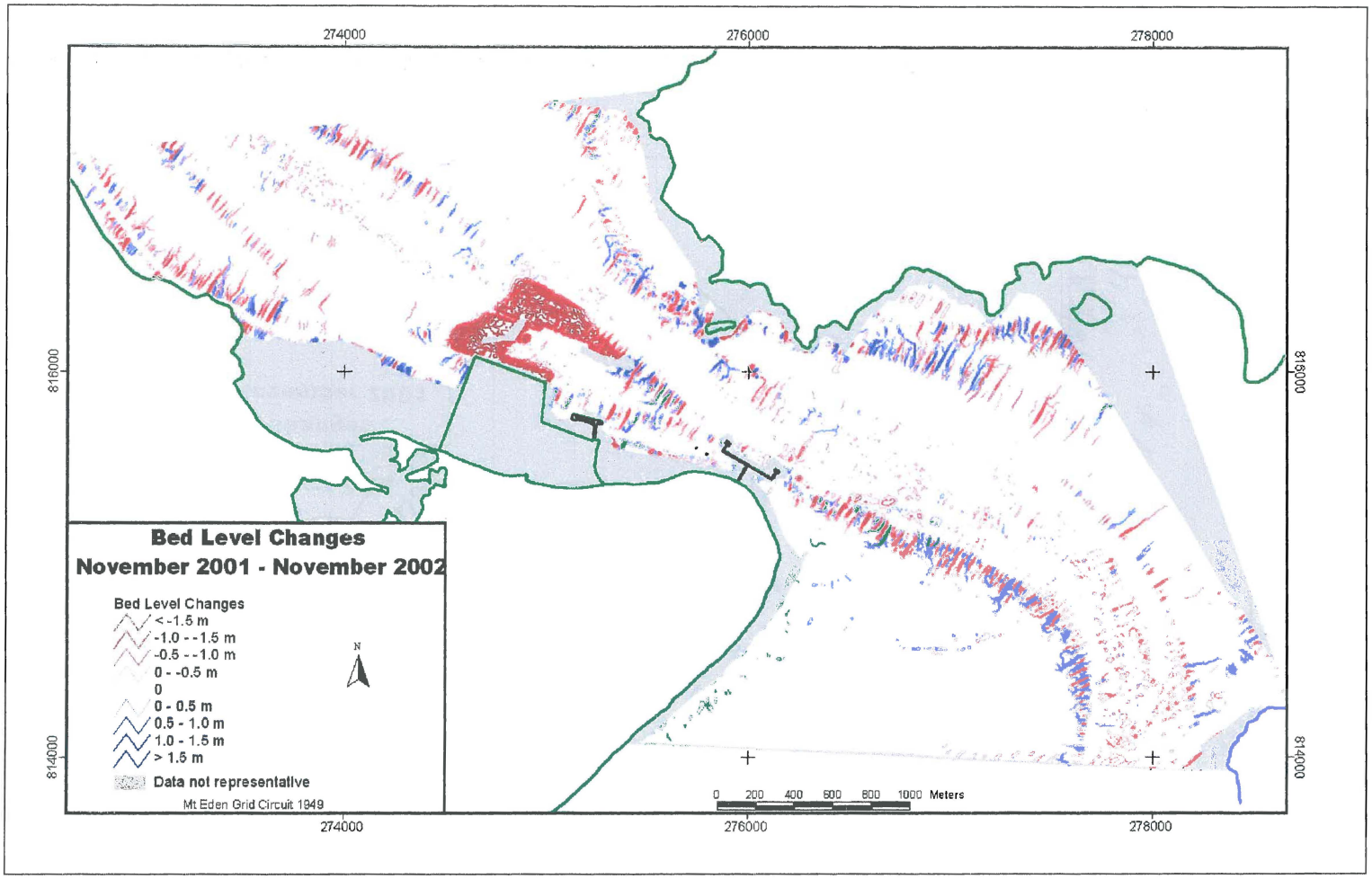


Figure D.15 - *Contours of bathymetric change at lower Whangarei Harbour, November 2001 to November 2002*

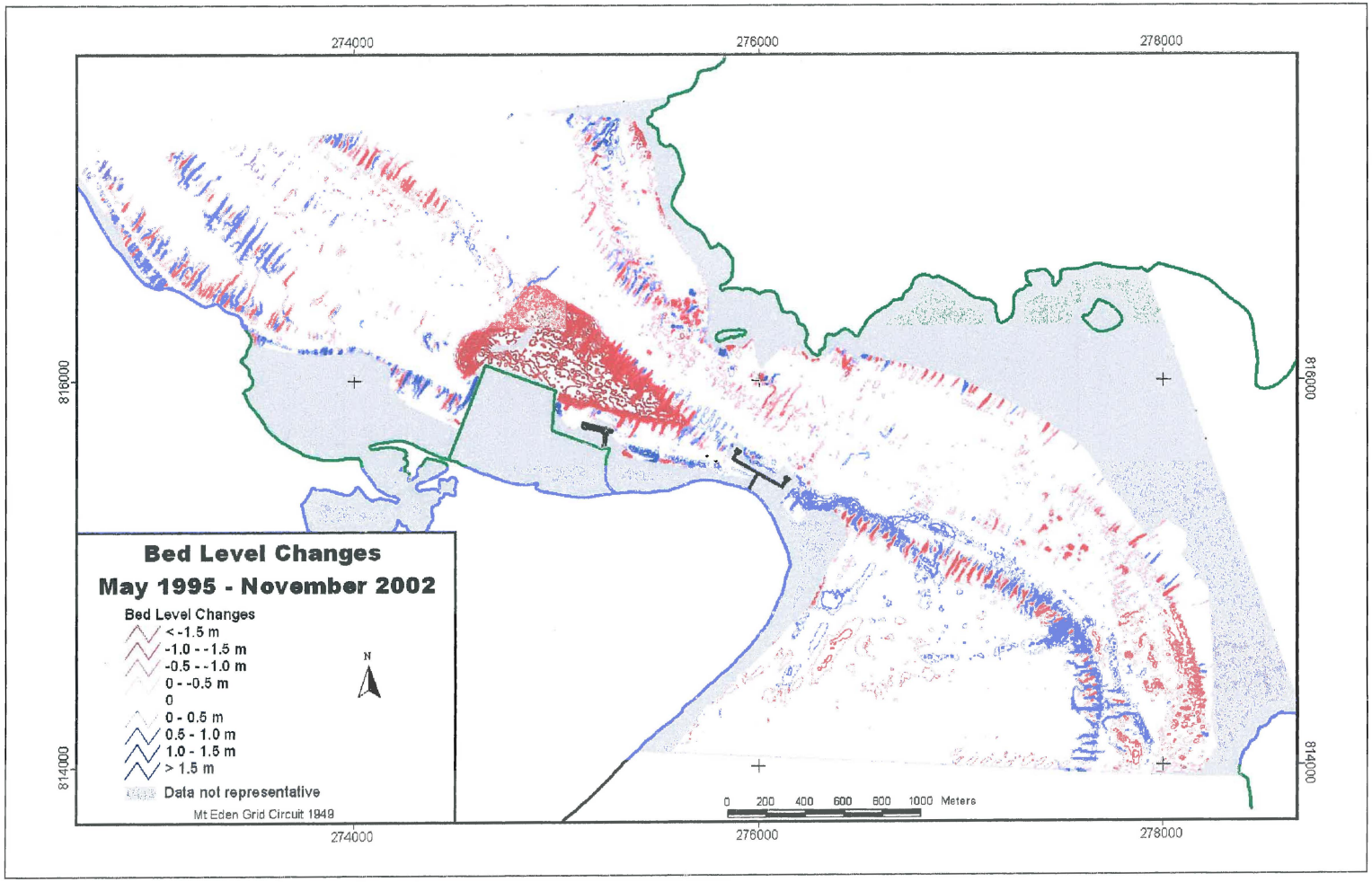


Figure D.16 - *Contours of bathymetric change at lower Whangarei Harbour, May 1995 to November 2002*

Appendix E

SIDE SCAN SONAR DATA PROCESSING

SSS image quality was improved through post-processing of the data. Post-processing involves correcting for slant-range and speed variations using the tow-fish altitude (above bed) and navigation data respectively. Corrections undertaken remove image distortions and are described below.

Across-track (range) resolution is the resolution allowing the separation of objects perpendicular to the direction of boat movement. The resolution of the image in the across-track direction is related to the pulse length of the acoustic signal and its relationship to tow-fish velocity. Shorter pulses have better resolution but are more prone to noise interferences in the water column. The energy of the beam incident on the sea floor is greater closer to the sonar due to the angle of incidence (Figure 7.1). Across-track resolution increases as the footprint of the beam approaches the actual pulse length (with increasing range from the tow-fish) (Klein Associates, 1985). In order to maximise the resolution the 500 kHz channels were used for playback during post processing. This, along with the relatively deep water being surveyed, allowed a maximum useful across track range of about 160 m.

Along-track resolution is the resolution allowing separation of objects in the same direction as boat movement. It is strongly dependent on the sonar's horizontal beam width. As with across-track, resolution increases closer to the transducer due to the greater amount of energy incident on the seabed (Figure 7.1). Other influences on the along-track resolution include pulse frequency and tow-fish speed. Increased speed acts to distort the image in the along-track direction by reducing the amount of reflected energy per pulse and also the number of echoes received by the tow-fish. The greater the tow velocity the shorter an object will appear on the trace and apparent angles of features will also increase.

By towing the transducer at a certain depth below the surface an oblique view of the seabed is recorded. The slant-range (distance between tow-fish and a feature of the seabed) recorded is always greater than the true horizontal distance (distance between seabed directly beneath tow-fish and a feature on the seabed). The slant-range distortion is greater for areas immediately beneath the tow-fish as the difference between the slant range and horizontal distance is at a maximum (compared with objects farther away in the across track direction). This results in features close to the sonar appearing more compressed.

Slant-range and vessel speed distortions in the image were corrected for during post processing. While replaying the raw data in Isis DelpMap® software the tow-fish altitude is determined by tracking the first bottom return echo, identified as a strong pulse in the signal. The bottom (and therefore tow-fish altitude) is tracked for the entire survey and saved back to the original data file. Tow-fish velocity is calculated from the GPS positional data. The DelpMap® software then corrects for slant-range and speed distortions on each run line. These corrections allow rectilinear rendering of the image resulting in an equal scale both along-track and across-track.

A mosaic of the rectilinear run line files was created in DelphMap®. The mosaic was geo-referenced based on the navigational GPS data. The sole output projection available is Universal Transverse Mercator, Zone 60 South. The geo-referenced mosaics are exported in a black and white, 8-bit GeoTIFF format with 0.25 m pixel width. The GeoTIFF format allows the SSS image to be displayed in its actual geographic position in many useful spatially referenced software programs (e.g. CAD, GIS etc).

The GeoTIFF image was plotted on an A0 size sheet of paper at a scale of 1:2500. This hardcopy was then used to delineate various units from the image. The image is a greyscale image in which the pixel value (from 0 to 255, or various shades from black to white respectively) represents the intensity of the backscatter of the sonar waves from the seafloor. Reflected wave intensity is dependent on:

i. The properties of the surface materials – their shape and orientation (hard surfaces such as rock provides a stronger reflection than soft unconsolidated fine material) and
ii. The angle of incidence of the sonar beam on the reflector.

Interference patterns may manifest themselves in the data from sources such as surface waves, dolphin noise, quenching due to air bubbles trapped in the water, mirror effects from surface reflections, refraction from density stratifications and ship wakes (Klein Associates, 1985). Issues can also arise with bottom tracking where waves have stirred up bottom sediment preventing an accurate determination of tow fish altitude (D. Immenga pers. com.), as was experienced in the initial SSS record from December 2002.

Appendix F

SEDIMENT TRANSPORT RELATED DATA, METHODS AND PROGRAMS

ADCP data collection methods

The ADP collected data on:

- Water velocity,
- Location from the Global Positioning System (GPS) in WGS84,
- Boat velocity from the GPS and
- Boat velocity from bottom tracking when the depth was less than 28 meters (range of the ADP).

Data was collected using SONTEK Real-Time Data Acquisition Software, a DOS based program 'ADPSA.exe' (Sontek, 1997b). This software is designed for the collection of boat mounted ADP data.

The data were collected without a correction from Magnetic to True North, as this was accounted for in post-processing. For the duration of the survey the internal battery powered the ADP.

The ADP transducers received estimates of three components of velocity, signal to noise ratio and standard deviation throughout the water column for the duration of the averaging period. An internal compass/tilt sensor provided heading, pitch and roll data. The sensor was calibrated amidships, following the manufacturers instructions (Sontek, 1997a). The sensor also had bottom-tracking capabilities, providing a depth value when the bottom was within range (~28 m).

Throughout the survey, data were transmitted in ENU (East-North-Up) coordinate units through a communication cable to the serial port of the controlling on-board PC computer running DOS. The controlling PC also received GPS information from a TRIMBLE Real Time Kinematics (RTK) GPS unit. Corrections for the position fixes were transmitted twenty times a second to the boat by radio, from a base station set up at the Harbour Lights Motel near One Tree Point.

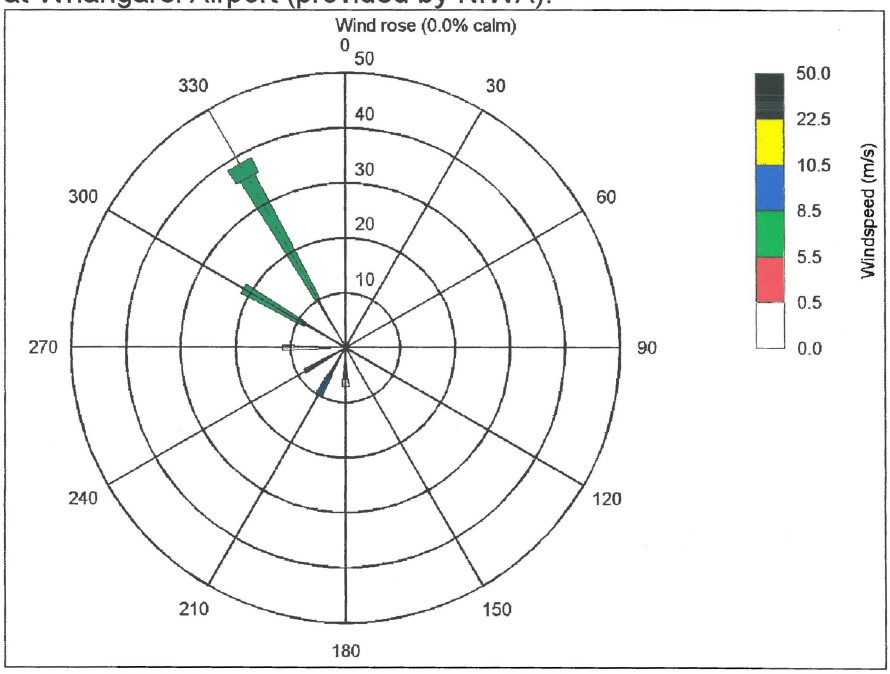
The program 'ADPSA.exe' (Sontek, 1997b) was utilised for the real time data collection. This Data Acquisition Software (DAS) is designed to receive both ADP and GPS information and store each in a single binary file. The binary file is later analysed, boat velocity calculated and then removed from the apparent water velocities. Whenever the bottom was in the 'visible' range of the ADP (< 28 m), the bottom-tracking algorithm (Sontek, 1997a) was used to calculate boat velocities and apply the correction to the apparent water velocities.

Where the depth was greater than the range of the ADP (>28 m), the RTK GPS position fixes in the binary file were used to calculate boat velocities and correct the water velocities recorded, as per the SONTEK formulations (Sontek, 1997a).

GPS data were also passed to the navigation computer, a Panasonic ToughBook, running HydroPRO® Navigation Software through a second serial port. This software displayed the transect lines, sites, boat position and boat velocity relative to these in real time. The software allowed the boat to be driven as close as possible to the intended lines or sites.

Additional data collected during the survey included records on the movements of large ships in the vicinity and the presence of tankers berthed at either the Northport wharf or the NZRC Jetties. Tidal records were obtained and digitised at 15 min intervals from the pen on paper trace recorded at the Northport Wharf (Figure 8.3). Wind data were obtained from the NZRC anemometer, located at Marsden Point.

Wind conditions during measurement of velocities and waves at Sites I-1 to I-4. Data recorded at Whangarei Airport (provided by NIWA).



Wind conditions for January 1st, 1981 to December 31st, 1987. Data supplied by NIWA via Northport.

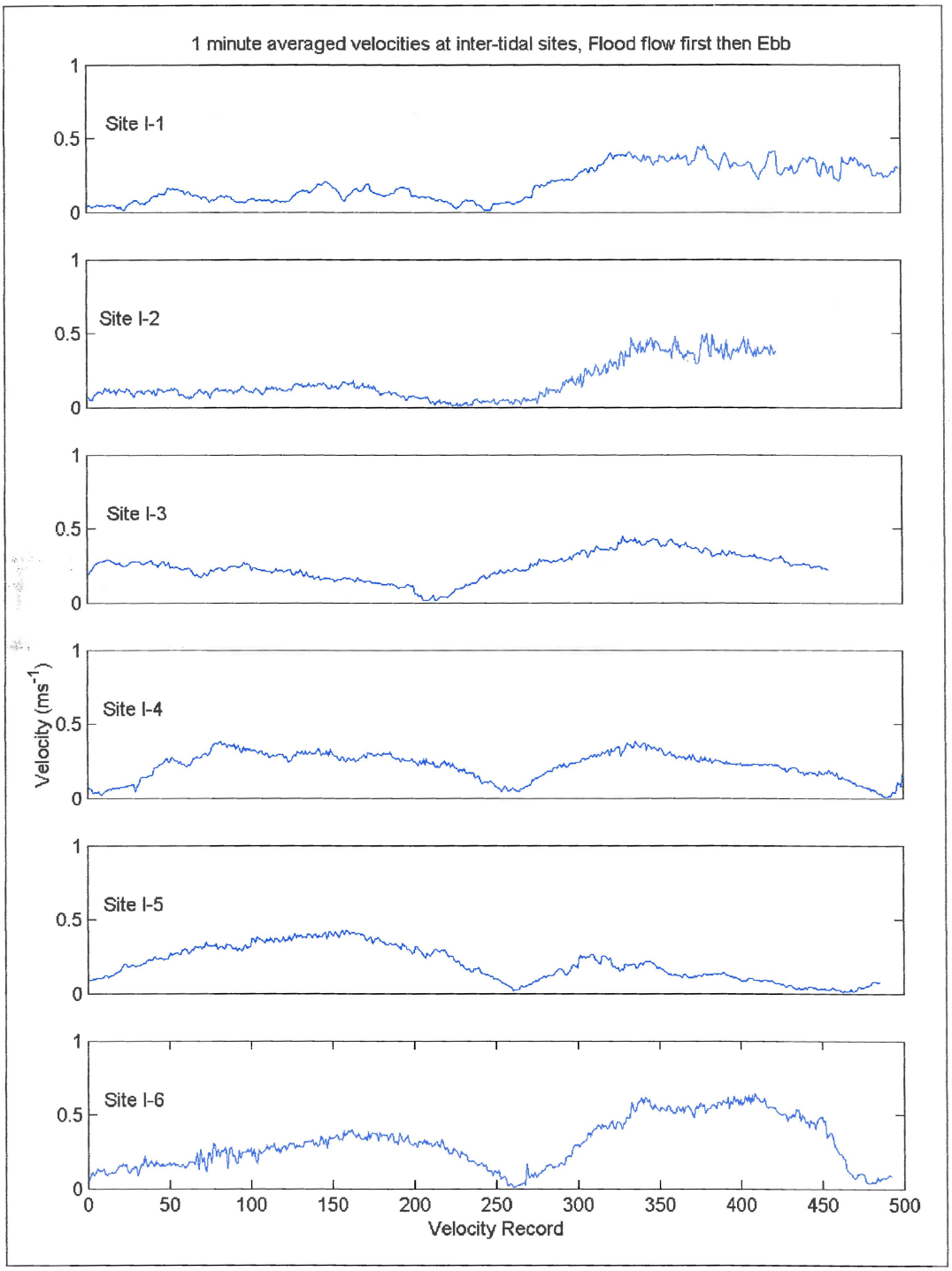
Frequencies (per thousand) For: Marsden Point A54840
Months: ALL Hours: ALL

Data from Period 1 JAN 1983 to 31 DEC 1987

SPEED (KT) DIR	1-5	6-10	11-15	16-20	21-25	26-30	31-35	36-40	41-45	46-50	ALL-S
N	18	50	28	12	2	1					110
NE	6	26	18	19	5	4					80
E	10	35	32	27	7	5	1				116
SE	5	19	14	8	1	1					48
S	8	24	10	3	1						45
SW	29	54	34	16	1						134
W	73	76	28	16	3	1					197
NW	32	45	21	9	2						108
*											
ALL DRNS	180	329	186	110	22	11	1				839

*UNSPECIFIED DIRECTION
CALM 161

Water Velocities measured at Sites I-1 to I-6 at 1 m above the bed.



Longshore transport (energy flux method) from wave hindcasting.

Site	**I-1**						
Wind	**0**						
fetch (m)	1700						
wind/crest angle	0						
beach angle	86						
time on beach face (hrs)	5						
% time on beach face	40%						
no. of wind records	1000						
D_{50} (mm)	0.17						
w=fall velocity (D_{50}) (m/s)	0.0442						
water depth (m)	1						
breaker angle(α_b)	-86						
$\sin(\alpha_b)*\cos(\alpha_b)$	-0.070						
U_s= Surface wind Speed (Kts)	3	8	13	18	23	28	33
Wind occurrence per 1000	18	50	28	12	2	1	0
Wind % Occurrence	1.80%	5.00%	2.80%	1.20%	0.20%	0.10%	0.00%
U_s= Surface wind Speed (ms^{-1})	1.5	4.1	6.7	9.3	11.8	14.4	17.0
U_A = wind stress factor	1.2	4.0	7.4	11.0	14.8	18.9	23.1
gd/U^2=	6.692	0.599	0.182	0.082	0.045	0.027	0.018
gF/U^2=	11376	1019	309	139	76	47	31
$\tanh[0.530\{gd/U^2\}^{0.75}]$=	0.9760	0.3461	0.1463	0.0807	0.0514	0.0358	0.0264
$gH_{sd}/U^2=[0.0016\{gF/U^2\}^{0.5}]$	0.1707	0.0511	0.0281	0.0188	0.0139	0.0109	0.0089
H_{sd}=	0.03	0.09	0.15	0.23	0.31	0.40	0.49
gH_{ss}/U^2=	0.1517	0.0469	0.0245	0.0155	0.0108	0.0080	0.0062
H_{ss}=	**0.02**	**0.08**	**0.13**	**0.19**	**0.24**	**0.29**	**0.34**
$\tanh[0.833\{gd/U^2\}^{0.375}]$	0.9353	0.5964	0.4131	0.3144	0.2538	0.2131	0.1839
gT/U=	5.0901	2.5385	1.7166	1.3128	1.0707	0.9084	0.7916
T=wave period (s)	**0.63**	**1.05**	**1.29**	**1.47**	**1.62**	**1.75**	**1.87**
L_d=deepwater=$gT/2\pi$	0.9807	1.6344	2.0081	2.2916	2.5267	2.7306	2.9122
L_s=shallow water = $T(gd)^{0.5}$	0.3355	1.0383	1.6742	2.2677	2.8254	3.3521	3.8516
h/L_d	1.0196	0.6119	0.4980	0.4364	0.3958	0.3662	0.3434
$d_b=0.78*H_{ss}$	0.02	0.06	0.11	0.15	0.19	0.23	0.26
C_{sg}=	0.4165	0.7736	1.0152	1.2049	1.3616	1.4948	1.6105
U_{mb} (linear wave theory)	0.1624	0.3017	0.3959	0.4699	0.5310	0.5830	0.6281
K (Bailard, 1984)/2	0.8065	0.9168	0.9914	1.0500	1.0984	1.1395	1.1752
$(EC_g)_b=pgH_{sb}^2/8$	0.27	5.95	23.15	54.53	100.47	160.23	232.55
$P_l=(EC_g)_b\sin\alpha_b\cos\alpha_b$	-0.02	-0.41	-1.61	-3.79	-6.99	-11.15	-16.18
$Q_l=K*P_l/((p_s-p)ga')$ (m^3/yr^{-1})	-50	-1251	-5265	-13135	-25320	-41890	-62704
$Q_{lw}=(m^3/yr^{-1})$	-0.36	-25.18	-59.35	-63.46	-20.39	-16.86	0.00

Site	**I-1**						
Wind	**45**						
fetch (m)	1000						
wind/crest angle	45						
beach angle	86						
time on beach face (hrs)	5						
% time on beach face	40%						
no. of wind records	1000						
D_{50} (mm)	0.17						
w=fall velocity (D_{50}) (m/s)	0.0442						
water depth (m)	1						
breaker angle(α_b)	-41						
$\sin(\alpha_b)*\cos(\alpha_b)$	-0.495						
U_s= Surface wind Speed (Kts)	3	8	13	18	23	28	33
Wind occurrence per 1000	6	26	18	19	5	4	0
Wind % Occurrence	0.60%	2.60%	1.80%	1.90%	0.50%	0.40%	0.00%
U_s= Surface wind Speed (ms^{-1})	1.5	4.1	6.7	9.3	11.8	14.4	17.0
U_A = wind stress factor	1.2	4.0	7.4	11.0	14.8	18.9	23.1
gd/U^2=	6.692	0.599	0.182	0.082	0.045	0.027	0.018
gF/U^2=	6692	599	182	82	45	27	18
$\tanh[0.530\{gd/U^2\}^{0.75}]$=	0.9760	0.3461	0.1463	0.0807	0.0514	0.0358	0.0264
$gH_{sd}/U^2=[0.0016\{gF/U^2\}^{0.5}]$	0.1309	0.0392	0.0216	0.0144	0.0107	0.0084	0.0069
H_{sd}=	0.02	0.07	0.12	0.18	0.24	0.31	0.37
gH_{ss}/U^2=	0.1218	0.0372	0.0198	0.0128	0.0091	0.0069	0.0054
H_{ss}=	**0.02**	**0.06**	**0.11**	**0.16**	**0.20**	**0.25**	**0.29**
$\tanh[0.833\{gd/U^2\}^{0.375}]$	0.9353	0.5964	0.4131	0.3144	0.2538	0.2131	0.1839
gT/U=	4.5359	2.2025	1.4867	1.1373	0.9283	0.7882	0.6874
T=wave period (s)	**0.56**	**0.91**	**1.11**	**1.27**	**1.40**	**1.52**	**1.62**
L_d=deepwater=$gT/2\pi$	0.8740	1.4180	1.7391	1.9854	2.1907	2.3693	2.5289

L_s=shallow water = $T(gd)^{0.5}$	0.2679	0.8024	1.3044	1.7856	2.2478	2.6922	3.1202
h/L_d	1.1442	0.7052	0.5750	0.5037	0.4565	0.4221	0.3954
$d_b=0.78*H_{ss}$	0.01	0.05	0.09	0.12	0.16	0.20	0.23
C_{sg}=	0.3732	0.6890	0.9133	1.0951	1.2494	1.3836	1.5024
U_{mb} (linear wave theory)	0.1456	0.2687	0.3562	0.4271	0.4873	0.5396	0.5859
K (Bailard, 1984)/2	0.2678	0.3653	0.4346	0.4908	0.5384	0.5798	0.6165
$(EC_g)_b=pgH_{sb}^2/8$	0.16	3.33	13.64	33.82	65.35	108.85	164.32
$P_l=(EC_g)_b\sin\alpha_b\cos\alpha_b$	-0.08	-1.65	-6.75	-16.74	-32.36	-53.90	-81.36
$Q_l=K*P_l/((p_s-p)ga')$ (m^3/yr^{-1})	-68	-1988	-9679	-27092	-57441	-103041	-165381
Q_{lw}=(m^3/yr^{-1})	-0.16	-20.81	-70.14	-207.23	-115.62	-165.93	0.00

Site	**I-1**						
Wind	**315**						
fetch (m)	6000						
wind/crest angle	315						
beach angle	86						
time on beach face (hrs)	5						
% time on beach face	40%						
no. of wind records	1000						
D_{50} (mm)	0.17						
w=fall velocity (D_{50}) (m/s)	0.0442						
water depth (m)	1						
breaker angle(α_b)	229						
$\sin(\alpha_b)*\cos(\alpha_b)$	0.495						
U_s= Surface wind Speed (Kts)	3	8	13	18	23	28	33
Wind occurrence per 1000	32	45	21	9	2	0	0
Wind % Occurrence	3.20%	4.50%	2.10%	0.90%	0.20%	0.00%	0.00%
U_s= Surface wind Speed (ms^{-1})	1.5	4.1	6.7	9.3	11.8	14.4	17.0
U_A = wind stress factor	1.2	4.0	7.4	11.0	14.8	18.9	23.1
gd/U^2=	6.692	0.599	0.182	0.082	0.045	0.027	0.018
gF/U^2=	40151	3596	1089	489	268	165	110
$\tanh[0.530\{gd/U^2\}^{0.75}]$=	0.9760	0.3461	0.1463	0.0807	0.0514	0.0358	0.0264
$gH_{sd}/U^2=[0.0016\{gF/U^2\}^{0.5}]$	0.3206	0.0959	0.0528	0.0354	0.0262	0.0206	0.0168
H_{sd}=	0.05	0.16	0.29	0.43	0.59	0.75	0.91
gH_{ss}/U^2=	0.2268	0.0737	0.0354	0.0209	0.0138	0.0098	0.0073
H_{ss}=	**0.03**	**0.12**	**0.20**	**0.26**	**0.31**	**0.36**	**0.40**
$\tanh[0.833\{gd/U^2\}^{0.375}]$	0.9353	0.5964	0.4131	0.3144	0.2538	0.2131	0.1839
gT/U=	6.2245	3.3738	2.2956	1.7534	1.4264	1.2069	1.0489
T=wave period (s)	**0.77**	**1.39**	**1.72**	**1.96**	**2.16**	**2.32**	**2.47**
L_d=deepwater=$gT/2\pi$	1.1993	2.1721	2.6854	3.0608	3.3662	3.6278	3.8589
L_s=shallow water = $T(gd)^{0.5}$	0.5015	1.7306	2.6942	3.5173	4.2486	4.9149	5.5328
h/L_d	0.8338	0.4604	0.3724	0.3267	0.2971	0.2757	0.2591
$d_b=0.78*H_{ss}$	0.03	0.10	0.15	0.20	0.24	0.28	0.31
C_{sg}=	0.5092	0.9701	1.2216	1.3993	1.5369	1.6497	1.7459
U_{mb} (linear wave theory)	0.1986	0.3784	0.4764	0.5457	0.5994	0.6434	0.6809
K (Bailard, 1984)/2	0.6868	0.8291	0.9068	0.9616	1.0041	1.0390	1.0687
$(EC_g)_b=pgH_{sb}^2/8$	0.74	18.45	58.41	115.15	184.06	262.29	348.22
$P_l=(EC_g)_b\sin\alpha_b\cos\alpha_b$	0.364	9.134	28.921	57.017	91.135	129.871	172.414
$Q_l=K*P_l/((p_s-p)ga')$ (m^3/yr^{-1})	824	24969	86468	180779	301722	444887	607510
Q_{lw}=(m^3/yr^{-1})	10.62	452.33	731.01	654.99	242.93	0.00	0.00

Site	**I-3**						
Wind	**0**						
fetch (m)	4300						
wind/crest angle	0						
beach angle	124						
time on beach face (hrs)	6						
% time on beach face	48%						
no. of wind records	1000						
D_{50} (mm)	0.25						
w=fall velocity (D_{50}) (m/s)	0.0442						
water depth (m)	1						
breaker angle(α_b)	-124						
$\sin(\alpha_b)*\cos(\alpha_b)$	0.464						
U_s= Surface wind Speed (Kts)	3	8	13	18	23	28	33
Wind occurrence per 1000	18	50	28	12	2	1	0
Wind % Occurrence	1.80%	5.00%	2.80%	1.20%	0.20%	0.10%	0.00%
U_s= Surface wind Speed (ms^{-1})	1.5	4.1	6.7	9.3	11.8	14.4	17.0
U_A = wind stress factor	1.2	4.0	7.4	11.0	14.8	18.9	23.1
gd/U^2=	6.692	0.599	0.182	0.082	0.045	0.027	0.018
gF/U^2=	28775	2577	781	351	192	118	79
$\tanh[0.530\{gd/U^2\}^{0.75}]$=	0.9760	0.3461	0.1463	0.0807	0.0514	0.0358	0.0264

gH_{sd}/U^2= [0.0016{gF/U^2}$^{0.5}$]	0.2714	0.0812	0.0447	0.0300	0.0222	0.0174	0.0142
H_{sd}=	0.04	0.14	0.25	0.37	0.50	0.63	0.77
gH_{ss}/U^2=	0.2082	0.0666	0.0328	0.0197	0.0132	0.0095	0.0071
H_{ss}=	**0.03**	**0.11**	**0.18**	**0.24**	**0.30**	**0.35**	**0.39**
tanh[0.833{gd/U^2}$^{0.375}$]	0.9353	0.5964	0.4131	0.3144	0.2538	0.2131	0.1839
gT/U=	5.9657	3.1568	2.1439	1.6381	1.3337	1.1294	0.9823
T=wave period (s)	**0.74**	**1.30**	**1.61**	**1.83**	**2.02**	**2.17**	**2.31**
L_d=deepwater=gT/2π	1.1495	2.0324	2.5079	2.8596	3.1473	3.3948	3.6139
L_s=shallow water = T(gd)$^{0.5}$	0.4606	1.5389	2.4228	3.1967	3.8929	4.5310	5.1242
h/L_d	0.8700	0.4920	0.3987	0.3497	0.3177	0.2946	0.2767
d_b=0.78*H_{ss}	0.02	0.09	0.14	0.19	0.23	0.27	0.30
C_{sg}=	0.4880	0.9220	1.1763	1.3612	1.5061	1.6252	1.7265
U_{mb} (linear wave theory)	0.1903	0.3596	0.4588	0.5309	0.5874	0.6338	0.6733
K (Bailard, 1984)/2	0.2201	0.3541	0.4327	0.4897	0.5345	0.5713	0.6026
$(EC_g)_b$=pgH_{sb}^2/8	0.59	14.30	48.36	100.32	166.36	243.41	329.34
P_l=$(EC_g)_b$sin$\alpha_b$cosα_b	0.28	6.63	22.42	46.51	77.12	112.84	152.68
Q_l=K*P_l/((ρ_s-p)ga') (m^3/yr^{-1})	200	7742	31979	75099	135915	212545	303334
Q_{lw}=(m^3/yr^{-1})	1.74	187.01	432.57	435.36	131.32	102.68	0.00

Site	**I-3**						
Wind	**45**						
fetch (m)	3500						
wind/crest angle	45						
beach angle	124						
time on beach face (hrs)	6						
% time on beach face	48%						
no. of wind records	1000						
D_{50} (mm)	0.25						
w=fall velocity (D_{50}) (m/s)	0.0442						
water depth (m)	1						
breaker angle(α_b)	-79						
sin(α_b)*cos(α_b)	-0.187						
U_s= Surface wind Speed (Kts)	3	8	13	18	23	28	33
Wind occurrence per 1000	6	26	18	19	5	4	0
Wind % Occurrence	0.60%	2.60%	1.80%	1.90%	0.50%	0.40%	0.00%
U_s= Surface wind Speed (ms^{-1})	1.5	4.1	6.7	9.3	11.8	14.4	17.0
U_A = wind stress factor	1.2	4.0	7.4	11.0	14.8	18.9	23.1
gd/U^2=	6.692	0.599	0.182	0.082	0.045	0.027	0.018
gF/U^2=	23421	2098	635	285	156	96	64
tanh[0.530{gd/U^2}$^{0.75}$]=	0.9760	0.3461	0.1463	0.0807	0.0514	0.0358	0.0264
gH_{sd}/U^2= [0.0016{gF/U^2}$^{0.5}$]	0.2449	0.0733	0.0403	0.0270	0.0200	0.0157	0.0128
H_{sd}=	0.04	0.12	0.22	0.33	0.45	0.57	0.70
gH_{ss}/U^2=	0.1959	0.0621	0.0311	0.0189	0.0128	0.0092	0.0070
H_{ss}=	**0.03**	**0.10**	**0.17**	**0.23**	**0.29**	**0.34**	**0.38**
tanh[0.833{gd/U^2}$^{0.375}$]	0.9353	0.5964	0.4131	0.3144	0.2538	0.2131	0.1839
gT/U=	5.7887	3.0196	2.0485	1.5656	1.2752	1.0804	0.9401
T=wave period (s)	**0.71**	**1.25**	**1.54**	**1.75**	**1.93**	**2.08**	**2.22**
L_d=deepwater=gT/2π	1.1153	1.9441	2.3964	2.7329	3.0093	3.2475	3.4587
L_s=shallow water = T(gd)$^{0.5}$	0.4336	1.4213	2.2520	2.9904	3.6610	4.2789	4.8549
h/L_d	0.8966	0.5144	0.4173	0.3659	0.3323	0.3079	0.2891
d_b=0.78*H_{ss}	0.02	0.08	0.13	0.18	0.22	0.26	0.30
C_{sg}=	0.4733	0.8902	1.1443	1.3324	1.4814	1.6044	1.7092
U_{mb} (linear wave theory)	0.1846	0.3472	0.4463	0.5196	0.5777	0.6257	0.6666
K (Bailard, 1984)/2	0.9945	1.1233	1.2017	1.2598	1.3058	1.3438	1.3762
$(EC_g)_b$=pgH_{sb}^2/8	0.51	12.00	42.12	90.15	153.14	228.22	313.15
P_l=$(EC_g)_b$sin$\alpha_b$cosα_b	-0.10	-2.25	-7.89	-16.88	-28.68	-42.75	-58.65
Q_l=K*P_l/((ρ_s-p)ga') (m^3/yr^{-1})	-313	-8327	-31257	-70136	-123494	-189395	-266140
Q_{lw}=(m^3/yr^{-1})	-0.91	-104.59	-271.80	-643.76	-298.30	-365.98	0.00

Site	**I-3**
Wind	**90**
fetch (m)	600
wind/crest angle	90
beach angle	124
time on beach face (hrs)	6
% time on beach face	48%
no. of wind records	1000
D_{50} (mm)	0.25
w=fall velocity (D_{50}) (m/s)	0.0442
water depth (m)	1
breaker angle(α_b)	-34
sin(α_b)*cos(α_b)	-0.464

U_s= Surface wind Speed (Kts)	3	8	13	18	23	28	33
Wind occurrence per 1000	10	35	32	27	7	5	1
Wind % Occurrence	1.00%	3.50%	3.20%	2.70%	0.70%	0.50%	0.10%
U_s= Surface wind Speed (ms^{-1})	1.5	4.1	6.7	9.3	11.8	14.4	17.0
U_A = wind stress factor	1.2	4.0	7.4	11.0	14.8	18.9	23.1
gd/U^2=	6.692	0.599	0.182	0.082	0.045	0.027	0.018
gF/U^2=	4015	360	109	49	27	16	11
$\tanh[0.530\{gd/U^2\}^{0.75}]$=	0.9760	0.3461	0.1463	0.0807	0.0514	0.0358	0.0264
gH_{sd}/U^2= $[0.0016\{gF/U^2\}^{0.5}]$	0.1014	0.0303	0.0167	0.0112	0.0083	0.0065	0.0053
H_{sd}=	0.02	0.05	0.09	0.14	0.19	0.24	0.29
gH_{ss}/U^2=	0.0970	0.0294	0.0158	0.0104	0.0075	0.0057	0.0046
H_{ss}=	**0.01**	**0.05**	**0.09**	**0.13**	**0.17**	**0.21**	**0.25**
$\tanh[0.833\{gd/U^2\}^{0.375}]$	0.9353	0.5964	0.4131	0.3144	0.2538	0.2131	0.1839
gT/U=	4.0032	1.9042	1.2836	0.9823	0.8022	0.6815	0.5947
T=wave period (s)	**0.49**	**0.79**	**0.96**	**1.10**	**1.21**	**1.31**	**1.40**
L_d=deepwater=$gT/2\pi$	0.7713	1.2260	1.5016	1.7147	1.8930	2.0486	2.1878
L_s=shallow water = $T(gd)^{0.5}$	0.2110	0.6167	1.0076	1.3890	1.7613	2.1244	2.4786
h/L_d	1.2965	0.8157	0.6660	0.5832	0.5283	0.4881	0.4571
d_b=$0.78*H_{ss}$	0.01	0.04	0.07	0.10	0.13	0.16	0.19
C_{sg}=	0.3330	0.6125	0.8171	0.9864	1.1329	1.2627	1.3795
U_{mb} (linear wave theory)	0.1299	0.2389	0.3187	0.3847	0.4418	0.4925	0.5380
K (Bailard, 1984)/2	1.1760	1.2623	1.3255	1.3778	1.4230	1.4631	1.4992
$(EC_g)_b$=$pgH_{sb}^2/8$	0.09	1.85	7.82	20.05	40.06	68.91	107.24
P_l=$(EC_g)_b \sin\alpha_b \cos\alpha_b$	-0.041	-0.858	-3.625	-9.295	-18.573	-31.946	-49.716
Q_l=$K*P_l/((p_s-p)ga')$ (m^3/yr^{-1})	-158	-3572	-15841	-42223	-87143	-154107	-245742
Q_{lw}=(m^3/yr^{-1})	-0.76	-60.39	-244.88	-550.73	-294.69	-372.24	-118.72

Site	**I-3**						
Wind	**315**						
fetch (m)	6000						
wind/crest angle	315						
beach angle	124						
time on beach face (hrs)	6						
% time on beach face	48%						
no. of wind records	1000						
D_{50} (mm)	0.25						
w=fall velocity (D_{50}) (m/s)	0.0442						
water depth (m)	1						
breaker angle(α_b)	191						
$\sin(\alpha_b)*\cos(\alpha_b)$	0.187						
U_s= Surface wind Speed (Kts)	3	8	13	18	23	28	33
Wind occurrence per 1000	32	45	21	9	2	0	0
Wind % Occurrence	3.20%	4.50%	2.10%	0.90%	0.20%	0.00%	0.00%
U_s= Surface wind Speed (ms^{-1})	1.5	4.1	6.7	9.3	11.8	14.4	17.0
U_A = wind stress factor	1.2	4.0	7.4	11.0	14.8	18.9	23.1
gd/U^2=	6.692	0.599	0.182	0.082	0.045	0.027	0.018
gF/U^2=	40151	3596	1089	489	268	165	110
$\tanh[0.530\{gd/U^2\}^{0.75}]$=	0.9760	0.3461	0.1463	0.0807	0.0514	0.0358	0.0264
gH_{sd}/U^2= $[0.0016\{gF/U^2\}^{0.5}]$	0.3206	0.0959	0.0528	0.0354	0.0262	0.0206	0.0168
H_{sd}=	0.05	0.16	0.29	0.43	0.59	0.75	0.91
gH_{ss}/U^2=	0.2268	0.0737	0.0354	0.0209	0.0138	0.0098	0.0073
H_{ss}=	**0.03**	**0.12**	**0.20**	**0.26**	**0.31**	**0.36**	**0.40**
$\tanh[0.833\{gd/U^2\}^{0.375}]$	0.9353	0.5964	0.4131	0.3144	0.2538	0.2131	0.1839
gT/U=	6.2245	3.3738	2.2956	1.7534	1.4264	1.2069	1.0489
T=wave period (s)	**0.77**	**1.39**	**1.72**	**1.96**	**2.16**	**2.32**	**2.47**
L_d=deepwater=$gT/2\pi$	1.1993	2.1721	2.6854	3.0608	3.3662	3.6278	3.8589
L_s=shallow water = $T(gd)^{0.5}$	0.5015	1.7306	2.6942	3.5173	4.2486	4.9149	5.5328
h/L_d	0.8338	0.4604	0.3724	0.3267	0.2971	0.2757	0.2591
d_b=$0.78*H_{ss}$	0.03	0.10	0.15	0.20	0.24	0.28	0.31
C_{sg}=	0.5092	0.9701	1.2216	1.3993	1.5369	1.6497	1.7459
U_{mb} (linear wave theory)	0.1986	0.3784	0.4764	0.5457	0.5994	0.6434	0.6809
K (Bailard, 1984)/2	1.3713	1.5136	1.5913	1.6462	1.6887	1.7235	1.7532
$(EC_g)_b$=$pgH_{sb}^2/8$	0.74	18.45	58.41	115.15	184.06	262.29	348.22
P_l=$(EC_g)_b \sin\alpha_b \cos\alpha_b$	0.138	3.455	10.940	21.568	34.475	49.128	65.221
Q_l=$K*P_l/((p_s-p)ga')$ (m^3/yr^{-1})	622	17243	57401	117064	191943	279171	377010
Q_{lw}=(m^3/yr^{-1})	9.62	374.85	582.33	508.97	185.45	0.00	0.00

Site	**I-4**
Wind	**0**
fetch (m)	4000
wind/crest angle	0
beach angle	129

time on beach face (hrs)	10						
% time on beach face	81%						
no. of wind records	1000						
D_{50} (mm)	0.27						
w=fall velocity (D_{50}) (m/s)	0.0526						
water depth (m)	1						
breaker angle(α_b)	-129						
$\sin(\alpha_b)*\cos(\alpha_b)$	0.489						
U_s= Surface wind Speed (Kts)	3	8	13	18	23	28	33
Wind occurrence per 1000	18	50	28	12	2	1	0
Wind % Occurrence	1.80%	5.00%	2.80%	1.20%	0.20%	0.10%	0.00%
U_s= Surface wind Speed (ms^{-1})	1.5	4.1	6.7	9.3	11.8	14.4	17.0
U_A = wind stress factor	1.2	4.0	7.4	11.0	14.8	18.9	23.1
gd/U^2=	6.692	0.599	0.182	0.082	0.045	0.027	0.018
gF/U^2=	26767	2397	726	326	178	110	73
$\tanh[0.530\{gd/U^2\}^{0.75}]$=	0.9760	0.3461	0.1463	0.0807	0.0514	0.0358	0.0264
$gH_{sd}/U^2=[0.0016\{gF/U^2\}^{0.5}]$	0.2618	0.0783	0.0431	0.0289	0.0214	0.0168	0.0137
H_{sd}=	0.04	0.13	0.24	0.35	0.48	0.61	0.75
gH_{ss}/U^2=	0.2040	0.0650	0.0322	0.0195	0.0131	0.0094	0.0071
H_{ss}=	**0.03**	**0.11**	**0.18**	**0.24**	**0.29**	**0.34**	**0.39**
$\tanh[0.833\{gd/U^2\}^{0.375}]$	0.9353	0.5964	0.4131	0.3144	0.2538	0.2131	0.1839
gT/U=	5.9049	3.1088	2.1104	1.6127	1.3132	1.1122	0.9675
T=wave period (s)	**0.73**	**1.28**	**1.58**	**1.80**	**1.99**	**2.14**	**2.28**
L_d=deepwater=$gT/2\pi$	1.1377	2.0015	2.4688	2.8152	3.0990	3.3432	3.5596
L_s=shallow water = $T(gd)^{0.5}$	0.4512	1.4974	2.3629	3.1247	3.8123	4.4436	5.0309
h/L_d	0.8789	0.4996	0.4051	0.3552	0.3227	0.2991	0.2809
$d_b=0.78*H_{ss}$	0.02	0.08	0.14	0.19	0.23	0.27	0.30
C_{sg}=	0.4829	0.9110	1.1654	1.3515	1.4979	1.6184	1.7210
U_{mb} (linear wave theory)	0.1883	0.3553	0.4545	0.5271	0.5842	0.6312	0.6712
K (Bailard, 1984)/2	0.3377	0.4488	0.5148	0.5631	0.6011	0.6324	0.6590
$(EC_g)_b=pgH_{sb}^2/8$	0.56	13.47	46.15	96.81	161.89	238.37	324.06
$P_l=(EC_g)_b\sin\alpha_b\cos\alpha_b$	0.28	6.59	22.57	47.35	79.18	116.58	158.49
$Q_l=K*P_l/((p_s-p)ga')$ (m^3/yr^{-1})	307	9747	38310	87901	156913	243058	344339
Q_{lw} =(m^3/yr^{-1})	4.45	392.39	863.66	849.29	252.68	195.70	0.00

Site	**I-4**						
Wind	**45**						
fetch (m)	3800						
wind/crest angle	45						
beach angle	129						
time on beach face (hrs)	10						
% time on beach face	81%						
no. of wind records	1000						
D_{50} (mm)	0.27						
w=fall velocity (D_{50}) (m/s)	0.0526						
water depth (m)	1						
breaker angle(α_b)	-84						
$\sin(\alpha_b)*\cos(\alpha_b)$	-0.104						
U_s= Surface wind Speed (Kts)	3	8	13	18	23	28	33
Wind occurrence per 1000	6	26	18	19	5	4	0
Wind % Occurrence	0.60%	2.60%	1.80%	1.90%	0.50%	0.40%	0.00%
U_s= Surface wind Speed (ms^{-1})	1.5	4.1	6.7	9.3	11.8	14.4	17.0
U_A = wind stress factor	1.2	4.0	7.4	11.0	14.8	18.9	23.1
gd/U^2=	6.692	0.599	0.182	0.082	0.045	0.027	0.018
gF/U^2=	25429	2277	690	310	170	104	70
$\tanh[0.530\{gd/U^2\}^{0.75}]$=	0.9760	0.3461	0.1463	0.0807	0.0514	0.0358	0.0264
$gH_{sd}/U^2=[0.0016\{gF/U^2\}^{0.5}]$	0.2551	0.0764	0.0420	0.0282	0.0208	0.0164	0.0134
H_{sd}=	0.04	0.13	0.23	0.35	0.47	0.59	0.73
gH_{ss}/U^2=	0.2009	0.0639	0.0318	0.0193	0.0130	0.0094	0.0071
H_{ss}=	**0.03**	**0.11**	**0.18**	**0.24**	**0.29**	**0.34**	**0.39**
$\tanh[0.833\{gd/U^2\}^{0.375}]$	0.9353	0.5964	0.4131	0.3144	0.2538	0.2131	0.1839
gT/U=	5.8609	3.0746	2.0867	1.5946	1.2986	1.1000	0.9570
T=wave period (s)	**0.72**	**1.27**	**1.56**	**1.78**	**1.96**	**2.12**	**2.26**
L_d=deepwater=$gT/2\pi$	1.1292	1.9795	2.4410	2.7836	3.0646	3.3065	3.5209
L_s=shallow water = $T(gd)^{0.5}$	0.4445	1.4681	2.3203	3.0733	3.7545	4.3808	4.9638
h/L_d	0.8855	0.5052	0.4097	0.3592	0.3263	0.3024	0.2840
$d_b=0.78*H_{ss}$	0.02	0.08	0.14	0.18	0.23	0.27	0.30
C_{sg}=	0.4793	0.9031	1.1574	1.3444	1.4918	1.6133	1.7167
U_{mb} (linear wave theory)	0.1869	0.3522	0.4514	0.5243	0.5818	0.6292	0.6695
K (Bailard, 1984)/2	1.4420	1.5520	1.6180	1.6665	1.7048	1.7363	1.7631
$(EC_g)_b=pgH_{sb}^2/8$	0.54	12.89	44.59	94.27	158.60	234.59	320.04
$P_l=(EC_g)_b\sin\alpha_b\cos\alpha_b$	-0.06	-1.34	-4.64	-9.80	-16.49	-24.39	-33.27

$Q_l=K*P_l/((p_s-p)ga')$ (m^3/yr^{-1})	-268	-6859	-24730	-53849	-92674	-139614	-193412
$Q_{lw}=(m^3/yr^{-1})$	-1.30	-143.59	-358.41	-823.78	-373.09	-449.64	0.00

Site	**I-4**						
Wind	**90**						
fetch (m)	3000						
wind/crest angle	90						
beach angle	129						
time on beach face (hrs)	10						
% time on beach face	81%						
no. of wind records	1000						
D_{50} (mm)	0.27						
w=fall velocity (D_{50}) (m/s)	0.0526						
water depth (m)	1						
breaker angle(α_b)	-39						
$\sin(\alpha_b)*\cos(\alpha_b)$	-0.489						
U_s= Surface wind Speed (Kts)	3	8	13	18	23	28	33
Wind occurrence per 1000	10	35	32	27	7	5	1
Wind % Occurrence	1.00%	3.50%	3.20%	2.70%	0.70%	0.50%	0.10%
U_s= Surface wind Speed (ms^{-1})	1.5	4.1	6.7	9.3	11.8	14.4	17.0
U_A = wind stress factor	1.2	4.0	7.4	11.0	14.8	18.9	23.1
gd/U^2=	6.692	0.599	0.182	0.082	0.045	0.027	0.018
gF/U^2=	20075	1798	545	245	134	82	55
$\tanh[0.530\{gd/U^2\}^{0.75}]$=	0.9760	0.3461	0.1463	0.0807	0.0514	0.0358	0.0264
$gH_{sd}/U^2=[0.0016\{gF/U^2\}^{0.5}]$	0.2267	0.0678	0.0373	0.0250	0.0185	0.0145	0.0119
H_{sd}=	0.03	0.11	0.21	0.31	0.41	0.53	0.65
gH_{ss}/U^2=	0.1865	0.0587	0.0297	0.0182	0.0124	0.0090	0.0069
H_{ss}=	**0.03**	**0.10**	**0.16**	**0.22**	**0.28**	**0.33**	**0.37**
$\tanh[0.833\{gd/U^2\}^{0.375}]$	0.9353	0.5964	0.4131	0.3144	0.2538	0.2131	0.1839
gT/U=	5.6486	2.9162	1.9768	1.5111	1.2312	1.0434	0.9082
T=wave period (s)	**0.70**	**1.20**	**1.48**	**1.69**	**1.86**	**2.01**	**2.14**
L_d=deepwater=$gT/2\pi$	1.0883	1.8775	2.3125	2.6378	2.9054	3.1364	3.3415
L_s=shallow water = $T(gd)^{0.5}$	0.4127	1.3350	2.1244	2.8342	3.4835	4.0846	4.6465
h/L_d	0.9188	0.5326	0.4324	0.3791	0.3442	0.3188	0.2993
$d_b=0.78*H_{ss}$	0.02	0.08	0.13	0.17	0.22	0.26	0.29
C_{sg}=	0.4618	0.8658	1.1186	1.3084	1.4599	1.5858	1.6932
U_{mb} (linear wave theory)	0.1801	0.3377	0.4363	0.5103	0.5694	0.6184	0.6603
K (Bailard, 1984)/2	0.4883	0.5931	0.6587	0.7080	0.7473	0.7799	0.8078
$(EC_g)_b=pgH_{sb}^2/8$	0.45	10.44	37.60	82.31	142.38	215.26	298.76
$P_l=(EC_g)_b\sin\alpha_b\cos\alpha_b$	-0.220	-5.107	-18.387	-40.253	-69.635	-105.280	-146.114
$Q_l=K*P_l/((p_s-p)ga')$ (m^3/yr^{-1})	-355	-9987	-39933	-93959	-171573	-270734	-389172
$Q_{lw}=(m^3/yr^{-1})$	-3	-281	-1029	-2043	-967	-1090	-313

Site	**I-4**						
Wind	**315**						
fetch (m)	7500						
wind/crest angle	315						
beach angle	129						
time on beach face (hrs)	10						
% time on beach face	81%						
no. of wind records	1000						
D_{50} (mm)	0.27						
w=fall velocity (D_{50}) (m/s)	0.0526						
water depth (m)	1						
breaker angle(α_b)	186						
$\sin(\alpha_b)*\cos(\alpha_b)$	0.104						
U_s= Surface wind Speed (Kts)	3	8	13	18	23	28	33
Wind occurrence per 1000	32	45	21	9	2	0	0
Wind % Occurrence	3.20%	4.50%	2.10%	0.90%	0.20%	0.00%	0.00%
U_s= Surface wind Speed (ms^{-1})	1.5	4.1	6.7	9.3	11.8	14.4	17.0
U_A = wind stress factor	1.2	4.0	7.4	11.0	14.8	18.9	23.1
gd/U^2=	6.692	0.599	0.182	0.082	0.045	0.027	0.018
gF/U^2=	50188	4495	1362	611	335	206	138
$\tanh[0.530\{gd/U^2\}^{0.75}]$=	0.9760	0.3461	0.1463	0.0807	0.0514	0.0358	0.0264
$gH_{sd}/U^2=[0.0016\{gF/U^2\}^{0.5}]$	0.3584	0.1073	0.0590	0.0396	0.0293	0.0230	0.0188
H_{sd}=	0.05	0.18	0.33	0.49	0.66	0.84	1.02
gH_{ss}/U^2=	0.2378	0.0782	0.0369	0.0214	0.0140	0.0099	0.0074
H_{ss}=	**0.04**	**0.13**	**0.20**	**0.26**	**0.31**	**0.36**	**0.40**
$\tanh[0.833\{gd/U^2\}^{0.375}]$	0.9353	0.5964	0.4131	0.3144	0.2538	0.2131	0.1839
gT/U=	6.3765	3.5134	2.3938	1.8279	1.4862	1.2567	1.0916
T=wave period (s)	**0.79**	**1.45**	**1.79**	**2.04**	**2.25**	**2.42**	**2.57**
L_d=deepwater=$gT/2\pi$	1.2286	2.2620	2.8004	3.1909	3.5073	3.7776	4.0160

L_s=shallow water = $T(gd)^{0.5}$	0.5261	1.8563	2.8675	3.7180	4.4689	5.1517	5.7847
h/L_d	0.8139	0.4421	0.3571	0.3134	0.2851	0.2647	0.2490
d_b=0.78*H_{ss}	0.03	0.10	0.16	0.21	0.25	0.28	0.31
C_{sg}=	0.5214	0.9993	1.2468	1.4188	1.5515	1.6606	1.7540
U_{mb} (linear wave theory)	0.2034	0.3897	0.4863	0.5533	0.6051	0.6476	0.6840
K (Bailard, 1984)/2	1.3619	1.4859	1.5502	1.5948	1.6292	1.6575	1.6818
$(EC_g)_b$=$pgH_{sb}^2/8$	0.83	21.39	64.69	123.41	193.00	271.07	356.36
P_l=$(EC_g)_b \sin\alpha_b \cos\alpha_b$	0.086	2.224	6.724	12.829	20.063	28.179	37.045
Q_l=K*P_l/((ρ_s-p)ga') (m^3/yr^{-1})	386	10894	34369	67457	107774	153997	205411
Q_{lw}=(m^3/yr^{-1})	9.95	394.70	581.11	488.82	173.55	0.00	0.00

Site	**I-5**						
Wind	**0**						
fetch (m)	3500						
wind/crest angle	0						
beach angle	146						
time on beach face (hrs)	6.5						
% time on beach face	52%						
no. of wind records	1000						
D_{50} (mm)	0.15						
w=fall velocity (D_{50}) (m/s)	0.0312						
water depth (m)	1						
breaker angle(α_b)	-146						
sin(α_b)*cos(α_b)	0.464						
U_s= Surface wind Speed (Kts)	3	8	13	18	23	28	33
Wind occurrence per 1000	18	50	28	12	2	1	0
Wind % Occurrence	1.80%	5.00%	2.80%	1.20%	0.20%	0.10%	0.00%
U_s= Surface wind Speed (ms^{-1})	1.5	4.1	6.7	9.3	11.8	14.4	17.0
U_A = wind stress factor	1.2	4.0	7.4	11.0	14.8	18.9	23.1
gd/U^2=	6.692	0.599	0.182	0.082	0.045	0.027	0.018
gF/U^2=	23421	2098	635	285	156	96	64
$\tanh[0.530\{gd/U^2\}^{0.75}]$=	0.9760	0.3461	0.1463	0.0807	0.0514	0.0358	0.0264
gH_{sd}/U^2= $[0.0016\{gF/U^2\}^{0.5}]$	0.2449	0.0733	0.0403	0.0270	0.0200	0.0157	0.0128
H_{sd}=	0.04	0.12	0.22	0.33	0.45	0.57	0.70
gH_{ss}/U^2=	0.1959	0.0621	0.0311	0.0189	0.0128	0.0092	0.0070
H_{ss}=	**0.03**	**0.10**	**0.17**	**0.23**	**0.29**	**0.34**	**0.38**
$\tanh[0.833\{gd/U^2\}^{0.375}]$	0.9353	0.5964	0.4131	0.3144	0.2538	0.2131	0.1839
gT/U=	5.7887	3.0196	2.0485	1.5656	1.2752	1.0804	0.9401
T=wave period (s)	**0.71**	**1.25**	**1.54**	**1.75**	**1.93**	**2.08**	**2.22**
L_d=deepwater=$gT/2\pi$	1.1153	1.9441	2.3964	2.7329	3.0093	3.2475	3.4587
L_s=shallow water = $T(gd)^{0.5}$	0.4336	1.4213	2.2520	2.9904	3.6610	4.2789	4.8549
h/L_d	0.8966	0.5144	0.4173	0.3659	0.3323	0.3079	0.2891
d_b=0.78*H_{ss}	0.02	0.08	0.13	0.18	0.22	0.26	0.30
C_{sg}=	0.4733	0.8902	1.1443	1.3324	1.4814	1.6044	1.7092
U_{mb} (linear wave theory)	0.1846	0.3472	0.4463	0.5196	0.5777	0.6257	0.6666
K (Bailard, 1984)/2	0.2685	0.4509	0.5620	0.6443	0.7095	0.7633	0.8092
$(EC_g)_b$=$pgH_{sb}^2/8$	0.51	12.00	42.12	90.15	153.14	228.22	313.15
P_l=$(EC_g)_b \sin\alpha_b \cos\alpha_b$	0.24	5.56	19.53	41.79	70.99	105.80	145.17
Q_l=K*P_l/((ρ_s-p)ga') (m^3/yr^{-1})	209	8273	36182	88782	166074	266273	387318
Q_{lw}=(m^3/yr^{-1})	1.97	216.48	530.20	557.57	173.83	139.35	0.00

Site	**I-5**						
Wind	**45**						
fetch (m)	4200						
wind/crest angle	45						
beach angle	146						
time on beach face (hrs)	6.5						
% time on beach face	52%						
no. of wind records	1000						
D_{50} (mm)	0.15						
w=fall velocity (D_{50}) (m/s)	0.0312						
water depth (m)	1						
breaker angle(α_b)	-101						
sin(α_b)*cos(α_b)	0.187						
U_s= Surface wind Speed (Kts)	3	8	13	18	23	28	33
Wind occurrence per 1000	6	26	18	19	5	4	0
Wind % Occurrence	0.60%	2.60%	1.80%	1.90%	0.50%	0.40%	0.00%
U_s= Surface wind Speed (ms^{-1})	1.5	4.1	6.7	9.3	11.8	14.4	17.0
U_A = wind stress factor	1.2	4.0	7.4	11.0	14.8	18.9	23.1
gd/U^2=	6.692	0.599	0.182	0.082	0.045	0.027	0.018
gF/U^2=	28106	2517	762	342	187	115	77
$\tanh[0.530\{gd/U^2\}^{0.75}]$=	0.9760	0.3461	0.1463	0.0807	0.0514	0.0358	0.0264

gH_{sd}/U^2= [0.0016{gF/U^2}$^{0.5}$]	0.2682	0.0803	0.0442	0.0296	0.0219	0.0172	0.0140
H_{sd}=	0.04	0.13	0.24	0.36	0.49	0.63	0.77
gH_{ss}/U^2=	0.2069	0.0661	0.0326	0.0197	0.0132	0.0095	0.0071
H_{ss}=	**0.03**	**0.11**	**0.18**	**0.24**	**0.30**	**0.34**	**0.39**
tanh[0.833{gd/U^2}$^{0.375}$]	0.9353	0.5964	0.4131	0.3144	0.2538	0.2131	0.1839
gT/U=	5.9461	3.1412	2.1330	1.6299	1.3270	1.1238	0.9775
T=wave period (s)	**0.73**	**1.30**	**1.60**	**1.82**	**2.01**	**2.16**	**2.30**
L_d=deepwater=gT/2π	1.1457	2.0224	2.4952	2.8451	3.1316	3.3780	3.5963
L_s=shallow water = T(gd)$^{0.5}$	0.4576	1.5254	2.4034	3.1733	3.8668	4.5027	5.0940
h/L_d	0.8728	0.4945	0.4008	0.3515	0.3193	0.2960	0.2781
d_b=0.78*H_{ss}	0.02	0.09	0.14	0.19	0.23	0.27	0.30
C_{sg}=	0.4863	0.9184	1.1728	1.3581	1.5035	1.6231	1.7248
U_{mb} (linear wave theory)	0.1897	0.3582	0.4574	0.5297	0.5864	0.6330	0.6727
K (Bailard, 1984)/2	1.0832	1.2722	1.3835	1.4646	1.5282	1.5805	1.6250
$(EC_g)_b$=pgH_{sb}^2/8	0.58	14.03	47.64	99.19	164.93	241.80	327.67
P_l=$(EC_g)_b$sinα$_b$cosα$_b$	0.11	2.63	8.92	18.58	30.89	45.29	61.37
Q_l=K*P_l/((p_s-p)ga') (m^3/yr^{-1})	391	11022	40701	89710	155650	236010	328825
Q_{lw}=(m^3/yr^{-1})	1.23	149.98	383.42	892.05	407.30	494.06	0.00

Site	**I-5**						
Wind	**90**						
fetch (m)	3000						
wind/crest angle	90						
beach angle	146						
time on beach face (hrs)	6.5						
% time on beach face	52%						
no. of wind records	1000						
D_{50} (mm)	0.15						
w=fall velocity (D_{50}) (m/s)	0.0312						
water depth (m)	1						
breaker angle(α$_b$)	-56						
sin(α$_b$)*cos(α$_b$)	-0.464						
U_s= Surface wind Speed (Kts)	3	8	13	18	23	28	33
Wind occurrence per 1000	10	35	32	27	7	5	1
Wind % Occurrence	1.00%	3.50%	3.20%	2.70%	0.70%	0.50%	0.10%
U_s= Surface wind Speed (ms^{-1})	1.5	4.1	6.7	9.3	11.8	14.4	17.0
U_A = wind stress factor	1.2	4.0	7.4	11.0	14.8	18.9	23.1
gd/U^2=	6.692	0.599	0.182	0.082	0.045	0.027	0.018
gF/U^2=	20075	1798	545	245	134	82	55
tanh[0.530{gd/U^2}$^{0.75}$]=	0.9760	0.3461	0.1463	0.0807	0.0514	0.0358	0.0264
gH_{sd}/U^2= [0.0016{gF/U^2}$^{0.5}$]	0.2267	0.0678	0.0373	0.0250	0.0185	0.0145	0.0119
H_{sd}=	0.03	0.11	0.21	0.31	0.41	0.53	0.65
gH_{ss}/U^2=	0.1865	0.0587	0.0297	0.0182	0.0124	0.0090	0.0069
H_{ss}=	**0.03**	**0.10**	**0.16**	**0.22**	**0.28**	**0.33**	**0.37**
tanh[0.833{gd/U^2}$^{0.375}$]	0.9353	0.5964	0.4131	0.3144	0.2538	0.2131	0.1839
gT/U=	5.6486	2.9162	1.9768	1.5111	1.2312	1.0434	0.9082
T=wave period (s)	**0.70**	**1.20**	**1.48**	**1.69**	**1.86**	**2.01**	**2.14**
L_d=deepwater=gT/2π	1.0883	1.8775	2.3125	2.6378	2.9054	3.1364	3.3415
L_s=shallow water = T(gd)$^{0.5}$	0.4127	1.3350	2.1244	2.8342	3.4835	4.0846	4.6465
h/L_d	0.9188	0.5326	0.4324	0.3791	0.3442	0.3188	0.2993
d_b=0.78*H_{ss}	0.02	0.08	0.13	0.17	0.22	0.26	0.29
C_{sg}=	0.4618	0.8658	1.1186	1.3084	1.4599	1.5858	1.6932
U_{mb} (linear wave theory)	0.1801	0.3377	0.4363	0.5103	0.5694	0.6184	0.6603
K (Bailard, 1984)/2	1.2568	1.4335	1.5441	1.6271	1.6934	1.7485	1.7955
$(EC_g)_b$=pgH_{sb}^2/8	0.45	10.44	37.60	82.31	142.38	215.26	298.76
P_l=$(EC_g)_b$sinα$_b$cosα$_b$	-0.209	-4.841	-17.429	-38.156	-66.007	-99.795	-138.502
Q_l=K*P_l/((p_s-p)ga') (m^3/yr^{-1})	-866	-22881	-88732	-204700	-368547	-575315	-819921
Q_{lw}=(m^3/yr^{-1})	-5	-419	-1486	-2893	-1350	-1505	-429

Site	**I-5**
Wind	**135**
fetch (m)	900
wind/crest angle	135
beach angle	146
time on beach face (hrs)	6.5
% time on beach face	52%
no. of wind records	1000
D_{50} (mm)	0.15
w=fall velocity (D_{50}) (m/s)	0.0312
water depth (m)	1
breaker angle(α$_b$)	-11
sin(α$_b$)*cos(α$_b$)	-0.187

U_s= Surface wind Speed (Kts)	3	8	13	18	23	28	33
Wind occurrence per 1000	5	19	14	8	1	1	0
Wind % Occurrence	0.50%	1.90%	1.40%	0.80%	0.10%	0.10%	0.00%
U_s= Surface wind Speed (ms^{-1})	1.5	4.1	6.7	9.3	11.8	14.4	17.0
U_A = wind stress factor	1.2	4.0	7.4	11.0	14.8	18.9	23.1
gd/U^2=	6.692	0.599	0.182	0.082	0.045	0.027	0.018
gF/U^2=	6023	539	163	73	40	25	17
$\tanh[0.530\{gd/U^2\}^{0.75}]$=	0.9760	0.3461	0.1463	0.0807	0.0514	0.0358	0.0264
$gH_{sd}/U^2 = [0.0016\{gF/U^2\}^{0.5}]$	0.1242	0.0372	0.0205	0.0137	0.0101	0.0080	0.0065
H_{sd}=	0.02	0.06	0.11	0.17	0.23	0.29	0.35
gH_{ss}/U^2=	0.1164	0.0355	0.0189	0.0123	0.0088	0.0066	0.0052
H_{ss}=	**0.02**	**0.06**	**0.10**	**0.15**	**0.20**	**0.24**	**0.29**
$\tanh[0.833\{gd/U^2\}^{0.375}]$	0.9353	0.5964	0.4131	0.3144	0.2538	0.2131	0.1839
gT/U=	4.4251	2.1387	1.4432	1.1041	0.9013	0.7654	0.6676
T=wave period (s)	**0.55**	**0.88**	**1.08**	**1.23**	**1.36**	**1.47**	**1.57**
L_d=deepwater=$gT/2\pi$	0.8526	1.3770	1.6883	1.9274	2.1270	2.3008	2.4560
L_s=shallow water = $T(gd)^{0.5}$	0.2554	0.7608	1.2383	1.6980	2.1411	2.5687	2.9815
h/L_d	1.1729	0.7262	0.5923	0.5188	0.4701	0.4346	0.4072
$d_b=0.78*H_{ss}$	0.01	0.05	0.08	0.12	0.15	0.19	0.22
C_{sg}=	0.3648	0.6728	0.8932	1.0727	1.2257	1.3594	1.4782
U_{mb} (linear wave theory)	0.1423	0.2624	0.3483	0.4184	0.4780	0.5302	0.5765
K (Bailard, 1984)/2	0.1847	0.3194	0.4159	0.4944	0.5614	0.6199	0.6718
$(EC_g)_b=pgH_{sb}^2/8$	0.14	2.96	12.20	30.49	59.40	99.67	151.50
$P_l=(EC_g)_b\sin\alpha_b\cos\alpha_b$	-0.026	-0.554	-2.285	-5.711	-11.125	-18.669	-28.377
$Q_l=K*P_l/((p_s-p)ga')$ (m^3/yr^{-1})	-16	-584	-3134	-9310	-20591	-38153	-62856
Q_{lw} =(m^3/yr^{-1})	-0.04	-5.80	-22.96	-38.98	-10.78	-19.97	0.00

MATLAB® programs

function find_residual_distance.m

```
function [s1_residuals,s2_residuals]=find_residual_distance;
sediment_threshold=0.33;
%for sites 1 and 2
for site=1:2;
   [ebb,flood] = separate_ebb_flood(site);
   [me,ne]=size(ebb);
   [mf,nf]=size(flood);
   %first ebb_profile is bad at site 1
   %now find means of each consecutive flood/ebb cycle
   for i=1:nf-1
      %remove the zeroes from the matricies so they are not taken into account during
      %the averaging
      last_gd_fld_vel=min(find(flood(:,i) == 0))-1;
      if  isempty(last_gd_fld_vel) == 1
         last_gd_fld_vel=length(flood(:,i));
      end
      flood_vels=flood(3:last_gd_fld_vel,i);
      last_gd_eb_vel=min(find(ebb(:,i) == 0))-1;
      if  isempty(last_gd_eb_vel) == 1
         last_gd_eb_vel=length(ebb(:,i));
      end
      ebb_vels=ebb(3:last_gd_eb_vel,i);
      %join ebb and flood matircies togeather
      flood_ebb=flood_vels;
      flood_ebb(length(flood_vels)+1:length(flood_vels)+length(ebb_vels))=ebb_vels;
      if  isnan(flood(2,i)) == 1 | isnan(ebb(2,i)) == 1;
         %skip as no tidal range data
         flood_ebb=NaN;
      end
      %now consider only velocities above the threshold
      %Find the excess velocity CUBED.
      %convert to polar coordinates, remove threshold then convert back
      [theta,rho]=cart2pol(real(flood_ebb),imag(flood_ebb));
      rho=(rho-sediment_threshold)^3;
      rho(find(rho < 0))=0;
      [x,y]=pol2cart(theta,rho);
      flood_ebb=complex(x,y);
      %we now need to remove the zeros from where the velocity was below the
      %threshold
      %as these should not be taken into account when we take the mean
      non_zero_indicies=find(abs(flood_ebb) > 0);
      for ii=1:length(non_zero_indicies)
         non_zero_flood_ebb(ii)=flood_ebb(non_zero_indicies(ii));
      end
      clear non_zero_indicies
      %non_zero_flood_ebb=flood_ebb;
      %10 mins between profiles =600s
      %time over threshold =number of non zero 'rhos' or magnitudes(over %threshold)*600
      no_of_vels_over_thres=length(non_zero_flood_ebb);
      time_over_threshold(i)=600*no_of_vels_over_thres;
      %find the residual_velocity of the tidal cycle
      residual_velocities(i)=mean(non_zero_flood_ebb);
      if abs(residual_velocities(i)) > 0.1
         residual_velocities(i)=0;
      end
      %to get residual_distance we need to multipy the magnitude (rho) of the velocity
      %by the time over thereshold.
      %therefore convert to polar co-ords, multiply the excess, then convert back.
[x,y]=pol2cart(angle(residual_velocities(i)),abs(residual_velocities(i))*time_over_threshold(i));
```

```
    residual_distances(i)=complex(x,y);
  end
  %       figure
  %       compass(real(res_dist),imag(res_dist))
  %       view(90,270)
  if site==1
    s1_residuals=residual_distances;
    figure
    compass(real(residual_distances),imag(residual_distances))
    view(90,270)
    figure
    h_to_get_axes=compass(real(residual_distances),imag(residual_distances));
    hold on
  elseif site ==2
    s2_residuals=residual_distances;
    good_h=compass(real(residual_distances),imag(residual_distances));
    set(h_to_get_axes,'linestyle','none')
    view(90,270)
  end
end
```

FUNCTIONS CALLED WITHIN FIND RESIDUAL DISTANCES:

separate_ebb_flood.m

```
function [ebb,flood] = separate_ebb_flood(site)
%         [ebb,flood] = separate_ebb_flood
%
%      separate original velocity data into ebb and flood components with the
%      1/2 tidal height given and time of the high/low tide at the beginning
%      of the measurements
load high_low
load profiletimes
if site ==1
   load s1velcmplx
%now need to separate the velocities in to ebb and flood for each 1/2 tidal period
ii=1;
for i=1:2:length(high_low(:,1))-4
   high_time1=high_low(i,1);
   low_time=high_low(i+1,1);
   high_time2=high_low(i+2,1);
   ebb_height=high_low(i,2)-high_low(i+1,2);
   flood_height=high_low(i+1,2)-high_low(i+2,2);
   %find the times of the profiles for the first ebb half tide.
   ebb_tide_profiles=find(s1times >= high_time1 & s1times <= low_time);
   flood_tide_profiles=find(s1times >=low_time & s1times <= high_time2);
   ebb(1,ii)=high_time1;
   ebb(2,ii)=ebb_height;
   ebb(3:length(ebb_tide_profiles)+2,ii)=s1bot(ebb_tide_profiles);
   flood(1,ii)=low_time;
   flood(2,ii)=flood_height;
   flood(3:length(flood_tide_profiles)+2,ii)=s1bot(flood_tide_profiles);
   ii=ii+1;
end
elseif site ==2
   load s2velcmplx
   ii=1;
for i=1:2:length(high_low(:,1))-4
   high_time1=high_low(i,1);
   low_time=high_low(i+1,1);
   high_time2=high_low(i+2,1);
   ebb_height=high_low(i,2)-high_low(i+1,2);
   flood_height=high_low(i+1,2)-high_low(i+2,2);
   %find the times of the profiles for the first ebb half tide.
```

```
    ebb_tide_profiles=find(s2times >= high_time1 & s2times <= low_time);
    flood_tide_profiles=find(s2times >=low_time & s2times <= high_time2);
    ebb(1,ii)=high_time1;
    ebb(2,ii)=ebb_height;
    ebb(3:length(ebb_tide_profiles)+2,ii)=s2bot(ebb_tide_profiles);
    flood(1,ii)=low_time;
    flood(2,ii)=flood_height;
    flood(3:length(flood_tide_profiles)+2,ii)=s2bot(flood_tide_profiles);
    ii=ii+1;
end
end
```

Rotate_to_north.m

```
function [rotated_vector]=rotate_to_north(matlab_vector)
[theta,rho]=cart2pol(real(matlab_vector),imag(matlab_vector));
new_theta=(theta-pi/2)*-1;
[x,y]=pol2cart(new_theta,rho);
rotated_vector=complex(x,y);
```

function scale_to_constant_tr.m

```
function [scaled_velocities]=scale_to_constant_tr(unscaled_velocities,...
tidal_range_observed,standard_tidal_range)

%
%SCALE_TO_CONSTANT_TR      scales velocity measurements in flood and ebb
%                          to a standard tidal range.
% assumes unscaled velocities is complex number
 %uses linear relationship as described in Black(1983) p80-81.
 %u2=u1.(H2/H1)

 %pre allocate matricies
 [m,n]=size(unscaled_velocities);

 scaled_velocities=(zeros(m,n))*NaN;

 %the for loop is only required if n >1, iw there are many columns
 for i=1:n
    scaled_vel_magnitude=abs(unscaled_velocities(:,i))*...
(standard_tidal_range/abs(tidal_range_observed));
    [x,y]=pol2cart(angle(unscaled_velocities(:,i)),scaled_vel_magnitude);
    scaled_velocities(:,i)=complex(x,y);
 end
```

function bm_residuals.m

```
function
[residual_distance]=bm_residuals(days_data,data_indicies,high_low,range,standard_tidal_rang
e,threshold)

%make matrix of appropriate velocities to site and times they were taken
velocities(:,1)=days_data(data_indicies,1);
velocities(:,2)=complex(days_data(data_indicies,6),days_data(data_indicies,7));
%append the times of high_low tides with ZERO velocities to the recorded data
%also sort the rows of the new data using the time as the basis for the sorting
all_velocities=sortrows(cat(1,velocities,high_low),1);
%set up matrix to interpolate velocity on to
%from min time to max time, using gaps of 10 mins
time_i=min(all_velocities(:,1)):datenum(0,0,0,0,10,0):max(all_velocities(:,1));
velocities_i=interp1(all_velocities(:,1),all_velocities(:,2),time_i);
%now scale the velocities to a standard tidal range (2.2m)
vel_i_scaled=vels_std_tr(velocities_i,range,standard_tidal_range);
%find the excess_velocities cubed above the threshold
```

```
[all_excess_velocity]=vels_above_threshold(vel_i_scaled,threshold);
all_excess_velocity=all_excess_velocity(:);
%remove the zeros from the excess velocity matrix
[excess_velocities]=remove_zeros(all_excess_velocity);
%at the interpolation stage we used 10 minutes as the interval between interpolated velocities
%therefore the time over threshold is the length of the excess_velocities*600 (seconds)
time_over_threshold=length(excess_velocities)*600;
%find the residual_velocity of the excess_velocities
residual_velocity=mean(excess_velocities);
%to get residual_distance we need to multipy the magnitude (rho) of the velocity
%by the time over thereshold.
%therefore convert to polar co-ords, multiply the excess, then convert back.
[x,y]=pol2cart(angle(residual_velocity),abs(residual_velocity)*time_over_threshold);
residual_distance=complex(x,y);
```

function tidal_cycle_transport.m

```
function [tc_transport]=tidal_cycle_transport(velocities,threshold)

%calcualte excess velocities above the threshold velocity
%Where velocities are under threshold, 0 is reported.
power=3;
sediment_density=2650;
sediment_porosity=0.45;
%convert to polar coordinates, remove threshold then convert back
[theta,rho]=cart2pol(real(velocities),imag(velocities));
rho=rho-threshold;
rho(find(rho < 0))=0;
rho=rho.^power;
[x,y]=pol2cart(theta,rho);
excess_velocities_cubed=complex(x,y);
%*****************************************************************
clear theta rho x y
%now find the tidal cycle transport

%Black's equation of bedload is qm=0.145(u1-u1cr)^3 qm is in kg/m/s.
%we need to mulitply our excess velocities cubed by 0.145, then sum
%over the tidal cycle
%each mesurement represents 1.5 minutes or 90 seconds
[theta,rho]=cart2pol(real(excess_velocities_cubed),...
   imag(excess_velocities_cubed));

%from Black's qm=0.145(u1-u1cr)^3
%and also each of our measurements represents a certain period of
%the tidal cycle(depends on length)
rep_time=(12.42*60*60)/length(velocities);
rho=rho*0.145*rep_time;
%now find the sum of these, must be in x-y form
[x_qm_tc,y_qm_tc]=pol2cart(theta,rho);
tidal_cycle_transport=complex(sum(x_qm_tc),sum(y_qm_tc));
%the tidal cycle transport is in kg/m/tidal_cycle
%now we need to convert this to m^3/m/year
%change to m3/m/tidal_cycle
[theta_tct,rho_tct]=cart2pol(real(tidal_cycle_transport),...
   imag(tidal_cycle_transport));
rho_tct=rho_tct/(sediment_density*(1-sediment_porosity));

[x,y]=pol2cart(theta_tct,rho_tct);
tc_transport=complex(x,y);
```

function weighted_mean.m

```
function [t]=weighted_mean(t_1_4,t_1_9,t_2_4)
mu=1.87;
sigma=0.347;
tidal_ranges=linspace(1.1,2.2,100);
tides_per_year=365*24/12.42;
probability=normpdf(tidal_ranges,mu,sigma);
probability(:);
probability=probability/sum(probability);
probability(:);
sum(probability);
for i=1:100;
   if tidal_ranges(i) < mu
      if t_1_4 == 0
         [a,b]=find_a_b(t_1_9,t_2_4,1.9,2.4);
         transport(i)=a*(tidal_ranges(i)^b)*probability(i);
      else
         %need to find the coefficients a and b
         [a,b]=find_a_b(t_1_4,t_1_9,1.4,1.9);
         transport(i)=a*(tidal_ranges(i)^b)*probability(i);
      end
   elseif tidal_ranges(i) > mu
      [a,b]=find_a_b(t_1_9,t_2_4,1.9,2.4);
      transport(i)=a*(tidal_ranges(i)^b)*probability(i);
   end
end
t=sum(transport)*tides_per_year;
%INTERNAL FUNCTION find_a_b
function [a,b]=find_a_b(t1,t2,del_h1,del_h2);
%transport is not linearly related to tidal range
%better approximated by the power curve phi_m=a(del_H)^b
%take log of both sides to get
%log10(phi_m)=log10(a)+b*log10(del_H);
a=10^(((log10(t1)*log10(del_h2))-(log10(t2)*log10(del_h1)))...
   /(1-log10(del_h1)));
b=(log10(t1)-log10(a))/log10(del_h1);
%END OF INTERNAL FUNCTION
```

function wave2HV.m

```
%find the wave heights that match the velocities and match them up.
function [Vl_with_wave]=waveH2V(Vl,Hs)
[m,n]=size(Vl);
Vl_with_wave=zeros(m,3)*NaN;
Vl_with_wave(:,1:2)=Vl;
for i=1:length(Vl(:,1))
   %this gives us the closest Hs_1 to the time of the velocity measurement
   time_diff=abs(Hs(:,3)-Vl(i,2));
   wave_i_closest_2_current=find(time_diff==min(time_diff));
   Vl_with_wave(i,3)=Hs(wave_i_closest_2_current,1);
end
```

function get_Ql.m

```
function Ql=get_Ql(Vl)
%Now assess the longshore sediment transport using the equation of
%Ql=0.044*density*gravity*(significant_breaker_height^2)*longshore_velocity
seawater_density=1020;
sediment_density=2650;
gravity=9.81;
constant=0.044;
a_prime=0.6;
Il=constant*seawater_density*gravity*Vl(:,3).^2.*Vl(:,1);
Ql=Il/((sediment_density-seawater_density)*gravity*a_prime);
```

function net_gross_transport

```
function [N_Ql,G_Ql]=net_gross_transport(Ql)
del_time=(12.42*60*60)/length(Ql);
tides_per_year=364*24/12.42;
%trapezoidal numerical integration
for i=1:length(Ql)-1
   area_net(i)=(del_time*Ql(i))+((del_time/2)*(Ql(i+1)-Ql(i)));
   area_gross(i)=(del_time*abs(Ql(i)))+((del_time/2)*(abs(Ql(i+1))-abs(Ql(i))));
end
N_Ql_tide=sum(area_net);
G_Ql_tide=sum(area_gross);
N_Ql=N_Ql_tide*tides_per_year;
G_Ql=G_Ql_tide*tides_per_year;
```

Appendix G

Beach Nourishment Analysis

Interval frequency (%) of particle sizes at potential nourishment sites and dredge basin. Data obtained from RSA (Appendix A). For site locations see Appendix A.

Patricle Size		Marsden Bay		One Tree Point				Dredge Basin				
		Central	West	South		Central						
Phi	mm	Profile-6	Profile-7	Profile-8	Profile-9	Profile-10	Profile-11	Dredge-A	Dredge-B	Dredge-C	Consent-E	Consent-F
-1.5	2.83	0	0	0	0	0	0	0	0	0	0	0
-1.25	2.38	0.54	0.12	0.05	0	0.07	0	2.53	0	0.17	0	0
-1.00	2.00	0	0	0.1	0	0	0	3.33	0	0.75	0.09	0
-0.75	1.68	0	0	0.15	0	0	0.07	4.82	0.09	2.25	0.09	0
-0.50	1.41	0	0	0.15	0	0	0.34	2.41	0.14	3.08	0	0
-0.25	1.19	0	0	0	0	0.14	0.34	1.84	0.14	0.92	0.09	0
0.00	1.0	0	0.06	0.39	0	0	0.14	1.72	0	0.58	0.09	0
0.25	0.84	0	0.23	1.41	0	0.47	0.27	1.95	0.18	0.25	0.27	0
0.50	0.71	0	0.12	0.58	0	1.36	1.16	1.72	0.32	0.08	0.27	0
0.75	0.59	2.54	0.46	0.29	0	1.02	0.07	1.84	0.99	0.08	0.09	0.54
1.00	0.50	0.72	0.81	1.12	2.41	0	0.62	5.28	2.12	1.42	0.18	0.75
1.25	0.42	0.97	0.87	1.51	1.98	29.58	66.03	3.56	0.9	0.58	0.36	0.75
1.50	0.35	8.15	6.38	0.63	0	39.28	14.32	1.15	1.36	4.83	0.91	3.75
1.75	0.30	5.43	1.16	6.91	0	4.55	3.97	1.49	53.37	3.91	6.2	4.29
2.00	0.25	0	60.29	49.66	74.13	4.75	4.66	3.21	19.2	0	15.86	8.58
2.25	0.210	51.87	13.28	17.02	9.43	3.73	2.19	14.93	11.21	0	17.23	21.89
2.50	0.177	15.04	8.41	8.8	5.95	5.43	1.92	11.14	5.2	65.11	0.09	25
2.75	0.149	9.18	3.94	5.64	4.11	3.39	1.85	8.96	3.12	8.83	52.21	16.09
3.00	0.125	4.11	2.67	3.65	2.13	2.71	1.3	5.51	0.99	4	4.1	9.44
3.25	0.105	1.57	1.39	2.04	0.43	1.76	0.75	6.66	0.5	1.33	1.64	5.26
Median (Φ)		2.25	2.00	2.00	2.00	1.50	1.25	2.25	1.75	2.5	2.75	2.25

Location of Transects for Beach Profile Monitoring

	Transect start point (NZMG)		
Transect I.D.	Easting	Northing	Orientation (^{o} true)
MB-1	2643397	6595381	55
MB-2	2643416	6595343	55
MB-3	2643431	6595298	55
MB-4	2643455	6595264	55
MB-5	2643488	6595227	55
MB-6	2643517	6595185	55
Mb-7	2643547	6595155	55